8th International Conference

M2D 2019

Mechanics and Materials in Design

Bologna/Italy, 4-6 September 2019

SOCIETÀ EDITRICE ESCULAPIO

ISBN 978-88-9385-155-8

Società Editrice Esculapio s.r.l.
Via Terracini, 30 – 40131 Bologna
www.editrice-esculapio.com – info@editrice-esculapio.it

Layout design: Carlotta Lenzi, Laura Tondelli, Laura Brugnoli

Editors:
Prof. **Dario Croccolo**, University of Bologna, Italy
Prof. **J.F. Silva Gomes**, University of Porto, Portugal
Prof. **S.A. Meguid**, University of Toronto, Canada

SOCIETÀ EDITRICE ESCULAPIO

TABLE OF CONTENTS

AUTHOR INDEX

KEYNOTE 1

CAN A JET ENGINE SURVIVE A BIRDSTRIKE?

Shaker A. Meguid*

Mechanics and Aerospace Design Laboratory
University of Toronto, Canada
(*)*Email:* meguid@mie.utoronto.ca

ABSTRACT

The extreme operating conditions present inside a turbofan engine, foreign object damage and birdstrike increase the likelihood of catastrophic failure of the blades, referred to as blade-out. Blade-out can involve the failure of compressor, turbine, or fan blades and can cause severe damage to the engine, wing, or fuselage and result in the loss of lives. The failure of fan blades, referred to as fan blade-out (FBO) is the most severe, since the fan blades are the largest blades in the engine and have the most kinetic energy. Due to the potential severity of a FBO event, all engine manufacturers include a containment structure (ring) which surrounds the rotating sections of the engine. This structure is designed to absorb the energy of a released blade and to contain the blade fragments so that they do not pierce fuel tanks, hydraulic control lines, and/or the fuselage. Unfortunately, current accidents show that containment structure designs are inadequate and better designs are needed.

Accordingly, this study is concerned with the design and analysis of a novel containment ring for turbofan engines using dynamic nonlinear finite element (FE) simulations and a blade-out testing apparatus. Three aspects of the work were accordingly examined. The first is concerned with the response of multilayered targets to normal and oblique impacts by a blade-like projectile. This enabled the selection of the most appropriate material combination for the containment ring. The second is concerned with the response of the selected target to blade-out impacts with partially and fully bladed fan disk. The third is concerned with the design and instrumentation of a novel test rig to calibrate the finite element simulations and examine the true response of blade-out in turbofan engines. The predictions of the finite element method reveal that Kevlar is suitable for use in containment rings. It further shows that the optimal multilayered target is the one where the exposed surface is made of aluminum foam and backing is made of Kevlar fabric. This is also confirmed in the containment of blade-out with a single trailing blade and fully bladed fan disk.

Keywords: Birdstrike, Turbofan, FBO, Containment ring, Modeling, Novel rig design

Biographical Sketch

Professor Shaker Meguid is an internationally renowned scholar with significant contributions in computational and experimental mechanics at varied length scales. Undoubtedly, his research activities have contributed significantly to the areas of multiscale modelling, advanced and smart nanocomposites, crashworthiness, fracture mechanics and failure prevention. He has published 295 papers in leading tier-1 scientific journals, 240 presentations in international conferences of significance with a large number being invited as keynote and plenary speaker. He authored 4 books on fracture mechanics, nanomechanics and micromechanics, edited17 international conference proceedings and contributed 17 book chapters.

He is the Founding Editor-in-Chief of Int. J of Mechanics and Materials in Design, former Technical Associate Editor of ASME J. of Engineering Materials and Technology (for two consecutive terms), former Associate Editor of IMechE Journal of Mechanical Process Engineering, Guest Editor to a number of Journals including Mechanics of Materials and a member of the editorial board of numerous journals. He is also the Founding Head of the Aerospace Engineering Division of Nanyang Technological University, Singapore. He taught different branches of mechanics in 4 continents: Europe (Manchester, Oxford (England) and Milano Polytecnico (Italy)), North America (Toronto, Canada), and Asia (NTU, Singapore), Hunan, Peking, and BIT (China), and Africa (Cairo University, Egypt).

He is an Engineering Consultant to the United Nations, a lifetime senior member of AIAA, member of the American Academy of Mechanics, Professional Engineer in the Province of Ontario (PEng), Chartered Engineer in Great Britain (CEng), Fellow of ASME, Fellow of IMechE and Fellow of the Engineering Institute of Canada. He works closely with the aerospace and automotive industries and is regularly approached by members of the media for clarification of engineering issues and accidents.

Professor Meguid and his research team won numerous awards, with the most recent honor being the nomination by his department for the gold medal by the Governor General of Canada, holder of the Robert Hooke Award bestowed by the European Society for Experimental Mechanics, Engineering Award-Research and Development by the Professional Engineers of Ontario for his significant contribution to research and development in Canada.

KEYNOTE 2

TOPOLOGY OPTIMIZATIONS OF SOLIDS AND FLOW CHANNELS BASED ON LEVEL SET METHOD USING BOUNDARY ELEMENT METHOD AND LATTICE BOLTZMANN METHOD

Toshiro Matsumoto*

Department of Mechanical Systems Engineering, Nagoya University, Japan

(*)*Email:* t.matsumoto@nuem.nagoya-u.ac.jp

ABSTRACT

This keynote lecture presents some application of boundary element method (BEM) and lattice Boltzmann method (LBM) to topology optimization problems in heat conduction, acoustic, elastodynamic, electromagnetic, and flow problems. Topology optimization is a structural design method to obtain the optimum shape allowing its topological change. The optimum shape can be considered as the optimum distribution of material, therefore, numerous works have treated topology optimization problems as the optimum material arrangement problems. However, the conventional works assume the existence of materials with small material constant values also in the area where the material should not exist, and the resulting material configuration is in fact different from the optimum one. Also, it is difficult to give explicit boundary conditions to the newly generated boundary of the material. Therefore, our laboratory employs a level-set based approach with which the boundary of the material is explicitly generated from the isosurface of the level set function. In the first part of this lecture, numerical scheme of topology optimization based on the level set method and BEM is presented. This approach has been applied to topology optimization of sound scatterer designs in acoustic problems. Sound pressure is measured at some points in a three-dimensional acoustic field and the optimum layout of the sound scatterers has been obtained so that the sum of the sound pressure levels at the measuring points is minimized. Another example of BEM application has been done for the topology optimization of the arrangement of dielectrics for cloaking of objects. The layout of the dielectrics with which the scattered waves were finally reconstructed to become the same incident plane wave in order to cloak the object. It turned out that, by defining the objective functional appropriately, objects of any shapes and material properties can be cloaked by using the same layout of the dielectrics.

In the second part, I will show some topological designs of flow channels. For such problems, it is crucial to employ a fast flow solver because we have to repeat flow analysis many times until we obtain the optimum topology of the channel. The LBM and its variant, lattice kinetic scheme (LKS), have been used for solving primary problem and newly derived adjoint lattice Boltzmann equation. LBM and LKS are rather fast because they are explicit methods for calculating the values of the velocity distribution function in the fixed design domain. The flow velocity, pressure, density, and internal energy are calculated from this distribution function directly. Memory requirement in LBM is heavy but is improved dramatically in LKS. The level set method was used again to control the boundary of the flow channel. This computation scheme was applied successfully to designs of flow channels to minimize the pressure drop between the inlet and outlet flows. The method was also applied to maximization of the dissipation energy of the fluid in the channel under transient but time harmonic inlet and outlet flows to design vibration damping devices based on fluid mechanism.

Keywords: Topology optimization, Level set method, Boundary element method, Lattice Boltzmann method

Biographical Sketch

Professor Toshiro Matsumoto is a professor of Nagoya University since 2004 and has a laboratory in the Department of Mechanical Systems Engineering. He has dedicated his study to boundary element methods (BEM) and its application to engineering problems. His contributions have been in the application of the boundary element method to fracture mechanics, development of BEM for inhomogeneous material, shape sensitivity analysis, BEM for piezoelectric materials, and application of BEM to topology optimizations. In recent years he is also interested in topology optimization related to flow problems using lattice Boltzmann method. He has published more than 200 journal papers and also more than 200 presentations in international conferences. He wrote two books on BEM and chapters of 7 books.

He is an editor of Engineering Analysis with Boundary Elements, former director of the Japan Society of Mechanical Engineers (JSME), Vice Chairman of the Computational Mechanics Division of JSME, Fellow of JSME, and Director of Japan Society for Computational Methods in Engineering (JASCOME). He has been a visiting professor at Wessex Institute, University of Pisa, École Polytechnique, and London University. He taught in China and Italy on BEM and topology optimization. He and his research group won many awards from JSME and JASCOME. He is nominated as the next president of JASCOME.

KEYNOTE 3

THE DEVELOPMENT OF DUCATI PANIGALE 1299 SUPERLEGGERA: LIGHTWEIGHT DESIGN IN THE MOTORBIKE SECTOR

Leonardo Bagnoli*

Head of Vehicle Simulation Dept.,
Ducati Motor Holding s.p.a., Bologna , Italy
(*)*Email:* leonardo.bagnoli@ducati.com

ABSTRACT

The purpose of the presentation is to show the development of Ducati 1299 Panigale Superleggera, an exclusive limited edition motorcycle that is the first production bike in the world to feature carbon fibre frame, rear seat frame, single sided swing arm and wheels.

First of all it will be introduced the Panigale product brief in order to understand the target of the original project launched back in 2012. Then there will be a brief explanation of the so called monocoque frame, one of the most effective new design concepts that allowed a consistent weight saving on the bike.

Moreover, it will be shown the 1199 Panigale Superleggera launched in 2014, the first limited edition motorcycle based on Panigale project. The challenging target on kerb weight was reached using magnesium alloys on frame and wheels and carbon fibre for the rear seat frame. The latest limited edition motorcycle, the 1299 Panigale Superleggera, is even lighter than its precursor thanks to the widespread use of composite materials on structural parts.

The development of those parts was done completely in house, sharing specific knowledge with Ducati Corse that has a long time expertise on composite materials. Dealing with composite materials, the design of the parts is strictly related to their manufacturing process so it was necessary to work together with the suppliers. Structural optimization, bonding design, temperature monitoring and heat insulation where also important to achieve reliability and stiffness targets, fulfilling a significant weight saving.

Keywords: Lightweight, Design, Aluminum, Magnesium, Carbon Fiber, Composite, Structure

Biographical Sketch

Leonardo Bagnoli has been in charge of Vehicle Simulation Dept. of Ducati Motor Holding s.p.a. since 2012. He joined Ducati Motor Holding s.p.a. back in 2007 and started his career as a structural analyst. He has gained particular expertise in the field of structural design, reliability assessment and innovative materials usage for structural applications. Now his team deals with most of the structural, dynamics, fluid-dynamics, NVH and optimization issues that are peculiar of motorcycles and cooperates with the other R&D Depts. in the development of production bikes.

KEYNOTE 4

DESIGN FOR PERFORMANCE AND RELIABILITY OF A REAR SUSPENSION OF A FORMULA ONE CAR

Marco Civinelli*
Head of Chassis Mechanical Design Dept.,
Scuderia Ferrari, Modena, Italy
(*)*Email:* marco.civinelli@ferrari.com

ABSTRACT

This keynote lecture focuses on the rear suspension and rear wheel group of the SF71H, the car that Scuderia Ferrari designed for the 2018 FIA Formula 1 World Championship. The first part offers an overview of the main components of the outboard suspension, in particular wishbones, uprights, hubs, rims and brake calipers.

The second part will treat the main design process for these components, with an introduction on the targets and the constraints of the project, followed by a description of the methodologies that have been used to define the final shapes and technical specifications.. The experimental activity that followed the production of the first parts will be presented to describe in which way the initial target indexes were measured in real components.

The third part will focus on the design of a specific suspension bracket, realized with additive manufacturing process, highlighting the opportunities but also the limitations that characterized this technology on that project.

Keywords: Design, Suspension, Lightweight, Stiffness, Titanium, Additive Manufacturing

Biographical Sketch

Marco Civinelli is Head of Chassis Mechanical Design Dept of Scuderia Ferrari since 2015.

He joined Scuderia Ferrari in 2005 as mechanical design engineer and from 2006 to 2015 he worked as member of the Research and Development group. During these ten years he had the opportunity to be project leader for innovative projects related to various areas of the F1 car, with particular attention for braking system, suspension design, wheel groups, pitstops, hydraulic systems, car launch strategies, following the activities for the concept to car introduction.

The mechanical design group he is currently coordinating has the responsibility of the design of suspensions, brakes system, wheel groups and steering system, working with the target to deliver to the races the best technical solutions, defined as compromise between performance and reliability.

PAPER REF: 002

ANALYSIS OF THE COLD FORMING PROCESS

Sigitas Kilikevičius[1(*)], Ramūnas Česnavičius[2], Kristina Liutkauskienė[2], Andrius Juodsnukis[2]

[1]Department of Transport Engineering, Kaunas University of Technology, Kaunas, Lithuania
[2]Department of Mechanical Engineering, Kaunas University of Technology, Kaunas, Lithuania
[(*)]*Email:* sigitas.kilikevicius@ktu.lt

ABSTRACT

This article is aimed to investigate how the quality of a part manufactured by the cold forming process is affected by the cold forming process parameters. A numerical simulation based on the finite element method (FEM) was carried out in order to investigate the influence of the blank-holding force, the friction coefficient and the matrix radius on the quality of the part. The most suitable values of the cold forming process were found based on the results of the numerical simulation. Multiple linear regression analyses were carried out in order to identify the relationships between the quantities related to the quality of the part and the cold forming process parameters.

Keywords: cold forming process, blank-holding force, wrinkles, springback, regression analysis.

INTRODUCTION

Cold forming is a very effective process which offers low material losses and very short manufacturing duration as the part can be made by only one press cycle. However, if the cold forming parameters are not adjusted properly, some defects might occur having negative effect on the quality of the parts. Thinning, wrinkling and springback determine the quality of cold formed parts (Atul, 2018). The springback value depends on the material and the geometry of part being formed (Baùon, 2016). Therefore, it is very important to determine the most suitable values of the cold forming parameters before manufacturing the die for the part. A numerical simulation is very effective way to optimise the cold forming parameters, which gives an advantage over the trial-and-error approach (Liu, 2018).

The main aim of this article is to analyse how the quality of a cover for a beer barrel is influenced by the blank-holding force, the matrix radius and the friction coefficient.

RESULTS AND CONCLUSIONS

A numerical model of the cold forming process of the part was created using AutoForm R7 software. The material of the cover is 1.4301 grade stainless steel. The part was meshed using elasto-plastic shell type elements (Fig. 1, a). The overall dimensions and thickness of the formed part are shown in Fig. 1, b. The numerical simulation results are shown in Fig. 2. The simulation showed that the part thickness value was the lowest (0.74 mm) when the blank-holding force value was the highest (250 kN). The holding force did not have such a significant influence on the wrinkle height. The possible form deviation was increasing when the blank-holding force was increasing.

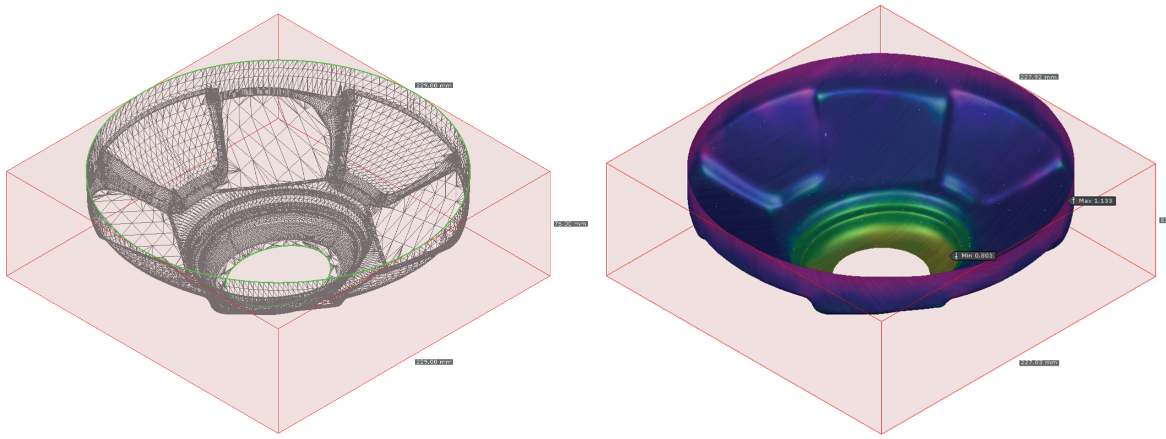

Fig. 1 - 3D model with FE mesh (a); overall dimensions and thickness of formed part (b)

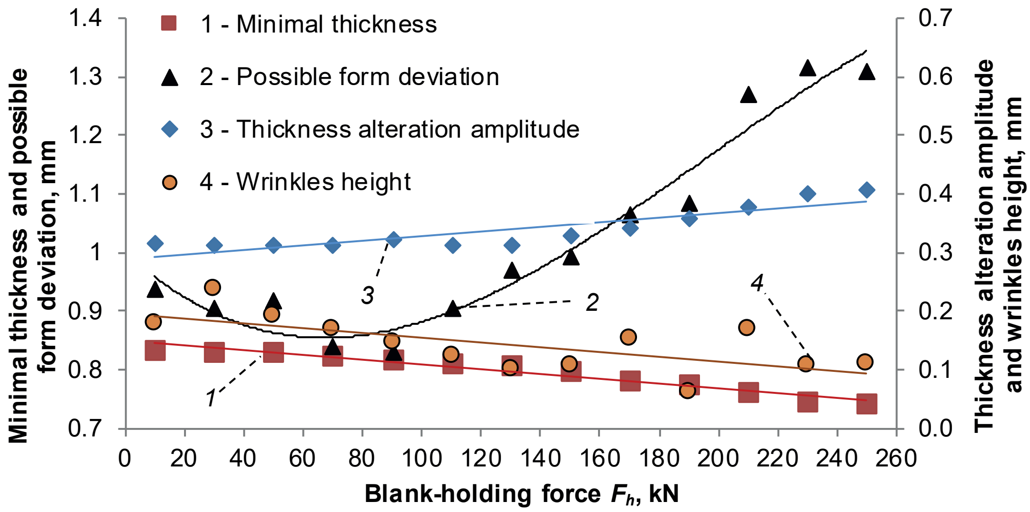

Fig. 2 - Minimal thickness (*1*), possible form deviation (*2*), thickness alteration amplitude (*3*) and wrinkles height (*4*) depending on the blank-holding force

When the blank-holding force was increasing, the minimal thickness was decreasing and the thickness alteration amplitude was increasing. The most relevant blank-holding force is 90 kN as the possible form deviation is the lowest and the minimum thickness is over 0.8 mm.

Multiple linear regression analyses were carried out in order to identify the relationships between the quantities related to the quality of the part and the cold forming process parameters. The blank-holding force had the largest effect on the quality of the part.

REFERENCES

Atul ST, Babu ML. A review on effect of thinning, wrinkling and spring-back on deep drawing process. Proceedings of the Institution of Mechanical Engineers, Part B: Journal of Engineering Manufacture, 2018. 0954405417752509.

Baùon P, Úwiàtoniowski A, Szostak J. Improved method of springback compensation in metal forming analysis. Strength of Materials, 2016, 48(4), p. 2016540-550.

Liu XL, Cao, JG, Chai XT, He ZL, Liu J, Zhao RG. Experimental and numerical prediction of the local thickness reduction defect of complex cross-sectional steel in cold roll forming. The International Journal of Advanced Manufacturing Technology, 2018, 95(5-8), p. 1837-1848.

PAPER REF: 004

MECHANICAL AND THERMAL PROPERTIES OF LIGHT-WEIGHT CONCRETE WITH INCORPORATED WASTE TYRE RUBBER AS COARSE AGGREGATE

Martina Záleská[1], Milena Pavlíková[1], David Čítek[2], Zbyšek Pavlík[1(*)]

[1] Department of Materials Engineering and Chemistry, Faculty of Civil Engineering, Czech Technical University in Prague, Prague, Czech Republic
[2]Department of Experimental Methods, Klokner Institute, Czech Technical University in Prague, Prague, Czech Republic
[(*)]*Email:* pavlikz@fsv.cvut.cz

ABSTRACT

The amount of waste tyres is still growing worldwide. This paper is focused on the experimental investigation of tyre rubber-based aggregate, which was used as a partial replacement of coarse natural aggregate to develop light-weight rubberized concrete with improved thermal insulation properties. The basic structural properties, mechanical resistance, and thermal conductivity measurements were conducted for rubber concrete assessment. The thermal conductivity was studied from dry to fully water saturated state.

Keywords: scrap tyre rubber, light-weight concrete, mechanical properties, thermal properties.

INTRODUCTION

In Europe, the total amount of used tyres in 2015 was 3868 kilotons (WBCSD, 2018). The possible reuse of material coming from scrap tyres in construction industry can solve disposal problems and allow production of light-weight concrete with enhanced thermal insulation parameters (Záleská, 2018; Aliabdo, 2015). As concrete performance is very dependent on the aggregate properties, the previous studies reported decrease in strength and thermal conductivity with increased rubber content (Pacheco-Torgal, 2012).

In this paper, samples of rubberized concrete (RC), where natural aggregate of 4/8 mm particle size was replaced by rubber-based aggregate of the same size fraction in the weight ratio of 10 %, 20 %, and 30 % were studied. Portland cement CEM 52.5 R was used a binder, and silica sand of fraction 0/4 and 4/8 mm as natural aggregate. The water/cement ratio was 0.5 for all concrete mixes. After 28 days of water curing, the tests of the compressive and flexural strength and dynamic modulus of elasticity were performed together with the measurement of the bulk and specific densities. The mechanical tests were done in accordance with EU standards for concrete testing. The bulk density was determined from measured sample volume and its dry mass. For the specific density test, helium pycnometry was used. The open porosity was calculated on the basis of densities values. The concrete thermal conductivity was measured from the dry to fully water saturated state using the transient impulse method.

RESULTS AND CONCLUSIONS

Table 1 shows the specific and bulk densities values that were for rubberized concrete lower compared to the reference material. Accordingly, the mechanical resistance decreased with higher dosage of rubber-based aggregate in concrete mix. The thermal conductivity decreased with rubber replacement ratio, and increased with the moisture content (Fig. 1).

Table 1 – Basic physical and mechanical properties of rubberized concrete

Material	Bulk density [kg/m^3]	**Matrix density [kg/m^3]**	**Open porosity [%]**	**Compressive strength [MPa]**	**Flexural strength [MPa]**	**Young´s modulus [GPa]**
Ref	2134	2453	13.0	61.5	6.8	39.0
RC10	1914	2249	14.9	26.0	5.1	17.0
RC20	1760	2101	16.3	13.0	2.7	5.8
RC30	1543	1902	18.9	4.5	1.7	3.1

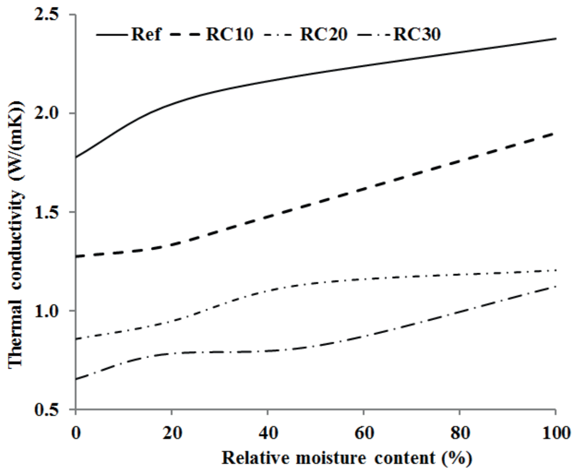

Fig. 1 - Thermal conductivity of samples in dependence on relative moisture content

In comparison with reference concrete, all studied rubberized concrete materials showed improved thermal insulation performance, even in the presence of moisture. Achieved mechanical resistance of rubberized concrete is sufficient for non-structural applications in civil engineering.

ACKNOWLEDGMENTS

The authors gratefully acknowledge the financial support received from the Czech Science Foundation, under project No 17-04215S – Thermal insulation composites containing waste plastic based fillers.

REFERENCES

Aliabdo AA, Elmoaty AEMA, Abdelbased MM. Utilization of waste rubber in non-structural applications. Construction and Buildings Materials, 2015, 91, p. 195-207.

Pacheco-Torgal F, Ding Y, Jalali S. Properties and durability of concrete containing polymeric wastes (tyre rubber and polyethylene terephtalate bottles): An overview. Construction and Buildings Materials, 2012, 30, p. 714-724.

WBCSD. Global ELT Management – A global state of knowledge on collection rates, recovery routes, and management methods. Published January 2018, www.wbcsd.org, accessed January 2018.

Záleská M, Čítek D, Pavlíková M, Pavlík Z. Thermal properties of lightweight concrete with scrap tire rubber-based aggregate. AIP Conference Proceedings, 2018, 1988, p. 020036.

PAPER REF: 005

PROPERTIES OF ALKALI-ACTIVATED COMPOSITES CONTAINING WOODEN BIOMASS ASH

Jaroslav Pokorný[1(*)], Lucie Zemanová[1], Milena Pavlíková[1], Zbyšek Pavlík[1(*)]

[1] Department of Material Engineering and Chemistry, Faculty of Civil Engineering, Czech technical university in Prague, Prague, Czech Republic

[(*)]*Email*: pavlikz@fsv.cvut.cz

ABSTRACT

This work is aimed at the possible use of wooden biomass ash in composition of geopolymer mortars. In mortar mix design, coal fly ash was partially substituted with biomass ash. The fly ash replacement ratio was 50 %, whereas the dosage of batch water remained the same. For the reference fly ash-based geopolymer mortar and mortar with incorporated biomass ash, basic structural, mechanical, and thermo-physical parameters were measured. As the porosity and mechanical parameters values were for geopolymer mortar with biomass ash similar as results obtained for reference geopolymer, it was concluded, the tested wooden biomass ash is usable as an alternative precursor for geopolymerization.

Keywords: alkali-activated composite, coal fly ash, wooden biomass ash, geopolymer mortar.

INTRODUCTION

Cement-based composites are the most utilized building materials all over the world. The cement production exceeds globally 4 billion tons annually (220 million tons in the EU), which releases from 5 % to 7 % of global CO_2 emissions (Ukrainczyk, 2016). Alkali-activated silica and alumina rich materials in the form of different wastes or industrial by-products can provide reasonable alternative to traditional cement-based materials (Galzerano, 2018) and mitigate negative economic and carbon footprints of their production. Presently, the main precursor applied for geopolymerization is coal fly ash, in most cases supplemented with ground granulated blast-furnace slag, silica fume, metakaolin, etc. (Hassan, 2019). Nevertheless, increased interest is devoted to biomass fly ashes generated by combustion of wooden/plant fuel sources in heating plants (Záleská, 2018). Currently, there is produced a considerable amount of biomass ash suitable to supplement excessively utilized and in the future hardly available coal fly ash.

Geopolymer mortars studied in this paper contained coal fly ash GM-FA or coal/wooden biomass ash GM-FA/WA and silica sand mixed together in the weight ratio 1/3. Silica sand used was a mix of three fractions (0.0/0.5, 0.5/1.0, and 1.0/2.0) combined in a weight ratio 1/1/1. In both mortars mixtures, the water to geopolymerization precursor ratio was 0.4. The dosage of water comprised of admixed tap water and water contained in alkali activator solution having app. 32.4 wt% of dry matter. Activator, with molar ratio SiO_2/Na_2O equals1.5, in equivalent sodium oxide content of 10 wt% of the activated components was applied. Casted mortar specimens (prisms 40 × 40 × 160 mm and 70 mm cubes) were for 24 h covered by PE foil and then stored for 27 days at high relative humidity of 98 % and temperature of (21 ± 1) °C. For hardened mortar samples, basic structural properties, mechanical parameters, and thermo-physical properties were accessed. Bulk density was determined with the use of gravimetric method. Specific density was tested using a helium pycnometer Pycnomatic ATC (Thermo Scientific). Total open porosity was calculated from the bulk and specific density values. Flexural strength tests were carried out on prismatic samples with mechanical press PF 100 when loading rate 40 N/s was employed. On the rest of broken prisms, compressive strength was measured. In this case, the loading rate was 500 N/s. The portable apparatus ISOMET 2114 (Applied precision) was used for the thermo-physical parameters measurement.

The basic structural and mechanical parameters data is summarized in Table. 1. A half weight replacement of coal fly ash by wooden biomass ash resulted in a slight increase in the total open porosity and thus strength reduction. However, the differences were very small, especially taking into account the measurement uncertainties. Thermo-physical properties data, given in Tab. 2, indicated an effect of wooden biomass ash on the deceleration of heat transport and decreased heat storage.

Table 1 – Basic physical properties and strength results

Material	**Bulk density [kg/m^3]**	**Matrix density [kg/m^3]**	**Total open porosity [%]**	**Flexural strength [MPa]**	**Compressive strength [MPa]**
GM-FA	2 084	2 545	18.0	3.8	8.8
GM-FA/WA	2 062	2 533	18.6	3.2	8.0

Table 2 – Thermo-physical properties

Material	**Thermal conductivity [W/(mK)]**	**Thermal diffusivity [(m^2/s) × 10^{-6}]**	**Volumetric heat capacity [(J/(m^{3}K)) × 10^6]**
AC-FA	1.95	1.06	1.84
AC-FA/WCH	1.71	0.94	1.80

Based on experimental results it can be concluded, the investigated wooden biomass ash is feasible, low-cost alternative material for production of alkali-activated construction materials.

ACKNOWLEDGMENTS

The authors gratefully acknowledge the funding by the Czech Science Foundation, under project No 17-02815S, and by the CTU in Prague under project No SGS17/166/OHK1/3T/11.

REFERENCES

Ukrainczyk N, Vrbos N, Koenferd EAB. Reuse of Woody Biomass Ash Waste in Cementitious Materials. Chemical nad Biochemical Engineering Quarterly, 2016, 30, p. 137-148.

Samadhi TW, Wulandari W, Prasetyo MI, Fernando MR, Purbasari A. Synthesis of Geopolymer from Biomass-Coal Ash Blends. AIP Conference Proceedings, 2017, 1887, p. 1-7.

Hassan HS, Abdel-Gawwad HA, Vásquez-García SR, Israde-Alcántra I, Flores N, Rico J. Cleaner production of one-part white geopolymer cement using pretreated wood biomass ash and diatomite. Journal of Cleaner Production, 2019, 209, p. 1420-1428.

Záleská M, Pavlík Z, Scheinherrová L, Pokorný J, Trník A, Svora P, Fořt J, Jankovský O, Suchorab Z, Černý R. Biomass ash-based mineral admixture prepared from municipal sewage sludge and its application in cement composites. Clean Technologies and Environmental Policy, 2018, 20, p. 159-171

PAPER REF: 006

TRIBOLOGICAL PROPERTIES BETWEEN a-C:H COATINGS AND SiO_2 AT HIGH TEMPERATURE

Kota Konishi[1], Noritsugu Umehara[1(*)], Motoyuki Murashima[1], Takayuki Tokoroyama[1]

[1] Department of Mechanical Science and Engineering, Nagoya University, Furo-cho, Chikusa-ku, Nagoya 464-8603, Japan

[(*)]*Email:* ume@mech.nagoya-u.ac.jp

ABSTRACT

Tribological properties of a-C:H coatings has been investigated in various friction conditions. It is clear that temperature and mating materials give effects on tribological properties. In this study, we especially focus on the effect of mating material on its tribological properties of a-C:H coatings. Ball-on-disk friction test is conducted between a-C:H coating and 5 kinds of mating material, which is SiC, SiC(O)_800(SiC oxidized at 800^oC), SiC(O)_1050^oC, SiC(O)_1300^oC, and Quartz glass. It is found that a-C:H coatings shows low friction coefficient and low specific wear rate when O/Si ratio of the element content of mating material is 2, in other words, mating material is SiO_2. In the wear scar of a-C:H coating after friction test with SiC, severe damage was confirmed. It is considered that a-C:H coating and SiO_2 show low adhesion even at high temperature, which leads low friction and wear. Compared SiC(O) with Quartz, the friction coefficients with a-C:H coatings are respectively 0.013 and 0.038. Even though SiC(O) and Quartz are both SiO_2, the tribological properties are different. On the wear track of SiC(O), transferred things from a-C:H coating are confirmed. It is considered that this graphitized transferred things make the friction coefficient lower by working as solid lubricant.

Keywords: a-C:H coatings, SiO_2, high temperature, oxidized SiC, low friction.

INTRODUCTION

DLC as a-C:H have a keen attention according to its low friction, high hardness and high wear resistance properties. There are needs to apply carbon coatings into ceramic mechanical parts, such as mechanical seal. The tribological properties of a-C:H when slid against ceramics as SiC, Si_3N_4 and Al_2O_3 were studied (Yamanouchi 2017). On the basis of their results, a-C:H when slid against SiC after annealing at 1000C showed low friction from 23^oC to 140 ^oC in air. However the low friction mechanism is still not unclear. Therefore, in order to know the effect of oxidation of SiC for reduction of friction at high temperature in air, 5 kinds of mating materials which are related to oxidized SiC were prepared. In this research, tribological behaviors of a-C:H when slid against various counterpart materials at various temperatures in air have been investigated.

EXPEIMENTAL APPARATUS NAD PROCUDURE

Friction pair is a-C:H coated steel ball which dimeter is 8 mm and 5 kinds of mating materials, which is SiC, SiC(O)_800(SiC oxidized at 800^oC), SiC(O)_1050^oC, SiC(O)_1300^oC, and Quartz glass. Hydrogenated amorphous carbon as a-C:H was coated on the high chromium carbon steel ball as SUJ2 bearing steel ball with ionized evaporation method. The a-C:H has 1 μm in thickness, 25.5 GPa in hardness and 5 nm in average surface roughness. Table 1 shows the properties and compositions of mating SiC related mating materials.

Table. 1 - Element composition and oxide thickness of specimen

Specimen	SiC	SiC(O)_800	SiC(O)_1050	SiC(O)_1300	Quartz glass
C	54.0	44.0	<0.1	<0.1	-
O	2.2	9.6	67.5	67.5	-
Si	43.8	46.4	32.5	32.5	-
O/Si	0.05	0.2	2	2	2
Thickness of oxidation film, nm	0	2.2	32.4	327.6	-

RESULTS AND CONCLUSIONS

Figure 1 shows variation of average friction coefficient between a-C:H and SiC oxidized mating materials during 20-30 m of sliding distance at 170 °C in air. When the annealing temperature is more than 800 °C, friction coefficient decreased less than 0.02. Figure 2 shows variation of specific wear rate of a-C:H between a-C:H and SiC oxidized mating materials. Also SiC(O)_1050 after the annealing at 1050 °C showed minimum wear rate. After Table 1, it can be considered which property is governing parameter for low friction and wear. It can be considered that 2 of O/Si ratio is more important than thickness of oxidation film.

If the SiO_2 is important to reduce friction and wear at 170 °C in air, SiO_2 glass should show the low friction and wear as mating materials for a-C:H. However SiO_2 quartz glass could not show lower friction and wear than SiC(O)_1050. After the friction test, the wear scar of SiC(O) was observed carefully with optical microscope as shown in Fig.3. Figure 3 shows many blue spots residue on wear truck of SiC(O)_1050. After the Raman spectroscopy analysis, the blue spots were decided as a graphite like materials. So it was found that low friction and wear need the transfer of graphite-like materials from a-C:H to mating material.

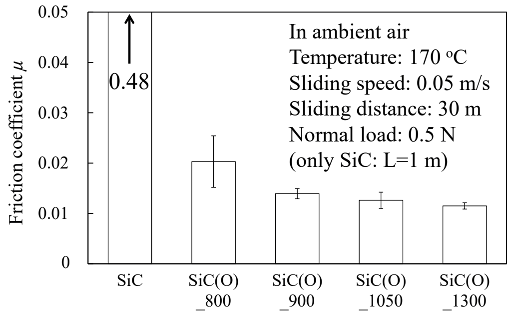

Fig. 1 - Friction coefficient between a-C:H and SiC and SiC(O) at 170oC in air

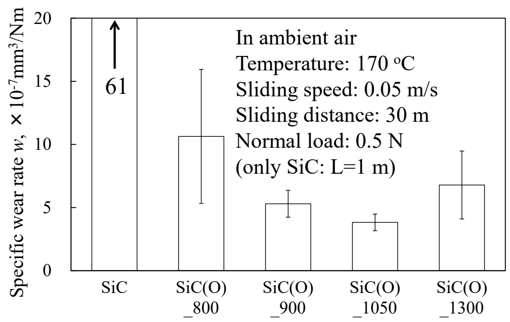

Fig. 2 - Specific wear rate of a-C:H between a-C:H and SiC and SiC(O) at 170oC in air

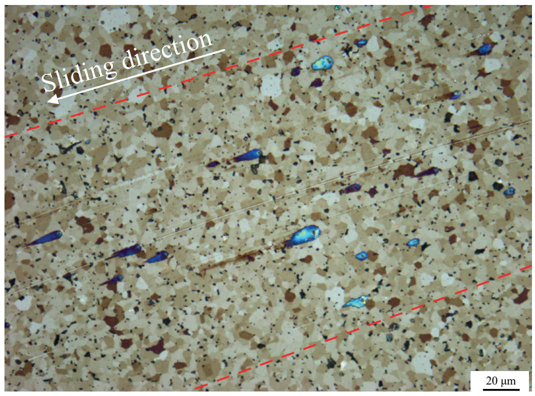

Fig. 3 - Optical microscope images of wear truck of SiC(O) against a-C:H

REFERENCES

Yamanouchi, T., Deng, X., Tanaka, Y., Umehara, N., Kousaka, H., Effects of Ceramic Counterpart materials on wear properties of a-C:H coatings at several temperature, Journal of Japanese Society of Tribologist, 62, 1(2017) pp.52-58.

PAPER REF: 007

STRUCTURAL, MECHANICAL AND THERMAL PROPERTIES OF LIGHTWEIGHT MAGNESIUM OXYCHLORIDE CEMENT CONCRETE

Martina Záleská[1], Zbyšek Pavlík[1], Milena Pavlíková[1(*)]

[1] Department of Materials Engineering and Chemistry, Faculty of Civil Engineering, Czech Technical University in Prague, Prague, Czech Republic

[(*)]*Email:* milena.pavlikova@fsv.cvut.cz

ABSTRACT

Considering the environmental sustainability in the construction industry, there is a need to look for alternatives to Portland cement and natural aggregates used for concrete production. This paper is aimed at the investigation of the use of crushed waste expanded polypropylene (EPP) in the magnesium oxychloride (MOC) cement-based composites. EPP was used for a full replacement of natural aggregate. Testing of air-cured MOC composites included experimental assessment of their structural, mechanical, and thermal parameters.

Keywords: magnesium oxychloride cement, waste expanded polypropylene, mechanical properties, thermal properties.

INTRODUCTION

MOC cement, also known as Sorel cement, belongs to non-hydraulic cements and is formed by the reaction of magnesia oxide (MgO) powder, magnesium chloride ($MgCl_2$) and water (Zhou and Li, 2012). MgO is obtained by calcination of $MgCO_3$ at temperature of 750-800 °C, which is considerably lower than the temperature required to produce Portland cement (1450 °C) and moreover MOC cements exhibit high carbonation capability in concrete products (Ruan and Unluer, 2016). MOC cement is further characterized by the ability to incorporate a high amount of many types of aggregate; the use of waste EPP as aggregate allows the production of environmentally friendly material with improved thermal insulation properties (Záleská, 2018).

Two experimental mixtures of MOC concrete were prepared: R-MOC containing the silica sand as aggregate, where sand to MgO weight ratio was 3:1 and EPP-MOC, where shredded waste EPP was used as a full replacement of silica sand in the amount of 150 % by volume of silica sand. Caustic magnesite powder was mixed with the solution of $MgCl_2$ ($MgCl_2.6H_2O$ was dissolved in tap water to prepare solution with a specific gravity of 26 °Bé) and with the corresponding aggregate. For tests were used 28 days air-cured prismatic and cubic specimens. The compressive strength test was performed following the standard EN 14016-2 (2005). The bulk density was determined on the gravimetric principle from the sample volume and its dry mass. The matrix density was obtained using the helium pycnometry. From the bulk and matrix density values, the total open porosity was calculated. The transient impulse method was used to conduct the thermal conductivity and the volume heat capacity measurements. The optical microscopy was used for the evaluation of binding conditions between EPP particles and MOC matrix.

RESULTS AND CONCLUSIONS

Table 1 shows a significant decrease in both bulk and matrix densities, in the compressive strength, as well as in the thermal conductivity for the EPP-MOC sample in comparison with the R-MOC material. On the contrary, the open porosity has increased. The volumetric heat capacity of EPP-MOC decreased only slightly compared to reference concrete. It can be seen from the Fig. 1 that the EPP aggregate was well embedded in the matrix of the binder.

Table 1 - Basic structural, mechanical and thermal properties of MOC composites

Material	Bulk density [kg/m^3]	Matrix density (kg/ m^3]	Open porosity [%]	Compressive strength [MPa]	Thermal conductivity [W/(m·K)]	Volumetric heat capacity [×10^6 J/(m^3·K)]
R-MOC	2124	2455	13.5	63.2	2.05	1.69
EPP-MOC	879	1411	37.7	7.5	0.30	1.60

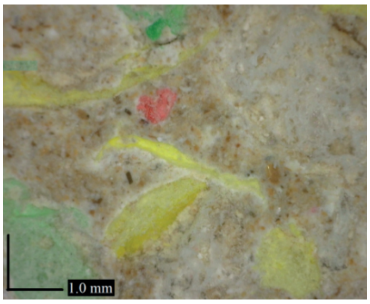

Fig. 1 - Optical microscopy image of EPP-MOC composite

Application of shredded EPP in MOC composites allows the utilization of a large amount of this plastic waste and has led to a great improvement of the thermal insulation parameters of developed material, which can serve as a part of floor, roof or wall for saving buildings energy consumption. Moreover, the high specific capacity of reference MOC composite remained almost unaffected by EPP incorporation what can help in heat accumulation and mitigate the energy demands for buildings conditioning. Using MOC cement as a binder can help reduce the CO_2 emissions associated with the cement production. In this respect, EPP-MOC composite can be considered as eco-efficient material for construction use.

ACKNOWLEDGMENTS

The authors gratefully acknowledge the financial support received from the Czech Science Foundation, under project No 19-00262S.

REFERENCES

EN 14016-2 Binders for magnesite screeds – Caustic magnesia and magnesium chloride – Part 2: Test methods, CEN, 2004.

Ruan S, Unluer C. Comparative life cycle assessment of reactive MgO and Portland cement production. Journal of Cleaner Production, 2016, 137, p. 258-273.

Záleská M, Pavlíková M, Jankovský O, Lojka M, Pivák A, Pavlík Z. Experimental analysis of MOC composite with a waste-expanded polypropylene-based aggregate. Materials, 2018, 11, 931.

Zhou X, Li Z. Light-weight wood-magnesium oxychloride cement composite building products made by extrusion. Construction and Buildings Materials, 2012, 27, p. 382-389.

PAPER REF: 008

COMPARATIVE STUDY OF VIBRATION MEASURING TECHNIQUES APPLIED TO ALUMINUM BEAMS WITH LOCALIZED DAMAGE

Edson V. G. da Silva[1(*)], Manuel T. B. César[2], João E. P. C. Ribeiro[3], Giovanni Bratti[4]

[1]Master in Industrial Engineering, Instituto Politécnico de Bragança, Bragança, Portugal
[2]Department of Applied Mechanics, Instituto Politécnico de Bragança, Bragança, Portugal
[3]Department of Industrial Engineering, Instituto Politécnico de Bragança, Bragança, Portugal
[4]Department of Mechanical Engineering, Universidade Tecnológica Federal do Paraná, Pato Branco, Brazil
[(*)]*Email:* a40929@alunos.ipb.pt

ABSTRACT

This work analyses the feasibility of using a commercial sound level meter (SLM) to measure the dynamic properties of a structural element, i.e., vibration frequencies, using acoustic output data obtained during a rover impact test carried out with rover impact hammer on small beams. The acoustic measurements are compared with those obtained with the accelerometer during the impact tests. In this case, four small aluminum beams were tested under undamaged and damaged conditions. The latter was simulated using drilled holes with different diameters at the mid span of the aluminum beams. Data from acoustic and acceleration measurements were processed to obtain the frequency content of each signal. The results allowed demonstrating if the sound level meter is able to capture the natural frequencies and monitor the damage effects on the natural frequencies of the beams.

Keywords: vibrations, natural frequency, sound level meter, acoustic, damage.

INTRODUCTION

Usually, modal data is acquired using piezoelectric sensors located on the system under analysis although frequency measurements can also be done measuring the acoustic response of the system (Randall J Allemang & Shapton, 1979). Every system has a set of vibration characteristics, such as the natural frequencies, mode shapes and damping (Ewins, 2000). These modal characteristics are affected by the physical characteristics of the system, in particular the stiffness and mass properties. A damage usually causes changes that can affect stiffness and/or mass, which directly affects the vibration properties of the system (Humar, Bagchi, & Xu, 2006).

Thus, in this study, 56 individual tests were performed to determine the effect of induced damage in the dynamic properties of small aluminum beams. The length and width of the prototype beams is 300 mm and 40 mm, respectively, with a thickness of 5 mm. From the total tests, 28 were performed using an accelerometer to measure the output data and the remaining 28 tests were performed using a sound level meter to measure the acoustic response. At first, the beams were undamaged and were tested to measure its natural frequency. Then, the beams were sequentially drilled with different diameter holes to simulate damage. The holes were located at the mid span with diameter range from 15 to 38 mm. A Finite Element Method (FEM) simulation was performed to obtain the mode shapes and the estimated natural frequencies. The main goal is to verify if the sound level meter is reliable enough to capture the natural frequencies. The secondary goal is to analyze the influence of the damage on the natural frequencies and damping ratios.

THEORY SECTION

Ewins (Ewins, 2000) defines modal testing as "the processes involved in testing components or structures with the objective of obtaining a mathematical description of their dynamic or vibration behavior". Perhaps the most used application of modal testing is measuring the system's vibration properties (natural frequencies, mode shapes and damping ratios), allowing verifying the measured data and the one used during the theoretical project (Ewins, 2000) but, also, it is an extremely important method to identify vibrations of a structure and to detect structural modifications (R. J. Allemang, 1983).

Although the Experimental Modal Analysis (EMA) is a relatively easy and cheap test to perform, some mechanisms require a special attention: the excitation mechanism, the sensing mechanism and the data acquisition mechanism (Maia et al., 1998). The excitation mechanism is, usually, a shaker or an impact hammer (Rao, 2010). The sensing mechanism is the one that obtains the vibration data from the system (usually an accelerometer) and the data acquisition and processing mechanism is responsible to obtain the signal generated by the sensing mechanism, digitize (if required) and processing it (Maia et al., 1998).

The correlation between the input signal and the output signal is usually shown as a Frequency Response Function (FRF) (Ewins, 2000). When talking about modal analysis, the FRFs represent the correlation between the input condition (usually an initial condition, such as displacement or velocity) and the system's response to it (the system's vibration). For most of materials, Maxwell's reciprocity principle can be applied to the FRFs, i.e., applying the initial condition on a point p and measuring its response on a point q provides the same result than applying the initial condition on the point q and measuring its response on the point p (Maxwell, 1890). The reciprocity of the FRFs implies that measuring a full row of the FRF matrix will provide a full column and vice-versa (Schwarz & Richardson, 1999).

Sound is defined as the variation on mass density, pressure, temperature and particle's position on a fluid along the time (Fahy, 2000). These variations can be due to a mechanical variation. A vibrating plate is an example, its vibration provokes displacement along the plate, the displacement dislocates the air particles on the fluid medium, causing the variation quoted above, generating an acoustic response (Cardoso, 2010). It is possible noticing that there is a correlation between the vibrational response and the acoustic response of a vibrating system, making possible to analyze some modal parameters (natural frequencies and damping ratios) from the acoustic response (Elwali, Satakopan, Shauche, Allemang, & Phillips, 2010) (Fahy, 2000). Sometimes the approach using the acoustic response is not possible: when the analyzed system is heavily damped the vibration will be damped before the sensing mechanism measures its response (Silva, 2015).

Damage affects a system's initial mass and stiffness condition and these parameters affects the modal behavior, so, it is correct to say that a damage affects a system's modal behavior and modal properties (Meirovitch, 1997). The changes on the mass can be associated with material removal and the stiffness changes can be associated with the variation on the moment of inertia, for example.

MATERIALS AND METHODS

The beams used during the experimental procedures are made of Aluminum alloy 6082. These beams have a rectangular cross section with 300 mm length, 40 mm width and 5 mm thickness. Initially, the beams are undamaged. Aiming to inflict a controlled damage on the beam, centered holes were drilled at mid span. The diameter has the initial value of 15 mm and is increased by 1 mm until the final value of 38 mm, these holes were distributed along the four analyzed beams, and the final data is composed by 28 tests (one for the undamaged condition and one for each damage severity on each beam). All the values used for the drilled holes (for each individual beam) are shown in Table 1.

Table 1. Perforations' dimensions.

Beam nº	Perforation diameter [mm]						
	Test 1	Test 2	Test 3	Test 4	Test 5	Test 6	Test 7
1	0	15	16	17	18	19	20
2	0	21	22	23	24	25	26
3	0	27	28	29	30	31	32
4	0	33	34	35	36	37	38

The damage will affect the mass (material removal) and the moment of inertia (the area resisting to the mechanical efforts changes). The mass variation is less than 10% and the moment of inertia variation is 95% (considering the most affected area), both from the undamaged scenario to the most severe damage scenario. The variation of these parameters implies the bending stiffness per unit of mass (EI/m), where E is the Young's modulus of the material, I ($I = bh^3/12$) *is* the moment of inertia and m the system's mass, will decrease along the tests performed, decreasing the stiffness on the affected area. IT is noticeable that the damage goes from a low severity level (d = 15 mm) to a high severity level (d = 38 mm), allowing monitoring the damage effects on the modal parameters along the tests.

Aiming to facilitate the measuring procedure and have a standard orientation for the input and output points, a grid was drawn on each beam. The grid is composed by squares (1 cm length) and was drawn using a permanent marker, avoiding damage infliction and mass loading. Figure 1 shows a damaged beam, with the grid and the excitation and measurement points drawn.

The excitation and measurement points must be chosen according to the mode shapes to be measured. Figure 1-(a) shows the input and output point chosen to the tests performed, they are very good to detect the bending modes but they are positioned on a modal line (i.e., there is no displacement on this nodes during some modes of vibration) when analyzing the torsional modes. In order to detect the torsional modes, a different position is required for the input and output points (distant from the modal line). The points shown in Figure 1-(b) were used to measure the torsional modes when required.

The numerical method used in this paper was a FEM simulation using Ansys' "modal" package and aims obtaining the mode shapes and the expected values for the natural frequencies of the beams. Every beam was tested individually and the results were obtained considering the interval between 0 and 2000 Hz.

The experimental method was composed by two parts: impact tests using an accelerometer to measure the output data (accelerometer method) and impact tests using a Sound Level Meter (SLM) to measure the acoustic response (SLM method). The experimental part aims to obtain the values of the natural frequencies for the same range used during the numerical method (i.e., 0 to 2000 Hz). During the tests using the accelerometer method, the acoustic response was measured simultaneously; allowing comparing the results obtained using both methods. Detailed tables containing the values obtained and errors associated can be seen in Silva (Silva, 2019). For both methods, an impact hammer (model E086C40) was used to provide the input signal and the beams were tested on a foam surface, simulating a "free" support condition.

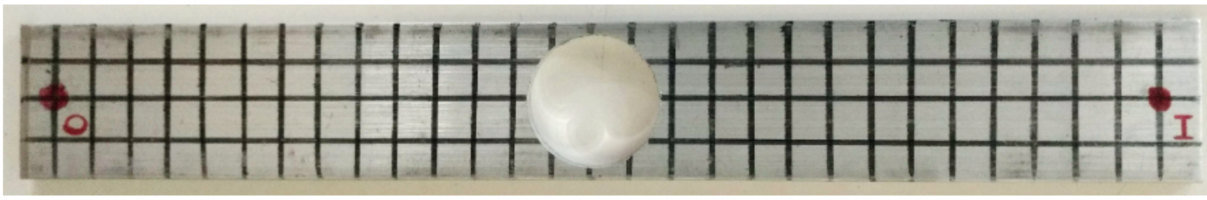

(a). Excitation and output points (“I” represents the excitation and “O” the output point).

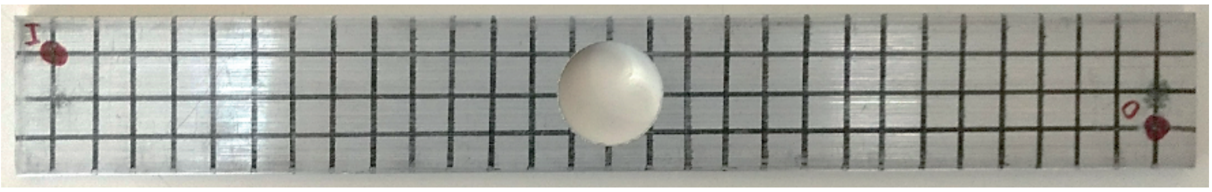

(b). Excitation and output points (“I” represents the excitation and “O” the output point).

Figure 1. Location of excitation (input) and output points for the rover impact tests.

The impact tests using the accelerometer method was carried out using an uniaxial accelerometer (type 4508, made by Brüel & Kjær), plugged into a PHOTON+ dynamic signal analyzer which was connected to a pc via an USB cable, allowing the data processing using the RT Pro Photon software. The tests performed using the accelerometer method was carried out using a Single-Input Single-Output, i.e., only one input and one output was used during these tests.

Looking Figure 1 it is possible noticing that two sets of points were used to provide the input and measure the output signal: one using two aligned points (a) and other using points dislocated from the centerline (b). The setup using the (a) points as a reference are not capable of obtaining the torsional modes of vibration when using the accelerometer method so, in order to obtain the torsional modes, the setup showed in (b) was adopted. Figure 2 shows the difference between the setups during a real simulation using the accelerometers to obtain the output signal.

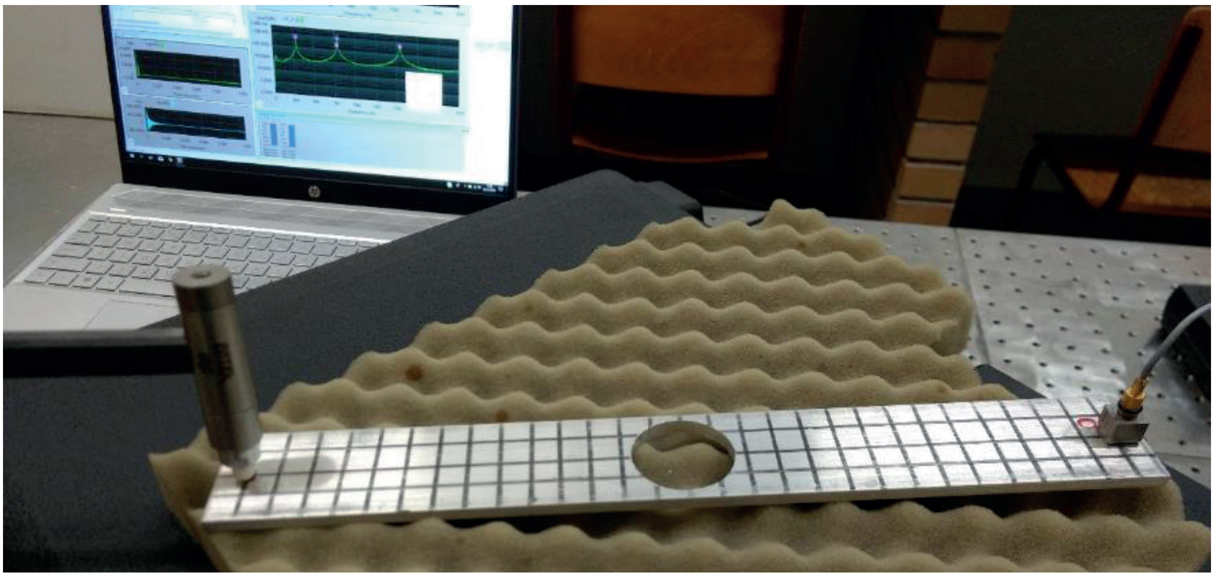

(a). Representation of a standard test using an accelerometer as an output source.

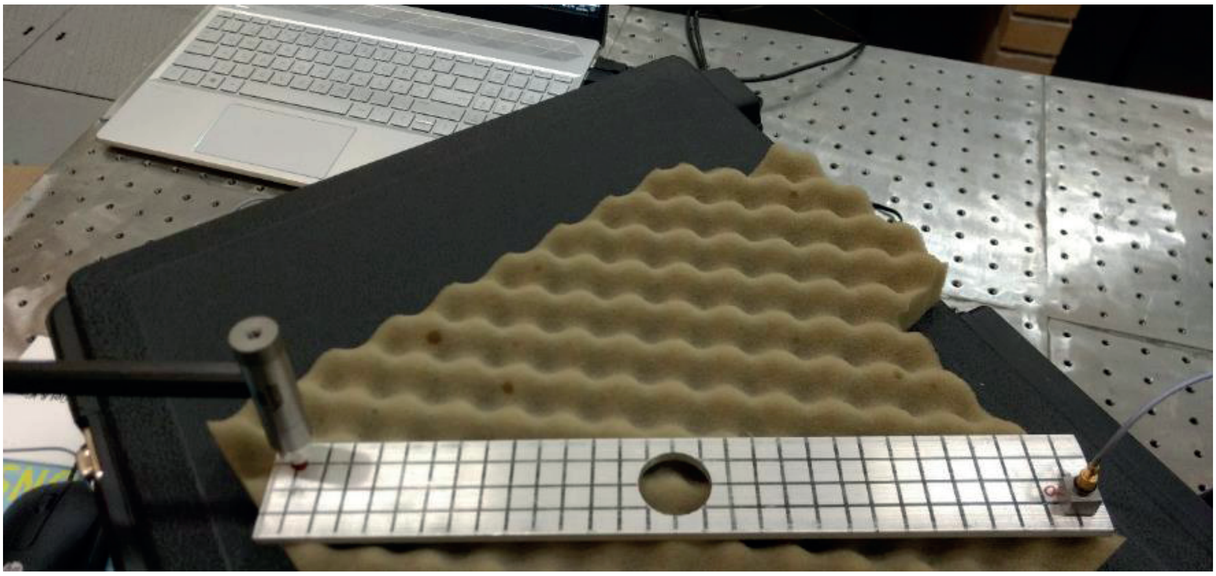

(b). Representation of a test to obtain the torsional natural frequencies.

Figure 2. Impact test using an accelerometer as an output source.

The impact tests using a SLM to measure the output data aims to capture the acoustic signal generated by the beam's vibration when it is impacted. To obtain the acoustic signal a free-field microphone (type 4189, manufactured by Brüel & Kjær), connected to a Hand-held analyzer (type 2250, G-4, manufactured by Brüel & Kjær) were used. This method allows obtaining the natural frequencies of the analyzed beam. This method discards the need of using two setups of points (unlike the tests using the accelerometer method) because every mode acting on the beam's vibrations contribute to the sound generated and it is captured by the microphone. The microphone was positioned perpendicular to the beam's surface, 5 cm distant from it. A representation of a test performed on the beams can be seen on Figure 3.

The acoustic response was processed using the hand-held analyzer and returned the values of the natural frequency on the analyzed range. It is possible to compare the data obtained using both methods and to calculate the error between them.

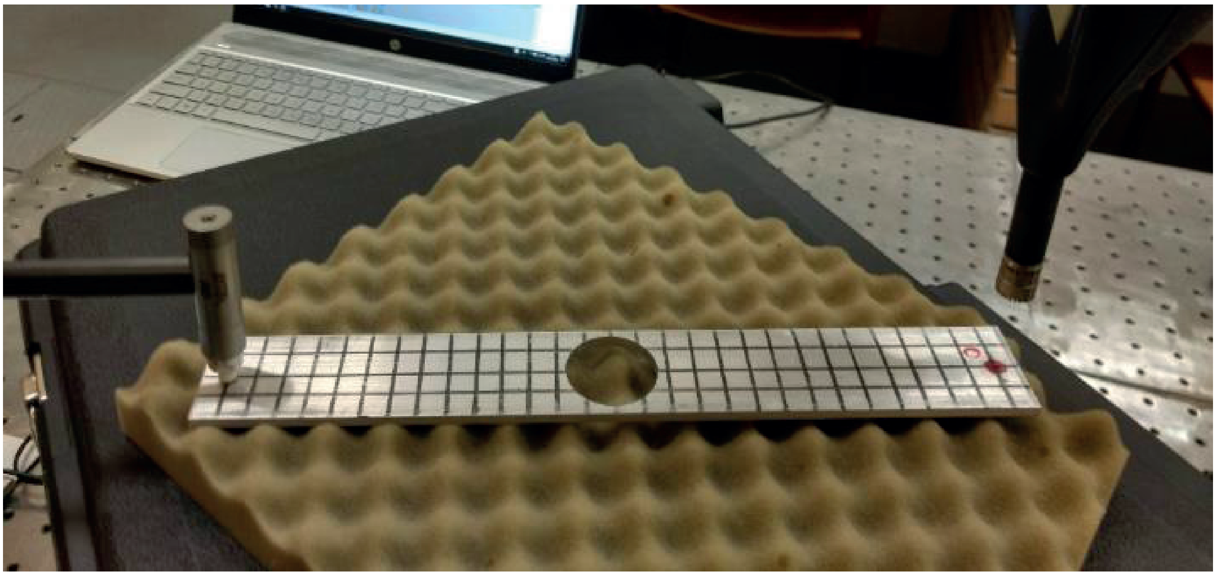

Figure 3. Impact test using a sound level meter to measure the output data.

RESULTS AND ANALYSIS

The variation of the natural frequencies due to the damage for the vibration modes detected between 0 and 2000 Hz are shown in Figure 4 to Figure 7. As expected, the natural frequencies decrease with an increase of the damage, i.e., the diameter of the drilled hole at the mid span. As can be seen, the most significant change of the natural frequencies occurs on the first and fourth modes.

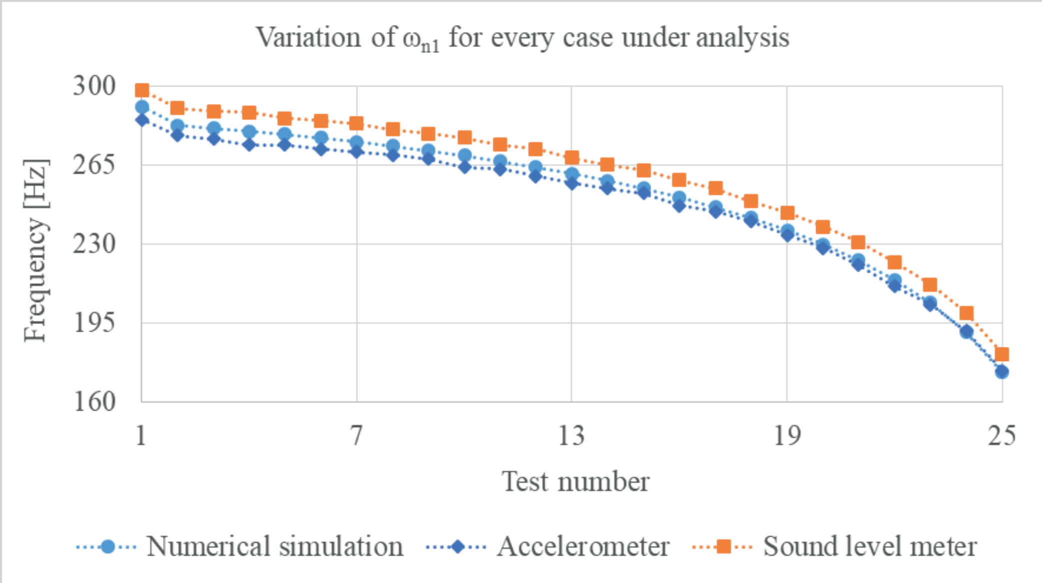

Figure 4. First natural frequency variation along the tests.

Observing Figure 4 it is noticeable a decrease of the values of the first natural frequency related with the first bending mode when the damage or hole diameter increases. The decrease between the natural frequencies measured for the undamaged case scenario and the last one is, approximately, 39.2%.

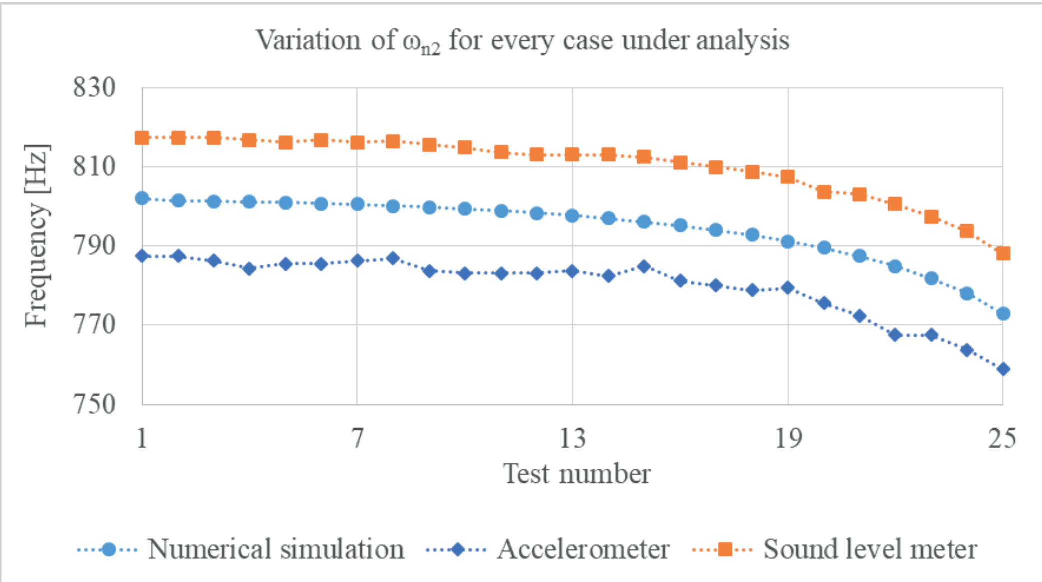

Figure 5. Second natural frequency variation along the tests.

Similarly to the variation of the first natural frequency, the second natural frequency related with the second bending mode (see Figure 5) decreases when the damage severity increases. Although this natural frequency is not as much affected as the first one (with a decrease of approximately 3.6%), a decrease is visible and can be associated with the type of damage used in this study.

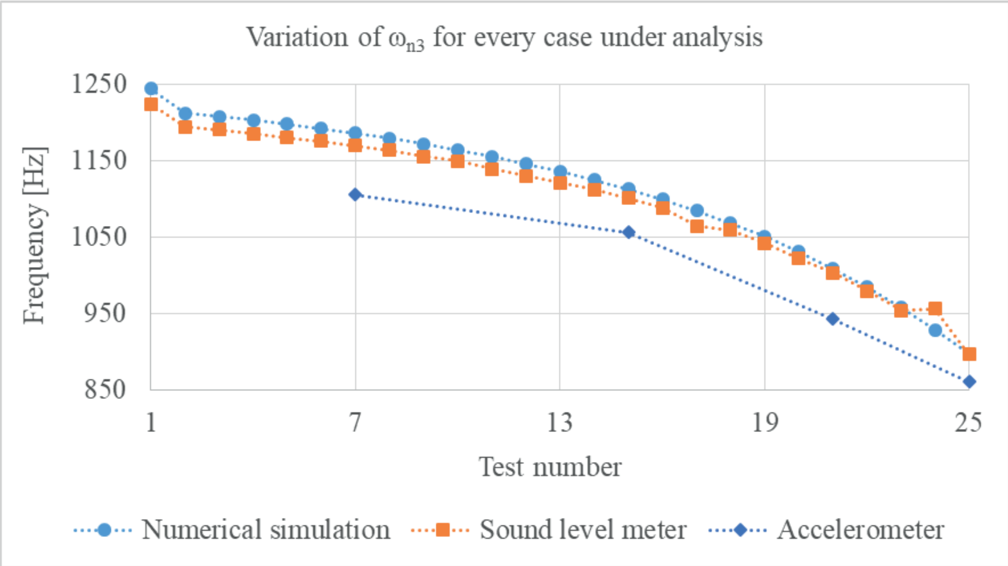

Figure 6. Third natural frequency variation along the tests.

Figure 6 shows the variation of the natural frequencies associated with the first torsional mode of vibration (with a decrease of approximately 26.7%). The lack of data obtained using the accelerometer is due to the points chosen to apply the input and measure the output, which are not able to measure the torsional mode vibration response (see Figure 1a). Some tests were repeated using the points shown in Figure 1b) and they were able to measure the output, resulting on the plot shown in Figure 6. Even with a small data sample, it is still possible to see a decrease on the value of the natural frquency.

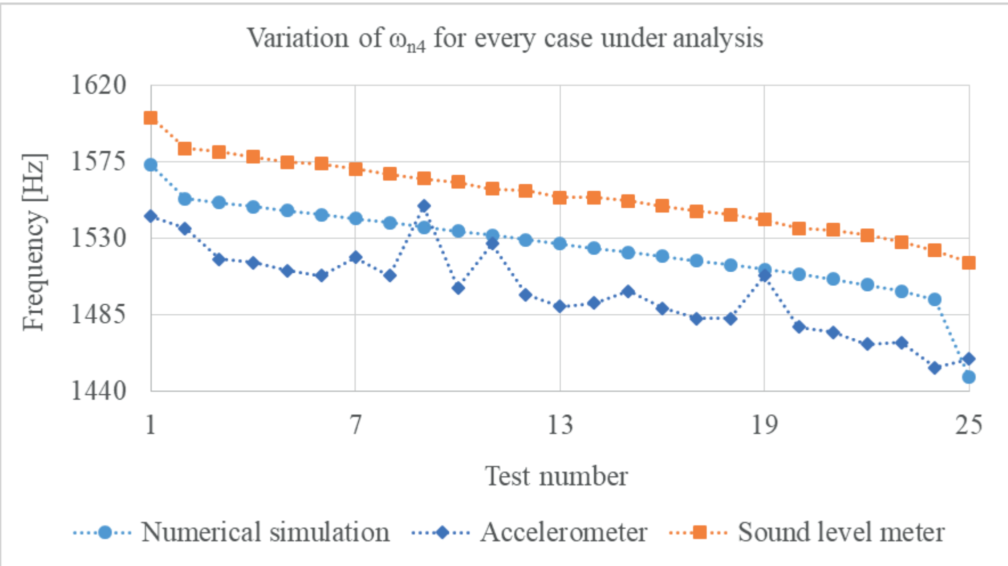

Figure 7. Fourth natural frequency variation along the tests.

Figure 7 displays the variation on the values measured for the fourth natural frequency (third bending mode). The difference of the value measured for the undamaged case to the value measured on the last test (most damaged) is around 5.4%. Some measurements mismatch the expected values (peaks) due to poor data obtained during the experimental tests. The average error between the measurements performed using the accelerometer and the SLM is of 4.0%.

CONCLUSIONS

Analyzing the data obtained with this experimental research it is possible to conclude that the SLM is a reliable equipment to measure the natural frequencies with some restrictions such as heavily damped systems in which the measurements must be done without background noise and the measurement time must be large enough to capture the frequency content of the sound wave. Also, the damage inflicted to the beams affects the natural frequencies and its value decreases when the damage severity increases, and finally the measuring points using the accelerometer (input and output) must be chosen carefully according to the modes that are been measured when.

REFERENCES

Allemang, R. (1983). *Experimental modal analysis. [for vibrating structures]*. Cincinnati.

Allemang, R. & Shapton, W. (1979). Using Modal Techniques to Guide Acoustic Signature Analysis. In *SAE 780106*, pp. 385–393.

Cardoso, L. (2010). *Interacção Vibroacústica do Sistema Placa-Cavidade Fechada:* Universidade do Porto.

Elwali, W., Satakopan, H., Shauche, V., Allemang, R., & Phillips, A. (2010). Modal Parameter Estimation Using Acoustic Modal Analysis. In *Proceedings of the IMAC-XXVIII* (Vol. 3, pp. 23–33). Jacksonville. https://doi.org/10.1007/978-1-4419-9834-7

Ewins, D. (2000). *Modal Testing* (2nd ed.). Philadelphia: Research Studies Press Ltd.

Fahy, F. (2000). *Foundations Of Engineering Acoustics*. Southampton: Academic Press.

Humar, J., Bagchi, A., & Xu, H. (2006). Performance of vibration-based techniques for the identification of structural damage. *Structural Health Monitoring*, *5*(3), 27.

Maia, N., Silva, J., He, J., Lieven, N., Lin, R, Skingle, G., Urgueira, A. (1998). *Theoretical and Experimental Modal Analysis*. Philadelphia: Research Studies Press Ltd.

Maxwell, J. (1890). Scientific Papers, *1*, 598.

Meirovitch, L. (1997). *Principles and techniques of vibrations*.

Rao, S. (2010). *Mechanical Vibrations*. *Recherche* (5th ed.). Upper Saddle River: Pearson.

Schwarz, B., & Richardson, M. (1999). Introduction to operating deflection shapes, pp. 1–7.

Silva, E. (2015). *Determinação do amortecimento de materiais por meio da técnica de excitação por impulso*. Pato Branco.

Silva, E. (2019). *Comparative study of vibration measuring techniques applied to Aluminum beams with localized damage*. Instituto Politécnico de Brangaça.

PAPER REF: 009

MINIMUM WEIGHT AND MAXIMUM FEASIBILITY ROBUSTNESS APPROACH FOR COMPOSITE STRUCTURES DESIGN

Carlos Conceição António[1 (*)], Luísa Natália Hoffbauer[2]

[1] INEGI/LAETA, Faculty of Engineering, University of Porto, Porto, Portugal
[2] INEGI/LAETA, Instituto Superior de Engenharia, P.Porto, Porto, Portugal
[(*)]*Email:* cantonio@fe.up.pt

ABSTRACT

A robust design optimization (RDO) of composite structures addresses the design as a bi-objective optimization problem with following objectives: (1) the weight of the structure which optimality is associated with performance robustness; and (2) the variability of structural response, which is associated with feasibility robustness of design constraints. Therefore, a bi-level dominance Multi-Objective Genetic Algorithm (MOGA-2D) solves the RDO of composite structures. The numerical tests show the capabilities of the approach.

Keywords: multi-objective optimization, composite structures, weight, feasibility robustness.

INTRODUCTION

In this paper, the RDO of composite structures addresses the design as a bi-objective optimization by considering the following objective functions: a function describing the performance/cost of the structure and a function describing the feasibility robustness of constraints related to the variability of the structural response. The design and uncertainty rules are controlled by following classes of variables and parameters: the vector of deterministic design variables $\mathbf{d} \in \Re^k$, the vector of random design variables, $\mathbf{z} \in \Re^m$, and the vector of random parameters, $\boldsymbol{\pi} \in \Re^p$. The nominal values of random design variables and random parameters are taken to be the expected values $\boldsymbol{\mu}_\mathbf{z}$ and $\boldsymbol{\mu}_\boldsymbol{\pi}$ respectively, and the associated uncertainties are given by their standard deviations. The design variables of the optimization procedure are the deterministic variables, $\mathbf{d}$ and the nominal values $\boldsymbol{\mu}_\mathbf{z}$ of the random design variables $\mathbf{z}$. The standard deviation of $\mathbf{z}$ is kept constant during the optimization. The performance/cost of the structure is given by its weight $W(\mathbf{d},\boldsymbol{\mu}_\mathbf{z})$. The functional $V(\mathbf{d},\boldsymbol{\mu}_\mathbf{z}, var(\bar{u}), var(\bar{R}), cov(\bar{u}, \bar{R}))$ is a measure of feasibility robustness associated to the constraint's variability. The bi-objective optimization problem follows as

$$\min_{over\ \mathbf{d},\,\boldsymbol{\mu}_z} \mathbf{OBJ}\left(\mathbf{d},\boldsymbol{\mu}_\mathbf{z},\mathbf{C}_\boldsymbol{\varphi}\right) = \left(f_1, f_2\right)$$

$$\text{with} \quad f_1 = W\left(\mathbf{d},\boldsymbol{\mu}_\mathbf{z}\right) \quad \text{and} \quad f_2 = V\left(\mathbf{d},\boldsymbol{\mu}_\mathbf{z}, var\left(\bar{u}\right), var\left(\bar{R}\right),\ cov\left(\bar{u},\bar{R}\right)\right) = \det \mathbf{C}_\varphi\left(\boldsymbol{\mu}_\mathbf{z},\boldsymbol{\mu}_\boldsymbol{\pi}\right)$$

$$\text{subject to } g_1\left(\mathbf{d},\boldsymbol{\mu}_\mathbf{z}\right) = \frac{\bar{u}\left(\mathbf{d},\boldsymbol{\mu}_z\right)}{u_a} - 1 \le 0 \quad , \quad g_2\left(\mathbf{d},\boldsymbol{\mu}_\mathbf{z}\right) = 1 - \frac{\bar{R}\left(\mathbf{d},\boldsymbol{\mu}_z\right)}{R_a} \le 0$$

$$\text{and } d_j^l \le d_j \le d_j^u,\ j = 1,\ldots,\bar{N}_d \qquad \mu_{z_j}^l \le \mu_{z_j} \le \mu_{z_j}^u\ ,\ j = 1,\ldots,\bar{N}_z \tag{1}$$

being $\bar{u}$ and $\bar{R}$ the critical displacement and critical Tsai number (António and Hoffbauer 2016, 2017). The MOGA-2D performs based on four genetic operators: mutation, crossover, replacement due to genetic similarity and selection. A binary code format emulates the phenotype of the design variables. The stopping criterion follows a minimum number of generations without improvement of Pareto front of enlarged population.

RESULTS AND CONCLUSIONS

To study the capabilities of the proposed approach for bi-objective optimization based on weight minimization and feasibility robustness maximization, an engine hood of a car built using a laminated shell structure is considered. The structure divided into eight macro-elements, as shown in Fig.1, presented one laminate per each macro-element. The laminates on engine hood shell follow a distribution according rational sense. The design variables are the ply angles and the laminate thicknesses.

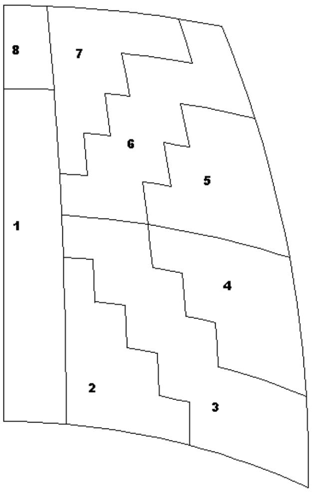

Fig. 1 - Composite laminates distribution on engine hood shell.

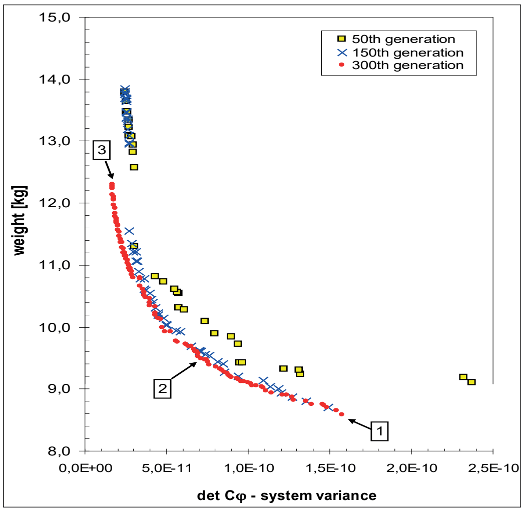

Fig. 2 - Optimal Pareto front for three generations of the evolutionary process.

The proposed approach considering weight minimization and feasibility robustness maximization (minimum variability) performed by MOGA-2D show its effectiveness, with the solutions shared along the optimal Pareto front as shown in Fig. 2. This figure shows the evolution of the of optimal Pareto front showing non-dominated solutions at three generations driven by MOGA-2D. Three solutions located on the optimal Pareto front will be analysed for further sensitivity analysis. The profiles of optimal solutions along the Pareto front show a constant optimal ply angle and three types of laminate thicknesses according the trade-off minimum weight and minimum variability. Therefore, the analysis of the partial effects of the variability is very important to make a design decision.

ACKNOWLEDGMENTS

The authors acknowledge the financial support provided by the Fundação para a Ciência e a Tecnologia (FCT), Portugal, through the funding of LAETA laboratory.

REFERENCES

Conceição António C, Hoffbauer LN. Bi-level dominance GA for minimum weight and maximum feasibility robustness of composite structures. Composite Structures 2016, 135, p. 83-95.

Conceição António C, Hoffbauer LN. Optimal design of composite shells based on minimum weight and maximum feasibility robustness. International Journal of Mechanics and Materials in Design 2017, 13, p. 287-310.

PAPER REF: 010

APPLICATION OF ARTIFICIAL NEURAL NETWORKS FOR ESTIMATION OF THE MASS OF THE WASTE POWDER DURING SELECTIVE LASER SINTERING

Zlatan Šoškić[1(*)], Jelena Tomić[1], Nenad Drvar[2], Michele Monti[3], Marco Cardu[3]

[1] Faculty of Mechanical and Civil Engineering in Kraljevo, University of Kragujevac, Kraljevo (Serbia)
[2]Topomatika d.o.o., Zagreb (Croatia)
[3]Studio Pedrini s.r.l, Bologna (Italy)
[(*)]*Email:* soskic.z@mfkv.kg.ac.rs

ABSTRACT

The paper presents results of the efforts to improve the accuracy of cost calculation of the selective laser sintering technology using an artificial neural network as a tool for estimation of the mass of the waste powder, based on the masses of the powder that will be, and the powder that will not be, built into products during a production process.

Keywords: additive manufacturing, selective laser sintering, manufacturing costs.

INTRODUCTION

An important characteristic of the selective laser sintering (SLS) technology is the ability to re-use a part of the powder that remains after a production process. The waste powder is the part of the powder that is not built into products, but still may not be used again. There are two main sources of the waste powder during SLS, a fixed amount of the powder that remains spread over the powder bed after a production process, and a variable amount of the powder that remains attached to the products after they are removed from the product bin.

While the costs of the waste powder are not assessed in the most important studies of the additive manufacturing costs (an overview is given by Costabile et al, 2017), their importance grows with the recent technology improvements that increase the ratio between the used and fresh powder in the production powder mixture. A recent effort (Soskic et al, 2017) was aimed at development of a rough, but simple, analytic expression for estimation of the mass of a waste powder during a production job. The conclusion was that for a rather typical production job the mass of the attached powder may be very roughly estimated to be proportional to the mass of the used powder that is not built into products (“non-product mass”). This paper presents an effort to develop a more complex method, an artificial neural network (abbreviated as ANN, a computational tool inspired by biological neural systems that is often used for data pattern recognition), which would use the same input data (the product mass and the non-product mass) to estimate the mass of the attached powder with more accuracy.

METHOD

An ANN consists of artificial neurons (nodes) which are organized into multiple layers and connected to each other via synapses. The relationships between ANN input and output parameters are established in a network training process, by tuning the values of synaptic weights based on data sets with known outputs.

The structure of the developed feedforward ANN for estimation of the mass of the attached powder has one hidden layer with five nodes. The bipolar sigmoid function and the linear function are used as the transfer functions of the hidden layer and the output layer, respectively. During the neural network training process, backpropagation algorithm based on Levenberg-Marquardt optimization has been used for updating the synaptic weights and bias values.

For the presented study were used 181 data sets obtained in exploitation conditions, which were also used in the previous study (Soskic et al, 2017). 127 of the data sets were used for training of the network, while the remaining 54 data sets were used for testing.

RESULTS AND CONCLUSIONS

The results show that the correlation coefficient between the measured masses of attached powder and predicted values, as well as the distribution of the relative errors (Fig. 1 left), seem to be very close for both methods (simple analytic expression and ANN). However, the convergence of the total relative error of the subsets of production processes towards zero is much faster for the ANN, as it becomes smaller than 5% for subsets than contain more than 20 production processes, which is achieved only for subsets larger than 90 production processes (Fig. 1 right) if the simple analytic expression is used.

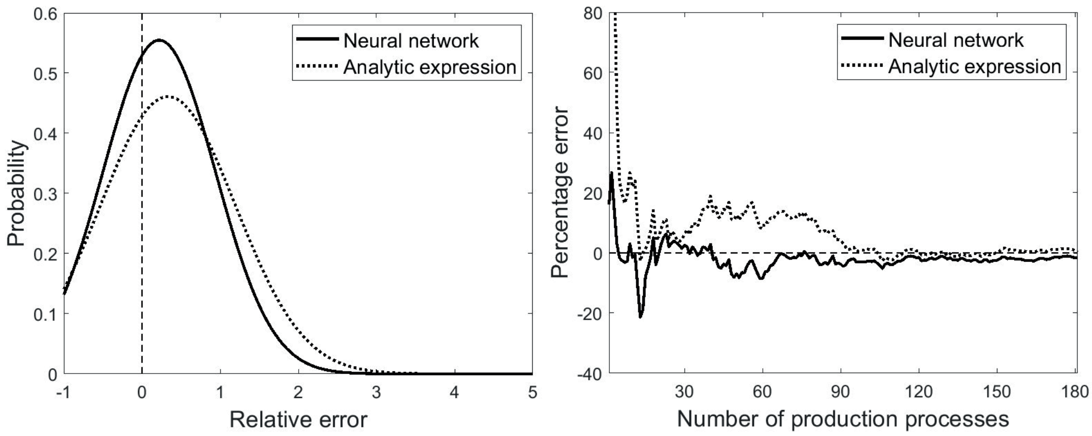

Fig. 1 – Relative errors of estimation and convergence of error of the two methods

The obtained result means that the ANN should be used by manufacturers who have less than 90 production processes within a supply cycle, i.e., those with small number of production machines that use SLS technology.

ACKNOWLEDGMENTS

The authors wish to acknowledge the support of European Commission through the project "Advanced design rules for optimal dynamic properties of additive manufacturing products – A_MADAM", which has received funding from the European Union's Horizon 2020 research and innovation programme under the Marie Skłodowska-Curie grant agreement No. 734455. The first two authors also acknowledge the support of the Serbian Ministry of Science, Education and Technology through the grant No. TR37020.

REFERENCES

Costabile C., Fera M., Fruggiero F., Lambiase A., Pham D. Cost models of additive manufacturing: A literature review. International Journal of Industrial Engineering Computations, 2017, 8, no. 2, pp. 263-283

Soskic Z., Montanari S., Monti G.L., Monti M. A Heuristic Approach to the Estimation of the Mass of the Waste Powder During Selective Laser Sintering of Polyamide PA2200. Proceedings of IX International Conference "Heavy Machinery-HM 2017", Zlatibor, 28 June – 1 July 2017, 2017, pp.D37-D44

PAPER REF: 011

STATIC ANALYSIS OF THE DRIVE SHAFT OF MANUAL GEARBOX

Tomas Petr(*)

[1],Department of Vehicles and Engines, Technical University of Liberec (TUL), Liberec, Czech Republic
(*)*Email:* tomas.petr@tul.cz

ABSTRACT

This article describes the static analysis of the shaft of the five-speed manual gearbox MQ100, which is used in New Small Family vehicles (Škoda Citigo, Volkswagen Up! or Seat Mii). Shaft deflection analysis was first verified by numerical methods and then a stress test on the test machine was performed. The values obtained by numerical methods were compared with the values obtained in the real test.

Keywords: drive shaft, MQ100, static analysis.

INTRODUCTION

The gearbox is an integral part of every car and every driver perceives it while driving. Whether it's the smoothness of gearshift, the gearshift lever's accuracy when shifting or its noise.

Due to the force applied to the shaft of the gear unit, there is a slight deflection. This deflection adversely affects the aforementioned riding comfort, especially the rolling noise of the individual gears and thus also their wear.

This paper describes the static analysis of the drive shaft of the 5-speed manual gearbox MQ 100. The gearbox MQ100 is a mechanical, five-speed manual transmission. It was designed for the VW group's "New Small Family" (Škoda Citigo, Volkswagen Up! Seat Mii). The gearbox is designed as a two-shaft for engines with a transverse installation and a maximum torque of 120 Nm.

The drive shaft transfers energy from the engine by means of gearing of a particular gear to the driven shaft. Shafts include first and second gear drive gears and direct reverse gearing. Drive gears (FestRad) of other adjustable gears are further pressed on the drive shaft. The drive and driven shaft is housed in a pair of tapered roller bearings in the "X" configuration. These bearings consist of an outer and inner ring with conical and conical cogs.

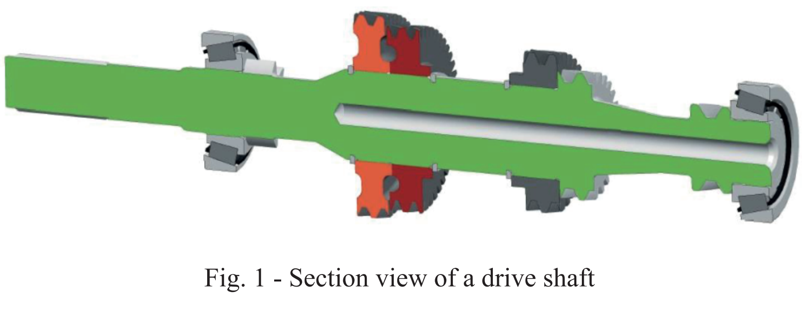

Fig. 1 - Section view of a drive shaft

RESULTS AND CONCLUSIONS

When simulating a load of 2.1 kN, which corresponds to the maximum force acting from the sprocket at a maximum torque of 120 Nm, the shaft displacement in the Y direction was 0.06 mm. The housing of the gearbox in which the shaft was mounted was deformed at the bearing location in the Y-direction by 0.016 mm on one side or on the one hand, 0.01 mm on the other. This means that the shaft deflection is 0.05 mm.

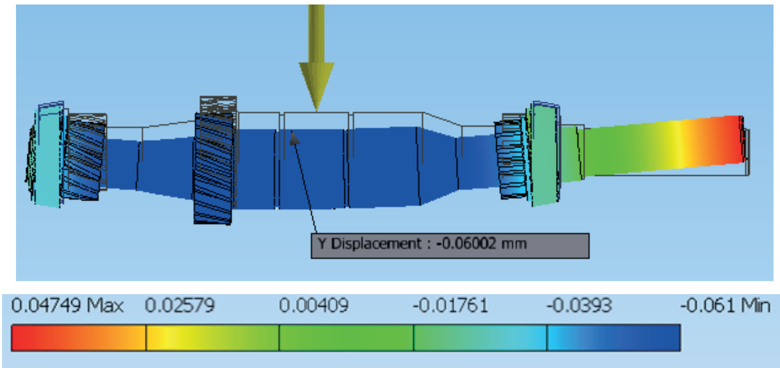

Fig. 2. Analysis of drive shaft deflection.

In the case of shaft load on the test machine, the shaft deflection was 0.056 mm.

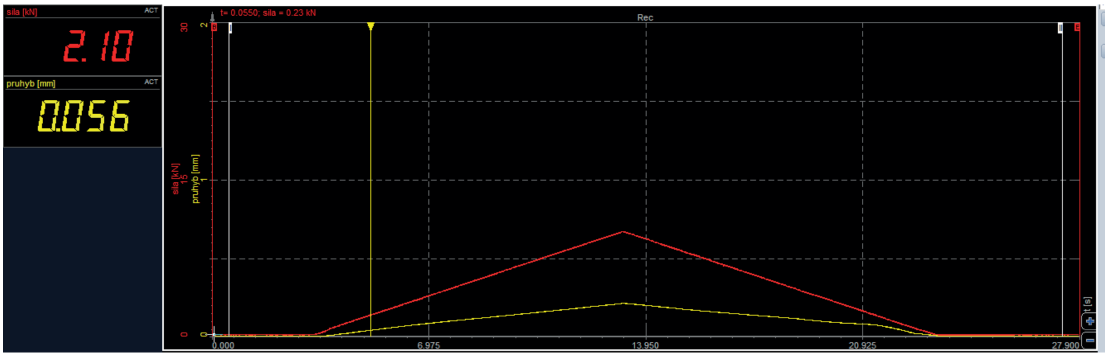

Fig. 3. Shaft deflection measured on the test machine.

ACKNOWLEDGMENTS

This publication was written at the Technical University of Liberec as part of the project 21276 with the support of the Specific University Research Grant, as provided by the Ministry of Education, Youth and Sports of the Czech Republic in the year 2019.

REFERENCES

LOEWENTHAL, Stuart H, 1984. *Design of Power-Transmitting Shafts* [online]. [vid. 2019-02-11]. Dostupné z: https://ntrs.nasa.gov/search.jsp?R=19840018973

VUČETIĆ, Nikola, 2017. STATIC ANALYSIS OF GEARBOX DRIVE SHAFT. *International Journal of Engineering* [online]. 4 [vid. 2019-02-10]. ISSN 1584-2673. Dostupné z: http://annals.fih.upt.ro/pdf-full/2017/ANNALS-2017-2-10.pdf

ŠKODA SERVICE, Pětistupňová mechanická převodovka 0CF a automatizovaná

pětistupňová převodovka ASG, Dílenská učební pomůcka č. 93, 2012, 48 s.

PAPER REF: 012

NON-DESTRUCTIVE EVALUATION OF COMPOSITE HELMETS BY ULTRASONIC IR THERMOGRAPHY

Monika Pracht, Waldemar Swiderski (*)

Military Institute of Armament Technology (MIAT), Zielonka, Poland

(*)*Email:* waldemar.swiderski@wp.pl

ABSTRACT

The paper presents selected results of non-destructive testing of composite helmets with deliberately introduced defects. Ultrasound pulsed infrared thermography was used for the tests and, in order to determine the initial possibilities of this method, artificial defects of Teflon with different sizes of surface to simulate delamination were placed between layers of the aramid composite from which the helmet was made. The obtained results confirmed the effectiveness of the method used in this application.

Keywords: non-destructive testing, IR thermography, ultrasonic.

INTRODUCTION

In recent years, composite materials have been used more frequently in lightweight ballistic armor designs. This is because advances in polymer chemistry have enabled the production of materials able to protect against impacts from small arms and other fragments. Woven (textile) materials combined with plastic are usually used, creating multi-layer composite materials used for personal ballistic armor (vests and helmets), armored vehicles, and solid objects. This type of composite material is largely manufactured on the basis of highly resistant aramid and polyethylene fibers combined with phenolic and polyurethane resins and other flexible blends. These materials are characterized by being lightweight, corrosion-resistant, and easily moldable which allows them to be adapted to the surface they are to protect. Material layers can be very different from their physical properties, therefore, as such, they are a difficult control task for many traditional non-destructive testing techniques. Defects that may appear in this type of multilayer composite are usually inaccuracies in gluing composite layers and delamination also resulting from the impact of fragments and projectiles.

One of the most effective methods of non-destructive testing in the study of fiber-reinforced composite materials is infrared thermography. As shown in many works (Pracht, 2018, Umara, 2019), ultrasound can be a particularly effective source of thermal stimulation of this type of material.

RESULTS AND CONCLUSIONS

In this work, an ultrasonic source with max. 2 kW and a frequency range from 15 to 25 kHz was used. Infrared image sequences were recorded using a FLIR 7600 SC infrared camera, both in heating and cooling phases. Pulse Phase Thermography (Maldague, 2001) was used in the analysis of the thermograms. Teflon defects in the shape of squares inserted into the helmet, had a thickness of about 0.1 mm and a surface difference of 0.5 cm^2 (defects D1, D2 and D3), 1 cm^2 (D4, D5, D6), and 1.5 cm^2 (D7, D8, D9). Eight defects were placed at a height of 100 mm from the top of the helmet, and one defect at a height of 150 mm. The layout of the defects in the helmet is shown in Figure 1. Selected results are shown in Figure 2.

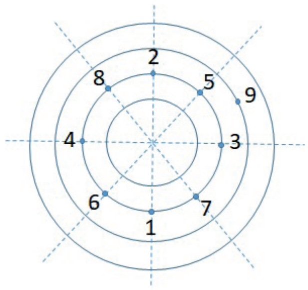

Fig. 1 - Diagram of the location of defects in the helmet

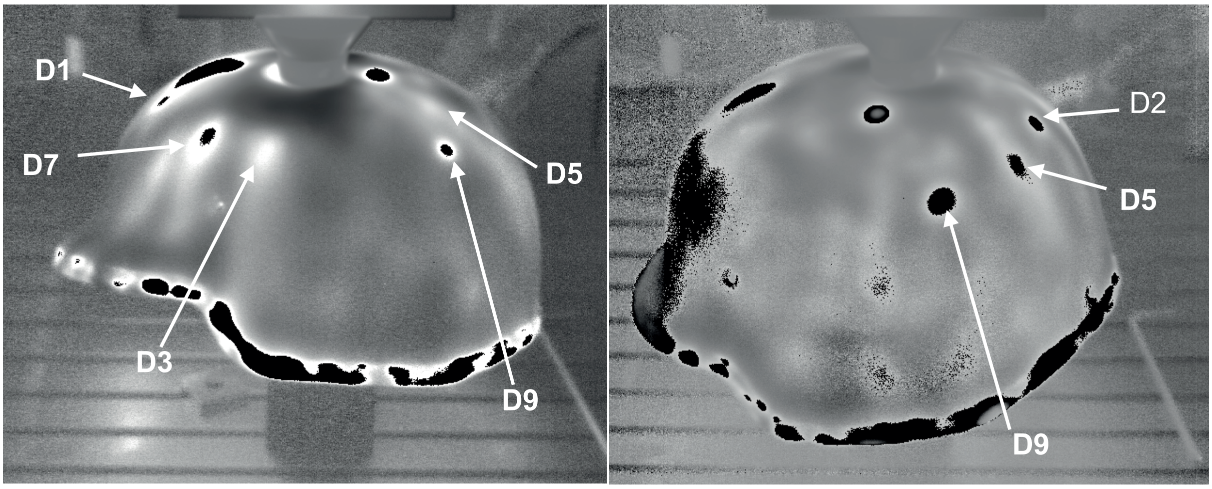

Fig. 2 - Phase images of helmets obtained for various test parameters:
a - generator power 0.9 kW, stimulation time 100 s, registration time 240 s;
b - generator power 0.9 kW, stimulation time 80 s, registration time 240 s.

Analysis of the results obtained from thermographic testing of helmets with deliberately introduced defects showed that phase image defects are more clearly visible and the area of their occurrence in the helmet is more easily identified.

REFERENCES

Pracht M, Swiderski W. Detection of defects in composite helmets using ultrasonic IR thermography: Proc. of Integrity/Reliability/Failure, 2018, p. 491-492.

Umara MZ, Vavilov V, Abdullah H, Ariffin AK. Quantitative study of local heat sources by Ultrasonic Infrared Thermography: An approach for estimating total energy released by low energy impact damage in C/C composite: Composites Part B, 2019, 165, p.167-173.

Maldague XPV. Theory and Practice of Infrared Technology for Non-Destructive Testing: John Willey & Son Inc. New York, 2001

PAPER REF: 015

STRUCTURAL HEALTH MONITORING OF THE RIBOU ARCH DAM USING ASYNCHRONOUS DATA AND INTERNET OF THINGS FOR DATA TRANSMISSION

Farouk Frigui[1 (*)], Sebastien Judenhrec[1], Jean Pierre Faye[2], Sylvain Genet[3]

[1]STANEO SAS, 154, route de Seysses, 31100 Toulouse, France
[2]Ecole Nationale d'Ingenieurs de Tarbes, LGP, 47 avenue d'Azereix, 65016 Tarbes, France
[3]Direction de l'environnement, Agglomeration de Cholet, France
[(*)]*Email:* farouk.frigui@staneo.fr

ABSTRACT

The Structural Health Monitoring (SHM) of civil engineering structures faces several challenges and presents a very important stake for human and material security. The main issue lies in defining a powerful and precise methodology of damage detection. This work deals with continuous monitoring of a concrete arch dam Eigen frequencies using a new SHM system architecture. From asynchronous ambient vibration measurements, data are compacted in-situ and the most significant information is kept. Using Internet of Things (IoT), reduced data are transmitted to a central computer. Eigen frequencies are then identified employing the Covariance-Driven Stochastic Subspace Identification method (SSI-COV). A simplistic big data approach has been carried out to identify correlations between Eigen frequencies, concrete temperature and air temperature.

Keywords: Structural Health Monitoring, Operational Madal Analysis, Internet of Things, Asynchronous acquisition.

INTRODUCTION

Civil engineering structures are confronted to several hazards that can cause their degradation. The monitoring of these structures presents a very important challenge in order to ensure human and material safety. The control and the follow-up, also called Structural Health Monitoring (SHM), are generally carried out by monitoring the dynamic characteristics using vibrational measuring means (Yan YJ, 2007). The instrumentation system is composed of sensors, an acquisition system, GPS, cables to ensure synchronization, and means of data transfer (ADSL). Data processing is performed ex-situ using Operational Modal Analysis technics (OMA) in order to evaluate structure performances subjected to ambient vibration conditions. This classical architecture has several drawbacks. In fact, for some civil engineering structures, such as historical monuments, cabling can become a crippling problem. In addition, time synchronization requires a certain number of satellites to be visible for the GPS antenna, which is not always possible in a large building or in a tunnel. Finally, continuous monitoring requires the processing of a large quantity of data, a powerful computing center and a large amount of memory (Zhu, 2018). The aim of this work is to develop new monitoring system architecture in order to facilitate the monitoring process and to ensure gain in terms of feasibility and economy. Based on the ergodic nature of the signals, this goal can be achieved by reducing the amount of data, by using Internet of Things for data transfer and by adapting Operational Modal Analysis algorithms (Tokognon, 2017). In this article, a new SHM system architecture is set up for the identification and the monitoring of the natural frequencies of Ribou arch dam. The Eigen frequencies identification method used is the COVariance-driven Stochastic Subspace Identification method (SSI-COV) for its accuracy (Frigui, 2018).

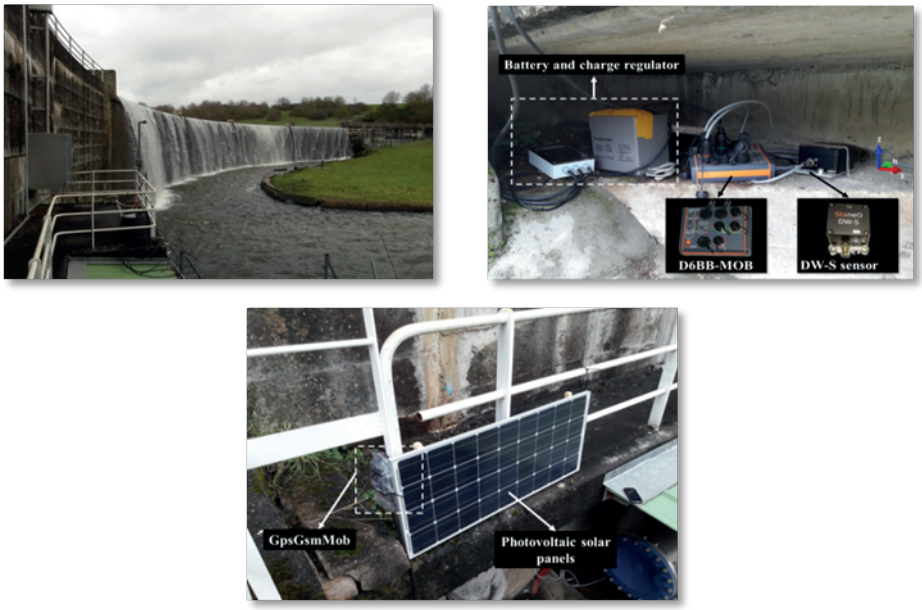

Fig. 1 - Installation of monitoring equipment on the Ribou dam

RESULTS AND CONCLUSIONS

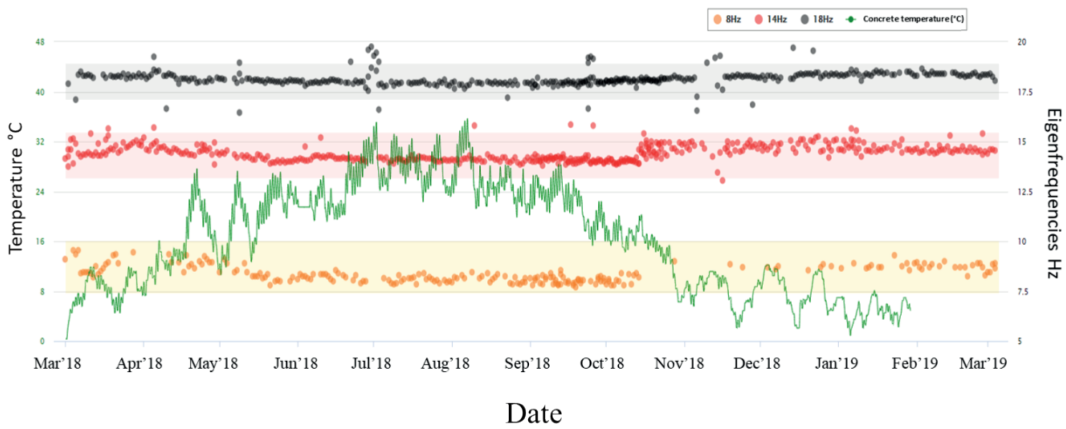

Fig. 2 - Concrete temperature and Ribou arch dam Eigen frequencies variations over a period of one year (March 2018 – March 2019)

The measurement results on the Ribou arch dam helped make the following conclusions:

– the compression rate of in-situ information was very important (1: 300000)
– the identification of the Eigen frequencies did take place from reduced data (2 SMS / day)
– there was a slow variation of Eigen frequencies during one year and which was mainly related to temperature changes.

Further measures on the dam are planned in order to identify higher frequencies and to study their variations according to several parameters (water level, concrete temperature, ambient temperature, etc.).

REFERENCES

Yan YJ, Cheng L, Wu ZY, Yam LH. Development in vibration based structural damage detection technique. Mechanical Systems and Signal Process J, 2007, 21(5), p.2198-2211

Zhu Y-C, Au S-K. Bayesian operational modal analysis with asynchronous data, part I: Most probable value. Mechanical Systems and Signal Processing, 2018, 98, p.652-666.

Tokognon C-A, Gao B, Tian G-Y, Yan Y. Structural health monitoring framework based on Internet of Things: A survey. IEEE Internet of Things Journal, 2017, 4(3), p.619-635.

Figui F, Faye J-P, Martin C, Dalverny O, Peres F, Judenherc S. Global methodology for damage detection and localization in civil engineering structures. Engineering Structures J, 2018, 171, p. 686-695.

PAPER REF: 016

ULTRASHORT PULSED LASER TEXTURING OF METALS FOR ENHANCED SURFACE FUNCTIONALITY

Adrian H.A. Lutey[(1,*)], Laura Gemini[2], Luca Romoli[1], Gianmarco Lazzini[1], Marc Faucon[2] & Rainer Kling[2]

[1]Dipartimento di Ingegneria e Architettura, Università degli Studi di Parma, Parma, Italy

[2]ALPhANOV Centre Technologique Optique et Lasers, Talence, France

[(*)]*Email:* adrian.lutey@unipr.it

ABSTRACT

Ultrashort pulsed laser texturing has been performed on stainless steel specimens to achieve hydrophobic and antibacterial properties. Surfaces characterised by nanoscale laser-induced periodic surface structures (*LIPSS*) and larger *spikes* structures are compared in terms of topography, wettability and bacterial attachment with control samples representing current practises within the food handling industry (S_a = 0.37 μm) and mirror-polished samples (S_a = 30 nm). It is shown that *LIPSS* provide the ideal combination of low wettability, low surface roughness and a topography with a high density of peaks to reduce attachment of both *Escherichia coli* (*E. coli*) and *Staphylococcus aureus* (*S. aureus*) bacterial cells.

Keywords: Laser Materials Processing, Ultrashort Pulses, Wettability, Bacterial Attachment.

INTRODUCTION

Ultrashort pulsed laser processing is an effective approach for achieving specific surface functionalities such as very low wettability (hydrophobicity) and self-cleaning or antibacterial behaviour (Kietzig *et al.*, 2009). At low pulse fluence, ultrashort laser pulses produce laser-induced periodic surface structures (*LIPSS*) perpendicular to the polarisation orientation with a feature size similar to the laser wavelength (Gnilitskyi *et al.*, 2017). Such structures have been shown to be appropriate for anti-bacterial surfaces due to their low wettability, low surface roughness and nano-scale topography that limits the available contact area for bacterial cells (Lutey *et al.*, 2018). At moderate fluence, laser interaction leads to larger *bumps* and *spikes* with superimposed LIPSS that become superhydrophobic over time and therefore highly water repellent.

The present work sees texturing of mirror-polished 316L stainless steel specimens with linearly polarised 350 fs laser pulses of wavelength 1030 nm for the production of superhydrophobic and antibacterial surfaces destined for the food production industry. Two different structure types, *LIPSS* and *spikes*, were produced with optimised parameters at low and moderate pulse fluence, respectively. The surfaces were analysed with a Taylor Hobson Talysurf optical profiler and custom-made shear force microscope (ShFM) to acquire the surface topography and derive the average areal roughness and density of peaks. Wettability tests were performed with a Dataphysics Instruments OCA20 goniometer to determine the static water droplet contact angle and sliding angle for all surfaces. Bacterial attachment tests were then performed by submerging samples into separate solutions containing *Escherichia coli* (*E. coli*) and *Staphylococcus aureus* (*S. aureus*) bacteria for two hours and quantifying residual micro-organism numbers in terms of colony forming units (cfu) in line with ISO 18593 for horizontal sampling methods. Laser-textured surfaces were compared to control samples representing current practises within the food handling industry (S_a = 0.37 μm) and mirror-polished samples (S_a = 30 nm) of the same composition.

RESULTS AND CONCLUSIONS

The results of surface roughness and wettability analyses are summarised in Tab. 1. Large differences can be seen between all tested samples. Laser-textured *spikes* exhibit high roughness and a low density of peaks but are superhydrophobic with a very high static contact angle and low sliding angle. *LIPSS* samples instead exhibit relatively low surface roughness and a lower static contact angle but are characterised by a very high density of peaks, greater than the minimum threshold value for reduced bacterial adhesion, 1 μm^{-2} (Lutey *et al.*, 2018). Both control and mirror-polished samples have a static water contact angle less than 90°.

Table 1 – Roughness and wettability parameters of all tested surfaces.

Parameter	*Control*	*Mirror-Polished*	*Spikes*	*LIPSS*
Areal roughness, S_a (nm)	370	30	8600	90
Density of peaks (μm^{-2})	-	-	0.002	1.1
Static water contact angle (°)	71	85	160	119
Water sliding angle (°)	-	-	14	-

The results of bacterial attachment tests are presented in Fig. 1. *E. coli* displays strong dependence on surface topography and little dependence on wettability or surface roughness, as bacterial adhesion increases for polished samples and laser-induced *spikes*. *E. coli* adhesion is instead more than two orders of magnitude lower for *LIPSS* due to the high density of peaks. *S. aureus* instead shows stronger dependence on wettability and surface roughness, with attachment being lower than control samples for both mirror-polished samples and laser-induced *spikes*. *LIPSS* perform the best due to the optimum combination of low surface roughness, small structure size and low wettability. Ultrashort pulsed laser texturing is therefore a promising method for producing hydrophobic and antibacterial surfaces.

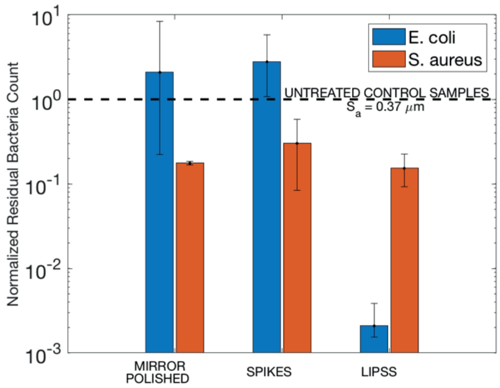

Fig. 1 – Bacterial attachment on mirror polished and laser-textured surfaces.

ACKNOWLEDGMENTS

This project has received funding from the European Union's Horizon 2020 Research and Innovation Programme under Grant Agreement No. 687613.

REFERENCES

Gnilitskyi I, Derrien TJ-Y, Levy Y, Bulgakova NM, Mocek T, Orazi L. High-speed manufacturing of highly regular femtosecond laser-induced periodic surface structures: physical origin of regularity. Scientific Reports, 2017, 7, p. 8485.

Kietzig A-M, Hatzikiriakos SG, Englezos P. Patterned superhydrophobic metallic surfaces. Langmuir, 2009, 25(8), pp. 4821-4827.

Lutey AHA, Gemini L, Romoli L, Lazzini G, Fuso F, Faucon M, Kling R. Towards laser-textured antibacterial surfaces. Scientific Reports, 2018, 8, p. 10112.

PAPER REF: 017

USE OF DIGITAL TWINS IN ADDITIVE MANUFACTURING DEVELOPMENT AND PRODUCTION

André Bergmann, Kai Lindow

Fraunhofer Institute for Production Systems and Design Technology IPK, Berlin, Germany, Department of Production Systems

ABSTRACT

The megatrend of the digitization of the industry is picking up speed. Today, the digital twin is an important component in the strategic positioning of a manufacturing company. The Gartner Report predicts that more than 50% of large industrial companies will be using the digital twin and that the effectiveness of the companies can be increased by up to 10% by 2021. For this, it is necessary on the one hand that the products are equipped with sensors, in order to be able to provide the data for the digital twin. On the other hand, it is also necessary to be capable to evaluate the data unambiguously with regard to the products and to be able to initiate appropriate measures to control them. In addition, insights can be gained into the improvement of subsequent product generations and their production.

The virtual representation of the product over its lifecycle requires a coupling with the real environment, in which lifecycle data are recorded via sensory systems and continuously imported into the virtual environment. Thus, the information and actual properties in the digital twin are mapped to the real conditions and the product condition in a dynamic data model. For this, it is necessary to integrate the information into the data systems of the product development and manufacturing processes. Based on this data, the behavior can be virtually tested, analyzed and predicted before actual production and use. This enables the engineer and manufacturer to further develop the product at reduced costs as early as the design phase.

The virtual validation is significantly extended by the collected database in the digital twin. For companies, this means a reduction of costs by reducing material and time expenditures as well as process times - for example, with increased utilization time.

On the basis of this study, a product example will be used to show which framework conditions are necessary for the use of the digital twin and which effects can be achieved in product development. It is also estimated to what extent the quality of the product and the process can be improved.

In the area of additive manufacturing, for example, the question arises how quality data can be used either to control the machine parameters of the printing process in a targeted manner (feedback-to-planning) so that the desired product quality is achieved, or to adapt the product models before manufacturing (feedback-to-engineering) so that the desired product quality can be produced with existing parameters.

The data alone is of little use to the companies. In addition to methodological and organizational issues, it is also necessary at the technological level to prepare the data for the various lifecycle phases of the product development process. This is where automated data evaluation in the form of AI comes in. Algorithms allow data evaluation by identifying patterns and deviations and consequently interpreting them for feedback-to-planning and feedback-to-engineering.

Keywords: Additive Manufacturing, Digital Twin, Intelligent Manufacturing System

PAPER REF: 018

INTUITIVE DESIGN OF SUPPORTS FOR SELECTIVE LASER MELTING

André Bergmann[1], Mattia Mele[2], Giampaolo Campana[2], Eckhart Uhlmann[1]

[1] Fraunhofer Institute for Production Systems and Design Technology IPK, Berlin, Germany, Department of Production Systems

[2] University of Bologna, Bologna, Italy, Department of Industrial Engineering

ABSTRACT

For the manufacture of products in selective laser melting, the components must be fixed on the construction platform (Zaeh and Branner, 2010). Depending on the type of component, support structures corresponding to its geometry are used in construction process planning for this purpose. The placement method depends on the geometry of the component itself. Straight downward surfaces must be fixed by support structures(Gan and Wong, 2016).

Only in rare cases the component can be manufactured as a self-supporting structure(Hussein et al., 2013). For a simple design of the supporting structures, the construction direction and the possible distortion of the components have to take into account when in the design process. In addition, the shape of the support structure plays a central role(Calignano, 2014).

The support structures can be manufactured in different thicknesses and cell types depending on the required stiffness. For example, it makes sense to use light support structures for low-stress and almost distortion-free components and very solid support structures for a secure connection of the component to the construction platform in the case of distortion-rich components. The required support volume and the stiffness of the support structures depend on the material and geometry of the component.

Several commercial software has been developed in order to aid the design of supporting structures. Nevertheless, these tools do not provide hints about the best auxiliary geometries to be adopted, leaving this decision to the experience of the user.

For this reason, a Computer Aided Engineering (CAE) tool (referred in the following as generator) has been developed to aid the decision-making problem concerning the design of supporting structures. This study compares and evaluates the various possibilities for using the generator, the achievable properties of the support structures and their influence on component quality.

In particular, the tool has been developed in relation to Selective Laser Melting (SLM) of metal powders

The aim is to provide the user with different classes of support structures and also to propose an optimized connection depending on the geometric characteristics of the components. For this propose, some generative parameters of the supporting structures (such as the pattern type and the support density) are managed by the user.

The intuitive tool for generating the support structures enables the operator to place his component in an optimized way during the construction process and to produce it afterwards minimizing the part distortion. The shape and amount of supporting structures contributes to determinate the time required for part construction (Lindemann *et al.*, 2013; Nopparat, 2015; Kellens *et al.*, 2017). Nonetheless, the adoption of supporting structures requires additional

energy during the process and leads to the transformation of material that can not be reused in next processes. For this reason, both the weight of support and the estimated building time are direct indicators of the process sustainability in terms of environmental and economic impact.

These indicators are automatically calculated by the generator to determine the optimal orientation of the part under given support structures generative parameters. In particular, a Genetic Algorithm (GA) based approach is adopted to determinate the optimal orientation according to weighted aims imposed by the user(Phatak and Pande, 2012).

The tool is applied to a case study in order to evaluate its applicability.

The impact indicators related to different manufacturing conditions are presented, thus showing the influence of supporting structures in determining the sustainability of parts obtained by the mean of SLM.

Furthermore, the efficiency of the supporting structures in reducing part distortion is evaluated for the different cases.

Keywords: Additive Manufacturing, Selective Laser Melting, Build-orientation, Intelligent Manufacturing System

REFERENCES

Calignano, F. (2014) ‘Design optimization of supports for overhanging structures in aluminum and titanium alloys by selective laser melting’, *Materials and Design*. Elsevier Ltd, 64, pp. 203–213. doi: 10.1016/j.matdes.2014.07.043.

Gan, M. X. and Wong, C. H. (2016) ‘Practical support structures for selective laser melting’, *Journal of Materials Processing Technology*. Elsevier B.V., 238, pp. 474–484. doi: 10.1016/j.jmatprotec.2016.08.006.

Hussein, A. *et al.* (2013) ‘Finite element simulation of the temperature and stress fields in single layers built without-support in selective laser melting’, *Materials and Design*. Elsevier Ltd, 52, pp. 638–647. doi: 10.1016/j.matdes.2013.05.070.

Kellens, K. *et al.* (2017) ‘Environmental Impact of Additive Manufacturing Processes: Does AM Contribute to a More Sustainable Way of Part Manufacturing?’, *Procedia CIRP*. The Author(s), 61(Section 3), pp. 582–587. doi: 10.1016/j.procir.2016.11.153.

Lindemann, C. *et al.* (2013) ‘Impact and Influence Factors of Additive Manufacturing on Product Lifecycle Costs’, *Proceedings of the 24th Solid Freeform Fabrication Symposium*, pp. 998–1009.

Nopparat (2015) ‘Resource Consumption of Additive Manufacturing Technology .’, (JUNE 2012).

Phatak, A. M. and Pande, S. S. (2012) ‘Optimum part orientation in Rapid Prototyping using genetic algorithm’, *Journal of Manufacturing Systems*. The Society of Manufacturing Engineers, 31(4), pp. 395–402. doi: 10.1016/j.jmsy.2012.07.001.

Zaeh, M. F. and Branner, G. (2010) ‘Investigations on residual stresses and deformations in selective laser melting’, *Production Engineering*, 4(1), pp. 35–45. doi: 10.1007/s11740-009-0192-y.

PAPER REF: 019

AUTOMATIC RECONSTRUCTION OF THE LUMINAL CAROTID BIFURCATION AXIS USING TRANSVERSE ULTRASOUND IMAGES

Catarina F. Castro[1,2(*)], Luisa C. Sousa[1,2], Ricardo Fitas[1], Carlos C. António[1,2], Rosa Santos[3], Elsa Azevedo[3,4]

[1]Faculty of Engineering of the University of Porto (FEUP), Porto, Portugal
[2]Institute of Science and Innovation in Mechanical and Industrial Engineering (INEGI), Porto, Portugal
[3]Hospital de S. João, Porto, Portugal
[4]Faculty of Medicine of the University of Porto (FMUP), Porto, Portugal
[(*)]*Email:* ccastro@fe.up.pt

ABSTRACT

Feature and structure identification in medical images allows a faster identification of certain anomalies and diseases. The study presented here enables the automatic reconstruction of the arterial bifurcation lumen axis using carotid B-mode ultrasound images. The segmentation methodology introduces new indexes in the automatic process aiming better accuracy in the selection of the correct artery structure as compared to previously published developments.

Keywords: Doppler ultrasound, carotid artery, B-mode images, segmentation algorithms.

INTRODUCTION

Carotid sonography, a fast and inexpensive technique, is extremely useful in the initial evaluation of symptomatic patients who present nonspecific symptoms related to stenotic or embolic accidents. Transverse ultrasound images of the carotid artery bifurcation and image segmentation provides data for reconstructing carotid luminal surface (Castro et al. 2018). The aim of the ongoing project is to convert morphologies of patient-specific vascular domains into flow domain used to simulate blood flow by means of computational fluid dynamics (Sousa et al. 2014). Nevertheless, automatic segmentation of the lumen is still a challenge due to low quality of images and presence of other elements such as stenosis and malformations that compromise the accuracy of the results (Jodas et al. 2018).

RESULTS AND CONCLUSIONS

Image assessment of the arterial system plays an important role in the diagnosis of cardiovascular diseases (Goddi et al. 2017). Doppler image segmentation relies on blood structures associated with the lowest values for luminance and on luminance grading from top to bottom of the images. Low contrast, shadows and echo artifacts degrade medical images. It is crucial to carry out a pre-processing step provided features of interest for lumen segmentation are not lost. Gaussian low-pass filters have been applied attenuating high-intensity noise points in the intensity distribution and reducing speckle noise, improving the signal to noise ratio. A complementary approach for automatic identification of lumen and wall arteries introduces new mathematical indexes capable of keeping the segmentation process in the correct track. Circularity index, irregularity index and centrality index based on medical facts such as healthy arteries are circular, arteries present a non-disruptive smooth structure and medical specialists keep the artery as close as possible to the image centre. The new algorithm for image processing and analysis was implemented using Matlab 2018a.

Using a new ultrasound system Philips Affiniti 50G with a broadband linear array L12-4 transducer, a qualified medical technician acquired Doppler transversal images from two specific patients with severe carotid disease. Patient-specific 3D bifurcation models were reconstructed from segmented transversal B-mode images. The main difficulty is associated with bifurcation; the transition from the central axis of the common carotid artery to the central axis of the internal and external carotid arteries is a challenge. Figure 1 presents the central axis reconstruction using B-spline methodology.

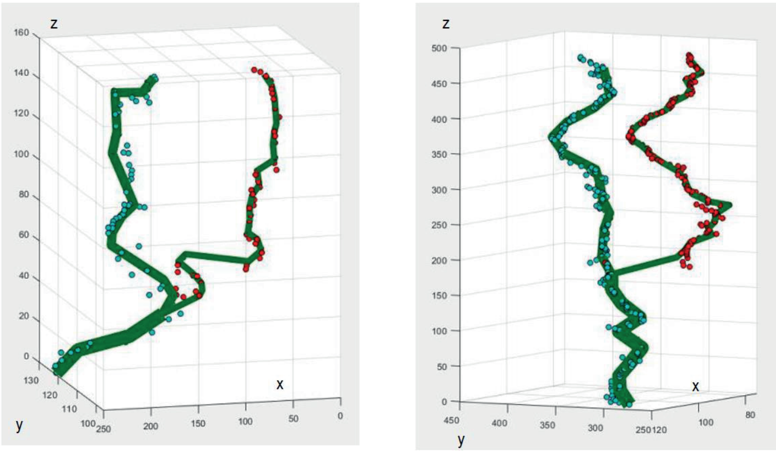

Fig. 1 – Carotid bifurcation reconstruction for two specific patients

The main advantage of the developed methodology is the user-independent ability to assign the correct number of regions of interest. This ability indicates the possibility of implementing a fully automatic segmentation algorithm even in images corrupted by noise. The difficulty remains on the correct identification of the artery centers for extremely irregular shapes. Despite of the good results applying the new proposed index methodology further study to perform accurate selection and segmentation is under development.

ACKNOWLEDGMENTS

The authors gratefully acknowledge the funding by FCT, Portugal, of the Research Unit of LAETA-INEGI.

REFERENCES

Castro CF, António CAC, Sousa LC (2018) Vessel detection in carotid ultrasound images using artificial neural networks. Proceedings of the 6th International Conference on Integrity, Reliability and Failure, 1169-1172.

Goddi A, Bortolotto C, Fiorina I, Raciti MV, Fanizza , Turpini E, Boffelli G, Calliada F (2017) High-frame rate vector flow imaging of the carotid bifurcation. Insights into imaging, 8(3), 319-328.

Jodas DS, Pereira AS, Tavares JMRS (2018) Automatic Segmentation of the Lumen in Magnetic Resonance Images of the Carotid Artery. Computers in Biology and Medicine 79:233-242. DOI: 10.1016/j.compbiomed.2016.10.021.

Sousa LC, Castro CF, António CC, Santos A, Santos R, Castro P, Azevedo E, Tavares JMRS (2014) Hemodynamic conditions of patient-specific carotid bifurcation based on ultrasound imaging. Computer Methods in Biomechanics and Biomedical Engineering: Imaging & Visualization, 157-166.

PAPER REF: 020

NOVEL DEGRADABLE ZN-BASE ALLOYS FOR STRUCTURAL BIOMEDICAL APPLICATIONS

Ehsan Mostaed[1*], Alessandra Fava[2], Roberto Montanari[2], Zahra Sajedi[1], Alessandra Varone[2], Maurizio Vedani[1(*)]

[1] Dipartimento di Meccanica, Politecnico di Milano, Via Giuseppe La Masa 1, 20156, Milan, Italy

[2] Department of Industrial Engineering, University of Rome "Tor Vergata", Rome, Italy

[*]current affiliation: Department of Materials Science and Engineering, Michigan Technological University, Houghton, USA

[(*)]*Email:* maurizio.vedani@polimi.it

ABSTRACT

Biodegradable metals (BMs) are selected and designed for their use in temporary implants, aimed at supporting tissue remodeling, regeneration and healing for limited time. The main constituents of BMs and related alloys should be essential metallic elements that can be safely metabolized by the human body. Their combination should also provide an appropriate degradation rate by homogeneous corrosion mechanisms as well as suitable strength and toughness properties to sustain static and dynamic loads.

BMs can be classified into three main groups: Fe-based, Mg-based and Zn-based alloys. In recent years Zn attracted increasing attention due to its biodegradation rate, the specific role as essential element in human nutrition and the effects on cell proliferation and in the immune and nervous systems. Despite these advantages, pure Zn is very soft and strengthening strategies have to be designed in Zn alloys for achieving the required combination of strength and ductility. They consist in tuning the chemical composition with the use of non-toxic elements, and on manipulating the alloy microstructure to refine grain size and promote a fine dispersion of second phases.

On this basis five Zn alloys (Zn-5.0Ag, Zn-5.0Ag-0.25Mn, Zn-5.0Ag-0.50Mn, Zn-7.5Ag-0.50Mn, Zn-7.5Ag-0.75Mn) have been prepared and characterized. They were cast on a laboratory scale by using pure ingredients (Zn: 99,995%; Mg: 99,95%; Ag: 99,5%; Al: 99,995%; Mn: 99,95%). Melting was performed in cylindrical graphite molds. The cast samples were annealed at temperatures ranging from 350 to 410°C, depending on alloy composition.

The microstructure of the alloys has been investigated through differential scanning calorimetry (DSC), X-ray diffraction (XRD) and optical microscopy (OM) and scanning electron microscopy (SEM), while the mechanical properties have been determined through hardness and tensile tests.

Analyses of microstructures depicted in Fig. 1 revealed that the Zn-5Ag alloy substantially consists in coarse η-Zn grains with evidence of twins at their interior. The addition of 0.25 wt.% Mn to form Zn-5.0Ag-0.25Mn alloy promoted the appearance of grain boundary precipitates having a tiny lamellar structure, presumably based on the Zn-$Zn_{13}Mn$ eutectics. Increasing the concentration of Ag and Mn led to a significant grain refinement and to the increase in volume fraction of both the eutectic constituent (in case of alloy Zn-5.0Ag-0.5Mn) and of the fraction of primary ε-$AgZn_3$ phase (visible in Figure 1 for Zn-7.5Ag-0.75Mn alloy).

Zn-5.0Ag Zn-5.0Ag-0.25Mn Zn-5.0Ag-0.50Mn Zn-7.5Ag-0.75Mn

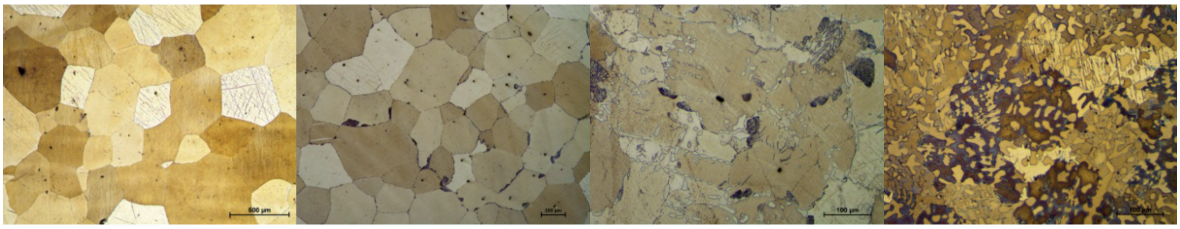

Fig. 1 - Optical micrographs of the Zn-5.0Ag, Zn-5.0Ag-0.25Mn, Zn-5.0Ag-0.50Mn and Zn-7.5Ag-0.75Mn alloys after annealing

DSC scans collected on cooling from liquid stage allowed identifying the sequence of alloy solidification. Fig. 2 summarizes the DSC scans collected at a cooling rate of 15°C/min. The cooling curve of the Zn-5.0Ag alloy confirms the presence of a peak visible at about 420°C (as a shoulder of the main peak) that corresponds to the formation of primary ε-$AgZn_3$ phase and of a wider peak centered at 400°C involving the peritectic transformation to produce the η-Zn solid solution. Adding Mn to the Zn-Ag alloy results in a shift of the peritectic reaction to slightly higher temperature (to about 410°C in all the investigated alloys) while the increase of the Ag content from 5 to 7,5 wt.% led to a widening and shift of the peak related to the primary ε-$AgZn_3$ phase, in accordance with the enrichment expected from phase diagrams.

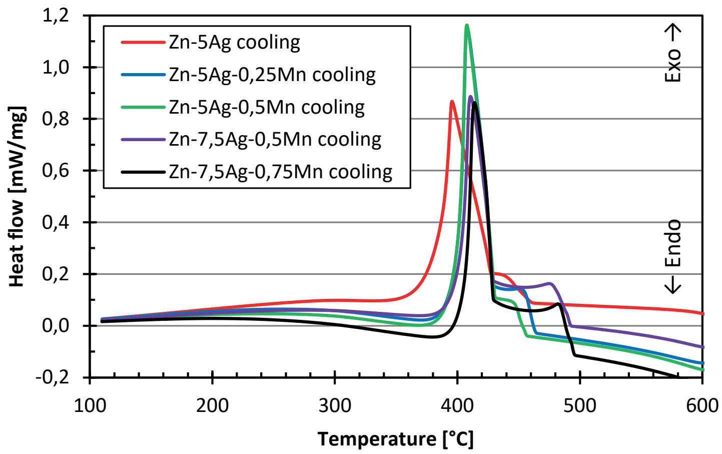

Fig. 2 - DSC curves recorded on cooling.

Table 1 summarizes the hardness of the alloys, both in as cast condition and after annealing. The results confirm that hardness can be significantly increased by alloying with Ag and Mn up to values of interest for the application as biodegradable devices. From hardness measurements, no distinct trend can be identified among the different investigated alloys.

Table 1 - Average Vickers micro-hardness and standard deviation.

Alloy	**As cast**	**Annealed**
Zn-5.0Ag	53.1±3.7	76.7±2.4
Zn-5.0Ag-0.25Mn	63.0±4.1	71.8±4.3
Zn-5.0Ag-0.50Mn	62.8±5.0	72.7±2,6
Zn-7.5Ag-0.50Mn	66.6±2.5	68.7±4.0
E (Zn-7,5Ag-0,75Mn)	69,3±4,4	74,9±5,0

PAPER REF: 021

ENVIRONMENTAL MANAGEMENT SYSTEMS: BENEFITS AND BARRIERS TO THE IMPLEMENTATION OF ISO 14001:2015

Federica Murmura[1], Laura Bravi[1], Gilberto Santos[2(*)]

[1] Department of Economics, Society, Politics; University of Urbino Carlo Bo, Via Saffi 42, 61029 Urbino, Italy
[2] School of Design, Campos do IPCA, Rua do Aldão, 4750-810, Barcelos, Portugal
[(*)]*Email:* gsantos@ipca.pt

ABSTRACT

The purpose of this study is to understand the perception of Italian companies with respect to the environmental management system standard ISO 14001:2015 in terms of motivations that have guided the adoption, benefits and barriers found. In addition to this, it has been tried to understand what was the perception of companies with respect to the new elements introduced by the latest version of the standard, also in terms of comparison with the previous version of 2004, in order to understand to what extent these changes have been perceived in terms of improvement by organizations.

Keywords: ISO 14001; Environmental Management Systems; Environmental management; Sustainability.

INTRODUCTION

The UNI EN ISO 14001 standard is part of the ISO 14000 family of standards; it offers practical tools to companies and organizations wishing to better manage the environmental impacts of their business. The ISO 14001 standard in particular establishes the criteria for the implementation of an effective Environmental Management System (EMS) (Murmura et al, 2018). To date, there are over 300,000 ISO 14001 certifications worldwide, present in 171 countries. Italy is the second country in the world for the number of ISO 14001 certifications, with 10.680 certifications at the end of 2017, preceded only by China which has 94.865 ones (www.isotc.iso.org). The ISO 14001 standard, thanks to its international diffusion, has become the main reference in the field of corporate environmental management for over twenty years (Boiral et al., 2018) and for this reason, it has always been widely debated by academics and managers. According to the study of Bansal and Roth (2000), Heras-Saizarbitoria et al., (2016) and Santos et al. 2015, three types of motivations can be identified that encourage companies to adopt an Environmental Management System based on an international standard: ethical, competitive and relational motivations. The literature also suggests that two main theoretical approaches can be distinguished regarding the motivations that drive companies to implement an EMS. The first refers to factors of an external nature, connected to the pressures that may come from the market, the company or national and international legislation (Heras-Saizarbitoria, et al., 2011), while the second approach, instead, focuses on the motivations related to the internal improvements that can be achieved through the implementation of the EMS, which include factors such as: the strategy and the internal capacities of the organization; human resources, such as management skills or ability to motivate environmental action paths. Considered that, the aim of the research is to understand the main motivations of Italian companies in implementing an EMS, the main benefits and barriers found in the adoption and the perception of companies with respect to the new elements introduced by the latest version of the standard ISO 14001:2015.

RESULTS AND CONCLUSIONS

From Table 1 it emerged that, the main motivations that guided companies in implementing an EMS were the improvement of corporate image (4.29), the possibility to work in respect of the environment (4.28), the alignment with environmental laws (4.22), the possibility to have continuous improvement of environmental performance (4.11) and to avoid potential negative environmental impacts (4.12).

Table 1 – Motivations that pushed companies to ISO 14001 implementation

Motivations	*Mean*	*St. Dev.*
Customer pressure satisfaction	3.17	1.39
Achievement of an environmental strategy	3.79	1.10
Operation in the respect of the environment	4.28	0.89
Integration with other management systems in the company	3.85	1.20
Spread of environmental skills and responsibilities at all levels of the company	4.02	0.94
Reduce in business costs	2.81	1.19
Maintain a competitive position in the reference market	3.71	1.22
Avoid potential negative environmental impacts	4.12	1.00
Improvement of corporate image	4.29	0.85
Alignment with environmental laws	4.22	0.91
Obtaining a continuous improvement of environmental performance	4.11	0.95
Improvement of employees' environmental awareness	3.85	1.06

The empirical survey conducted in this study has allowed to confirm the importance of the ISO 14001 environmental standard within the Italian economy. The motivations that lead companies to get certified are many and not always due to the desire to satisfy the strong environmental sensitivity of the entrepreneur.

REFERENCES

Bansal, P, Roth, K. Why companies go green: A model of ecological responsiveness. Academy of Management Journal, 2000, 43(4), p. 717-736.

Boiral, O, Guillaumie, L, Heras-Saizarbitoria, I, Tayo Tene, CV. Adoption and outcomes of ISO 14001: a systematic review. International Journal of Management Reviews, 2018, 20(2), p. 411-432.

Heras-Saizarbitoria, I, Arana Landín, G, Molina-Azorín, JF. Do drivers matter for the benefits of ISO 14001? International Journal of Operations & Production Management, 2011, 31(2), p. 192-216.

Heras-Saizarbitoria, I, Boiral, O, Arana, G. Renewing environmental certification in times of crisis. Journal of Cleaner Production, 2016, 115, 214-223.

Murmura, F, Liberatore, L, Bravi, L., Casolani, N. Evaluation of Italian Companies' Perception About ISO 14001 and Eco Management and Audit Scheme III: Motivations, Benefits and Barriers. Journal of Cleaner Production, 2018, 174, 691-700.

Santos, G, Rebelo, M, Lopes, N, Alves, MR, Silva, R, Implementing and certifying ISO 14001 in Portugal: motives, difficulties and benefits after ISO 9001 certification. Total Quality Management & Business Excellence, 2015, 27(11-12), 1211-1223.

PAPER REF: 022

IMPROVED FORMULATION FOR SIMULATING ALLOYS WITH THE SMOOTHED MOLECULAR DYNAMICS (SMD) METHOD

Yan Liu[1(*)], **Leiyang Zhao**[1], **Shuai Wang**[1]

[1]School of Aerospace Engineering, Tsinghua University, Beijing 100084, China
[(*)]*Email:* yan-liu@tsinghua.edu.cn

ABSTRACT

The smoothed molecular dynamics (SMD) method can use much larger time step size than traditional molecular dynamics (MD) with the aid of a background mesh and the mappings between the mesh nodes and the atoms. However, the original SMD method was only well validated for pure metals. This work investigates the influences of the mass ratio between different atoms and the potential parameter on the accuracy when the alloy is simulated. Based on the simulation results, novel schemes are developed to improve the accuracy of the SMD method for alloys. Novel mapping functions with much better accuracy are also employed to improve the local accuracy.

Keywords: smoothed molecular dynamics, molecular dynamics, alloys, shape function.

INTRODUCTION

The MD method is widely used in nanoscience and problems under extreme condition. However, the temporal and spatial scales in MD simulation are too limited due to huge number of atoms and tiny time step sizes. The smoothed molecular dynamics (SMD) method was proposed in our previous work (Liu, 2007) by introducing one set of background mesh into MD flowchart, and the time step of SMD method can be one order higher than that of MD method. Recently, improvement schemes, such as the coupling scheme with MD, the parallel scheme, and the alternating SMD method, have been developed. SMD also serves to bridge the MD method and the continuum-based material point method to a seamless multiscale method (He, 2017).

The original SMD method was only thoroughly studied for pure metals. In this work, we examine the accuracy of SMD for alloys. The influences of the mass ratio and the parameters of interaction potential of two types of atoms are investigated. A multigrid technique is developed in SMD framework to improve the accuracy for systems with two types of atoms. Furthermore, the linear mapping function is used in the original SMD method, which limits local accuracy due to the excessive smoothing of high-frequency modes. Some higher-order mapping functions are employed to replace the linear mapping function in SMD method, and their performance is examined in detail.

RESULTS AND CONCLUSIONS

The examples of impact of 1D atoms chains and the propagation of wave are examined. Cases using different mass ratios and interaction potential parameters are simulated by MD method and SMD method, respectively. The results show that the mass ratio between two types of atoms has much less effect on the accuracy while the interaction potential parameter dominates the accuracy. Both the SMD method and the developed multigrid scheme can give nice results when the interaction parameters of different atoms are close. The multigrid scheme can obtain much better accuracy than original SMD method when the difference of interaction parameters of different atoms is large.

The accuracy loss by the linear mapping function can be well reduced by using higher-order functions. An example of wave propagation in a plate is shown in Fig. 1. The region below the red dotted line is simulated by MD method while the region above is simulated by SMD method. The result in Fig. 1(b) (using higher-order function) is much better than that in Fig. 1(a) (using the linear mapping function).

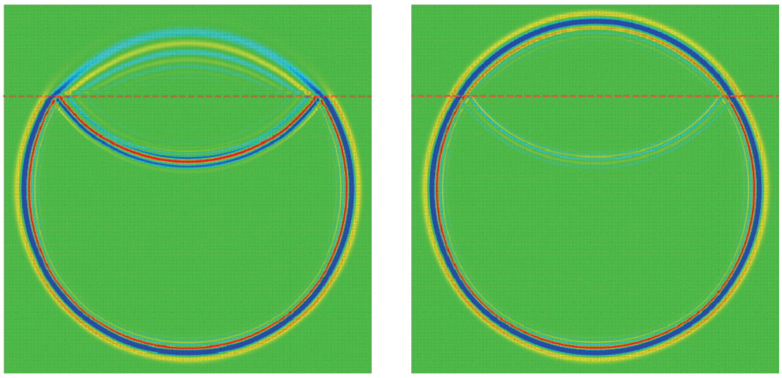

(*a*) (*b*)

Fig. 1 - Wave propagation in a plate using different mapping functions

ACKNOWLEDGMENTS

The authors gratefully acknowledge the support from the National Natural Science Foundation of China (Grant Nos. 11772171 and 11672154) and Science Challenge Project (Grant No. TZ2018001).

REFERENCES

Liu, Y., Zhang, X., Sze, K. Y., Wang, M.. Smoothed molecular dynamics for large step time integration. CMES-Computer Modeling in Engineering & Sciences, 2007, 20(3), p. 177–191.

He, N., Liu, Y., Zhang, X.. Seamless coupling of molecular dynamics and material point method via smoothed molecular dynamics. International Journal for Numerical Methods in Engineering, 2017, 112(4), p. 380–400.

PAPER REF: 023

ROTATING BENDING FATIGUE TESTS ON UNCOATED AND DLC COATED 7075-T6 ALUMINUM ALLOY

Sergio Baragetti[1,2(*)], Emanuele Borzini[3], Emanuele Vincenzo Arcieri[2]

[1]GITT – Centre on Innovation Management and Technology Transfer, University of Bergamo, Via Salvecchio 19, Bergamo 24129, Italy

[2]Department of Management, Information and Production Engineering, University of Bergamo, Viale Marconi 5, Dalmine 24044, Italy

[3]Machine Designer, Via Lagrange 26, Novara 28100, Italy

[(*)]*Email:* sergio.baragetti@unibg.it

ABSTRACT

7075-T6 aluminum alloy is commonly used in high strength-to-mass ratio applications. However, its usage in corrosive environments, with fatigue loads, is still under investigation. Physical Vapor Deposition (PVD) coatings can improve the tribological properties of the surface. R=-1 rotating bending tests on uncoated and PVD Diamond Like Carbon (DLC) coated 7075-T6 specimens were carried out in laboratory air in order to evaluate the contribution of the coating deposition on the fatigue strength of the alloy.

Keywords: light alloys, 7075-T6, rotating bending fatigue, PVD, DLC.

INTRODUCTION

7075-T6 aluminum alloy is a light alloy used in aerospace, marine, automotive sectors (VVAA, 2001). However, the alloy is susceptible to Stress Corrosion Cracking and Corrosion Fatigue (Brown, 1972). The deposition of PVD coatings improve the corrosion resistance and the 7075-T6 wear behavior (Puchi-Cabrera, 2008). The elevated deposition temperatures of some PVD coatings can produce detrimental effects in terms of fatigue strength (Puchi-Cabrera, 2008). DLC coating is a low temperature PVD coating. Here a study on the fatigue strength of uncoated and DLC coated 7075-T6 at different stress levels is presented.

MATERIALS AND METHODS

R=-1 rotating bending fatigue tests were carried out on 7075-T6 hourglass specimens. The fatigue limit was found by means of a step loading procedure (Baragetti, 2016): for a prefixed number of cycles, a load is applied, if the rupture does not occur within this number of cycles, the test is repeated with an increased load. The fatigue limit at N cycles is defined by Eq.1:

$$\sigma_{max} = \sigma_{prior} + N_f\,(\sigma_{final} - \sigma_{prior})/N \qquad (1)$$

where σ_{final} is the maximum nominal stress at the failed load block, σ_{prior} at the previous one and N_f is the number of cycles at which failure occurs during the failed block.

RESULTS AND CONCLUSIONS

In Fig. 1 the results are displayed. A small fatigue strength loss occurs for the coated specimens within the 2e5 - 1e7 number of cycles range. This reduction could be caused by the thermal load of the coating deposition. The residual compressive stress state due to the coating deposition could induce the small slope of the coated specimens' data points.

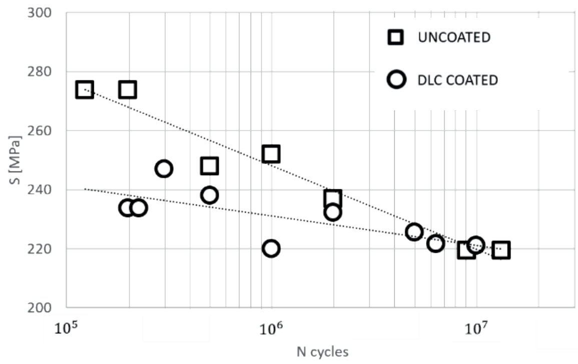

Fig. 1 – Results.

The fracture surfaces of two DLC coated specimens at different stress levels (Fig. 2) point out a greater number of fracture lines for the specimen ruptured at the smallest stress level. A flake can be noticed in Fig. 2B. It is due to high plastic deformation before the rupture (high stress).

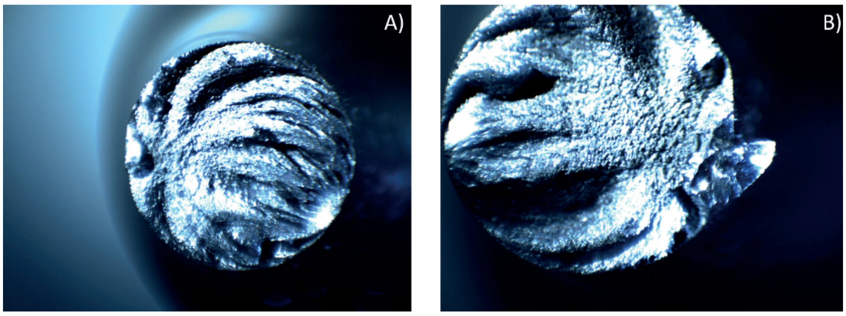

Fig. 2 – Surfaces: A) DLC, 240 MPa, 1083723 cycles; B) DLC, 290 MPa, 48543 cycles.

ACKNOWLEDGMENTS

The authors wish to thank Lafer S.p.A. for the coating deposition and the technical advice.

REFERENCES

Baragetti S, Gerosa R, Villa F, Step loading corrosion fatigue testing of 7075-T6 WC/C coated specimens in air and methanol. Engineering Fracture Mechanics, 2016, 164, p. 106-116.

Brown BF, Stress-Corrosion Cracking in High Strength Steels and in Titanium and Aluminum Alloys. Washington, D.C.: Naval Research Laboratory, 1972.

Puchi-Cabrera ES, Staia MH, Lesage J, Gil L, Villalobos-Gutiérrez C, La Barbera-Sosa J, Ochoa-Pérez EA, Le Bourhis E, Fatigue behavior of AA7075-T6 aluminum alloy coated with ZrN by PVD. International J of Fatigue, 2008, 30, p. 1220–1230.

VVAA, ASM Metals Handbook: Properties and Selection: Nonferrous Alloys and Special-Purpose Materials, vol. 2. ASM International, 2001.

PAPER REF: 024

HYBRID EVOLUTIONARY ALGORITHM FOR GLOBAL STRUCTURAL RELIABILITY ASSESSMENT

Gonçalo das Neves Carneiro[1(*)], **Carlos Conceição António**[1]

[1] LAETA/ INEGI, Faculty of Engineering, University of Porto, Porto, Portugal

[(*)]*Email:* em09077@fe.up.pt

ABSTRACT

Composite laminate structures are prone to probabilistic catastrophic failure due to uncertainty in material and strength properties. The Reliability Index Approach (RIA) estimates the failure probability as a function of the reliability index and is formulated as a minimization problem. For highly dimensional problems and discontinuous implicit structural response functionals, gradient-based optimization methods suffer from premature local convergence, or even divergence. A new hybrid evolutionary algorithm is developed, to achieve global convergence of the RIA problem with practical efficiency.

Keywords: Reliability assessment, Evolutionary Algorithms, Composite Structures.

INTRODUCTION

Consider deterministic design variables, $\mathbf{d} \in \mathbb{R}^{N_\mathbf{d}}$, and random design variables and random parameters, $\mathbf{z} \in \mathbb{R}^{N_\mathbf{z}}$. Now, let $\mathbf{y}(\mathbf{z}) \sim N(0,1)$ be the set of independent standard normal random variables, obtained through transformation of $\mathbf{z}$ (Melchers, 1999). The Reliability Index Approach (RIA) problem is defined as follows

$$\begin{aligned} \min_{\mathbf{y}} \quad & \beta \equiv \| \mathbf{y} \| \\ \text{subject to} \quad & G(\mathbf{y} \,|\, \mathbf{d}, \boldsymbol{\mu}_\mathbf{z}) = 0 \end{aligned} \tag{1}$$

where $G(\cdot)$ is the transformed limit-state function, in the standard normal uncertainty space and $G(\cdot) = 0$ is the failure surface. The solution of this problem is the point on the failure surface with the minimum reliability index, β, named the most probable failure point (MPP).

Gradient-based methods only guarantee local convergence and may diverge in high dimensional problems and in the presence of discontinuous response functionals. To achieve global convergence with efficient computing times a new evolutionary algorithm, named Hybrid micro-Genetic Algorithm (HmGA), is proposed with the following novelties: random variables are decomposed into magnitude and direction components, the RIA problem is redefined as dual problem, with a mixed real-binary coded genotype, and two new evolutionary operators are introduced, one for the genetic repair of the solutions, to impose the equality constraint of the RIA, and another for the progressive reduction and reallocation of the search domain, implicitly guiding the evolutionary process to a region of the failure surface with higher probabilistic failure content.

To study the ability of the proposed EA, the reliability indexes of a set of Pareto-optimal solutions, from a multi-objective design optimization of shell composite laminate structures, are calculated (das Neves Carneiro and António, 2018). Random uncertainty is considered in material and strength properties. Results are compared with a gradient-based method and with Monte Carlo Sampling (MCS).

RESULTS AND CONCLUSIONS

The results show very good accuracy of the HmGA in predicting the both the values of β and the location of the MPP's, in the failure surface. Comparing the performance of the HmGA with a gradient-based method, the maximum relative difference between the estimates of the reliability index is inferior to 4.5%. The maximum relative difference in the components of the MPP vector is about 4%. MCS was executed for 3 representative Pareto-optimal solutions. For each solution $3E^6$ random samples were evaluated, in the uncertainty space, after which two-sided confidence intervals of the probability of failure were calculated. The probability of failure estimated by the HmGA, resulting from the predicted reliability index, falls inside the confidence intervals calculated after MCS. The downside of MCS is requiring 35 hours to evaluate each solution. The computing times of the proposed method are considered to be practical, varying between 4 and 12 minutes, attesting the efficiency of the method. Even though it performs slower than gradient-based methods, the advantages of the HmGA have to be taken into account, mainly the ability to guarantee global convergence, to deal with discontinuities and not requiring sensitivity analyses. The proposed method is expected to set the basis for further developments on the design optimization of more complex structures with multiple probabilistic failure criteria, where gradient-based methods are likely to fail.

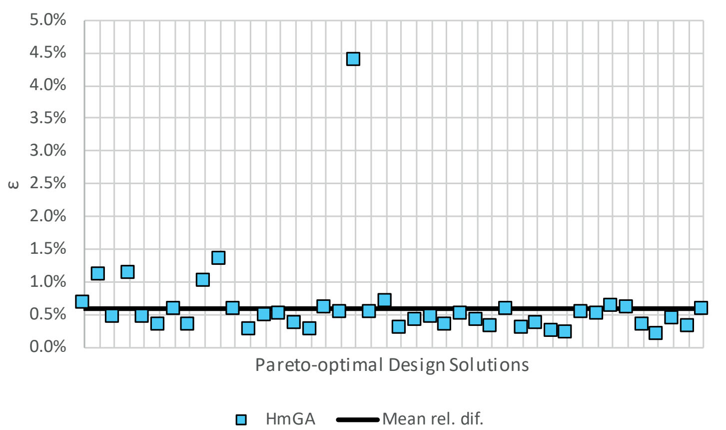

Fig. 1. Relative difference of β, between the proposed EA and a gradient-based method.

Table 1. Accuracy of the proposed EA against MCS.

	β	$p_f = \Phi(-\beta)$	Nº failures	p_f^{low}	p_f^{up}
(1)	3.552	1.913E-04	587	0.000182384	0.000208949
(2)	4.002	3.144E-05	90	1.67174E-05	3.52014E-05
(3)	4.508	3.266E-06	6	0	3.34302E-06

ACKNOWLEDGMENTS

The authors acknowledge the financial support provided by the Fundação para a Ciência e a Tecnologia (FCT), Portugal, through the funding of LAETA laboratory.

REFERENCES

das Neves Carneiro G, António CC. A RBRDO approach based on structural robustness and imposed reliability level. Struct Multidisc Optim, 2018, 57(6), p. 2411-29.

Melchers RE. Structural Reliability Analysis and Prediction. Ltd. JWS, 1999.

PAPER REF: 025

IMPROVING THE EFFICIENCY OF MECHATRONIC SYSTEMS IN ORDER TO ENSURE INTENSIVE REFORM "INDUSTRY-4.0"

Raul Turmanidze [1(*)], Vasili Bachanadze [2], Giorgi Popkhadze[3]

[1, 2, 3] GTU, Department of Mechanical Engineering Manufacturing Technologies, Tbilisi, Georgia
[(*)]*Email:* inform@gtu.ge

ABSTRACT

The presented work will show the highest relevance of solving all the issues related to this problem and present the results of the analysis of the main expected potential problems, which may occur in the implementation of the INDUSTRY - 4.0 reform. It is proved that the pace and level of development of this reform will be determined to a large extent by the effectiveness of the individual nodes used and the entire mechatronic system.

It has also been established that as a result of systematic miniaturization of the nodes of radio-electronic equipment and microelectronic equipment and microelectronic technology, the main problem of these reforms and the implementation of complex technological processes is instrumental and technological support, especially with cutting micro-tools and equipment. Therefore, on the example of these investigations, methods for improving their performance are shown.

Keywords: "industry - 4.0", mechatronic systems, micro tools for electro technical industry, optimization of the design and geometrical parameters of various tools and technological equipment.

INTRODUCTION

To date, almost every scientist in any country knows and is unequivocally recognized that at the beginning of the XXI century the whole world is at the turn of the fourth scientific and technological revolution, which fundamentally should change the style and level of thinking, the rules of life for every person and especially the young generation in all countries of the world. This is due to the fact that according to many scholars and authors of large-profiled studies on the state of the necessary conditions for a worthy meeting of major reforms impending change is evaluated as the most comprehensive and ambitious in the history of mankind. It will be held under the abbreviated name "Industry - 4".

During the first industrial revolution, which lasted for more than two centuries for the mechanization of certain operations of industry water and steam were used. As a result, the second revolution based on electricity were created mass production of many products in different areas of the economy. During the third revolution using electronic and information technology production processes have become automated. Now, based on the results of the third revolution is developing the fourth revolution, which is based on digital technologies, the development of which was started in the second half of the last century. It involves a merger of several modern technologies and the disappearance of all boundaries between physical, digital and biological spheres, is the creation of a cyber - physical systems.

In other words, the final goal of the “Industry 4.0” reform is full automation and remote control of complex technological processes and administrative and financial operations by using super modern mechatronic systems.

RESULTS

To create the above-mentioned mechatronic systems, that determine the level and pace of the development of the “Industry 4.0” reform it Requires high-precision technological equipment and special micro-tools for different purposes.

The presented report will show the classification of the micro-tools used for the production of the main units of modern mechatronic systems, as well as ways of systematically improving the efficiency of the used individual instrument groups, taking into account the process of intensive miniaturization of radio electronic equipment and increasing the level of requirements for their performance characteristics.

CONCLUSIONS

- It is established that the rate of development of the INDUSTRY-4.0 reform in a strong degree depends on the efficiency of the Operational characteristics of the used mechatronic systems.
- It is proved that the output characteristics of individual nodes of the used mechatronic systems can be significantly improved by optimizing the design and geometric parameters of technological equipment and the manufacturing processes. For example, the hardness of hard-alloy precision spiral drills with a working diameter of less than 1 mm and the productivity of drilling of printed circuit boards can be increased by at least 25-30%.
- By optimizing the geometric parameters of carbide micro-drills, it is possible to significantly improve the chip formation process and their free removal from the cutting zone when drilling printed circuit boards, which positively affects the quality of the treated surface and subsequently its metallization.

REFERENCES

Снова перемены. Как выглядит Индустрия 4.0? available at: http://hi-news.ru/business-analitics/industriya-4-0-chto-takoe-chetvertaya-promyshlennaya-revolyuciya.html

Карпушевски Б., Дюбнер Л., О. Кушнаренко О., Турманидзе Р.С. Erhöhung der standzeit und prozesssicherheit von mikrobohrern durch die entwicklung neuer werkzeuggeometrien. Сборник научных трудов «Современные технологии в машиностроении». Харьковский национ. техн. университет «Харьковский Политехни-ческий Институт», Харьков, Украина. Выпуск 2. 2008 г. стр. 27-32.

R.TurmanidzeV.Bachanadze, G.Popkhadze International saintific journal “Inovations”. Year V, Issu 3/2017, Sofia, Bulgaria,ISSN Print 1314-8907,ISSN WEB 2534-8469123-128.Basic technological processes required to create mechatronic sistems to meet today’s needs and problems of their instrumental support of “Industry 4.0” challenges

PAPER REF: 026

COMPUTER MODELING OF PROGRESSIVE DAMAGE OF HYBRID METAL-PLASTIC SHELLS OF REVOLUTION UNDER EXPLOSIVE LOADING

Leonid Igumnov[1], Nikolay Abrosimov[1(*)], Nadezhda Novoselceva[1]

[1]Research Institute for Mechanics, National Research Lobachevski State University of Nizhniy Novgorod, Nizhny Novgorod, Russian Federation

[(*)]*Email:* abrosimov@mech.unn.ru

ABSTRACT

A methodology for numerically analyzing nonlinear dynamic deformation and progressive damage of multilayered metal-plastic shells of revolution, accounting for the strain-rate dependence of their strength characteristics, is developed.

Keywords: composite materials, shells of revolution, strength, failure, numerical methods, explosive loading hybrid.

INTRODUCTION

Due to their effective energy absorption, increased crack-resistance and non-splintering character of possible failure, composite materials are widely used in constructing protective structures suffering from intensive pulsed loading effects. In this connection, experimental and theoretical studies on analyzing the processes of progressive damage, starting from the time of initial damage of an elementary layer up to macro-damage of multilayered composite structural elements, appears to be vital.

A kinematic model of deformation of a multilayered package is based on the non-classical theory of shells, where displacement vector components are approximated by finite series through the shell thickness. Geometrical relations are constructed based on the relations of the simplest quadratic version of the nonlinear elasticity theory. The stress-strain tensor correlation in a composite macro-layer is described based on Hooke's law for an orthotropic body in combination with the theory of effective moduli, and in a metallic one it is described in the framework of bilinear strain-hardening yield. The energy-consistent resolving system of dynamic equations of hybrid metal-plastic shells of revolution is derived by minimizing the total energy functional of a shell as a three-dimensional body. The process of layer-by-layer progressive damage of multilayered shells of revolution is described in the framework of the model of degradation of their rigidity characteristics, accounting for the strain-rate dependence of the strength characteristics of composite materials (Abrisimov N.A., 2018). The method of numerical analysis of the formulated initial boundary-value problem is based on an explicit variational-difference scheme (Abrisimov N.A., 2002).

RESULTS AND CONCLUSIONS

The reliability of the introduced methodology for analyzing dynamic strength of hybrid metal-plastic shells of revolution was assessed by analyzing the problem of nonstationary deformation and progressive damage of a two-layer metal-plastic cylindrical shell loaded with a pressure pulse imitating an explosion of a spherical explosive charge in the center of the shell. The results of the comparative experimental-theoretical analysis of the strain-rate effect on the strength of the two-layer metal-plastic cylindrical shells are summarized in the Table 1.

Table 1 - Comparison of the numerical and experimental data (Fedorenko A.G., 2005) for two-layer metal-plastic cylindrical shells

Reinforcement pattern	**Condition of the shell**		
	Experiment	Constant strength characteristics	Accounting for strain-rate dependence of strength characteristics
$\left(\pm 45;90^0\right)_8$	not failed, loss of stability of the steel layer of the shell	failed during the first vibration cycle	not failed, partial damage of individual layers

It is evident in the Table 1 that the results of numerical analysis of dynamic strength of the two-layer metal-plastic cylindrical shells, using the model accounting for the strain-rate dependence of strength characteristics, are in closer agreement with the experimental data than the numerical results obtained using the model with constant strength characteristics.

ACKNOWLEDGMENTS

The work is financially supported by the Federal Targeted Program for Research and Development in Priority Areas of Development of the Russian Scientific and Technological Complex for 2014-2020 under the contract No. 14.578.21.0246 (unique identifier RFMEFI57817X0246).

REFERENCES

Abrisimov N.A., Novoseltsev N.A. Chislrnnoye modelirovaniye vliyaniya skorostey deformatsii na dinamicheskuyu prochnost stekloplastikobyh tsilindricheskih obolochek (in Rus.), Mehanika kompozitnyh materialov, 2018, 54 (6), p. 1063-1078.

Abrosimov N. A., Bazhenov V. G. Nelineynye zadachi dinamiki kompozitnyh konstruktsiy. (in Rus.), N.Novgorod: Izd-vo NNGU, 2002. 400 p.

Fedorenko A.G., Sysurin M.A., Ivanov A.G. Kriterii vybora kompozitnyh materialov dlya obolochechnyh konstruktsiy, lokaliziruyushih vzryv (obzor) (in Rus.), FGiV, 2005, 41 (5), p. 3-13.

PAPER REF: 027

CREEP AND LONG-TERM STRENGTH OF STRUCTURAL ELEMENTS UNDER HIGH-TEMPERATURE THERMAL-MECHANICAL LOADING

Ivan Volkov[1], Leonid Igumnov[1(*)], Francesco Dell'Isola[1], Igor Vorobtsov[1], Aleksandr Ipatov[1]

[1]Research Institute for Mechanics, National Research Lobachevsky State University of Nizhny Novgorod, Nizhny Novgorod, Russian Federation

[(*)]*Email:* igumnov@mech.unn.ru

ABSTRACT

The paper discusses the issue of evaluating strength and service life of critical engineering objects, exploitation properties of which are characterized by multi-parametric nonstationary thermal-mechanical effects. The main degradation mechanisms characteristic of such objects are considered. Basic requirements to the mathematical models of the processes are formulated. A mathematical model is developed in the framework of mechanics of damaged media. The model describes processes of inelastic deformation and damage accumulation in creep (Volkov I.A., 2017).

Keywords: nonstationary creep, long-term strength, modeling, structural element, mechanics of damaged media, temperature, damage degree, durability, failure, service life.

INTRODUCTION

The model consists of three interrelated parts: defining relations describing inelastic behavior of the material, accounting for its dependence on the unloading process; kinetic equations of damage accumulation; a criterion of strength of damaged material. The relations of nonstationary creep are defined by a family of equipotential creep surfaces in the stress space. The surfaces have a common center and different radii. The principle of orthogonality of the creep strain rate vector to the corresponding surface at the loading point holds. The defining relations describe transient and stable parts of the creep curve and the main effects of the creep process in metals for various temperatures and multiaxial stressed states. The version of kinetic equations of damage accumulation is based on introducing a scalar parameter of damage degree. Energy principles are used, and the main effects of nucleation, growth and merging of microdefects of the degrading material according to the long-term strength mechanism are taken into account. The point at which damage degree reaches its critical value is taken as a strength criterion of damaged material.

RESULTS AND CONCLUSIONS

The results of numerically modeling the carrying capacity of the reactor vessel of a nuclear power plant in the conditions of a hypothetical emergency are presented. The emergency conditions were modeled with the effects of pressure from meltdown, constant internal pressure and temperature varying within the analyzed part of the reactor vessel. An axisymmetric reactor vessel consisting of a cylindrical sidewall with an elliptical bottom was analyzed. The emergency situation was modeled by an effect of internal hydrostatic pressure p_1, changing from zero at a height of h = 1,5 m above the lowest point from the bottom and modeling a force effect from the meltdown, internal pressure p_2 and temperature T varying within the analyzed part of the reactor vessel from 184° to 1510° C. Two values of temperature T on the region in the apex of the outer surface of the elliptical bottom were used in the analysis: $T = 594°$ C (Kazakov D.A., 1994); and $T = 800°$ C (E.A. Frizen, 2014). The geometrical dimensions and the version of temperature distribution over the reactor vessel surface is shown in Fig. 1.

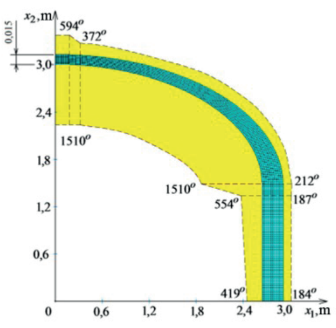

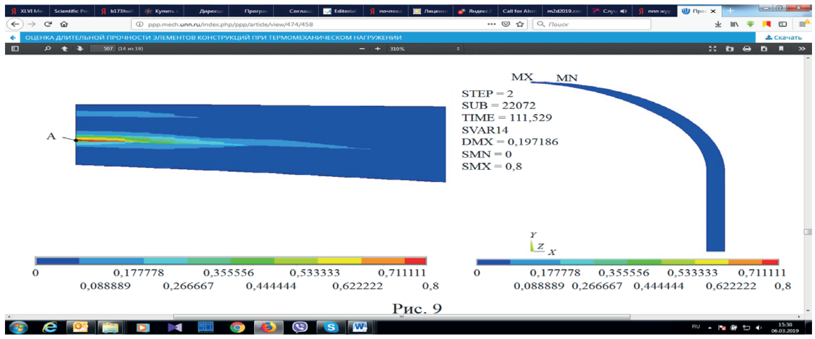

Fig. 1

Fig. 2

The four following values of pressure p_2 were used in the analysis for the version of the temperature field shown in Fig. 1 p_2 = 1,25; 1,35; 1,5 and 2 MPa. The damage degree distribution over the reactor vessel cross-section at the moment of nucleation of a macroscopic crack is shown in Fig. 2. The macroscopic crack for both versions of the analysis is nucleated in the central part of the elliptical bottom in the vicinity of the median surface of the structural element. In Figs. 2 the portion of the zone where the macroscopic crack is nucleated is shown separately. Fig. 3 depicts damage degree ω as a function of time of the process in the most critical zone (point A in Fig. 2): the curve 1 corresponds to p_2 = 2 MPa, the curve 2 - p_2 = 1,5 MPa, the curve 3 - p_2 = 1,25 MPa. The numerical results obtained in the paper agree with the analogous results from (E.A. Frizen, 2014).

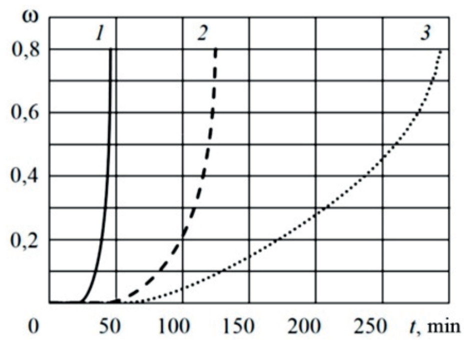

ACKNOWLEDGMENTS

This work was supported by a grant from the Government of the Russian Federation (contract No. 14.Y26.31.0031)

REFERENCES

Volkov I.A., Igumnov L.A. Vvedenie v kontinualnuyu mehaniku povrezhdennoy sredy. (in Rus.), Moscow, Fizmatlit, 2017, 304 p.

Kazakov D.A., Kapustin S. A., Korotkikh Yu. G. Modelirovalie protsessov deformirovaniya i razrusheniya materialov i konstruktsiy. (in Rus.), N. Novgorod: Izd-vo Nizhegorodskogo Un-ta, 1994, 225 p.

E.A. Frizen, V.P. Semishkin, S.I. Pantyushin. Termomehanicheskiy analiz povedeniya korpusa reaktora sredney moshnosti v usloviyah tyazholoy zaproektnoy avarii (in Rus.), Gidropress, 2014.

PAPER REF: 028

A CONTINUAL MODEL OF DAMAGED MEDIA FOR DESCRIBING CREEP FAILURE PROCESSES

Ivan Volkov[1], Sergey Vlasov[2], Svetlana Litvinchuk[1(*)]

[1]Research Institute for Mechanics, National Research Lobachevsky State University of Nizhny Novgorod, Nizhny Novgorod, Russian Federation

[2]Federal State Institution «Scientific Research Institute for System Analysis of the Russian Academy of Sciences», Moscow, Russian Federation

[(*)]*Email:* litvinchuk@mech.unn.ru

ABSTRACT

High-temperature deformation of structural materials (metals and their alloys) is considered, as well as the degradation of initial strength properties of structural alloys according the long-term strength mechanism. The main laws of deformation and damage accumulation processes in creep are studied.

Keywords: nonstationary creep, long-term strength, modeling, defining relations, mechanics of damaged media, temperature, stress, strain, damage degree, numerical and full-scale experiment.

INTRODUCTION

In the framework of mechanics of damaged media, a mathematical model of long-term strength is developed, that describes processes of inelastic deformation and damage accumulation in creep (Volkov I.A., 2017). The version of the defining relation of nonstationary creep is based on introducing into the stress space a family of equipotential creep surfaces having a common center and different surface radii and the principle of orthogonality of the creep strain rate vector to the corresponding surface at the loading point. The effect of the accumulated damage degree on the physical-mechanical material properties and on the parameters of the deformation process is accounted for through effective stresses, based on the concept of degrading continua. The version of kinetic equations of damage accumulation is based on introducing a scalar parameter of damage degree. The point when the damage degree reaches its critical value is taken as a strength criterion of the damaged material.

RESULTS AND CONCLUSIONS

The results of studies of a number of structural alloys at constant temperatures and varying values of the stresses assigned in specimens (transfer from one stress level to another) are presented. Paper (Kapustin S.A., 2008) presents the results of experimental study of the processes of short-range high-temperature creep of the VZh-159 heat-resistant alloy. The tests were conducted with cylindrical specimens of solid cross-section with the working part of the length $l = 50$ *mm* and diameter $d = 8$ *mm* in the conditions of uniaxial tension for various levels of normal stresses σ_{11} and temperatures T. Numerical modeling of non-isothermal process of short-term creep under irregular nonstationary thermal-mechanical loading up to the nucleation of a macrocrack according to the long-term strength mechanism was analysed using the «EXPMODEL» program (Volkov I.A., 2016). Figs. 1–2 depict some plotted creep curves, the solid lines on which show numerical modelling, whereas the dotted lines represent the corresponding experimental results. The figures demonstrate agreement between the experimental and numerical results. For the experiment shown in Fig. 2 the dependences of effective stresses $\tilde{\sigma}_{11}$ (Fig. 3) and damage degree ω (Fig. 4) as a function of time of the process are given.

The analysis of the obtained model showed that it describes the main effects observed in nonstationary creep of structural materials (metals and their alloys) and degradation of the initial strength characteristics of the materials according to the long-term strength mechanism.

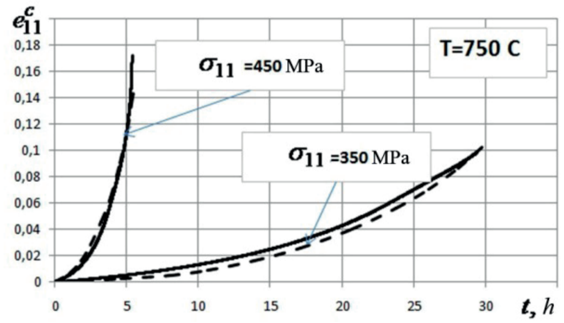

Fig. 1

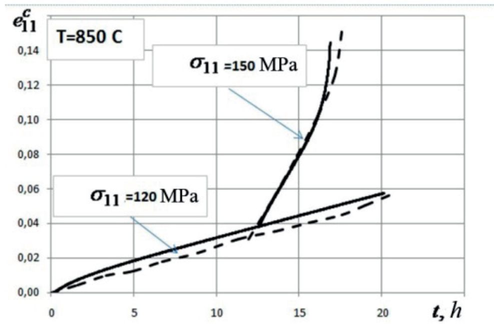

Fig. 2

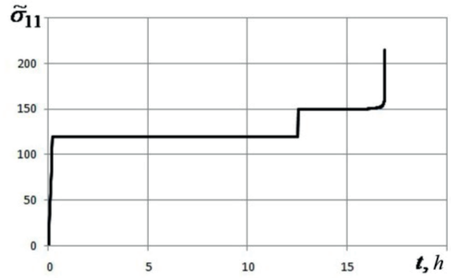

Fig. 3

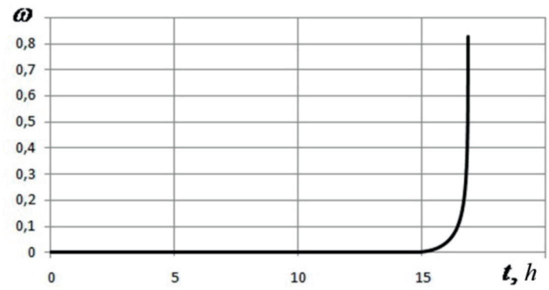

Fig. 4

ACKNOWLEDGMENTS

The work is financially supported by the Federal Targeted Program for Research and Development in Priority Areas of Development of the Russian Scientific and Technological Complex for 2014-2020 under the contract No. 14.578.21.0246 (unique identifier RFMEFI57817X0246).

REFERENCES

Volkov I.A., Igumnov L.A. Vvedenie v kontinualnuyu mehaniku povrezhdennoy sredy. (in Rus.), Moscow, Fizmatlit, 2017. 304 p.

Kapustin S.A., Kazakov D.A., Churilov Yu.A., Galushenko A.I. i dr. Eksperimentalno-teoreticheskoye izuchenoye povedeniya izdeliy iz zharoprochnogo splava v usloviyah vysokotemperaturnoy polzuchesti (in Rus.), Problemy prochnosti i plastichnosti: Mezhvuzovskiy sbornik, N.Novgorod, 2008, 70. p. 100-111.

Volkov I.A., Igumnov L.A., Kazakov D.A., Emelyanov A.A., Tarasov I.S., Guseva M.A. Programmnaya realizatsiya processov vyazkoplasticheskogo deformirovaniya I nakopleniya povrezhdeniy v konstruktsionnyh splavah pri termomehanicheskom nagruzhenii (in Rus.), Problemy prochnosti i plastichnosti: Mezhvuzovskiy sbornik, N.Novgorod, 2016, 78(2), p. 188-207.

PAPER REF: 029

STRUCTURE-ACOUSTIC COUPLING ANALYSIS IN SHALLOW SEA BY COUPLED FINITE ELEMENT AND SINGULAR BOUNDARY METHOD

Zhuo-Jia Fu [1,2,3(*)], Qiang Xi [1,2]

[1]Key Laboratory of Coastal Disaster and Defence (Ministry of Education), Hohai University, Nanjing 210098, China

[2]Center for Numerical Simulation Software in Engineering and Sciences, College of Mechanics and Materials, Hohai University, Nanjing 211100, China

[3]State Key Laboratory of Structural Analysis for Industrial Equipment, Dalian University of Technology, Dalian 116024, China

[(*)]*Email:*paul212063@hhu.edu.cn

ABSTRACT

In this article the coupled finite element and singular boundary method are given to obtain the numerical solution of the structure-acoustic coupling response of three-dimensional spherical shell structure excited by simple harmonic force in shallow water. The finite element method (FEM) is employed to obtain the vibration response of spherical shell structure, and the singular boundary method (SBM) with Pekeris waveguide Green function is applied to calculate the external acoustic field of spherical shell structure. To facilitate the FEM–SBM coupling, the fluid-solid coupled boundary conditions are adopted on the surface of spherical shell structure. Several numerical examples are carried out to demonstrate the accuracy and efficiency of the proposed coupling solver in the solution of acoustic-vibration coupling response of spherical shell structure.

Keywords: Structure-acoustic coupling response, Singular boundary method, Finite element method, Pekeris waveguide Green function, Simple harmonic force.

INTRODUCTION

In recent years, the vibration noise and acoustic wave propagation of structures in shallow sea has attracted great attention in marine engineering. The most popular numerical methods for structural-acoustic coupling analysis are statistical energy analysis method, the coupled finite element-boundary element method, etc. The statistical energy analysis method is to statistically analyze the average structural-acoustic coupling response in the high frequency range, but cannot obtain the structural-acoustic coupling response of localized regions of complex structure. In comparison, the coupled finite element-boundary element method has been widely used in the structural-acoustic coupling analysis at low and moderate frequency range, and it is based on the fact that the vibration response of localized regions can be clearly described.

However, it should be mentioned that the BEM needs to treat the singular and near-singular integrals, which is mathematically complex and requires extensive computational resources. In order to overcome these shortcomings of the BEM, the singular boundary method (SBM) is proposed in 2009. This method avoids the complex singular integration problem in BEM by introducing the origin intensity factor.

In this study, we establish the coupled model of finite element and singular boundary method by the sono-elasticity theory of ships, the fluid-solid coupling boundary condition and the boundary integral equation. Then, the coupled model has been employed in the structural-acoustic coupling analysis of three-dimensional spherical shell structure excited by simple harmonic force in shallow water.

RESULTS AND CONCLUSIONS

Here consider the acoustic radiation of spherical shell structure under two different simple harmonic forces: (a) vertically downward axial harmonic force $F_1 = 100N$, (b) vertically upward cyclic harmonic force $F_2 = 1N$. The numerical results of the proposed coupled model are compared with COMSOL simulation.

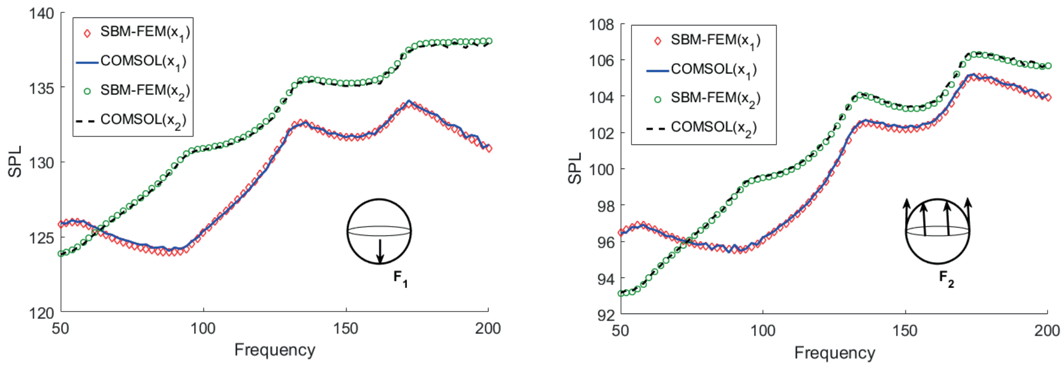

(a) Vertically downward axial harmonic force (b) Vertically upward cyclic harmonic force

Fig. 1 the sound pressure level at different test points ($x_1 = (2, 0, -2.5)$, $x_2 = (2, 0, 2.5)$) under two different simple harmonic forces with different frequencies

Numerical results demonstrate that the proposed coupled model works well for the structure-acoustic coupling response of three-dimensional spherical shell structure excited by simple harmonic force in shallow water.

ACKNOWLEDGMENTS

The work described in this paper was supported by the National Science Funds of China (Grant No. 11772119), the Foundation for Open Project of State Key Laboratory of Structural Analysis for Industrial Equipment (Grant No. GZ1707), Qing Lan Project.

REFERENCES

Fu Z J, Chen W, Wen P H, et al. Singular boundary method for wave propagation analysis in periodic structures[J]. Journal of Sound and Vibration, 2018, 425: 170-188.

Zou M S, Wu Y S, Liu S X. A three-dimensional sono-elastic method of ships in finite depth water with experimental validation[J]. Ocean Engineering, 2018, 164: 238-247.

Chen L L, Zheng C J, Chen H B. FEM/wideband FMBEM coupling for structural–acoustic design sensitivity analysis[J]. Computer Methods in Applied Mechanics and Engineering, 2014, 276:1-19.

Fritze D, Marburg S, Hardtke H J. FEM–BEM-coupling and structural–acoustic sensitivity analysis for shell geometries[J]. Computers & Structures, 2005, 83(2-3):143-154.

PAPER REF: 030

MEASURING MECHANICAL LOSSES OF PISTON COMBUSTION ENGINE BY SPINNING AT VARIOUS WORKING PRESSURES IN ENGINE CYLINDERS

Radek Procházka[1(*)], Aleš Dittrich[2]

[1]Faculty of Mechanical Engineering, Program Machines and Equipment, Department of Vehicles and Engines, Specialization Pistons internal combustion engines, Technical University of Liberec, Liberec, Czech Republic

[2]Faculty of Mechanical Engineering, Program Machines and Equipment, Department of Vehicles and Engines, Specialization Pistons internal combustion engines, Technical University of Liberec, Liberec, Czech Republic

[(*)]*Email:* radek.prochazka@tul.cz

ABSTRACT

This work deals with measurement of mechanical losses by spinning on a test station. It is the current widely used procedure for detecting the effect of various measures to reduce mechanical losses in the piston combustion engine. From the point of view of mechanical losses on the piston group, these measurements show, as the main deficiency, a greater difference between cylinder pressure at engine spinning and cylinder pressure in standard engine operation (i.e. combustion of the mixture). A new way of measuring passive resistances by spinning on a test station in the laboratory of the Department of Vehicles and Engines (DVE), Technical University of Liberec (TUL) eliminates the above-mentioned deficiency for the most part by the fact that even when spinning it is possible to increase the pressure in the cylinder by means of a proportional pressure valve on the values common during normal operation of the engine.

Keywords: spinning the piston combustion engine, mechanical losses, loss torque, measuring.

INTRODUCTION

In recent years, are manufacturers of piston combustion engines (PCE) have been constantly pushing by legislation to reduce emissions of exhaust pollutants and reduce fuel consumption. We are particularly interested in the emission of CO2 emissions in the testing of piston combustion engines, which depends on the overall efficiency of the PCE. The overall efficiency is determined by the thermal efficiency of the working cycle and mechanical efficiency PCE. In research and development of engines is an effort to increase the thermal efficiency of PSM and reduce mechanical losses in the engine. The largest share of about 40-50% of mechanical losses in the PCE are friction losses on the piston group (piston + sealing piston rings). That is why the research of the influence of the construction and material design of the piston group in PCE is given a great deal of attention.

The often-used procedure for detecting the effect of various measures to reduce mechanical losses in PCE is the measurement of “passive engine resistances” by spinning on a test engine station with a dynamometer. The test station must be suitably equipped with a high quality torque sensor, stabilization of coolant and lubricating oil temperature in the engine, automated recording and evaluation of monitored quantities.

RESULTS AND CONCLUSIONS

The measurements were performed on a special DVE test station for the measurement of passive resistances by spinning the 4-cylinder spark-ignition engine 1.6MPI, series EA211 from the VW group. The valve control mechanism has been disabled (the suction and exhaust valves are closed). In the cylinder head were placed instead a fully multifunctional screw fitting (with self-acting single-way valves) instead of spark plugs. Operating modes verification measurement at the test station: coolant temperatures 85 °C and lubricating oil temperature 90 °C, various engine speed (1000, 1500, 2000, …, 5500 rpm), various air pressure at the inlet to automatic single-way valves (1, 2, 3, …, 5 bar- the maximum possible pressure 5,5 bar).

The measured torque of the engine has a linear course depending on the maximum cylinder pressure (see Fig. 2). This includes friction losses in the engine and negative work of "cycle" due to differences in compression and expansion pressure and its magnitude is determined by a double frequency of compression and expansion against the actual 4-stroke engine. Measurement of passive engine resistances spinning with increasing pressure fillings in the cylinder provides important information about properties and behavior of piston rings in conditions close to real engine operation. A new way of measuring passive engine resistors by spinning can thus become an effective tool in research piston rings.

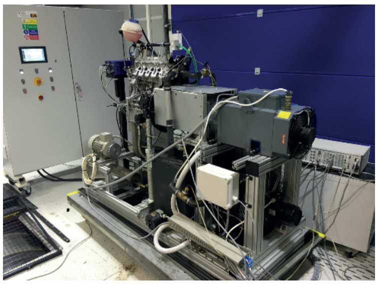

Fig. 1 – The measurement of "passive engine resistances" by spinning on a test engine station with dynamometer.

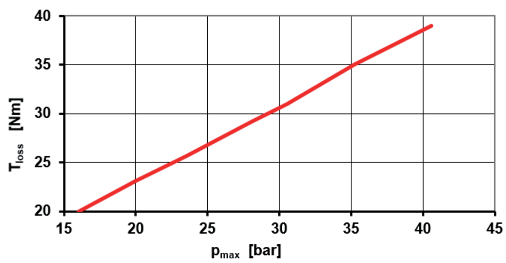

Fig. 2 – The losses torque dependence on the maximum cylinder pressure

ACKNOWLEDGMENTS

This publication was written at the Technical University of Liberec as part of the project Center of Competence of the Automotive Industry Josef Božek with the support of the Specific University Research Grant, as provided by the Ministry of Education, Youth and Sports of the Czech Republic in 2019.

REFERENCES

BEROUN S., VOŽENÍLEK R.: Measurement of passive engine resistances (complete engine and its selected groups) by cranking. Research report SM 617/2009. Department of Vehicles and Engines, Technical University of Liberec, 2009, 13.

NOVOTNÝ P., PÍŠTĚK V., DRÁPAL L.: Modelling of Piston Ring Pack Dynamics. MECCA IX/02, ČVUT v Praze, 2011, p. 8-12. ISSN 1214-0821.

VOŽENÍLEK R., BEROUN S., DITTRICH A.: Measuring the passive resistance of the piston combustion engine by cranking with increase pressure in cylinder. XLVIII. International Scientific Conference of Czech and Slovak University Departments and Institutions Dealing with the Research of Combustion Engines. 2017 Liberec, 8, p. 191-198. ISBN 978-80-7494-354-6

PAPER REF: 031

OPTIMIZATION METHODOLOGY FOR CASTED VEHICLE NODE STRUCTURES

Ralf Sturm(*), Michael Schäffer, Marco Münster

[1]Institute of Vehicle Concepts, German Aerospace Center, Stuttgart, Germany
(*)*Email:* Ralf.Sturm@dlr.de

ABSTRACT

New optimization strategies are developed at the German Aerospace Center (DLR) as part of the Next Generation Car META-project. Within this project novel vehicle concepts are being investigated as the Urban Modular Vehicle (UMV). A high grade of modularity is the main design specification of the UMV concept. This significantly influences the design of the main structural components. In the presented contribution, the focus lies on the development of a new optimisation methodology for casted vehicle node structures. By directly applying load distributions obtained for crash simulations, an optimal structural topology can be directly obtained considering all applied load cases.

Keywords: crashworthiness, safety, topology optimization, vehicle safety

INTRODUCTION

Today's vehicles and their body structures are characterised in particular by their drive train technology, package and the given crash certification requirements. Currently, many concepts have a traditional combustion engine at the front of the vehicle and a gearbox in the transmission tunnel. Due to the electrification of vehicles, vehicle concepts and their body-in-white structures must be rethought.

The UMV concept is a highly modular and intelligent battery-electric vehicle. The modularity of the UMV mainly affects the development of its structural design [1]. By dividing the structure into a central stretchable floor region (with an integrated battery box) and exchangeable crash elements in the front and at the sides of the vehicle, a modular platform can be obtained, on which different vehicle concepts (from a basic sub-compact up to a cargo version) can be built without significantly changing the global structural architecture of the vehicle.

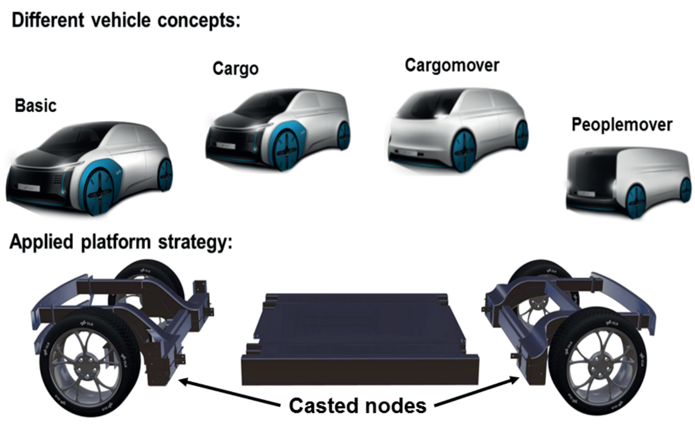

Fig. 1 – Modularisation concept of the UMV

A new methodological approach for the design process of this modular battery-electric vehicle was developed. These optimisations and virtual testing strategies were applied to design the body structures of the vehicle.

In the floor concept the variable mass of the different vehicle concepts can be directly addressed by adapting the trapezoidal crash element, which is positioned at the location of the door sills [2]. The functionality and the required energy absorption characteristics of the floor concept could be proven in an experimental campaign.

Other important structural components for passive safety are the frontal crash structures. In this concept the frontal crash - and floor structures are connected by casted nodes. These elements must sustain all loadings from frontal and lateral crash load cases without failing. For the identification of an optimized structural topology a process chain was developed to directly identify an optimized structural topology by applying quasi static crash load representations to the available design space.

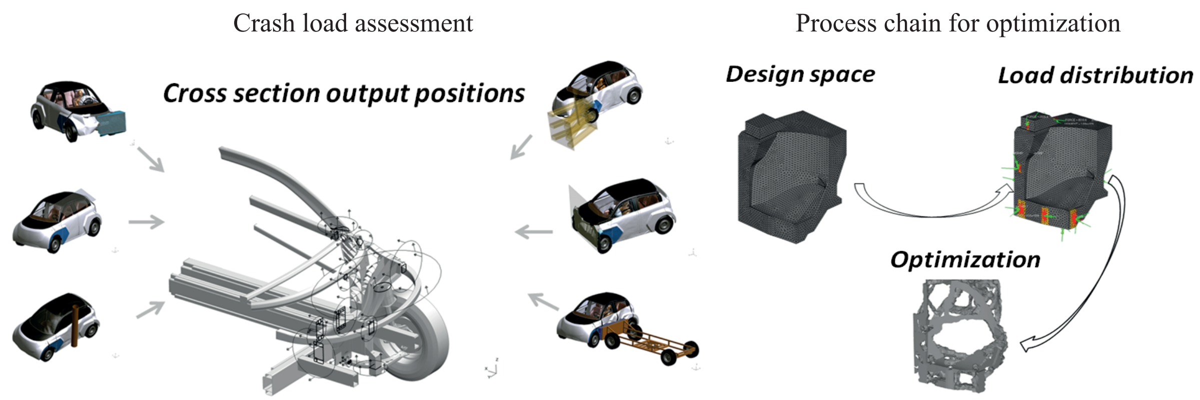

Fig. 2 – Identification of the quasi static crash load representations [left] and the applied process chain for topology optimization [right]

In the talk the methodological approach and the derived process chain for the identification of the optimized structural topology is presented. The main focus lies on the developed optimisation approach to obtain an optimized casted node design fulfilling all stiffness and strength requirements identified by crash simulations.

REFERENCES

[1] Schäffer M, Münster M, Sturm R, Friedrich H, Development of an optimised side crash concept for the battery-electric vehicle concept Urban Modular Vehicle, Deutsches LS-Dyna Forum, 2016

[2] Münster M, Schäffer M, Sturm R, Friedrich H, Methodological development from vehicle concept to modular body structure for the DLR NGC-Urban Modular Vehicle, 16TH Stuttgart international symposium automotive and engine technology, Volume 1, 581-596, 2016

PAPER REF: 032

INVESTIGATION OF MIXED MODE I AND II FRACTURE MECHANICAL BEHAVIOUR OF SLS PRINTED IASCB SPECIMENS BY DIGITAL IMAGE CORRELATION

Ivo Campione[1(*)], Tommaso Maria Brugo[2], Giangiacomo Minak[3], Josip Kos[4], Jelena Janković Tomić[5], Snežana Ćirić-Kostić[6]

[1,2,3]Department of Industrial Engineering (DIN), University of Bologna, Bologna (UNIBO), Italy
[4]Topomatika d.o.o., Zagreb, Croatia
[5,6] Faculty of Mechanical and Civil Engineering in Kraljevo, University of Kragujevac, Kraljevo, Serbia
[(*)]*Email:* ivo.campione@unibo.it

ABSTRACT

This work focuses on the fracture mechanics properties of polyamide (PA) for selective laser sintering (SLS) and investigates the capability of additive manufacturing process to build 3D artificial cracks, otherwise impossible to create by classic methods.

IASCB semi-circular specimen with tilted crack subjected to asymmetric three-point bend loading were tested in order to cover a wide range of stress intensity factors (KI, KII and mixed modes) and T-stress. Moreover, Digital Image correlation (DIC) technique was used by full strain field analysis with the purpose of evaluating the fracture behaviour.

Keywords: Additive manufacturing, Fracture mechanics, Stress intensity factor, Mixed mode, IASCB specimen, Elasto-plastic crack, Digital image correlation.

INTRODUCTION

Additive manufacturing is a recent and promising technology which in the last decades has become widespread in many different fields. However, the mechanical behavior of the used materials has not been completely investigated, especially for what concerns fracture behavior. Brugo et al. (2016) have shown on CT specimens that it is possible to insert intentionally cracks in any desired direction during the AM process and that the building direction influences the fracture toughness.

IASCB specimens (Saghafi, 2010) were manufactured by SLS with an EOS Formiga P100 using polyamide PA 2200 powder. This specimen is a semi-circular disk of radius R that contains a radial edge crack tilted with respect to the load direction. Cracks were initiated in two different ways: they were manufactured during the sintering process or manually initiated after the manufacturing (only for mode I). A total of 15 SLS specimens were manufactured with different crack angles with respect to a vertical axis (0°, 10° and 50°) and tested with different support spans in order to obtain different crack opening mode combinations. The stress intensity factors were obtained by the classic mechanical test and by the DIC measurement of the displacement and strain field developed at the crack tip. This approach was already used in literature (McNeill, 1987) on various types of specimens and proved to be feasible for linear elastic fracture problems.

RESULTS AND CONCLUSIONS

The experimental fracture tests conducted on IASCB specimens are summarized in the graph of Fig. 1, where red and blue circles represent SLS and manually induced crack, respectively.

The KIs of the manually induced crack specimens result to be about 10% lower than the SLS ones, because the crack tip is sharper than the printed one due to the limit of the printing resolution (0.1mm). The experimental data points of the SLS printed cracks were compared with the theoretical criterion MTS (Maximum Tangential Stress) and GMTS (Generalized Maximum Tangential Stress). Cleary the GMTS curve fits better because of the fact it also takes into account the effect of T-stress.

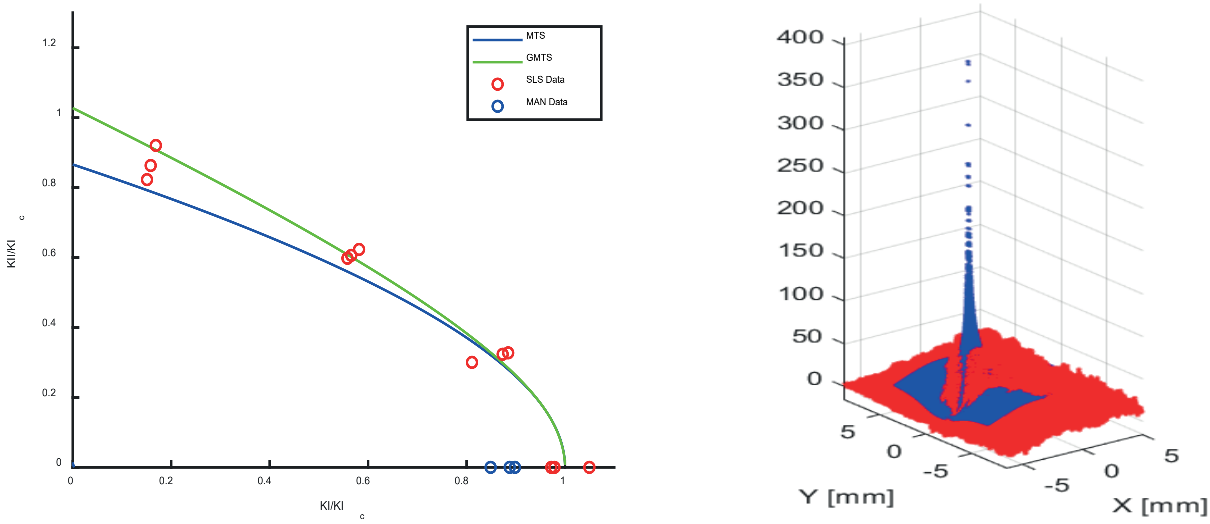

Fig 1 - Mode I and II fracture mechanical results, compared with MTS ang GMTS model (left). Experimental stress field developed at the crack tip compared with Irwin theoretical model for stress (right).

As can be seen in Fig. 1 (right), due to the elasto-plastic behavior of the material, the Irwin theoretical model does not fit well the DIC data. In order to overcome this issue an approach based on the J Integral can be utilized and will be the next development of the research.

ACKNOWLEDGMENTS

The research was realized with the support of the A_MADAM project, funded by the European Union's Horizon 2020 research and innovation program, under the Marie Skłodowska-Curie grant agreement No 734455.

REFERENCES

Brugo T et al. Fracture mechanics of laser sintered cracked polyamide for a new method to induce cracks by additive manufacturing. Polymer Testing, 2016, 50, p. 301-308.

Saghafi H, Monemian SA. A new fracture toughness test covering mixed-mode conditions and positive and negative T-stresses. Int. J.Fract, 2010, 165, p. 135-138.

McNeill SR, Peters WH, Sutton MA. Estimation of stress intensity factor by digital image correlation, Eng. Fract. Mech, 1987, 28, p. 101-112.

PAPER REF: 033

EFFECT OF FRACTURE TOUGHNESS ON THE WEAR BEHAVIOUR OF TETRAHEDRAL AMORPHOUS CARBON (ta-C) COATING

Mohd Muhyiddin Bin Mustafa[1,3(*)], Noritsugu Umehara[1], Takayuki Tokoroyama[1], Motoyuki Murashima[1], Akinori Shibata[2], Yoshiharu Utsumi[2], Hideki Moriguchi[2]

[1]Department of Micro-Nano Mechanical Science and Engineering, Nagoya University, Furo-cho, Chikusa-ku, Nagoya, Aichi 464-8603, Japan
[2]Technology Development Center, Nippon ITF Inc., 47, Umezu-Takase-cho, Ukyo-ku, Kyoto 615-8686, Japan
[3]Faculty of Mechanical and Manufacturing Engineering Technology, Universiti Teknikal Malaysia Melaka, Hang Tuah Jaya, 76100 Durian Tunggal, Melaka, Malaysia
[(*)]*Email:* muhyiddin@ume.mech.nagoya-u.ac.jp

ABSTRACT

Fracture-induced wear is one of the major reasons for the DLC coating failures in the tribological application, which involve rubbing of two components that create contact pressure. The performance of the DLC was restricted by the fracture toughness which is the ability of the material to resist the growth of the pre-existing crack. This study presents the analysis of fracture toughness and its mechanism on the novel Pillar and Mesh ta-C coating, as well as the conventional ta-C coating for comparison by employing a micro-indentation method. Mesh ta-C shows the highest fracture toughness value with 16.6 MPa $m^{1/2}$, followed by Pillar ta-C with 13.4 MPa $m^{1/2}$, and conventional ta-C 11.7 MPa $m^{1/2}$. Increased of fracture toughness result in higher wear resistance of the Mesh ta-C and Pillar ta-C coating. The improved fracture toughness and wear resistance of Mesh and Pillar ta-C is explained by the enhancement of crack propagation inhibition by the intersection effect and soft sp^2 structure in both coatings.

Keywords: diamond-like carbon, material structure, fracture toughness.

INTRODUCTION

Diamond-like carbon (DLC) coatings are known as remarkable features applied as the solid lubricants because of low friction, high hardness as well as wear resistance and chemical inertness. Commonly, DLC is deposited with a layer of homogeneous structure except for multilayer coating design. The current study investigate the tribological features of the as-deposited pillar/mesh structure of ta-C coating under base-oil lubrication conditions together with conventional ta-C coatings. Pillar and Mesh ta-C coating properties are unique for its' pillar-like and mesh-like-structure, which is characterized by the hardness controlled DLC in the direction of the coating thickness. This novel DLC consists of softer topmost surface layer sp^2–rich pillar/mesh structure and substrate-side sp^3–rich conventional ta-C, Fig. 1(a) proposed to improve fracture toughness as well as friction and wear resistance of the coating.

Three types of ta-C were characterized by the structure where conventional ta-C having the uniform structure, while the Pillar ta-C and Mesh ta-C are developed with pillar and mesh structure deposited on Si-wafer were provided by the Nippon ITF Inc. Indentation tests were performed using the micro Vickers hardness testing machine with loads of 0.1, 0.2, 0.3, 0.5 and 1.0 kgf. The determination of fracture toughness from radial crack formed on the DLC/Si system method was established by M. Nastasi et al. (Nastasi et al., 2001). The friction tests were performed via the ball-on-disk tribo-tester under boundary lubrication regime with a constant normal load of 1 N. The speed and temperature of the tests were fixed at 0.042 m/s for 60 minutes that corresponds to 172.8 m of sliding distance and 80°C, respectively. Wear volume loss and specific wear rates of the DLC-coated Si-wafer were quantified via Archard wear equations by calculating the width and depth of the worn area.

RESULTS AND CONCLUSIONS

Specific wear rates of the ta-C, Pillar ta-C, and Mesh ta-C is plotted against fracture toughness of the coating as in Fig. 1(b). The characterization of the coating by means of its mechanical properties is importance to understand the tribological process in the boundary lubrication regime since direct contact of coating surface asperities occur. Fig. 1(b) shows that the fracture toughness of the coating is inversely proportional to the specific wear rates. Increase of fracture toughness result in higher wear resistance of ta-C coating which reduces the effect of fracture induced wear.

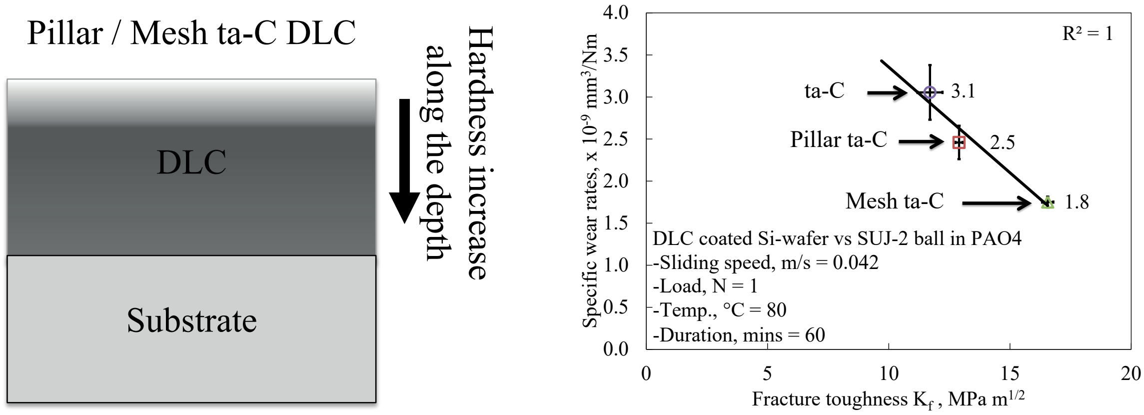

(a) (b)

Fig. 1 - (a) Material concept of Pillar/Mesh ta-C, and
(b) Specific wear rates plotted against fracture toughness of the coating

Fracture toughness of the Pillar and Mesh ta-C coating increased as a result of soft structure sp^2 phase that terminates the crack propagation through energy release by plastic deformation. In addition, Mesh ta-C provides higher fracture toughness as compared to the Pillar ta-C coating as a result of combination of intersection effect and soft sp^2 structure restraints the crack propagation. Introduction of Pillar and Mesh structure to the ta-C coating eliminates the brittle characteristics of the conventional ta-C. The soft structure sp^2 phase terminates the crack propagation through energy release by plastic deformation leads to film toughness enhancement.

ACKNOWLEDGMENTS

The author Mohd Muhyiddin Bin Mustafa would like to thank Ministry of Education, Malaysia and Universiti Teknikal Malaysia Melaka for his doctorial study financial support.

REFERENCES

Nastasi M, Kodali P, Walter KC, Embury JD, Raj R, Nakamura Y. Fracture toughness of diamond-like carbon coatings. Journal of materials research, 1999, 14(5), p. 2173-2180.

PAPER REF: 034

EVALUATING THE SOIL-STRUCTURE INTERACTION (SSI) EFFECTS ON THE PERFORMANCE POINT OF STEEL FRAMED TUBE TALL STRUCTURES EQUIPPED WITH BELT TREUSSES

Armen Assatourians[1(*)], Mohammad Reza Mehrdoust[2], Sohrab Fallahi[3]

[1] Earthquake Engineering Research Consultant, Yerevan Project Co., Yerevan, Armenia
[2] Earthquake Engineer, Building and Housing Research Center., Mashhad, Iran
[3] Senior Structural Designer, E.S.S. Consulting Eng. Co., Tehran, Iran
[(*)] *Email:* ar_ast@mail.ru

ABSTRACT

Current research is carried out on Steel Framed Tube Tall Structures with Truss Belts, consisting of welded connections. The main goal of this research is to illustrate the effects of Soil-Structure Interaction on the Performance Point of such structures. For this purpose, two dimensional 40, 50 & 60 stories Framed Tube Structures, equipped with belt trusses are modeled, analyzed and designed according to ASCE 7-10 code, based on 3 soil categories of Rock (Vs>800m/s), Dense Soil (500<Vs<800m/s) and Loose Soil (150<Vs<500m/s), taking into account the spectral acceleration level of S_a=0.40g. On the next step, Modal Pushover Analyses are carried out on models according to FEMA440 guideline, due to which the Capacity Spectrums and Performance Point characteristics are computed for each model, using USB97 pseudo-acceleration spectrums. Finally, the Performance Point characterestics are computed once more, taking into account the Soil-Structure Interaction (SSI) for each soil category, according to FEMA440 guideline and at last the final results are compared.

Keywords: Soil-Structure Interaction, Framed Tube Tall Structures, Capacity Spectrum, Modal Pushover Analysis, Pseudo-Acceleration Spectrum

INTRODUCTION

Previous experience of earthquakes illustrate that the structures behave nonlinearly during a severe earthquake, due to which a huge amount of input energy is dissipated through the form of damping and hysteresis. In this research, the Performance Point of framed tube structures equipped with belt trusses for models in Fig.1 are computed due to Fig.2, which shows the

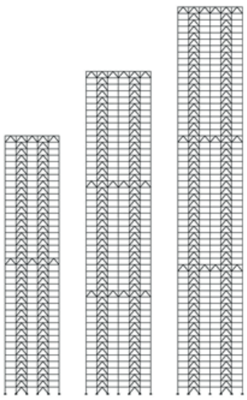

Fig. 1 - Proposed finite element models

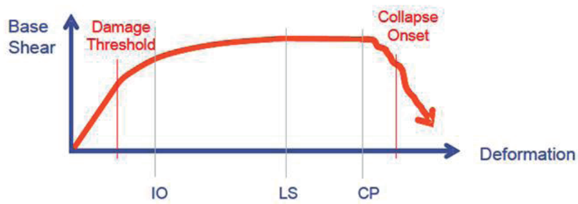

Fig.2 - Performance Levels based on FEMA440

general performance point levels according to FEMA440 guideline and are completed using Nonlinear Static Pushover Analyses. After completing the requested Analysis on each finite element model, the final results for performance points of both with and without taking into account the soil-structure interaction are indicated in Table 1.

Table 1 – Performance Point results according to FEMA440 guideline.
V = base shear force (Ton) and D = displacement (cm)

Soil Type	P.P.	40		50		60	
		w SSI	w/o SSI	w SSI	w/o SSI	w SSI	w/o SSI
Rock	V	118.9	129.8	162.5	175.9	183.1	197.1
	D	51.6	56.3	73.2	80.1	90.1	98.5
Dense Soil	V	176.2	187.3	219.9	235.1	257.3	278.1
	D	74.1	80.1	109.0	119.0	134.6	147.1
Loose Soil	V	251.1	268.0	351.8	372.3	440.2	465.3
	D	104.1	113.6	145.3	158.2	179.7	195.8

RESULTS AND CONCLUSIONS

According to the results in Table 1, the Performance Point Displacement average reduction percent is about 8.3% for all soil categories when the SSI is taken into account, which shows that the different soil categories have almost the same effect on P.P. displacement reduction. In case of P.P. Base shear Force, one could observe variations in reduction when SSI is taken into account. For Rock category, the P.P. base shear force reduction percent decreases when the height of the structure raises from 40 to 60 stories. This starts from 8.4% for 40 St. to 7.1% for 60 St. structures. The situation is just the opposite for Dense soil category, in which one can observe an amplification from 5.9% for 40 St. to 7.5% for 60 St. structures. For Loose soil category, the situation is again similar to Rock, in which it could be observed a base shear force reduction of 6.3% for 40 St. to 5.4% for 60 St. In general it could be concluded that the P.P. displacement reduction percent mean value is about 8.3% regardless of the soil category. On the other hand, unlike the P.P. displacement reduction percent, the base shear force reduction percent is obeying a variation, which is an amplification based on height for Dense soil, and is a reduction based on height for Rock and Loose soil categories.

REFERENCES

ASCE7-10, “Minimum Design Loads for buildings and other Structures”, Published by American Society of Civil Engineers, 1801 Alexander Bell Drive, Reston, Virginia

Bungale S. Taranath, 2005, “Wind and Earthquake Resistant Buildings”, John A. Martin & Associates, Inc. Los Angeles, California

Chopra A.K.,2012, Dynamics of Structures: “Theory and applications to Earthquake Engineering” (4th ed.), Prentice Hall, Englewood Cliffs

Naeim. F, (2001), “Seismic Design Handbook”, Springer Science + Business Media, New York, pp. 754-792

Nassar, A.A., and Krawinkler. H., 1991, “Seismic Demands for SDOF & MDOF Systems”, John A. Blume Earthquake Eng. Center, Report No. 95. Department of Civil Engineering, Stanford University

FEMA 440 (2005). Improvement of Nonlinear Static Seismic Analysis Procedures, (ATC-55 Project) FEMA 440. Federal Emergency Management Agency, Washington, D.C.

PAPER REF: 035

A NOVEL METHODOLOGY TOWARD INDIVIDUALIZING 3D-RUNNING SHOES

Bahador Keshvari[1(*)], Marc Solé Lamich[2] and Veit Senner[3]

[1] Professorship of Sport Equipment and Sport Material, Mechanical faculty, Technical University of Munich
[(*)] *Email:* bahador.keshvari@tum.de

ABSTRACT

This work establishes a new method for individualizing running shoes. The main idea of this work is to create 3D printed midsole which has similar cushioning characteristics in objective and subjective measurements. The first impact of the traditional running shoes were measured by an impactor device. The impact force of different lattice structures which has close rate to the traditional running shoes are simulated. Then the lattice structure which provides the lowest impact force similar to the traditional running shoe was printed and employed in the midsole. A subjective measurement using questionnaire compared traditional running shoe with 3D printed running shoe to find the perceived cushioning and stiffness factors. The finding shows that the subjective results confirm the objective measurements.

Keywords: 3D printer, running shoes, lattice structure, cushioning, perception

INTRODUCTION

Endurance running (ER) originated about 2 million years ago with the purpose of surviving, but todays it is well known as a sport. 'ER can be most injurious at the moment the foot strikes the ground. Runners repeatedly cope with the impact transient of the vertical ground reaction force, an abrupt collision force of approximately 1.5–3 times body weight, within the first 50ms of stance phase'(Bramble, 2004). To decrease the collision force, a 3D printer technology employing lattice structure's modification may provide individualized midsole shape and cushioning properties. It makes designing more effective by allowing engineers to focus on cell topologies rather than overall midsole. The aim of this study is to establish a methodology to achieve a personalize running shoe by fulfilling individual comfort requirement. The methodology is as follows: *Step 1.* To produce lattice structures which have cushioning properties comparable with running shoes on the market, the cushioning feature of eight traditional running shoes were evaluated using an impact device. This device provides time-acceleration profiles by dropping 4.3 kg sphere on the sample in a defined number of times. *Step 2***.** To reduce the number of printed samples, the impact test conditions were modeled and simulated with finite elements (Figure 1.a). To verify the reliability of the simulation model, six midsoles were designed (using Rhinoceros 3D-Crystallon) and printed with 3D printer namely Selective laser sintering (SLS). *Step 3.* from 15 beam-based and four shell-based structures offered by Rhinoceros 3D-Crystallon, eight different samples were selected as follows: Body Centred (BC), Body Centred Cubic (BCC), Edge Octahedron (EO), Star Tetrahedron (ST), Face Centred Cubic (FCC), Dodecahedron (DO), Truncated Octahedron (TO) and Vertex Octahedron (VO). The first impact of each midsole (Figure 1.a) was simulated and compared with the first impact of eight traditional running shoes (refer to step1).*Step 4.* The closest first impact to traditional running shoes among the eight simulated midsoles were chosen for midsole printing. *Step 5***.** After printing the prototype, the 3D printed running shoes were compared with traditional running shoes by seven participants. Each participant compared two shoes (traditional running shoe and 3D running shoe) with a questionnaire which included the discomfort perception. In addition, for each participant, the sensitivity of foot plantar in six regions was measured using the Monofilament Test (0.4 grams, size 3.61)

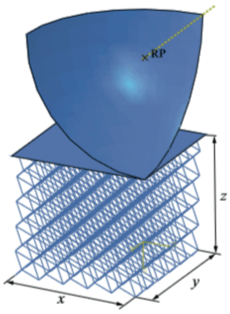

a

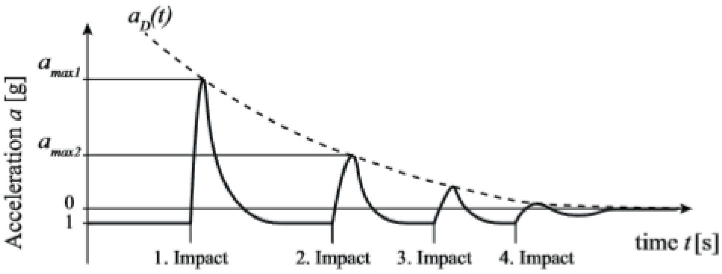

b

Figure 1.a impact test simulation 1.b the schematic of the result from impactor device

RESULTS AND CONCLUSIONS

Among 8 structures in Figure 2, the edge octahedron (EO) had the lowest first impact and was closest to the traditional running shoes (Figure 2). The average acceleration of first impact of all of the traditional running shoes and the EO running shoe were 15G and 30 G respectively. The data of only participants (4 females) who sensed all 6 regions in the Monofilament test were measured. The perception of cushioning and the stiffness of the EO shoe were estimated to be two times greater than the traditional shoe which support the result gained in the impact test of cushioning.

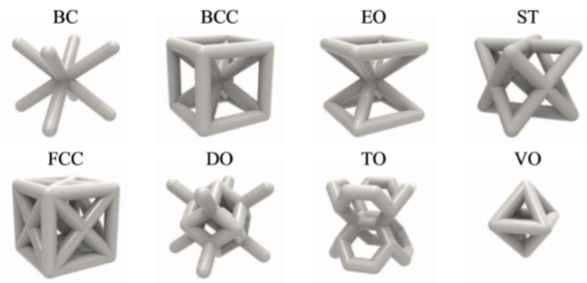

a

b

Figure 2.a eight lattice structure 2.b the printed running shoe

This finding shows that future work should make more of an effort to individualize a shoe using individual perceived discomfort to determine their optimal lattice structure. The author believes that the mass production of footwear may decline due to the higher potential comfort level which 3D shoes can provide.

REFERENCE

Bramble, D. M., & Lieberman, D. E. Endurance running and the evolution of Homo.2004. Nature.

PAPER REF: 036

FORMATION AND ELECTROCHEMICAL CHARACTERIZATION OF SELF-ORGANIZED TITANIUM NANOTUBES FOR BIOMEDICAL APPLICATIONS

Annalisa Acquesta(*), Anna Carangelo, Tullio Monetta

Department of Chemical Engineering, Materials and Industrial Production (DICMAPI), University of Napoli Federico II, Napoli, Italy

(*)*Email:* annalisa.acquesta@unina.it

ABSTRACT

In this paper, the formation of nanotubes on titanium CP2 dental implants and the influence of the nanotubes geometrical features on the electrochemical behaviour in Hank's solution are presented. Different kind of electrolytes, from acid to organic-based solutions both containing fluoride compounds, have been used to grow the nanotubes on titanium CP2 implants. The acid solutions limited the growth of the nanotubes due to the high dissolution rate of the titanium oxide (TiO_2), while the organic electrolyte allowed to obtain nanotubes more higher, with smoother side walls and smaller diameters. The electrochemical characterization has revealed a more active behaviour for nanotubes-covered samples compared to samples not covered by nanotubes, due to the higher extent area developed by nanostructures.

Keywords: metallic biomaterials, titanium nanotubes, electrochemical characterization, dental implants.

INTRODUCTION

The biocompatibility and the high corrosion resistance of the titanium and its alloys make them the ideal devices for biomedical applications [1]. In order to improve the interactions between the implants and the host tissues different surface treatments have been studied to modify the morphology and chemical composition of devices. The anodic oxidation treatment allows to obtain nanostructures able to stimulate osseointegration processes or antibacterial activity, as depicted by various papers. On the other hand, the nanostructures with their large surface area could affect the corrosion resistance of titanium. In this paper, the morphological and electrochemical analysis, carried out by scanning electron microscopy (SEM) and potentiodynamic polarization and electrochemical impedance spectroscopy (EIS), respectively, of nanotubes formed on dental implant made of commercially pure titanium alloy (CP2), by using a solution with hydrofluoridric acid and an organic solution with ammonium fluoride, is presented.

RESULTS AND CONCLUSIONS

The results from the morphological analysis are shown in Fig. 1. The nanotubes grown in acid solution presented more larger diameter (in the range of 130–170 nm) than the nanotubes produced in organic-based solution (about 70 nm), which presented also smoother side walls and major length, as reported elsewhere [2].

a) b)
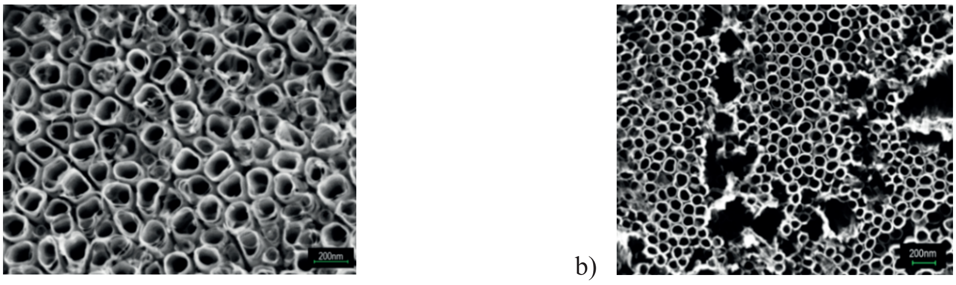

Fig. 1 – SEM top-view pictures of nanotubes formed a) in acid solution and b) in organic-based solution.

The potentiodynamic polarization curves of the nanotubes samples are depicted in Fig. 2a and compared with the untreated sample, TiCP2. The nanotubes samples show both a higher corrosion potential, due to the presence of the anodic oxide and its thickness, but the "organic nanotubes" sample exhibit also the highest passive current density for the greater area exposed, due to their longer nanostructures and their higher density.

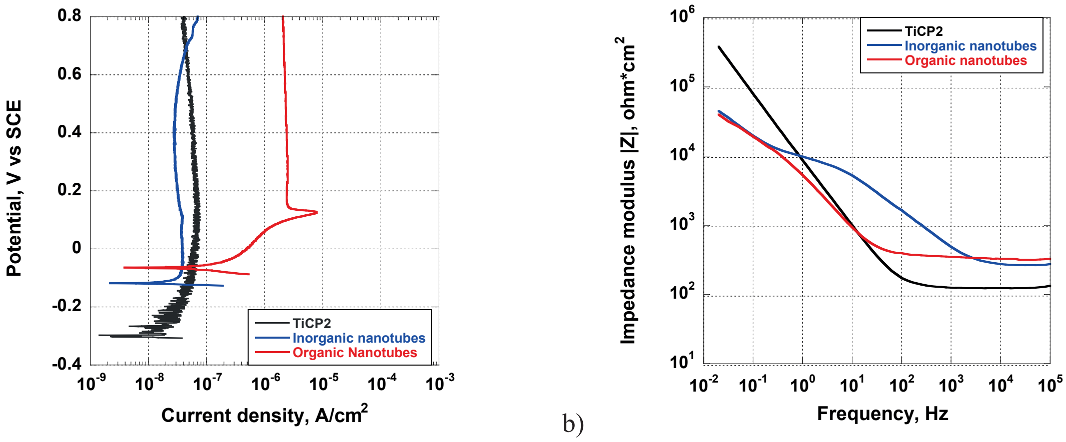

Fig. 2 – Electrochemical analysis of samples carried out in Hank's solution: a) potentiodynamic polarization and b) impedance modulus curves, respectively.

The impedance modulus curve for the nanotubes samples, recorded at the beginning of immersion in Hank's solution and reported in Fig. 2b, show the presence of two-time constants, due to the structure of double-layer titanium anodic oxide, made of a porous outer layer and a dense inner layer. The effect is more significant for the inorganic one, due to its morphology. The lower density and the minor length of the inorganic nanotubes sample than of the organic nanotubes sample, allow the Hank's solution to easy penetrate in the bottom of the nanotubes and in the gap between them, where precipitation/dissolution processes of chemicals, containing Ca, P, Mg, can occur. While, the organic nanotubes with their topography, narrower and longer, allow a much slower replacement of the electrolytic solution. In conclusion, the nanotubes geometrical features can be optimized to improve the corrosion resistance of dental implants.

REFERENCES

[1] M. Long, H.J. Rack, Titanium alloys in total joint replacement--a materials science perspective, Biomaterials 19(18) (1998) 1621-39.

[2] A. Acquesta, A. Carangelo, T. Monetta, TiO2 Nanotubes on ti dental implant. Part 3: Electrochemical behavior in hank's solution of titania nanotubes formed in ethylene glycol, Metals 8(7) (2018).

PAPER REF: 037

DUCTILE MATERIAL STRESS-STRAIN CURVE DETERMINATION BY USING TAYLOR TEST

Anatoly Bragov(*), Aleksandr Konstantinov, Svetlana Litvinchuk, Andrey Lomunov, Artem Basalin
Research Institute for Mechanics, National Research Lobachevsky State University of Nizhni Novgorod, Russia
(*)*Email:* bragov@mech.unn.ru

ABSTRACT

This work describes the stress-strain curve determination procedure by using Taylor test. The stress-strain relation is determined by minimizing the difference between experimental and modelled specimen shapes after impact. The deformation diagrams for cupper C101 (as received and annealed) obtained using described procedure and using well-known SHPB method are compared.

Keywords: deformation diagram, strain rate, Taylor, modelling, impact, high velocity.

INTRODUCTION

To determine the characteristics of materials at high strain rates, Taylor and Winnie [Taylor, 1934] developed a method that allows estimating the flow stress based on the analysis of residual strains in a cylindrical specimen after hitting a rigid barrier. Widespread approach in which the characteristics of the strain hardening of the material is determined by the results of the Taylor experiment using numerical simulation. A set of model parameters describing the behavior of the yield surface radius is found using an iterative procedure, minimizing the deviation of the experimental profile of the sample from the profile obtained in numerical simulation. A similar procedure is implemented in this paper.

To find the optimal set of parameters corresponding to the minimum of the objective function, the Nelder – Mead method is used [Nelder, 1965]. This is a simple and at the same time effective method for optimizing functions without using gradients.

RESULTS AND CONCLUSIONS

The implemented procedure is demonstrated by determining deformation diagrams of the high-purity copper (C101). Tested sample in the state of delivery (bar with a diameter of 10 mm) and after annealing. Comparisons of the residual profiles of the samples after the impact at different speeds are shown in Figure 1. The left side of the Figure 1 corresponds to samples in the state of delivery, right side - samples of annealed copper.

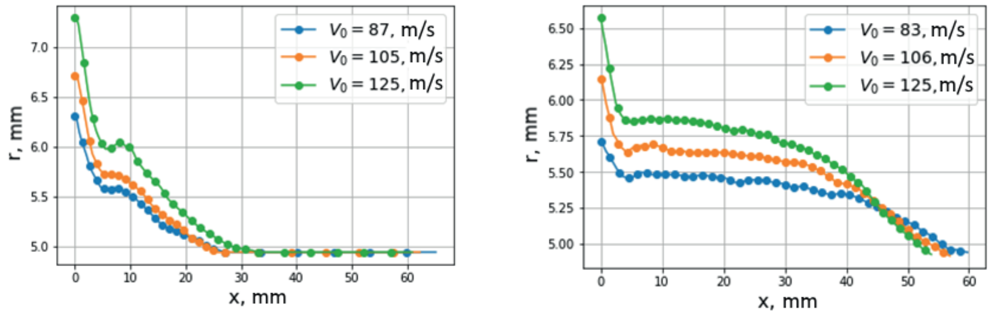

Fig. 1 - Profiles of C101 Taylor samples. Left side – state of delivery, right – annealed

Figure 2 shows a comparison of the experimental profiles (markers) with the profiles obtained in the numerical simulation (solid lines) at the last iteration of the optimization procedure for copper samples in the delivery state (left) and after annealing (right). The corresponding formulas connecting deformations and stresses among themselves are also given in the figures. The curves obtained by solving the inverse problem (color lines) were compared with the diagrams determined using the Kolsky method (black lines) [Kolsky, 1949] (Fig. 3). A pretty good match is obtained.

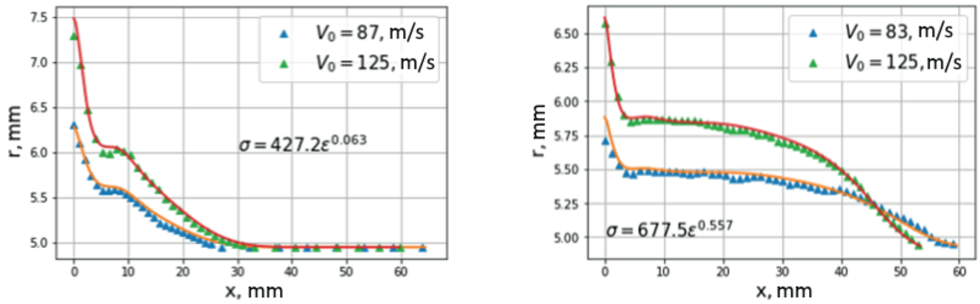

Fig. 2 - Comparison of experimental (markers) and calculated profiles of samples (solid lines)/ Left side – state of delivery, right – annealed

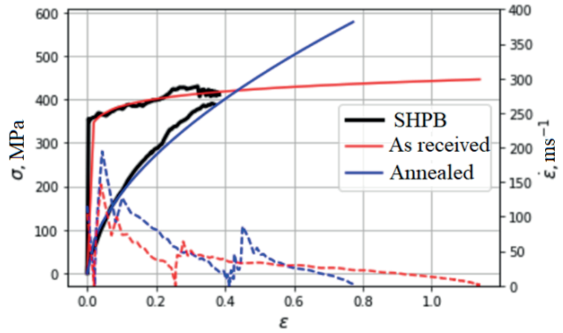

Fig. 3 – Comparison of curves obtained using Taylor and SHPB methods

The implemented procedure allows the construction of material deformation curves, at strain rates of more than 10^4 s^{-1}, and in combination with other experimental methods, it is possible to investigate the deformation characteristics of materials in a wide range of the strain rates.

ACKNOWLEDGMENTS

The work is financially supported by the Federal Targeted Program for Research and Development in Priority Areas of Development of the Russian Scientific and Technological Complex for 2014-2020 under the contract No. 14.578.21.0246 (unique identifier RFMEFI57817X0246).

REFERENCES

Taylor G.I., Quinney A. The latent energy remaining in a metal after cold working. Proc. Roy. Soc., 1934, 143, p. 307-326.

Nelder J.A., Mead R. A Simplex Method for Function Minimization. The Computer Journal, 1965, 7, p. 308-313.

Kolsky H. An investigation of the mechanical properties of materials at very high rates of loading. Proc. Phys. Soc. London, Sect. B 62, 1949, p. 676–700.

PAPER REF: 038

FRACTURE OF TITANIUM ALLOYS AT HIGH STRAIN RATES AND STRESS TRIAXIALITY

Vladimir V. Skripnyak[1(*)], Vladimir A. Skripnyak[1], and Evgeniya G. Skripnyak[1]

[1]National Research Tomsk State University, Tomsk, Russia

[(*)]*Email:* skrp2012@yandex.ru

ABSTRACT

This work compares mechanical behaviour of alpha, alpha+beta and beta titanium alloys in a range of strain rates from 0.001 to 1000 1/s and stress triaxiality (0.3–0.6) at room temperature. Specimens of titanium alloys were studied under tension using an Instron VHS 40 / 50-20 servo hydraulic test machine. Analysis of stress state and strain distribution in smooth and notched samples under tension was carried out by computer simulation. The damage accumulation model, complemented with phenomenological laws for voids nucleation, growth and coalescence, was adopted for describing the fracture process of single and multiphase titanium alloys. It was shown that stress triaxiality is important for prediction of damage evolution and fracture of titanium alloys at high strain rates. It was obtained that strain localization phenomena play a major role in the fracture process at lower triaxiality factor. It is found that the strain to fracture of titanium alloy is strongly depended on the stress triaxiality and strain rate above 100 s^{-1}. The strain to failure of alpha titanium alloys at room temperature decrease by 3.7 times with increasing stress triaxiality from 0.3 to 0.6 in wide range of strain rates.

Keywords: computer simulation, mechanical behaviour, ductility, titanium alloys, high strain rate, stress triaxiality

INTRODUCTION

Frost (Frost, 1983) showed that the generality of the laws of deformation and resolution of materials is realized in isomechanical groups with the same crystal lattice. Alpha-titanium alloys belong to the isomechanical group of alloys with hexagonal close-packed (HCP) crystal lattice, and beta-titanium alloys belong to another group of alloys with body-centered cubic (BCC) lattice. Materials belonging to the same mechanical group possess the similarity in mechanical behavior in wide ranges of strain rates and temperature owing to the similarity in mechanisms of plastic deformation and fracture. Generalization of data on the laws of deformation and fracture of alpha titanium alloys in a wide range of strain rates will allow developing a method for prediction of titanium structural elements under dynamic loadings (Skripnyak VA, and Skripnyak EG, 2017). It was shown that the ductility and strength of titanium alloys in a wide range of strain rates depends on the grain size and a grain size distribution (Sharkeev, 2018, Skripnyak, 2017, Skripnyak, 2014). Studies of the effect of the triaxiality parameter of the stress state on the mechanical behavior of titanium alloys over a wide range of strain rates are necessary for the development of adequate constitutive equations and fracture models of alloys with HCP and BCC phases. In this study, we study the effect of different values of stress triaxiality factor ($0.33 < \eta < 0.6$) on ductile failure over a wide range of strain rates using experimental tests and numerical simulation.

RESULTS AND CONCLUSIONS

In this paper, mechanical behavior of titanium alloy Grade 6 (this is an analog of VT5-1 or Ti-5Al-22,5Sn), Grade 2 (VT1-0), Grade 4 (Ti-6Al-4V), and Ti-45Nb was studied under tension in a wide range of strain rates and stress triaxiality (0.0–0.6) at room temperature. Smooth and notched specimens were tested at tension velocity from 0.04 m / s to 20 m/s using an Instron VHS 40/50-20 servo-hydraulic test machine. Analysis of the experimental results is supported by numerical simulations. Detailed information, complementary to the test results, is obtained on the stress and strain distribution close to the fracture. A ductile fracture at high strain rates occurs in smooth and notched samples. A coupled elastic-plastic-damage model based on continuum damage theory used to simulate the mechanical behavior of alpha titanium alloys with HCP crystal structure. The Gurson-Tvergaard-Needleman damage model is adopted for alpha titanium alloys, complemented with phenomenological laws for void nucleation, growth and coalescence. The model can accurately predict both deformation and damage behaviors of alpha titanium alloys at strain rates from 0.001 to 1000 s^{-1} and stress triaxiality from 0.3 to 0.6. The obtained experimental data indicate that there is a very strong correlation between the characteristics of the plastic deformation and the rate of damage growth. The constitutive and failure model parameters can be determined on the base of tensile test results. The constitutive and fracture models have been validated by simulating the tension tests.

ACKNOWLEDGMENTS

This work was supported by the Russian Science Foundation (RSF), grant № 16-19-10264. The authors are grateful for the support of this research.

REFERENCES

Frost HJ, Ashby MF. Deformation Mechanism Maps. Oxford, Pergamon Press, 1983, 166 p.

Sharkeev YP, Vavilov VP, Belyavskaya OA, Skripnyak VA, Nesteruk DA, Kozulin AA, and Kim VM Analyzing deformation and damage of VT1-0 titanium in different structural states by using infrared thermography. Journal of Nondestructive Evaluation, 2016, 35(3), art. no.42.

Skripnyak NV, Skripnyak EG, Skripnyak VA, Skripnyak VV, Vaganova I.K. Failure mechanisms of light alloys with a bimodal grain size distribution 11th World Congress on Computational Mechanics, WCCM 2014, 5th European Conference on Computational Mechanics, ECCM 2014 and 6th European Conference on Computational Fluid Dynamics, ECFD, 2014, p. 3915-392.

Skripnyak VA, and Skripnyak EG. Mechanical behaviour of nanostructured and ultrafine-grained metal alloy under intensive dynamic loading, In: Nanomechanics, Eds.by A. Vakhrushev, 2017, Intech open. 68291.

Skripnyak VA, Skripnyak NV, Skripnyak EG, Skripnyak VV. Influence of grain size distribution on the mechanical behavior of light alloys in wide range of strain rates, AIP Conference Proceedings, 2017, 1793, art. no. 110001.

Verleysen P. and Peirs J. Quasi-static and high strain rate fracture behaviour of Ti6Al4V, International Journal of Impact Engineering, 2017, 108, p.370-388.

PAPER REF: 039

THE MECHANICAL BEHAVIOR OF A MAGNESIUM ALLOY AT HIGH STRAIN RATES IN THE TEMPERATURE RANGE FROM 295 K TO 673 K

Vladimir V. Skripnyak[1(*)], Vladimir A. Skripnyak[1], Evgeniya G. Skripnyak[1]

[1]National Research Tomsk State University, Tomsk, Russia
[(*)]*Email:* skrp2012@yandex.ru

ABSTRACT

The paper presents the results of experimental and numerical simulation studies of the mechanical behavior of the Mg−3Al−1Zn alloy at high strain rates at room and temperatures up to 673 K. The flat samples with a smooth working part and with the notch radius of 10 mm, 5 mm and 2.5 mm were used. Experimental studies were carried out on the high-velocity servo hydraulic test machine Instron VHS 40/50-20. Heating the samples with flat ceramic infrared emitters to the set temperatures took on average from 60 seconds to 160 seconds. Temperature control in the working part of the samples was carried out in real time using a K-type thermocouple (chromel–alumel). It was found that the value of tensile strain to fracture of magnesium alloy is decreased twice when stress triaxiality factor increased from 0.33 to 0.5. This effect is realized in a wide range of strain rates and homologous temperatures T/T_m from 0.32 to 0.73 (T_m=923 K is the melting point of magnesium alloy Mg−3%Al−1%Zn).

Keywords: high-strain rates, damage, fracture under tension, stress triaxiality factor, elevated temperatures, and magnesium alloys.

INTRODUCTION

Magnesium alloys belong to the isomechanical group of alloys with a hexagonal close-packed lattice, possess enhanced specific strength characteristics and are used to create metallic lightweight and reliable structures in aerospace, automotive, biomedicine, and many others engineering fields. The mechanism of the ductile fracture of magnesium alloys significantly depends on a grain sizes distribution, concentration and sizes hardening intermetallic phases. The development of theoretical base for the prediction of ductile fracture of magnesium alloys taking into account structural factors in wide loading conditions remains an urgent problem. In the last decade, the physical mechanisms of plastic deformation of a number of magnesium alloys in a wide range of temperatures and strain rates have been studied (Pan,2016, Skripnyak,2018). It is found that the difference in the response of magnesium alloys to tensile and compressive loads is due to the peculiarities of the development of plastic deformations as a result of twinning and dislocation slip. One of the most important areas of research is the development of linked models of plasticity and damage. In these models, the values of inelastic deformations and the distribution of micro pores in the material are taken into account when predicting changes in the damage parameter (Ulacia,2011, Skripnyak,2018). Results of fracture tests of alloy samples with different geometry and notch radius were used for the calibration of these models. This article presents the results of experimental and theoretical studies of the mechanical behavior of magnesium alloy MA2-1 under tension in a wide range of strain rates at room and elevated temperatures, which were used to determine the parameters of elastic-plastic deformation and damage models.

RESULTS AND CONCLUSIONS

Smooth and notched specimens of polycrystalline MA2−1 magnesium alloy were tested at tension velocity from 0.04 m/s to 20 m/s using an Instron VHS 40/50-20 servo-hydraulic test machine. Grain size distribution of alloy was obtained by EBSD method using scanning electron microscope TESCAN. The average grain size of the alloy was ~40 microns. Strain to fracture of the magnesium alloy Mg−3%Al−1%Zn under tension at strain rates of 0.001 s^{-1} and 100 s^{-1} and temperatures of 295K, 473 K, and 673 K versus the stress triaxiality factor is shown in Fig.1.

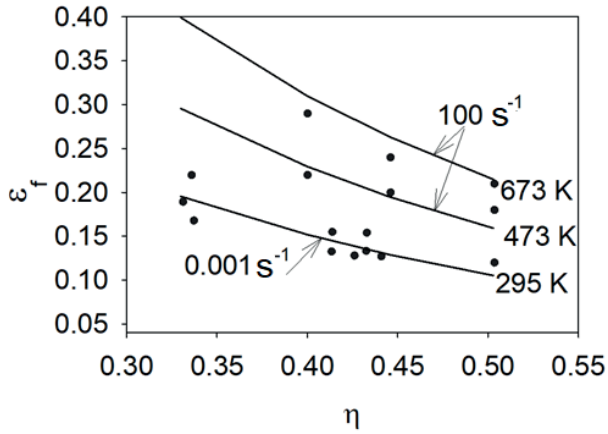

Fig. 1 − Strain to fracture under tension versus the stress triaxiality factor

The obtained data showed that the increasing the stress triaxiality factor from 0.33 to 0.5 leads to decreasing the strain to fracture of MA2-1 alloy twice under tension in the temperature range from 295 K to 673 K. The complex of the obtained experimental data made it possible to determine the parameters of the Zerilli-Armstrong and Gurson-Tvergaard-Needleman models to describe the mechanical behavior of the magnesium alloy MA2-1 at high-speed tension at room and elevated temperatures.

ACKNOWLEDGMENTS

This work was supported by the Russian Science Foundation (RSF), grant № 18-71-00117. The authors are grateful for the support of this research..

REFERENCES

Pan H, Wang F, Jin L, Feng M, Dong J. Mechanical Behavior and Microstructure Evolution of a Magnesium Alloy AZ31B under Low Stress Triaxiality. Journal of Materials Science and Technology, 2016, 32, p. 1282–1288.

Skripnyak VA, Skripnyak VV, Skripnyak EG. Ductility of titanium alloys in a wide range of strain rates In: Proc. IRF2018: 6th International Conference on Integrity-Reliability-Failure Lisbon/Portugal, 22-26 July 2018. FEUP-INEGI: Porto, Portugal, 2018, p.813-822.

Ulacia I, Salisbury CP, Hurtado I, Worswick MJ. Tensile characterization and constitutive modeling of AZ31B magnesium alloy sheet over wide range of strain rates and temperatures. Journal of Materials Processing Technology, 2011, 211 (5), p. 830-839.

PAPER REF: 040

APPLICATION OF MECHANICAL SPECTROSCOPY TO THE STUDY OF BIOLOGICAL TISSUES. THE CASE OF HUMAN DENTIN

Roberto Montanari[1(*)], Maria Richetta[1]

[1] Department of Industrial Engineering, University of Rome "Tor Vergata", Rome, Italy
[(*)]*Email:* roberto.montanari@uniroma2.it

ABSTRACT

Mechanical Spectroscopy (MS), i.e. damping and dynamic modulus measurements, provides information on microstructural features of materials not obtained by other techniques. MS is commonly used for investigating physical phenomena and solving practical problems related to industrial processes. This work shows that the technique can be fruitfully used to investigate also biological tissues and reports the case of human dentin.

Dentin is a complex hydrated biological composite consisting of about 50 vol% mineral in the form of apatite, 30 vol% of collagen, and about 20 vol% fluid. Other non-collagenous proteins and other organic components are also present in small amounts.

On a macro scale dentin can be modelled as a continuous fibre-reinforced composite, with the intertubular dentin forming the matrix and the tubule lumens forming the fibre reinforcement. On a meso scale intertubular dentin is formed by fibres randomly oriented in a plane perpendicular to the direction of dentin formation. On a nanoscale the characteristic features are collagene fibrils, apatite crystals and water. Each fibre consists of several fibrils (50-100 nm in diameter) which exhibit periodically spaced gaps. Three polypeptide chains are wound together in a triple helix. The mineral is either within the fibrils or between the fibrils. Water is the third major component and is located within and between the fibrils, between fibres and between triple-helical molecules.

A lot of work has been devoted to investigate the mechanical properties of dentin, however few papers deal with its anelastic behaviour. Here we present the results of MS tests carried out from room temperature to 673 K.

Human molars were longitudinally sectioned in order to obtain 0.8 mm-thick slices. From these sections bar-shaped samples (length L = 13÷16 mm) have been cut for the tests. The samples, mounted in free-clamped mode, have been tested with the method of frequency modulation.

Dynamic modulus E is proportional to the resonance frequency f:

$$f = \frac{m^2 h}{2\pi\sqrt{12}L^2}\sqrt{\frac{E}{\rho}} \tag{1}$$

where m is a constant (m=1.875), ρ the material density, L and h are the length and thickness of the sample, respectively. The damping parameter (Q^{-1}) has been determined from the logarithmic decay of flexural vibrations. MS runs has been made on 15 samples by performing heating-cooling cycles from 300 to 673 K with constant heating rate of 3.33 x 10^{-2} K s^{-1}.

Figure 1 (a) shows the Q^{-1} and E curves measured along a heating-cooling cycle. From 300 to 373 K modulus exhibits an increasing trend while Q^{-1} behaves in the opposite way. It is known that heating up to 373 K affects only residual water present in the pores of dentin without altering the molecular structure of collagen. Since hydrated dentin has a lower modulus and a higher Q^{-1} than dried dentin the initial water loss leads to an increase of E and a decrease of Q^{-1}. If the samples are cooled down from 373 K and rewetted, the original characteristics are completely restored thus the process is reversible.

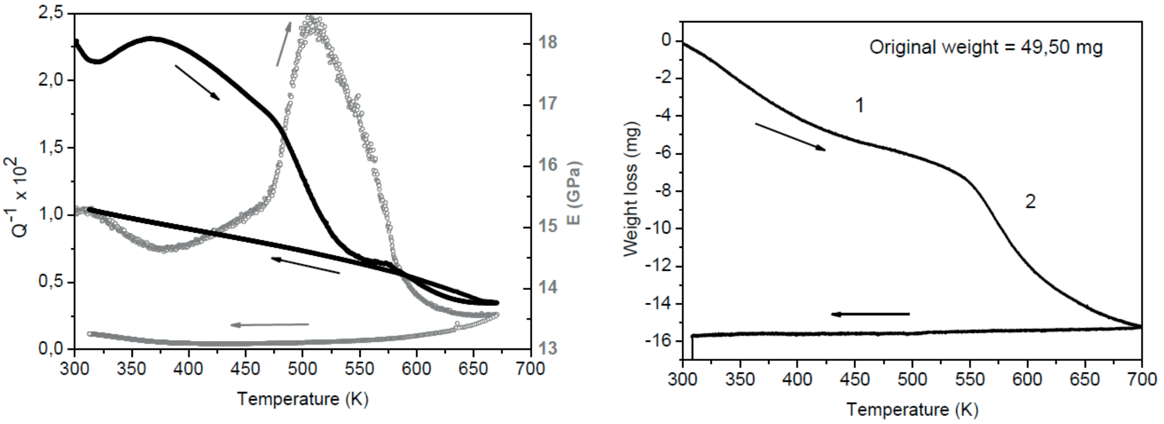

a) b)

Figure 1. a) Q^{-1} and dynamic modulus of dentin measured during heating up to 673 K and subsequent cooling. b) Thermo-gravimetric curve of dentin during a heating-cooling cycle.

Above 373 K Q^{-1} progressively increases and a maximum at 523 K is observed. Modulus decreases and exhibits two slope changes around 473 and 573 K. These phenomena are not present during cooling to room temperature and successive cycles. After a heating-cooling cycle up to 673 K both Q^{-1} and E decrease with respect the original values.

TGA shows a remarkable weight loss in the same temperature range of Q^{-1} maximum (Figure 1 b). Two stages can be identified, which basically correspond to the ascending (stage 1) and descending (stage 2) parts of the Q^{-1} maximum. The two TGA stages have been related to water loss (1) and protein degradation (2), respectively.

The collagen denaturation begins when temperature exceeds 393 K and occurs within the triple helix by cleaving intramolecular hydrogen bonding. From 473 to 673 K the main change is due to structural water that has a strong chemical interaction with the proteins. The backbone of the proteins starts to break into fragments after 523 K, degradation and combustion of collagen occur from 573 to 673 K. The Q^{-1} maximum is connected to water loss and collagen degradation.

Damping behaviour can be explained by considering the specific structure of dentin which is made of several fibres consisting of bundles of fibrils. Fibres, fibrils and molecular chains forming the helix structure are like strings subjected to a complex system of constraints, i.e. bonds fiber-fiber, fibril-fibril and helix structure, which are progressively modified as temperature increases with a consequent effect on the anelastic properties of the organic phase.

Damping and modulus depend on the number of oscillating strings and on their mean length:

$$Q^{-1} \propto \rho l^4 \omega \tag{2}$$

$$\frac{\Delta G}{G} \cong -\beta\rho\, l^2 \tag{3}$$

where β is a constant, ρ the density of vibrating strings, l the average string length, $\omega/2\pi$ the frequency. The ascending part of maximum is ascribed to the loss of water in the gaps between fibres and between fibrils. Despiralization of tridimensional helix structure of collagen molecule occurs so molecules become free to oscillate and to contribute to the damping. Therefore, the increased number of oscillating strings leads to Q^{-1} increase and E decrease.

Above 523 K the water loss regards that inside the fibrils, i.e. water that guarantees the continuity of the peptide chain, so fibrils degrade and the chain is broken in fragments. The damping decreases owing to the shorter length of the vibrating strings. At 573 K combustion occurs further contributing to decreasing the damping and producing the second slope change of modulus.

PAPER REF: 041

MECHANICAL BEHAVIOR OF Zr-Nb ALLOYS AT A HIGH STRAIN RATES

Vladimir A. Skripnyak[1], Nataliya V. Skripnyak[1,2(*)], Vladimir V. Skripnyak[1], and Evgeniya G. Skripnyak[1]

[1]National Research Tomsk State University, Tomsk, Russia
[2]Linköping University, Linköping, Sweden
[(*)]*Email:* skrp2012@yandex.ru

ABSTRACT

The results of the development of a physical-mechanical model for predicting the mechanical and deformation properties of Zr−Nb in a wide range of strain rates are presented. The model was used to study the mechanical behavior of coarse-grained and ultrafine Zr-Nb alloys under quasi-static and dynamic loading conditions. It was shown that the creation of bimodal grain structures in Zr−Nb alloys causes an increase in the flow stress while maintaining the ductile fracture in a wide range of strain rates. It was shown the strain rate sensitivity of the yield stress of Zr–Nb alloys strongly depends on the concentration of Nb. The concentration of Nb in Zr−Nb alloys, temperature and pressure determine the phase state. Martensitic phase transitions α→ω and β→ω cause not only changes in the elastic properties and parameters of the Hugoniot adiabat of Zr−Nb alloys, but also their strain hardening and the spall strength. The results can be used in engineering analysis of designed technical systems for nuclear reactors.

Keywords: computer simulation, mechanical behavior, ductility, zirconium-niobium alloys, high strain rate

INTRODUCTION

Improvement in technology of fabrication of fuel claddings and some constructional elements of nuclear reactors is connected with computer simulation of mechanical properties and structural evolution of radiation-resistant alloys Zr–Nb. In this regard, there is an increasing need to develop computational models of the mechanical behavior of advanced Zr−Nb in loading conditions close to operating ones. The Zr–Nb has a unique complex of physical and mechanical properties and is considered as promising structural alloys for nuclear reactors of IV generation. Zirconium alloys with a concentration of Nb below 2.5 weight % and additionally doped with Mo, Fe, Cr for the stabilization of precipitations of beta-phase Zr were studied during last decade (Xiao, 2010). A new precipitation-strengthening theory was present by Fang and coworkers (Fang,2019). This theory describes a probability-dependent precipitation-strengthening mechanism, to more accurately predict the yield strength of alloys. Precipitation strengthening of Zr-Nb alloys requires detailed investigation. It is known that the mechanical behavior of Zr-Nb alloys during the α→β phase transformation changes significantly (Hazell, 2014, Kazakov,2015, Skripnyak,2014, Skripnyak,2017). In this regard, the mechanical behavior of α, and α+β Zr–Nb alloys was studied in a wide strain rates.

RESULTS AND CONCLUSIONS

Mechanical behavior of Zr−1%Nb and Zr−2,5 % Nb alloys (Grades E110, E625, E125) was studied in the strain rate range from 10^{-3} to 10^{6} s^{-1} by the numerical simulation method. The model took into account the multiphase state of Zr−Nb alloys, different resistance of α, β and ω phases to plastic flow. Simulation of plastic flow, evolution of damages and destruction of alloys at uniaxial tension and compression of samples in quasi-static conditions, loading of samples by plane shock waves was carried out. It was shown the strain rate sensitivity of the flow stress of alpha Zr−1%Nb in the range from 10^{-3} to 10^{3} s^{-1} is less then at strain rates above 10^{3} s^{-1}. The creation of the three-wave configuration was predicted in Zr−1%Nb due to polymorphous α → ω transition at ~11 GPa. The Hugoniot elastic limit (σ_{HEL}) and spall strength of Zr−x%Nb alloys strongly depends on beta phase concentration. Calculations have shown that the increase in the dynamic yield strength $\sigma_{sd} = 1.5\sigma_{HEL}(1 - (c_b/c_l)^2$ can be caused by an increase in the volume concentration of the beta phase in Zr−x%Nb alloys (c_b, and c_l are the bulk and the longitudinal sound velocity, respectively). The increase in the β phase concentration at elevated temperatures causes an increasing of the dynamic yield strength of Zr−1%Nb alloys. It was shown that $ZrFe_3$ and βNb precipitations in Zr−2,5%Nb caused increasing of σ_{sd} and the spall strength.

ACKNOWLEDGMENTS

This work was supported by the Russian Science Foundation (RSF), grant № 18-71-00117. The authors are grateful for the support of this research.

REFERENCES

Fang Q, Li L, Li J, Wu H, Huang Z, Liu B, Liu Y, Liaw PK. A statistical theory of probability-dependent precipitation strengthening in metals and alloys. Journal of the Mechanics and Physics of Solids, 2019, 122, p. 177–189.

Hazell PJ, Appleby-Thomas GJ, Wielewski E., and Escobedo J. P. The shock and spall response of three industrially important hexagonal close-packed metals: magnesium, titanium and zirconium. Philosophical Transactions of The Royal Society A, 2014, 372: 20130204.

Kazakov DN, Kozelkov OE, Mayorova AS. Dynamic behavior of zirconium alloy E110 under sub microsecond shock-wave loading. EPJ Web of Conferences, 2015, 94, p.1–5.

Skripnyak N.V., Skripnyak E.G., Skripnyak V.A., Skripnyak V.V., Vaganova I.K. Failure mechanisms of light alloys with a bimodal grain size distribution 11th World Congress on Computational Mechanics, WCCM 2014, 5th European Conference on Computational Mechanics, ECCM 2014 and 6th European Conference on Computational Fluid Dynamics, ECFD, 2014, p. 3915-392.

Skripnyak VA and Skripnyak EG. Mechanical behaviour of nanostructured and ultrafine-grained metal alloy under intensive dynamic loading. In: Nanomechanics. Eds.by A. Vakhrushev, 2017. Intech open. 68291.

Skripnyak VA, Skripnyak NV, Skripnyak EG, Skripnyak VV. Influence of grain size distribution on the mechanical behavior of light alloys in wide range of strain rates, AIP Conference Proceedings, 2017, 1793, art. No. 110001.

Xiao D, Li Y, Hu S. High Strain Rate Deformation Behavior of Zirconium at Elevated Temperatures. Journal of Materials Science & Technology, 2010, 26, p. 878-882.

PAPER REF: 042

INFLUENCE OF GRAIN SIZE DISTRIBUTION ON THE MECHANICAL BEHAVIOUR OF Ti–Nb ALLOYS

Vladimir A. Skripnyak[1(*)], Vladimir V. Skripnyak[2], and Evgeniya G. Skripnyak[1]

[1]National Research Tomsk State University, Tomsk, Russia

[(*)]*Email:* skrp2006@yandex.ru

ABSTRACT

This article presents the results of modelling of the mechanical behaviour of coarse grained (CG) and ultrafine-grained (UFG) Ti–Nb alloys in the range of strain rates from 10^{-3} to 10^{3} s^{-1} at temperatures from 297 K to 1273 K. Modification of the micro-dynamical model was proposed for the description of Ti–Nb ultrafine grained and coarse grained α+β and β alloys. It was shown that the HCP → BCC phase transformation in Ti–Nb alloys leads to a sharp changing in resistance to plastic flow and kinetics of growth of damage. The results can be used for engineering analysis of designed constructive elements of technical and biomedical applications.

Keywords: mechanical behaviour, ultra-fine grained, titanium alloys.

INTRODUCTION

Last years a number of α+β and β Ti-Nb-Zr alloys were developed and studied. These alloys have remarkable properties such as low density, high melting point, good oxidation resistance and high specific strengths, low elastic moduli, biocompatibility, etc. (Sharkeev,2018, Bobbili,2017, Bobbili, 2016, Nikonov,2015). Understanding of the mechanical behavior of Ti-Nb-Zr alloys in wide temperature range is extremely essential for the numerical modeling of various applications and manufacturing technologies. It has been shown that beta titanium alloys have low modulus of elasticity (Nikonov,2015). The effect of bimodal grain size distribution on plastic flow stress and deformation to fracture of GPU alloys in a wide range of strain rates has been shown (Skripnyak,2017). Deformation mechanisms and mechanical behavior of UFG metastable titanium alloys β at high strain rates are of great interest. In this regard, the mechanical behavior of Zr-1%Nb alloy was studied by numerical simulation method in the practically important temperature range from 297 K to 1243 K. Mechanical behavior of Ti-13Nb-13Zr alloy was simulated in strain rate range from 0.01 to 10^{3} s^{-1} at room temperature.

RESULTS AND CONCLUSIONS

Fig. 1a shows the calculated stress versus strain curves of coarse grained Ti-13Nb-13 Zr alloy at the tensile strain rate of 10^{-2} s^{-1}. Results of simulation agree with experimental data within temperature range from 298 K to 873 K. In this temperature range, the Ti-13Nb-13Zr alloy remains two-phase. The strong increasing of the ultimate tensile strength of Ti-45Nb alloy was predicted. It was shown that the dependence of the normalized yield strength of Ti-13Nb-13Zr from normalized temperature can be approximated by a bilinear relation. The change in slope is due to phase transition α → β.

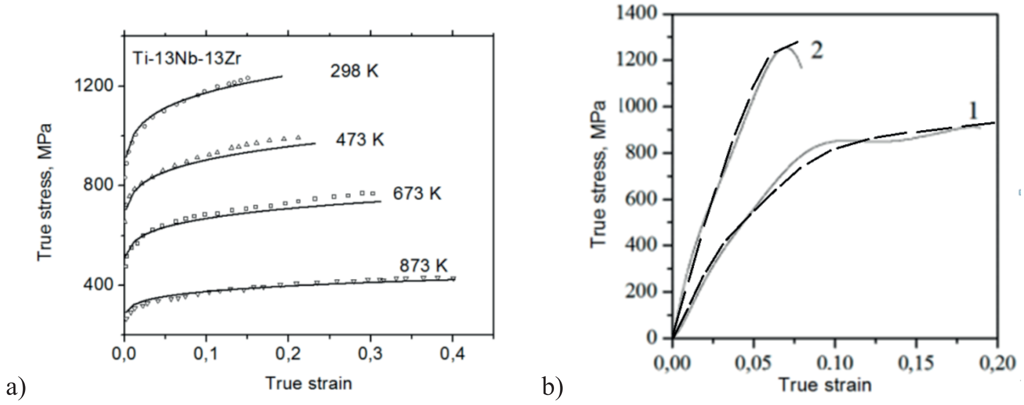

Fig. 1.a – Calculated stress versus strain of Ti-13Nb-13Zr alloy at the tensile strain rate of 10^{-2} s^{-1}. Symbols are experimental data (Bobbili, 2017); b. True stress–true strain diagrams for Ti–45Nb alloy in the CG (curves 1) and UFG (curves 2) states

The effects of strain hardening and thermal softening were considered in the computational model. Results of numerical simulation of quasi static loading of Ti-13Nb-13Zr alloys have a good correlation with experimental data. The calculated stress-strain curves were obtained for UFG alloys taking into account changes in coefficient of the Hall-Petch relation in comparison with the value for GC alloys.

ACKNOWLEDGMENTS

This work was supported by the Russian Science Foundation (RSF), grant № 18-71-00117. The authors are grateful for the support of this research.

REFERENCES

Bobbili R, and Madhu V. Constitutive modeling and fracture behaviour of a biomedical Ti–13Nb-13Zr alloy // Materials Science and Engineering A. 2017, 700, p. 82-91.

Bobbili R, and Madhun V. Flow and fracture characteristics of near alpha titanium alloy. Journal of Alloys and Compounds 2016, 684, p.162-170.

Nikonov AY, Zharmukhambetova AM, Skripnyak NV, Ponomareva AV, Abrikosov IA, Barannikova SA, and Dmitriev AI. Calculation of mechanical properties of BCC Ti-Nb alloys. AIP Conference Proceedings, 2015, 1683 (020165).

Sharkeev Y, Vavilov V, Skripnyak VA, Belyavskaya O, Legostaeva E, Kozulin A, Chulkov A, Sorokoletov A, Skripnyak VV, Eroshenko A, and Kuimov M. Analyzing the Deformation and Fracture of Bioinert Titanium, Zirconium and Niobium Alloys in Different Structural States by the Use of Infrared Thermography. Metals, 2018, 8, 703, 15p.

Skripnyak VA, Skripnyak NV, Skripnyak EG, Skripnyak VV. Influence of grain size distribution on the mechanical behavior of light alloys in wide range of strain rates, AIP Conference Proceedings, 2017, 1793, art. No. 110001

PAPER REF: 043

POSSIBILITIES OF USE OF NANOMATERIALS IN BUILDINGS MASONRY WALLS. SOME EXAMPLES

Hipólito Sousa[1(*)], Rui Sousa[1]

1 CONSTRUCT (Gequaltec), Faculty of Engineering (FEUP), University of Porto, Portugal

[(*)]*Email:* hipolito@fe.up.pt

ABSTRACT

Masonry is an ancient solution used in construction for thousands of years. Nowadays faces to important challenges to improve performance and compare properly with more modern and clean solutions used in building enclosures. In this work, after a short review of the evolution of masonry walls and applied performance requirements, some examples of improved industrial masonry systems are presented, some of them already with new materials like PCM's and aerogel. The improvement and optimizations process is presented, underlining the contributions of external and internal mortar including render, masonry units geometry and raw-material and, yet, the mortar laying. Thermal and mechanical simulations and tests are presented to illustrate this evolution.

Keywords: energy efficiency, masonry, new materials, nanomaterials.

INTRODUCTION

The pressure to reduce the energy consumption and thermal comfort in buildings is high, mainly in developed countries. This increasing demand changed the buildings enclosure/envelope walls solutions. Over the last 30 years, the most relevant indicator for the thermal performance of enclosure walls, U value, increased in Portugal more than 250% pushing the walls to achieve higher levels of thermal insulation.

This evolution is changing the way the walls are made and the materials industry is investigating and innovating in this domain. Besides the obvious application of conventional thermal insulations layers, solution that may cause environmental sustainability issues, other strategies to improve the thermal performance of walls can also be used, such as using constituents (units, joints and rendering) made with thermal improved raw-materials or/and optimizing the geometry of the constituents (joints and units). These actions usually involve a "trade-off" between thermal and mechanical performance. It is fundamental to improve thermal performance without compromise the mechanical robustness/strength of the wall. This improvement research is usually developed based on experimental tests and advanced numerical simulations using optimization routines (Fig.1).

Within the scope of research activities in cooperation with the construction industry, thermal enhanced products born for masonry walls were developed recently. The main focus was to develop efficient wall constituents (masonry units and renderings) with optimized thermal and mechanical behaviour to be used in enclosure/external walls.

RESULTS AND CONCLUSIONS

Under the scope of research activities, some new materials and constituent were developed with promising results:

- High thermal performance renderings using cement/lime mortars mixed with micro-encapsulated PCMs (Vaz Sá et al, 2012 and Vaz Sá et al, 2014) or mixed aerogel/perlite aggregates (Pedroso, 2018; Sousa 2019);
- Thermal enhanced masonry assembled with units made with thermal/mechanical optimized geometry and insulation/open structure lightweight concrete (Sousa, 2019);
- Multifunctional and thermal efficient wall system constructed with thermal enhanced masonry and high thermal performance renderings (Sousa, 2019; Sousa, 2018).

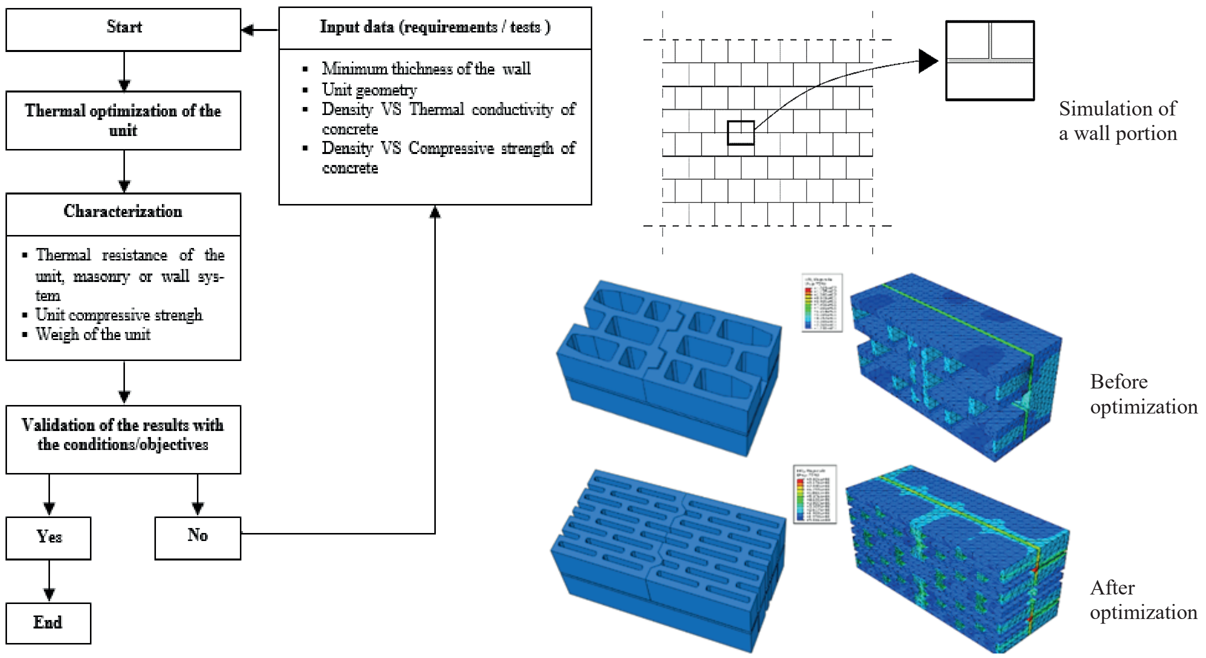

Fig.1 - Example of thermal/mechanical numerical simulations and optimization of masonry units (Sousa, 2018)

ACKNOWLEDGMENTS

This work was financially supported by Project POCI-01-0145-FEDER-007457 - CONSTRUCT - Institute of R&D In Structures and Construction, funded by FEDER funds through COMPETE2020 - Programa Operacional Competitividade e Internacionalização (POCI) – and by national funds through FCT - Fundação para a Ciência e a Tecnologia and Project POCI-01-0247-FEDER-017417 - PEP - Efficient Wall Plus Saint-Gobain Weber, funded by FEDER funds through COMPETE2020 - Programa Operacional Competitividade e Internacionalização (POCI).

REFERENCES

Vaz Sá A, Azenha M, Sousa H, Samagaio A. Thermal enhancement of plastering mortars with Phase Change Materials: Experimental and numerical approach. Energy and Buildings, 2012, 49, p.16-27.

Sousa H, Sousa R, Silva L, Colen I. Development of Energy Efficient Masonry System. 10th International Masonry Conference, Milan, Italy, 9-11 July 2018, p.1198-1218.

Sousa R, Sousa H, Silva L, Flores-Colen I, Pedroso M. Development of a Wall System Made with Thermally Optimized Masonry and Super Insulation Mortar Render. Masonry International Journal, 2019 (accepted for publication).

PAPER REF: 044

MICROSTRUCTURE AND TRIBOCORROSION CORRELATIONS ON A DIRECTIONALLY SOLIDIFIED Al-Sn-Cu ALLOY

Felipe Bertelli[1(*)], Maria Angeles Arenas[(2)], Ana Conde[(2)], Juan de Damborenea[(2)], Emmanuelle Sá Freitas[(3)], Noé Cheung[(4)], Amauri Garcia[(4)]

[1]Post-graduated Program in Mechanical Engineering, Santa Cecilia University (Unisanta), Santos, Brazil

[2]Department of Surface Engineering, Corrosion and Durability, National Center for Metallurgical Research (CENIM-CSIC), Madrid, Spain

[3]Institute of Marine Sciences, Federal University of São Paulo, UNIFESP, Santos, Brazil

[4]Department of Manufacturing and Materials Engineering, University of Campinas, UNICAMP, Campinas, Brazil

[(*)]*Email:* felipe.berteli@gmail.com

ABSTRACT

A careful study, permitting correlations between the microstructural parameters of alloys directionally solidified under transient heat flow conditions and tribocorrosion behaviour is fundamental in the pre-programming of final properties of as-cast components. This study aims to establish correlations between quantitative parameters of different microstructure scales of an Al-Sn-Cu ternary alloy (e.g. dendritic or interphase spacings) and tribocorrosion behaviour. It was found that the wear volume increases with decreasing interdendritic spacing and the product of corrosion may directly affect this behaviour.

Keywords: Tribocorrosion, Al-Sn-Cu ternary alloy, interdendritic spacing

INTRODUCTION

The wear by tribochemical reaction can be characterized by exposing the tribological system to a reactive environment, i.e. the surfaces in contact will react with the surrounding environment (Mischler, 2008). The process is developed by the continuous removal of material formed on one or both surfaces of the tribological pair generating a layer, and the formation of more material in that layer, which is the result of the corrosive action of the medium on the surfaces in contact. Removal of metallic material resulting from the peeling off of the surface roughness of the lower hardness element of the pair, and the rupture of the surface layer formed by the reaction of the environment on the surfaces in contact, generate wear debris, which are formed by metallic and non-metallic particles, thus increasing the abrasive action of the wear (Salinas, 1999; Frutos, 2010).

Tribocorrosion tests were performed on a pin-on-disk device containing a ceramic ball on the tip of the pin for contact with the samples, coupled to an Autolab PGSTAT 128N potentiostat/galvanostat. A load of 0.5N and a speed of 60 revolutions per minute were adopted. At the same time, a system with three electrodes was used, that is, an Ag/AgCl reference electrode, one counter electrode with a platinum wire, and samples of the Al-Sn-Cu ternary alloy as the working electrode. Four samples with different interdendritic spacings were obtained from different positions (P) along the length of a transient unidirectionally solidified casting: P = 5, 10, 30 and 50mm, considering P = 0 as the cooled surface of the casting. The delimited test area was 0.2 cm^2 and the electrolyte had a concentration of 0.06M NaCl at 25 ° C.

RESULTS AND CONCLUSIONS

Fig 1 shows the evolution of the Wear volume as a function of Position from the cooled bottom of an Al-10Sn-10Cu alloy casting directionally solidified under transient heat flow conditions and electrochemical noise curves with Potential Density as a function of Time. Four samples, characterized by different values of interdendritic spacings (λ_1), were chosen and subjected to wear tests under corrosion conditions, as described in the introduction section, with a view to evaluating the role of microstructural effects on the tribocorrosion behaviour.

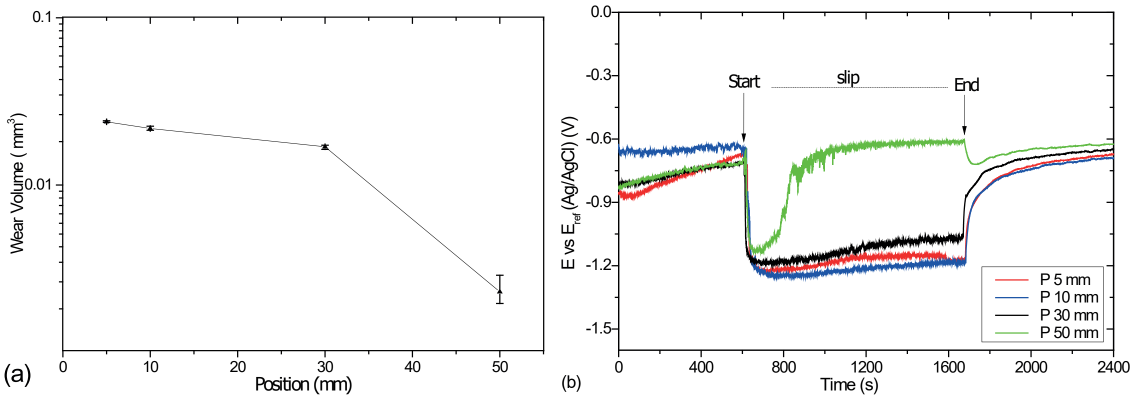

Fig. 1 – Wear volume as a function of position in a directionally solidified Al10Sn10Cu alloy casting and electrochemical noise curves with Potential Density as a function of Time

Considering that samples extracted from positions farthest from the cooled surface of the casting have larger interdendritic spacings (λ_1), the last position analyzed, P = 50 mm, has the largest λ_1 value of all samples analyzed. At the same time, it can be observed in Fig. 1a that the smaller wear volume is associated with such sample. Therefore, the wear volume is shown to decrease with the increase in λ_1 for the Al-10Sn-10Cu alloy, that is, regions with coarser α-Al dendritic phase and interdendritic regions composed by larger Sn pockets were shown to be the best microstructural arrangement for tribocorrosion resistance. Fig. 1(b) shows the influence of the corrosion product that directly affects the Potential density behavior. For the sample P 50 mm, it can be seen that the passive layer, probably formed during the slip of the pin over the sample, promoted a continuous protection of the tribological pair.

ACKNOWLEDGMENTS

The authors acknowledge the financial support provided by FAPESP- São Paulo Research Foundation, Brazil (grants 2012/16328-2) and CNPq - National Council for Scientific and Technological Development.

REFERENCES

Frutos A, Arenas MA, Fuentes GG, Rodríguez RJ, Martínez R, Avelar-Batista JC, Damborenea JJ. Tribocorrosion behaviour of duplex surface treated AISI 304 stainless steel, Surface and Coatings Technology, 2010, 204, p. 1623-1630.

Mischler S. Triboelectrochemical Techniques and Interpretation Methods in Tribocorrosion: A Comparative Evaluation, Tribology International, 2008, 41, p. 573-583.

Salinas DR, Garcia SG, Bessone JB. Influence of Alloying Elements on Aluminium Sacrificial Anode Performance: Case of Al-Zn, Journal of Applied Electrochemistry, 1999, 29, p.1063-1071.

PAPER REF: 045

NUMERICAL COMPUTATION OF CALIBRATION COEFFICIENTS FOR INTEGRAL HOLE DRILLING METHOD. APPLICATION TO THICK THERMAL SPRAYED COATINGS

Harouche Mohamed Karim(*), Hattali Lamine[2], Mesrati Nadir [3]

[1]Ecole Militaire Polytechnique, Algiers, Algeria
[2]Universit Paris Sud, laboratoire FAST, Dpartement GMP, France
[3]Ecole Nationale Polytechnique d'Alger, Algeria
(*)*Email:* harouche_karim@outlook.fr

ABSTRACT

Thermal spray is the most used technique to produce coatings on structural materials. Such coatings are used as protection against: high temperature, corrosion, erosion and wear. Due to the simultaneous action of high pressures, temperatures and spraying conditions, the process of elaborating such materials often generates non-uniform residual stresses with respect to coating thickness. A 120µm AlNi bond-coat was first deposited on a 2017A Aluminium substrate of 6mm thickness. Final coating consisted of X10CrNi18-8 wire stainless steel of different thicknesses. We propose in this work, a numerical method for calibration coefficients to asses residual stress field by the integral hole drilling technique based on relaxed strains. A correlation between calibration coefficients, drilling sequence and coating thicknesses is proposed.

Keywords: thermal spray, residual stresses, incremental hole drilling, calibration coefficients.

INTRODUCTION

Residual stresses can be present in any mechanical structure because of many causes. Manufacturing processes are the most common causes of residual stress. To avoid their unwanted results, they must be accurately characterized which is usually a thought thing to do because they can have random intensity and distribution. The incremental hole drilling method is the most used technique for computing stress fields when it is assumed to vary significantly with depth. A numerical analysis is necessary to compute the calibration coefficients in order to calculate the residual stress caused by the removal of material layers (G. S. Schajer, 1988). All non-uniform stress fields were calculated with respect to the prescription of the ASTM E837 norm in his integral variant (A.Ajovalasit, M.Scafidi,...,2010). Elaborated coatings were industrially deposited. The spraying process was carried out using an AWS equipment (Arc Wire Spraying) gun type and the final approximate coating thicknesses were 300, 350, 700, 750 µm. Aluminium substrates were bond-coated with a 120µm AlNi bond-coat. Final coating consisted of X10CrNi18-8 wire stainless steel. Before deposition, surfaces were grit blasted to ensure correct roughness for mechanical bonding (P. V. Grant, J.D. Lord and P.S. Whitehead, 2006).

RESULTS AND CONCLUSIONS

Figure(4) shows contour plots for calibration coefficients a and b for a drilled hole of 2mm of diameter and a 300 µm coating thickness. For both coefficients a and b, the curves show that the more the drilling is deeper, the more coefficient a and b are larger. Another interesting point lies in that both contour family well behaved over the range plotted. The fact that no singularity was observed in the substrate / coating interface in terms of strains is of practical interest and justifies the trusted range of half diameter of the drilled hole where non-uniform stress fields can be computed.

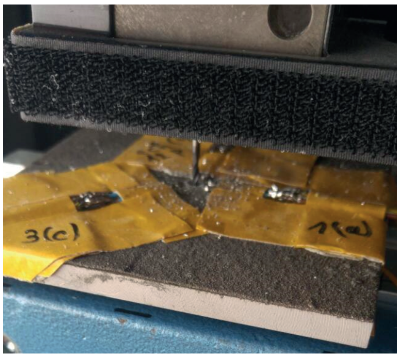

Fig. 1 – Experimental setup for incremental hole drilling technique.

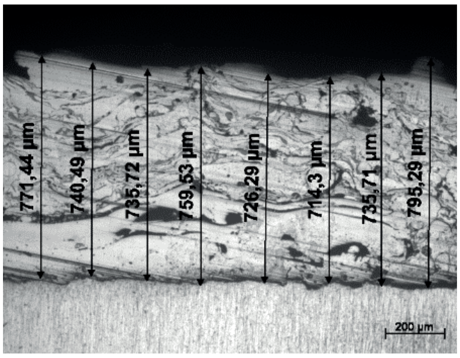

Fig. 2 – Example of a coated 2017A substrate with approximate 750µm stainless steel.

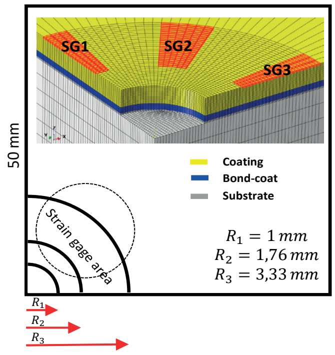

Fig. 3 – Finite element model for calibration coefficient computation

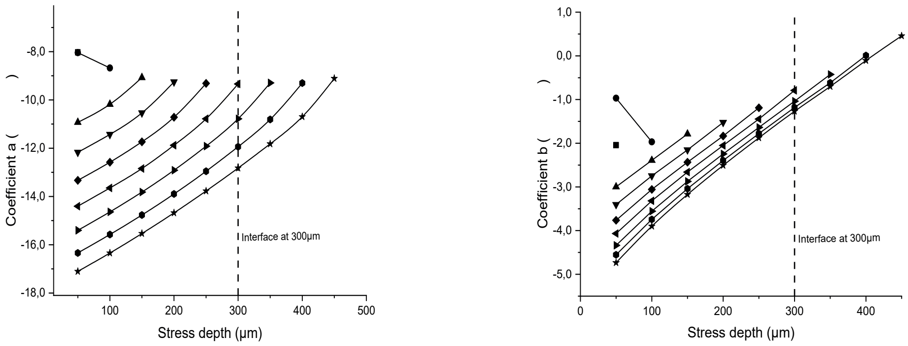

Fig. 4 – Calibration coefficients with respect to stress depth in the case of 300µm coating thickness.

Table 1 - Uniaxial tension test results

Thickness(µm)	**300**	**350**	**700**	**750**
Mean equivalentVon Mises stress (MPa)	84,47	46,02	24,44	18,93

Table(1) gives a simple correlation between the mean equivalent von mises computed stress and coatings thicknesses. Values shows that the more the deposit is thicker, the more the average stress acting in the deposit is lower. This fact is explained by the loss of adhesion strength with increasing thickness.

REFERENCES

G. S. Schajer. Measurement of Non-uniform Residual Stresses Using the Hole Drilling Method. Part II- Practical Application of the Integral Method, OCTOBER 1988, 344/Vol. 110.

A.Ajovalasit, M.Scafidi, B.Zuccarello, M.Beghini, L.Bertini, C.Santus, E.Valentini, A.Benincasa, L.Bertelli. The hole-drilling strain gauge method for the measurement of uniform or non-uniform residual stresses 2010, AIAS – TR01.

P. V. Grant, J.D. Lord and P.S. Whitehead. Measurement Good Practice Guide No. 53 -Issue2- The Measurement of Residual Stresses by the Incremental Hole Drilling Technique 2006, ISSN 1744-3911.

PAPER REF: 046

THE INTEROPERATION AMONG EXERGY ANALYSIS AND LIFE CYCLE THINKING: A SYSTEMATIC LITERATURE REVIEW IN SUSTAINABILITY ASSESSMENT

Michele Dassisti[1(*)], Concetta Semeraro[1], Valeria Selicati[2]

[1]Department of Mechanics, Management & Mathematics (DMMM), Polytechnical University of Bari, Bari, Italy
[2]Department of European and Mediterranean Cultures (DICEM), University of Basilicata, Matera, Italy
[(*)]*Email:* michele.dassisti@poliba.it

ABSTRACT

Presently, the Life Cycle Assessment is still the most used tool to evaluate the sustainability of products, processes and activities, even in a social and economic perspective. Still, there are some gaps between the interpretation of the results of the assessment and the real behaviour of the system.

Exergy is defined by literature as the amount of useful work extractable from a real system when it is brought to equilibrium with its environment through a series of reversible processes in which the system can only interact with such environment. In literature it is considered an excellent concept that can be developed in order to improve the effectiveness of ordinary evaluation models as LCA.

The aim of the paper is to conduct a wide review of the methodologies for the assessment of energy sustainability in processes. More precisely, the intent is to set an analysis of the Integration Degree (ID) between conventional LCA and exergetic models with the purpose of constructing an analytical path that can highlight the gaps (calculation uncertainties, lack of updated data and related sources, transition from linear to non-linear conditions and vice versa, etc.) that arise during the implementation of the steps of the life cycle analysis.

The framework of exergy-based strategies of investigation have been largely developed in literature, as illustrated by the huge number of scientific papers and books presented so far. Among the well-known strategies, the Cumulative Exergy Consumption (CExC) can be appointed, or Exergetic Life Cycle Assessment (ELCA), Cumulative Exergy Extraction from the Natural Environment (CEENE), Life Cycle Exergy Analysis (LCEA), Industrial/Ecological Cumulative Exergy Consumption (ICEC/ECEC) and Extended Exergy Accounting (EEA) as well.

Recently, literature proposes different hybrid approaches that combines exergetic balancing with LCA like Hybrid Exergetic-LCA analysis and Exergoenvironmental Analysis, or combines costs and environmental impacts in exergetic terms as Thermoeconomics and Environomics.

Nonetheless, there are limitations that seem too hard to overcome: the link with old techniques that refers to obsolete and incomplete databases due to the difficulty in finding data that suit to the updated goals and scopes. Plus, in order to carry out an assessment affected by the least possible uncertainty, the sub-phases in which to divide the process must match to the steps of “from cradle to grave” thinking; any further phases that occur during the life cycle are accompanied by a high level of uncertainty and cannot be subjected to a detailed analysis, especially since there are no reference databases.

The striking thing that emerges from the review is that any methodology above mentioned would be more effective if joined (not replaced) to the conventional LCA, because it turned out that they are in such a way complementary. Explicitly, the results together can outline a transdisciplinary framework of the behaviour of the system case of the study. This assumption is long-established by many authors in their study cases, as validation of what Gutowski et.al wrote in 2009: no single alternative criteria or subsidiary model, regardless how well aggregated, could provide a fulfilling solution for all conditions.

The integration of all strategies contributing to the construction of the analytical path is beyond the purpose of this paper which requires a strong conciseness, as it will be object of a further investigation.

Keywords: exergy, life cycle assessment, sustainable manufacturing, sustainability.

PAPER REF: 047

NUMERICAL ANALYSIS OF CYCLIC LOADED SHAPE MEMORY ALLOYS WITH AN ADAPTED ALGORITHM FOR ANSYS

Jean C. Hilário[1(*)], Andrade; C. A. R.[1], Manuel T. B. César[1], Adailton S. Borges[2]

[1] School of Technology and Management (ESTiG), Polytechnic Institute of Bragança, Bragança, Portugal l

[2] Department of Mechanical Engineering (DAMEC), Federal University of Technology – Paraná, Brazil.

[(*)]*Email:* a39513@alunos.ipb.pt

ABSTRACT

This work presents an adapted numerical model using as basis Ansys Mechanical solver to simulate the behaviour of a shape memory alloy (SMA) circular beam. The analysis includes quasi-static and traction-compression cyclic cases. Since the Ansys Mechanical solves mainly the first case, the other result is obtained using the adapted algorithm based in a developed theory. The final results show the superelastic behaviour through stress-strain diagram for the material and displacement-time curve of a free vibration system.

Keywords: shape memory alloys, superelasticity, numerical methods, dynamic response.

INTRODUCTION

The SMA are a kind of alloy classified as smart materials. It receives this rating because of two main characteristics, the shape memory effect (SME) and superelasticity (SE). The important material properties that produces the two characteristics mentioned are detailed in Lagoudas (2008). In the case of numerical simulations, there are different models that propose to predict the structure's behaviour. More details about them can be found in and Auricchio (2001).

The software Ansys uses the Auricchio's model to solve static problems, since the generated stress-strain diagram bring the hysteresis loop, when the material is used in a vibration system, there is a hysteretic damping condition, soon the adapted algorithm aims to simulate an adopted ideal free vibration system with only hysteretic damping based on multiple simulations in the commercial software and be able to present the material's properties caused by cyclic loadings as mentioned by Tobushi et al. (1992).

The routine consists in an Ansys's simulation with the system's initial condition, displacement and velocity, to obtain the stress-strain data for the movement first half-cycle that is used by Matlab's algorithm to calculate the hysteretic damping parameters and predict the next behavior of the second half-cycle. These steps are repeated until the system reach a steady-state condition. The characteristics of the material are present in Table 1, being used to calculate the effect of the SMA application in a dynamic situation, with the dynamic system having a 1 [kg] mass coupled, the SMA element radius and length being 10^{-3} and 10^{-2} meters respectively and the simulation considering an environment temperature of 60 [ºC].

RESULTS AND CONCLUSIONS

The displacement-time curve in Fig. 1a presents the vibration behaviour of the system studied and Fig. 1b shows the respective stress-strain that is caused by the movement. It is possible to see the influence of the energy loss due to the hysteresis loop and the alteration in the hysteretic damper parameters produced over the cycles, including the changes in the characteristic's temperatures due to cyclic loading-unloading.

Table 1 – Adopted system parameters

Young's modulus [GPa]	Transformation temperatures [°C]	Transformation constants [MPa ºC^{-1}]	Transformation stress [MPa]	Maximum residual deformation
67	$M_F = 9$ $M_S = 18.4$ $A_S = 34.5$ $A_F = 49$	$C_M = 8$ $C_A = 13.8$	$\sigma_s^{crit} = 100$ $\sigma_f^{crit} = 170$	$\varepsilon_r = 0.067$

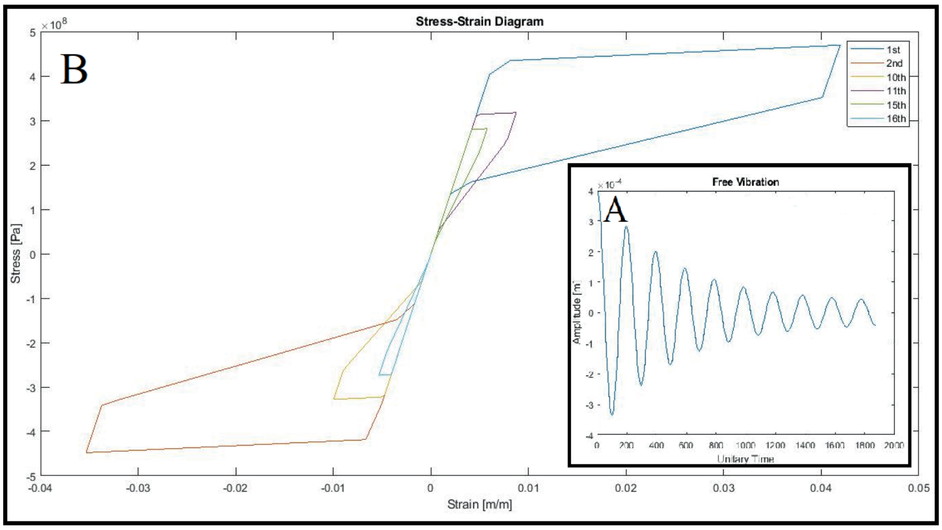

Fig. 1 – Results obtained with the adopted simulation procedure.

The presented research was developed with the goal to simulate the expected dynamic behavior of a shape memory alloy subjected to a free vibration system based on it stress-strain diagram obtained with Ansys. Future research is going to acquire experimental data to calibrate the model and obtain the dynamic behavior to validate the adapted algorithm utilized.

ACKNOWLEDGMENTS

The authors gratefully acknowledge the support by Universidade Técnológica Federal do Paraná – Cornélio Procópio and Instituto Politécnico de Bragrança.

REFERENCES

Auricchio, F. "A robust integration-algorithm for a finite-strain shape-memory-alloy superelastic model". International Journal of Plasticity, Vol. 17, pp. 971-990, 2001.

Lagoudas, D. C. (2008). ShapeMemory Alloys- Modeling and Engineering Applications. (D. C. Lagoudas, Ed.). New York: Springer.

Tobushi, H., Iwanaga, H., Tanaka, K., Hori, T. Sawada, T., "Stress-Strain-Temperature Relationships of TiNi Shape Memory Alloy Suitable for Thermomechanical Cycling". JSME International Journal, Series 1, Vol. 35, No. 3, 1992.

PAPER REF: 048

SIMULATION OF A MECHANICAL VIBRATORY SYSTEM UNDER ROTATING UNBALANCE EXCITATION AND DAMPED BY SHAPE MEMORY ALLOY

Michel A. da Silva[1], Andrade; C. A. R.[1], Vinícius Piccirillo[2], Jean C. Hilário[1(*)]
[1]School of Technology and Management (ESTiG), Polytechnic Institute of Bragança, Portugal.
[2]Department of Mathematics, Federal Technological University of Paraná, 84016-210, Brazil
[(*)]*Email : a39513@alunos.ipb.pt*

ABSTRACT

This work presents a numerical simulation of mechanical vibratory systems (MVSs) under rotating unbalance and damped by a shape memory alloy (SMA) element. Due to pseudoelastic hysteretic behaviour, SMAs can dissipate energy and provide damping capabilities to the structure, which leads to a passive structural vibration control. The algorithm utilizes was implemented in Matlab, based in Helmholtz free energy deduction that results in a cosine constitutive model. The results made clear the dissipative capability of SMAs due to their hysteretic behavior.

Keywords: shape memory alloys, rotating unbalance, vibration, structural integrity.

INTRODUCTION

In an industrial environment, there are a lot of different rotating machines that are subject to unbalance due to an unsymmetrical mass distribution. The vibration analysis field is responsible to study this behavior, and technicians do the maintenance of this machines over the operating time. However, to prevent structural damage between the balancing, other techniques to easy vibration ought to be considered.

Several authors have been researching ways to dissipate mechanical vibratory energy. One of those ways is the use of smart materials, in particular the SMAs that present the pseudoelastic hysteretic behavior. For Brinson (1993), the main goals where the development of a constitutive model to simulate the behavior of SMA elements.

Since there is a high cost involved with the fabrication of different damping element's prototypes, the development of mathematical models able to simulate the behavior of these elements are essential. This work presents a study of a MVS solved by a numerical model based in a method that come from Helmholtz free energy using cosine constitutive model implemented in Matlab to obtain the dynamic behavior presenting qualitative comparations with literature, Machado (2007).

The material properties and system features are exhibited in Table 1, being utilized as input in the developed algorithm to obtain the stress-strain and displacement-time diagrams.

RESULTS AND CONCLUSIONS

Figure 1 shows the literature data and the result obtained with the algorithm implemented. Both cases consider the same MVS, however the properties from the alloy are different. Thus, a qualitative comparison of the graphical shape exhibits a similar behavior, showing the energy loss over the time of the vibration cycle.

Table 1 – System features and material properties

m (Kg)	**r (m)**	**ω (RPM)**	**A_{SMA} (mm^2)**	**C (Nsm^{-1})**	**M (Kg)**	**L_{SMA} (m)**	**T (°C)**	**g (ms^{-2})**
0.3	0.32	1000	2.5	36	27	0.55	51, 61 and 71	9.81

Young's modulus (GPa)	**Transformation temperatures (°C)**	**Transformation constants (MPa ºC^{-1})**	**Transformation stress (MPa)**	**Maximum residual deformation**
$D_A = 67$	$M_F = 9$ $M_S = 18.4$	$C_M = 8$	$\sigma_s^{crit} = 100$	$\varepsilon_r = 0.067$
$D_M = 26.3$	$A_S = 34.5$ $A_F = 49$	$C_A = 13.8$	$\sigma_f^{crit} = 170$	

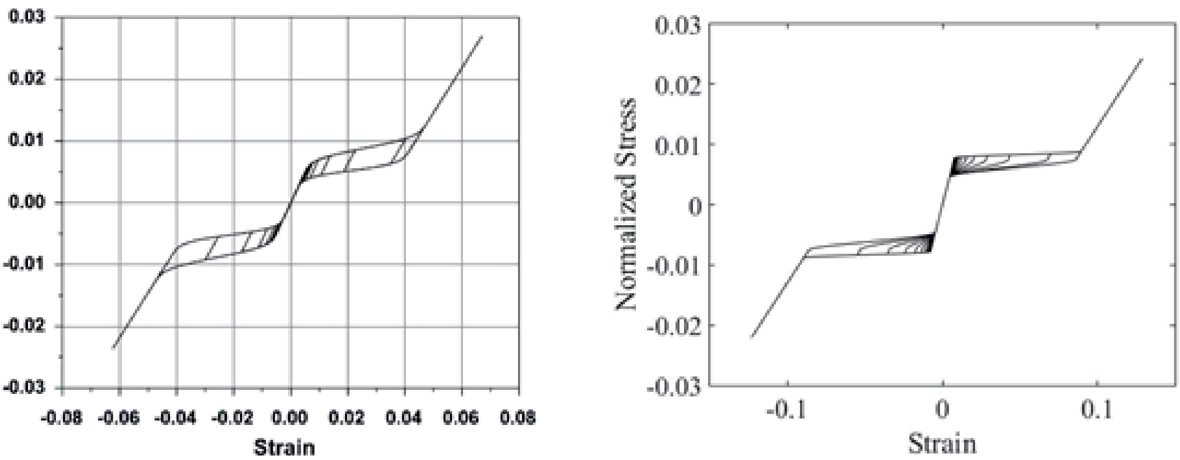

Fig. 1 – a) literature's result and b) obtained result for a free vibration case of a MVS.

This study shows that, by a qualitative analysis, the implemented algorithm presents an acceptable behavior of the MVS with SMA for a free vibration case. Future research aims to expand the analysis to forced vibration case and comparison with other authors to see the influence in the results of the different constitutive models developed over the years.

ACKNOWLEDGMENTS

The authors gratefully acknowledge the support by Universidade Técnológica Federal do Paraná – Cornélio Procópio and Ponta Grossa and Instituto Politécnico de Bragrança.

REFERENCES

Brinson, L. C., "One-Dimensional Constitutive Behavior of Shape Memory Alloys: Thermomechanical Derivation - Non-Constant Material Functions and Redefined Martensite Internal Variable," J. Intell. Mater. Syst. Struct., vol. 4, no. 2, pp. 229–242, Apr. 1993.

Machado, L. G., "Shape memory alloys for vibration isolation and damping", Thesis, Texas A&M University, Dec. 2007.

PAPER REF: 049

CONCEPT FOR LOW FRICTION HYDROGEN END DLC SURFACE GENERATED BY PHOTOCATALYST REACTION

Motoyuki Murashima[1(*)], Yusuke Imaizumi[1], Takazumi Yamada[1], Katsuno Shotaro[2], Tomoki Yoshida[2], Noritsugu Umehara[1], Takayuki Tokoroyama[1]

[1]Department of Micro-Nano Mechanical Science and Engineering, Nagoya University, Nagoya, Japan
[2]Mechanical and Aerospace Engineering, Nagoya University, Nagoya, Japan
[(*)]*Email:* motoyuki.murashima@mae.nagoya-u.ac.jp

ABSTRACT

This study shows a feasibility of using a diamond-like carbon (DLC) coating in water lubricated components with photocatalyst. The hydrogen-end of the DLC carbon structures reduces friction of DLC due to a repulsive force generated by a dipole configuration. It is well known that electrolysis of water using photocatalyst generates hydrogen and oxygen molecules. In this research, we propose a new hydrogen terminating method to create hydrogen-ended DLC surface with photocatalyst in a water lubricated condition. The friction result shows a decrease in the coefficient which is associated with UV irradiation. The reduction in hydrogen-bonding component of surface energy can increase the repulsive force, resulting in lower friction.

Keywords: hydrogenated diamond-like carbon, photocatalyst, hydrogen end, low friction.

INTRODUCTION

Diamond-like carbon (DLC) coatings have variety of applications (e.g. cutting tools, automobile engine components, protect films for electric devices) because of their extraordinary tribological properties (e.g. low friction, high hardness and anti-wear properties). Some mechanisms lead to the low friction property of DLC; graphitization of the structure, transferred layer on a mating surface and hydrogen-ended surface (Erdemir 2001, Erdemir 2004). In an inert dry gas condition, highly hydrogenated DLC (a-C:H) sliding against a-C:H shows a super-low friction less than 0.003. One dominant mechanism showing the low friction can be attributed to promotion of hydrogen end, resulting in rather generating a repulsive force than an attractive force due to dipole configurations. A result that higher hydrogen containing DLCs show lower friction coefficient can be a reasonable proof of the super-low friction mechanism. Hereafter, an importance of developing a new method providing hydrogen into sliding surfaces can be a new challenge.

It is well known that electrolysis of water using photocatalyst generates hydrogen and oxygen molecules, which can be used in new clean energy source (i.e. fuel cell). In this research, we propose a new hydrogen terminating method to create hydrogen-ended DLC surfaces with photocatalyst in a water lubricated condition.

RESULTS AND CONCLUSIONS

We carried out friction tests using a a-C:H coated ball against a TiO_2 (photocatalyst material) disk. During a test, we irradiated a TiO_2 disk with ultraviolet light at wavelength of 365 nm. The disk was fully sunk under water.

The representative frictional revolutions are shown in Fig. 1. The UV irradiation decreased friction coefficient from 0.13 (average friction coefficient value of the without irradiation condition in the last 150 s) to 0.11. The reduction in friction reached by more than 15%. We measured surface energy and its component by droplet observation in an ESEM. The result shows a decrease in surface energy associated with UV irradiation due to a decrease in hydrogen-bonding component, which corresponds to a previous research (Takata, 2003). The decrease in hydrogen-bonding component can reduce attractive force between a-C:H and TiO_2, resulting in a decrease in friction coefficient.

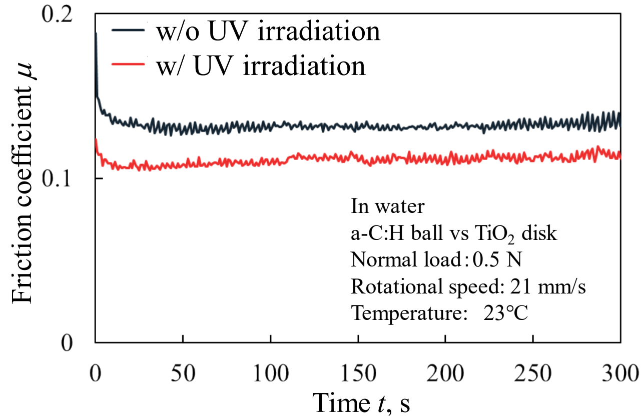

Fig. 1 – Friction revolution of a-C:H against TiO_2 disk with/without UV irradiation

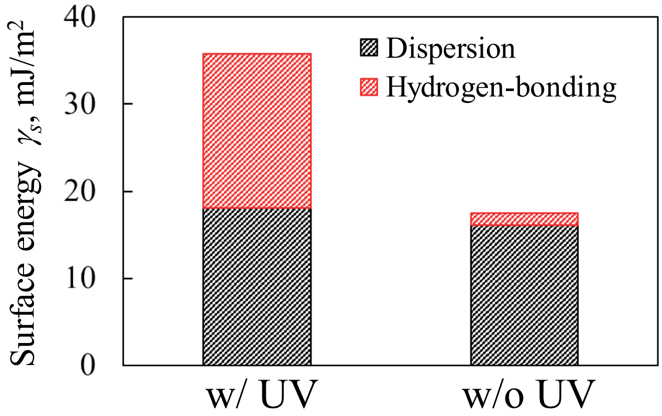

Fig. 2 – Surface energy and its component in the wear track

This study shows a feasibility of using a DLC coating in water lubricated components with photocatalyst. Further development to obtain lower friction, and research work clarifying precise mechanism of the friction reduction should be performed.

REFERENCES

Erdemir A. Genesis of superlow friction and wear in diamondlike carbon films. Tribology International, 2004, 37, p. 1005-1012.

Erdemir A. The role of hydrogen in tribological properties of diamond-like carbon films. Surface and Coatings Technology, 2001, 146-147, p.292-297.

Takata Y. Hidaka S. Masuda M. Ito T. Pool boiling on a superhydrophilic surface. International journal of energy research, 2003, 27, p. 111-119.

PAPER REF: 050

AN ALGORITHM TO INTEGRATE MPM AND SPH WITH NONLOCAL SOFTENING CONSTITUTIVE MODEL FOR FAILURE EVOLUTION

Lisha He[1]**, Zhen Chen**[2,*]**, Yong Gan**[3]

[1]School of Civil Engineering and Architecture, Nanchang University, China
[2]Department of Civil and Environmental Engineering, University of Missouri, Columbia, MO 65211, USA
[3]Department of Engineering Mechanics, Zhejiang University, Hangzhou, Zhejiang 310027, China
(*)*Email:* chenzh@missouri.edu

ABSTRACT

To develop an algorithm for predicting and evaluating the large deformation with failure evolution, a strain softening constitutive model must be incorporated to regularize softening with localization. The length of softening zone is typically related with the mesh size when a local constitutive model is applied. In this study, an integrated MPM (material point method) and SPH (smoothed particle hydrodynamics) numerical algorithm is proposed to implement a nonlocal constitutive model via the spatial gradient of plastic strain in [1], to describe strain softening state. Unlike the work reported in [2] that the SPH is coupled with the MPM, the algorithm proposed here is to integrate the MPM with the smoothing operator [3] and particle approximation for nonlocal modeling. The strengths of both methods can be inherited in the proposed method. The MPM can discretize the continuum region without the need for master/slave nodes at the contact surface. As the post-peak response is unstable due to bifurcation, the effect of numerical noise on the transient responses involving failure evolution could be reduced by using the smoothing operator in the MPM simulation. The particle approximation based on the SPH is adopted on the material points to facilitate the evaluation of strain gradient. A one-dimensional bar under tensile loading is considered to verify and demonstrate the performance of the proposed algorithm. A parametric investigation is then performed to illustrate the effects of controlling parameters on the evolution of localized softening. It is demonstrated that integrating nonlocal constitutive modeling with spatial discretization could yield an effective procedure for predicting and evaluating failure evolution.

Keywords: Material point method, Smoothed particle hydrodynamics, Strain softening, Impact, Transient responses

REFERENCES

[1] H.L. Schreyer and Z. Chen. One Dimensional Softening with Localization. *Journal of Applied Mechanics,* 53(4): 791-797, 1986.

[2] S.J. Raymond, B. Jones, and J.R. Williams. A strategy to couple the material point method (MPM) and smoothed particle hydrodynamics (SPH) computational techniques. *Computational Particle Mechanics*, 5(1):49–58, 2018.

[3] L. He, Y. Gan and Z. Chen. Preliminary Effort in Developing the Smoothed Material Point Method for Impact. *Computational Particle Mechanics,* 6: 45-53, 2019.

PAPER REF: 051

BALLISTIC PERFOMANCE MULTYLAYERED METAL PLATES IMPACTED BY 6.1 MM SMK PROJECTILE

Maxim Yu. Orlov, Viktor Glazyrin and Yuri N. Orlov

National Research Tomsk State University (TSU), Tomsk State University, Tomsk, Russia

(*)*Email:* orloff_m@mail.ru

ABSTRACT

In this work, numerical simulation of penetration of multilayer steel structures by a projectile is presented. The research objects were three-layer and four-layer steel plates. Projectiles had the same mass and diameter but different head part. The penetration of multilayer plates by a projectile was modeled in an elastic plastic lagrangian 2D statement using a non-commercial software package. Comparison of numerical results with experimental data was given. The post penetration analysis, including the time of the birth of the first foci of destruction, the time of penetration, the residual projectile velocity, the residual displacement were obtained numerically.

Keywords: multi-layered plates, projectile, post penetration analysis.

INTRODUCTION

At present time, multi-layer plates are used to protect civilian and military facilities. This is due to many reasons, including the unique ability of such structures to transform a falling shock pulse. Numerical results of the process of breaking through multilayer plates impacted by a 7.62 mm APM2 projectile are presented (Flores-Johnson, 2011). The influence of the shape of the projectile on the penetration of plates is studied in (Gupta N.K, 2008). According with a previous study impact resistance of steel bilayer plates was studied. The target was divided into the main layer and an additional layer. Moreover, the second layer was reinforcing. Ballistic performance steel plates impacted by 6.1 mm Smk projectile are presented (Glazyrin, 2006). The current research objects are multi-layered plates in which the reinforcing layer is bilayer one. The additional layer consisted of two identical steel plates.

Mathematical model is based on phenomenological macroscopic model of continuum mechanics. Governing equations is based on the fundamental laws conservation for: mass, momentum and energy. Elastic-plastic flow is given by the Prandl − Reis equations. The numerical solution is carried out in 2D statement for the axial symmetry by G.R. Johnson's modified method. This method is based on lagrangian approach, and it allows simulate the task of deep penetration into heterogeneous structures, including modern protective structure.

The modification of the method include: algorithm erosion of triangulation elements, nodes splitting algorithm, and free surface constructing algorithm (Gerasimov A.V., 2007). According to the terminology of acad. V. Fomin method contains a new way for isolating discontinuity surfaces of materials. Before the numerical simulation conducted internal, qualitative and quantitative tests. The calculations were performed on the non-commercial software package Impact 2D. Before the calculations were carried out quantitative test only.

RESULTS AND CONCLUSIONS

The initial projectile velocity is 700 m/s. Projectile's material is high-strength steel ShH-15, material's plate is Steel 3 (In accordance with the Russian nomenclature of Construction materials). Projectile's mass is 2.55 g. One diameter is 6.1 mm. The thickness of the layer in the multilayer plate was 2 mm.

Table 1 shows the numerical results. In addition to the values from Table 1, the time of the birth of the foci of fracture in materials, the air gap between the layers, the pressure at the control points, were obtained. The table shows the values for the three types of projectiles, including a projectile with an ogival nose, conical one and flat one. X is the designation of an additional layer. The first sample in the table is the homogeneous 6 mm plate.

Table 1 - Numerical simulation results

Sample	**Penetration time** [μs]	**Residual Velocity [m/s]**	**Damage [%]**	**Hole diameter [mm]**
(6)	44/35/70	444/349/240	10.3/10.3/9.8	6.9/7.8/9.1
(2+2+2)	47/49/48	472/382/226	10.4/10.3/8.3	7.4/9.1/8.5
(X+2+2)	37/42/40	493/302/232	11.2/9.9/10.2	7.4/8.5/9.2
(2+X+2)	42/38/45	483/390/238	10.7/10.3/9.3	7.1/8.9/9.4
(2+2+X)	32/40/48	528/392/237	9.47/11.1/9.5	6.8/9.2/8.9

Numerical values for **ogival nose/conical nose/flat nose/**.

Thus, the research presents the result of breaking through multilayer plate by projectile. Location additional layer in different parts of the plates have little effect on its impact resistance at a given initial velocity.

ACKNOWLEDGMENTS

The reported study was funded by RFBR according to the research project № 19-08-01152.

REFERENCES

Flores-Johnson E.A, Saleh M, Edwards L, Ballistic performance of multi-layered metallic plates impacted by a 7.62-mm APM2 projectile. Impact Engineering J, 2011, 38, p.1022-1032

Gupta N.K, Iqbal M.A, Sekhon G, Effect of projectile nose shape, impact velocity and target thickness on the deformation behavior of layered plates. Impact Engineering J, 2008, 35, p.37-60

Orlov M Yu, Glazyrin VP, Orlov Yu N, Golubatnikov VV Modelling of the process penetration of steel barriers by elongated impactors Proceedings of the 7th International Conference on Mechanics and Materials in Design, Albufeira/Portugal 11-15 June 2017. Editors J.F. Silva Gomes and S.A. Meguid. pp. 1019-1020

Theoretical and experimental research of high-speed interaction of bodies. In Gerasimov AV (ed)/ Tomsk State University Publishing House, 2007, p/ 564

PAPER REF: 052

MODELING OF THE PROCESS OF EXPLOSIVE LOADING OF ICE

Viktor P. Glazyrin, Maxim Yu. Orlov and Yuri N. Orlov
National Research Tomsk State University, 36, Lenin Avenue, Tomsk, 634050, Russia
(*)*Email:* glvp@list.ru, orloff_m@mail.ru

ABSTRACT

In this paper, the problem of the effect of detonation products of an explosive charge located in ice or under water under ice on an ice block was solved. The charge is considered to be an explosive such as TNT and liquefied gas ethane. The behavior of ice is described by the basic system of equations of the mechanics of a deformable solid. The effect of explosive loading on a material is given in the approximation of the model of instantaneous detonation of an explosive charge. The aim of the research is to study the process of ice destruction, including the formation of the first foci of destruction, the time ice destruction, pressure and velocity at control points under action of detonation products (DP). By means of the author's software package, computational experiments on modeling the process of explosive loading of ice cover were carried out and analyzed.

Keywords: ice, model, modelling, velocity, barrier, penetration, detonation, destruction

INTRODUCTION

The modern development of the Arctic and the northern territories of Russia requires the deepening of our knowledge in the field of physics and ice mechanics by conducting theoretical and experimental studies on the behavior of ice under various types of loading, in particular under impulse action. Certain results in this direction can be obtained by conducting large-scale model and field experiments. However, it is necessary to note the technical complexity and high cost of such experiments, as well as the impossibility of obtaining detailed information on the spatial and temporal distribution of stress fields, deformations and areas of damage in the ice samples under consideration. Therefore, a theoretical approach based on mathematical modeling of processes is of particular importance in terms of these studies (Gerasimov, 2007). In the paper (Orlov, 2017) with the help of the original computer program (Glazyrin, 2018), penetration metal ball into the ice block was studied. The calculated values of stresses and strains in the samples correspond to the experimental data.

RESULTS AND CONCLUSIONS

The physical formulation of the problem is formulated as the action on the ice plate of detonation products of an explosive charge placed in ice or in water under ice. As a charge, explosives of the TNT type and liquefied gas ethane SZHG are considered. Ice thickness is 80 cm.

The medium considered is assumed to be compressible, isotropic with the absence of mass forces, internal heat sources and heat conduction (Zelepugin, 2017). An elastic-plastic model is used with the Prandtl − Reis plastic flow equations associated with the von Mises yield condition. The equation of state of Walsh is used. The effect of porosity on the stress-strain state of bodies and their strain hardening is taken into account by correcting the yield strength and shear modulus (Skripnyak, 2018). The model takes into account the kinetics of destruction, the gradient distribution of strength, the initial anisotropy, as well as the effect of temperature on the strength and fragmented selection of zones of destruction. The model of destruction is based on a deterministic approach and takes into account the joint formation of damage by the type of spall and damage by the type of shift. The effect of explosive loading on the material is set in the approximation of the model of instantaneous detonation of the explosive charge.

The numerical solution of the stated boundary value problem is carried out in 2D for axial symmetry by the Johnson's method. The method contains a modified algorithm for splitting nodes, erosion triangle elements, restructuring the free surface, etc. (Gerasimov, 2007). To test the mathematical model and determine the necessary constants, task of penetration of 4.5 mm steel ball into the ice block was solved. The impact velocity varied from 100 m/s to 200 m/s. The objects of study were the freshwater ice block, as well as thick ice (300 cm) and ice on the water. By means of author's uncommercial software package, the task of the destruction of an ice block by an explosive charge placed under ice in water was solved. The modelling was carried out for the "Ice − Water – Explosives" system at different detonation velocity and explosive substance masses. The depth of explosive laying was 80, 50, 40 and 0 cm, the masses of explosives were 6, 10 and 14 kg, the detonation velocity was 4.6 km/s and 6.9 km/s.

The numerical results allow us to estimate the degree of damage to the ice cover, to determine the values of the velocity of the elements of the free ice surface and the pressure at any point of water and ice, depending on the depth of the explosive charge. It has been established that the action of DP of a TNT charge, which is equal in mass to the charge of SZHG, under the same initial conditions, causes almost two times more ice destruction.

ACKNOWLEDGMENTS

The reported study was funded by RFBR according to the research project № 19-08-01152.

REFERENCES

Gerasimov A.V., GlazyrinV.P., Orlov M. Yu. and others. Theoretical and experimental research of high-speed interaction of bodies/ Tomsk State University, 2007, pp. 564.

Orlov M.Yu, Orlova Yu.N., Bogomolov G.N., Glazyrin V.P. Research of the behavior of ice on water under explosive loads. IOP Conf. Series: Journal of Physics: Conf. Series 919 (2017) 012006 doi :10.1088/1742-6596/919/1/012006.

Viktor P. Glazyrin, Maxim Yu. Orlov, Yuri N. Orlov Analysis of the penetration of the barriers by impactors with an explosive substance // Proceedings IRF2018: 6th International Conference Integrity-Reliability-Failure, Lisbon/Portugal 22-26 July 2018, p. 893-898.

Zelepugin S.A., Ivanova O.V., Yunoshev A.S., Zelepugin A.S. Numerical simulation for the propagation and action of shock waves during explosive synthesis // IOP Conf. Series: Materials Science and Engineering, 2017, Vol.894, no. 012033, p. 1-8. doi: 10.1088/1742-6596/894/1/012033.

Skripnyak V.V., Skripnyak V.A., Skripnyak E.G. and Vaganova I.K. Mechanical response of ZrB2–based ultra-high temperature ceramics to shock pulse loadings in a wide temperature range. IOP Conf. Series: Journal of Physics: Conf. Series 1115 (2018) 042016, https://doi:10.1088/1742-6596/1115/4/042016.

PAPER REF: 053

DESIGN OF CFRP INFILL STRUCTURE FABRICATED BY ADDITIVE MANUFACTURING FOR CONTROLLING ANISOTROPY OF MECHANICAL PROPERTIES

Koki Jimbo[1], Tomohiro Tanaka[2] and Toshitake Tateno[3(*)]

[1] Graduate School of Science and Engineering, Meiji University, Kanagawa, Japan
[2] Honda Motor Co., Ltd., Tokyo, Japan
[3] Department of Mechanical Engineering Informatics, Meiji University, Kanagawa, Japan
[(*)]*Email:* tateno@meiji.ac.jp

ABSTRACT

By Additive Manufacturing (AM), it is easy to fabricate complicated structures with composite materials such as CFRP. In AM, infill structures are fabricated with hollow spaces inside an object, which is usually two-dimensional pattern shapes. Because the reinforcement material is placed along the two-dimensional pattern, the orientation and pattern of the reinforcement material is constrained by the infill structure, and the mechanical properties are anisotropic. In this study, a design method of CFRP infill structure for controlling the anisotropy of mechanical properties by combining different orientation pattern layers was proposed.

Keywords: additive manufacturing, composite material, CFRP, infill structure, mechanical strength, anisotropy.

INTRODUCTION

Additive Manufacturing (AM) is easy to fabricate complicated structures with composite materials such as CFRP. However, it is known that the orientation of the reinforcement material much influences on the mechanical properties of parts (Barile, 2017). In AM, infill structures including spaces inside an object is fabricated. Usually, two-dimensional pattern shapes are used. The infill structures enable to reduce the weight of objects, fabrication time, and material cost (Smith, 2017). In infill structures with composite materials, the reinforcement material is placed along the two-dimensional pattern. Reinforcement materials such as continuous carbon fiber in CFRP need to be placed to satisfy a required mechanical property. However, infill walls fabricated by AM are thin and multiple reinforcement materials is difficult to set in a layer. Therefore, the orientation of the reinforcement material is constrained by the infill structure. Such anisotropy makes it difficult to design machine parts.

DESIGN METHOD AND FUDAMENTAL EXAMINATION

In this study, honeycomb structure, that is widely used for infill structure, was adopted. CFRP that consists of nylon and continuous carbon fiber is used for a composite material. As shown in Fig. 1, One layer has carbon fiber in a certain orientation pattern and the orientation patterns are different at each layer. By laminating them, the infill structure is fabricated. By using different orientation pattern of the carbon fibers at each layer, the anisotropy of the mechanical strength can be controlled.

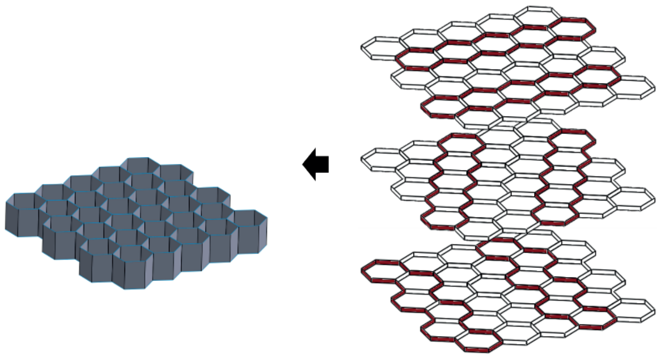

Fig. 1 - An image of proposed method.

First of all, in order to investigate the influence on the mechanical strength of carbon fibers in each orientation pattern, as shown in Fig. 2, specimens are fabricated. In the specimens, carbon fibers are placed only in a certain orientation pattern. Additionally, specimens including all orientation pattern is fabricated. And tensile test is conducted.

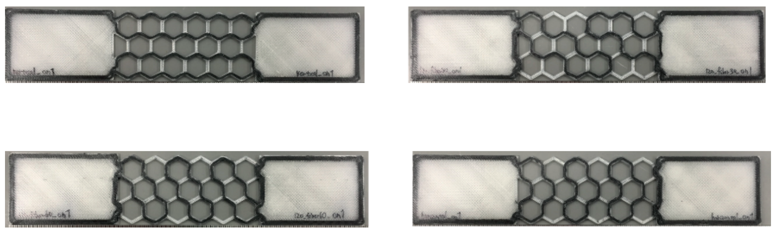

Fig. 2 - Photos of specimens of each orientation pattern.

ACKNOWLEDGMENTS

This work was supported by JSPS KAKENHI Grant Number 17K06126.

REFERENCES

Smyth, C., Functional Design for 3D Printing: Designing 3d printed things for everyday use - 3rd edition, Clifford Smith, 2017.

Claudia B., Caterina C. and Carmine P., The influence of stitching and unconventional fibres orientation on the tensile properties of CFRP laminates. Composites Part B, 110, 2017, 248-254.

PAPER REF: 054

OBSERVATION OF DYNAMIC DEFORMATION AND FRACTURE BEHAVIOR OF BONDED MATERIAL BY DIGITAL IMAGE CORRELATION AND INVESTIGATION OF FRACTURE TOUGHNESS

Shuichi Arikawa[1(*)], Yuta Kimura[2], Tomohisa Kojima[3]

[1]Department of Mechanical Engineering Informatics, Meiji University, Kanagawa, Japan
[2]Graduate School of Science and Technology, Meiji University, Kanagawa, Japan
[3]Department of Mechanical Engineering, Meiji University, Kanagawa, Japan
[(*)]*Email:* arikawa@meiji.ac.jp

ABSTRACT

A dynamic deformation and fracture behavior of a bonded material is observed by digital image correlation. A three-layered specimen used in this study consists of an aluminum part placed as the middle layer and of acrylic resin layers bonded on the top and the bottom surfaces of the middle layer. An impact load is applied to the end of the middle layer using a split-Hopkinson pressure bar. The dynamic shear deformation and fracture behavior of the three-layered specimen is observed by a high-speed camera with the frame rate of 1 Mfps. The fracture occurs along the bonded interface. The dynamic displacement field is obtained by digital image correlation. Strain fields are obtained from the measured displacements. The dynamic fracture toughness of the interface crack is investigated using the measured displacements and strains.

Keywords: dynamic deformation, interface, crack, stress intensity factor, digital image correlation.

INTRODUCTION

There are interfaces of different materials in composites and bonded materials. The strength and the toughness of the interface are keys of the strength of such materials. Therefore, a lot of evaluation method of the interface strength have been investigated. Above all, stress intensity facture of interface crack is one of the effective parameters and has been investigated by many researchers (Tan, 1990), (Nehar, 2017). Furthermore, impact or dynamic loading often occurs. The variation of the strain field becomes complex in dynamic phenomenon, because there is an effect of the inertial force and usually different materials have different sound velocities. On the other hand, recently performances of computers and digital high-speed cameras have been improved. Also noncontact full-field measurement techniques such as optical measurement methods have been improved. One of the useful techniques is digital image correlation (Sutton, 1983). This method can measure displacement fields of object surfaces in various conditions. Hence, it is very effective for measuring complex dynamic deformations using digital image correlation with a high-speed camera.

EXPERIMENT

A three-layered specimen is made as shown in Fig 1. The three-layered specimen consists of an aluminum part placed as the middle layer and of acrylic resin layers bonded on the top and the bottom surfaces of the middle layer. An acrylic adhesive is used for the bonding. An impact load is applied to the end of the middle layer as shown in Fig. 1 using a sprit-Hopkinson pressure bar. The dynamic shear deformation and fracture behavior of the three-layered specimen is observed by a high-speed camera with the frame rate of 1 Mfps.

RESULTS AND CONCLUSIONS

Dynamic displacement fields were obtained by the experiment. The fracture occured along the interface. Strain fields were obtained from the measured displacement fields. The interface stresses near the propagating crack were calculated with considering the special averaging of the displacements and strains. The stress intensity factor as the dynamic fracture toughness of the interface crack is obtained from the calculated stresses. The results are shown in Fig. 2.

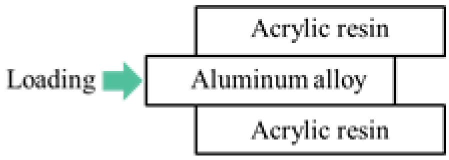

Fig. 1 – Specimen construction and loading condition

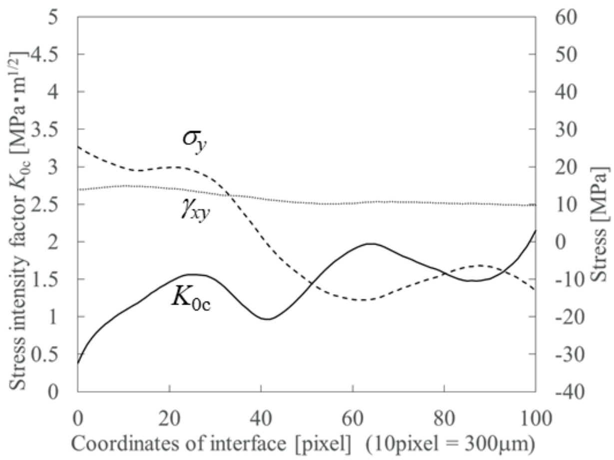

Fig. 2 – Obtained stress intensity factor and interface stresses

In this study, the interface stress intensity factor can be obtained using digital image correlation under the dynamic load. Therefore, it is expected that evaluations of interface stress intensity factors under dynamic loads will be performed for various conditions.

REFERENCES

Tan CL, Gao YL. Treatment of bimaterial interface crack problems using the boundary element method, Engineering Fracture Mechanics, 1990, 36, 6, p. 919-932.

Nehar KC, Hachi BE, Cazes F, Haboussi M. Evaluation of stress intensity factors for bi-material interface cracks using displacement jump methods, Acta Mechanica Sinica, 2017, 33, 6, p. 1051-1064.

M. A. Sutton, W. J. Wolters, W. H. Peters, W. F. Ranson, McNeill SR. Determination of displacements using an improved digital correlation method, Optical, Image and Vision Computing, 1983, 1, 3, p.133-139.

PAPER REF: 055

LATTICE STRUCTURES REPRESENTATION IN 2D DRAWINGS: A PROPOSAL FOR A STANDARD

Antonio Bacciaglia[1(*)], Alessandro Ceruti[1], Alfredo Liverani[1]

[1]Department of Industrial Engineering (DIN), University of Bologna, Bologna, Italy
[(*)]*Email:* antonio.bacciaglia2@unibo.it

ABSTRACT

The interest in the Additive Manufacturing (AM) technology is surging due to its capability of printing components with complex optimized shapes that fit industrial engineering necessities better than traditionally manufactured parts. However, conventional Computer Aided Design (CAD) software packages are often limited to deal with such complex parts, especially when the AM part is designed using lattice structures: these are structures composed of repeated small elements, called cells, across a domain which generate a light and stiff component. The scope of this work is to analyze the problem of the lattice bidimensional representation and propose a standard for representation in assembly and 2D drawings. Rules useful to handle such hierarchic structures in CAD tools is developed, and a code in Python for the open-source software FreeCad™ has been developed to evaluate the effectiveness and usability of the standard. Simplified symbols to describe complex lattice structures instead of drawing all the small elements forming the lattice have been developed. The standard is useful in technical drawings for assembly representation where lattice components are used (assembly operators, maintenance, parts catalogues). A case study is included to describe how the proposed standard could be integrated in a 2D drawing following technical product documentation production typical workflow.

Keywords: Design, Lattice structure, Drawing standards, Additive Manufacturing.

INTRODUCTION

Additive Manufacturing (AM) technology shows well-established advantages: time reduction in the design-to-manufacturing cycle, capability to generate complex biomimetic shapes with a high strength to weight ratio, and reduction of parts thus avoiding bolted connections or welding. Complex 3D components with nature inspired efficient structures can be easily manufactured by adding material layer by layer, operating in contrast respect to the traditional manufacturing processes based on chip removal processes. Bibliography (Ian, et al. 2015) define the fact that a high freedom of shaping is given to the designer with the expression: “What You See Is What You Build”. To exploit the AM potentials, engineers and practitioners must change the way in which a component is designed and sketched to exploit the AM advantages: topological optimization must be adopted to obtain light and stiff structures whose shape can hardly be guessed without optimization codes. With AM “the design drives the shape” concept is valid, opposed to the strategy “manufacturing drives the shape” which applies to traditional parts. Cellular structures, also called hierarchic structures, may be included in AM parts where lightweight, stiffness and strength are needed. In literature, there are different types of cellular structures like foams (stochastic structures), honeycombs and lattices (periodic structures) (Azman, et al. 2015).

Lattices are composed of simple small elements, as cylindrical beams, forming a representative volume called “unit cell” that is repeated thousands of times along the body (Figure 1).

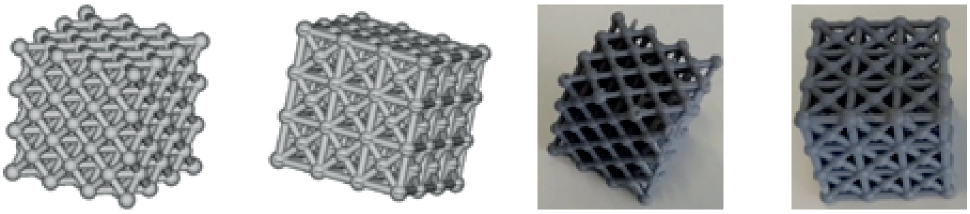

Figure 1 - FCC and Octet lattice CAD model in the left and 3d printed in the right with SLA technique

This unit cell can have different shapes and different topologies, but the easiest to implement are based on cubic unit cell, where the eight vertices are linked following different schemes (Nguyen, et al. 2016). Even if the advantages of such structures are clear, common design tools available to the engineer, such as CAD tools, still shows large limitations because they often use boundary representation technology (B-rep) that is not well suited for lattices where the external surface is quite complex (McMillan, et al. 2017). There are some contributions in literature where tools for the lattice generation is addressed (Rosen, 2013), but the largest part of them are stand-alone applications not embedded in CAD systems. Moreover, the lack of easy interface with Finite Element Method solvers can be noticed. The paper (Ceruti, et al. 2017) is an example of the development of environments embedded in opensource FreeCad™ software packages, to automate the design of different type of lattices and honeycombs in 3D. Commercial CAD tools like PTC’s CREO® includes functions to model lattice structures too. However, in literature there is no mention on how to represent in a 2D technical drawing a lattice component; neither the ISO standards suggests how to deal with this type of structure, nor national standards. AM machines require the 3D model of the part to be manufactured in STL format: however, in case of 2D assembly or single part constructive drawings, the representation of lattice structures could be a challenging task. With modern CAD the sketching of the 3D model of the part is the first step of the modelling loop; in the following these parts are assembled together and finally 2D constructive (including GD&T symbols and tooling details) and assembly drawings are obtained in an automatic way: tools and pre-set functions support quoting, tolerances, and roughness symbols. But if the part is modelled with small elements (such as lattice cells made of cylinders, beams, spheres) the representation on the 2D drawing would be hardly understandable because of too small details. Moreover, the quoting of such a structure would be confusing and operator dependant. This paper suggests a new standard for the 2D representation of lattice structures based on conventional symbols. The proposed standard has been embedded in a new add-on for FreeCad™: a dedicated environment has been implemented programming the CAD in Python language. This new tool implements the representative standard proposed in this paper and allows the representation in a 2D technical documentation of different types of lattice structures.

Once an assembly (i.e. 2 rods linked with a pin, Figure 2) with one or more components constituted by lattice structures is available, the user can obtain a 2D drawing in an automatic way using standard tools of the CAD. In the following, the user has to click on the icon shown in Figure 3 with a red circle and a red label “1” to add the proposed lattice notation. Then, according to the right cross-sectional shape of the lattice, the designer chooses the specific command in the new window that appears in the screen, based on the truss cross-section shape (label “2” in Figure 3).

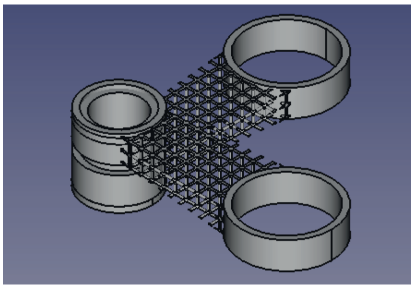

Figure 2 - 3D assembly in FreeCad™ of lattice components

Finally, the user inserts all the lattice specifications in a new window, such as: the lattice component label, the characteristic dimensions and the lattice type among the available ones (Figure 3). By confirming the inputs, FreeCad™ automatically generates the table and places it over the title block (label "4" in Figure 3).

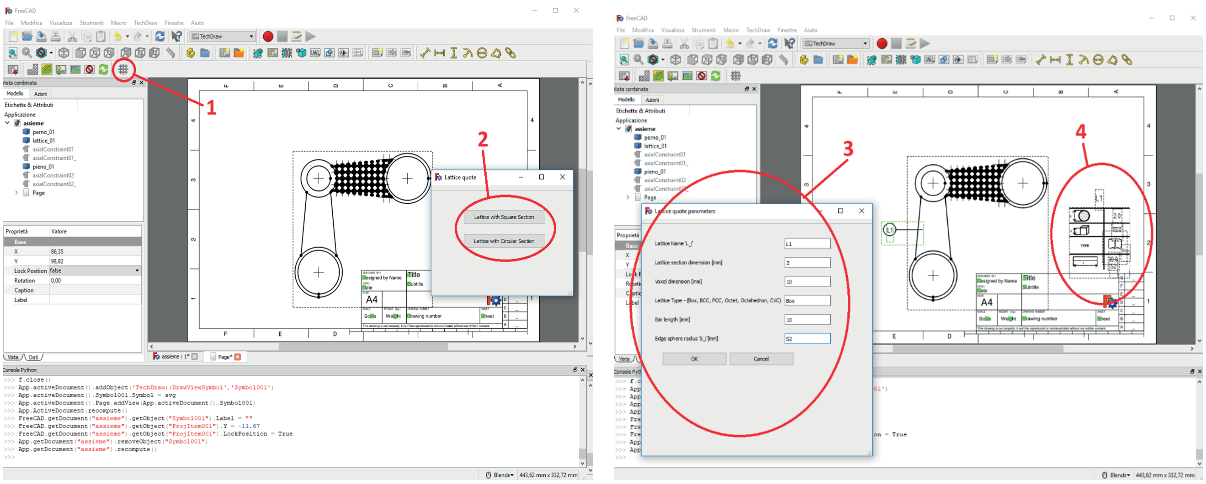

Figure 3 - Print screen of TechDraw environment with additional command (1) for lattice quotes. A new window appears, and the user has to select the right cross-sectional shape (2). Another window appears (3) where all the lattice specifications have to be declared by the user. A new table is automatically created with lattice specifications (4).

REFERENCES

Azman, A. H., Vignat, F., & Villeneuve, F. (2015). Design configurations and creation of lattice structures for metallic additive manufacturing. *14eme Colloque National AIP PRIMECA*. La Plagne.

Ceruti, A., Ferrari, R., & Liverani, A. (2017). Design for additive manufacturing using LSWM: A CAD tool for the modelling of lightweight and lattice structures. *SDM 2017: Sustainable Design and Manufacturing 2017* (p. 756-765). Springer, Cham.

Ian, G., Rosen, D., & Stucker, B. (2015). *Additive manufacturing technologies*. Springer, Boston, MA.

McMillan, M. L., Furg, M., Leary, M., & Brandt, M. (2017). Programmatic generation of computationally efficient lattice structures for additive manufacture. *Rapid Prototyping Journal*, 486-494.

Nguyen, D. S., & Vignat, F. (2016). A method to generate lattice structures for additive manufacturing. *2016 IEEE International Conference on Industrial Engineering and Engineering Management (IEEM)*, (p. 966-970).

Rosen, D. (2013). Computer-Aided Design for Additive Manufacturing of Cellular Structures. *Computer-Aided Design and Applications*.

PAPER REF: 056

ADDITIVE MANUFACTURING IN AUTOMOTIVE: ADVANTAGES AND CRITICALITIES

Antonio Bacciaglia[1(*)], Alessandro Ceruti[1], Alfredo Liverani[1]

[1]Department of Industrial Engineering (DIN), University of Bologna, Bologna, Italy
[(*)]*Email:* antonio.bacciaglia2@unibo.it

ABSTRACT

Additive Manufacturing (AM) is becoming an important alternative to traditional manufacturing processes based on chip removal. In AM "the design drives the shape" concept is valid, opposed to the strategy "manufacturing drives the shape" which applies with traditional parts obtained through casting, milling, lathing processing where several design constraints should be respected. In many industries, aerospace and automotive, the lightweight design plays an important role on the means of transport performances. Owing to AM potentialities, a wide-range of researches are focused on methodologies to obtain structurally optimized shapes: structures obtained through topology optimization algorithms can be manufactured only in AM due to their complex shape. The scope of this work is to analyze advantages and criticalities of AM in automotive applications: a case study to evaluate pros & cons of AM is included, together with a fuel reduction analysis which can be obtained thanks to proper lightweight design of automotive components.

Keywords: Additive Manufacturing, Automotive Industry, Topology Optimization.

INTRODUCTION

A significant growth of Additive Manufacturing (AM) technology in industrial engineering applications has been noticed in last few years due to its well-established advantages: time reduction in the design-to-manufacturing cycle, capability to generate even complex shapes in one piece through an additive process, weight saving just to mention the main significant. Even if in automotive industry the production volumes are very high compared to aerospace, AM usage is growing year by year and in 2013 automotive sector accounts for 17% of all expenditures in AM, namely for special cars, racing cars and all the application where there is a low volume production (Gibson, Rosen e Stucker 2015). It is worth nothing that if the production volumes are high, AM is currently too much expensive in the assembly lines: this is because tooling price becomes significant below 50,000 parts/year while its impact is small from 200,000 to 300,000 parts. On the other hand, costs reduce for customized consumer product. A key advantage of AM is an almost negligible investment in tooling machines compared to millions of dollars for traditional processes: this fact is attractive for new companies in the automotive sector (Bubna, et al. 2016). Moreover, even if the production costs are higher, it's important to spot the light on the time reduction of the design-to-manufacturing cycle that AM technology offers, together with the minimization of internal process logistics due to significant less operations (Leal, et al. 2017).

There are different types of AM technologies, each one showing pros & cons, but laser-based metal AM processes are the most used in automotive (Figure 1) making products with strong and stiff characteristics (Disner, Deschamps e Pinheiro De Lima 2016). This technique well matches with the shape complexity coming from the topology optimization techniques in order to reach an optimized and lightweight shape. The main idea behind this algorithm is to optimize local material density value by exploiting FEM analysis results, in order to add material only where is needed and leave it when not necessary. (Bendsoe e Sigmund 2004) (Reddy, et al. 2016).

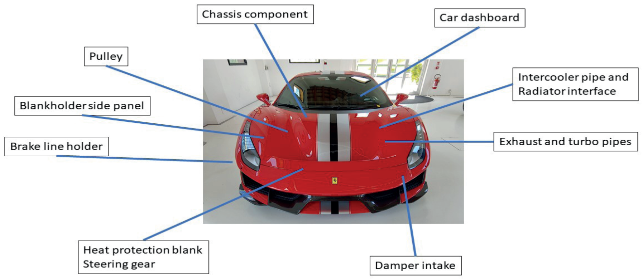

Figure 1 - Automotive components manufactured with AM

The material behaviour uncertainty is a major drawback of AM: this is the reason why certification processes are more complicated (Adam, et al. 2018). With AM more standard certification rules are necessary with respect to traditional manufacturing processes.

In order to highlight advantages and criticalities of AM in automotive industry, a topology optimization example will be included in this work using opensource software as FreeCad and Blender and a cost breakdown analysis will be performed to get the amount of fuel reduction and energy consumption during its service life (Hettesheimer, Hirzel e Rob 2018). This work is organized as follows: Section 2 highlights AM advantages applied to the automotive industry while Section 3 its criticalities and how they could be solved. Section 4 shows a topology optimization case study with weight and costs analysis to support the cause of AM usage. Section 5 reports conclusions and future works.

REFERENCES

Adam, Laurent, Roger Assaker, Philippe Hebert, Olivier Lietaer, and Sylvain Mathieu. “Additive manufacturing simulation solution as enabler for confident lightweight automotive design.” *5th Annual Composites and Advanced Materials Expo, CAMX 2018.* Kay Bailey Hutchison Convention CenterDallas, 2018.

Bendsoe, M. P., and O. Sigmund. *Topology optimization - Theory, methods and applications.* Springer, 2004.

Bubna, P., M. Humbert, M. Wiseman, and E. Manes. “Barriers to entry in automotive production and opportunities with emerging additive manufacturing techniques.” *SAE 2016 world congress and exibition.* Detroit, 2016.

Disner, Nairana Aparecida Alberton, Fernando Deschamps, and Edson Pinheiro De Lima. “A framework for applying additive manufacturing to consumable process parts.” *23rd ISPE Inc. International Conference on Transdisciplinary Engineering.* 2016. 651-661.

Gibson, Ian, David Rosen, and Brent Stucker. *Additive manufacturing technologies.* New York: Springer, 2015.

Hettesheimer, T., S. Hirzel, and H. B. Rob. “Energy savings through additive manufacturing: an analysis of selective laser sintering for automotive and aircraft components.” *Energy efficiency*, 2018: 1227-1245.

Leal, R., et al. “Additive manufacturing tooling for the automotive industry.” *International journal of advanced manufacturing technology*, 2017: 1671-1676.

Reddy, S. N., V. Maranan, T. W. Simpson, T. Palmer, and C. J. Dickman. “Application of topology optimization and design for additive manufacturing guidelines on an automotive component.” *ASME 2016 International design engineering technical conference and computers and information in engineering conference, IDETC/CIE 2016.* Charlotte, 2016.

PAPER REF: 057

INFLUENCE OF PISTON ENGINE INSERT ON TEMPERATURE DISTRIBUTION IN THE PISTON

Paweł Stężycki[1](*), Andrzej Żyluk[2], Antoni Jankowski[3]

[1]Institute of Aviation, Warsaw, Poland
[2]Air Force Institute of Technology, Warsaw, Poland
[3]Institute of Aviation, Warsaw, Poland
(*[1])Email: [1]pawel.stezycki@ilot.edu.pl, [2]andrzej.zyluk@itwl.pl, [3]antoni.jankowski@ilot.edu.pl

ABSTRACT

The subject of the research was test pistons having piston ring carrier with various discontinuities of bond with the material of the piston, a piston without discontinuities and a piston without a carrier. Static and dynamic temperature measurements on the engine indicate a change of the piston temperature field, which affects the thermal stress in the piston and the temperature in the sealing ring, which is associated with the coking of lubricating engine oil.

Keywords: piston ring carrier, bond discontinuity, temperature distribution, laboratory tests, engine tests.

INTRODUCTION

Pistons are highly loaded thermally and mechanically elements of internal combustion engines. The high pressure in the combustion chamber causes the upper sealing ring to be heavily loaded and there is intensive wear in the grooves of the piston ring made of aluminum alloys. Counteracting this is the use of a piston ring carrier [2]. The materials used on piston ring carriers are cast iron, steels, and special metal alloys. Commonly used on the piston ring carrier is a Ni-Resist alloy with a high Ni, Cu and Cr content, which is characterized by a high coefficient of thermal expansion (about 19.3 1E-6 / K) α, which is close to the coefficient of Aluminum alloys and greater by about 80% than the coefficient α of grey iron. In the technological process, the piston ring carriers are covered with a layer of Alfin alloy before joining with the piston material.

During work of piston with ring carrier, increased thermal stresses can lead to piston damage [1]. Increased stresses are caused by the occurrence of temperature differences in the piston and additionally by the temperature difference between the carrier and the main piston material. Thermal stresses increase due to the discontinuity of the carrier bond. The discontinuity of the bond is the result of an incorrect technological process of the piston.

RESULTS AND CONCLUSIONS

In order to determine the effect of the bond discontinuity of the ring piston ring carrier on the temperature distribution in the piston, which results in increased thermal loads, engine and laboratory tests were carried out. The engine tests allow the reproduction of working conditions of pistons, while the laboratory tests allow for placing a large number of temperature measurement points. In engine tests, temperature measurements are carried out by transmitting signals from sensors placed in the piston, which has reciprocating motion to receivers located outside the engine. For this purpose, the inductive devices for transmitting signals from the moving piston to the fixed engine block were used. The measuring device for one measuring point contained two coils, one of which was placed at the measuring point of the moving reciprocating piston, and the second inductive coil was placed in the fixed engine block and connected to the measuring apparatus outside the engine. Transmission of the temperature measurement signal took place during the coupling of the induction coils, which took place when the piston was at the bottom dead centre. The tests were carried out on the SB3.1 single-cylinder research engine with a cylinder diameter of 107.19 mm, a piston stroke of 120.65 mm and a nominal power of 15.8 kW. In the piston, 6 measuring sensors placed.

Laboratory tests were carried out on a test bench, where the temperature distribution was obtained by means of electric heating devices and cooling of the piston using a spray of lubricating engine oil. During the tests, the programmed temperature distribution in the piston in the test bench was similar to the temperature distribution of the piston in the running engine. For testing, pistons with different bond discontinuities of the piston ring carrier with the piston alloy, the piston without bond discontinuity of the piston ring carrier and piston without piston ring carrier were prepared. Engine tests have shown that the use of the piston ring carrier increased the temperature at the edge of the piston crown by 6 K, while under the piston ring carrier; it reduced the temperature by 19 K compared to the piston without a piston ring carrier for the nominal engine load. Piston testing with a 60 mm bond discontinuity showed an increase in temperature at the edge of the piston crown by 5 K and for a piston with a discontinuity of 25 mm bond, an increase in temperature of 3 K compared to a piston with no defects in the bond continuity. The results of laboratory tests are presented in Table 1 and engine results − in Table 2.

Table 1 – Temperature changes above and under piston ring carrier (Laboratory tests)

	Bond discontinuity length (% of perimeter)			
	50%	70%	90%	95%
Temp. increase above carrier	10.3 K	8.1 K	7.9 K	4.6 K
Temp. increase under carrier	8.8 K	7.6 K	5.7 K	3.9 K

Table 2 – Temperature changes above and under piston ring carrier (Engine tests)

Measuring point	**Discontinuity length**			
	60 mm	0	25 mm	0
	Above discontinuity	-	Above discontinuity	-
Temp. above carrier	585 K	589 K	583 K	584 K
Temp. under carrier	445 K	483 k	456 K	475 K

In conclusion, the piston ring carrier increases the temperature of the piston above the carrier by 6 K and decreases the temperature under by 19 K. The discontinuity of the bond causes a further temperature increase above the carrier and decrease under the piston ring carrier.

REFERENCES

[1] Kowalski M., An Analysis of Failure Symptoms of the Airscrew Drive in the PAL-130-TCI Olick Aircraft, Journal of vibration engineering & technologies, Volume: 2 Issue: 4 pp. 315-326, 2014.

[2] Manasijevic S., Dolic N., Djurdjevic, M., Mišic N., Davitkov N., The intermetallic bonding between a ring carrier and aluminum piston alloy, Revista de Metalurgia 51(3), July-September 2015, e048. ISSN-L: 0034-8570 doi: http://dx.doi.org/10.3989.

PAPER REF: 059

PROBABILISTIC APPROACH IN MODELING DYNAMIC FRACTURE PROBLEMS

Sergey A. Zelepugin[1,2(*)], Sergey V. Pashkov[2]

[1]Tomsk Scientific Center, Siberian Branch RAS, Tomsk, Russia

[2]Research Institute of Applied Mathematics and Mechanics, Tomsk State University, Tomsk, Russia

[(*)]*Email:* szel@yandex.ru

ABSTRACT

Using experimental data and numerical simulation results, it is shown, that the introduction of only one additional parameter - dispersion of the strength properties distribution, into the material model makes it possible to give a probabilistic character to the crack formation process at any scale level (macro-, meso-, microlevel), which corresponds to theoretical concepts and experimental data.

Keywords: probabilistic approach, dynamic fracture, numerical simulation.

INTRODUCTION

In many fracture problems, fragmentation is essentially a probabilistic process, which is determined by the stochastic nature of the distribution of inhomogeneities of the internal structure of material. In the paper the probabilistic approach is described, which allows to model structural heterogeneities of the material in a simple form, practically without complication of the model and additional experiments.

Distribution of materials strength characteristics (according to the selected distribution law) in the cells of the computational domain is used for initial heterogeneities and materials structure defects modeling. It is shown that the fragmentation spectra obtained using different distribution laws with the same dispersion coincide up to the probability factor, which allows to use any distribution law in the calculations.

RESULTS AND CONCLUSIONS

Expanding ring test (Diep, 2004; Lambert, 2012) is an illustrative example of the probabilistic approach. The experimental scheme provides a uniform radial velocity, so, the ring is fragmented due to the presence of internal inhomogeneities and deformations localized on the largest of materials structure defects. The final fragmentation spectrum obtained in the work (Gerasimov, 2013) using the described approach is qualitatively and quantitatively consistent with the experimental results (Diep, 2004) both in the number of fragments and in their masses (Fig. 1). It should be noted that (Diep, 2004) also come to the conclusion that the choice of the distribution law does not have a significant impact on the fragmentation spectrum.

Other example of the probabilistic approach is a petaling of a thin plate under ogive-nosed projectile impact shown in Fig. 2. The number of petals depends on the speed of the projectile and the properties of the material.

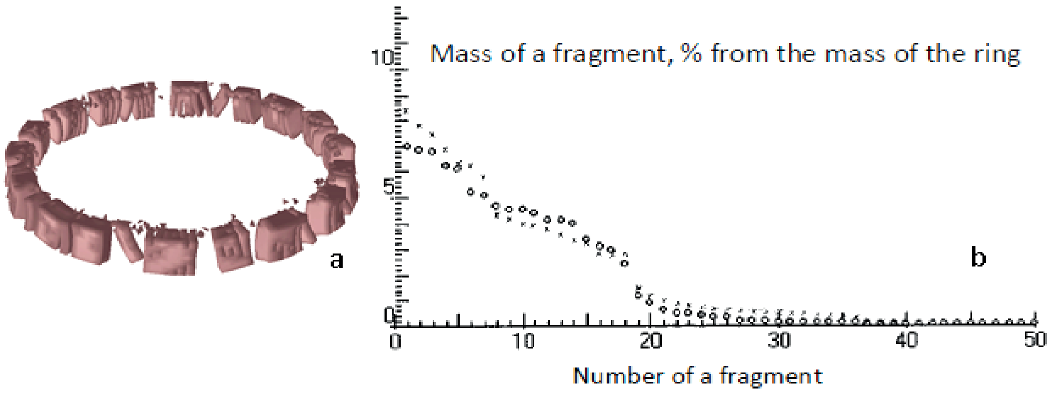

Fig. 1 - Expanding ring test: a) simulation (Gerasimov, 2013);
b) comparison of experimental data (Diep, 2004) and simulation.

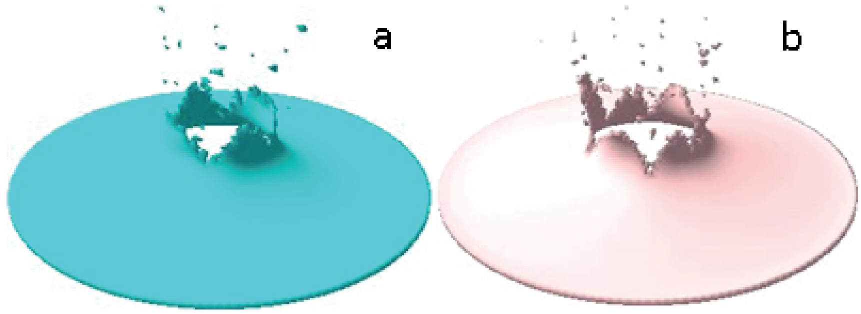

Fig. 2 – Petaling of a thin plate under ogive-nosed projectile impact:
a) copper plate, υ = 150 m/s; b) steel plate, υ = 300 m/s.

Thus, the introduction of only one additional parameter (dispersion of the strength properties distribution) into the material model makes it possible to give the process of crack formation a probabilistic character, which corresponds to the experimental data and allows to improve the accuracy of computations without preliminary study of the structure of the material. The proposed probabilistic approach can be used at any mesh step and at any level of multilevel modeling, providing the distribution of inhomogeneities of the characteristic size. This approach can be applied to any material models and fracture criteria.

ACKNOWLEDGMENTS

This work was supported by the Russian Science Foundation (RSF), project no. 16-19-10264.

REFERENCES

Gerasimov AV, Pashkov SV. Composites: Mechanics, Computations, Applications. An International Journal, 2013, 4(2), p. 97–111.

Diep QB, Moxnes JF, Nevstad G. Fragmentation of projectiles and steel rings using 3D numerical simulations. Proc. 21th Int. Symp. on Ballistics, 19–23 April 2004, Adelaide, Australia, 2004, p. 752.

Lambert DE, Weiderhold J, Osborn J, Hopson MV. Explosively driven fragmentation experiments for continuum damage modelling. Journal of Pressure Vessel Technology, Transactions of the ASME, 2012, 134(3), 031209.

PAPER REF: 060

SOLID-PHASE SYNTHESIS UNDER EXPLOSIVE LOADING: PROBLEMS AND THEIR SOLUTION

Oksana V. Ivanova, Sergey A. Zelepugin[(*)]
Tomsk Scientific Center, Siberian Branch RAS, Tomsk, Russia
[(*)]*Email:* szel@yandex.ru

ABSTRACT

The previous numerical and experimental studies of the behaviour of porous reactive mixtures (Al-S and Al-Tf) placed into cylindrical ampoules under explosive loading revealed the problems related to the fracture of cylindrical ampoules. This problem is solved by adding an inert porous aluminium layer to the bottom part of the mixture. The numerical computations have shown that in this case the fracture of the cylindrical ampoule is not observed.

Keywords: solid-phase synthesis, explosive loading, numerical simulation.

INTRODUCTION

By now the solid-phase synthesis of mixtures placed in cylindrical ampoules under explosive loading has been insufficiently studied and, therefore, it is of great interest for further research. This direction has not yet reached the level of technology due to the lack of experimental data and numerical techniques correctly describing the process. During shock-wave compression a significant energy release due to exothermic reactions in reactive mixtures takes place, which, on the one hand, can lead to self-sustaining propagation of chemical reactions in mixtures and, on the other hand, to the failure of ampoules, as well as to the complete fracture (Zelepugin, 2015; Zelepugin, 2016; Batsanov, 1994). Developed numerical models and available experimental data will provide the reliable information on reactive media and mechanisms and kinetics of physical and chemical transformations.

The goal of this work is to eliminate the problems of solid-phase synthesis such as the fracture of cylindrical ampoules during explosive loading.

RESULTS AND CONCLUSIONS

To study the explosive loading of reactive porous mixtures, numerical computations were carried out using a multicomponent medium model and the finite element method (Johnson, 2011). The axisymmetric explosive loading of a porous Al–S mixture placed in a cylindrical steel ampoule was considered. It should be noted that the previous numerical and experimental studies of the behavior of porous reactive mixtures (Al-S and Al-Tf) placed into cylindrical ampoules under explosive loading revealed the problems related to the fracture of cylindrical ampoules.

To solve this problem, it was assumed to add an inert porous aluminum layer to the bottom part of the Al-S sample. In this case, the height and diameter of the reactive Al-S sample were 49 mm and 14 mm, and the height and diameter of the inert aluminum layer were 16 mm and 14 mm, respectively.

In the computations the explosive surrounding the ampoule was simulated in terms of pressure acting on the upper part of the ampoule in an axial direction and on the lateral surface of the ampoule in a radial direction during the propagation of the detonation front. The detonation velocity used in the numerical computations was measured experimentally and was equal to 3.3 km/s.

Shock wave propagation in the Al-S reactive mixture with an inert bottom Al layer is characterized by the different dynamics during the explosive synthesis of aluminum sulfide as compared to the Al-S reactive mixture without addition of an inert bottom Al layer. In this case, the shock wave propagating along the ampoule does not reflect from the bottom lid of the ampoule. In addition, the inert aluminum layer does not contribute to pressure and temperature rise due to the absence of chemical reactions in it. The shock wave propagating along the ampoule encounters the shock compression wave in the inert layer, which leads to the increase in the pressure, but not as high as the pressure in the Al-S reactive mixture without inert additives. After the encounter, the shock waves propagate in opposite directions. The residual pressures are observed in the sample for short time.

The numerical computations have shown that in this case the fracture of the cylindrical ampoule is not observed.

ACKNOWLEDGMENTS

This work was carried out within the state task for Tomsk Scientific Center of the Siberian Branch of the Russian Academy of Sciences (project no. 0365-2019-0004).

REFERENCES

Zelepugin S., Ivanova O., Yunoshev A. and Zelepugin A. Letters on materials, 2015, 5(4), p. 468-472.

Zelepugin S.A., Ivanova O.V., Yunoshev A.S. and Zelepugin A.S. IOP Conf. Series: Materials Science and Engineering, 2016, 127(1), 012057.

Batsanov S.S. Effects of explosions on materials (New York: Springer-Verlag), 1994.

Johnson G.R. Int. J. Impact Eng., 2011, 38(6), p. 456-472.

PAPER REF: 061

NUMERICAL MODEL FOR SELECTIVE LASER AND ELECTRON BEAM MELTING OF TI POWDER

Roman Cherepanov(*), Maxim Krinitsyn, Vasiliy Fedorov, Maxim Gustomyasov

[1]National Research Tomsk Polytechnic University, Tomsk, Russia

(*)*Email:* RCherepanov82@gmail.com

ABSTRACT

This work presents a meshless numerical model of Ti powders melting with laser and electron beam. Numerical technique based on incompressible smoothed particle hydrodynamics (ISPH) with some improvements to avoid particle clustering.

Keywords: Additive manufacturing, electron beam melting, selective laser melting, Ti alloys, numerical modelling.

INTRODUCTION

When developing technologies for the additive production of metal powders, there is the problem of selecting fusion parameters and product cooling modes. To determine the parameters of the electron beam and the preheating temperature, we developed a numerical model for the melting of metal powders, taking into account heat transfer in the material, hydrodynamic effects in the molten bath, and surface radiation. The model is based on the meshless smoothed particle method (SPH) and the method of process splitting for hydrodynamics flows and heat transfer.

To calculate the hydrodynamic flows in the melt zone, we use incompressible smoothed particle hydrodynamics (iSPH) [1] with an algorithm for preventing the joining of particles. To calculate the process of heat conduction, an implicit stable numerical scheme based on the smoothed particles method has been developed. Both schemes use a conjugate gradients method as a background for solution of systems of linear equations.

As it proposed in [1], the pressure projection method is used to enforce incompressibility, and relies on Helmholtz-Hodge decomposition of the velocity field into a divergence free and a curl free part.

Pressure projection method invokes solution of linear equations system with sparse matrix, what can be done effectively with conjugate gradients method (CG). We use CG method without of preconditioner with relative error of 1.0e-7. Since CG method uses only matrix and vector multiplication, it was realized in parallel multi-threaded mode with significantly increased computational performance.

It is found in 3D-calculation particles are subjected to joining effect, which lead to ill-conditioned matrixes for equations of pressure projection method. To avoid such particle clustering an artificial repulsive force added if inter-particle distance becomes too small. This repulsive force do not affect main hydrodynamics flows and have no significant influence on local pressure distribution, but effectively prevent particle joining and stabilizes computations.

RESULTS AND CONCLUSIONS

The proposed method allows simulating the process of selective electron-beam melting of powders of titanium alloys, taking into account the hydrodynamic flow of the melted metal, thermal conductivity and the effect of surface tension on the shape of the surface of the melt pool. Effective parallel computation procedures can be used due to the use of the conjugate gradient method for solving systems of linear equations. Advantages of the meshless iSPH-method significantly simplify the calculation of the adhesion of powder particles during melting and allow calculation of melt mixing and heat transfer in the same computational framework.

Comparison of numerical simulation results with experimental studies of EBM melting VT1 powder (analogue alloy CI-2 (Japan), T-40 (France)) performed. This comparison show that the proposed model adequately describes the main stages of the process of melting and crystallization of the powder and allows you to qualitatively investigate the effect of electron beam parameters on fusion of layers and surface roughness [2] of products obtained by the method of selective electron beam melting. This model can be useful for predicting fatigue strength properties of Ti-6Al-4V manufactured by additive SLM and EBM manufacturing [3].

ACKNOWLEDGMENTS

The research was supported by RSF (project No. 18-79-10049)

REFERENCES

[1] A. Bockman, O. Shipilova, G. Skeie. Incompressible SPH for free surface flows. Computers & Fluids, 2012, 67, p. 138–151

[2] B. Vayssette, N. Saintier, C. Brugger, M. Elmay, E. Pessard. Surface roughness of Ti-6Al-4V parts obtained by SLM and EBM: Effect on the High Cycle Fatigue life. Procedia Engineering, 2018, 213, p. 89-97

[3] H. Masuo, Y. Tanaka, S. Morokoshi, H. Yagura, T. Uchida, Y. Yamamoto, Y. Murakami, Influence of defects, surface roughness and HIP on the fatigue strength of Ti-6Al-4V manufactured by additive manufacturing, International J of Fatigue, 2018,117, p. 163-179.

PAPER REF: 062

A THREE-DIMENSIONAL UNIT CELL MODEL WITH CONTROLLABLE IRREGULAR HELICAL STRUCTURE FOR INVESTIGATING FAILURE OF COLLAGEN FIBER REINFORCED BIOLOGICAL COMPOSITE

Li Liu[1], Dean Hu[1(*)], Xu Han[12(*)]

[1]State Key Laboratory of Advanced Design and Manufacturing for Vehicle Body, Hunan University, Changsha, P. R. China
[2]School of Mechanical Engineering, Hebei University of Technology, Tianjin, P. R. China
[(*)]*Email:* hudean@hnu.edu.cn, xhan@hebut.edu.cn

ABSTRACT

To explicitly account for the morphological structure of crimped fibers and reveal their damage mechanism at mesoscopic level, a three-dimensional (3D) unit cell model (UCM) is developed based on the microstructure of collagen fibers, in which a fiber with controllable irregular helical curve structure is explicitly embedded into the soft matrix. For reproducing the softening behavior and failure of the composite, the neo-Hookean and Holzapfel-Gasser-Ogden (HGO) models enhanced with different energy limiters and failure parameters are applied to the UCM with ABAQUS user subroutine. Moreover, the damage of fiber/matrix interface is simulated by cohesive elements. Finally, the effects of interfacial strength, material properties and morphological structure of crimped fibers on the mechanical properties and damage mechanism are discussed.

Keywords: morphological structure, collagen fiber, UCM, energy limiter, damage mechanism.

INTRODUCTION

The crimped fiber reinforced composites (Rezakhaniha, 2012 and Gattinger, 2018) play a significant role in advanced engineering applications. Connective tissue, as one of the most common fibrous composites, supports, connects or separates different types of tissues and organs in the body. There are many literatures on the constitutive model or numerical analysis of the tissues. Accordingly, the nonlinear constitutive behavior of the tissues is caused by the nanoscale material mechanism (Marino, 2017) and geometric nonlinearities (Cacho, 2007), but it is limited to two-dimensional or one-dimensional problems and the effect of the crimped geometric features on the local stress and strain fields of the composites cannot be obtained during the deformation. Moreover, the damage accumulation in the material is a consequence of micro-defects evolution, degradation of mechanical properties up to failure (Calvo, 2007 and Fathi, 2017). Therefore, a three-dimensional (3D) model with controllable geometric features is needed for investigating the geometric effects on the global or local mechanical responses of the composites and revealing the damage mechanism which is caused by the interfacial strength, material properties and morphological structure of crimped fibers.

RESULTS AND CONCLUSIONS

Fig. 1 gives the load-displacement curves and Fig. 2 gives the Mises stress contours. The influences of straightness *Ps* on mechanical property are discussed. This study shows that fibers with the same straightness exhibit the same overall mechanical properties. The overall mechanical properties of the material enhanced with the increase of fiber straightness, but the local stress level is non-monotonically correlated with it.

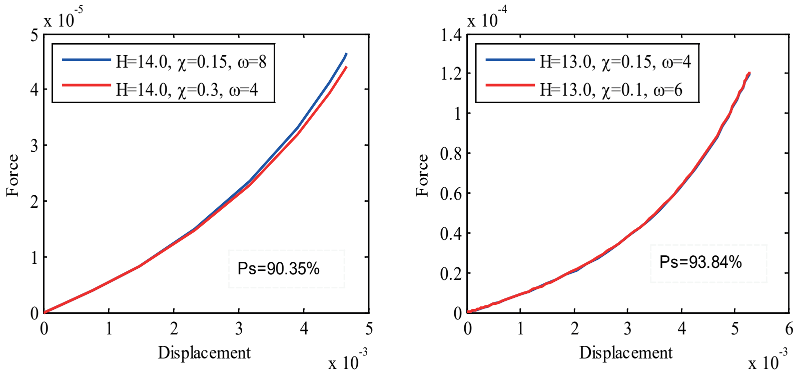

Fig. 1 - Load-displacement curves with different straightness

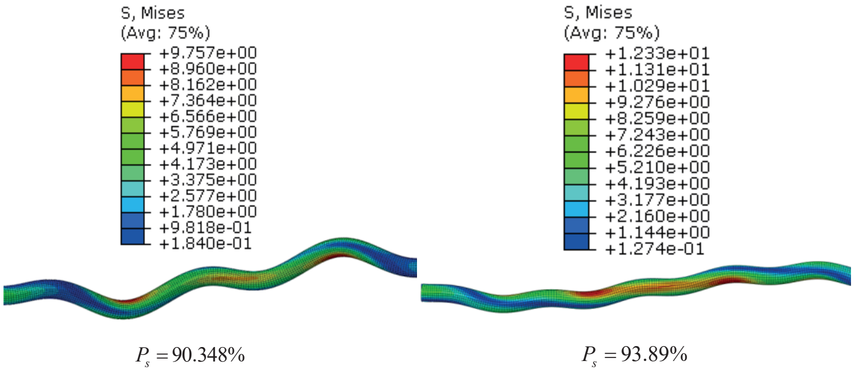

Fig. 2. – Mises stress contours

ACKNOWLEDGMENTS

The authors gratefully acknowledge the funding by National Natural Science Foundation of China (11672105, 11232004) and Natural Science Foundation of Hunan Province (2016JJ1009).

REFERENCES

Rezakhaniha R, Agianniotis A, Schrauwen JT, et al. Experimental investigation of collagen waviness and orientation in the arterial adventitia using confocal laser scanning microscopy. Biomechanics Model. Mechanobiol, 2012, 11(3–4), p. 461–473.

Gattinger J , Kirsch M , Kirchebner B. Flexible composite strands through extrusion of crimped fiber reinforced thermoplastic elastomers. Materials Today Communications, 2018, 15, p. 43-47.

Marino M, Wriggers P. Finite strain response of crimped fibers under uniaxial traction: an analytical approach applied to collagen. J. Mech. Phys. Solid, 2017, 98, p. 429–453.

Cacho F, Elbischger P J, J.F. Rodríguez, et al. A constitutive model for fibrous tissues considering collagen fiber crimp. International Journal of Non-Linear Mechanics, 2007, 42(2), p. 391-402.

Calvo B, Peña E, Martinez M A, et al. An uncoupled directional damage model for fibred biological soft tissues. Formulation and computational aspects. International Journal for Numerical Methods in Engineering, 2007, 69(10), p. 2036-2057.

Fathi F, Ardakani S H, Dehaghani P F, et al. A finite strain integral-type anisotropic damage model for fiber-reinforced materials: Application in soft biological tissues. Computer Methods in Applied Mechanics & Engineering, 2017, 322, p. 262-295.

PAPER REF: 063

ADDITIVE MANUFACTURING OF WC-CO CUTTING TOOLS FOR GEAR

Alessandro Fortunato[1], Giuseppe Valli[1], Erica Liverani[1], Alessandro Ascari[1]
[1]Dipartimento Ingegneria Industriale (DIN), Università di Bologna.

ABSTRACT

This article presents results relating to the production of a WC-Co gear cutting tool via selective laser melting (SLM). The influence of powder grain geometry and chemical composition on SLM process outcomes are firstly investigating by producing and testing simple cylindrical specimens, from which optimal process parameters and scanning strategies are establish for both the component itself and supporting structures. These parameters are then utilised to produce a real cutting tool that is subsequently employed for internal automotive gear fabrication.

Keywords: Selective Laser Melting (SLM), Additive Manufacturing, WC-Co Cutting Tools.

INTRODUCTION

Current powder sintering processes utilised for cutting tool production are limited by the fact that components must always be of full density and are moulded to produce the semi-finished form, which can take a very long time for tools with complex geometry. It is instead possible to produce semi-finished components via selective laser melting (SLM), a 3D printing technology that allows weight savings to be made through the creation of structures with the same stiffness but reduced mass. This ultimately leads to lower material consumption and allows traditional forming process to be avoided, with time savings in delivery and warehousing stocking. The production of WC-Co components via SLM is extremely complicated due to the different melting temperatures of WC and Co and optical absorptance at the laser beam wavelength; moreover, WC is very fragile, which makes the object susceptible to cracking as a result of thermal cycles that are induced during the SLM process. Many studies have been presented in the literature in relation to these problems [1-4]; however, to the authors' knowledge, none have yet demonstrated successful production of cutting tools via SLM, especially tools with large dimensions and complex geometry.

In order to optimize this process, components were produced by SLM using a SISMA MYSINT100 system with a 100 mm diameter cylindrical building chamber and fibre laser of wavelength 1030 nm, power up to 150 W and spot diameter of 50 µm. All tests were carried out in a nitrogen environment with a residual oxygen content of 0.2%. Process parameters and laser beam scanning strategies were implemented with the MARCAM AutoFab software. Layer thickness and hatch space were set to 20 µm and 60 µm, respectively, for all tests, while a 3 × 3 mm^2 checkerboard hatching style was utilised for the bulk volume. All samples for process optimisation were cylindrical in form with a diameter of 8 mm and a height of 10 mm. Hot Isostatic Pressing (HIP) was subsequently performed on all samples at a temperature of 1392°C and a pressure of 50 bar. Samples were analysed with optical microscopy (OM) and SEM coupled with energy dispersive spectroscopy (EDS) (X-Act/INCA, Oxford Instruments). Etching was carried out by exposing samples to Murakami reagent for 10 s.

The density of samples was determined both before and after HIP treatment based on Archimedes' principle using scales with a precision of ±0.0001 g. An experimental campaign was then developed, evaluating three different scanning strategies:

1. A single laser pass per layer, varying the laser power and scanning velocity to achieve increasing energy density over the range 140-450 J/mm^3.
2. Two laser passes per layer, varying the laser power and scanning velocity to achieve increasing energy density up to 520 J/mm^3.
3. Three laser passes per layer increasing energy density up to 680 J/mm^3.

RESULTS AND CONCLUSIONS

The first set of experiments conducted with a single laser pass per layer has demonstrate that the density of samples increases with increasing energy density, before reaching a horizontal asymptote for energy density above 375 J/mm^3. An energy density of 375 J/mm^3 was furthermore considered the maximum usable in the case of a single laser pass per layer, as higher energy density levels did not produce intact cylinders. With the second set of experiments, conducted with two laser passes per layer, the division of the total energy density into two successive laser passes allowed the maximum energy density per layer to be increased from 375 to 520 J/mm^3 and the density from 92.5 to 98.8%.

Upon increasing the number of passes from two to three, this value increased to 620 J/mm^3 (sample 3.4* in Fig.1). Microscopic analysis of all samples, moreover showed that an increase in total energy density led to a reduction in cracks due to minimisation of temperature differences during production and therefore minimisation of the rate at which thermal expansion and contraction took place. Sample 3.4* was almost completely crack-free, representing the best compromise between maximum component density, minimum crack formation and maximum production speed. Investigation into additional strategies for division of the total energy density was therefore not undertaken.

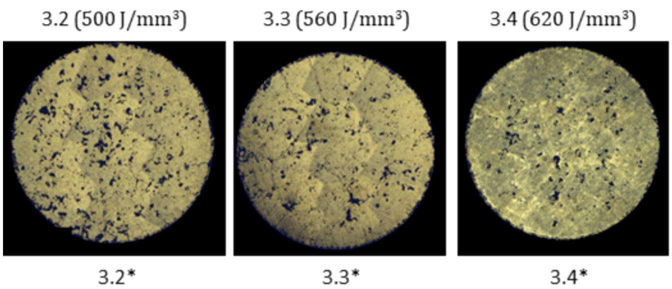

Figure 1: Microspose images of sample scanned with a triple-pass strategy.

REFERENCES

[1] Bourell, D., Kruth, J., P., Leu, M., Levy, G., Rosen, D., Beese, M., A., Clare, A., 2017, Materials for additive manufacturing, CIRP Annals, 66/2: 659-681.

[2] Uhlmann, E., Bergmann, A., Gridin, W., 2015, Investigation on Additive Manufacturing of tungsten carbide-cobalt by Selective Laser Melting, Procedia CIRP, 35: 8-15.

[3] Uhlmann, E., Bergmann, A., Boltz, R., 2018, Manufacturing of Carbide Tools, Procedia Manufacturing, 21: 765-773.

[4] Kruth, J., P., Levy, G., Klocke, F., Childs, T., 2007, Consolidation Phenomena in Laser and Powder-Bed Based Layered Manufacturing, CIRP Annals, 56/2: 730-759.

PAPER REF: 064

L5-S1 MINIMALY INVASIVE TRANSFORAMINAL LUMBAR INTERBODY FUSION: A FINITE ELEMENT MODEL

D. S. Fidalgo[1], B. Areias[2], L.C. Sousa[2(*)], M. Parente[2], R. Natal[2], H. Sousa[3], J. Gonçalbves[4]

[1]DEMec, Faculdade de Engenharia da Universidade do Porto, Porto, Portugal, Portugal
[2]INEGI e DEMec, Faculdade de Engenharia da Universidade do Porto, Porto, Portugal
[3]Centro Hospitalar de Vila Nova de Gaia / Espinho, Vila Nova de Gaia, Portugal
[4]Hospital da Luz Arrábida, Vila Nova de Gaia, Portugal
[(*)]*Email:* lcsousa@fe.up.pt

ABSTRACT

Transforaminal lumbar interbody fusion (TLIF) is an established treatment for structural instability associated some with spine instability and symptomatic disk degeneration. TLIF approach by a unilateral access to the intervertebral foraminal space, reduces direct dissection and surgical trauma to spinal muscles, so it and can be performed via “mini-open” technique. Stand-alone TLIF may increase the risk of non-fusion. This work presents a numerical model of a minimaly invasive transforaminal lumbar interbody fusion of the functional spine unit L5-S1 with bone graft and posterior instrumentation in order to increase fusion rate.

Keywords: minimally invasive lumbar fusion, transforaminal approach, T-Pal implant, finite element method.

INTRODUCTION

Lumbar spinal fusion (LIF) has evolved as a treatment option for symptomatic spinal instability, spinal stenosis, spondylolisthesis, and degenerative scoliosis. TLIF is a posterior approach that places the interbody implant after the unilateral removal of the pars interarticularis and facet complex without violating the spinal canal. TLIF enables placement of the graft within the anterior of the disc space to restore lumbar lordosis. Implants have radiopaque marker pins to allow the exact position of the implant, during and after surgeries (Skovrlj, 2015) which increases radiation exposure. The chief advantages of the TLIF procedure include an improvement in lordotic alignment due to graft placement within the anterior column, decrease in potential neurological injury, and preservation of posterior column integrity and the posterior and anterior longitudinal ligaments (Cole, 2009).

METHODS

A finite element model of the L5-S1 FSU was created using computer tomography images. In order to define the geometry of the two vertebrae surface, Mimics software (version 10.0, Materialise Inc., Belgium) was used. Then the smoothed surface was imported into Abaqus/CAE (2007) software to perform meshing with four node tetrahedral elements C3D4 and finite element analysis. The definition of the intervertebral disc of the L5-S1 FSU was performed using the intervertebral space between the two vertebrae and lower surface of L5 and the upper surface of S1 geometries. Then ligaments were modelled using tension-only spring connector elements, truss elements T3D2, and intervertebral joint layers were meshed with eight-noded hexahedral elements and a hybrid formulation C3D8H.

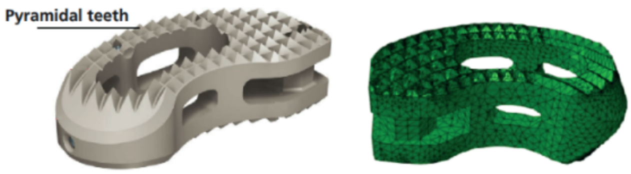

Fig. 1 - TPal Cage anatomic shape and finite element mesh

Fig. 1 shows T-Pal cage (DePuy Synthes GmbH) geometry characterized by 28 mm length, insertion depth 10 mm, total depth 14 mm, 11 mm thickness and a lordotic angulation equal to 0º. It is manufactured with a biocompatible polymer (PEEK) with Titanium alloy marker pins. It was modelled with 14217 nodes and 65775 four node tetrahedrical elements, C3D4. In order to make possible the T-PAL cage insertion, a discectomy was performed at the L5-S1 FSU level: the left inferior facet joint of L5 and the superior facet joint of S1 were removed and considering the intervertebral disk only 1/3 of the annulus fibrosus was preserved. Consequently, left facet capsular ligament was not considered in this model. Before implant insertion, the central window and the anterior disk space were filled with autogenous bone graft to improve fusion rate. Fig. 2 shows the finite element model of the TLIF considering supplemental fixation.

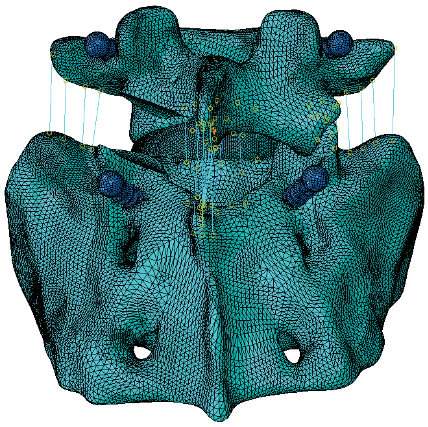

Fig. 2 – L5-S1 transforaminal lumbar interbody fusion finite element model

ACKNOWLEDGMENTS

The authors gratefully acknowledge the funding by FCT, Portugal, the Research Unit of LAETA-INEGI, Engineering Faculty of University of Porto, and to Dr. Maia Golçalves of Hospital da Luz Arrábida**.**

REFERENCES

Cole CD, McCall TD, Schmidt MH, Dailey AT. Comparison of low back fusion techniques: transforaminal lumbar interbody fusion (TLIF) or posterior lumbar interbody fusion (PLIF) approaches. Curr Rev Musculoskelet Med, 2009, 2, p.118–126.

Skovrlj B. 2015. Minimally invasive procedures on the lumbar spine. World J Clin Cases, 2015, 3(1), p. 1–9.

PAPER REF: 065

NUMERICAL MODELING AND EXPERIMENTAL INVESTIGATION OF PROTECTIVE PROPERTIES OF 3D-PRINTED SHIELDS REINFORCED WITH ARAMID FIBER AGAINST LOW VELOCITY IMPACTORS

Roman Cherepanov[1,2(*)], Yuriy Dontsov[1], Maxim Krinitsyn[1], Vasiliy Fedorov[1], Maxim Gustomyasov[1].

[1] National Research Tomsk Polytechnic University, Tomsk, Russia

[2] Tomsk scientific center, Sibirian branch of Russian Academy of Science. Tomsk, Russia.

[(*)]*Email:* RCherepanov82@gmail.com

ABSTRACT

This work proposes a model for prediction of protective properties of 3d-printed plastic shield reinforced with aramid fiber against low velocity debris generated in a process of electric motor destruction. Results of numerical computations and comparison with experimental data presented.

Keywords: 3D-print, protection, destruction, reinforcement fiber, shield.

INTRODUCTION

There is erosion phenomena associated with destruction of technical equipment. This phenomenon produces low velocity debris that is potentially dangerous to personnel. Creating protection against such debris is an important task. This paper is dedicated to research of protective properties of 3D-printed shields reinforced with aramid fiber against debris produced at electrical motor destruction process. 3D-printed plastic shields and cases is cheap, fast manufactured and effective elements of cases for electrical equipment, but low strength is one of important disadvantages of this technology. Reinforcement fibers are widely used to improve strength of additively manufactured plastic products and it is important task to optimize cost when manufacturing fiber reinforced products. This leads to importance of theoretical investigation of fiber reinforced 3D-printed products and to importance of numerical models for prediction of strength properties of reinforced 3D-printed plastic materials.

RESULTS

This paper presents a numerical method for modeling of destruction of fiber reinforced plastic for low deformation rates which is typical for low velocity impact in application to protection of technical equipment.

Proposed model uses smooth particle hydrodynamics [1,2] as computational base. Restoring of particle consistency [3] improves approximation accuracy. Reinforcement fiber are modeled as 1D strings with given strength, acting as anisotropic reinforcement factor. This reinforcement fibers connects computational nodes (smoothed particles) in long lines and acts as additional forces for this nodes.

It allow to represent full stress in material of matrix as two parts

$$\sigma = \sigma_m + \sigma_F \tag{1}$$

where σ_m – stress in isotropic plastic materials of matrix, σ_F – highly anisotropic stress in fibers.

A criterion of destruction for this media also splits for two parts:

$$\left[f_1\left(\sigma_m, Y_m\right) < 0 \right] \vee \left[f_1\left(\sigma_F, Y_F\right) < 0 \right] \tag{2}$$

where f - destruction functional, Y_m, Y_F - critical stress of destruction for plastic matrix and reinforcement fibers respectively.

In our model we do not take into account slippage of the fibers relative to the plastic matrix.

Destruction of fiber lead to redistribution of stresses in local point. Due to high difference in elastic modulus of fiber and plastic, it is reasonable to assume that after fiber break corresponding parts of fiber relax and stretch matrix near point of break. Corresponding deformations of matrix should compensate elastic energy of cracked fiber, and therefore additional deformation of matrix near point of crack get form of:

$$\delta\varepsilon_{ij} = \frac{3 d_i d_j}{4\pi H^3} \cdot \sqrt{\delta E_{fiber} \cdot S_{ijkl} \left(d_i d_j \right)^{-1} \left(d_k d_l \right)^{-1}} \tag{3}$$

where $\delta\varepsilon_{ij}$ – additional deformations of plastic matrix, δE_{fiber} – released energy of fiber, S_{ijkl} – compliance modulus of plastic matrix, d_i – components of vector of fiber direction, H – radius of influence of fiber break. This additional deformation lead to local stress change near point of fiber break and may initiate plastic flow of matrix.

CONCLUSIONS

Computational results of proposed model was compared with experimental data of shield destruction for different count of reinforcement fibers and quantitative agreement is observed.

REFERENCES

[1] Li Shaofan, Liu Wing Kam, Meshfree Particle Methods, Springer Science & Business Media, 2007, 502p.

[2] R .A. Gingold, J.J. Monaghan, Smoothed particle hydrodynamics: theory and application to non-spherical stars, Mon. Not. R. Astron. Soc. 181 (1977) 375–389

[3] M.B. Liu, G.R. Liu, Restoring particle consistency in smoothed particle hydrodynamics Appl. Numer. Math., 56 (2006), pp. 19–36

PAPER REF: 066

STUDY OF MASS-INERTIAL CHARACTERISTICS OF MALES IN BASIC POSITIONS OF THE BODY

Gergana Nikolova[1(*)], Vladimir Kotev[2], Daniel Dantchev[1]

[1]Institute of Mechanics, Bulgarian Academy of Sciences, Acad. G. Bonchev Str. Bl. 4, 1113 Sofia, Bulgaria
[2]University of National and World Economy, Student Town, UNWE, 1700, Sofia, Bulgaria
[(*)]*Email:* gergana1973@gmail.com

ABSTRACT

The purpose of the present paper is to propose a 16-segmental biomechanical model of the Bulgarian male and to determine the mass-inertial characteristics of the body based on anthropometric parameters available in the literature. In addition, we provide a 3D generation of the model within SolidWorks media. The computer realization allows the determination of the mass-inertial characteristics of the body in any position of interest. We report data for two selected such positions. The basic idea of the study is to support mainly sports, rehabilitation, ergonomics and human body motion in microgravity.

Keywords: biomechanics, human body modeling, mass-inertial characteristics, CAD design.

INTRODUCTION

The human movement is a subject of analysis from ancient times. To do this analysis scientifically grounded, one obviously needs knowledge of geometric and mass-inertial characteristics of the body, as well as of the various segments of the human body. This field of research has been the subject of intensive simulations and mathematical modeling, see, e.g., (Hanavan, 1964; Winter, 2009; Herman, 2016).

In the current article, we propose an approach to the problem based on a mathematical model realized in a suitable computer media. The design of the 3D model of the human body needs knowledge of anthropometry and biomechanics. One should successively solve specific problems, related to i) proper body decomposition; ii) select of necessary anthropometric points; iii) organization of data that give the geometrical and mass-inertial characteristics of the human body and its segments; iv) model generation within a CAD system (e.g. SolidWorks); v) verification of the model via analytical results. The 3D model should allow performing fast individualization using a small range of parameters that could be easily determined. In the current study, we suggest such a model and provide data for the mass-inertial parameters of the human body in two basic positions and compare our results with those accessible from the literature. In order to do that we are going to use a realization of the model within a CAD system - Solid Works.

RESULTS AND CONCLUSIONS

We use a mathematical model of the human body explained in detail in (Nikolova, 2007). There this model has been used to define the mass inertial parameters of the different segments of the body. The model encompasses 16 segments representing: head + neck, the upper, middle and lower part of the torso, thigh, shank, foot, upper arm, lower arm, and hand, assumed to be relatively simple geometrical bodies. We accept full body symmetry with respect to the sagittal plane. The geometrical data needed is taken from a detailed anthropological investigation of the Bulgarian population (Yordanov, 2006). A total of 2435 males were measured. We take the average values and design a model, which represents the so defined average Bulgarian male. After determining the mass inertial parameters of the segments, one can also study the corresponding characteristics of the total body assuming the body to be in each position of interest.

With the aim of realizing the goals described above, we have accomplished a realization of the model in the CAD system – SolidWorks. We have verified the computer realization by comparing the results it delivers for the mass-inertial parameters of the segments of the body with those reported in (Nikolova, 2007). The program reproduces segment-by-segment data about volume, mass, center of mass and moments of inertia. That gives us confidence that this model could be used to calculate these characteristics at different body positions of the body. The basic positions of the body have been classified long ago in the literature – see, e.g., (Hanavan, 1964). NASA has classified eight principal body position of interest. Here, we will present data for two of these positions: the so-called “standing position” and the so-called “relaxed (weightless)”. Wherever possible we present a comparison of our results with data available in the literature for other Caucasian men. The inspection shows a reasonably good agreement between our results and those previously reported in the literature.

Let us finally stress, that the model proposed can be used in related sport, rehabilitation, and ergonomics. It can be applied also in other areas such as simulation of the human behavior in space, medicine (orthopedics, orthotics and prosthetics design), criminology and other areas.

ACKNOWLEDGMENTS

The authors gratefully acknowledge the financial support by Bulgarian National Science Fund: Contract DN-07/5 “Study of anthropometric and mass-inertial characteristics of the Bulgarian men and women via mathematical models of the human body”.

REFERENCES

Hanavan, P A mathematical model of the human body. AMRL-TR-64-102. Aerospace Medical Research Laboratories, Wright-Patterson Air Force Base, Ohio, 1964.

NASA-STD-3000, The man_system integration standards, Anthropometry and biomechanics at: https://msis.jsc.nasa.gov/sections/section03.htm#3.2.1.

Nikolova G, Toshev Y. Estimation of male and female body segment parameters of the Bulgarian population using a 16-segmental mathematical model. Journal of Biomechanics, 2007, 40, p. 3700-3707.

Herman I. P. Physics of the Human Body. Springer, 2016.

Winter D.A., Biomechanics and Motor Control of Human Movement. 4th Edition, John Wiley & Sons, Hoboken, 2009.

Yordanov Y. et al. Anthropology of the Bulgarian population at the end of the 20-th century (30-40 years old persons). Professor Marin Drinov Academic Publishing House, Sofia, Bulgaria, 2006.

PAPER REF: 067

WINDING DEPOSITION METHOD OF ADDITIVE MANUFACTURING FOR FABRICATION OF FUNCTIONAL CYLINDRICAL PARTS

Toshitake Tateno[1(*)], Koki Jimbo[2] and Mitsuhiro Kosaka[3]

[1]Department of Mechanical Engineering Informatics, Meiji University, Kawasaki, Japan
[2]Graduate School of Meiji University, Kawasaki, Japan
[3]Koito Manufacturing Co., LTD., Tokyo, Japan
[(*)]*Email:* tateno@meiji.ac.jp

ABSTRACT

This work proposes a new deposition path for Fused Filament Fabrication (FFF) in Additive Manufacturing (AM). In the proposed method, a material is extruded from a nozzle on a rotating cylindrical bed to make a winding deposition, which is designed toward a different direction at each layer. This method can fabricate 3D parts without plane layer that lead to weakness between layers. Additionally, the method can adopt composite materials with continuous fiber strings for reinforcement, such as CFRP. In this study, a FFF machine was developed to realize the winding deposition and bending tests of cylindrical parts fabricated with this method were conducted. The experimental results showed that the parts have higher strength and toughness than that of conventional FFF methods. The proposed method is valuable in low-volume production for functional parts receiving heavy loads.

Keywords: additive manufacturing, fused filament fabrication, winding deposition.

INTRODUCTION

Additive Manufacturing (AM) has a lot of merits in low-volume production. Fused Filament Fabrication (FFF) is a well-known type of AM, where plastic material is extruded form a heated nozzle to a designed position. FFF machines are widely used for making not only prototypes but also practical functional parts such as aircraft parts. However, there is a problem as that the strength between extruded paths is weak. The problem exists even on CFRP AM machines, which use continuous carbon fiber with a plastic. There is two important conditions to avoid the problem. One is to use curved surface as a deposition layer. Another is to use different orientation path at each layer. Singamneni (Singamneni, 2012) proposed a curved layer fused deposition to ensure inter-road and inter-layer connectivity.

In this paper, winding deposition path is adopted because it can envelop a 3D object. In case of cylindrical parts, the winding FFF AM machine can be realized simply. The curved layer is achieved by using rotational cylindrical bed. The different orientation path is achieved by generating a different directional motion at each layer. The prototype machine was developed.

In order to confirm the effect of the winding deposition method, the experiments of bending test using a pipe shape object with a single material of ABS are conducted. The bed consists of a core part having a cylindrical shape and a sacrifice part having a pipe shape attached to the core part. The deposition in AM is performed on the surface of a sacrifice part. In the bending test, both the sacrifice part and the deposited object are treated as one test piece to avoid influence of removing operation on the surface of deposited object.

RESULTS AND CONCLUSIONS

Four types of pipe shape test pieces are fabricated with different winding orientation, of which the angles to the cross-sectional plane are 0˚, 13˚, 25˚, and 90˚. It is known that the bending strength of pipe shape objects deposited toward the longitudinal direction becomes weak (Tateno, 2016). Fig. 1 shows a photograph and the size of a test piece. The test results of typical test pieces for each winding orientation are shown in Fig. 2. They had similar stiffness, but the test piece of 25˚ had a significant result, in which the breaking load is about 40% stronger and the stroke at breaking point is approximately twice larger than that of 0˚. It is confirmed that the winding deposition method can fabricate objects compensate weakness between deposition paths in strength and toughness by fabrication with various direction paths.

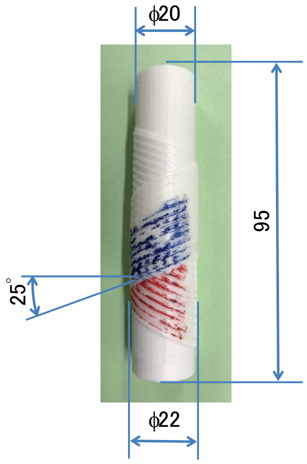

Fig. 1 Photograph of a test piece (25˚)

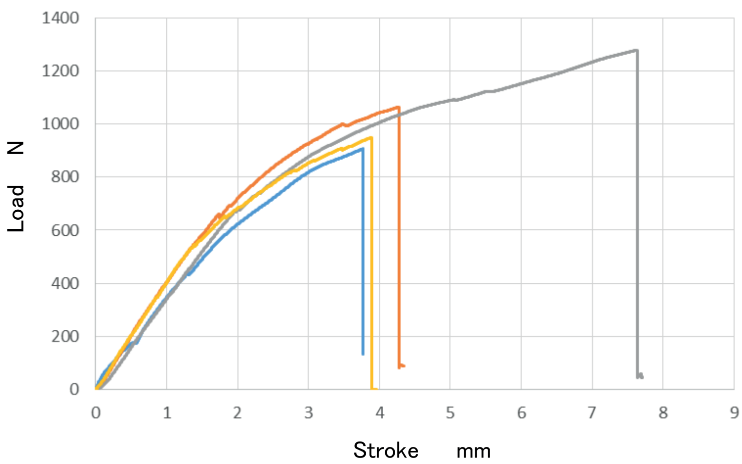

Fig. 2 3-points bending test results

Further tests should be performed to evaluate the effect of the winding orientation on mechanical properties qualitatively. The machine should be improved to use CFRP and to realize 5-axis motion for enveloping arbitral 3D convex shape objects.

ACKNOWLEDGMENTS

This work was supported by JSPS KAKENHI Grant Number 17K06126.

REFERENCES

Singamneni S, Roychoudhury A, Diegel O, Huang B, Modeling and evaluation of curved layer fused deposition, Journal of Materials Processing Technology, Vol.212, 2012 pp.27-35.

Tateno T, Yaguchi Y, Fujitsuka M, Study on parallel fabrication in additive manufacturing (Connector design considering anisotropic strength by deposition direction), Journal of Advanced Mechanical Design, Systems, and Manufacturing, Vol.10, No.7, 2016 Paper No.15-00716.

PAPER REF: 068

DESIGNING A HYBRID SAMPLER FOR GYNECOLOGICAL CANCER SCREENING

Paola Ulacia[1(*)], Lucy Gilbert[2], Ramses Galaz[3], Rosaire Mongrain[1]

[1]Department of Mechanical Engineering, McGill University, Montreal, Canada

[2]Department of Obstetrics & Gynaecology, Gynaecologic Oncology, McGill University Health Centre, Montreal, Canada

[3]GSE Biomedical, Hermosillo, Mexico

(*) *Email:* paola.ulaciaflores@mail.mcgill.ca

ABSTRACT

Ovarian and endometrial cancers are the deadliest gynecological cancers in women over 45 years of age with an overall survival rate of 46.5%. Available diagnostic tools are not specific or sensitive enough for early detection. We designed a triple modality hybrid sampling device for the collection of genetic material from the uterine cavity. Preliminary *in vitro* results show the device is safe for *in vivo* testing. Further *in vitro* testing is needed for performance validation prior to its use in an *in vivo* feasibility trial.

Keywords: medical devices, device design, device validation, liquid cytology, gynaecologic oncology, ovarian cancer.

INTRODUCTION

Ovarian and endometrial cancers are the deadliest gynecological cancers in women over 45 years of age with an overall survival rate of 46.5% (The American Cancer Society, 2018) (Ovarian Cancer Research Alliance, 2018). Current standards of care include CA125 test and transvaginal sonography (TVS) both of which are not specific and sensitive enough for the disease (Pinsky et al. n.d.) (Wang & al., 2018). Due to the low concentrations of tumoral DNA available in blood samples, liquid biopsies still yield a high number of false positives (Jung & Kirhcner, 2018).

Increasing tumoral DNA concentrations available in liquid cytology samples, could yield higher sensitivity and specificity rates due to a better sample quality. For this, we developed a minimally-invasive, triple modality hybrid sampling device, for the collection of genetic material from the uterine cavity, table 1 summarizes design specifications and criteria.

Ongoing *in-vitro* and *in-vivo* testing for safety and performance, include dislodgement tests for critical components, torquability, navigability, volume collection, sample quality, simulated use and determination of pain threshold (Table 1).

PRELIMINARY RESULTS AND CONCLUSIONS

Four concepts were generated to comply with design criteria and specifications. Two were selected for prototyping based on manufacturability. Materials were chosen for biocompatibility, manufacturability and regulatory compliance. All concepts comprise a tapered tip for cervical dilation, a soft surface for cell recovery, a suction port and a sheath for sample protection. Suction is achieved by means of a standard syringe (Fig 1).

Table 1 - Design criteria, specifications and associated tests

	Criteria	Target specification	Associated test
Efficacy[a,b]	*Volume collection*	≥ 0.1-0.5 mL	*In vitro* volume
	Sample quality	High DNA concentration	*Post In vivo* DNA quality
	Sample contamination	Minimize presence of cervical cells	*In vitro* simulated use[e]
	Suction	-150 to -349 mmHg	*In vitro* volume
Usability	*Ease of use*	Simple / No need of specialized training[c]	*In vitro* simulated use
	Pain reduction	≤ 3.5 on a 0-10 scale[d]	*In vitro* Pain threshold
	Affordable	Yes	NA — Cost analysis
	Reusable	No	NA
Technical	*Sterilization*	EO gas / Gamma rays	NA — Sterilization validation
	DNA interaction	Inert	NA — Material selection
	Biocompatibility	ISO 10993	NA — Material sourcing

[a] as per DOvEEgene Haloplex assay; [b] Target 99% Specific & 80% sensitive; [c] User perception questionnaire [d] Patient pain perception scale correlated to *in vitro* pain threshold test results; [e] Using a dedicated experimental setup.

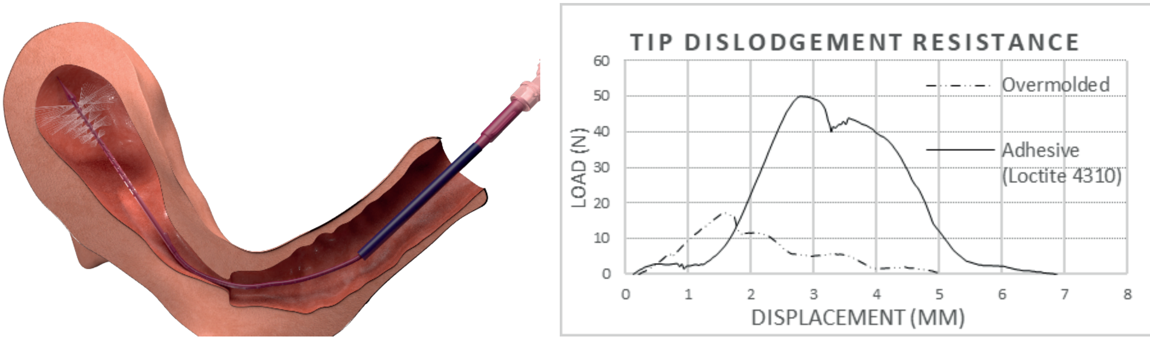

Fig. 1 – Left—Concept in utero. Right —Tip dislodgement test - Preliminary results

Preliminary results show the concepts are easily manufacturable and deployable. Ongoing analyses include cell collection efficiency assessment and navigability. Further testing is required for design optimization on the critical specification for intended use, using a dedicated experimental setup.

ACKNOWLEDGMENTS

The authors gratefully acknowledge the support from Ms. Valerie Josset and the Valerie Josset & Gary Aitken Cancer Research Award.

REFERENCES

Jung, A. & Kirhcner, T., 2018. Liquid Biopsy in Tumor Genetic Diagnosis. *Deutsches Arzteblatt International,* pp. 169-174.

Ovarian Cancer Research Alliance, 2018. *Statistics — Ovarian Cancer Research Alliance.* Available at: https://ocrahope.org/patients/about-ovarian-cancer/statistics/

The American Cancer Society, 2018. *Cancer Facts & Statistics.* Available at: https://cancerstatisticscenter.cancer.org/#!/cancer-site/Ovary

Wang, Y. & al., e., 2018. Evaluation of Liquid from the Papanicolaou Test and Other Liquid Biopsies for the Detection of Endometrial and Ovarian Cancers. *Science Translational Medicine,* p. eaap8793.

PAPER REF: 069

WASTE PRODUCTION AND MANAGEMENT IN THE STEEL SECTOR: A CASE STUDY

Veronica Novelli, Paola Geatti, Alice D'Odorico
Department of Economics and Statistics, University of Udine, Italy
[(*)]*Email:* veronica.novelli@uniud.it

ABSTRACT

The iron and steel manufacturing is considered one the most ancient activity of the human history, playing a strategic and fundamental role for the development of the world economy. The main goal of this paper is the implementation of an environmental management system of the steel sector, through the analysis of the organizational, technological and structural characteristics of a steel plant located in San Giorgio di Nogaro, in the province of Udine (Italy). According to the Directive 2010/75/EC, related to the industrial emissions of the "cast iron and steel production", and by the adoption of best practices, the plant is able to take care of the environment reducing the pollution.

Keywords: Steel production**,** emission law limits**,** environmental protection, waste management.

INTRODUCTION

Because of its availability, versatility (Foraboschi, 2016), limited cost, easy manufacturing, resistance to corrosion, excellent mechanical characteristics and recyclability, steel is one of the favourite materials of the industrial sectors (Blair M., Stevens L., 1995). Furthermore, it is an essential material for those sectors involved in sustainable development for improving green economy: steel productive processes allow wide possibility of industrial synergies for an efficient use of resources, by the use of by-products and heat and energy recovery. Multiple recycling is an important aspect of steel (Brimacombe et al., 2005), nevertheless steel production has a great environmental impact (Its and Least 2017), generating solid, liquid and gaseous waste; it needs a high consume of energy, generates acoustic (Golmohammadi, et al. 2014) and electromagnetic pollution; furthermore, it constitutes a serious problem adversely affecting public health (Qing et al., 2015). Nunki Steel S.p.A., a plant operating in Friuli-Venezia Giulia region, is engaged to minimize its negative impact on environment, through the obtainment of ISO 14001 certification (2013), and other solutions that allow to improve the quality of the work and the environmental protection.

RESULTS AND CONCLUSIONS

Nunki Steel is an iron and steel plant that operates with an electric arc furnace, where steel ingots are manufactured from iron cast and iron scraps fusion. The ingots are principally destined to the forges belonging to the Group, but also to free market, in particular foreign market. The productive activity began in 2010, after the takeover of a previous iron and steel plant. This study concerns the waste management of the plant. Waste incoming are constituted by the metal scraps that can be received as End of Waste (EoW), (Directive 2008/98/EC); scrap-waste coming from European countries, submitted to control activities, before its transformation in EoW; iron scraps in quality of waste in simplified procedure, according to Ministerial Decree February

5th 1998. Waste typologies are classified according to the Directive 2008/98/EC (Revision 4 of Analisi Ambientale Iniziale-Initial Environmental Review). In Table 1 the main characteristics of some typology of waste produced by Nunki Steel plant from 2010 to 2015 are listed.

Table 1. Outgoing waste. Period 2010-2015

EWC*	Name	Physic state	Store	Origin	2010 kg	2011 kg	2012 kg	2013 kg	2014 kg	2015 kg
100202	Not treated slags	Solid	Heaps	Ladle Furnace (LF)-prod.	-	2,834,740	2,133,760	3,850,090	4,181,510	5,371,220
100207	Solid waste from fumes with dangerous substances	Solid	Silo	Fume treatment plant	-	1,079,000	914,270	1,304,420	1,174,170	2,077,980
100903	Fusion slags	Solid	Heaps	Electric arc furnace/LF- prod.	470,740	7,379,320	5,851,230	12,366,520	11,656,840	12,927,880
130208	Exhaust oils, others oils for gears and oiling	Liquid	Oils store-covered and floored area	Maintenance	-	37,650	16,040	2,780	1,620	1,520
150103	Wood packaging	Solid	Melted in container	Logistics	34,160	49,340	28,500	100,860	83,500	85,800
170405	Iron and steel	Solid	Heaps	Maintenance, production	398, 800	121,750	55,970	2,050,220	1,619,340	1,276,710

*EWC= European Waste Catalogue

In addition to law requirements, the plant has achieved positive goals related to the environmental protection, realizing important activities to reduce its pollution. Among them, the system of thermo-resistances and insulation on the hoppers of bag filter and the extractor hood, to reduce the diffused emissions, the re-use of iron scraps coming from close industrial activities, the realization of a new partition wall, to improve the acoustic insulation. These solutions improve the quality of work and at the same time the environmental protection.

REFERENCES

Blair M, Stevens L. Steel Castings Handbook. ASM International, 1995.

Brimacombe L, Coleman N, Honess C. Recycling, reuse and sustainability of steel. Millennium Steel, 2005, p. 31-36.

EC Directive, 2008. Directive 2008/98/EC of the European Parliament and of the Council of 19 November 2008 on waste and repealing certain Directives.

Foraboschi P. Versatility of steel in correcting construction deficiencies and in seismic retrofitting of RC buildings. Journal of Building Engineering, 2016, p. 107-122.

Golmohammadi R, Giahi O, Aliabadi M, Darvishi E. An Intervention for Noise Control of Blast Furnace in Steel Industry. Journal of Research in Health Science, 2015, 14(4), p. 287-290.

Its WR, Least EBA. The road from Paris: the European Union's progress towards its climate pledge. Natural Resources Defence Council (NRDC), 2017, on line at: https://www.nrdc.org/sites/default/files/parisclimate-agreement-progress-2017-eu-ib.pdf

Ministerial Decree, 1998. Ministerial Decree February 5th 1998. Individuation of not dangerous waste submitted to simplified recovery procedures according Articles n°31 and 33 of Legislative Decree 22/1997.

Qing X, Yutong Z, Shenggao L. Assessment of heavy metal pollution and human health risk in urban soils of steel industrial city (Anshan), Liaoning, Northeast China. Ecotoxicology and Environmental Safety, 2015, 120, p. 377-385.

PAPER REF: 070

ANTHROPOMETRIC DIMENSIONS AND MODEL ESTIMATION OF MASS-INERTIAL PARAMETERS OF THE HUMAN UPPER AND LOWER EXTREMITIES

Gergana Nikolova[1], Vladimir Kotev[1,2(*)], Daniel Dantchev[1]

[1]Institute of Mechanics, Bulgarian Academy of Sciences, Acad. G. Bonchev Str. Bl. 4, 1113 Sofia, Bulgaria
[2]University of National and World Economy, Student Town, UNWE, 1700, Sofia, Bulgaria
[(*)]*Email:* vladokotev@gmail.com

ABSTRACT

We present an approach for determining the mass-inertial parameters of the upper and lower arm, thigh and shank of the human body using 3D geometrical modeling. The method is based on our own anthropometric measurements of 100 Bulgarian men that complement the representative anthropological investigation (Yordanov, 2006) of 2435 males of the Bulgarian population aged 30-40 years. These additional measurements are needed for the determination of some of the parameters of the geometrical bodies involved in the model. The segments are modeled via three-dimensional versions of right elliptical stadium solids. The comparison performed between our model results and data reported in literature demonstrates that the suggested modeling is successful being closer to the real shape of the segments envisaged.

Keywords: body segment parameters, anthropometry, 3D human body modeling.

INTRODUCTION

The biomechanical analysis of human movement demands knowledge of the geometric and mass-inertial properties of the body segments. Different methods for estimation of the parameters of the human body are available, e.g., geometrical modeling techniques representing the shape of body segments by means of standard geometric solids (Yeadon, 1990; Zatsiorsky, 2002). In the current study, we present a specific 16-segmental simplified 3D biomechanical model of the human body, which provides a possibility to calculate the mass-inertial parameters of all segments of the body. The main purpose of the present article is to improve the 16-segmental mathematical model of the human body of the average Bulgarian man and woman (Nikolova, 2007) by modeling the upper arm, lower arm, thigh and shank with versions of right elliptical stadium solids instead of using the frustum of a cone.

We begin with a 3D model of the human body which consists of 16 segments (Zatsiorsky, 2002; Nikolova, 2007): head + neck, upper part of torso, middle part of torso, lower part of torso, thigh, shank, foot, upper arm, lower arm, and hand, assumed to be relatively simple geometrical bodies. The explanation how one determines the numerical values of the geometrical parameters, the choice of the anthropometric landmarks, the way the segments are modeled, etc., is described in (Nikolova, 2007), to which we refer the interested reader for details. However, in the model used in the current study, we change the geometrical modeling of the thigh, shank, upper and lower arm representing them via three-dimensional versions of right elliptical stadium solids. Furthermore, we compare the results of the new model with data from literature and verify that the model suggested describes the inertial parameters of changed segments better than the model used in (Nikolova, 2007).

RESULTS AND CONCLUSIONS

In (Nikolova, 2007) the main part of the geometrical data needed to determine the geometrical parameters of the segments of the body is taken from a detailed representative anthropological investigation of the Bulgarian population (Yordanov, 2006) where the authors measured a total of 2435 males. Unfortunately, the data collected does not include all the data needed to model the thigh, shank, upper and the lower arm as right elliptical solids. For that reason, we made our own complementary anthropometric measurements of these segments on additional 100 Bulgarian men. The average data for the directly measured independent geometrical parameters of these segments, as well as their standard and mean deviations are summarized. These average values define the so-called average man - height 1.71.m and weight 77.7 kg.

Using the novel experimental data measured and the analytical properties of the solid bodies involved in modeling the segments of the human body, we calculate the volumes, masses, the positions of the centers of the masses and the corresponding principal moments of inertia of the average Bulgarian man. The model used can be considered as a modification of the one applied in (Nikolova, 2007) along with some suggestions made in (Yeadon, 1990). Let us stress that in this new model we found the geometrical parameters of the body segments approximating them by elliptical solids, which are closer to the real shape of some of the segments of the human body. For these geometrical bodies, we derived analytically, and estimated numerically, the positions of the segment mass centers, as well as their inertial characteristics. The comparison between our simple model results and those experimentally found and reported in the available literature for other Caucasian allows us to conclude an, in general, very good agreement. The method, described above, has been applied to the “average” Bulgarian man aged 30-40 years. We do not use any regression equations or adjustments of the measured parameters. The last leads to an interesting advantage, namely that our approach shall be working reasonably well also for determination of the corresponding characteristics of a given specific individual, and not only to the “average person”, provided some relatively simple geometrical measurements for this individual are performed.

ACKNOWLEDGMENTS

The authors gratefully acknowledge the financial support by Bulgarian National Science Fund: Contract DN-07/5 “Study of anthropometric and mass-inertial characteristics of the Bulgarian men and women via mathematical models of the human body”.

REFERENCES

Nikolova G, Toshev Y. Estimation of male and female body segment parameters of the Bulgarian population using a 16-segmental mathematical model. Journal of Biomechanics, 2007, 40, p. 3700-3707.

Yeadon MR. The simulation of aerial movement-II. A mathematical inertia model of the human body. Journal of Biomechanics, 1990, 23, p. 67-74.

Yordanov Y. et al. Anthropology of the Bulgarian population at the end of the 20-th century (30-40 years old persons). Prof. M. Drinov Academic Publishing House, Sofia, 2006.

Zatsiorsky VM. Kinetics of human motion. Human Kinetics, Champaign, IL, 2002.

PAPER REF: 071

WALL SHEAR STRESS DESCRIPTION IN PATIENT-SPECIFIC RIGHT CORONARY ARTERIES WITH STENOSIS – CFD

I.S. Saraiva[1], C.F. Castro[1,2], C.C. António[1,2], R. Ladeiras-Lopes[3,4], N.D. Ferreira[4], N. Bettencourt[3], L.C. Sousa[1,2], S.I.S. Pinto[1,2(*)]

[1]Engineering Faculty, University of Porto, Porto, Portugal
[2]Institute of Science and Innovation in Mechanical and Industrial Engineering (LAETA-INEGI), Porto, Portugal
[3]Cardiovascular R&D Unit, Faculty of Medicine, University of Porto, Porto, Portugal
[4]Department of Cardiology, Gaia/Espinho Hospital Centre, Vila Nova de Gaia, Portugal
[(*)]*Email:* spinto@fe.up.pt

ABSTRACT

The present work shows the relative residence time spatial distribution, the strongest metric of hemodynamic descriptors for assessing atherosclerotic plaque formation, for completely different patient cases: different geometry configuration, different percentage of lumen stenosis and different locations of the stenosis. The stenosis tends to increase, even more, when located between two side-branch bifurcations. Moreover, locations with high roughness have a high tendency to atherosclerosis appearance.

Keywords: right coronary artery, stenosis, hemodynamics, wall shear stress-based descriptors, computational fluid dynamics.

INTRODUCTION

Cardiovascular diseases have been one of the leading causes of mortality in developed countries (Mozaffarian et al. 2015). Atherosclerosis develops due to the accumulation of lipoproteins in the arterial wall and the migration of smooth muscle cells to the intima and leukocyte infiltration. Numerical studies of blood flow in patient-specific right coronary arteries (RCA) with atherosclerosis has not been well explored in the literature, probably, due to the extremely irregular geometry of the main artery, of its side-branches and of the atherosclerotic plaque. Myers et al. 2001 suggested that the hemodynamic behaviour of the RCA complex geometry is dominated by its geometric configuration. However, a detailed study of the hemodynamic in patient-specific RCAs with atherosclerosis is still a challenge in the diagnosis and treatment of atherosclerotic disease.

The use of geometric models of the RCA, with its side-branches and atherosclerotic plaque, as close as possible to reality is essential for simulations. Moreover, some authors have been used the Fluid-Structure Interaction (FSI) method, considering a deformable wall of the artery, during the cardiac cycle, for hemodynamic simulations (Zhou et al. 2018). However, when the differences considering deformable wall or rigid wall are not significant, FSI should not be used due to the high computational time.

The present work focuses on a detailed hemodynamic study of each patient-specific case with different percentage of lumen stenosis. The goal is to conclude about the tendency of atherosclerosis appearance around the stenosis depending on its location: near or far side-branch bifurcations. Since these patient-specific arteries have rigid atherosclerotic plaque, results considering rigid wall, with faster computational time, are considered accurate.

METHODOLOGY

The DICOM (*Digital Imaging and Communications in Medicine*) were provided by Vila Nova de Gaia / Espinho Hospital Centre. The patient-specific cases are males, mean age 54.7 ± 8.8 years old, with different locations and percentages of lumen stenosis in the right coronary artery: Patient 1 with 70% lumen stenosis far from bifurcations, Patient 2 with 20% lumen stenosis just before a bifurcation and Patient 3 with 40% lumen stenosis between two bifurcations. The computed tomography (CT) examinations were performed with a third generation 2 × 192-section dual-source CT system (SOMATOM Force; Siemens Healthcare Sector, Forchheim, Germany) and the mean effective radiation dose was 1.133 ± 0.2035 mSv.

The CT images were transferred and imported to *Mimics* software to start the segmentation process, for the 3D geometry reconstruction of the RCAs with its side-branches and atherosclerotic plaque. Therefore, a 3D mask was obtained (Fig. 1a) and imported to *3-Matic* software in order to reduce abnormalities (Fig. 1b) from the segmentation process. This method considers the non-modification of the specific configurations of the patient, namely the shape and anatomic dimensions.

Then, a uniform tetrahedral mesh was reconstructed in *Meshing Ansys* software, through a Path Independent method (Fig. 1c). The statistical parameter Skewness was used to verify the accuracy of the mesh. Following the *Ansys* tutorial, the mesh is accurate if the Maximum Skewness is lower than 0.95. Patient 1 has a Max. Skewness equal to 0.63, Patient 2 a Max. Skewness equal to 0.59 and Patient 3 a Max. Skewness equal to 0.60. So, all the meshes obtained were considered accurate for numerical simulations.

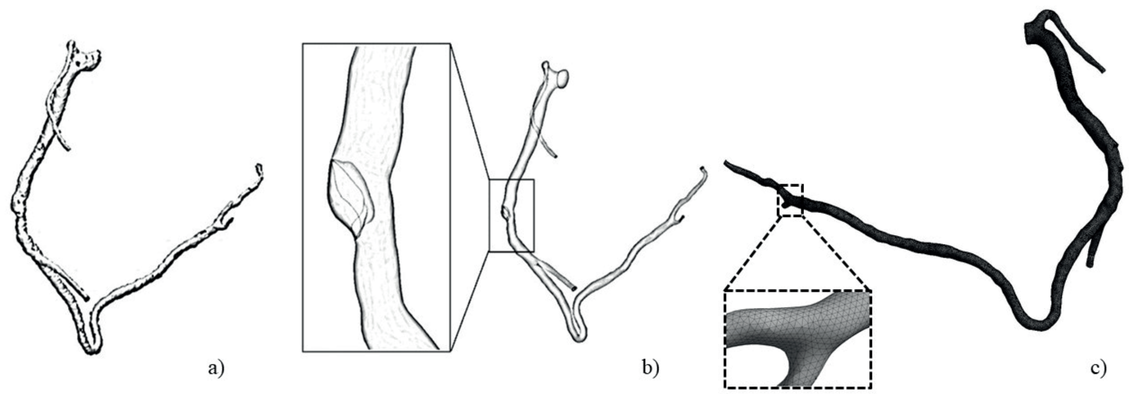

Fig. 1 – a) 3D mask obtained thought *Mimics* software, b) 3D geometric model of the RCA obtained after the minimization of abnormalities through *3-Matic* software, c) 3D mesh of the RCA obtained through *Meshing Ansys* software.

In the present work, blood was considered as isotropic, impressible and homogeneous fluid with the purely shear-thinning non-Newtonian property. Carreau model fits well this property for blood at 37ºC and parameters are defined in the literature (Yilmaz and Gundogdu 2008).

The inlet boundary condition, in Ostium, was a Womersley velocity profile, depending on the instant time of the cardiac cycle, the position at the inlet and the Womersley number ($\propto = R\sqrt{\frac{\rho\,\omega}{\mu}}$). Consequently, the Womersley number depends on the radius of the artery (R), the blood density (ρ), the cardiac frequency (ω) and the viscosity of blood (μ) at infinite shear rate. At the outlet branches, pressure profiles were taken into account depending on the instant time of the cardiac cycle and radius-independent. These boundary conditions were implemented in User-Defined Functions (UDFs) in *Ansys* software. Fig. 2 shows the mean velocity profile imposed at the inlet (ostium) and the pressure profile imposed at the outlet branches.

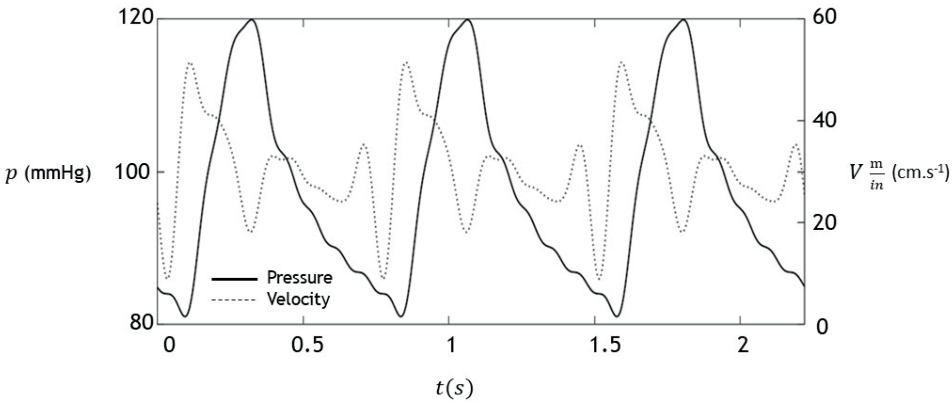

Fig. 2 - Mean velocity profile imposed at the inlet (ostium) and pressure profile imposed at the outlet branches.

Afterward, *Ansys* software was used to perform blood flow simulations. Navier–Stokes equations are solved considering a laminar flow. Reynolds number in the systolic peak, maximum velocity, has a maximum of 1000. The velocity–pressure coupled equations were solved by SIMPLE algorithm and the momentum equations were discretized by the second-order upwind scheme.

The time step size considered was 0.005 s/time step, the number of iterations for each time step was 20 and the time step number defined as 444, corresponding to the time of three cardiac cycles (3 cardiac cycles × 0.74 s/cardiac cycle = 2.22 s). The process is completed when the 444 time steps are achieved.

RESULTS AND CONCLUSIONS

The wall shear stress (WSS) hemodynamic descriptors - time average wall shear stress (TAWSS), oscillating shear index (OSI) and relative residence time (RRT) - highlight the tendency for atherosusceptible regions in patient-specific arteries. TAWSS lower than 0.4 Pa (Malek et al. 1999), OSI between 0.25 and 0.5 (Soulis and Fytanidis 2010) and RRT higher than 8 Pa^{-1} (Lee et al. 2009) indicate propitious regions to atherosclerosis development. Fig. 3 shows the relative residence time (RRT) spatial distribution, the most reliable metric for assessing atherosclerotic plaque formation (Knight et al. 2010), for the three right coronary arteries of the patients in study.

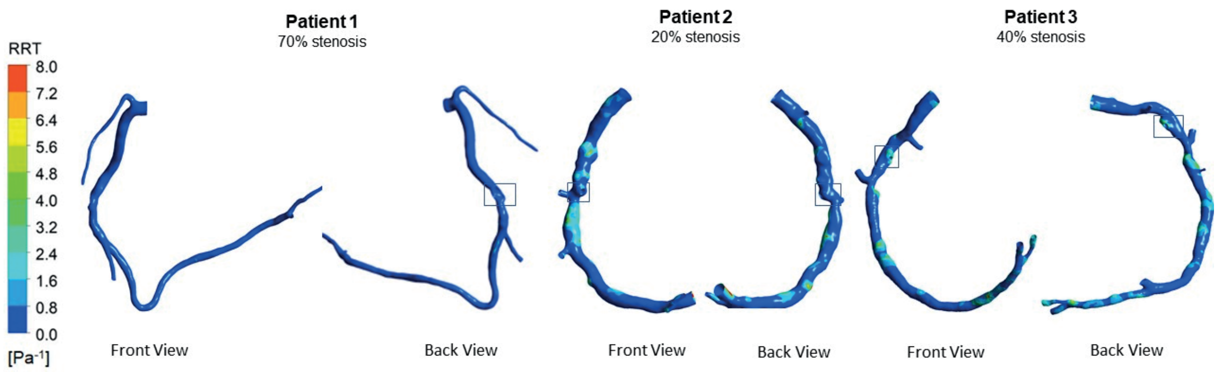

Fig. 3 – RRT spatial distribution for each patient-specific RCA with atherosclerotic plaque.

Regions closer to 8 Pa^{-1} are considered more propitious to atherosclerotic plaque formation (Lee et al. 2009). The highest tendency for atherosclerosis appearance around the stenosis occurs in Patient 3 since the 40% lumen stenosis is located near and between the first side-branch bifurcations. The tendency to increase the 20% lumen stenosis in Patient 2 is lower than in Patient 3. The stenosis of Patient 2 is found before the second side-branch and far from the first side-branch. Patient 1, with 70% of lumen stenosis, has no tendency to enlarge its stenosis due to the geometric configuration. The stenosis in Patient 1 is far from the bifurcations and the geometry has not roughness. However, this patient has, in reality, 70% of stenosis, perhaps, due to conventional risk factors (smoking, no physical activities, etc.). In order to obtain accurate conclusions about the influence of the geometric configuration in the tendency of atherosclerosis formation, the study should be further developed: study other patient-specific cases with different locations of the stenosis, study other degrees of the stenosis in the same patient, etc.

It is well-known that blood has complex properties: not only the shear-thinning but also the viscoelastic property. Therefore, in future work, authors should implement, in UDFs of *Ansys*, constitutive equations defining the viscoelastic property of blood. This property will certainly influence the wall shear stress based descriptors distribution in the patient-specific arteries, and so, influence critical regions prone to atherosclerosis appearance.

ACKNOWLEDGMENTS

Authors gratefully acknowledge the financial support by FCT, Portugal, the Engineering Faculty of University of Porto, the Institute of Science and Innovation in Mechanical and Industrial Engineering, the Cardiovascular R&D Unit of the Medicine Faculty of University of Porto and the Cardiology Department of Gaia/Espinho Hospital Centre.

REFERENCES

Knight J, Olgac U, Saur SC, Poulikakos D, Marshall W, Cattin PC, Alkadhi H, Kurtcuoglu V. Choosing the optimal wall shear parameter for the prediction of plaque location – A patient-specific computational study in human right coronary arteries. Atherosclerosis, 2010, 211, p. 445-450.

Lee S-W, Antiga L, Steinman DA. Correlations among indicators of disturbed flow at the normal carotid bifurcation. J. Biomech. Eng., 2009, 131, 061013.

Malek AM, Alper SL, Izumo S. Hemodynamic shear stress and its role in atherosclerosis. JAMA, 1999, 282, p. 2035-2042.

Mozaffarian D, Benjamin EJ, Go AS et al. Heart disease and stroke statistics. Circulation, 2015, 131, p. e29-322.

Myers JG, Moore JA, Ojha M, Johnston KW, Ethier CR. Factors influencing blood flow patterns in the human right coronary artery. Ann. Biomed. Eng., 2001, 29, p. 109-120.

Soulis JV, Fytanidis DK. Oscillating shear index, wall shear stress and low-density lipoprotein accumulation in human RCAs. Acad. Sci. USA, 2010, 32, p. 867-877.

Yilmaz F, Gundogdu MY. A critical review on blood flow in large arteries; relevance to blood rheology, viscosity models, and physiologic conditions. Korea-Australia Rheology Journal, 2008, 20, p. 197-211.

Zhou Y, Lee C, Wang J. The computational fluid dynamics analyses on hemodynamic characteristics in stenosed arterial models. J. Healthc. Eng., 2018, p. 1-6.

PAPER REF: 072

A NEW DESIGN FOR A MAGNETIC LEVITATION SYSTEM WITH HORIZONTAL MOVEMENT

R.J.S. Maia[1], P.T.C. Peixoto[3], S.I.S. Pinto[1,2(*)]

[1]Engineering Faculty, University of Porto, Porto, Portugal

[2]Institute of Science and Innovation in Mechanical and Industrial Engineering (LAETA-INEGI), Porto, Portugal

[3]Centre for Nanotechnology and Smart Materials (CeNTI), Vila Nova de Famalicão, Portugal

[(*)]*Email:* spinto@fe.up.pt

ABSTRACT

This work presents a developed design solution to produce a magnetic levitation system with horizontal movement, using permanent magnets. The permanent magnets on top of the rail create the necessary lift force, while lateral permanent magnets are responsible to control the position of the structure. The presented design was optimized in terms of dimensions and magnets to serve different applications, for example, an opening door system.

Keywords: Magnetic levitation, static levitation, horizontal movement, maglev, design.

INTRODUCTION

The conventional methods used in slide doors, windows or other types of structures that require horizontal movement are usually associated with great loss of power and material deterioration due to dissipative forces, such as friction. This problem can be solved with a magnetic levitation system, allowing the movement of heavy bodies with low propulsion forces and almost no need for maintenance combined with the low noise production. This system becomes a viable option to use at home, office or industrial environments (Hyung-Suk and Dong-Sung 2016, Yaghoubi 2013).

The developed design consists of using a track with incorporated permanent magnets that provide the required forces to levitating the intended object. By using only permanent magnets, a simpler structure was obtained. This structure does not need active control, discarding the use of sensors and computing resources, resulting in a low cost production and a functional system even when there is no electrical power available. It is expected to exist small oscillations since it is impossible to obtain a stable magnetic using only static forces, like magnetostatic, electrostatic or static gravitation forces, stated in the Earnshaw Theorem, developed in 1842 (Cazacu et al. 2014, Reusch 1994). However, considering that the developed system is designed to be used in structures like windows, doors and other simple moving structures, small and limited oscillations and vibrations does not require much of concern. They are compensated by the manufacturing cost reduction and the simplification of the installation process.

METHODOLOGY

In order to obtain the most efficient design, several magnetic levitation systems were created using *Solidworks* software and post analyzed using *Ansys 19.2* software, specifically the

Magnetostatic analysis system, existing in the *Workbench Ansys*, and Maxwell 3D of the electromagnetics package.

In the first place, the geometry was created in *Solidworks*, since it is user-friendly software to create complex designs. Then, the geometry was imported in IGS or STEP format to Workbench *Ansys*, where the materials of each component were defined. Since different materials interact differently with magnetic fields, bringing more variables into the project, it was chosen materials which have a reduced impact on magnetic forces (Hilzinger and Rodewald 2013). These materials are paramagnetic and have good mechanical properties that guarantee a safe usage, ending up using aluminum for the supports united to the structure intended to levitate and stainless steel for the rails. Regarding the magnets, it was chosen neodymium magnets, since they are the most powerful permanents magnets and can operate at higher temperature scales (Coey 2002), with a magnetization of grade N42. It is also important to emphasize that the top support of the structure was dimensioned regarding the tensions involved and possible deformations. It was also considered the thermal expansion of aluminum when subjected to variations of temperature it would be normally subjected when used in a house front.

Once the material selection is done, the simulation parameters were input. A region of air was created, distancing itself 200 mm of the edges in every direction. Using the Magnetostatic option, the static study was performed considering a general mesh of 1/3 mm associated with a refinement in critical areas. For the dynamic study, it was used the Maxwell 3D, considering a movement velocity of 60 mm/s.

After the running process of the simulations, in different equilibrium points, it is necessaire to validate the results. With that in mind, analytical methods and laboratory methods were used to verify the simulated results. As analytical methods, formulas from the classical literature like Maxwell, Gauss and Lorentz laws were taken into account. For the laboratory test, a 3D model was printed with scaled dimensions and, after the installation of the magnets, the magnetic fields were measured using Gauss probes.

RESULTS AND CONCLUSIONS

Fig.1 shows the created and optimized design for a magnetic levitation system with horizontal movement, using SolidWorks software. The system is projected to have an air gap of 5 mm, constant in the horizontal direction, and variable in the vertical direction, since the vertical gap depends on the weight lifted. It is also easy to substitute the magnets used if we intend greater lifting forces. The top rail is expected to be fixedly in a wall or some other stable structure, supporting the magnetic forces, while the lower rail can be mounted on the floor or embedded to be hidden, resulting in a more appealing appearance.

Due to the difficulty created by the determination of the magnetic fields and the lift forces created, it is important to establish certain operating ranges to a series of magnets, in order to prevent the necessity of calculation new magnetic fields and their lift forces.

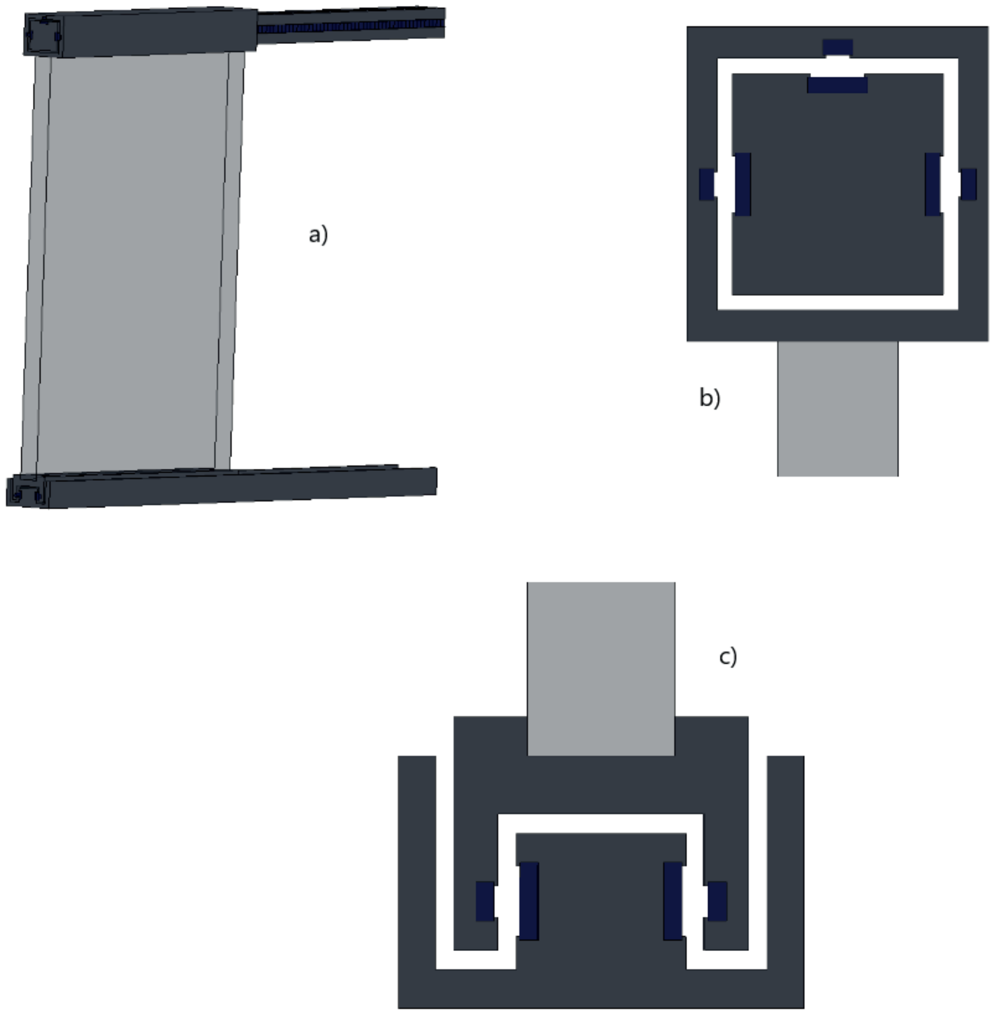

Fig. 1 - Magnetic Levitation System a) full view b) cut view, top rail c) cut view, lower rail.

The present configuration is designed to support 215 kg/m up to 280 kg/m. The biggest gap between the rails and the levitating structure is for the lowest weight (10 mm). The air gap is, also, as lowest as possible (0.2 mm) to the higher mass.

It is recommended using an air gap of 5 mm for the most stable configuration, corresponding to a levitation force of 226 kg/m. These results were validated by the analytical calculus, which was 240 kg/m for the air gap of 5 mm. The difference was small, only 5%, and can be explaining with the mesh used in the simulations. If the mesh was more refined, the simulated results would certainly be even more coherent. However, that was not possible because of the limitation of hardware resources.

The magnetic flux of the designed system is represented in Fig.2, where the maximum value is 0.935 T. This value does not represent a risk to humans, and therefore this type of structures can be implemented in offices, houses and similar environments.

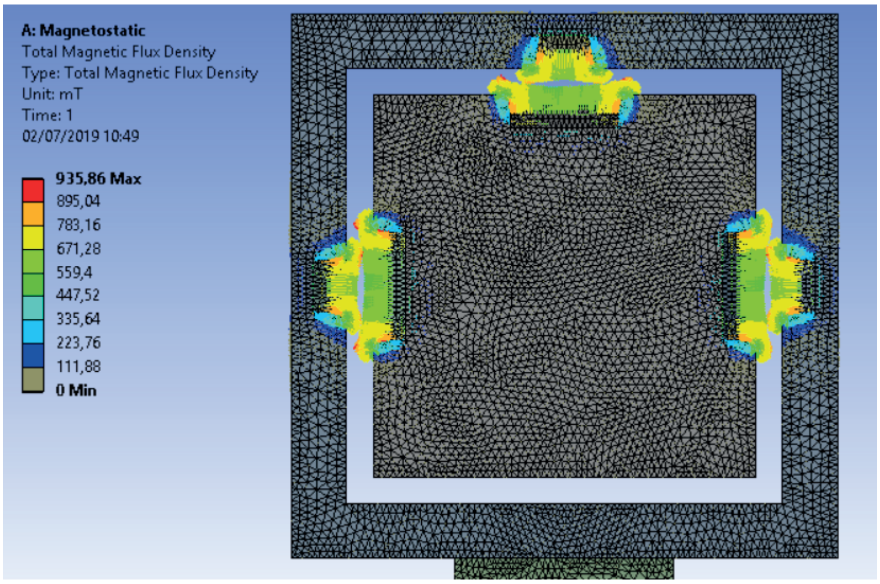

Fig. 2 - Magnetic Flux Density of the designed system

The design can also incorporate a system to automate the horizontal movement of the levitating structure using electromagnets (Long et al. 2011, Nam and Long 2013). This subject will be further analyzed and tested using computational mechanics and compared with conventional methods to evaluate its efficiency.

ACKNOWLEDGMENTS

Authors gratefully acknowledge the Engineering Faculty of University of Porto (FEUP), the Department of Mechanical Engineering (DeMEC) of FEUP, the Institute of Science and Innovation in Mechanical and Industrial Engineering (LAETA-INEGI) and the Centre for Nanotechnology and Smart Materials (CeNTI).

REFERENCES

Cazacu E, Maricaru M, Stanciulescu A, Stanculescu M. Escaping from Earnshaw Theorem,2014, pp. 59-65.

Coey JMD. Permanent magnet applications. Journal of Magnetism and Magnetic Materials, 2002, 248, p. 441–456

Hilzinger R, Rodewald W. Magnetic Materials: Fundamentals, Products, Properties, Applications. Wiley, 2013.

Hyung-Suk H, Dong-Sung K. Magnetic Levitation, 2016.

Long Z, He G, Xue S. Study of EDS & EMS Hybrid Suspension System With Permanent-Magnet Halbach Array. IEEE Transactions on Magnetics, 2011, 47, p. 4717-4724.

Nam K, Long G. Dynamic modelling of electromagnetic suspension system. Journal of Vibration and Control, 2013, p. 729-741.

Reusch MF. A problem related to Earnshaw's theorem. IEEE Transactions on Magnetics, 1994, 30, p. 1324–1326.

Yaghoubi H. The Most Important Maglev Applications. Journal of Engineering, 2013, p. 1-19.

PAPER REF: 073

EXPERIMENTAL MODAL ANALYSIS OF A FRICTION WELDED Al 6013-Al 7075 BIMATERIAL BEAM

Erhan Baysal[1], Oguz Kocar[2,3], H. Alper Ozyigit[2,3], Mehmet Yetmez[3(*)]

[1]Alapli Vocational School, Zonguldak Bulent Ecevit University, 67850 Zonguldak, Turkey
[2]Department of Mechatronics Engineering, Bulent Ecevit University, 67100 Zonguldak, Turkey
[3]Department of Mechanical Engineering, Bulent Ecevit University, 67100 Zonguldak, Turkey
[(*)]*Email:* yetmez@beun.edu.tr

ABSTRACT

In this study, modal analysis of a friction welded Al6013-Al7075 bimaterial aluminum alloy beam is considered. For this purpose, two different friction welding parameters (i.e., rotational speed and welding pressure) and two constant friction welding parameters (i.e., friction pressure and contact time) are taken into account. Effects of the speed and the welding pressure on the vibration characteristics/structural performances are examined experimentally. Vibration tests are performed to present free vibration characteristics of the bimaterial aluminum alloy beams under free-free boundary conditions. Results are given in tabular and graphical forms.

Keywords: friction welding, bimaterial, modal analysis, displacement response function.

INTRODUCTION

There are many studies on friction welded materials in structures. On one hand, according to mechanical control of a friction welded beam, design works indicate that the boundary conditions are very important key whether natural frequencies of a component of the beam tend to be reduced by dissimilar material zone. Many procedures are used to analysis modal stresses of such those structures with respect to optimization procedures (Vigneshwar, 2018). On the other hand, it can be noted that due to the bimaterial effect, behavior of displacement response function is of great importance. Normalized fundamental natural frequency, normalized displacement response function and normalized damping ratio values with respect to each material are actually main important parameters of a friction welded Al 6013-Al 7075 bimaterial aluminum alloy beam to understand variations of vibration characteristics in frequency domain (Ahmad, 2009).

In this study, modal analysis of a friction welded Al6013-Al7075 bimaterial aluminum alloy beam is considered. For this purpose, two different friction welding parameters (i.e., rotational speed and welding pressure) and two constant friction welding parameters (i.e., friction pressure and contact time) are taken into account. Effects of the speed and the welding pressure on the vibration characteristics/structural performances are examined experimentally. Vibration tests are performed to present free vibration characteristics of the bimaterial aluminum alloy beams under free-free boundary conditions.

MATERIALS AND METHOD

Friction welded Al6063-Al7075 bimaterial beams possess welding location at the middle of the beams. Each circular bimaterial beam with 30 mm in diameter is 300 mm in length.

Consequently, half of the beam is Al6063 and the other part is Al7075. According to friction welding parameters, eight bimaterial beam groups are taken into consideration. Details of the welding parameters of the bimaterial beam groups are given in Table 1.

Table 1 – Friction welding parameters of the bimaterial beam groups.

Group #	**Welding pressure (MPa)**	**Friction pressure (MPa)**	**Contact time (s)**	**Rotational speed (rpm)**
1	3	1.4	10	1000
2	1	1.4	10	1000
3	5	1.4	10	1000
4	10	1.4	10	1000
5	3	1.4	10	2000
6	1	1.4	10	2000
7	5	1.4	10	2000
8	10	1.4	10	2000

Vibration measurements are conducted such a way that an impact hammer with a force transducer (Model No: 5800B2, Dytran Instruments, Inc., USA) is used to excite the welded Al6063-Al7075 bimaterial beams through the selected node. After the excitations, the responses are obtained by an accelerometer (Model No: 3093B, Dytran Instruments, Inc., USA). The vibration measurements are completed using a microprocessor-based data acquisition system, namely SoMat™ eDAQ-lite and nCode GlyphWorks software (HBM, Inc., USA).

RESULTS AND CONCLUSION

Mean values of all results are normalized by the results of control groups Al6013 cylindrical aluminium beam (ω=4.98 Hz, X(ω)= 10.4E-9 and ζ=0.95 Hz/Hz) and Al7075 cylindrical aluminium beam (ω=4.92 Hz, X(ω)= 14.4E-9 and ζ=0.97 Hz/Hz) respectively.

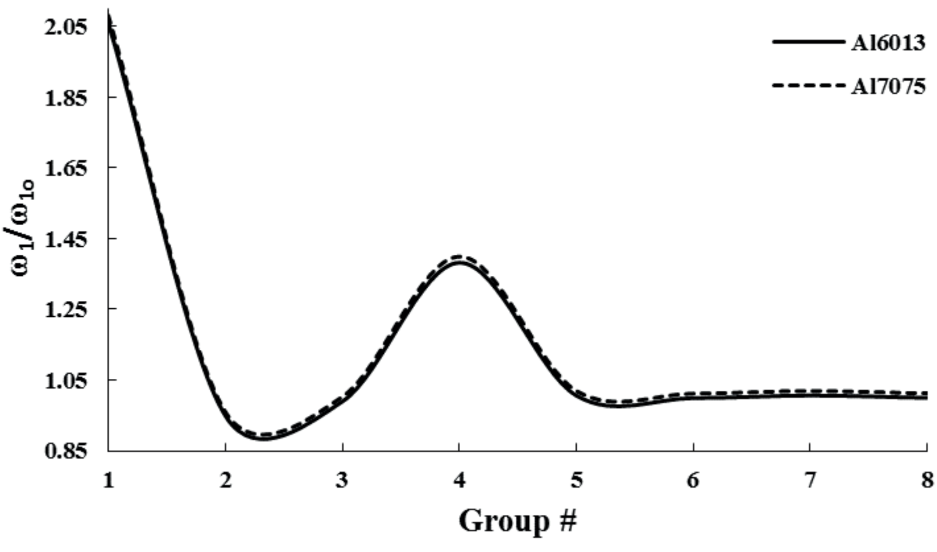

Figure 1. Variation of fundamental natural frequency values with the bimaterial beam groups.

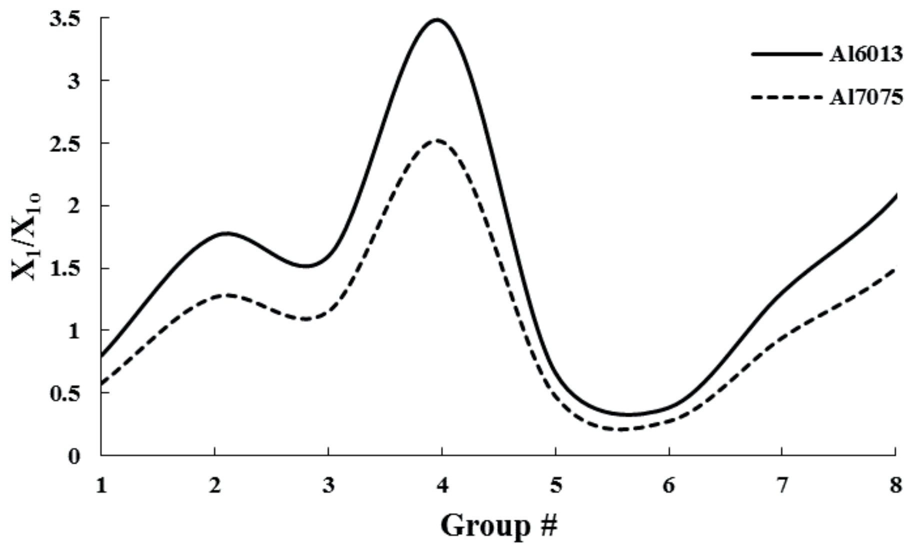

Figure 2. Variation of displacement response function values with the bimaterial beam groups.

Variation of fundamental natural frequency values with the bimaterial beam groups are given in Figure 1. It is clearly seen that (i) rotational speed influences the effect of welding pressure, (ii) variation of welding pressure does not affect the fundamental natural frequency under rotational speed of 2000rpm, (iii) variation of welding pressure directly affect the fundamental natural frequency in a fluctuating trend under rotational speed of 1000 rpm.

Variation of displacement response function values with the bimaterial beam groups are given in Figure 2. It is noted that (i) rotational speed influences the effect of welding pressure, (ii) variation of welding pressure affect the displacement response function values linearly under rotational speed of 2000rpm, (iii) similar with the behavior in Figure 1, variation of welding pressure affect the displacement response function values in a fluctuating trend under rotational speed of 1000 rpm.

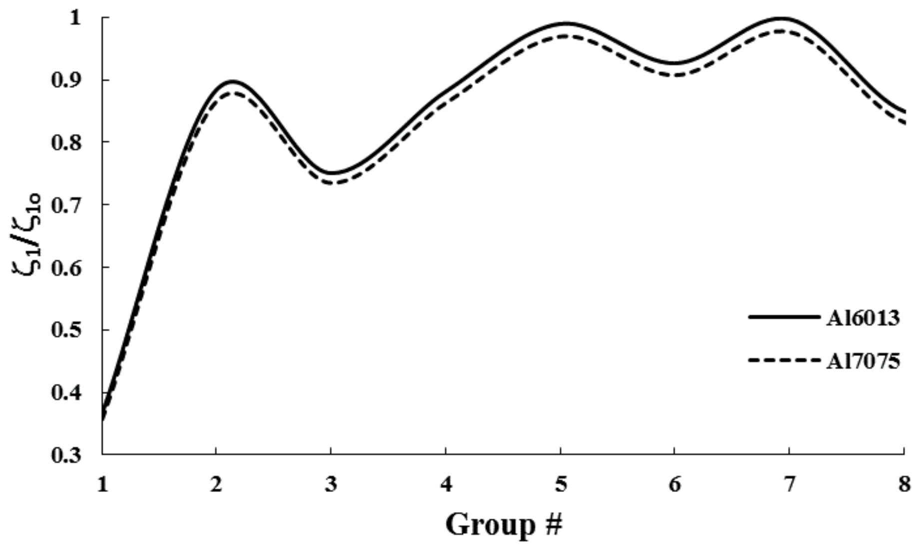

Figure 3. Variation of damping ratio values with the bimaterial beam groups.

Variation of damping ratio values with the bimaterial beam groups are given in Figure 3. It is concluded that (i) rotational speed influences the effect of welding pressure, (ii) variation of welding pressure affect the damping ratio values in sinusoidal trend under rotational speed of 2000rpm, (iii) similar to the behavior in both Figure 1 and 2, variation of welding pressure affect the displacement response function values in a fluctuating trend under rotational speed of 1000 rpm.

REFERENCES

Vigneshwar M, Selvamani ST, Hariprasath P, Palanikumar K. Analysis of mechanical, metallurgical and fatigue behaviour of friction welded AA6061-AA2024 dissimilar aluminium alloys in optimized condition. Materials Today: Proceedings, 2018, 5, p.7853-7863.

Ahmad Z, Abdul Aleem BJ. The effect of inhibitors on the susceptibility of Al 6013/SiC interface to localized corrosion. Journal of Materials Engineering and Performance, 2009, 18, p.129-136.

PAPER REF: 074

POLYMER RE-CYCLING FOR ADDITIVE MANUFACTURING THROUGH THE ARBURG PLASTIC FREEFORMING PROCESS

Gregorio Pisaneschi[1], Mattia Mele[1], Maurizio Fiorini[2], Giampaolo Campana[1], Andrea Zucchelli[1]

[1] University of Bologna, Department of Industrial Engineering (DIN), Bologna, Italy

[2] University of Bologna, Department of Civil, Chemical, Environmental, and Materials Engineering (DICAM), Bologna, Italy

ABSTRACT

The Freeformer Additive Manufacturing process by Arburg is characterized by the fact that inexpensive, qualified standard polymeric granulate can be processed to manufacture fully functional parts (Gaub, H., 2016). The process is based on the Arburg Plastic Preeforming (APF) concept where the base material is prepared with a screw as for the injection moulding and is discharged on the part layer as a droplet through a nozzle that is served by a piezo actuator that performs a pulsed nozzle closure. The molten material is prepared and collected in a reservoir under pressure between the screw and the nozzle tip. The working area can be served by two or three independent screws and nozzles and different polymers can be processed in the same moment, for example one of them can be used to build supporting structures that can be easily eliminated at the end.

The Freeformer Additive Manufacturing process has already found important application like, for example, for the additive production of sintered metal components (Spiller, Q., Fleischer, J., 2018). In this case the Arburg freeformer replaces the injection moulding machine in the (Metal Injection Moulding) MIM process chain. The metal powder is charged together with the binder in the screw and a part is realised without the need of a mould. This approach allows the MIM process to be applied also for a small amount of parts. Obviously, after the production of the parts, debinding and sintering is necessary as in the conventional MIM process.

The possibility to use inexpensive, qualified standard polymeric granulate also helps to enhance a sustainable approach for the additive manufacturing. Particularly, a recycle of the polymers is simple because easily scraps or also old components and parts can processed to be melted a second time. Polymer recycling is an important aspects that is already investigated for other technology like, for example, the Fused Filament Fabrication (FFF) process. (Lee, Y., Lee, D., Ko, Y., Lee, K., Kim, N., 2018). The number of applications for 3D printers has increased significantly and consequently the use of thermoplastic resins such as acrylonitrile butadiene styrene (ABS) and poly lactic acid (PLA), which are typical filament materials for FFF. Thus, the interest of designing procedures for making recycled filaments from waste polymer is large.

Plastic waste contains often a mixture of polymers; for example, water bottles and caps comprised of polyethylene terephthalate (PET) and polypropylene (PP) are quite a common wasted material and complete separation is rarely implemented. (Zander, N.E., Gillan, M., Burckhard, Z., Gardea, F., 2019) investigated the use of blends of waste PolyEthylene Terephthalate (PET), PolyPropylene (PP) and PolyStyrene (PS) for 3D FFF.

In the present study, Acrilonitrile butadiene stirene (ABS) has been investigated by considering the attitude of this polymer to be recycled through the Freeformer Additive Manufacturing process by Arburg. A benchmark part was designed to test chemical-physical properties and

mechanical performances of the recycled material. The Drop Aspect Ratio and the Discarge Rate were the controlled process parameters to investigate the effect of multiple material transformation.

Keywords: Additive Manufacturing, Arburg plastic freeforming process, Polymers, re-Cycling

REFERENCES

Gaub, H., 2016. Customization of mass-produced parts by combining injection molding and additive manufacturing with Industry 4.0 technologies. Reinforced Plastics 60, 401–404. https://doi.org/10.1016/j.repl.2015.09.004

Spiller, Q., Fleischer, J., 2018. Additive manufacturing of metal components with the ARBURG plastic freeforming process. CIRP Annals 67, 225–228. https://doi.org/10.1016/j.cirp.2018.04.104

Lee, Y., Lee, D., Ko, Y., Lee, K., Kim, N., 2018. Development and Evaluation of a Distributed Recycling System for Making Filaments Reused in Three-Dimensional Printers. Journal of Manufacturing Science and Engineering 141, 021007. https://doi.org/10.1115/1.4041747

Zander, N.E., Gillan, M., Burckhard, Z., Gardea, F., 2019. Recycled polypropylene blends as novel 3D printing materials. Additive Manufacturing 25, 122–130. https://doi.org/10.1016/j.addma.2018.11.009

PAPER REF: 075

METHODS TO OBTAIN THERMOELECTRIC COOLER PROPERTIES AND PERFORMANCE EVALUATION AS GENERATOR

J.M. Ferraz[1], P.T.C. Peixoto[3], S.I.S Pinto[1,2(*)]

[1]Engineering Faculty, University of Porto, Porto, Portugal

[2]Institute of Science and Innovation in Mechanical and Industrial Engineering (LAETA-INEGI), Porto, Portugal

[3]Centre for Nanotechnology and Smart Materials (CeNTI), Vila Nova de Famalicão, Portugal

[(*)]*Email:* spinto@fe.up.pt

ABSTRACT

This work compares three different methods (Lineykin, Luo, Palacios) to obtain the properties of a thermoelectric cooler through a developed numerical tool in *Visual Basic*. Then, the obtained results were compared with the manufacturer information as power generators. The Palacios model is aligned, more closely, with the manufacturer data. Later, the properties obtained were introduced in an analytical power prediction model and compared with experimental data. The same model (Palacios) shows more reliable results.

Keywords: thermoelectrity, TEC, TEG, thermoelectric generator, properties estimation, numerical tool development.

INTRODUCTION

Recovery of waste energy has become a topic of increased interest due to the increased energy needs and efficiency demand. In addition, nowadays, increased use of portable or remotely located sensors and communication systems creates the need for reliable, self-sufficient power sources. Thermoelectric generators (TEG) are a suitable candidate to solve these problems, due to its abilities to generate electrical power with very small temperature differences and its solid-state construction that implies maintenance free operations. The high price of dedicated generators is a disadvantage. However, thermoelectric coolers (TEC) are much cheaper and can also be used as TEG (Nesarajah, 2016). Given its purpose, thermoelectric properties of TEC are rarely made available to users. Therefore, methods need to be employed to enable performance prediction.

In order to evaluate the thermoelectric properties, three methods were tested, relying on the manufacturer performance curves - Palacios et al., 2009 - or maximum performance values - Lineykin and Ben-Yaakov, 2007; Luo, 2008. The information obtained, through a developed tool in *Visual Basic*, was then compared with the data provided by the manufacturer or measured in the laboratory. A commercially available TEC was used for the tests.

METHODOLOGY

In the first part of the test, the thermoelectric properties of a commercially available module, Marlow NL1013T, were calculated from its performance curves as a TEC. Given the module is designed to be used both as a TEC and a TEG, the manufacturer also provides performance curves for the module's capability as a TEG. The module's properties according to the three different methods - Lineykin, Luo and Palacios - are used to calculate the module's performance as a TEG and the data compared.

In the second part of the test, a commercially available TEC module, CUI CP40136, is placed on a heating band, as presented in Fig. 1, to be used as a TEG. The thermoelectric properties were calculated according to the three methods - Lineykin, Luo and Palacios - through the developed tool and the results were compared. The experimental setup was chosen to enable temperature readings with a thermal camera, screenshot seen in Fig. 2, with the objective of eliminating thermal contact resistance in the temperature measurement.

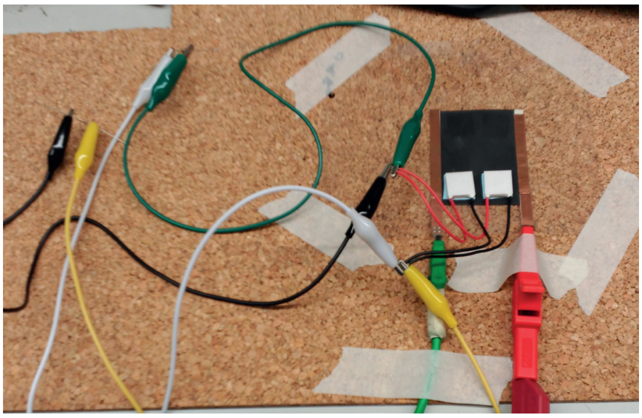

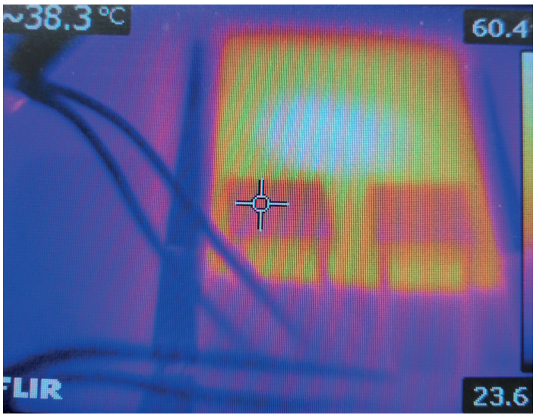

Fig. 1 - Experimental setupFig. 2 - Thermal camera screenshot

RESULTS AND CONCLUSIONS

Table 1 shows the results of the properties estimation, for the NL1013T module, with the analytical method identified by the authors, using the data from the spec sheet for 50˚C hot side. The generated power was predicted by:

$$P = \left(\frac{S \Delta T}{R_i + R_L} \right)^2 \times R_L \tag{1}$$

where R_L is the electrical resistance of the load attached to the module and ΔT is the temperature difference across the module. The load resistance was equalled to the internal resistance, a common practice known as "load matching" and believed to have been used by the manufacturer. The comparison between the calculated values obtained by the developed numerical tool and manufacturer data is presented in Table 2 for the generated power and in Table 3 for the open circuit voltage. Cold side is maintained at 27˚C while hot side temperature is varied. The method that shows closer results to the manufacturer's claim is Palacios' method.

Table 1 - Calculated properties according to the different methods for the NL1013T module

Property	Lineykin	Luo	Palacios
S (V/K)	0.0297	0.0276	0.0310
R_i (Ω)	7.55	7.00	9.20
R_{th} (K/W)	18.28	19.72	21.14

Table 2 - Generated power [W] at different hot side temperatures according to the different methods and the manufacturer

	T_H=35˚C	T_H=55˚C	T_H=85˚C
Lineykin	0.002	0.024	0.096
Luo	0.002	0.022	0.089
Palacios	0.002	0.021	0.085
Manufacturer	0.002	0.021	0.087

Table 3 - Open circuit voltage [V] at different hot side temperatures according to the different methods and the manufacturer

	T_H=35˚C	T_H=55˚C	T_H=85˚C
Lineykin	0.231	0.822	1.734
Luo	0.214	0.762	1.608
Palacios	0.241	0.857	1.809
Manufacturer	0.24	0.85	1.79

The thermoelectric properties, for the CUI CP40136 module, used in the experimental tests, are shown in Table 4. For this test, the heating band was powered by a power source. The temperature of the heating band and of the cold side of the module was measured, as well as the open circuit and closed circuit voltage. The measured values were compared with those obtained by the developed numerical tool. Hot side temperature varied between 52.3˚C and 51.3˚C and cold side temperature varied between 47.9˚C and 47.4˚C. The circuit was closed using a 1.10Ω load (including wires and contact electric resistance) for a single module, 2.15Ω for two modules in series and 0.60Ω for two modules in parallel. The results are presented in Table 5, Table 6 and Table 7.

Table 4 - Calculated properties according to the different methods for the CP40136 module

Property	Lineykin	Luo	Palacios
S (V/K)	0.0127	0.0111	0.0131
R_i (Ω)	0.74	0.65	0.95
R_{th} (K/W)	11.13	12.74	14.21

Table 5 - Calculated and measured voltage in open-circuit and closed-circuit assemblies for a single module

	Open-circuit voltage [V]	Closed-circuit voltage [V]
Lineykin	0.0426	0.0193
Luo	0.0383	0.0187
Palacios	0.0463	0.0177
Experimental results	0.0422	0.0167

Table 6 - Calculated and measured voltage in open-circuit and closed-circuit assemblies for modules in series

	Open-circuit voltage [V]	Closed-circuit voltage [V]
Lineykin	0.0953	0.0414
Luo	0.0840	0.0400
Palacios	0.1014	0.0399
Experimental results	0.0901	0.0348

Table 7 - Calculated and measured voltage in open-circuit and closed-circuit assemblies for modules in parallel

	Open-circuit voltage [V]	Closed-circuit voltage [V]
Lineykin	0.0466	0.0184
Luo	0.042	0.0177
Palacios	0.0507	0.0179
Experimental results	0.0453	0.0164

In these tests, the Lineykin method shows, on average, the smallest error. However, the measured voltage, both in open-circuit and closed-circuit, presents deviations in different directions. The Palacios method shows higher differences between calculated and measured values, but consistent in direction and module. Therefore, it is believed that this is due to several circumstances, not taking into consideration, in the experimental method. The difference in values, with predictions using values according to the Palacios method showing higher voltage in every scenario, might be due to poorly calculated thermal contact resistance. It was considered a value of 3,5K/W – Nesarajah and Frey, 2016; Hansson et al.,2016 - accounting for the low contact pressure applied. It is possible that this value might have been even higher, as the modules separated more than once from the thermal pads. Comparison between the numerical results with the manufacturer data for the NL1013T module (see Table 2 and Table 3) also leads that Palacios method is the most accurate.

ACKNOWLEDGMENTS

Authors gratefully acknowledge the Engineering Faculty of University of Porto (FEUP), the Department of Mechanical Engineering (DEMec) of FEUP, the Institute of Science and Innovation in Mechanical and Industrial Engineering (LAETA-INEGI) and the Centre for Nanotechnology and Smart Materials (CeNTI).

REFERENCES

Nesarajah M, Frey G. Thermoelectric power generation: Peltier element versus thermoelectric generator. Thermoelectric power generation: Peltier element versus thermoelectric generator, 2016, p. 4252-4257.

Hansson J et al. Review of Current Progress of Thermal Interface Materials for Electronics Thermal Management Applications. 2016 IEEE 16th International Conference on Nanotechnology (IEEE-NANO), 2016, p. 371-374.

Lee S et al. Thermal Interface Material Performance in Microelectronics Packaging Applications. Microelectronics Journal, 1997, volume 28, nº 1, p. xiii-xx.

Lineykin S, Ben-Yaakov S. Modelling and Analysis of Thermoelectric Modules. IEEE Transactions on Industry Applications, 2007, vol. 43, no. 2, pp. 505-512.

Luo Z. A Simple Method to Estimate the Physical Characteristics of a Thermoelectric Cooler from Vendor Datasheets. Electronics Cooling, 2008, 14, p. 22-27

Palacios R. et al. Analytical procedure to obtain internal parameters from performance curves of commercial thermoelectric modules. Applied Thermal Engineering, 2009, 29, p. 3501-3505.

PAPER REF: 076

AIR FLOW RESISTANCE OF POLYAMIDE 12 MADE BY SELECTIVE LASER SINTERING

Nebojša Bogojević[1(*)], Nusret Muharemović[2], Branko Radičević[1], Aleksandar Vranić[1], Snežana Ćirić-Kostić[1]

[1]Faculty of Mechanical and Civil engineering in Kraljevo, University of Kragujevac, Kraljevo, Serbia
[2]Plaming d.o.o., Gračanica, Bosnia and Herzegovina
[(*)]*Email:* bogojevic.n@mfkv.kg.ac.rs

ABSTRACT

This paper presents the measurements of the air flow resistance of polyamide 12 samples made by selective laser sintering. The results have shown that, due to the porosity of the microstructure, the samples with thickness smaller than 1.7 mm cannot be considered airtight, while the samples with thickness 2.2 mm are airtight. The airflow resistance of the samples that allow airflow increases with air speed.

Keywords: *air flow resistance, porosity*, *additive manufacturing, polyamide*.

INTRODUCTION

Selective laser sintering (SLS) is one of the most popular additive manufacturing (AM) technologies because of the superior mechanical properties of the produced parts in comparison with other AM technologies. The basic material used for production of plastic parts by SLS is polyamide 12 (PA 12). However, the measurements have shown that the densities of parts produced by SLS are around 10% smaller than the densities of the parts made by injection moulding. Microscopic analyses revealed that the parts produced by SLS have grainy structure and contain porosities. According to the specifications of the manufacturer of the PA12 powder with trade name PA2200, the parts produced from that material by SLS with thicknesses under 1.5 mm, due to the porosity, are not watertight. Since the SLS are used for production of various pneumatic components, as well as to other components which are exposed to air flow and air pressure, the influence of the porosity of the polyamide 12 to the air flow and air pressure is of practical interest.

METHODOLOGY

Air resistance is one of the main parameters that describe the behaviour of the porous materials exposed to air flow (Wittstock, Schmelzer 2018). The air resistance (measured in Pa·s/m^3) is defined as a quotient of pressure difference on two sides of an obstacle to air flow (measured in Pa) and the volumetric airflow through the obstacle (measured in m^3/s). This paper presents the measurements of air flow resistance of 40 samples made from PA 2200 using the SLS technology. All the samples had shape of disk with diameter of 100 mm and were divided into four sets with different thicknesses, 0.7 mm, 1.2 mm, 1.7 mm and 2.2 mm. Each set consisted of 10 samples. The air flow resistance of the samples was measured according to ISO 9053 standard using steady state air flow method. The volumetric airflow varied between 12.5 mm/s and 36 mm/s.

RESULTS AND CONCLUSIONS

The air flow resistance of the samples with thickness of 2.2 mm was too high to be measured by the described methodology, which means that the samples with the thicknesses higher than 2.2 mm may be considered airtight.

The results of the measurements of the airflow resistance for the samples with thicknesses smaller than 1.7 mm are presented in the Figure 1. Each data point in the diagram represents a mean value of the airflow resistance of the set of 10 samples with the same thickness. While each of the samples under the study allowed airflow, it may be noted that the samples with thickness 1.7 mm showed substantial increase of the airflow resistance with increase of the air speed. Since this may be of interest for the applications with high-frequency dynamics (e.g. sound absorption and audio technics), further frequency analysis of the obtained results will be made.

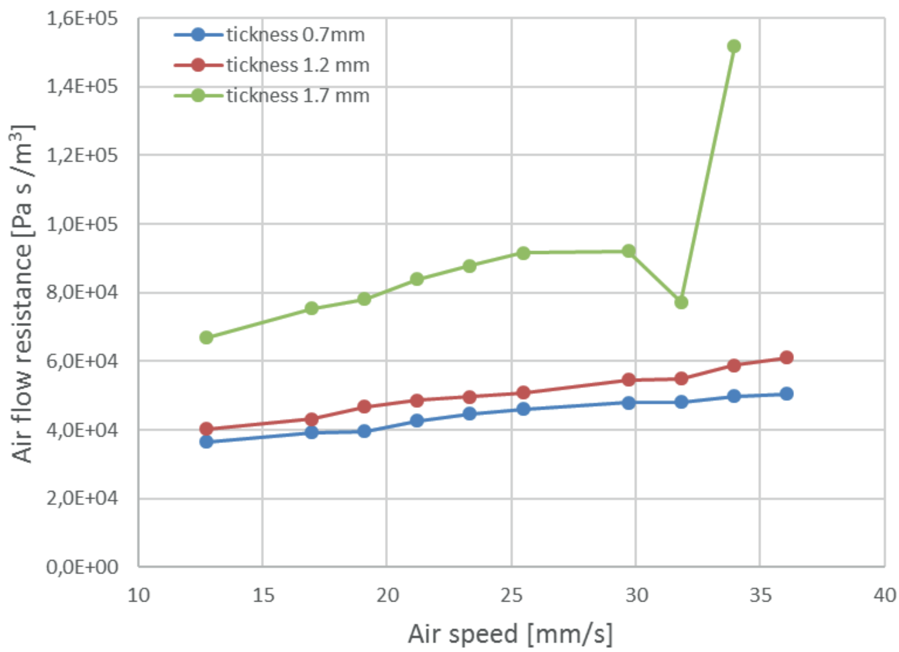

Fig. 1 – Air flow resistance

The presented results lead to the conclusion that the limiting thickness to consider the products made from polyamide 12 by SLS to be airtight is between 1.7 mm and 2.2 mm, and is certainly higher than the limiting thickness to consider the products to be watertight.

ACKNOWLEDGMENTS

The authors wish to acknowledge the support of European Commission through the project “Advanced design rules for optimal dynamic properties of additive manufacturing products – A_MADAM”, which has received funding from the European Union’s Horizon 2020 research and innovation programme under the Marie Skłodowska-Curie grant agreement No. 734455. The third author (B.R.) acknowledges the support of the Serbian Ministry of Science, Education and Technology through the grant No. TR37020.

REFERENCES

Acoustics - Determination of airflow resistance, ISO 9053:2018

Wittstock V, Schmelzer M, Measurement of airflow resistance by the alternating flow method, Euronoise 2018, Heraklion, Crete - Greece | 27-31 May 2018, p 625-629

PAPER REF: 077

RESEARCH OF FUEL INJECTION EQUIPMENT FOR COMBUSTION ENGINES WITH LASER METHODS

Antoni Jankowski[1(*)], Paweł Stężycki[2], Dariusz Ćwik[3]

[1]Air Force Institute of Technology, Warsaw, Poland
[2]Institute of Aviation, Warsaw, Poland
[3]Military University of Technology, Warsaw, Poland
[(*1)]*Email*: [1]antoni.jankowski@itwl.pl [2]pawel.stezycki@ilot.edu.pl, [3]dariusz.cwik@wat.edu.pl

ABSTRACT

The article presents the original results of fuel atomization tests with measurements of droplet size in a fuel stream. The test results indicate that in addition to the Sauter diameter (D_{32}) the fuel atomization process from the point of view of combustion and emission processes, a better assessment can be obtained using the Herdan diameter (D_{43}), which is similar to the volume median of droplets of fuel. Laser methods can be used to evaluate injection apparatus for internal combustion engines.

Keywords: combustion engine, fuel injection equipment, fuel atomization, laser method.

INTRODUCTION

Fuel injection systems are dominant in spark-ignition and Diesel engines. These systems allow for accurate metering of fuel and feeding it to the combustion chamber. They also allow for the appropriate shaping of the injection process for the shape of the spray, the dimensions of droplets, and the dosing of the amount of fuel. The use of optical methods using lasers to measure droplets' diameters and speed allow for significant progress in this field of research [1]. In tests of atomised fuel spray, in conditions reflecting the conditions of the internal combustion engine, the size of droplets, their distribution in the spray and the velocity of individual droplets are possible to determine. Droplets in the spray have different diameters, depending on the discharge conditions and fuel properties. From the point of view of the economics of the combustion engine operation and the emission of toxic exhaust components, differences in the size of droplets should be within a narrow range [2]. To determine the quality of the fuel spray, two substitute diameters Sauter (D_{32}) and Herdan (D_{43}) were selected, the first of which refers to heat transfer and the second to combustion processes.

RESULTS AND CONCLUSIONS

The paper presents Laser Doppler Velocimeter and Phase Doppler Particle Analyser. The stand allows measurements of droplets in the range from 0.5 μm to 2.0 mm, and when the optical system parameters change, even up to 3.822 mm. Exemplary results of studies of droplet size distribution in a homogeneous spray are shown in Fig. 1, and in a spray with a dispersion of droplets − in Fig. 2. Figures 1 and 2 indicate that the Sauter diameter is 18.41 μm / 20.99 μm respectively and the Herdan diameter − 20.4 μm / 25.94 μm. The differences between the Herdan and Sauter diameters are respectively 1.99 μm / 4.95 μm, which is 9.7% / 19.1%. The smaller the average diameters between diameters, the greater the homogeneity of the fuel stream. An important role in assessing the fuel injection stream has a volume median of droplets, which is 20.14 / 24.94 μm respectively, which is 99% / 94% of the Herdan diameter, respectively.

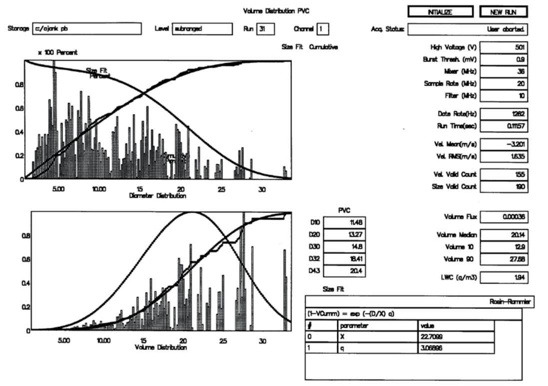

Fig. 1 – Diametr distrubiution in fuel homogeneous spray

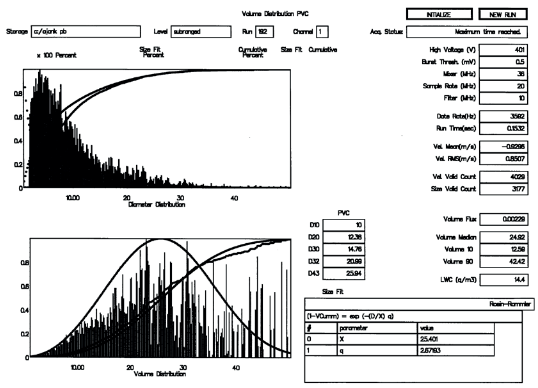

Fig. 1 – Diametr distrubiution in fuel spray with dispersion

The Sauter diameter (D_{32}) is determined by the relationship (1):

$$D_{32} = \frac{\sum_{i=1}^{n} c_i d_i^3}{\sum_{i=1}^{n} c_i d_i^2} \tag{1}$$

The Herdan diameter (D_{43}) is determined by the relationship (2):

$$D_{43} = \frac{\sum_{i=1}^{n} c_i d_i^4}{\sum_{i=1}^{n} c_i d_i^3} \tag{2}$$

where:
c_i – the number of drops with a given diameter,
d_i – diameter of the i-th droplet,
n – number of measured droplets.

The most harmful droplets of fuel in the spray are large droplets. Even a few such droplets significantly change the combustion process and emission of toxic exhaust components, mainly (NO_x). The atomization process from the point of view of combustion and ignition processes, as well as emission levels, is characterized by the best substitute diameter D_{43}, which value is close to the median volume. The main reasons for excessive fuel consumption and the emission of toxic exhaust components are inaccurate metering of fuel and improper preparation of the mixture. For proper fuel metering as well as fuel preparation the fuel atomization process has the main influence. For the evaluation of the fuel apparatus, measurement of the Herdan diameter (D_{43}) should take place along the length of the stream at a distance of 2/3 of the spray range from the injector and 2/3 of the stream radius value from the spray axis.

REFERENCES

[1] Doerr, T., The Significance of Fuel Preparation for Low Emissions Aero-Engine Combustion Technology, ICLASS 2012, 12th Triennial International Conference on Liquid Atomization and Spray Systems, Heidelberg, Germany, September 2-6, 2012.

[2] Kowalski M., An Analysis of Failure Symptoms of the Airscrew Drive in the PZL-130-TCI Orlik Aircraft, Journal of vibration engineering & technologies, Volume: 2 Issue: 4 pp. 315-326, 2014.

PAPER REF: 078

STEERING COLUMN SUPPORT TOPOLOGY OPTIMIZATION INCLUDING LATTICE STRUCTURE FOR METAL ADDITIVE MANUFACTURING

Sara Mantovani[1(*)], Giuseppe Alessio Campo[1]

[1]Engineering Department "Enzo Ferrari" (DIEF), University of Modena and Reggio Emilia, Italy

[(*)]*Email:* sara.mantovani@unimore.it

ABSTRACT

This work is focused on Finite Element (FE) modelling of lattice structures applied to optimization process of an automotive Steering Column Support (SCS). Topology Optimization (TO) with and without lattice structure are considered to obtain the lightest feasible solution. The constraints considered for the optimization problem are modal frequencies and Equivalent Local Stiffness. Finally lattice TO results are compared with traditional TO varying penalty factor *p*.

Keywords: lattice structure, finite element modelling, topology optimization, steering column support, additive manufacturing.

INTRODUCTION

Weight reduction is a crucial goal for car manufacturers. In the literature, several articles demonstrate the usefulness of TO applied to structural components in order to increase stiffness-to-weight ratio (Mantovani, 2017). However, TO results often present a continuous relative density distribution which might be meaningless in terms of feasibility. In fact, with traditional manufacturing process only void or solid areas are available. Feasible solution could be obtained penalizing the intermediate element densities with high *p*. This solution could compromise the minimization of objective function *e.g. weight*.

Brackett *et al.* (Brackett, 2011) individuate in lattice structures a possible solution to create volumes with intermediate relative densities. The recent improvements in additive manufacturing for metals allow the creation of micro lattice structures, that can be used to reduce the total bulk material and thus the overall weight. Mechanical properties of lattice cells are studied by Ashby (Ashby, 2006) and used in optimization of structural components (Cheng, 2017) (Mantovani, 2018)

In present paper, the SCS is optimized considering 4 Equivalent Local Stiffness (ELS) constraints and 2 modal frequencies constraints. The minimization of SCS mass is imposed as TO objective function. The design space of TO is discretized in 5 mm tetrahedral elements. The lattice optimization process is subdivided in three steps. The first one adopts a traditional TO. From the outcome of first step, the elements with relative density above a certain threshold are considered as bulk material, otherwise the edges of tetra elements are converted with beams to create tetrahedral lattice structures. The radii of these beams are optimized by size optimization. Finally, the beams with radius below a specified limit are deleted. On TO results, the influence of *p* is investigated.

RESULTS AND CONCLUSIONS

The masses obtained from 4 significant TO results are reported in Table 1. As expected, the minimum mass is achieved in the traditional TO with lowest *p*, but this solution is unfeasible. The TO with lattice allows feasible solution with good level of mass reduction. The comparison between TO with and without lattice, adopting *p* equal 1.8, highlights that the first one is 107 g heavier than the second solution, Fig.1.

Table 1 – Topology optimization results

Type of optimization	Penalty factor	mass [g]	Δ mass [%]
TO	1	485	-60
TO (reference)	3	1225	0
TO	6	1489	+22
TO	1.8	868	-29
TO + lattice	1.8	975	-20

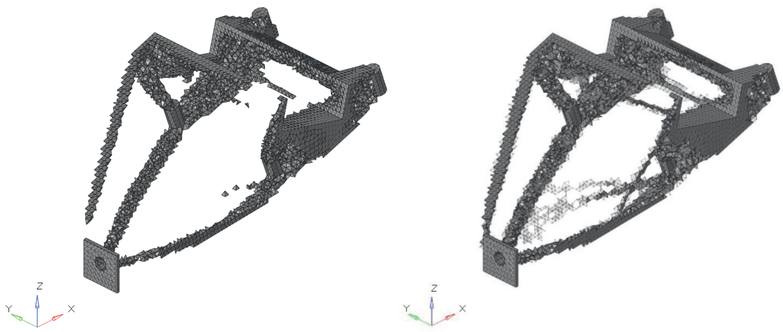

(a) (b)

Fig. 1 – Topology optimization (*p*=1.8) of steering column support: without lattice structures (relative density ≥ 0.5) (a); with lattice structures (b)

This study stresses the introduction of lattice structures to the optimization of automotive structural components. Further approaches of FE modelling of lattice structures, such as hexahedral repetitive cells or homogenization, could be investigated .

REFERENCES

Ashby, M. F. (2006) ‘The properties of foams and lattices’, *Philos Trans A Math Phys Eng Sci*, 364(1838), pp. 15–30.

Brackett, D., Ashcroft, I. and Hague, R. J. M. (2011) ‘Topology optimization for additive manufacturing’, *SFF Symposium*, pp. 348–362.

Cheng, L. *et al.* (2017) ‘Efficient design optimization of variable-density cellular structures for additive manufacturing: theory and experimental validation’, *Rapid Prototyping J*, 23(4), pp. 660–677.

Mantovani, S. *et al.* (2017) ‘Influence of Manufacturing Constraints on the Topology Optimization of an Automotive Dashboard’, *Procedia Manufacturing*. 11, pp. 1700–1708.

Mantovani, S. *et al.* (2018) ‘Optimization methodology for automotive chassis design by truss frame: A preliminary investigation using the lattice approach’, Advances in Transdisciplinary Engineering, 7, 2018, pp. 984-992

PAPER REF: 080

SSC, SCC, and GHSC CORROSION RESISTANCE OF PRECIPITATION HARDENED UNS N06625 FORGED BARS

Andrea Febbrari[1(*)], Marcello Gelfi[1], Annalisa Pola[1], Chiara Veronesi[2], Raimondo Montani[2]

[1]Università degli Studi di Brescia, Via Branze 38 25123 Brescia (BS), Italia
[2]Italfond S.p.A, Via Industriale 1, 25121 Bagnolo Mella (BS)
[(*)]*Email:* a.febbrari002@unibs.it

ABSTRACT

Stress Corrosion Cracking (SCC), Galvanic induced Hydrogen Stress Cracking (GHSC) and Sulphide Stress Cracking (SSC) of metals exposed to environments containing H_2S, common in oilfield applications, are recognized as material failure problems. Specific tests have been developed in order to demonstrate the resistance of materials to the corrosion mechanisms which are introduced above. A material can be applied in Oil & Gas field only if it is resistant to SCC, GHSC and SCC. This work investigates the microstructure, mechanical properties and resistance to SSC, SCC and GHSC of precipitation hardened UNS N06625 forged bars. Precipitation hardening heat treatment is not considered by international specifications applied in Oil & Gas field *(NACE MR 0175 ISO 15156, 2015) (NACE MR 0103 ISO 17945, 2015)* which permit only annealing or solution annealing conditions. In order to consider the size effect, three different bar diameters were investigated: 152 mm, 203 mm and 254 mm to prove the applicability of UNS N06625 in Oil & Gas field in this not standard heat treatment condition.

Keywords: UNS N06625, Age Hardening, Mechanical Properties, Sulphide Stress Cracking, Galvanic induced Hydrogen Stress Cracking, Stress Corrosion Cracking.

INTRODUCTION

UNS N06625 is widely applied in form of forged products for applications in Oil and Gas field in annealed or solution-annealed condition, the prescribed heat treated conditions allow maximizing the alloy corrosion resistance and ductility *(Floreen, 1994)*, with the limit of a rather low tensile strength. Another feasible heat treatment for UNS N06625 is age hardening that produces the strengthening by precipitation of metastable tetragonal γ” phase Ni_3(Nb,Mo) *(Tehovnik, 2015)*. The relationship between ageing parameters, microstructure and mechanical properties has been studied in literature *(Floreen, 1994)*. In particular, it is shown that a controlled ageing for 80 hours in a temperature range between 650°C and 700°C causes the precipitation of γ” phase, improving the yield strength to values higher than 750 MPa *(Mataveli, 2014) (Kohler, 1991)*. Considering the UNS N06625 time-temperature transformation (TTT) curves from literature, it is possible to define an ageing treatment cycle able to produce the γ” phase strengthening, giving a combination of high mechanical strength with corrosion resistance comparable to the annealed condition that would be a great advantage for the application of UNS N06625 alloy in Oil and Gas field.

Starting from these considerations, the aim of the present work is to study the effect of a specific ageing treatment on the mechanical and corrosion properties of large forged bars. Three different diameter age-hardened forged bars were tested to determine their mechanical properties and their corrosion resistance to environmental conditions typically used to qualify materials for Oil and Gas applications.

RESULTS AND CONCLUSIONS

The age hardening treatment was performed on the whole forged bar, with increasing diameters, i.e. 152 mm, 203 mm and 254 mm. The heat treatment consists into a first annealing followed by an aging treatment between 600°C and 700°C. Bars were tested on top and bottom positions, corresponding to the hot-top and to the base sides in the starting ingot. Figure 1 shows the yield and tensile strength of aged bars. In general, the average values are 50% higher than the annealed ones. Hardness and ductility of the material tested remain acceptable as per international applicable standards applicable in Oil & Gas field *(NACE MR 0175 ISO 15156, 2015) (NACE MR 0103 ISO 15156, 2015)*.

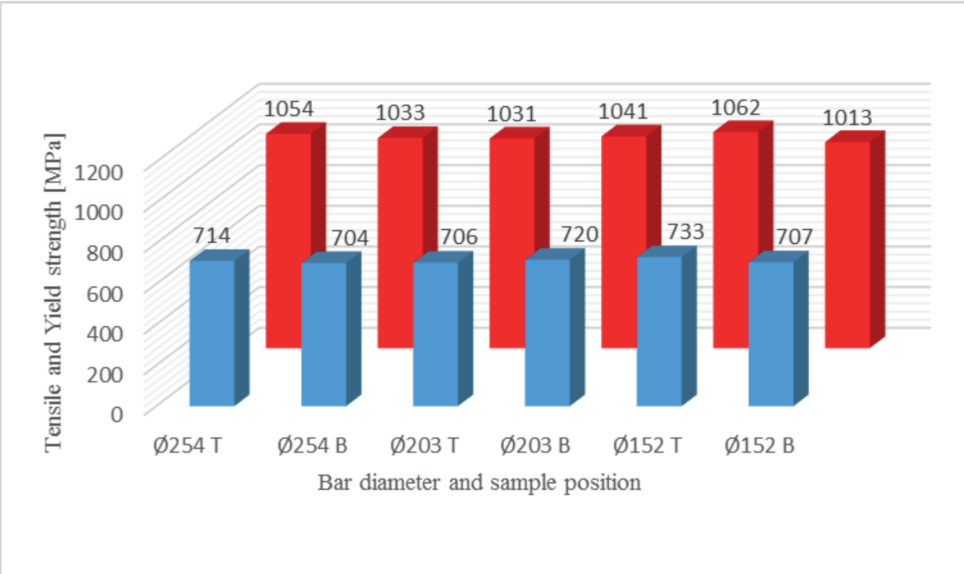

Fig. 1 Tensile test results, in blue yield strength, in red tensile strength

The corrosion resistance of the age hardened material, investigated through SSC, SCC and GHSC test according to NACE TM 0177 in the most challenging environment, level VII, is comparable to the annealed one and all mentioned tests were successfully passed. Additional corrosion test commonly performed in Oil & Gas field, ASTM G28 and ASTM G48 showed the good corrosion resistance of UNS N06625 in aged condition.

Test results showed the possibility of the application of the aged UNS N06625 as a precipitation hardenable material for Oil & Gas field according to NACE requirements.

REFERENCES

S. Floreen, G.E. Fuchs, W. J. Yang, presented at Superalloys 718, 625, 706 and Various Derivatives, Pittsburgh, USA, 26 – 29 June, **1994**, p. 13.

M. Kohler, presented at Superalloys 718, 625, 706 and Various Derivatives, Pittsburgh, USA, 23 – 26 June, **1991**, p. 363.

L. Mataveli Suave, J. Cormier, P. Villechaise, A. Soula, Z. Hervier, D. Bertheau, J. Laigo, *Met. and Mat. Trans. A*, **2014**, *45A*, 2963.

NACE MR0175/ISO15156:2015

NACE MR 0103/ISO 17945: 2015

F. Tehovnik, J. Burja, B. Podgornik, M. Godec, F. Vode, *Mat. and Tech.*, **2015**, *49*, 801.

PAPER REF: 081

SOLID CIRCULAR PLATE UNILATERALLY SUPPORTED ALONG TWO ANTIPODAL EDGE ARCS AND DEFLECTED BY A CENTRAL TRANSVERSE CONCENTRATED FORCE

Antonio Strozzi[1(*)]

[1]Department Enzo Ferrari, University of Modena and Reggio Emilia, Italy

[(*)]*Email:* antonio.strozzi@unimore.it

ABSTRACT

Protracted attention has been paid by the researchers to the mechanical analysis of circular plates subjected to non axisymmetric boundary conditions. A critical review of the works addressing circular plates statically loaded and subjected to mixed boundary conditions is presented in Strozzi & Vaccari (2001). The first study on this kind of problems has been carried out by Sherman (1955a,b); more recent contributions are those by Monegato and Strozzi [2001-2009]. An example of mechanical component that may be idealised as a circular plate non-axisymmetrically supported along its boundary is a resin reinforced cutting wheel, for which the mean values of the elastic constants are determined by comparing the deflection of a resin circular plate irregularly supported along its edge to a similar isotropic model, Milton (1966).

Keywords: circular plate, influence function, integral equation, Chebyshev polynomials.

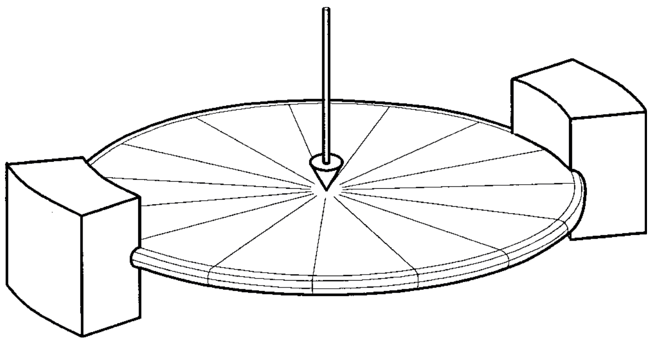

Figure 1

INTRODUCTION

This paper considers a thin solid circular plate, unilaterally supported along two antipodal boundary arcs, and statically loaded by a central point force. The supports are idealized as rigid and frictionless. The Kirchhoff plate theory is employed, and the extent of the contact zones as well as the contact reaction are determined. For limited angular extents of the supporting arcs, the plate does not lifts from the arcs, whereas for higher extents the plate loses it contact with the supports, and it may also come again in contact with the arcs along a central zone.

METHODOLOGY

This receding contact problem is formulated in terms of a singular integral equation. The kernel adopted is the influence function describing a Kirchhoff plate deflected by two antipodal transverse forces, and equilibrated by a central load. The integral equation is of the Prandtl type, for which solutions of ample validity are not available. The integral equation is therefore solved numerically with a series expressed in terms of Chebyshev polynomials.

The results retrieved suggest that, for the analysis of the title problem, the Kirchhoff theory constitutes a practically relevant trade-off between simplicity and accuracy.

The problem of a similarly supported plate, loaded by a uniform pressure or, more generally, by an axisymmetrically distributed pressure, is mathematically analogous, and it is relatively simple to extend to this configuration the present solution. Instead, if the plate is loaded non-axisymmetrically, for instance by an eccentric point force, this problem becomes appreciably more complex, since the Green function is more complex.

It is finally observed that this kind of mathematical problems is in these years mainly treated with the aid of Finite Elements. The present author, however, feels that the determination of the regrouped variables describing the plate mechanical response takes advantage from an analytical approach.

REFERENCES

Milton, C.S. Principles of abrasive processing. Clarendono Press, Oxford, 1966.

Strozzi, A. & Vaccari, P. 2001 Circular solid plate supported along and edge arc and deflected by a central transverse force. Proc. Instns Mech Engrs Part C 215, 389-404.

Sherman, D.I. 1955a On the bending of a circular plate partially clamped and partially supported along the contour. Doklady Akad. Nauk SSSR 101, 623-626.

Sherman, D.I. 1955b On the bending of a circular plate partially supported and partially free along the contour. Doklady Akad. Nauk SSSR 105, 1180-1183.

Monegato, G. & Strozzi, A. 2001 On the existence of a solution for a solid circular plate bilaterally supported along two antipodal boundary arcs and loaded by a central transverse concentrated force. ASME J. Appl. Mech. 68, 809-812.

Monegato, G. & Strozzi, A. 2002 On the Form of the Contact Reaction in a Solid Circular Plate simply Supported along two Antipodal Edge Arcs and Deflected by a Central Transverse Concentrated Force. J. Elasticity 68, 13-35.

Strozzi, A. & Monegato, G. 2009 Solid Circular Plate clamped along two Antipodal Edge Arcs and Deflected by a Central Transverse Concentrated Force. J. Elasticity 97, 155-171.

PAPER REF: 082

DESIGN OF AN INSTRUMENTED EXTENSIBLE AXIAL LOAD BAR FOR THE CONFORMITY ASSESSMENT OF ELEVATOR CARS ACCORDING TO EN 81-20:2014

Piero Morelli

Department of Industrial Engineering, Alma Mater Studiorum Università di Bologna, Italy
e-mail: piero.morelli@unibo.it

ABSTRACT

This work presents the design of an instrumented extensible bar for the axial loading of elevator car walls, used to certify the compliance of the car frame within the strength requirements of the EN standard 81-20:2014. A prototype of the bar was manufactured in the mechanical laboratory of the University of Bologna. The experimental validation of the system was performed in the workshop of Cabine Europa – Rebo, which is an Italian company addicted to elevator car manufacturing for worldwide commercial and luxury applications. Eventually, the performance of the loading procedure was analysed to get indications for the optimum re-design of the extension actuation system of the bar.

Keywords: EN 81-20:2014, elevator car, conformity assessment, extensible axial load bar.

INTRODUCTION

The safety requirements for the elevator cars are governed by the European standard 81-20, which prescribes a complete set of qualifying tests to assess the mechanical strength and stiffness of the different parts, such as walls, roof protections, top balustrade and bottom apron. The maximum allowable deformations on the measuring points are also defined. A device for applying the required loadings was specifically designed for this purpose and optimized after the experimental evaluation of its operational effectiveness.

CONCEPT DESIGN

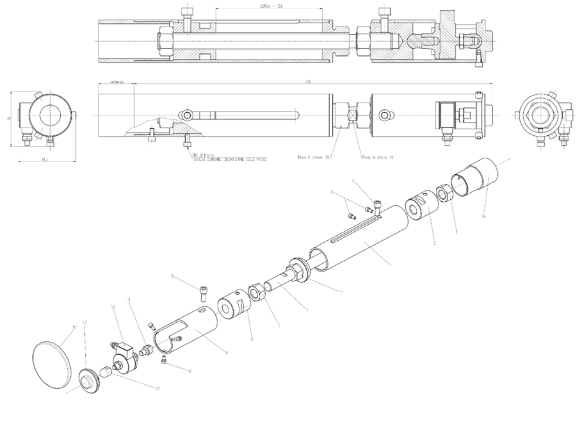

The concept of this extensible bar is based on a hand actuated screw-nut coupling that controls the length of the loading device. Consequently, the intensity of the applied load is controlled by the axial extension ramp that allows smooth loading rates due to the relatively low bending stiffness of the profiled sheet metal panels of the car walls. A load cell model HBM U2A is lodged inside the bar head, which was designed in a tubular shape giving both axial and bending stiffness, in order to prevent buckling. The bar head can be equipped with interchangeable thrust disks that meet the requirements of the 81-20 standard concerning the size of the contact area (5 cm^2 for the case of 300 N load tests and 100 cm^2 for the case of 1000 N load tests).

EXPERIMENTAL PERFORMANCE OF THE SYSTEM

The prototype of the load bar is shown in the figure, applied to a measuring point during the execution of a bending load test on a lateral wall. In the diagram on the side, the elastic mechanical characteristic of the panel is shown.

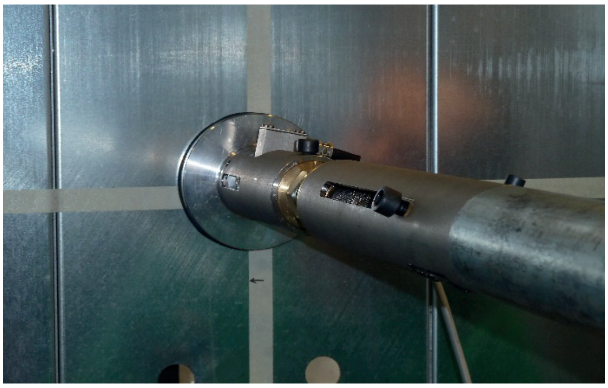

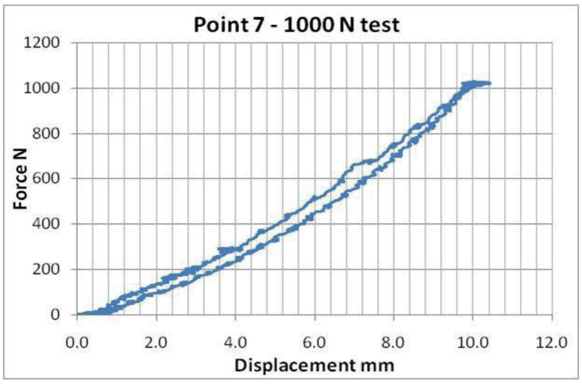

However, the wrench hand drive has not proven to be optimal, since the lack of continuity in the actuation caused load vibrations and general irregularities.

REDESIGN OF THE EXTENSION ACTUATION SYSTEM

A helical wheel and worm mechanism with motion reduction was designed in order to provide a continuous and more regular actuation of the extension system of the bar. This implementation is expected to reduce signal vibrations in the reading of the applied load and avoid stepped discontinuities related to stick-slip phenomena that can occasionally occur due to friction.

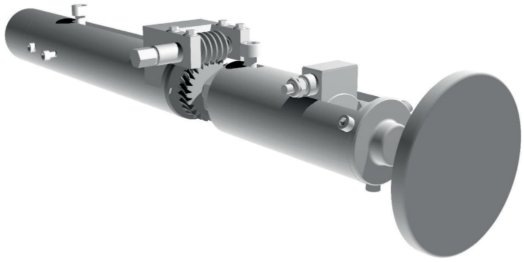

CONCLUSIONS

The experimental check on the operativity of this prototype of axial load bar was overall satisfactory, since the effectiveness of the system was proven against all requirements of the different kinds of tests and measurements that must be performed for the assessment of conformity to the standard. Moreover, the re-design of the actuation system of the bar is expected to improve the efficiency and regularity of the application profile of the load, which could guarantee a better quality and repeatability of the measurements.

ACKNOWLEDGMENTS

The author gratefully acknowledges Cabine Europa – Rebo for funding this project and for having made available the workshop and all necessary components required to carry out the experimental validation of the system.

REFERENCES

EN 81-20:2014. Safety rules for the construction and installation of lifts – Lifts for the transport of persons and goods – Part 20: Passenger and goods lifts.

PAPER REF: 083

QUALITY ATTRIBUTES FOR COLLABORATIVE PRODUCT DEVELOPMENT

Marcel Randermann[1(*)], Till Blüher[2], Theo Giese[1], Roland Jochem[1], Rainer Stark[2]

[1]Institute for Machine Tools and Factory Management, Department of Quality Science, Technische Universität Berlin, Berlin, Germany

[2]Institute for Machine Tools and Factory Management, Department of Industrial Information Technology, Technische Universität Berlin, Berlin, Germany

[(*)]*Email:* marcel.randermann@tu-berlin.de

ABSTRACT

This work proposes quality attributes for collaborative product development by aggregating best practices of collaborative engineering and synthesizing interoperability frameworks. A systematic literature review provided literature for best practice identification. The results were condensed and displayed in four areas of interest for collaborative product development (orgnization, data, IT infrastructure and social aspects).

Keywords: quality attributes, collaborative engineering, interoperability, product development.

INTRODUCTION

In today's globalised value creation, an increasing number of companies collaborate in distributed product development projects. This requires a high degree of interoperability between partners regarding processes, IT-systems and shared data (Pasch et al., 2013). To develop products successfully, the quality of processes and systems has to assessed and assured. Quality attributes of collaborative engineering or interoperability may be defined by extracting parameters of frameworks as well as condensing knowledge from industrial practice. Most frameworks for interoperability in literature are too generic, while existing best practices that could guide companies are too detailed in specific aspects and not structured systematically. Therefore, in this paper, existing frameworks for interoperability were analysed and unified to a suitable structure for collaborative engineering. The structure considers the four areas of organizational aspects, data-driven aspects, IT infrastructural aspects and social aspects. Secondly, best practices in collaborative engineering and product development have been aggregated to an applicable level and represented condensely in the aforementioned structure. In result, quality attributes for collaborative product development were obtained allowing companies to assess the quality of their collaborative product development environment.

METHODOLOGY

First, five frameworks (i.e., AWG, 1998; Clark/Jones, 1999; Berre et al, 2007; Chen, 2009; European Union, 2017) for interoperability were compared and analyzed in order to synthethize and define a domain structure, which address the common areas that indicate relevance for collaborative product development. Secondly, a systematic literature review regarding the best practices in collaborative product development was performed using the databases SCOPUS and Web of Science with the search terms "best practice", "product development", "engineering" and "collaboration" within title, abstract and keywords. From each database the twenty most cited publications were taken. Furthermore, the list of references in appropriate papers were screened as well as prevalent best practice literature (i.e. Stoekert, 2010) assessed to detect additional results. In total, 37 publications could be identified to include material for quality attribute aggregation.

RESULTS AND CONCLUSIONS

The four areas of interest for collaborative engineering with the aggregated quality attributes from best practice literature are shown in Tab. 1.

Table 1 – Quality attributes for collaborative product development

Organization		Data	IT Infrastructure	Social Aspects
– conjoint performance monitoring – conjoint risk management – comprehensive compliance – explicit roles and responsibilities – joint process design – resource availability	– joint continual improvement process – awareness of dependencies – consistent performance – adaptability – conjoint strategy	– capability of purposive data exchange – conjoint knowledge management – data traceability and consistency – coordinated data access	– purposive definition of interfaces – compatibility – reliable communication	– transparency – trust – mutual cultural appreciation – precise communication – preparedness – applying conflict management

These quality attributes that indicate parameters for successful interoperability in product development may be used for performance management in collaboration projects. Further studies need to ascertain the validity and completeness of our results.

ACKNOWLEDGMENTS

The IGF promotion plan 19793 N of the Research Community for Quality (FQS), August-Schanz-Straße 21A, 60433 Frankfurt/Main has been funded by the AiF within the programme for sponsorship by Industrial Joint Research (IGF) of the German Federal Ministry of Economic Affairs and Energy based on an enactment of the German Parliament.

REFERENCES

AWG, Levels of Information Systems Interoperability (LISI), 1998

Chen, David. Framework for Enterprise Interoperability, 2009

Clark, Thea; Jones, Richard. Organizational Interoperability Maturity Model for C2, 1999

European Union. European Interoperability Framework, 2017

Berre A.J. et al. The ATHENA Interoperability Framework. In: Gonçalves R.J., Müller J.P., Mertins K., Zelm M. (eds) Enterprise Interoperability II. Springer, 2007, London

Stoekert, H., et al. Collaborative Engineering – Issues and Evidence from Industrial Practice. In: Proc of Int Design – Design 2010, Dubrovnik, Croatia, 17.–20.5.2010, pp 1199-1208.

Pasch, F. et al. Anforderungen an Kollaboration zur Sicherung der Prozess- und Produktqualität in der Entwicklung. In: Jochem, R. and Rößle, D. (eds) Qualitätsmanagement nachhaltig gestalten und umsetzen, Berlin, 2013, pp 103-130

PAPER REF: 084

VISCOELASTIC CHARACTERIZATION OF DACRON GRAFT AND AORTIC TISSUE

Rosaire Mongrain[1], Christopher Zikry[1], Raymond Cartier[2], Gilles Soulez[4]

[1]Department of Mechanical Engineering, McGill University, Montreal, Canada
[2]Montreal Heart Institute, University of Montreal, Montreal, Canada
[3]CHUM, University of Montreal, Montreal, Canada
[(*)]*Email:* rosaire.mongrain@mcgill.ca

ABSTRACT

In this work, we present the elastic and viscoelastic characterization of aortic tissue and a synthetic material used for the fabrication of artificial vessels (Dacron). Using high deformation and an oscillating mechanical testing protocols, we assessed the hyperelastic and viscoelastic properties and observed significant differences between the biological and the synthetic materials.

Keywords: Artificial vessel, hyperelastic properties, viscoelastic properties, mechanical bio-integration, graft design

INTRODUCTION

Vascular grafts are implanted in the human body in order to replace damaged or blocked vessels [1]. The development of synthetic grafts began in 1940s [1]. In the 1950s, the concept of porous, fabric vascular grafts were introduced (using PVC, polyacrylonitrile). By the 1960s, most fabrics were abandoned except for Dacron and Teflon. Prosthetic Dacron grafts are widely used as a synthetic substitute following aortic resection in cases of aorta aneurysms, aortic dilatations, and aortic dissections. While these polyester grafts are readily available, extremely durable, and biocompatible. They exhibit mechanical properties inconsistent with native aortic tissue. From a bio-engineering perspective, there are important geometrical and mechanical constraints that the synthetic replacements need to mimic to properly replace the aorta it needs to be compliant to function with the soft environment tissue and avoid causing damaging local stresses (pressure, friction).

RESULTS AND CONCLUSIONS

<u>Hyperelastic characterization:</u> The samples are fastened to an EnduraTEC Electro Force ELF 3200 Biaxial Tensile Tester (TA Instruments, New Castle, DE, USA) and equipped with a displacement transducer and a 1 Kg load-cell (Model 31, Sensotec Honeywell). The tests are performed on patches of 15×15 mm^2 affixed with four silk surgical threads model 4-0 (Ethicon, USA) with adjusted suture hooks. The biological samples are immersed in buffered solution at 37°C. Tissue are preloaded to a force of 0.05 N in both directions and pre-cycles (13 cycles) before testing. Equi-biaxial loading-unloading cycles are performed to 60% strain at 0.1 mm/s strain rate. The incremental (tangent) modulus is calculated at 15% and 45 % strain. <u>Viscoelastic Characterization:</u> The ELF 3200 also allows for frequency characterization (it can perform a frequency sweep from 0.1–100 Hz). Briefly, an oscillating force (load) is generated ($\sigma=\sigma_0\sin(\omega t)$,

with amplitude σ_0 and frequency ω) and produce an out-of-phase displacement ($\varepsilon=\varepsilon_0\sin(\omega t+\delta)$, with amplitude ε_0 and phase lag δ). From this, the complex viscoelastic stiffness is assessed: $E^*=E_s+iE_l$, where $E_s=\sigma_0/\varepsilon_0\cos(\delta)$ is the storage modulus and $E_l=\sigma_0/\varepsilon_0\sin(\delta)$ is the loss modulus, from which $\tan(\delta)= E_l/E_s$. It can be shown that for a Kelvin-Voigt model, $E^*=E+i\omega\mu$ with E and μ are the elasticity and viscosity respectively (then $|E^*|^2= E^2+\omega^2\mu^2$ and $\tan(\delta)=\omega\mu/E$) and the corresponding hyteresis is modeled as an ellipse (with an area $W_d=\pi\mu\omega\varepsilon^2$). The Loss Factor (or energy loss) is defined as the ratio of the area of the hysteresis over the storage deformation energy LF=(Energy hysteresis)/(Storage energy) or $LF=W_d/(W_e-W_d)$ with W_e the elastic deformation energy [2-4]. In Figure 1, we summarize the results for the incremental modulus (or tangent modulus) at 15% and 45% and the viscoelasticity characterization assessed with the energy loss. They are both shown for healthy aortic tissue, aneurysmal tissue and Dacron. One can note the significant differences between the synthetic material and the biological tissues. Disease tissue appears less stiff and has more energy loss than healthy tissue [4]. Current synthetic Dacron material have intrinsic stiffness and viscoelastic properties that are significantly different from the biological tissue. Improvement in terms of biomechanical integration would require adjustments of the viscoelastic properties to achieve closer properties to native tissue.

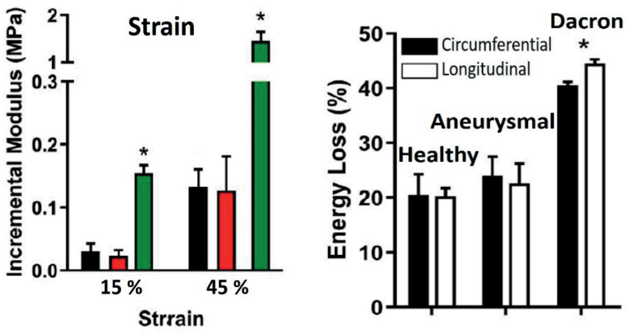

Fig 1 - Incremental modulus (left) and energy loss (right) for healthy, aneurysmal and Dacron

ACKNOWLEDGMENTS

The authors gratefully acknowledge the funding by NSERC National Science and Engineering Council of Canada RDCPJ 510049-17.

REFERENCES

1. Puskas JE, Chen Y, Biomacromolecules. 5(4):1141-54, 2004

2. Shahmansouri N, Alreshidian M, Emmot A, et al. Investigation on the regional loss factor and its anisotropy for aortic aneurysms. Materials 2016;9:867

3. Chung J, Lachapelle K, Wener E, et al. Energy loss, a novel biomechanical parameter, correlates with aortic aneurysm size and histopathologic findings. J Thorac Cardiovasc Surg 2014;148:1082-8; discussion 8-9

4. Zikry C, Evaluation of poly(vinyl alcohol) cryogel as viscoelastic reconstruction graft for the ascending aorta, Master Thesis, Department of Mechanical Engineering, McGill University, 2018

PAPER REF: 085

SURVEY PAPER ON PROTOTYPES APPLIED ON RESISTANCE, STRENGTH AND AGILITY TESTS

Francieli Fidler[1(*)], José Gonçalves[2], João E. Ribeiro[3], Fábio Mandello[4]

[1]Academic of Mechanical Engineering, Polytechnic Institute of Bragança, Bragança, Portugal
[2]Department of Electrical Engineering, Polytechnic Institute of Bragança, Bragança, Portugal
[3]Department of Mechanical Engineering, Polytechnic Institute of Bragança, Bragança, Portugal
[4]Department of Mechanical Engineering, Federal University of Paraná, Pato Branco, Brasil
[(*)]*Email:* francielifidler@alunos.utfpr.edu.br

ABSTRACT

The use of mobility, resistance and strength tests in physiotherapy treatments brings a continuous improvement of the conditions of mobility and strength of the individuals. The objective of this study is to carry out a systematic review in the literature on how these tests are performed. The used methodology is a featuring Timed Up and Go, Sit to Stand and Hand Force tests and instrumented chairs were searched in the SciELO and Pub Med databases, among others, from March to January 2019, being selected according to the inclusion or exclusion classification criteria. The results show all the articles that were chosen after the classification approach one of the three tests, or even of instrumented chairs. In all the articles it is noticed the presence of some alteration in the equipment used for the tests or even the inclusion of technologies for the same. In this work, it is concluded that the used of new technologies based on network communication is very important to improve test systems and are beneficial to the quality of results.

Keywords: physiotherapy, mobility test, strength test, instrumented chair.

INTRODUCTION

Biomechanics studies shows how human body performs the movements, that is, the way it reacts to the performance of any physical activity. Posture is known as the position that the body segments relate to each other due to the joint configuration and the state of balance of muscles and bones, for (Bragança, Arezes, Carvalho and Ashdown, 2016), the human being is able to adopt different postures according to the activity that they perform during the day, which, in order to be maintained, requires interactions between all parts of the body, besides the neural and biomechanical regions.

Tests to assess mobility and balance are widely used to control and suggest improvements for posture correction and greater mobility. Among them there are Timed Up and Go (TUG), Sit to Stand (STS) and Hand Force, the latter evaluates only the strength of the hand and not the lower limbs like the others. Each of this tests follow the same principle as the first ones performed with time (Podsiadlo and Richardson, 1991), but Mathias *et al.* (Mathias, Nayak, & Isaacs, 1986), have argued that the tests suffer some variations depending on the purpose of the test, for who is applied and the conditions of the environment that are performed.

This article has as main objective to present a comprehensiveness of how the mobility tests are performed and how the aids of the technologies have brought benefits for the results thus increasing reliability, accuracy and repeatability. The studies considered for this research should contain the way how the tests are performed or how the sensors are used, or even the instrumented chair that are used for similar physiotherapy tests.

During this work was made a type of questionnaire aimed at health professionals such as physiotherapists, physiatrists, rehabilitation therapists among others, to know if the prototype, that is present in a laboratory on IPB (Polytechnic Institute of Bragança), it is according to the reality when the tests are made.

This work shows the results of the bibliographic searches being a synthesis of the main works found, which have similar systems of the tests or a similar instrumented chair, being performed the SWOT analysis of the existing prototype.

RESULTS AND CONCLUSIONS

The diverse approaches report different means of carrying out the tests. The first techniques to perform these tests were simple, only with a chronometer and a chair in good condition, and with dynamometers in the case of the Hand Force test. More recent research highlights that is necessary to know all the response times for each command of the TUG steps, the time of get up, go to the cone, make the return, return to the chair and sit down again, the same for the STS, the time spent to get up and then sit down again.

Differences were found for the performance of these tests in people with reduced mobility or with some specific disease, such as Alzheimer's and Parkinson's. These people require a longer period of time to respond to commands, therefore, longer test times are considered, when compared to those who do not suffer any disease, also in the Hand Force where the type of force that is intended to be analyzed, can change the method of obtaining or even the equipment to perform the tests.

The evolution of the equipment is also a factor that influences the results. For lower limb mobility tests some more advanced studies employ motion and force sensors, while the most traditional ones use only a chronometer, not considering the variables beyond the total time. In the Hand Force, the more adapted the measurement system to the shape of the hand, the better are the results that the load cells, or the force sensors, will show.

ACKNOWLEDGMENTS

The authors gratefully acknowledge the Polytechnic Institute of Bragança.

REFERENCES

Bragança S., Arezes P., Carvalho M., Ashdown S. Effects of Different Body Postures on Anthropometric Measures. Advances In Ergonomics In Design, 2016. Springer International Publishing, p.313-322.

Podsiadlo D., Richardson S. The Timed "Up & Go": A Test of Basic Functional Mobility for Frail Elderly Persons. Journal of the American Geriatrics Society, 1991, 39(2):142-148.

Mathias S., Nayak U. & Isaacs B. Balance in elderly patients: the "get-up and go" test. Archives of Physical Medicine and Rehabilitation, 1986, 67(6):387-389.

Gonçalves J., Batista J., Costa P. Fully-Automated Strength, Agility and Endurance Tests Assessment: An Integrated Low Cost Approach Based on an Instrumented Chair. 19th IEEE International Conference on Emerging Technologies and Factory Automatio (ETFA'2014) Barcelona (Spain), 16 to 19 September 2014.

PAPER REF: 086

MICROGRAPHIC STUDY OF WELDED JOINTS IN ALUMINUM ALLOYS BY MIG PROCESS

Sharlane da Costa[1(*)], João E. Ribeiro[2], José Gonçalves[3], Bruno B. Medeiros[4], Eduardo Izeda[5]

[1]Academic of Mechanical Engineering, Polytechnic Institute of Bragança, Bragança, Portugal
[2]Department of Mechanical Technology, Polytechnic Institute of Bragança, Bragança, Portugal
[3]Department of Electrical Engineering, Polytechnic Institute of Bragança, Bragança, Portugal
[4]Department of Mechanical Engineering, Federal University of Paraná, Pato Branco, Brasil
[5]Investigador of Mechanical Engineering, Polytechnic Institute of Bragança, Bragança, Portugal
[(*)]*Email:* sharlane@alunos.utfpr.edu.br

ABSTRACT

The objective of this work is to analyze and evaluate the influence of thermal treatments of solubilization, tempering and aging sequence, made in the 6082 - T6 alloy, previously welded by the MIG (Metal Inert Gas) welding process.

In this work, a microscopically analysis of the welded and a thermally treated joint is realized, to evaluate the microstructure quality and the results found by varying the time and temperature during the treatment. In addition, it is intended to verify the influence of the waiting time amongst the heat treatment of quenching and artificial aging.

Keywords: Robotic welding, MIG welding, Alloy AA-6082-T6, Solubilization, Quenching, Artificial aging, Thermal treatments, Micrographic analysis.

INTRODUCTION

Aluminum is a lightweight, ductile, corrosion resistant, non-toxic, good heat conductor, good conductor of electricity and processable, to have good flow and resistance limits (Souza, 2015), thus, due to its good characteristics and properties it is so widely employed.

The welding is a very usual and important, which is why, it is essential to acknowledge the effects and problems generated during the welding process to guarantee the quality of the joint and the final product. The main defects of the welds are porosities, oxide inclusions, formation of surface oxide films, hot cracking during solidification, non-melting, and reduction of corrosion resistance (Mathers, 2012). In aluminum alloys, heat treatment is of great importance as it is commonly used to recover the mechanical properties after the welding process. Heat treatment improves the strength of aluminum alloys by a process known as precipitation hardening, which occurs during heating and cooling of an aluminum alloy and in which forms the precipitates in the aluminum matrix (Mohamed, Samuel, 2012).

This work carries out 18 different cycles of thermal treatments and after that, it holds a micrographic analysis to evaluate which cycle presented the best results in the matter of recovery of the mechanical properties after the welding.

RESULTS AND CONCLUSIONS

The best-performing thermal cycle was found for the combination one (test 1), in which the sample was solubilized for 90 minutes at temperature of 520 ° C, then tempered and finally aged at 190 ° C for 20 hours. Test one shows an ideal micrograph, presenting uniform precipitates in size and distribution throughout the matrix and thus displacements are unable to cut precipitates, increasing strength and hardness.

Presented below are the micrographs of assay number one, in Figure 1, where they indicate the micrographs of the base metal, Heat Affected Zone – HAZ, and melt zone, respectively.

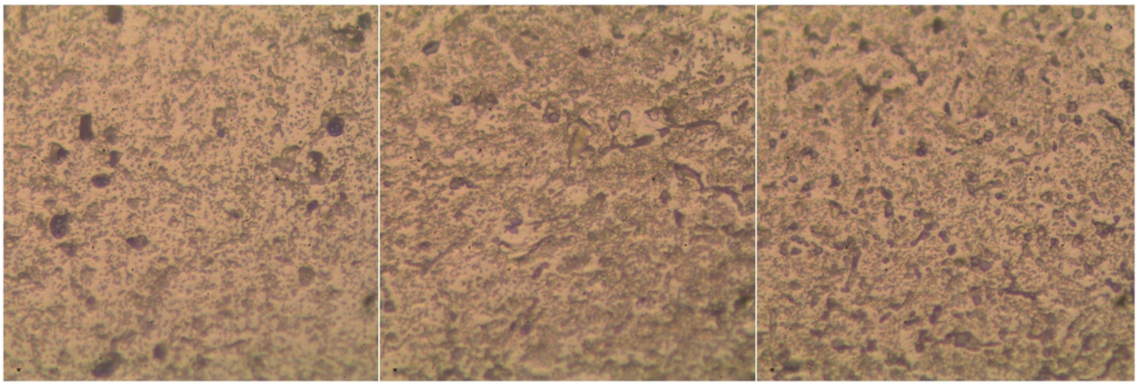

Figure 1 - Micrographs of the test number 1

The regions with the most noticeable changes in micrography were HAZ and weld. In Figure 1, in these regions, it is possible to observe a microstructure with an optimal size and distribution of the precipitates for the hardening and where, theoretically, the maximum hardness value is reached.

ACKNOWLEDGMENTS

The authors gratefully acknowledge the funding by PORTUGAL2020: SI I&DT Individual – Call 16/SI/2015 (Proj. nº 9703): “Automatização de Processos de Soldadura de Estruturas Hiperestáticas em Ligas de Alumínio (APSEHAL)”.

REFERENCES

F. M. Souza, “O Alumínio e suas ligas: Destaque na liga AA4006 produzida por lingotamento contínuo e semicontínuo”, pp 15, 2015.

G. Mathers, “The welding of Aluminium and its alloys. The effects of brief mindfulness intervention on acute pain experience: An examination of individual difference”, Vol. 1, 2012.

Mohamed, A.M.A. and F.H. Samuel, A Review on the Heat Treatment of Al-Si-Cu/Mg Casting Alloys. Heat Treatment - Conventional and Novel Applications. 2012.

PAPER REF: 087

THE IMPORTANCE OF STARTING AN AIRCRAFT ENGINE DURING A FLIGHT

Antoni Jankowski[1](*), Paweł Stężycki[2], Andrzej Żyluk[3]

[1]Air Force Institute of Technology, Warsaw, Poland
[2]Institute of Aviation, Warsaw, Poland
[3]Polish Air Force University, Deblin, Poland
Email: (*)[1]antoni.jankowski@itwl.pl [2]pawel.stezycki@ilot.edu.pl, [3]a.zyluk@law.mil.pl

ABSTRACT

The paper presents the analysis of the drive unit start-up process of training aircrafts during flight, which are equipped by the Deblin's "School of Eaglets" and intended for a flight training of officer cadets. The analysis of the start-up process was conducted using data from on-board flight recorders recorded during a flight training, whose aim was an emergency launch of particular drive units, and with the help of the so-called phase diagrams of the selected operating parameters of the particular flight drive systems. The construction principle of typical start-up systems was presented schematically presenting their base subassemblies. The importance of proper selection of the start-up system for the particular aircraft was emphasised and the basic indicators, which must be taken into account in the process, were cited. The basic mathematical dependences necessary in designing and determining the basic characteristics of the engine start-up process were explained. At the end, the obtained results and the main problems that need intervention as well as the proposal of preventive activities were shortly commented.

Keywords: engine start-up during flight, flight safety.

INTRODUCTION

The start-up process of drive units during the flight of training aircrafts, which are equipped by the Deblin's "School of Eaglets" and intended for flight training of future pilots, is a very important element in terms of flight safety. The construction of the aircraft engine start-up system is often an indicator of ranges of the aircraft's possible applications. The start-up system – regardless of the type – consists of three main systems: start-up automatics, a basic generator, and a power supply. The power source can be an integral part of the aircraft or engine. In modern turbine jet engines, start-up is automatic in accordance with the specially tailored programme of the generator turn-on/turn-off, ignition, and start fuel. The type of start-up system determines also its weight and dimensions, which is especially important for small aeroplanes, as well as the necessary actions to be performed by the pilot during its launch. This is especially important during the flight training in the air, of the future pilots and it is directly related to flights' safety.

The research and analysis of the start-up processes were conducted on (among other):

- the PT6A-25C engine by the Pratt & Whitney Company constituting a drive unit of the PZL-130TC-II „Olik" aircraft,
- the PZL-10WM engine constituting the drive unit of the W-3 "Sokół" helicopter,
- the SO-3 turbojet engine of the TS-11 "Iskra" aircraft.

These are the basic aircrafts equipped by the Deblin's School Eaglets. The task of the start-up system of the area engine is to give the necessary rotational speed of the engine power transmission (an air compressor and turbine unit), at which the power developed by the turbine N_t is greater than the sum of the power pulled by the air compressor N_s and other engine subassemblies – in accordance with the balance of the power of the turbine specified by the dependency [1]:

$$N_t > N_s + N_{agr} \tag{1}$$

where: N_{agr} – the power needed for the units' drive and overcoming the frictional resistances.

The analysis was conducted mainly using the so-called phase diagrams of the selected engine operation parameters, described with the general dependency [2, 3, 4]:

$$\frac{dX}{dt} = f\left(X\right) \tag{2}$$

where: X – tested parameter,

t – time (s)

CONCLUSION

The executed analyses of the drive units' start-up processes analysis show that the start-up systems of the drive units are effective and provide good operational (practically) in all conditions. However, they are not devoid of minor flaws, whose existence directly affects the safety of flights and requires taking preventive actions or even modernisation of certain elements of the given start-up system.

Particular attention was paid to cases of failed engine start-ups during the flight, which were affected by mainly additional activities, without which it is impossible to launch the engine during the flight, imposed on the pilot.

It is also important to keep the current verification of state of control of aircraft drive unit start-up processes, which allows avoiding unnecessary loads (e.g. thermal ones) of the engine drive units. The method of phase mapping of the rotational speed growth is a very good way of such monitoring of engine control state. It pretty accurately indicates the points of excessive loads of aircraft drive units' elements.

REFERENCES

[1] Dzierżanowski P., Kordziński W., Łyżwiński M., Otyś J., Szczeciński A., Wiatrek R.: Turbinowe silniki odrzutowe [Turbine jet engines]. WKŁ, Warszawa 1983.

[2] Kowalski M., An Analysis of Failure Symptoms of the Airscrew Drive in the PAL-130-TCI Olick Aircraft, Journal of vibration engineering & technologies, Volume: 2 Issue: 4 pp. 315-326, 2014.

[3] Kowalski M., Considerations on operation of a turbojet engine with the 'bypass' design. Ed.: Gomes, JFS; Meguid, SA, M2D2015: Proceedings of the 6th international conference on mechanics and materials in design, pp. 581-586, 2015.

[4] Kozakiewicz A., Kowalski M., Unstable operation of the turbine aircraft engine, Journal of theoretical and applied mechanics Volume: 51, Issue: 3, pp. 719-727, 2013.

PAPER REF: 088

EVALUATION OF NITROGEN OXIDES EMISSION IN THE COMBUSTION OF WATER AND FUEL MICROEMULSION

Andrzej Żyluk[1(*)], Paweł Stężycki[2], Antoni Jankowski[3]

[1]Air Force Institute of Technology, Warsaw, Poland
[2]Institute of Aviation, Warsaw, Poland
[3]Institute of Aviation, Warsaw, Poland
Email: [1(*)]andrzej.zyluk@itwl.pl, [2]pawel.stezycki@ilot.edu.pl, [3]antoni.jankowski@ilot.edu.pl

ABSTRACT

The paper presents the importance of the composition of gases emitted to the atmosphere. Among many methods of reducing the emission of nitrogen oxides, an important option is to provide fuel-water microemulsions to the engine. The components of the microemulsion are thoroughly dispersed, creating a mixture similar to a homogeneous mixture (molecular mixture). Water is a source of oxygen when burning a rich mixture, causing, among other things, a lowering of the temperature in the flame zone, which reflects the heat mechanism (Zeldovich mechanism) and reduces the emission of nitrogen oxides. The presented test results indicate that the lowest concentration of nitrogen oxides concerns the engine feeding with a microemulsion containing 10% and 20% water. Supplying the engine with both a microemulsion containing 10% and 20% concentration of nitrogen oxides in water has been significantly reduced throughout the entire working range of the engine. As the water increases, the NOx concentration also decreases. This concentration is reduced to 60% in the standard delivery. In summary, it was pointed out that the use of water lowers the temperature in the combustion chamber.

Keywords: combustion engines, combustion chamber, fuel microemulsion, nitrogen oxides emission.

INTRODUCTION

Air pollution, which occurs during the combustion process in the combustion chamber, is a very important problem for the environment [2, 3]. The most harmful to the environment and to humans are nitrogen oxides NOx.

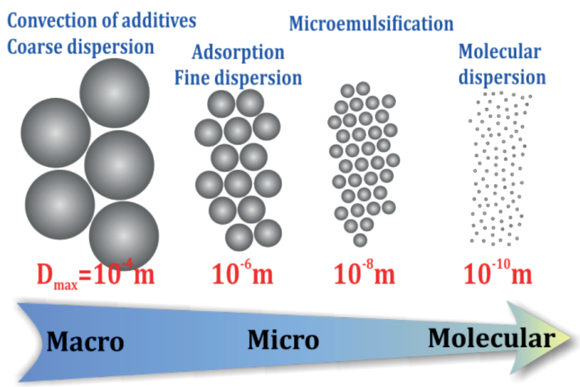

Fig. 1 − Mechanism of emulsions` formation with different degrees of dispersion (from the turbulent dispersion via turbulent diffusion to molecular dispersion)

They are carcinogenic and gathering in the atmosphere react creating a photochemical smog dangerous for health. Among many methods of reducing NOx emissions, an important option is supply the engine water-fuel microemulsion. Microemulsion's components are exactly dispersed to form a mixture similar to the homogeneous mixture (molecular mixture) [1]. The mechanism of microemulsion's formation with different degrees of dispersion shows Fig. 1.

TEST RESULTS AND DISCUSSION

The test results showing the engine loads for the three rotational speeds are shown in the drawings. The example is shown below.

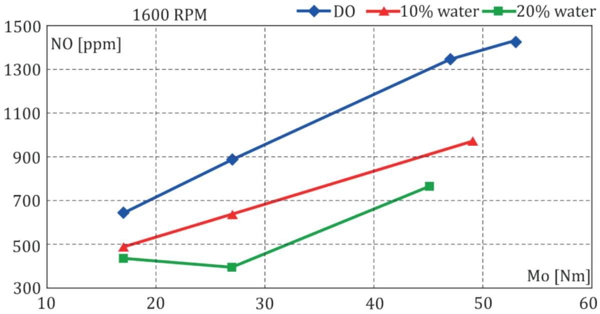

Fig.1 – Concentration of nitrogen oxides (NOx) in exhaust gases, for the engine load performance at the engine speed of 1600 RPM for supply with diesel oil (DO), microemulsion containing 10% and 20% of water

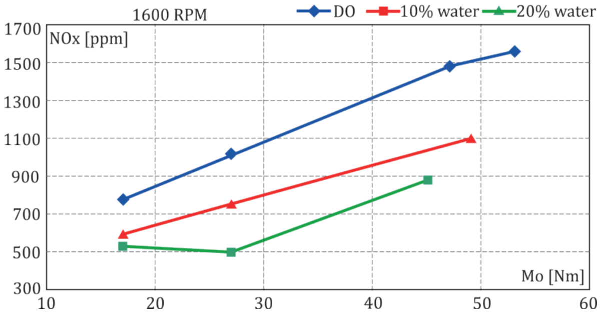

Fig.2 – Concentration of nitrogen monoxide (NO) in exhaust gases, for the engine load performance at the engine speed of 1600 RPM for supply with diesel oil (DO), microemulsion containing 10% and 20% of water

CONCLUSION

The maximum concentration of NOx for n = 1200 RPM for engine supplied with diesel oil was 2178 ppm, while the maximum concentration of NOx engine supplied with microemulsion of 10% water was 1448 ppm and 20% – 1132 ppm.

The engine supply both with the microemulsion containing 10% and 20% water concentration of nitrogen oxides was dramatically reduced in the entire operating range of the engine.

With the increase of the water, concentration of NOx is reduced, too. This concentration is reduced by up to 60% in the standard supply.

The use of water reduces the temperature in the combustion chamber. For maximum NOx concentration reduction, the microemulsion should be targeted flame zone.

REFERENCES

[1] Jankowski A., Kowalski M.: Mechanism of Formation of Toxic Substances Emission of Combustion Engines. Journal of KONBIN. 1(30) Warsaw 2015 (in Polish).

[2] Cheng A., Upatnieks A., and Mueller C.: Investigation of the Impact of Biodiesel Fuelling on NOx Emissions Using an Optical Direct Injection Diesel Engine, Int. J. Engine Res., 7(22), 297-318, 2006.

[3] Jankowski A., Kowalski, M., Design of a new alloy for internal combustion engines pistons, Ed. Gomes, JFS; Meguid, SA, Proceedings of the 7th international conference on mechanics and materials in design (M2D2017), pp. 607-618, 2017.

PAPER REF: 089

ANALYSIS OF FORCES IN THE BRYZA-1R ENGINE MOUNTING FRAME

Paweł Stężycki[1(*)], Antoni Jankowski[2]

[1]Institute of Aviation, Warsaw, Poland

[2]Air Force Institute of Technology, Warsaw, Poland

Email: [1(*)]pawel.stezycki@ilot.edu.pl, [2]antoni.jankowski@itwl.pl

ABSTRACT

The paper presents the results of tests carried out on the pipe of the engine-mounting frame to the Bryza-1R airframe, during the qualification tests of this aircraft. Strength sensors were used in the tests. Five outlets were made, carrying out selected flight elements, suggesting the possibility of significant increases in forces in the pipe. Analysis of existing forces in the frame was carried out using Fourier analysis. The results of the analysis are illustrated graphically. The paper presents only the elements of the flight in which the amplitude of the force was visible and showed the nature of the impact of the individual elements of the drive unit. Each display was described by the type of flight element being made and the scope of the drive unit's work. It has been proven that the dynamics of axial forces in the frame was small. However, no explicit reason for the break of the mounting bracket of the frame was indicated. It was found that the dynamics of forces occurring in the frame are decisively influenced by low frequency vibrations, originating from the airframe and the propeller shaft rotation. To a small extent from successive harmonics from propeller shaft rotation, from high-speed gearbox and drive turbine.

Keywords: aircraft, qualification tests, flight safety.

INTRODUCTION

During qualification tests prior to introducing aviation equipment to the inventory of the Air Forces of the Republic of Poland, the following, among others, are tested: equal types of fastening nodes for wings, vertical and directional empennage, propulsion units of an aircraft and others [1, 3, 4].

A similar case took place during qualification tests of the Bryza-1R aircraft, with an installed propulsion unit, consisting of a PWD-10B/PZL-10S engine, in the configuration with a HC-B5 propeller by Hartzell [2, 5]. During the test flights, the frame for mounting the engine to the airframe was tested (additionally). The reason was that during the tests, largest stretching forces were found in that tube of the engine frame. Besides, it is fastened to the lug, on which a crack appeared. The aim of these tests was to additionally check the dynamics of the axial force in the engine-mounting frame's tube, after broadening the frequency band from 200 to 400 Hz. The second objective was to determine the influence of variable flight conditions on the engine vibrations and its mounting frame in the airframe.

ANALYSIS OF TEST RESULTS

The study was based on Fourier's analysis, with the use of the Excel software for graphic presentation. It is a sufficient tool to effectively present a variable signal over time, in the frequency scale. Each analogue signal can be presented in the form of sinusoidal components with an appropriate amplitude, phase, and frequency.

It allows the determination of the influence of a particular element of an aircraft, propulsion unit on the presence of excess axial force amplitude in an engine-mounting frame′s tube of an aircraft. The example is shown in the figure below.

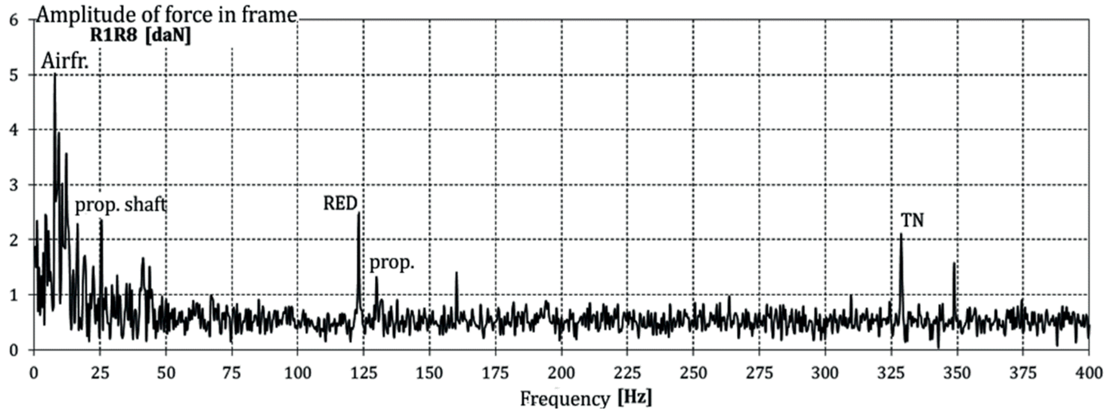

Fig. 1 – Flight 4, nominal operating range

CONCLUSION

The conducted analysis showed a quite small dynamics of axial forces in the R1R8 tube of the TWD-10B/PZL-10S engine-mounting frame, which was confirmed by the initial study. Broadening the band from 200 to 400 Hz, showed just a minor (order of several daN) influence on the dynamics of the forces in the frame′s pipe, coming from the propeller and the turbine. However, we need to remember that the applied band might not have shown the influence of the turbocharger, since its frequency band appears in the range of 350 to 526 Hz.

Anyway, it was concluded that the decisive influence on the dynamics of forces in that tube was by the low-frequency vibrations coming from the airframe (own vibrations of the plane) and the rotations of the propeller shaft. In a lesser extent, from subsequent harmonics of propeller shaft rotations (i.e., 2, 3 and 5), from the fast-running reducer and the drive turbine.

REFERENCES

[1] Jankowski A., Kowalski, M., Design of a new alloy for internal combustion engines pistons, Ed. Gomes, JFS; Meguid, SA, Proceedings of the 7th international conference on mechanics and materials in design (M2D2017), pp. 607-618, 2017.

[2] Kowalski M., An Analysis of Failure Symptoms of the Airscrew Drive in the PAL-130-TCI Olick Aircraft, Journal of vibration engineering & technologies, Volume: 2 Issue: 4 pp. 315-326, 2014.

[3] Kowalski M., Considerations on operation of a turbojet engine with the ‘bypass’ design. Ed.: Gomes, JFS; Meguid, SA, M2D2015: Proceedings of the 6th international conference on mechanics and materials in design, pp. 581-586, 2015.

[4] Kozakiewicz A., Kowalski M., Unstable operation of the turbine aircraft engine, Journal of theoretical and applied mechanics Volume: 51, Issue: 3, pp. 719-727, 2013.

[5] Technical description of the BRYZA-1R aircraft, part 1. Airframe, reference number PBD-1/5/2000 alb. 6. Mielec 2000.

PAPER REF: 090

BIOLOGICAL METAPHORS TO CONSTRUCT A NARRATIVE IN PRODUCT DESIGN

Pedro Bandeira Maia[1*], Maria João Felix[2], Gilberto Santos[2], Nuno Dias[3], George Stilwell[4]

[1] Polytechnic Institute of Coimbra, ESEC, DAT, Coimbra, Portugal
ID+ Research Institute for Design, Media and Culture, University of Aveiro
[2] Design School (ESD) Polytechnic Institute Cávado Ave, Barcelos, Portugal
[3] University of Aveiro
ID+ Research Institute for Design, Media and Culture, University of Aveiro,
[4] Faculty of Veterinary Medecine, University of Lisbon
[(*)]*Email*: bandeiramaia@esec.pt

ABSTRACT

Biomimetic is used in specific design projects, mainly as a methodology focused on the study of technical, mechanical and formal aspects. Our research aims to expand the biomimetic taxonomy, continuing the study of nature in a broader design perspective, not just on their mechanic and formal aspects, but in the study of animal behaviour in its aesthetic and symbolic dimension. In this context, the present paper advocates the need to deep in the exploration of this inspirational and methodological relationship between Design and Nature from the study of seduction biological behaviors of non-human.

We believe this approach could be an inspiration for new artefact human interaction paradigms.

Keywords: Biomimicry, Artefact, Interaction Design, Experience Design, Biological Inspiration, Seduction Rituals, Taxonomy.

INTRODUCTION

Whether in Design, as in Engineering and Art, inspiration in Nature within the framework of human creation has a relevant historical tradition that is lost by immemorial time. The methods of biological inspiration established in Design, such as biomimetics, focus mainly on finding innovative technical and formal solutions, not focusing on the poetic and aesthetic potential that Nature offers to think about the aesthetic qualification of technological mediation with products.

The development of new meanings in the human relationship with technology, presents itself as a major challenge in a post-digital society.

RESULTS AND CONCLUSIONS

We developed a taxonomy of behaviours based on animal´s seduction and mating rituals with the goal of building a conceptual framework that relate these behaviors with the design of inedited interactions and contribute to the construction of new metaphors in product design.

The study of techniques of rituals of seduction and dating found in the non-rational animals seeks to establish contact bridges between intangible concepts and timeless archetypes, and the possible relations generated between man and artifact. We believe that would be possible to build and develop the human imagination that enhances experiences, behaviors and seductions grounded in biological and timeless archetypes that promote new relationships with technological objects.

To structure the information related with biology and ethology, a "taxonomy of biological behaviors of seduction" has been developed, according to Design's perspective, based on Nathan Shedroff's (2010) "dynamic structure of experience".

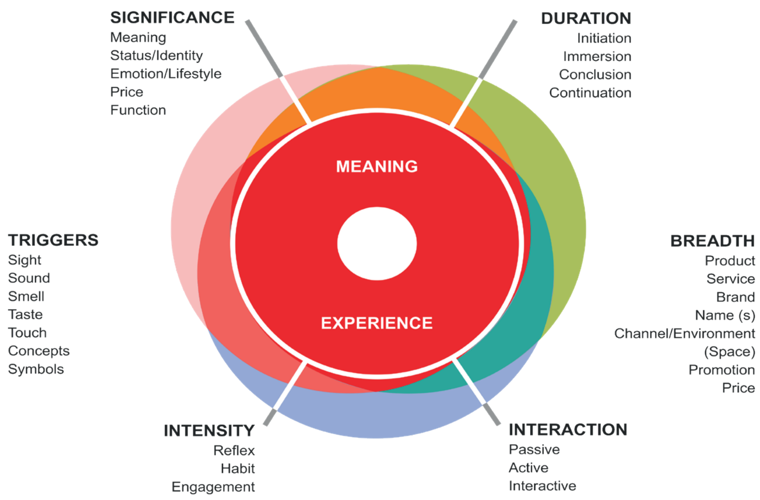

Fig. 1: Dynamic structure of experience (Shedroff, 2010)

This taxonomy should enable and support the design of new interfaces with technologically rich artifacts, as well as new forms of human social interaction through technological mediation, inspired by seduction rituals of animals.

The concepts developed show that inspiration in seduction rituals can support and foster the development of innovative Design solutions, as well as a new awareness of Nature's inspirational potential regarding the mediation between humans and technology, but also the technological mediation between humans.

REFERENCES

Shedroff, N. (2001). Experience design 1. Indianapolis, Indiana, USA: New Riders.

Shedroff, N. (2010). Meaningful Innovation Relies on Interaction and Service Design. Interaction Design Association. Rocovery on 22, may, 2013 from https://vimeo.com/9659499

PAPER REF: 091

GUIDING PRINCIPLES OF MATERIALS SELECTION FOR PRODUCT DESIGNERS

Maria João Félix[1(*)], Pedro Ferreira[2], Gilberto Santos[2], Ricardo Simões [2], João Martins[3]

[1] CIAUD, Lisbon School of Architecture, Universidade de Lisboa, Lisbon, Portugal, and Design School (ESD) Polytechnic Institute Cávado Ave, Barcelos, Portugal

[2] Design School (ESD) Polytechnic Institute Cávado Ave, Barcelos, Portugal

[3] *School of Technology and Management* (ESTG) Polytechnic Institute of Viana do Castelo, Portugal

[(*)]*Email:* mfelix@ipca.pt

ABSTRACT

This work intends to analyze the importance of the materials selection process for the development of a new product.

The aspects that influence the selection of materials in the Design process are due to the fact that these collaborate in the materialization of a project, stimulating a better interaction in the utilization of the products and consequently in the improvement of the people's quality of life.

The strategic use of a material is one the most influential means designers have to communicate and create emotional connections with its users; however, the materials classification in simple and definitive categories is complex, due to the diversity of options available in the market. This study can provide a significant contribution to the field of the product Design. As such, the general objectives of this work are to identify, analyze and understand the importance of the selection of materials in the development of a new product

Keywords: Materials selection; Material properties databases; Product design

INTRODUCTION

It is extremely important to provide the necessary information so that the designer can make decisions in the selection of materials in the initial phases of a product's development. By using woods, metals, plastics, or ceramics, (Lefteri, 2007)the designer will have a variety of books and technical manuals available applied to several environments and usage conditions. However, as it can be seen in the study of the selection of materials in Design, there are gaps in the selection methods as well as in the way these are available.

Facing an empirical, subjective and quantitative review of the materials selection area in Product Design, it is urgent, to create a library equipped with methods and instruments that allows to follow the development of product design projects, prioritizing a usage reflection and the proposals for the utilization of the best materials and sustainable (Ljungberg, 2007) transformation processes.

Mostly, the supports that the designers have upon this theme are developed by engineering experts, in which the used technical language isn't well interpreted by the designer language. It has come the time to break this current paradigm that exists by the universities as well as by the companies. The Designer should indeed, comprehend and understand the concepts related to the materials being applied to the products, but they don't need to enunciate physical properties, analyze and interpret graphical data, as for example, it is presented to us through the program

CES (M F Ashby & Cebon, 2007), selection of materials, developed by the professor Mike Asbhy (Michael F. Ashby & Johnson, 2014) and the respective cooperators of the Cambridge University. Despite the program validating positive results, it adds more value to the engineering area than to the product Design.

The research focuses on an exploratory and quantitative research, which consists of reformulating events, comparing ideas and reflecting on some later studies to the proposed theme building new hypotheses.

After a literature review on the subject, interviews are scheduled to be conducted with alumni of product design and designers (van Kesteren, 2008) who are in the market, with the objective of making a survey of the difficulties in the selection of the materials and the way they have overcome them in their work. A critical analysis of the existing educational materials and a proposal to update them will then be performed.

RESULTS AND CONCLUSIONS

The chances are temporary, considering that we are still in the initial phase of the study, but facts and theories are being analyzed, making the problem less complex. We intend to demonstrate that the methods and instruments of the materials selection aren't easily available and that there are gaps in the way these are used by the product designer. The selection tools aren't intuitive to the Designer and he finds difficulties in the data interpretation, thus the existing tools use a specific language the Designer isn't used to, being necessary to clarify the language, turning to simple and explanatory concepts, with few physical properties.

It is necessary for the Designer to understand the importance of the materials selection for the development of a product, in a way to validate his choices.

It is essential to understand beyond the material inner characteristics, the subjective characteristics, putting himself in the place of the possible user. And, finally, understand as well that the selection of materials is part of the creative process, being adopted as well as a methodology to be used in a specific phase of the project, or in the proposal progression, in cycles.

This study intends to propose supporting guidelines to the product designer, in the selection of materials, taking into consideration aspects as seen in the study, selection of materials in Design. It will be taken into consideration the contribution for the development of useful objects; for the increase of the product lifespan; the product's cycle of life; the culture valorization, materials that can be recycled; the substitution of raw materials, which are harmful for human health and the environment and the use of materials that come from natural resources.

REFERENCES

Ashby, M. F., & Cebon, D. (2007). Teaching Engineering Materials : the CES EduPack. *Cambridge University*.

Ashby, M. F., & Johnson, K. (2014). *Materials and Design: The Art and Science of Material Selection in Product Design: Third Edition*. *Materials and Design: The Art and Science of Material Selection in Product Design: Third Edition*. https://doi.org/10.1016/C2011-0-05518-7

Lefteri, C. (2007). *Making It: Manufacturing Techniques for Product Design*. *Continuum*.

Ljungberg, L. Y. (2007). Materials selection and design for development of sustainable products. *Materials and Design*. https://doi.org/10.1016/j.matdes.2005.09.006

van Kesteren, I. E. H. (2008). Product designers' information needs in materials selection. *Materials and Design*. https://doi.org/10.1016/j.matdes.2006.11.008

PAPER REF: 092

TECHNOLOGICAL INNOVATION AND PEDAGOGICAL PROCESSES, FOR THE FASHION AND TEXTILE DESIGN HIGHER EDUCATION COURSES IN PORTUGAL.

Maria João Félix[1(*)], Sónia Seixas[2], Fernando Moreira da Silva[3]

[1] CIAUD, Lisbon School of Architecture, Universidade de Lisboa, Lisbon, Portugal, and Design School (ESD) Polytechnic Institute Cávado Ave, Barcelos, Portugal

[2] Design School (ESD) Polytechnic Institute Cávado Ave, Barcelos, Portugal

[3] CIAUD, Lisbon School of Architecture, Universidade de Lisboa, Lisbon, Portugal

[(*)] *Email:* mfelix@ipca.pt

ABSTRACT

Higher education degrees in Fashion and Textile Design are relatively recent in Portugal, however, advances in the Textile and Clothing Industry, regarding technological innovation, are increasingly fast and demanding. On the other hand, particularly in the consumer society – the individual – aspires to the consumption of products that correspond to innovations and that can improve their quality of life, without neglecting environmental, social and economic concerns. Considering the importance of Fashion and Textile products under this perspective, this research evidences it as its universe of study. Thus, it is important to consider the academic curricula in the field of Fashion and Textile Design, in order to proceed with its analysis, and contribute with some suggestions for the improvement regarding this change fostered not only by the industry but also by the consumers' desires.

Keywords: Fashion Design, Textile Design, Design Education, Higher Education, Portugal

INTRODUCTION

Teaching in Fashion Design in Portugal, comes from an empirical learning process from one professional to another trained at the workplace at the tailor, designer and seamstresses' studios, without the attribution of a vocational academic degree (de Wet, 2017). Industrialization and the following evolution of the textile and clothing industry came to foster the systematization of academic knowledge in technical subjects in the fashion area to suppress the needs of the sector. With the appearance and proliferation of courses in the area in the 80s, (Fletcher, 2010)fashion Design comes closer to the Design field, associated with the economic pressure as a result of the evolution in the clothing and textile industry(Hameed & Umer, 2017). It is assigned to the designer an increasingly value associated with the use of knowledge and the management of new technologies, seen as productivity and international differentiation factors.

This study will start from an holistic vision of the Higher Education state of art in Fashion and Textile Design courses in Portugal to the definition of a strategic vision. Its main objective is to analyze the existence of gaps in the academic curricula, (Sinclair & Hong Kong Polytechnic, 2008) of Fashion and Textile Design courses in Portugal, proposing a curricular revision which responds to the real needs of the sector and future designers' ambitions, culminating in a new curricular proposal for the Integrated Master's Degree in the field. In addition to the collection of information through documentary research, an active research methodology will be used, mostly qualitative, using quantitative methods to analyze some data. The obtained results will justify this study.

For these purposes, the research begins by identifying fourteen academic curricula from six Portuguese Institutions: Instituto Politécnico do Cávado do Ave (IPCA), Escola Superior de Artes e Design (ESAD), Escola Superior em Artes Aplicadas (ESART), Faculdade de Arquitetura da Universidade de Lisboa (FAUL), Universidade da Beira Interior (UBI), Universidade do Minho (UMINHO) and, four institutions and European curricula will be reviewed: Central Saint Martins, École Supérieure des Arts et Techniques de la Mode (ESMOD), Institut Français de la Mode (IFM) e Parsons. The review of these curricula will allow to compare and identify differences that will support the construction of a new curricular proposal.

The methodology of this research will be based on a literature review and a collection from the involved entities, universities and the (Clothing and Textile Industry- CTI) sector agents, placed in the North and Centre of Portugal, where most of the sector agents are placed. It will be developed a grid of the national and European curricula correlation and at last, there will be the cross-checking of the obtained results, contributing this way to the conclusions, analysis of the results and recommendations.

The main findings of the survey are, among others, the contribution to improve Higher Education Studies (Cowan, 2000)in the field of Fashion and Textile Design, pointing out suggestions for improvement, favoring the competitiveness of the national economy, enhancing the relationship between universities and industry by developing more adjusted programs to the needs of the sector, future designers and consumers.

RESULTS AND CONCLUSIONS

In a first analysis it is concluded that in the first cycle of studies (Degree) all curricula include the Design scientific area, some integrate the technology and art areas, but the remain areas are different, without standardization. In the second cycle of studies (Master's Degree), the majority integrates the design and textile technologies scientific areas, being the remain ones equally different.

This study intends to show that there are substantial differences in the scientific areas of the academic curricula of the Textile and Fashion Design courses in Portugal, existing, therefore, the need for an uniformization. The previously mentioned curricula of the European Institutions will be equally analyzed, allowing to perform a comparison, and thus, propose suggestions to improve with the proposal of a new academic curriculum.

It will be proposed the development of an Integrated Master's Degree in Textile and Fashion Design, interdisciplinary in the first two years, with common subjects from creative process, fashion and consuming trends, weaving/knitwear/stamping/manufacturing, industry 4.0, marketing, circular economy, green textile, among others. The last two years will be specialized in a sector of the clothing and textile industry: fashion (men; women; children), textile (knitwear/weaving/stamping), manufacturing and modelling, footwear and fashion accessories, home and functional textiles.

REFERENCES

Cowan, J. (2000). Designing courses for higher education. *British Journal of Educational Technology*.

de Wet, A. J. C. (2017). An educational tool to encourage higher level thinking skills in the selection of images for fashion design mood boards: an action research approach. *International Journal of Fashion Design, Technology and Education*. https://doi.org/10.1080/17543266.2016.1173236

Fletcher, K. (2010). Design History Society Book Reviews Sustainable Fashion and Textiles Journeys Fletcher's approach in Sustainable Fashion and Textiles crosses disciplines: she looks at fashion and. *Journal of Design History*.

Hameed, U., & Umer, S. (2017). Comparative study on fashion & textile design higher education system, Pakistan vs UK. In *IOP Conference Series: Materials Science and Engineering*. https://doi.org/10.1088/1757-899X/254/22/222005

Sinclair, R., & Hong Kong Polytechnic, U. (2008). *Exploring textiles futures: textiles and fashion education for generation x, y and z, negotiating the digital transition. 86th Textile Institute World Conference, Vol 2, Conference Proceedings*.

PAPER REF: 093

PLANE STRAIN FRACTURE TOUGHNESS BY COMPACT-TENSION SPECIMENS OF DIMENSIONS COMPLETED BY WELDED ATTACHMENTS

M.A. Beltrán-Zúñiga[1*], J.L. González-Velázquez[1], D.I. Rivas-López[1], F. Hernández-Santiago[2], H.J. Dorantes-Rosales[1]

[1]Instituto Politécnico Nacional, Escuela Superior de Ingeniería Química e Industrias Extractivas, Departamento de Ingeniería en Metalurgia y Materiales, Ciudad de México, México.
[2]Instituto Politécnico Nacional, Escuela Superior de Ingeniería Mecánica y Eléctrica, Ciudad de México, México.
**Correspondent author*: mabz_2205@hotmail.com

ABSTRACT

The plane strain fracture toughness values were obtained by the use of compact tension specimens completed by welded attachments. The results were compared to those obtained from one-piece CT specimens, observing differences within the acceptable experimental error (less than 5%). At first, these results demonstrate that the proposed method of completing the dimensions of a standard specimen with welded attachments is a viable alternative for the experimental determination of the plain strain fracture toughness in directions where the component geometrical limitations do not allow to obtain one-piece specimens that meet the dimensions established in the ASTM E1820 standard, as is the case of the short transverse directions of steel pipes. Additionally, it is experimentally determined that the short transverse directions RL in steel pipes of API 5L specifications, fabricated by the UOE process are weaker than the CL and LC directions. This result is attributed to the orientation of the pearlite bands with respect to the plane of cracking.

***Keywords**:* Welding, fracture toughness, fracture mechanics, pipeline steel

INTRODUCTION

The plane strain fracture toughness (K_{IC}) of low carbon steel has been widely studied, due to its great importance in integrity assessments of components containing crack-like defects. However, in most cases, the studies are conducted with specimens oriented in the longitudinal (CL) and circumferential (LC) standard directions; owing to the fact that the geometry and dimensions of the test specimens, specified in the ASTM E-1820 [1] standard, are only met in those orientations. All the standard procedures to determine K_{IC}, require that the sample size to be large enough, so that the results depend only on the properties of the material and not on the geometry or size of the specimen.

Studies have been carried out to prevent the thickness limitation of the specimen geometries, through the use of constriction parameters [21-23]. On the other hand, researchers have proposed the use of miniature specimens, where the geometry of the notches is modified, in order to increase the stress triaxiality at the tip of the notch [24]. However, a scaling factor is required to obtain results close to the real ones. Other studies show the experimental results of the dynamic miniature Charpy impact tests, which adjust to a fracture resistance curve of a standard specimen and scale the characteristic values of miniature size tests from total fracture energy and energy consumed up to the maximum load.

In this work the use of compact tension specimens (CT), enlarged with welded segments, for the evaluation of K_{IC} in the short RL direction of the test material is proposed, in order to satisfy the size requirements of the ASTM E-399 and E-1820 standards. The results of K_{IC} obtained by this procedure are validated by comparison with the results obtained by standard test specimens.

RESULTS AND CONCLUSIONS

The results show non-significant variation (less than the 5%) of the K_{IC} values between the one-piece and the welded specimens, which demonstrate that the proposed method to achieve the standard CT dimensions by welded attachments is a feasible practice, when the geometrical limitations do not allow obtaining one-piece specimens to meet the ASTM E1820-18 and ASTM E399-17 requirements, as is the case of the short transverse directions of pipes.

Table 1 – Fracture toughness (K_{IC}) test results, for standard and welded specimens.

Steel	Orientation	Specimen type	K_I Values ($MPa\sqrt{m}$)	Total Fracture energy (J)
API 5L X46	CL	Standard	126	154
	LC	Standard	137	163
	CL	Welded	128	157
	RL	Welded	107	128

Neither the microstructure nor the hardness profile of the welding, along the crack propagation zone, showed any alterations, with respect to the base metal. Hence, the welding procedure to enlarge the CT specimens does not alter the microstructure or the mechanical properties.

The low carbon steel used showed the lowest K_{IC} value and total fracture energy along the short transverse direction RL, as compared to the standard directions CL and LC. On the other hand, the highest values are achieved in the LC direction of the steel.

ACKNOWLEDGMENTS

The authors acknowledge to the National Polytechnic Institute (IPN), the National Council of Science and Technology (CONACYT) and the Pipelines Integrity Analysis Group (GAID) for the financial support necessary to carry out this research.

REFERENCES

ASTM. “Standard Test Method for Measurement of Fracture Toughness, ASTM E1820-18”. American Society of Testing Materials Standards Handbook. Philadelphia, USA, (2018), pp. 1-55.

M. S. Joo, D. W. Suh, J. H. Bae and H. JBhadeshia. “Role of delamination and crystallography on anisotropy of Charpy toughness in API X80 steel”. Materials Science and Engineering A, Vol. 546, (2012), pp. 314–322.

MA Beltrán-Zúñiga, JL González-Velázquez, DI Rivas-López, HJ Dorantes-Rosales, F Hernández-Santiago, “Effect of microstructure and crystallographic texture on the toughness anisotropy of API 5L X46 STEEL”. Fatigue Fract Eng Mater Struct. 2018;41: 749–761. https://doi.org/10.1111/ffe. 12782.

PAPER REF: 094

THREEDIMENSIONAL RECONSTRUCTION OF THE FEMALE PELVIC ORGANS FOR BIOMECHANICAL MODELING.

Paola Ulacia[1(*)], Lucy Gilbert[2], Rosaire Mongrain[1]

[1]Department of Mechanical Engineering, McGill University, Montreal, Canada

[2]Department of Obstetrics & Gynaecology, Gynaecologic Oncology, McGill University Health Centre, Montreal, Canada

[(*)]*Email:* paola.ulaciaflores@mail.mcgill.ca

ABSTRACT

To date, most gynaecological models available focus on pregnancy. Using imaging data from pelvic MR, we extracted the specific anatomy of the non-pregnant uterine cavity and surrounding tissues through segmentation and created 3D reconstructed solid models. These models aid in the visualization of the anatomical features in silico and can easily be transferred by means of rapid prototyping to physical model and dedicated experimental setups that mimic not only the geometries but the mechanical properties.

Keywords: female pelvic organs, phantom model, segmentation, rapid prototyping

INTRODUCTION

Mechanical alterations of the female reproductive organs can lead to different pathological states (Baah-Dwomoh et al. 2016) hence the mechanical characterization of such biological tissues and the generation of mechanically accurate models is of great importance for the analyses of therapeutic interventions, simulation of surgical interventions as well as characterizing the onset of disease. PVA gels and silicone rubbers have been proven to mimic the mechanical properties of soft tissues, allowing for transparent models(Jiang et al. 2011; Jiang et al. 2013)

Using segmentation and 3D reconstruction of the female pelvic organs from MR images, anatomically correct structures were obtained for mould preparation by rapid prototyping techniques. Segmentation of the female pelvic organs requires a semi-automated approach due to the complexity of the female pelvic anatomy (Ma et al. 2013).

Using sagittal and axial T2 weighed FRFSE MR images, we proceeded to identify the bladder, uterus and vagina, as well as reference anatomic landmarks using semiautomated segmentation tools available in slicer 4.10.1 (“3D Slicer” 2019), followed by user auditing and correction. Three-dimensional solids will be generated for each structure and then smoothed to create a better solid model for rapid prototyping, and further mechanically accurate mock-up model reconstruction.

RESULTS AND CONCLUSIONS

Automatic segmentation of the female pelvic organs is not accurate in all planes, after an initial automation based on intensity for the different segments, a slice by slice audit and correction for image correlation was needed. Figure 1 shows the resulting three-dimensional reconstruction.

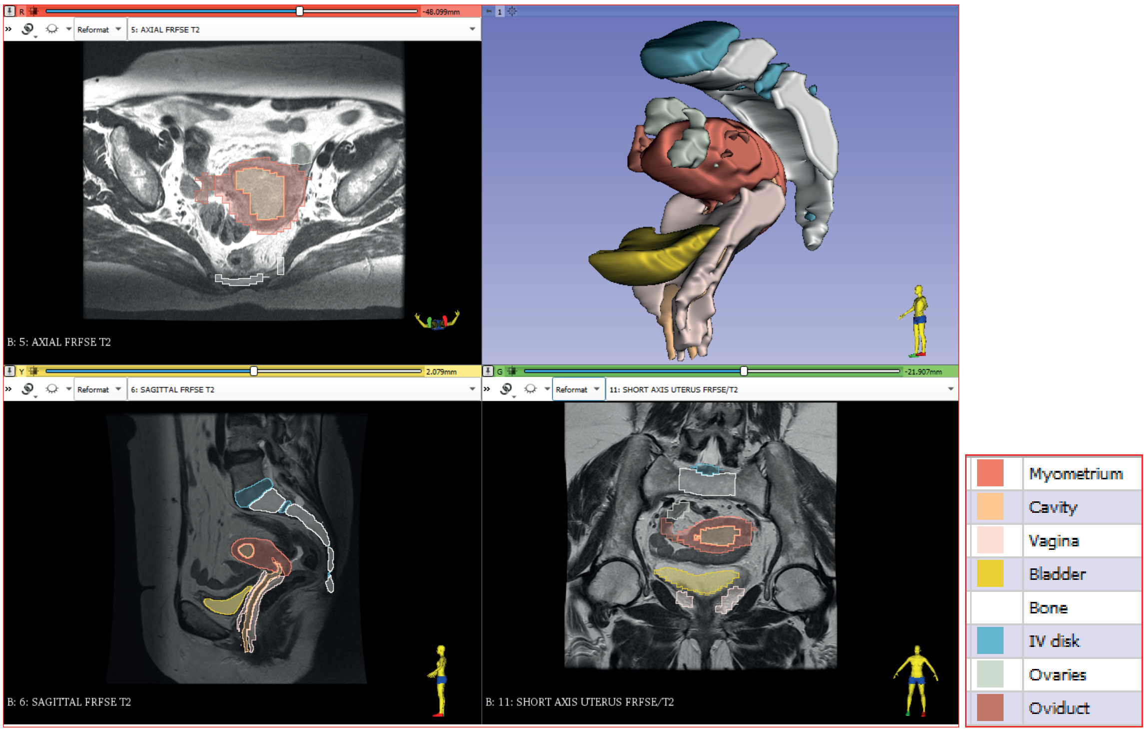

Fig. 1 – 3D reconstruction of the pelvic organs. R. Axial View, Y. Sagittal view, G. Coronal View. B. 3D volume.

After reconstructing the pelvic organs based on the sagittal view, we noted the correlation in other anatomical planes is not accurate, to achieve a better reconstruction we will repeat the process again on the axial and coronal planes to obtain three solids for each structure, which will then be merged to obtain a well-rounded structure containing information from all planes.

ACKNOWLEDGMENTS

The authors gratefully acknowledge the support from Ms. Valerie Josset and the Valerie Josset & Gary Aitken Cancer Research Award 2018.

REFERENCES

"3D Slicer." 2019. Accessed January 16. https://www.slicer.org/.

Baah-Dwomoh, Adwoa, Jeffrey McGuire, Ting Tan, and Raffaella De Vita. 2016. "Mechanical Properties of Female Reproductive Organs and Supporting Connective Tissues: A Review of the Current State of Knowledge." *Applied Mechanics Reviews* 68 (6): 060801..

Jiang, Shan, Sha Liu, and Wenhao Feng. 2011. "PVA Hydrogel Properties for Biomedical Application." *Journal of the Mechanical Behaviorof Biomedical Materials* 4: 1228–33.

Jiang, Shan, Zhiliang Su, Xingji Wang, Sha Liu, and Yan Yu. 2013. "Development of a New Tissue-Equivalent Material Applied to Optimizing Surgical Accuracy." *Materials Science and Engineering: C* 33 (7): 3768–74. doi:10.1016/j.msec.2013.05.001.

Ma, Zhen, Renato M Natal Jorge, Teresa Mascarenhas, and ao RS Manuel Tavares. 2013. "Segmentation of Female Pelvic Organs in Axial Magnetic Resonance Images Using Coupled Geometric Deformable Models." *Computers in Biology and Medicine* 43: 248–58.

PAPER REF: 095

EQUATION TO PREDICT THE KINETICS OF HYDROGEN INDUCED CRACKING OF TYPE API 5L STEELS

J.L. González-Velázquez[1], D.A Sigala-García[1], D.I. Rivas-López[1*], M.A. Beltrán-Zúñiga[1], F. Hernández-Santiago[2], H.J. Dorantes-Rosales[1]

[1]Instituto Politécnico Nacional, Escuela Superior de Ingeniería Química e Industrias Extractivas, Departamento de Ingeniería en Metalurgia y Materiales, Ciudad de México, México.
[2]Instituto Politécnico Nacional, Escuela Superior de Ingeniería Mecánica y Eléctrica, Ciudad de México, México.
**Correspondent author*: drivas_lopez@yahoo.com.mx

ABSTRACT

This work presents the sensitivity analysis of an empirical equation to estimate the hydrogen induced cracking (HIC) kinetics in steel plates, extracted form API 5L type pipes, obtained from the best-fit of experimental results. The correlation of the model's variables with the most significant microstructural characteristics of the steel plates used in the experimentation were identified. The results show that the HIC initiation time is at the point where the slope (derivative) of the cracked area vs. time plot (dA/dt) is equal or greater that 1E-2 mm2/h, while the maximum HIC rate and the time at which HIC slows down to near zero is when the value of dA/dt is equal or less than 1E-2 mm2/h. On the other hand, it was determined that that variables α and δ are the most sensible for the model´s curve fitting and they are related to the banding degree of the microstructure in the longitudinal section and the three-dimensional spacing parameter of non-metallic inclusions in the steel plates.

Keywords: HIC, kinetic model, metallurgical characteristics

INTRODUCTION

Hydrogen-induced cracking (HIC) is a damage mechanism that occurs in components such as tanks or steel pipes exposed to sour environments. The presence of cracks affects the integrity of these components, reducing its performance and capacity to withstand loads. Also, the location and length of the cracks or defects will determine if the component is suitable or not for the service, according to the evaluation criteria of API 579-1 / ASME FFS-1 (2016). However, this standard does not show a method to estimate the HIC crack propagation rate, as a result of there is not an equation or model to predict the rate of damage progression.

In this work, based on an empirical model, the growth kinetics of hydrogen-assisted cracks is adjusted using the microstructural metallurgical characteristics, such as the inclusions content and the banding degree, as well as mechanical properties such as the fracture toughness, the maximum tensile strength and the yield stress.

RESULTS AND CONCLUSIONS

The numerical variation of the parameters of the equation of used of the double exponential and its comparison with the metallurgical and mechanical characteristics allowed to establish that:

- From the sensitivity analysis it was determined that the constants of Amax, α and δ were the most significant for the adjustment of the mathematical model of the HIC phenomenon.

- The correlation of the adjustment constants of the mathematical model of hydrogen-induced growth with the microstructural characteristics is established, such as the band degree (Ai) and the three-dimensional spacing of the inclusions (λ).

ACKNOWLEDGMENTS

The authors acknowledge to the Instituto Politécnico Nacional (IPN), and the Pipelines Integrity Analysis Group (GAID) for the financial support necessary to carry out this research.

REFERENCES

API 579-1/ASME FFS-1 2016 *Fitness for Service*, Part 7, Assessment of Hydrogen blisters and hydrogen damage associated with HIC and SOHIC.

M. Elbjoudani, Uhlig´s Corrosion Handbook, third edition. USA: John Wiley & Sons, Inc. 2011. Pág. 183-192.

Wan Keun Kim, Seong Ung Koh, Boo Young Yang Kyoo Young Kim. Effect of environmental and metallurgical factors on hydrogen induced cracking of HSLA steels. *Corrosion Science* 50 (2008) 3336 – 3342.

Jorge Luis Gonzàlez Velàzquez. Agrietamiento Inducido por Hidrógeno. *Mecánica de la fractura* (2da. Ed.) Limusa S.A. de C. V. Pág. 165-170.

J. L. González, R, Ramírez, J. M. Hallen, R. A. Guzmán. Hydrogen-Induced Crack Growth Rate in Steel Plates Exposed to Sour Environments. *Corrosion Science* Vol. 53, No. 12, (1997), Pág 935-943.

M. Garet, A. M. Brass, C. Haut, F. Gutierrez Solana. Hydrogen Trapping on Non Metallic Inclusions in Cr-Mo Low Alloy steels. *Corrosion Science* Vol. 40, No. 7, (1998), Pág 1073-1086.

D. Rivas, E, Morlet, J. L. González, H. Dorantes, P. Velázquez, W. González. Modeling and Simulation of Cracked Area Growth Rate of Hydrogen Induced Cracking in Pipeline Steels, *10th international Symposium on Advanced Science and Technology in Experimental Mechanics, 1 – 4 November*, (2015).

J. L. González, E. M. Lazcano, D. I. Rivas, H. J. Dorantes. Modelling the effect of early and Late Nucleation Sites on Growth Rate of HIC in Low Carbon Steel Plates.

PAPER REF: 096

INFLUENCE OF HIGH-DENSITY ELECTRIC CURRENT ON QUASI-STATIC CRACK GROWTH OF SUS316

Sungmin Yoon[1], Rui Iwase[1], Shaojie Gu[1], Yuhki Toku[2], Yang Ju[2(*)]
[1]Graduate School of Engineering, Nagoya University, Nagoya, Japan
[2]Faculty of Engineering, Nagoya University, Nagoya, Japan
[(*)] *Corresponding email:* ju@mech.nagoya-u.ac.jp

ABSTRACT

We investigate an experimental and numerical approach to clarify a deceleration mechanism on quasi-static crack growth of SUS316 by applying high-density electric current (HDEC). To better understand this mechanism, one of general stainless steel was used to explain that, how much force is needed to propagate a crack under the different level of HDEC density. We are also interested in that how the modified material properties can be influenced on crack opening profiles. A series of experiments on crack extension of fracture mode I were conducted with single notched specimen to identify the resistance of crack growth at a constant strain rate, 0.003 s^{-1}, to the specimens prepared without and with the HDEC (0 A/mm^2 and 400 A/mm^2), respectively. *In-situ* measurements of equivalent force and crack profile were carried out to understand the alteration of power law related to the level of ductility. We also use a finite element model to confirm the crack profiles by the alteration of material property.

Keywords: SUS316, crack deceleration, ductility, J-integral.

INTRODUCTION

To improve material's property at micro-nano scale is always an important issue since most of mechanical failure is currently caused by a tiny defect inside the material. The defects like voids, flaws and crystallographic ones have great influence on the mechanical properties by stress concentration induced from the micro-nano scale to relatively large scale in metals (Hosoi, 2012, Yu, 2016, Van Dijk, 2018).

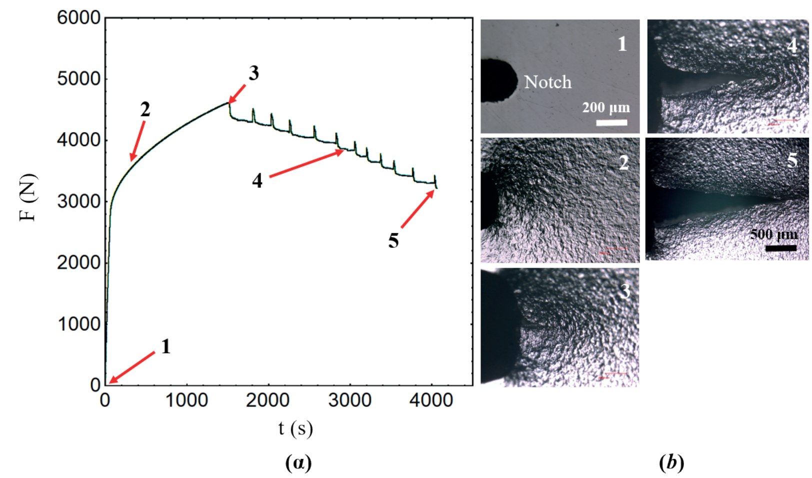

Fig. 1 *In-situ* observation of crack profiles at each equivalent force F with the electric current 400 A/mm^2 : (a) history of F vs time t ; (b) *in-situ* images from initial mirror-like surface to crack extension instantaneously captured at each equivalent force, the images 1-4 in scale bar of 200 μm and the image 5 of 500 μm.

In this study, to obtain the evidences, we are interested in relatively large scale with the comprehensive mechanism on the deceleration of crack growth which is significantly affected by applying HDEC. The comparison between the *in-situ* measurement (Fig. 1) and numerical calculation of crack profiles was employed to know how much differences they have for the material properties such as young's modulus, *E*, strain hardening exponent, *h*, by HDEC.

RESULTS AND CONCLUSIONS

The results of applied force versus quasi-static crack growth from *in-situ* measurement at the equilibrium state are shown in Fig. 2(α). The experimental measurements were fitted with an equation of inset in Fig. 2(α), namely Hutchinson-Rice-Rosengren, HRR singularity for J-integral approach (Anderson, 2005).

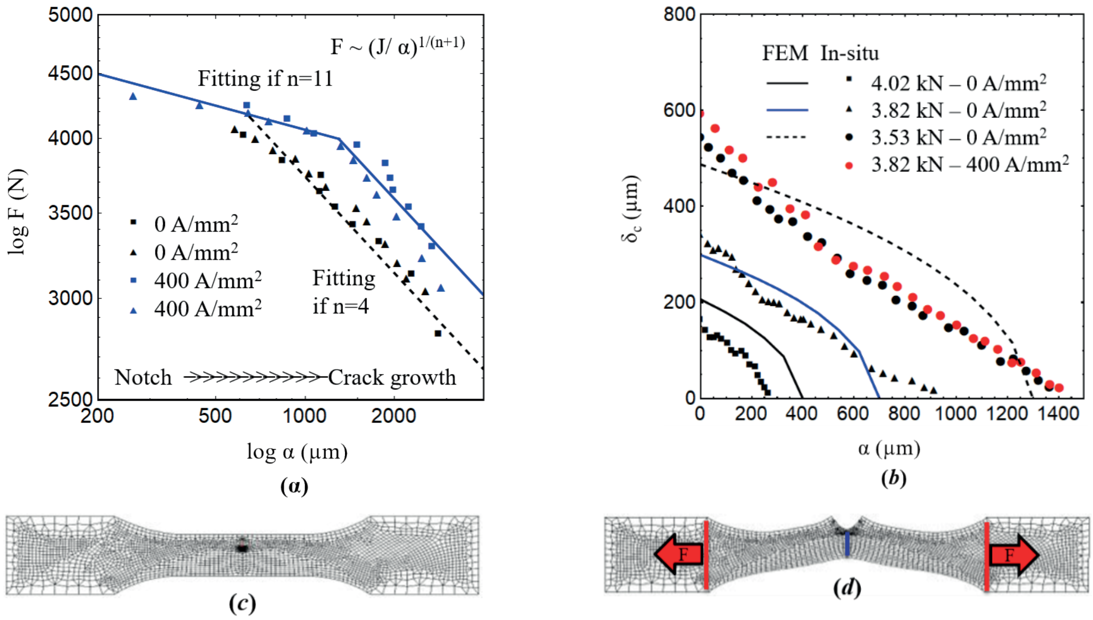

Fig. 2 Experimental and numerical results: (α) force F as a function of the crack length α, at each condition and different proportionality fitted with n=4 and n=11 from HRR singularity; (*b*) comparison of crack profiles δ_c between experiment and simulation and (*c-d*) finite element model before and after fracture at the crack tip, respectively.

With careful consideration of these experimental and numerical results as shown in Fig. 2, finally, why it is able to modify and what is the most influential reason into the modification of material properties, notably, influenced by applying HDEC were investigated.

REFERENCES

Hosoi A, Nagahama T, Ju Y. Fatigue crack healing by a controlled high-density electric current field. Materials Science and Engineering A, 2012, 533, p. 38-42.

Yu T, Deng D, Wang G, Zhang H. Crack healing in SUS304 stainless steel by electropulsing treatment. Journal of Cleaner Production, 2016, 113, p. 989-994.

Van Dijk N, Van der Zwaag S. Self-Healing Phenomena in Metals. Advanced Materials Interfaces, 2018, 1800226, p. 1-13.

Anderson TL. Fracture mechanics fundamentals and applications 3rd (ed). Taylor&Francis, 2005, p. 108-112.

PAPER REF: 097

MONITORING OF THERMAL DEFORMATION OF MACHINE TOOLS INDUCED BY ENVIRONMENTAL CONDITIONS

Christian Brecher[1], Tae Hun Lee[2], Filippos Tzanetos[2(*)], Daniel Zontar[2]

[1]Machine Tool Laboratory (WZL), RWTH Aachen University, Aachen, Germany
[2]Fraunhofer Institute of Production Technology (IPT), Aachen, Germany
[(*)]*Email:* filippos.tzanetos@ipt.fraunhofer.de

ABSTRACT

Many researchers have studied thermal issues in machine tools for several decades. Although many modelling techniques and sensor placement algorithms could lead to a good prediction of the overall dislocation due to internal heat sources, none was able to do the same for environmental effects. The complexity of environmental conditions, including the spatial distribution of environmental temperature, the air speed and the air humidity, make this task challenging even for neural networks and machine learning algorithms. This paper investigates the use of the Integral Deformation Sensors (IDS), developed by the Fraunhofer Institute of Production Technology. Their main advantage is that they measure the deformation of a machine tool component, which is the outcome of all thermal effects and heat transport phenomena that inflict the component. The second significant advantage is that they allow the use of a simple and interpretable physical model that reaches a high prediction accuracy.

Keywords: thermal deformation, machine tools, Tool Center Point, correction.

INTRODUCTION

There are many modelling techniques and sensor placement algorithms, whose prediction accuracy was investigated for environmental effects. However, only few research papers focused on the influence of environmental conditions. One approach (Tan, 2014) gathered temperature and Tool Center Point (TCP) data over a full year and built a phenomenological model, which was however valid only along one direction within the working space. Another approach (Mayr, 2015) derived relationships between temperature sensors and measurement data of the TCP dislocation from FEM simulations with the help of model order reduction methods. The authors derived that the environmental effects led to a distinctly inhomogeneous distribution of the TCP dislocation along the working space, which in turn shows that the first approach is inappropriate for this issue. A third approach (Zhang, 2017) builds a transfer function model based on the heat transfer equation and the dimensions of the machine tool, but parametrizes it with measurement data. Another obstacle is that the temperature sensors on this work are mounted on the tool holder, which cannot be implemented during operation. Finally, the order of magnitude of the measured TCP dislocation was less than 1 μm and may possibly lie within the measurement uncertainty of the used instrument measuring the TCP dislocation.

RESULTS AND CONCLUSIONS

The results from the experimental investigations are shown in Fig. 1. A middle-sized machine tool is located close to the machine hall door and thus strongly influenced by sudden drops of temperature. The measurement was held in September, where the environmental temperature drops during the day and rises up during the night, in contrast to the environmental conditions during the summer. The TCP dislocation was measured at four different positions in the working space with a simplified version of the R-test method. The combined measurement uncertainty of the TCP dislocation measurement is estimated to be 3,2 µm, while the uncertainty of each Integral Deformation Sensor (IDS) 1,4 µm. The prediction was derived with a physical model based on the theory of Euler-Bernoulli beams. The model uses the information from twelve IDS and the dimensions of the machine tool without any data training methods.

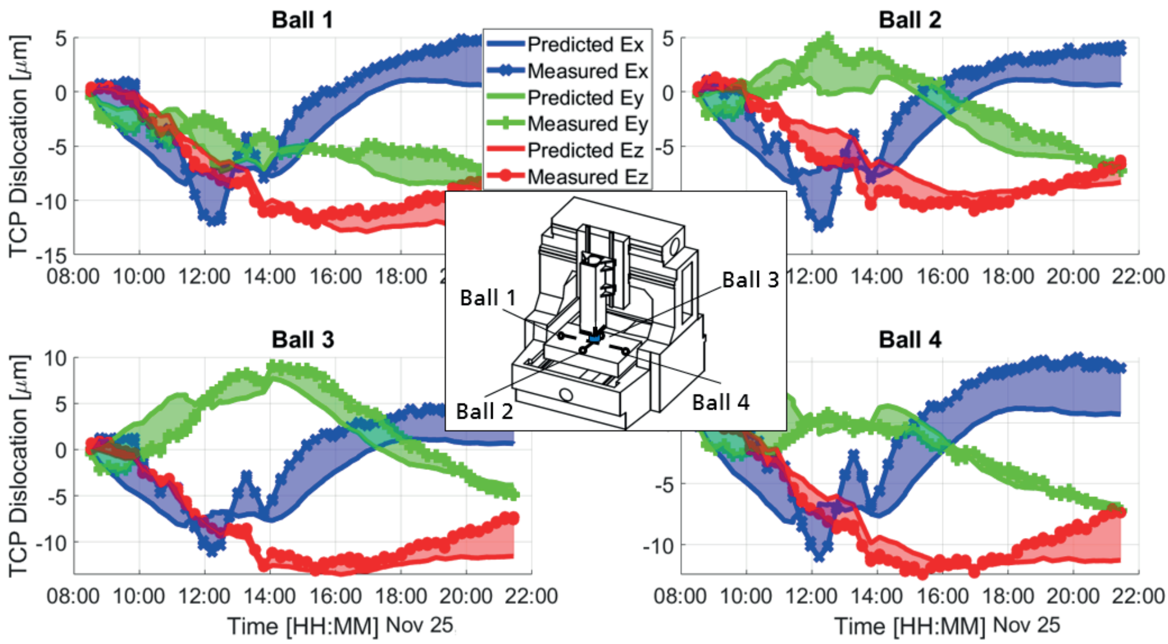

Fig. 1 – Prediction of the overall TCP dislocation at four positions in the working space under the influence of real machine hall environmental conditions

ACKNOWLEDGMENTS

The authors gratefully acknowledge the funding by the DFG (German Research Foundation) within the framework of the trans-regional special research field CRC/TR96 “Thermo-energetic Design of Machine Tools” in subproject C03 “Structurally Integrated Sensors”.

REFERENCES

Tan B, Mao X, Liu H, Li B, He S, Peng F, Yin L. A thermal error model for large machine tools that considers environmental thermal hysteresis effects. International Journal of Machine Tools & Manufacture, 2014, 82-83, p. 11-20.

Mayr J, Ess M, Pavlicek F, Weikert S, Spescha D, Knapp W. Simulation and measurement of environmental influences on machines in frequency domain. CIRP Annals - Manufacturing Technology J, 2015, 64, p. 479-482.

Zhang C, Gao F, Li Y. Thermal error characteristic analysis and modeling for machine tools due to time-varying environmental temperature. Precision Engineering J. 2017, 47, p. 231-238.

PAPER REF: 098

MATERIAL POINT METHOD FOR INCOMPRESSIBLE FLUID-STRUCTURAL INTERACTION PROBLEMS

Ming-Jian Li[1], Xiong Zhang[1(*)]

[1] School of Aerospace Engineering, Tsinghua University, Beijing, 100084, PR China

(*)*Email:* xzhang@tsinghua.edu.cn

ABSTRACT

This work presents an incompressible material point method (MPM) to deal with fluid-structural interaction (FSI) problems with free surface. The algorithm uses Eulerian background grids to solve fluid velocity and pressure, and transport the variables in a Lagrangian way. An immersed boundary idea was introduced to describes the fluid-structure interface, and the level-set function was advected on background grids, in order to eliminate numerical cavity caused by particles transportation. The proposed scheme has been successfully applied to FSI problems with free surface, such as water entry and sloshing problems. Numerical results suggested good agreement with analytical and experiment results.

Keywords: material point method, incompressible, fluid-structural interaction, immersed boundary.

INTRODUCTION

In the incompressible material point method, we use the Chorin projection scheme to solve velocity equation and pressure Poisson equation at Cartesian grids. Meanwhile, the level-set function is solved using WENO scheme, to capture the free surface and eliminate numerical cavity. Fluid particles will then be transported, and help to reconstruct velocity fields in the next time level. The structural velocity will then be solved using FEM, with pressure boundary conditions interpolated from the fluid grids.

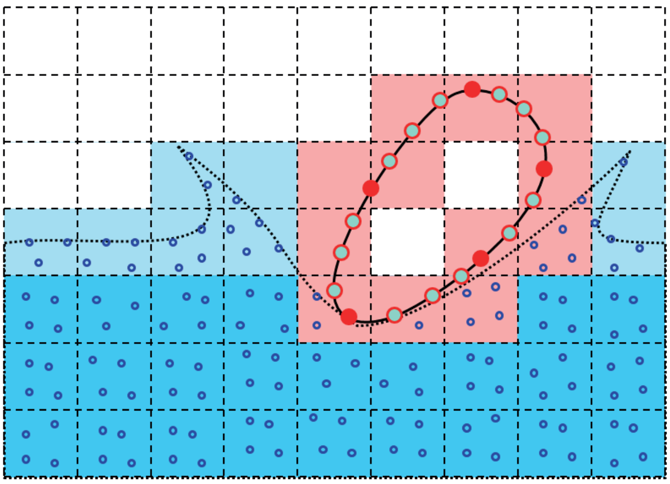

Fig. 1 – Background grids and particles in incompressible material point method

RESULTS AND CONCLUSIONS

The numerical case has been presented on an oblique cylinder falling into a water tank (Fig. 2). Results suggest that, the cylinder velocity time-history is in line with SPH simulation by Sun (2018), and experimental data by Wei (2015).

A sloshing problem under horizontal excitation has also been presented. Fig. 3 illustrates the pressure distribution as well as the free surface profile. Also, the surface elevation time-history at a certain position was compared with experimental work by Faltinsen (2000), and the results suggest good agreement.

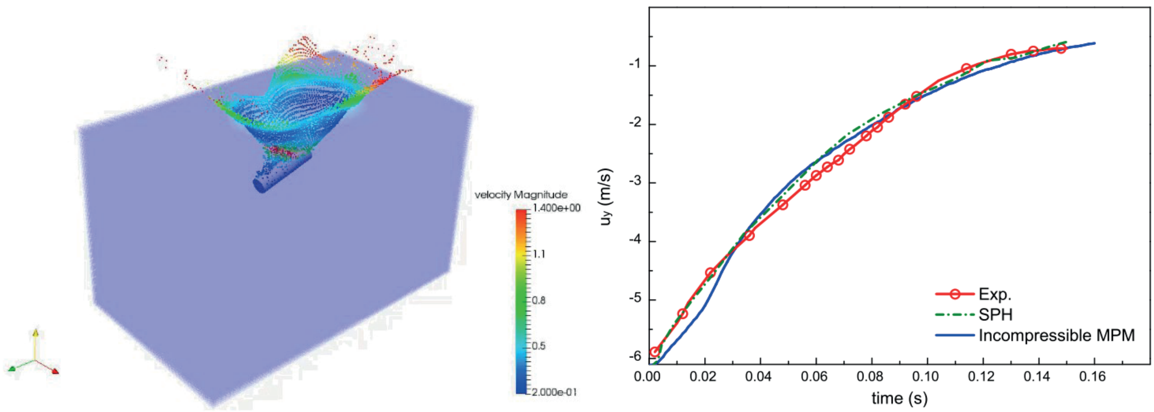

Fig. 2 – Water entry problem, velocity of the cylinder has been compared with experimental results and SPH results.

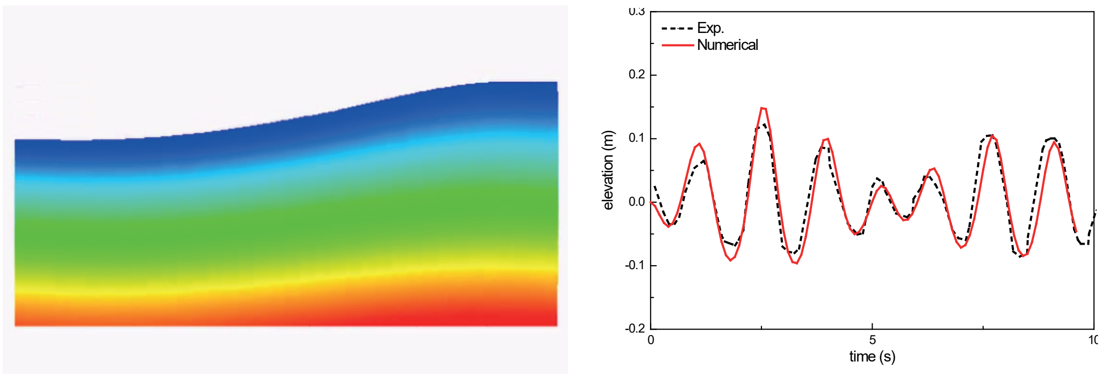

Fig. 3 – Sloshing problem with horizontal excitation, the free surface elevation time-history has been compared with experimental data.

REFERENCES

Zhang F, Zhang X, Sze KY, et al. Incompressible material point method for free surface flow: Journal of Computational Physics, 2017, 330, p. 92-110.

Faltinsen OM, Rognebakke OF, Lukovsky IA, et al. Multidimensional modal analysis of nonlinear sloshing in a rectangular tank with finite water depth: Journal of Fluid Mechanics, 2000, 407, p. 201-234.

Sun P, Zhang AM, Marrone S, et al. An accurate and efficient SPH modeling of the water entry of circular cylinders: Applied Ocean Research, 2018, 72, p. 60-75.

Wei Z, Hu C. Experimental study on water entry of circular cylinders with inclined angles: Journal of Marine Science and Technology, 2015, 20(4), p. 722-738.

PAPER REF: 099

EXPERIMENTAL INVESTIGATION OF STEEL T-STUB MACRO-COMPONENTS WITH FOUR BOLTS-PER-ROW

Daniel L. Nunes[1(*)], Adrian Ciutina[1], Ioan Both[1]

[1]University "Politehnica" of Timisoara, Timisoara, Romania

[(*)]*Email:* daniel.nunes@student.upt.ro

ABSTRACT

The paper summarizes an experimental study, performed on different steel joint macro-components with four bolts-per-row. These macro-components represent the tensile area of a steel beam-to-column extended end-plate connection. The scope of the work is to investigate the elasto-plastic behaviour of this type of four bolts-per-row configurations and to assess its behaviour in regard to the classic two bolts-per-row solutions.

Keywords: steel connection, four bolts-per-row, macro-component, ductility, robustness.

INTRODUCTION

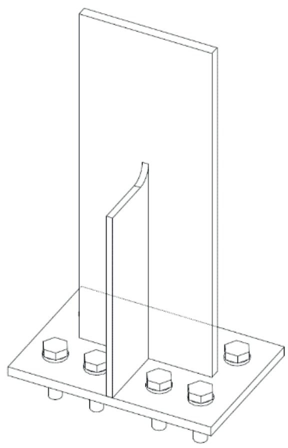

The widely used configuration for moment resisting beam-to-column connections usually employ two bolts-per-row in its most current configurations. This configuration has been not only extensively studied but is also the only configuration presented and detailed in the European design codes for moment resisting connection, despite its possible variants. However, this configuration can lead to poor post-flexural performance in cases of extreme loading (Dinu, Marginean and Dubina). According to Nunes (Nunes, Marginen and Ciutina), by adding a supplementary outer bolt, the connection's behavior can be enhanced not only in strength but also in ductility and improve its post-flexural behavior.

Despite the research made on this type of connections - (Demonceau, Jaspart and Weynand) and (Dreveny), accurate design procedures are still undeveloped and the current models maintain the classic t-stub analysis which fails to account for interaction between bolts of different rows, which represent a key failure mechanism for this type of connections (Nunes and Ciutina).

In this experimental study, a total of 54 macro-component (Figure 1) specimens are being tested and analysed. The specimens follow a recent parametric study where, based on an original connection configuration, for which several parameters were varied, such as bolt diameter, end-plate thickness, flange width and bolt disposition. The specimens are subjected to monotonic tensile tests in order to asses their mechanical properties and failure mechanisms.

RESULTS AND CONCLUSIONS

In order to identify the most relevant configurations and to evaluate the experimental testing setup, numerical tests have been performed in equivalent specimens. The preliminary results from the numerical study show considerable gains in strength and ductility for several 4 bolts per row (4B) configurations, which justify a closer analysis of this type of connection.

In order to assess the global behaviour differences between the 2B and 4B configurations, the response Force – Displacement curves are superposed in Figure 2.

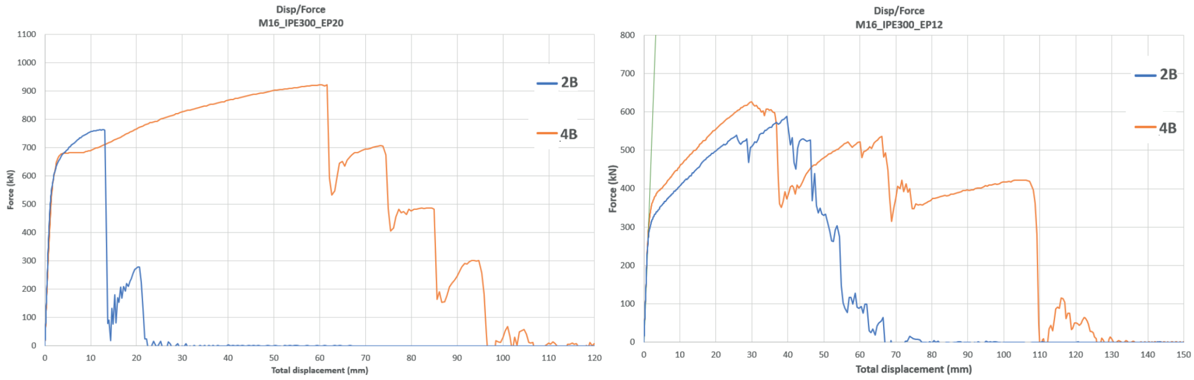

Figure 2. Behaviour curves for models 2B and 4B M16_IPE300_EP20 and M16_IPE300_EP12

Table 3. Exterior bolts participation ratio

			at F_y			at F_{max}		
Bolts	Beam	End Plate	$F_{eff,y}$ [kN]	$F_{t,Rd,y,b}$ [kN]	Difference [%]	$F_{eff,max}$ [kN]	$F_{t,Rd,max,b}$ [kN]	Difference [%]
M12	IPE300	12	19,6	105,7	18,5	50,3	105,7	47,6
M12	IPE300	15	30,6	105,7	28,9	79,7	105,7	75,4
M12	IPE300	20	58,5	105,7	55,3	115,1	105,7	100,0
M16	IPE300	12	18,6	196,9	9,4	53,8	196,9	27,3
M16	IPE300	15	21,7	196,9	11,0	55,4	196,9	28,1
M16	IPE300	20	44,0	196,9	22,3	124,6	196,9	63,3
M20	IPE300	12	20,2	307,2	6,6	95,9	307,2	31,2
M20	IPE300	15	17,7	307,2	5,8	63,2	307,2	20,6

The study also shows the difference in failure mechanism and identify the most efficient configurations in the new four bolts-per-row configurations, in relation to their key characteristics: strength, ductility and post-flexural behavior.

REFERENCES

Demonceau, J.-F., et al. "Connections with four bolts per horizontal row." EUROSTEEL 2011. Budapest, 2011.

Dinu, Florea, Ioan Marginean and Dan Dubina. "Experimental testing and numerical modelling of steel moment-frame connections under column loss." Engineering Structures 151 (2017).

Dreveny, Z. Behaviour of beam-to-column joints under large vertical displacements following the loss of a column, M.Sc. thesis. Timisoara, Romania: UPT, 2014.

Nunes, Daniel Luís and Adrian Ciutina. "Behaviour of end-plate steel connections with 4 bolts per row under large deformations." 9th International Conference on Steel and Aluminium Structures (ICSAS19). Bradford, 2019.

Nunes, Daniel Luís, et al. "Influence of four bolts per row connections on a steel frame building subjected to column." Integrity – Reliability – Failure 2018. Lisbon, 2018.

PAPER REF: 100

ULTRASONIC MEASUREMENT OF RESIDUAL STRESSES IN WELDED ELEMENTS

Yuri Kudryavtsev
Structural Integrity Technologies Inc., Markham, Ontario, Canada
Email: ykudryavtsev@sintec.ca

ABSTRACT

The objective of the study described in this paper is to identify the residual stress (RS) distribution and relaxation in standard welded specimens, large-scale welded panel and real structure. The RS were measured after welding and in the process of fatigue loading of welded elements by the UltraMARS system that is based on using ultrasound.

Keywords: residual stresses, welded elements, ultrasonic method.

INTRODUCTION

The RS are one of the main factors determining the engineering properties of materials, parts and welded elements and this factor should be taken into account during the design and manufacturing of different products. Although certain progress has been achieved in the development of different experimental techniques, a considerable effort is still required to develop efficient and cost-effective methods of residual stress analysis (Kudryavtsev, 2008). The application of an ultrasonic non-destructive method for residual stress measurements had shown that, in many cases, this technique is very efficient and allows measuring the residual stresses both in laboratory conditions and in real structures in field for a wide range of materials (Kudryavtsev, 1985, 2016).

RESULTS AND CONCLUSIONS

The measurements of welding residual stress were performed in standard welded samples for fatigue testing, large welded panel and real structures. The residual stress measurements in lab and field conditions were performed by using the UltraMARS system shown on Figure 1.

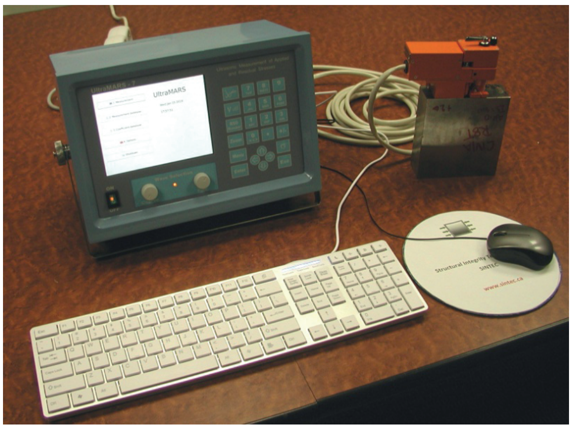

Figure 1. Ultrasonic Computerized Complex for residual and applied stress measurement UltraMARS-7

In field conditions the residual stresses were measured in a number of welded structures including the pressure hull of a submarine. Four zones were selected for RS measurement in the welded elements of the hull of submarine. Figure 2 shows the results of residual stress measurement in one of the selected zones of the hull of submarine. In this case both components of residual stresses are tensile at the distance from the weld toe of 20 mm. The longitudinal component of residual stresses reaches 295 MPa.

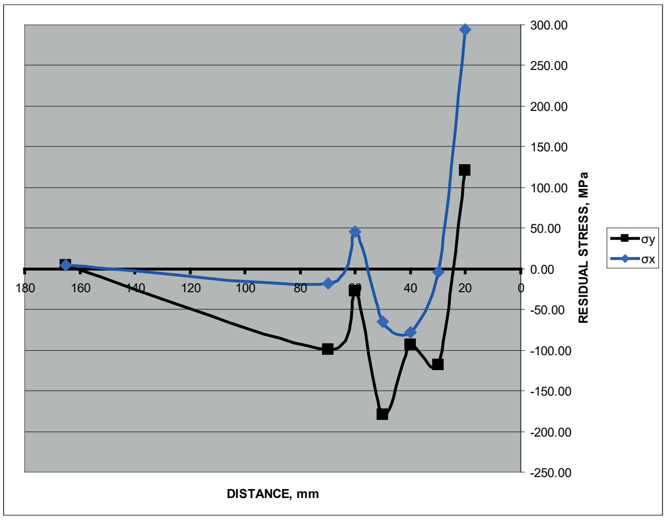

Figure 2. The distribution of residual stresses near the butt weld of pressure hull of submarine (horizontal axis represents the distance from the weld):
σx and σ_y – components of residual stresses that are parallel and perpendicular to the weld

A comparison of residual stresses determined by measurements using the ultrasonic method and by numerical simulations showed a reasonable agreement both for standard welded specimens and the large welded panel.

SUMMARY

Certain progress has been achieved during the past few years in improvement of traditional techniques and development of new methods for residual stress measurement. The developed advanced ultrasonic method, based on it portable instrument and the supporting software can be used for non-destructive measurement of applied and residual stresses in laboratory samples and real parts and structural elements in many applications for a wide range of materials.

REFERENCES

Kudryavtsev Y. Residual Stress. Springer Handbook on Experimental Solid Mechanics. Springer – SEM. 2008. P. 371-387.

Kudryavtsev Y. Application of the ultrasonic method for residual stress measurement. Development of fracture toughness requirement for weld joints in steel structures for arctic service. VTT-MET. B-89. Espoo. Finland. 1985. p.62-76.

Y. Kudryavtsev and J. Kleiman. Ultrasonic Measurement of Residual Stresses in Welded Elements and Structures. Proceedings of the 19th World Conference on Non-Destructive Testing 2016. Munich, Germany, June 13-17 2016.

PAPER REF: 101

FATIGUE IMPROVEMENT OF WELDED ELEMENTS BY ULTRASONIC PEENING

Yuri Kudryavtsev(*) and Jacob Kleiman

Structural Integrity Technologies Inc. (SINTEC), Markham, Ontario, Canada
(*)*Email:* ykudryavtsev@sintec.ca

ABSTRACT

The ultrasonic impact treatment (UIT) is one of the new and promising processes for fatigue life improvement of welded elements and structures. In most industrial application this process is also known as ultrasonic peening (UP). The fatigue testing of welded specimens showed that the UIT/UP is the most efficient improvement treatment as compared with traditional techniques such as grinding, TIG-dressing, heat treatment, hammer peening and laser peening. The description of UIT/UP technology and the results of fatigue testing of welded elements of steels and aluminum alloys in as-welded condition and after application of UIT/UP are discussed in this paper.

Keywords: fatigue improvement, welded elements, ultrasonic impact treatment.

INTRODUCTION

The UIT/UP technique is based on the combined effect of high frequency impacts of special strikers and ultrasonic oscillations in treated material (Kudryavtsev, 2008). The beneficial effect of UIT/UP is achieved mainly by relieving of harmful tensile residual stresses and introducing of compressive residual stresses into surface layers of material (Kudryavtsev, 1989) and also on smaller scale by decreasing of stress concentration in weld toe zones and enhancement of mechanical properties of the surface layers of the material. The basic system for UIT/UP treatment (total weight - 11 kg) includes an ultrasonic transducer, a generator and

Figure 1. Ultrasonic impact treatment system for fatigue improvement of welded elements and structures

a laptop (optional item) with software for optimum application of UP - maximum possible increase in fatigue life of parts and welded elements with minimum cost, labor and power consumption (Kudryavtsev, 2013). In general, the basic UIT/UP system UP-600U shown in Figure 1 could be used for treatment of weld toe or welds and base metal also if necessary.

RESULTS AND CONCLUSIONS

The welded specimens were fatigue tested in as-welded conditions and after UIT/UP. Investigated materials - steels and aluminum alloys of different strength. Parameters of fatigue testing: axial loading, R=0. The results of fatigue testing of welded joints made from aluminum alloy 5083 are presented in Figure 2.

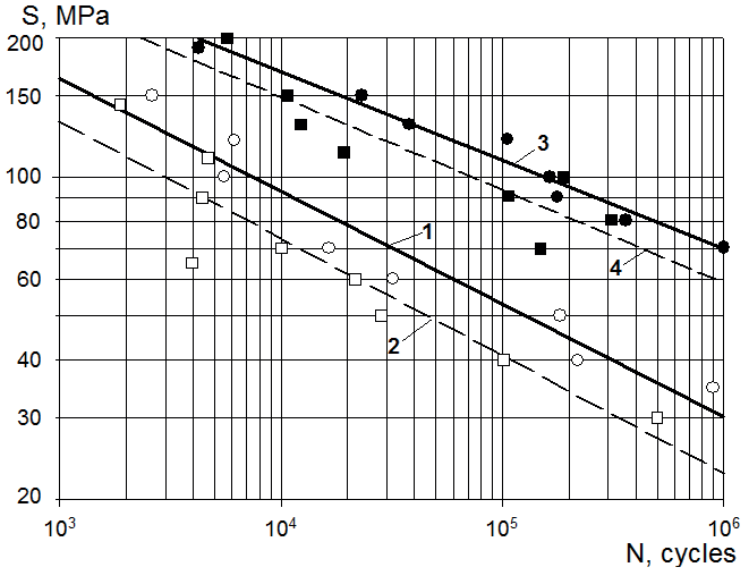

Figure 2. Results of fatigue testing of lap joints made from aluminum alloy 5083:
1, 2- in as-welded condition; 3, 4- after UIT/UP;
1, 3 – technology of welding A; 2, 4 – technology of welding B

These and other numerous results of fatigue testing of welded specimens made from steels and aluminum alloys showed that the UIT/UP provided significant increase in fatigue performance of all considered types of welded joints and materials and that the UIT/UP is the most efficient improvement treatment as compared with traditional techniques such as grinding, TIG-dressing, heat treatment, shot peening and hammer peening.

REFERENCES

Y. Kudryavtsev. Residual Stress. Springer Handbook on Experimental Solid Mechanics. Springer – SEM. 2008. P. 371-387.

Y. Kudryavtsev, V. Korshun and A. Kuzmenko. Improvement of Fatigue Life of Welded Joints by Ultrasonic Impact Treatment. Paton Welding Journal. 1989. No. 7. p. 24-28.

Y. Kudryavtsev and J. Kleiman. Fatigue Improvement of Welded Elements and Structures by Ultrasonic Peening. Proceedings of the ASME 2013 Pressure Vessels and Piping Conference PVP2013. Paper Number PVP2013-97185. July 14-18, 2013, Paris, France.

PAPER REF: 102

TESTING ENVIROMENT FOR THE CHARACTERIZATION OF ARTIFICIAL MEMBRANES – A CONCEPTUAL DESIGN

Erik Krumnow[1(*)], Steffen Zinn[1], Kai-H. Lietzau[1], Sergio Bernardini[2], Andreas H. Foitzik[1]

[1]Technical University of Applied Science Wildau, Hochschulring 1, 15745, Wildau, Germany

[2]University of Rome Tor Vergata, Department of Industrial Engineering, Via Orazio Raimondo, 18 - 00173 Roma, Italy

[(*)]*Email:* krumnow@th-wildau.de

ABSTRACT

The development of new medical procedures and products is a difficult as well as resource intense process, which always requires the developer verify the different stages in order to protect the future costumer and to ensure the functionalities of the product. As every day new technologies are being developed the necessity to provide customized testing environments rises exponentially. The presented work is focused on the development of a testing environment for the validation of injection needle geometries in dependence of different membrane surfaces.

For testing itself, the system will primarily utilize mechanical force to penetrate the surface, thereby characterizing the mechanical resistance properties of the membrane. Another aspect is the efficiency of the applied needle geometry as well as the punctuations of the membrane which is intended to be optically validated. Consequently, the developed system should be designed to utilize a variety of membranes as well as skin tissue mock-ups and needle systems.

Due to this intended modularity the developed system should be capable to support a broad spectrum of task and applications. These include for example the development of auto-injector system for non-medical personal in case of a hazardous event, a minimalistic blood extraction device as well as a tool to validate 3D printed multilayers of biological samples. The presented work shall provide an overview of the current development state of the testing environment and the further steps of development.

Keywords: mechanical analysis, artificial membranes, testing environment.

INTRODUCTION

Over the last decade, the so called personalized medical care moved more into the focus of our modern society and already helped to significantly improve the living conditions for a great variety of people. Personalized medical care is hereby often based on a dual approach which combines the processing of the patient specific data with an individual treatment strategy. (Snyderman, 2012) Additionally, simplified solutions for self-treatment in terms of home care are also in high demand. This approach requires an essential redevelopment of a great variety of already existing medical devices with a particular focus on efficiency and user-comfort. Consequently, a verification of the overall functionality of the developed product in a controlled and reliable environment is also highly needed.

Therefore, the presented work is focused on the development of an experimental setup for the validation of punctuation geometries in dependence of the utilized biological surface. It is intended to develop a modular environment which can address different tasks and support a broad spectrum of applications.

CONCEPT AND MEASUREMENT PROCESS

The developed experimental setup is designed to address two primarily functionalities. In terms of testing, the system will primarily utilize mechanical force to penetrate the surface of the membrane and thereby characterizing its mechanical resistance properties. The second aspect is the validation of the punctuation efficiency in dependence to the applied needle geometry and the resulting punctuation.

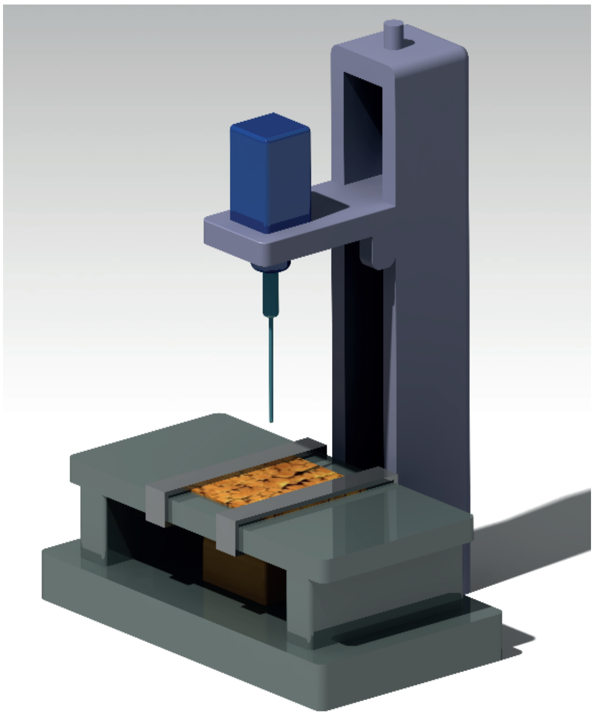

Figure 1: Concept the experimental setup in CAD

As shown in figure 1, the current modular approach consists of a test bed, a mechanical arm and a holder for the punctuation system itself. In terms of measurement, the selected biological sample will be placed onto the test bed directly under the punctuation system. The mechanical arm is lowered and constantly moved towards the test sample. The selected membrane resists the punctuation which results in an increase of force until a penetration is achieved.

In order to provide a reliable base line of the applied forces strain gauges will be also integrated into the setup. Therefore, the force mustered to penetrate the membrane can be utilized as a reference value by which the efficiency of the overall application is determined. Considering the penetration it is assumed, that a high penetration efficiency requires only a minimal amount of force depending on the applied biological membrane. Hereby, the movement speed, material resistance, initial tension and blade geometry should be regarded as the most significant factors. (Abolhassani, 2007 and Bader 1983) In order to reduce variance for the specific test setup it is intended to vary primarily the speed or the material resistance in regard to the scenario of application.

PLANNED TEST MEDIUM

As previously mentioned the material resistance should be considered a crucial factor for the testing procedure. In order to create a basic understanding of material behavior as well as to achieve an optimal experimentation setup it is intended to execute a three phase development procedure:

- Phase one will utilize different artificial membranes trying to mimic skin tissue of varying density and strength
- Phase two will attached those membranes to ballistic gel in order to approach a realistic organic mimic.

- Phase three will be focused on the behavior of biological test samples.

With the conclusion of phase three the developed experimental setup should be capable to verify the punctuation system, different membrane materials and mimic a realistic case of application.

FINALISATION AND CONCLUSIONS

The presented work is focused on the current development stage of a novel experimental system for the validation of punctuation systems (needles and lancets) in regard to different biological membranes or tissue. Due to the modular approach it should also be possible to imitate a broad set of applications possibilities. The designed system shall be transferred into a first prototype within this year, to create the baseline for further development. Afterwards, it is intended utilize the developed setup in three particular application examples, which include an auto-injector system for non-medical personal.

REFERENCES

N. Abolhassani et al., „Needle insertion into soft tissue: A survey“, Medical Engineering & Physics, 2007, Vol 29, Issue 4, 413-431, DOI: https://doi.org/10.1016/j.medengphy.2006.07.003

D.L. Bader, P. Bowker, „Mechanical characteristics of skin and underlying tissues in vivo“, Biomaterials, 1983, Vol. 4, Issue 4, 305-308, DOI: https://doi.org/10.1016/0142-9612(83)90033-9

R. Snyderman, „Personalized health care: From theory to practice“, Biotechnology Journal, 2012, Vol. 7, Issue 8, 973-979, DOI: https://doi.org/10.1002/biot.201100297

PAPER REF: 103

DATA ANALYSIS FOR THE VALIDATION OF DISPLACEMENT BEHAVIOUR

Josefine Johanna Gottschalk[1(*)], Erik Krumnow[1], Kai-H. Lietzau[1], Andreas H. Foitzik[1], Maria Richetta[2]

[1]Technical University of Applied Science Wildau, Institute for Materials, Development and Production, Hochschulring 1, 15745 Wildau, Germany

[2] University of Rome „Tor Vergata“, Department of Industrial Engineering, 00133 Rome, Italy

[(*)]*Email:* gottschalk@th-wildau.de

ABSTRACT

At the Technical University of Applied Science Wildau a novel screening procedure for cancer treatment is currently in development, which aims to use a biopsy sample without the need of further processing or cell separation for drug screening. It is based on the electronic speckle pattern interferometry (ESPI) method in form of a Micro-ESPI adaptation. The system is designed to incubate a certain amount of tissue over a prolonged period of time to validate different treatment strategies thoroughly. In order to provide reliable environmental conditions, the system contains an integrated heating module that is capable to automatically regulate the temperature of the applied medium. Furthermore, this first iteration of the system includes ports for a medium and gas supply. The complete system can be also sterilized by using an autoclave or disinfectants. Currently, the developed system is capable to sustain incubated cells for over 120 minutes doubling the current observation time inside the Micro-ESPI setup. Furthermore, simulations were carried out in order to improve the medium supply, which displayed necessary changes for the next iteration.

Keywords: Biomechanics, Interferometry, ESPI, Cancer treatment.

INTRODUCTION

Medical technology is nowadays in a constant flux of inventions and trends. One of those new trends is the so called personalized medicine. Personalized Medicine is aiming at the goal to treat a patient quick and efficient based on the available biological information. This confronts all technology fields in the medical branch with new challenges. In order to achieve the required safety and efficiency, the precise manipulation and targeting of microscopic structures such as cells is the logical next step. Especially in cancer treatment such an approach is very promising, in order to protect the patient from further physiological stress and treat the tumor directly. (Balis, 2018) Therefore, different methods are being developed such as the usage of nanoparticles (Rapoport, 2007) or antibodies (DiJoseph, 2004) that address tumor specific characteristics. Due to the differences between patients, cancer drugs and their individual effect need to be validated, to choose the best treatment strategy for the patient. (Wang, 2015) This task can be approached by different means; for example, by treating the tumor in vivo, where drugs are injected directly into the patient and tumor response is analyzed for further treatment. (Coombes, 2015) Or by the usage of single cell systems; those cells can originate from cell lines but could also be extracted via biopsy from a patient. The cells are afterwards incubated and exposed over a certain amount of time to the cancer drug while the resulting reactions are verified. One promising approach for a new mechanical based screening technique could be achieved by utilizing the electronic speckle pattern interferometry (ESPI). This optical method is capable of observing microscopic structure changes in the vicinity after an initial stimulus. (Lietzau, 2016) Due to the contact-free measurement, a biopsy sample could be used for a drug screening without the need of further processing.

RESULTS AND DISCUSSION

The experiments regarding the analysis of the apoptotic cellular reaction were performed utulizing a culture medium without fetal bovine serum (FBS). Hereby, the applied dosage of Halaven® corresponds to the therapeutic recommendation of the manufacturer. The chemical agent of Halaven®, Eribulin, binds to the beta subunits of the tubulins and overlaps the guanosine triphosphate (GTP) binding site. Thus, the tubulin polymerization is inhibited which causes the tubulins to degrade into non-productive aggregates. Thereby, the spindle apparatus can't be formed and inhibits the mitosis which as a consequence induces the apoptosis of the cell. (Moore, 2005) The apoptotic bodies represent itself in form of circular outgrowths of the cell membrane.

During a first set of experiments the induced effect of Halaven® was analyzed on a variety of cellular samples which included Fibroblasts. The following results are focused on the later. Fibroblasts are the main component of connective tissue and the primary source of most extracellular matrix components. Another important function is the production of collagen. In addition, fibroblasts are a key factor in wound healing and also involved in tumor progression. (Theerakittayakorn, 2011) For this reason, the experiment was carried out with fibroblast cell of

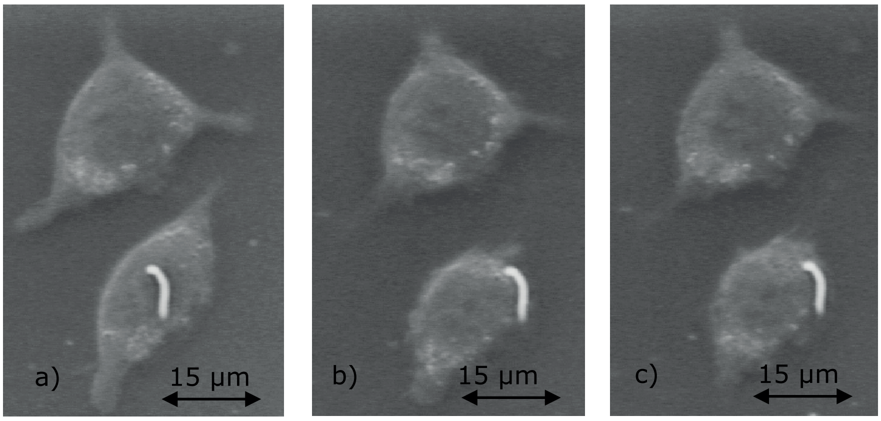

Figure 1: microscope images of apoptotic stages of the L929 cell after Halaven® injection. a) reaction time: 0 minutes b) reaction time: 10 minutes c) reaction time: 30 minutes

the cell line L929. The L929 are monolayer growing cells with an approximate cell cycle of 24 hours. They are often used for cytotoxicity tests since the cytotoxicity can be directly correlated with the cellular morphology and metabolic activity because these cells have a high cell division rate similar to degenerated cells. Thus, they are effective for degenerate cell experiments in terms of a negative control. As seen in figure 1, the apoptotic reaction was induced after the addition of halaven. However, the reaction is significantly slower in comparison to other tested cells. Overall the cellular displacement after a reaction time of 10 minutes (see fig. 1b) and 30 minutes (see fig. 1c) wasn't distinctive visible. Nevertheless, after a total reaction time of 60 minutes the apoptotic state of the observed L929 was clearly observed. Nevertheless, only a minimal change of the cell geometry as well as some developed apoptotic corpuscles were obtained. Based on these results it was concluded, that the overall effect of Halaven® was significantly reduced. An exemplary apoptotic reaction of the L929 cells obtained with ESPI are shown in figure 2.

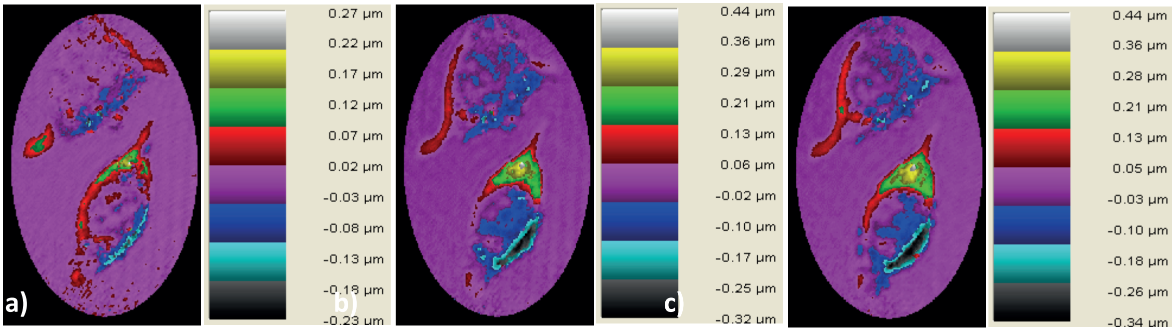

Figure 2: False phase images with color scale of apoptotic stages of the L929 cells after Halaven® injection. a) reaction time: 5 minutes b) reaction time: 10 minutes c) reaction time: 30 minutes

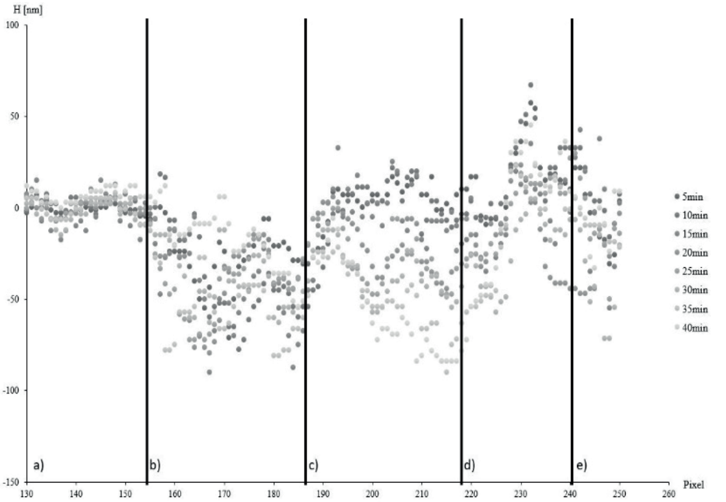

Figure 3: cellular deformation of the lower L929 cell over the reaction time with Halaven®. X-axes: amount of pixels; y-axes: displacement high in nm scale

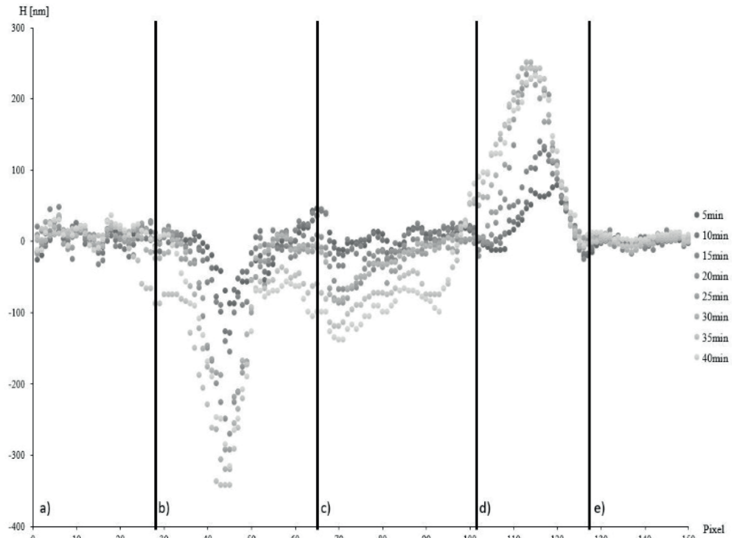

Figure 4: cellular deformation of the upper L929 cell over the reaction time with Halaven®. X-axes: amount of pixel; y-axes: displacement high in nm scale

In figure 2, both cells display distinctive areas of displacement which are indicated in yellow (positive) and blue (negative). Furthermore, the slow contraction of the cellular body, the loss of the spindle-shaped structure, the formation of the apoptotic bodies are clearly visible over time and shown in figure 2a to 2c. This is indicated by circular negative displacements also in the increasing positive deformation area. Based on the obtained deformation a linear scan was placed across the deformed cell (30 minutes) with the *ESPI-Result-Image-Comparser*. This self-designed program utilizes the intensity per pixel according to the measurement result and the corresponding color scale to generate the topographic scan which is shown in figure 3. Section a) represents the surface of the silicon chip without any cells. The obtained displacement in section b) indicates that the lower cell has contracted strongly compared to the initial position. The membrane invaginations formed by the apoptotic reaction are displayed in section c). Section d) represents the original cell position and thus indicates the occurred positive surface deformation.

In comparison, figure 4 contains an overlap of multiple scanlines for the upper cell. With advancing apoptosis, the increasing formation of the induced deformation is clearly shown in figure 4. As in the previous example, section a) contains the surface information of the silicone substrate which consequently displays no displacement. In comparison, the other sections b), c) and d) display an alternating patterns for each lines, which indicates the formation of the apoptosis corpuscles over the time.

CONCLUSION

Within this work, a new strategy for the investigation of such a cellular interactions after the application of external stress in form of a cytotoxic agent was demonstrated. After injection of the drug Halaven®, an apoptotic reaction of the different cells could be induced while the surface displacement of the cellular body was obtained utilizing the ESPI method. The main advantages of this method are the abilities to observe the biological samples in real-time, without sample contact and without sample destruction. Furthermore, the application of a modified ESPI setup allows a direct analysis of the cells in medium without additional influence by the measurement procedure. This approach provides a capable method to examine the cells in an almost natural environment which is fundamental to analyze complex cellular interactions in order to develop new therapeutic methods.

REFERENCES

Balis FM, “The Goal of Cancer Treatment”, Oncologist, 1998, 3(4), https://www.ncbi.nlm.nih.gov/pubmed/10388118; 21.09.2018, 10:30 am

R. C. Coombes, “Drug testing in the patient: Toward personalized cancer treatment” Science Translational Medicine, 2015, 7/284:284, http://stm.sciencemag.org/content/7/284/284ps10.full; 21.09.2018, 10:35 am

J. F. DiJoseph, et al. “Antibody-targeted chemotherapy with CMC-544: a CD22-targeted immunoconjugate of calicheamicin for the treatment of B-lymphoid malignancies”; blood; 2004; 103:1807-1814, http://www.bloodjournal.org/content/103/5/1807.short?sso-checked=true; 21.09.2018, 10:31 am

Kai-H. Lietzau; 2016; „Electronic Speckle Pattern Interferometry for cancer research”; University Tor Vergata Rome

T. R. Moore, A simple design for an electronic speckle pattern interferometer, American Journal of Physics 73, 2005

N. Rapoport, et al. , “Multifunctional Nanoparticles for Combining Ultrasonic Tumor Imaging and Targeted Chemotherapy”; Journal of the National Cancer Institute; 2007; 99/14, https://academic.oup.com/jnci/article/99/14/1095/938872; 21.09.2018, 10:30 am

K. Theerakittayakorn, T. Bunpraser, Differentiation Capacity of Mouse L929 Fibroblastic Cell Line Compare With Human Dermal Fibroblast, Engineering and Technology International Journal of Medical, Health, Biomedical, Bioengineering and Pharmaceutical Engineering, Ausgabe 5 Nr. 2, World Academy of Science, 2011

J. Wang et al. “Insider information: Testing cancer drug sensitivity for personalized therapy”, Genes & Diseases, 2015, 2/3:219-221, https://www.sciencedirect.com/science/article/pii/S2352304215000380?via%3Dihub; 21.09.2018, 10:32 am

PAPER REF: 104

ANALYSIS OF MATERIAL PARAMETERS OF DIFFERENT BIOMATERIAL BASED INKS FOR 3D

Volker Schlegel[1(*)], Andreas Engels[1], Steffen Zinn[1], Stefano Bifaretti[2], Andreas H. Foitzik[1]

[1]Technical University of Applied Science Wildau, Hochschulring 1, 15745, Wildau, Germany

[2]University of Rome Tor Vergata, Department of Industrial Engineering, Via Orazio Raimondo, 18 - 00173 Roma, Italy

[(*)]*Email:* VSchlegel@th-wildau.de

ABSTRACT

Innovative approaches of personalized medicine affect various areas of therapeutic treatment at the present days. These include application of surgical procedures, private point-of-care solutions, pharmaceuticals, as well as rehabilitation procedures. Beside these current existing strategies, the progression of patient specific models for training of clinical and surgical personal is currently inadequate. Such models are vital to prepare an individualized approach in medical care. The conversion of an established 3d printing technology to process suitable structural biopolymers could be a possible solution to approach the mentioned issue.

The focus of the presented work lies upon the development of a printing system utilizing multiple biomaterial based inks. Of highest interest are gelatine, collagen and agar due to their type of temperature dependent hardening. Therefore, it is intended to design several different extrusion heads which handle the material in regard to its specific processing parameters. In order to obtain the intended physiological properties of the final model, various experiments will be performed with several compositions of biomaterials to verify the fundamental mechanical and physical characteristics. Hereby, the force resistance, elasticity, thermal stability, haptic behaviour, as well as the visual appearance are of highest interest.

Afterwards, these received experimental results should be used to validate the extruder concepts and to simulate the extrusion process. In case of a positive evaluation these concepts are manufactured and realized by using rapid prototyping technologies. Eventually, this novel 3D bioprinter will be used to print first organic test structures with biomaterials based on individualized patient's data.

Keywords: 3D printing, biomaterials, bioprinting.

INTRODUCTION

Progression in the field of medicine and the political stability had a wide influence on the lifespan of humans in Europe and the western world within the last century. Novel inventions of vaccines, antibiotics as well as other medical products and the advance in the field of surgery nearly doubled the average lifespan of humans. At the very beginning of the 20th century the average age at death for females and males was 45.84 years and 43.65 years, whereas in 2008 the average ages increased up to 79.79 for females and 73.58 for males (Mackenbach, 2013). This trend leads to a permanent rise of diseases, such as cancer, diabetes and similar age-related medical conditions. In order to treat such diseases, multiple treatments need to be performed to patients, which influences the physical as well as the psychological conditions of the affected patients. One of the most challenging problems is the highly increased occurrence of cancer. E.g., within the years of 1999 to 2015 the number of patients developing a liver carcinoma in Germany drastically increased. In 1999, 2199 female and 3875 male patients were diagnosed with a liver carcinoma, whereas in 2015 the number of women increased to 2709 and of men to 6374 (Robert-Koch-Institut, 2017). Those numbers even continued to rise, while the technology and procedures to treat and cure cancer advanced even further. As the technology advances, the clinical personal, e.g. surgeons, needs to be trained for new approaches and surgical procedures. Currently most applied therapies are the removal of the carcinoma or transplants from organ donors. The survival rates for both methods are about 50 %, while the transplantation even contains a certain risk to the donor (Bismuth et al., 1993). In order to improve the survival rates, the operating surgeons need special training. Such training methods could be performed via simulation programs as well as artificial organ-like models. Consequently, artificial models need to have the same haptic and optical properties as the original organ and should be produced based on the patients' data. Therefore, the most important properties are the firmness and coloring of various tissues. Similar organ-like models are already produced through casting. However, using this technology, the models are cost intensive while the manufacturing is time-consuming and not customizable. A new approach for the production of those organ-like structures would be the adaption of a 3d printer utilizing a variety of biomaterial based inks, such as collagen. Another biomaterial, which is already used within 3d cell cultures and bioprinting, is agar. This gelable fluid is widely used as a basis for cell culture, due to its properties. Introduced to microbiological bacteriology in 1939 (Hitchens and Leikind, 1939), agar consists of two different main components, the polysaccharides Agarose and Agaropectin. Agar itself is produced from multiple types of algae, mostly from east Asia. In 3d bioprinting, agar is also used to construct base structures (Marga et al., 2012), as well as scaffolds for 3d cell culture (Landers et al., 2002), based on the natural behaviour and biological compatibility (Kyle et al., 2017).

RESULTS AND CONCLUSIONS

The gel point can be determined by measuring the storage modulus G` and the loss modulus G`` of the solutions. For this, six agar samples in the range of 0.5 to 3.0 % were prepared. The temperature was measure from 70 °C to 25 °C, with a cooling rate of 1 °C/min. Therefore, a rheometer (Anton Paar, Physica MCR 301) has been used. The measurement was done with the measuring system of cone/disk (50 mm) using oscillation with a frequency of 1 Hz and an amplitude of 10 %.

The illustrations (a) and (b) of Fig. 1 displays the design concepts of a syringe extruder using a revolver-like configuration for standardized syringes to achieve a high variability of compositions. The syringe revolver consists of several different main parts. At first, a rotatable revolver structure, which mounts the syringes, is located at the bottom of the extruder. The syringes are pre-filled with the already mixed and heated compositions of biomaterials. A base plate is located beneath the revolver, which is unmovable and carries the nozzle of the syringes. The revolver itself is rotatable via a belt driven by a stepping motor in order to align the nozzle with the correct syringe. Hereby, the axis is surrounded by a heater, which modulates the temperature of the syringes based on predefined values. In order to deplete the content of the syringes for extrusion, the stamp is forced down via a stepping motor.

Therefore, the gel point of multiple agar concentrations had to be examined. The gel point can be determined by measuring the storage modulus G` and the loss modulus G`` of the solutions.

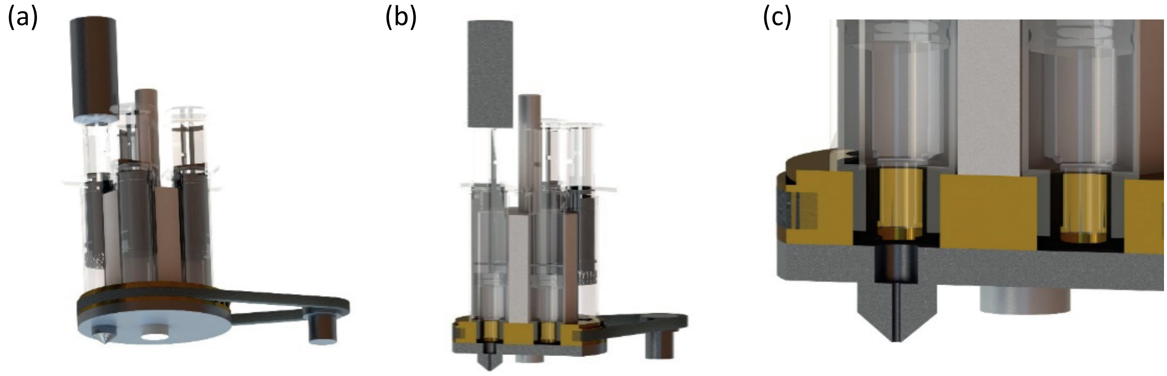

Fig 1 - Rendered images of the syringe extruder, as viewed from the bottom (a), the top (b), as well as zoomed onto the nozzle (c)

For this, six agar samples in the range of 0.5 to 3.0 % were prepared. The range of temperature reached between 25 °C and 70 °C, with a cooling rate of 1 °C/min. Two results are representatively shown in the diagrams of Fig. 2. At the beginning of the measurement, G` is higher than G``, while at the end it is beneath the values of G``. First, the viscous amount of the agar, which is described by G``, is minor to the elastic part. While cooling, both moduli rise based on the kinetics of the agar, since the process of solidification of the sol-gel slowly follows the lowering temperature, until a certain critical value is reached. The gel point is noticeable by the crossover of both graphs, when G``/G` = 1 (Labropoulos et al., 2002a). For example, the first gel point of a 1.5 % agar solution is at 68 °C and the second at 49.7 °C. The first gel point declares the initiation of the gel process, whereas the second marks the accurate gel point. As visible in Fig. 2, the gel point increases with the concentration of agar, because of the rising amount of agarose. The measurement of the viscosity of multiple agar samples in the range of 0.5 to 3.0 % was realized with the help of a rheometer using oscillation. The range of temperature reached between 25 °C and 70 °C, while the cooling rate was 1 °C/min. Decreasing the temperature increased the viscosity, until the sol-gel had formed completely. The result for 1.5 % and 3.0 % agar are also shown in Fig. 2. Within nearly all measurements, a sudden rise of the moduli is noticeable. This is caused by the kinetics of the gel of agar (Labropoulos et al., 2002a, b).

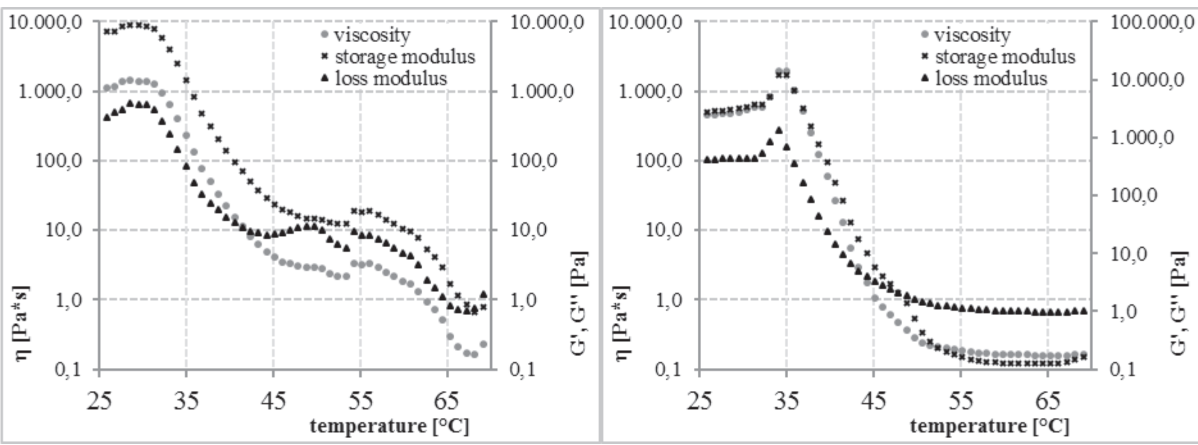

Fig. 2 - Plotted data of rheometric measurements of viscosity(●), storage modulus (G` represented as ▲) and the loss modulus (G`` represented as ○) of 1.5 % (left) and 3 % (right) agar against the temperature T

CONCLUSION

The aim of the presented ongoing work is to develop multiple extruders for a 3d printing system utilizing multiple biomaterials as inks. As mentioned, such extruders should be adaptable to the parameters needed for the liquefaction and polymerisation of e.g. agar and collagen, whereas the shear forces and temperature are of most importance for the extrusion process. The final objective is to print organ-like test structures. These look-alike should possess the same haptic and optical behaviours as the original patient organ. As a reference, agar was used and therefor, the gel points of multiple concentrations were determined, discovering a concentration dependency of the agar to the gel point. Eventually, an extruder design was presented. A revolver-like syringe extruder could hold multiple standardised syringes with pre-mixed biomaterial compositions. The revolver is turned via a stepping motor, while being mounted onto a base plate, where a nozzle is attached. Currently, the concept is realized by rapid prototyping and will be implemented afterwards in a functional laboratory setup.

REFERENCES

Bismuth, H., Chiche, L., Adam, R., Castaing, D., Diamond, T., and Dennison, A.: Liver resection versus transplantation for hepatocellular carcinoma in cirrhotic patients, Annals of surgery, 218, 145-151, 1993.

Di Lullo, G. A., Sweeney, S. M., Korkko, J., Ala-Kokko, L., and San Antonio, J. D.: Mapping the ligand-binding sites and disease-associated mutations on the most abundant protein in the human, type I collagen, The Journal of biological chemistry, 277, 4223-4231, 10.1074/jbc.M110709200, 2002.

Hitchens, A. P., and Leikind, M. C.: The Introduction of Agar-Agar into Bacteriology, J Bacteriol, 37, 485-493, 1939.

Kyle, S., Jessop, Z. M., Al-Sabah, A., and Whitaker, I. S.: 'Printability' of Candidate Biomaterials for Extrusion Based 3D Printing: State-of-the-Art, Adv Healthc Mater, 6, 10.1002/adhm.201700264, 2017.

Labropoulos, K. C., Niesz, D. E., Danforth, S. C., and Kevrekidis, P. G.: Dynamic rheology of Agar gels: theory and experiments. Part I. Development of a rheological model, Carbohydrate Polymers, 50, 393-406, https://doi.org/10.1016/S0144-8617(02)00084-X, 2002a.

Labropoulos, K. C., Niesz, D. E., Danforth, S. C., and Kevrekidis, P. G.: Dynamic rheology of Agar gels: theory and experiments. Part II: gelation behavior of Agar sols and fitting of a theoretical rheological model, Carbohydrate Polymers, 50, 407-415, https://doi.org/10.1016/S0144-8617(02)00085-1, 2002b.

Landers, R., Hubner, U., Schmelzeisen, R., and Mulhaupt, R.: Rapid prototyping of scaffolds derived from thermoreversible hydrogels and tailored for applications in tissue engineering, Biomaterials, 23, 4437-4447, 2002.

Mackenbach, J. P.: Political conditions and life expectancy in Europe, 1900-2008, Social science & medicine, 82, 134-146, 10.1016/j.socscimed.2012.12.022, 2013.

Marga, F., Jakab, K., Khatiwala, C., Shepherd, B., Dorfman, S., Hubbard, B., Colbert, S., and Gabor, F.: Toward engineering functional organ modules by additive manufacturing, Biofabrication, 4, 022001, 10.1088/1758-5082/4/2/022001, 2012.

PAPER REF: 105

SIMULATION AND EXPERIMENTATION OF MICRO-SINGLE POINT INCREMENTAL FORMING PROCESS OF THIN SHEET METALS

Belouettar Karim[1(*)], Ould Ouali Mohand[2], Sébastien Thibaud[3], Ramzi Ben Hmida[3]

[1]Advanced Manufacturing and Control Techniques Laboratory (AMCTL), Ecole Militaire Polytechnique, EMP, Algiers 16111, Algeria

[2]Laboratory of Elaboration and Characterization of Materials and Modeling (LEC2M), University of Tizi-Ouzou 15100, Algeria

[3]UBFC/ FEMTO-ST Institute /CNRS-UMR6174/UFC/ENSMM/UTBM, Department of Applied Mechanics, Besançon, France

[(*)]*Email*: karim.belouettar@emp.mdn.dz , belouettar_karim@yahoo.fr

ABSTRACT

Incremental sheet forming is a rapid prototyping process which used a forming tool to form a sheet metal according to a predetermined trajectory of tool controlled by a CNC machine. This article is dedicated to the study of the Single Point Incremental Forming (SPIF) process and more particularly to the numerical simulation of a pyramidal shape with the finite element calculation code ABAQUS/Explicit and in the validation of these numerical predictions using the results of experimental tests. In addition, force profile comparisons made during an incremental forming operation revealed a good correlation between the numerical simulation and the experimental.

Keywords: Incremental forming, numerical simulation, ductile damage model.

INTRODUCTION

Incremental sheet forming is a new technology allows to obtain complex parts using a hemispherical end tool by applying a locally deformation process in sheet metal. The desired geometry is provided by using a specific forming tool path controlled by a CNC machine. The main advantage of this process is the very low cost of tooling development compared to conventional processes as deep drawing (Jeswiet, 2005).

A second asset of this process is due to the important plastic strain level that it can be obtained. The main objective of this work is to develop a numerical tool by applying a GURSON-type ductile damage model with the finite element calculation code ABAQUS/Explicit and validating these numerical predictions using the results of experimental tests (Gurson, 1977- Tvergaard, 1984). A copper alloy material is considering with a controlled grain size (Ben Hmida, 2013). The comparisons made on the force prediction during a single-point incremental forming (SPIF), operation of a pyramidal shape (truncated) (Thibaud, 2012), and the results obtained are given in terms of axial forces evaluation and geometrics comparison.

RESULTS AND CONCLUSIONS

The work reported above has demonstrated the ability to predict correctly the materials behavior during the single-point incremental forming process SPIF. A micromechanical GTN model is chosen for the prediction of the damage and ductile fracture of materials applied to a single-phase copper alloy (Cu-0.1Fe). In a second step, experimental tests of this process were carried out in order to study the mechanisms involved in Figure 1.

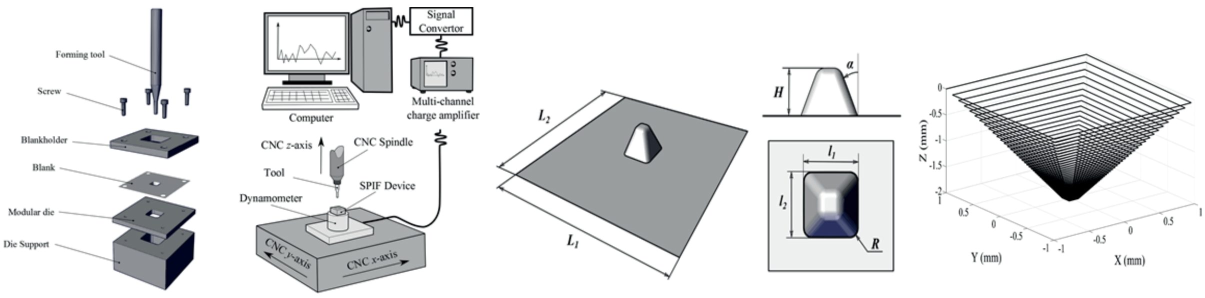

a b c

Fig. 1 - μ-SPIF test : a-testing device, b- pyramidal part shape, c-forming strategy

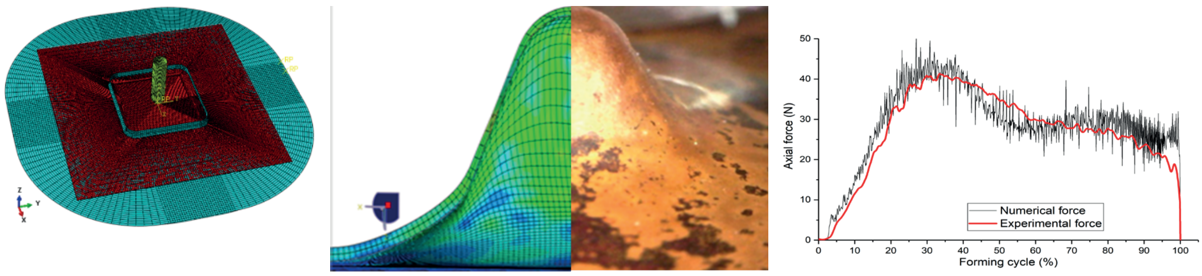

EF model of μ-SPIF Pyramidal form Forming force

Fig. 2 - Numerical and experimental comparisons results

The geometry and axial force results show a good correlation between the experiment and the numerical predictions for a pyramidal form (Figure 2). This comparison was very satisfactory and allowed us to validate our approach.

REFERENCES

[1] J. Jeswiet, F. Micari, G. Hirt, A. Bramley, J. Duflou, J. Allwood, Asymmetric Single Point Incremental Forming of Sheet Metal, CIRP Annals - Manufacturing Technology, 2005, 54, p. 88-114.

[2] A. L. Gurson, Continuum Theory of Ductile Rupture by Void Nucleation and Growth: Part I-Yield Criteria and Flow Rules for Porous Ductile Media, J. Eng. Mater. Technol, 1977, 99, p. 2-15.

[3] V. Tvergaard, A. Needleman, Analysis of the cup-cone fracture in a round tensile bar, Acta Metallurgica, 1984, 32, p. 157-169.

[4] R. Ben Hmida, S. Thibaud, A. Gilbin, F. Richard, Influence of the initial grain size in single point incremental forming process for thin sheets metal and micro parts: experimental investigations, Materials and Design, 2013, 45, p.155-165.

[5] S. Thibaud, R. Ben Hmida, F. Richard, P. Malécot, A fully parametric toolbox for the simulation of single point incremental sheet forming process: Numerical feasibility and experimental validation, Simul. Model. Pract. Theory, 2012, 29, p.32-43.

PAPER REF: 106

EFFECT OF LASER CLADDING PARAMETERS ON DILUTION AND WELD BED GEOMETRY IN 316L STAINLESS STEEL

Eriel Pérez Zapico[1(*)], Alessandro Ascari[2], Alessandro Fortunato[2]

[1]Welding Research Center (CIS), Central University of Las Villas, Villa Clara, Cuba

[2]Department of Industrial Engineering (DIN), University of Bologna, Italy

[(*)]*Email:* zapico@uclv.cu

ABSTRACT

This work studies the effect of laser cladding parameters on the dilution and weld bead geometry in 316L stainless steel. A series of experiments were carried out to know the effect of power, scanning speed, powder feed rate and hatch distance on dilution and weld bead geometry. The metallographic samples were polished and chemically etched to find the depth of penetration, height deposition and dilution. The results show the optimal values of the parameters studied to reduce the geometrical deposition imperfections.

Keywords: laser cladding, penetration depth, dilution, weld bed.

INTRODUCTION

Laser cladding is a modern additive manufacturing technology. The laser cladding consists in the fused metal deposition using a laser beam defocused on the workpiece. The powder is carried out by an inert gas through a coaxial or lateral nozzle and is projected into the melt pool. The processes involve moving the laser optics and powder nozzle assembly over a substrate to produce solidified tracks. A successful cladding needs a weld bead with a good geometric and minimum dilution. Laser power and speed are two important parameters to influence dilution in laser cladding with wire feeding (Kim J.D., 2000). Weld bed geometric and dilution increase with increasing the wire feed rate and decrease with increasing welding speed, but dilution increases (Nouri M, 2007). Methods of measuring dilution ratio can be calculated according the measured value of cross-section area of cladding bed (Song B, 2016). Higher level of dilution and lower concentration of carbon can be decrease the hardness of the coating (Kusmoko A, 2016).

A total of 9 individual test were performed. The experimental setup include a GTV Powder Feeder, Laserline LDF 4000 diode laser of 4 kW power source, the powder were injected using a coaxial GTV nozzle and the Motoman robotic arm controlled the laser beam scanning speed. The samples were performed following the scanning strategy consist in deposition of alternately parallel track to x-y and laser off return. The powdery additive was 316L. The substrate plate's material was a low carbon steel alloy. To simplify the laser cladding parameters, were combined laser power (W) and powder feed rate (g/min) with scanning speed (mm/s), resulting the parameters: specific energy (J/mm) and powder feed rate (g/mm).

RESULTS AND CONCLUSIONS

The tests 0,012 g/mm; 176 J/mm and 0,009 g/mm; 118 J/mm show in Fig. 1, have a high penetration depth, are characterized by a high energy/powder feed rate with a high heat that influences the substrate directly. The experiment 0,014 g/mm; 88 J/mm, having a low energy/ powder feed rate, has a lower depth.

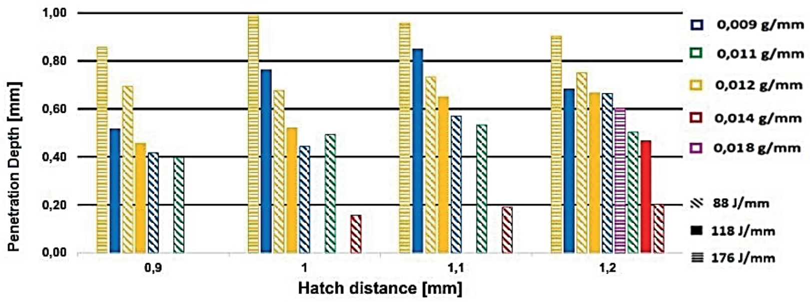

Fig. 1 - Effect of laser cladding parameters in the penetration depth

At the same gas flow rate and specific energy input, the height increases if the hatch distance decreases, due to the greater overlap.

The lower dilution was obtained for 0,014 g/mm tests; 88 J/mm, show in Fig. 2, is characterized by a low penetration depth and a high height. The higher dilution is obtained for 0,012 g/mm; 88 and 118 J/mm, tests with high penetration depth and limited height. With the same specific energy and powder feed rate, the dilution rate tends to increase as the hatch distance increases.

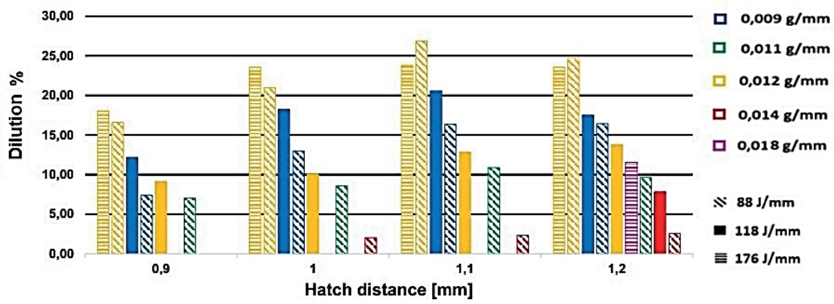

Fig. 2 – Effect of laser cladding parameters in the dilution rate

This study shows that the laser power and scanning speed are strong influence in the penetration depth and dilution. Further tests should be performed in order to analyze the influence of laser cladding parameters in the hardness and mechanical properties.

REFERENCES

Kim J.D., Peng Y. Melt pool shape and dilution of laser cladding with wire feeding. Journal of Materials Processing Technology, 2000, 104 284-293.

Kusmoko A, Dunne D, Li H. Measuring Dilution and Wear for Laser Cladding of Stellite 6 Produced on a P91 Steel Substrate using Two Different Heat Inputs. In MATEC Web of Conferences ICMIT 2016, 2016.

Nouri M, Abdollah-zadeh A, Malek F. Effect of Welding Parameters on Dilution and Weld Bead Geometry in Cladding. Journal of Materials Science & Technology, 2007, 23 (6).

Song B, Hussain T, Voisey K.T. Laser Cladding of Ni50Cr: A Parametric and Dilution Study. Physics Procedia, 2016, 83, 706-715.

PAPER REF: 107

THE WEAR EFFECT OF MOLYBDENUM-DERIVED PARTICLES ON HYDROGENATED DIAMOND-LIKE CARBON AT HIGH TEMPERATURE

K.A.M. Kassim[1]*, T. Tokoroyama[1], M. Murashima[1], N. Umehara[1]

[1] Department of Micro-Nano Mechanical Science and Engineering, Graduate School of Engineering, Nagoya University, Furo-cho, Chikusa-ku, Nagoya, Aichi 464-8603, Japan

(*)*Email:* khairul@ume.mech.nagoya-u.ac.jp

ABSTRACT

This research work focuses on the wear acceleration effect of Mo-derived particles on the hydrogenated amorphous carbon (a-C:H) DLC under boundary lubrication at 80 ºC. It shows that each Mo particles gave a different effect on the wear properties of a-C:H DLC. However, the inclusion of Silicon-doped onto a-C:H DLC reduces the wear acceleration.

Keywords: friction, wear, molybdenum, diamond-like carbon.

INTRODUCTION

Since decades ago, the control of friction and wear in the automotive engine system has been captured attention by many researchers. Literatures broadly reported that low friction coefficient under boundary lubrication leads to a vital decrement of fuel consumption, and also an increment of life expectancy and durability of the engine.

Diamond-Like Carbon (DLC) coating is one of the potential candidates to give low friction and long life span due to its high hardness and chemical inertness properties. It is now being prominently used in the automotive industry as a coating material especially on the sliding parts of automobile engine such as piston ring and cylinder liner.

In order to get an optimum operating condition under lubrication regimes, the DLC coatings are exposed to assorted lubricant additives. Liquid-type molybdenum dithiocarbamate (MoDTC) is a well-known friction modifier in the engine oil and very efficient in reducing friction between DLC/steel contacts surfaces under boundary lubrication. However, the MoDTC lubrication resulted in wear increment of DLC [1].

MoDTC is reported as an easily degradable compound and has tendency to change it physical and chemical structures. Previous research works presumed that the intermediate products from the degradation of the liquid MoDTC accelerate the DLC wear. Mo-derived compounds such as molybdenum disulfide (MoS_2) and molybdenum trioxide (MoO_3) are reported to form tribo-layers on hydrogenated DLC and promote chemical wear. The other Mo-derived compound, molybdenum carbide (Mo_2C) is revealed to cause an abrasive wear on DLC surface [2-3].

There are a lot of conclusion and assumption being made. However, which Mo compound precisely accelerates the wear; either MoDTC itself or the Mo-derived compounds from the MoDTC degradation has still been unknown. Therefore, it is very essential to identify which Mo-derived compound has a major role to enhance the wear. Thus, powder-type MoDTC and

Mo-derived compounds are used to divide their wear effect on DLC by dispersing each of them into base oil and tested under standard engine temperature of 80 ºC.

RESULTS AND CONCLUSIONS

Five types of Mo-derived particles; MoDTC, MoO_3, Mo_2C, MoS_2 and pure Mo are tested onto hydrogenated amorphous carbon (a-C:H) DLC and Si-doped a-C:H (Si-DLC) against steel ball. Fig.1 shows the specific wear rate of a-C:H and Si-DLC discs. Basically, a-C:H gives higher specific wear rate compared to Si-DLC. MoDTC which is known as the wear acceleration material shows a specific wear rate around 8.0 x 10^{-6} mm^3/N.m for a-C:H. However, Mo_2C reveals it has 8 times much higher specific wear rate compared to MoDTC, approximately 60 x 10^{-6} mm^3/N.m for a-C:H. MoO_3 and Mo also enhance modest wear acceleration on a-C:H and Si-DLC. MoS_2 which is famous as solid lubricant maintains its specific ware rate at the lowest level.

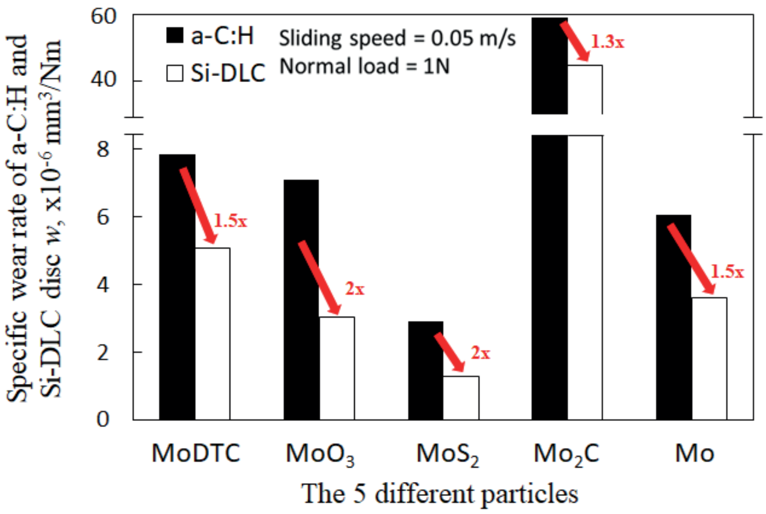

Fig.1 - The specific wear rate of a-C:H and Si-DLC disc under lubrication of 5 different particles with base oil

It can be concluded that each additive particles gives different wear effect on both a-C:H and Si-DLC discs. Based on the wear analysis, Mo_2C plays the main role to accelerate wear on hydrogenated DLC. It is suggested that the inclusion of Silicon-doped onto the a-C:H DLC reduces as much as two times the wear acceleration.

REFERENCES

De Barros'Bouchet MI, Martin JM, Le-Mogne T, Vacher B. Boundary lubrication mechanisms of carbon coatings by MoDTC and ZDDP additives. Tribology International, 2005, 38, p. 257–264.

Okubo H, Sasaki S. In situ Raman observation of structural transformation of diamond-like carbon films lubricated with MoDTC solution: Mechanism of wear acceleration of DLC films lubricated with MoDTC solution. Tribology International, 2017, 113, p. 399–410.

Ohara K, Hanyuda K, Kawamura Y, Omura K, Kameda I, Umehara N, et al. Analysis of Wear Track on DLC Coatings after Sliding with MoDTC-Containing Lubricants. Tribology Online, 2017, 12, p. 110–116.

PAPER REF: 109

CAROTID ULTRASOUND IMAGE ANALYSIS USING ARTIFICIAL NEURAL NETWORKS

Catarina F. Castro[1,2(*)], Carlos C. António[1,2], Luisa C. Sousa[1,2]
[1]Faculty of Engineering of the University of Porto (FEUP), Porto, Portugal
[2]Institute of Science and Innovation in Mechanical and Industrial Engineering (INEGI), Porto, Portugal
[(*)]*Email:* ccastro@fe.up.pt

ABSTRACT

This paper aims at developing an ultrasound-based diagnostic measure quantifying plaque activity and the likelihood of asymptomatic lesions to produce neurological symptoms. Based on echogenicity the methodology has been successfully applied on longitudinal ultrasound images of the carotid artery bifurcation. Transverse ultrasound images incorporate noise, artifacts, shadowing and reverberation. Nevertheless, transverse images are a resource not yet fully explored. The comparison of sequential transverse images minimizes the intrinsic scale variability between operators and ultrasound devices. Based on pixel level tissue classification, the use of an artificial neural network analysis applied to transverse images allows identifying vulnerable or unstable echolucent plaques.

Keywords: artificial neural network, ultrasound image, carotid plaque status.

INTRODUCTION

In carotid ultrasound images, detection and characterization of plaques is challenging even for an expert clinician, resulting in tedious and inconsistent assessments. Not only the degree of stenosis but also the carotid plaque instability are important determinants of stroke risk, triggering episodes of local thrombosis and leading to distal embolization of plaque debris. An automated technique is required to obtain fast, robust, and user-independent analyses for image segmentation and plaque composition. The anatomic superficial location of the extra-cranial carotid arteries favours their insonation. Advantages of studying from the non-invasive nature of the technique are the low cost and easy availability of the equipment. The aim of the ongoing project is analyse patient-specific ultrasound images for the study of plaque surface and contents, plaque volume, and vessel wall movement using artificial neural networks (Castro et al. 2018; Leclerc et al., 2018). The development of an artificial neural network model to address the feasibility of development of neurological complications based on pixel intensity information and the associated plaque risk score is the main project.

METHODOLOGY

Image analysis methodology is usually based on three sequential steps: image normalization, multiscale description, and classification. Performing multiscale description of image regions, the methodology can deal with the intrinsic scale variability of the image. Obtaining better pixel-level tissue classification allows providing a better plaque classification in terms of asymptomatic or symptomatic, and so, for determining the risk of diseases for the patient. Figure 1 represents the proposed methodology (Litjens et al. 2017; Pazinato et al., 2016).

Fig. 1 – Proposed methodology assuming that all pixels in each region are of the same tissue

The study of plaque contents is associated to the identification of the plaque constituents and their relative localization to the luminal surface. Lipids reflect ultrasound poorly and produce pixels predominantly dark in the grayscale B-mode ultrasound screen. Fibrotic tissue, which renders the plaque more stable, produces a stronger reflection of the ultrasound waves and appears lighter on the screen. Vulnerable or unstable echolucent plaques appear darker as in opposition to echogenic plaques that are denser and appear lighter on the screen (Molinari et al., 2007; Seabra et al., 2011). After image normalization, image regions were identified as in Figure 2. Image cuts removes unwanted information and selects the region of interest.

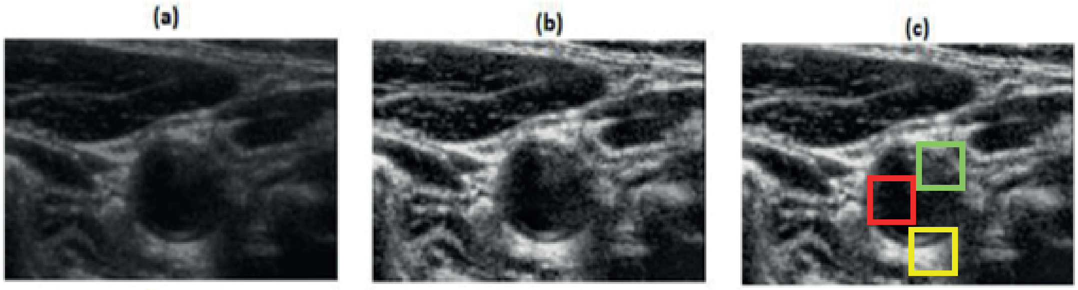

Fig.2 – (a) Original image; (b) image normalization; (c) tissue description with red square assigned as blood tissue, green square as echolucent plaque and yellow square as echogenic plaque.

In order to extract the information to differentiate blood from plaques, a dataset with selected images were considered. The considered methodology considers using different areas of the images in which all pixels belong to the same tissue. Verified by a specialist, images were cropped as having high prevalence of one particular tissue. The difficulty for establishing one threshold for classifying each type of plaque based on pixel intensity distribution of the tissues is due to unavoidable fact of class overlaps when using a histogram of frequencies.

Artificial neural networks (ANNs) are computer programs designed to simulate the way brain processes information. ANNs are trained based on examples and can be valuable to construct a decision maker based on knowledge only. There is no theoretically sound way of choosing the optimal ANN architecture for each separate model. The considered network has one hidden layer with N neurons. Synapses send data on to a hidden layer, which in turn sends to the output layer representing the dependent variables. Input and hidden layer biases need to be adjusted in all learning algorithms of neural networks and thus there exists dependency between different layers of parameters (weights and biases). The activation functions (hyperbolic tangent functions), the weights of the synapses and the bias applied to the neurons at the hidden and output layers are to be controlled during the supervised learning process.

For this paper, and due to the differences between the longitudinal and the transversal images, transversal images have been considered. A classifier has been established frame-wise, not considering transitions between frames when scanning tissues. Feeding the system with different areas of the ultrasound image allows different sort of plaques to be classified. Vessel candidate images of blood vessels and other non-vessel structures were used for training the neural network. Figure 3 gives an overview of the proposed developed artificial neural network. Due to the presence of connective tissue, it is impossible to ensure that 100% of the training images really contain only pixels of the labeled tissues.

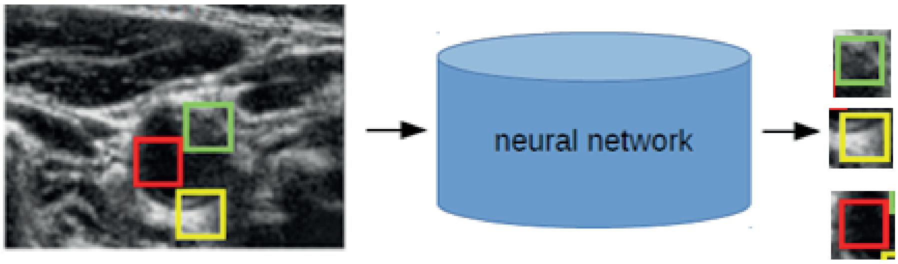

Fig. 3 – Overview of the proposed developed artificial neural network: sub-images are passed on to a neural network classifying vessels, echolucent plaques and echogenic plaques.

RESULTS AND CONCLUSIONS

It is important to highlight that this is a pixel-level classification; therefore, it is not easy to achieve a perfect classification score. Objective and quantitative evaluation of the ANN performance is crucial and usually difficult in medical applications. For each of the categories, blood vessels, echolucent plaques or echogenic plaques, success rates are usually based on: true positive (number of areas correctly identified), true negative (number of areas correctly identified as not belonging to the category), false positive (number of incorrectly identified areas) and false negative (number of incorrectly identified areas). Computed parameters are sensitivity reflecting in the ratio of areas correctly classified and specificity defined as the true negative rate. The mean value obtained for the sensitivity verifying the correct identification was 82%, 90% and 88% for blood vessels, echolucent plaques or echogenic plaques, respectively. As for the specificity, the ANN excludes 85%, 82% and 86% of the areas considered as not belonging to blood vessels, echolucent plaques or echogenic plaques, respectively. It should be noted that this algorithm solves the problem of poorly defined arterial wall and low quality images, works for different equipment and successfully identifies areas of the common carotid artery, bifurcation region (with a different topology) and the proximal internal carotid artery and external carotid artery. Pearson correlation values are $\rho = 0.45$, $\rho = 0.666$ and $\rho = 0.72$ for blood vessels, echolucent plaques or echogenic plaques, respectively. Figure 4 presents an overview of the intended results for two different transverse images of the same individual: (a) distal common carotid artery and external carotid artery and (b) carotid artery bifurcation region.

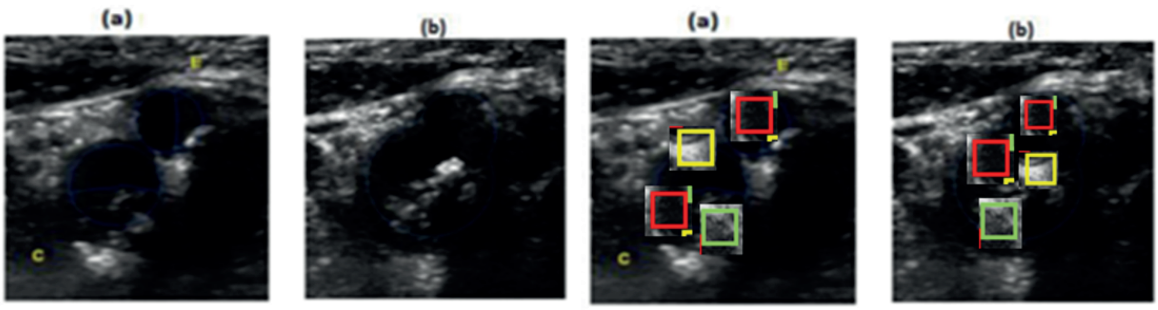

Fig. 4 – Overview of the results for two different transverse images of the same individual: (a) distal common carotid artery and external carotid artery and (b) carotid artery bifurcation region. On the left images with no area identification and on the right identified areas of blood vessels, echolucent plaques and echogenic plaques (color selection as in Fig. 2 and 3).

A good approximation considering the problem of low quality and poorly defined arterial walls in transverse images. Moreover, fibrous and calcium are tissues with a similar echogenicity and in this work they were included in the same category and for analyzing carotid plaque image, the two most important tissues are blood and lipids and both have different classes.

The implemented methodology is prepared to analyse different B-mode images from different sonographers allowing the user to load images and process and extract features enabling plaque detection an classification. With ultrasound imaging, a large amount of unlabeled data can easily be acquired from the target body regions. Thus, unsupervised pre-training will be a useful technique within ultrasound imaging. Limitations similar to other technologies are expected to be resolved with further studies and technical improvements. The present research contributes to the analysis of hemodynamic conditions of the carotid bifurcation stenosis and occlusion (Pinho et al. 2018; Sousa et al. 2014).

ACKNOWLEDGMENTS

The authors gratefully acknowledge the funding by FCT, Portugal, of the Research Unit of LAETA-INEGI.

REFERENCES

Castro CF, António CAC, Sousa LC (2018) Vessel detection in carotid ultrasound images using artificial neural networks. Proceedings of the 6th International Conference on Integrity, Reliability and Failure, 1169-1172.

Leclerc S, Smistad E, Grenier T, Lartizien C, OstvikA, Espinosa F, Jodoin P-M, Lovstakken L, Bernard O (2018) Deep Learning Applied to Multi-Structure Segmentation in 2D Echocardiography: A Preliminary Investigation of the Required Database Size, Ultrasonics Symposium (IUS) IEEE International 2018, 1-4.

Litjens G, Kooi T, Bejnordi BE, Setio AAA, Ciompi F, Ghafoorian, M et al., (2017) A survey on deep learning in medical image analysis, Medical Image Analysis, 42: 60-88.

Molinari F, Liboni W, Pavanelli E, Giustetto, P, Badalamenti S, Suri JS (2007) Accurate and automatic carotid plaque characterization in contrast enhanced 2D ultrasound images. Conf. Proc. IEEE Eng. Med. Biol. Soc. 2007, 335–338.

Pazinato DV, Stein BV, de Almeida WR, Werneck RO, Mendes Júnior PR, Penatti OA, Torres RS, Menezes FH, Rocha A (2016) Pixel-Level Tissue Classification for Ultrasound Images. IEEE J Biomed Health Inform, 20(1): 256-267.

Pinho N, Castro CF, António CAC, Bettencourt N, Sousa LC, Pinto SIS (2018) Correlation between geometric parameters of the left coronary artery and hemodynamic descriptors of atherosclerosis: FSI and statistical study. International Journal for Numerical Methods in Biomedical Engineering, 34 (e2972): 1-17.

Seabra J, Pedro L, Fernandes J, Sanches J. (2011) Ultrasound plaque enhanced activity index for predicting neurological symptoms, in Pattern Recognition and Image Analysis (Lecture Notes in Computer Science.Berlin, Germany: Springer-Verlag,, 184–191.

Sousa LC, Castro CF, António CC, Santos A, Santos R, Castro P, Azevedo E, Tavares JMRS (2014) Hemodynamic conditions of patient-specific carotid bifurcation based on ultrasound imaging. Computer Methods in Biomechanics and Biomedical Engineering: Imaging & Visualization, 157-166.

PAPER REF: 110

MECHANICAL CHARACTERIZATION OF CELL-SEEDED ANISOTROPIC SCAFFOLDS WITH/WITHOUT MECHANICAL STIMULATION FOR TISSUE ENGINEERED CARTILAGE

Ângela Semitela[1], André F. Girão[1], Gonçalo Ramalho[1], Paula A. A. P. Marques [1], António Completo[1(*)]

[1]Department of Mechanical Engineering, University of Aveiro, Portugal

[(*)]*Email:* completo@ua.pt

ABSTRACT

The purpose of this work was to analyse experimentally the influence of mechanical stimulation on four cell seeded anisotropic scaffolds architectures, by measuring the compressive modulus, cell viability, and extracellular matrix production for each scaffold architecture before and after mechanical stimulation.

Keywords: tissue engineered cartilage, anisotropic scaffolds, dynamic compression.

INTRODUCTION

It has been established that since mechanical stimulation is an essential part of the native cartilaginous tissue environment, it is vital to the development of functional tissue engineered-cartilage. To this effect, bioreactors have been developed to apply mechanical stimulation to cell-seeded constructs. A specific bioreactor chamber that uses dynamic compression was developed and used in this study. The purpose of this experiment was to verify the influence of mechanical stimulation on the cell seeded fibrous anisotropic scaffolds by measuring the force response and stiffness of the constructs, cell viability and extracellular matrix production. The cell-seeded scaffolds were subjected to a dynamic unconfined compression regime: 2 h of sinusoidal compression (0.5 Hz, 0-10% strain) and 10 h with no load. This regime was repeated during 7 weeks (1200h).

RESULTS AND CONCLUSIONS

The force responses for the cell-seeded anisotropic scaffolds during 7 weeks of mechanical stimulation showed that fibrous scaffolds architectures were able to withstand dynamic compression for 600 hours (25 days) with no significant changes in force response (Fig 1). Afterwards there was a slight decrease on the force response that can be attributed to scaffold degradation, but these values remained steady for nearly more than 1200 hours. The compressive moduli of the cell-seeded fibrous anisotropic scaffolds after 7 weeks of mechanical stimulation has increased in most of the architectures. The highest compressive modulus increase occurred for the H1 and H2 scaffolds architectures (Fig 1). Only H4 architecture revealed a lower value that can possibly be attributed to the scaffolds degradation throughout the long stimulation period. The cell-viability of articular cartilage progenitor cells seeded on anisotropic scaffolds H1, H2, H3 and H4 before and after 7 weeks of mechanical stimulation demonstrated that the mechanical stimulation regime was beneficial with a cell viability increase greater than 100% relatively to the static culture.

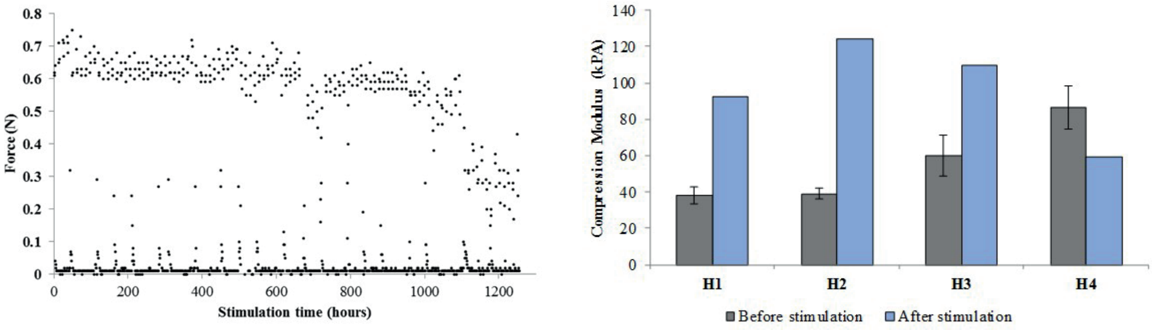

Fig. 1 – a) Force responses for the cell-seeded anisotropic scaffolds for 1255 hours (7 weeks) of mechanical stimulation; b) Compressive moduli of the anisotropic scaffolds H1, H2, H3 and H4

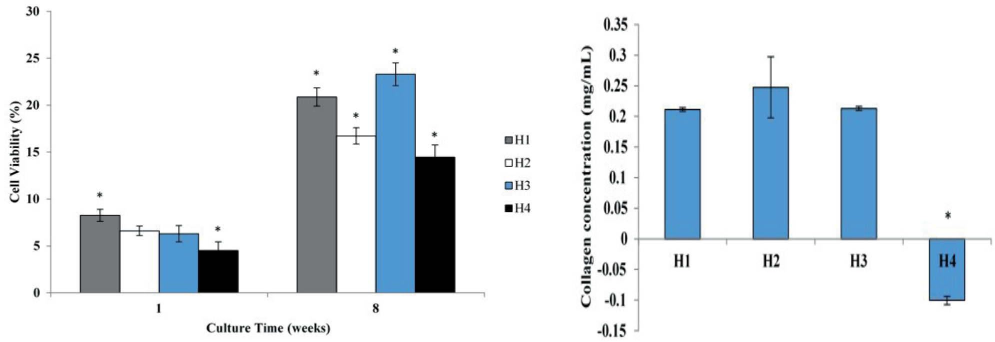

Fig. 2 – a) Cell viability of articular cartilage progenitor cells seeded on anisotropic scaffolds H1, H2, H3 and H4 after 7 weeks of mechanical stimulation; b) Collagen content measured by a Sirius red assay on cell-seeded anisotropic scaffolds H1, H2, H3 and H4 after 7 weeks of mechanical stimulation.

The collagen content has increased in the H1, H2 and H3 scaffolds architectures without statistical significance differences between them (Fig 2). The collagen concentration measured in H4 architecture was negative, possibly due to the degradation of the scaffold. There was evidence that H1, H2 and H3 anisotropic scaffolds architectures were able to withstand dynamic compression during nearly 1000 hours and the production of extracellular matrix components, as well as, the mechanical proprieties increased with the mechanical stimulation, suggesting that the mechanical stimulus regime applied is beneficial to the development of tissue-engineered cartilage.

ACKNOWLEDGMENTS

This work is supported by the project POCI-01-0145-FEDER-028424, funded by Programa Operacional Competitividade e Internacionalização (COMPETE 2020) on its component FEDER and by funding from FCT – Fundação para a Ciência e Tecnologia on its component OE. The authors thank to FCT for the PhD grant SFRH/BD/133129/2017.

REFERENCES

Girão, A., Semitela, A., Ramalho, G., Completo, A., Marques, P. Mimicking nature: Fabrication of 3D anisotropic electrospun polycaprolactone scaffolds for cartilage tissue engineering applications. Composites Part B: Engineering, 2018. 154, p. 99-107.

PAPER REF: 111

MICROSTRUCTURE CONTROL OF IRON SHEET SURFACE BY COMBINATION OF BURNISHING AND ANNEALING

Masahiko Yoshino[1(*)], Ryandanu Priwanta Wuryanjono[1], Yuki Nakagawa[1] and Motoki Terano[2]

[1] Tokyo Institute of Technology, Tokyo, Japan
[2] Okayama University of Science, Okayama, Japan
[(*)]*Email*: myoshino@mes.titech.ac.jp

ABSTRACT

In order to reduce environmental load, it is required to addopt various material properties on a mechanical parts made of material of simple chemical composition without adding alloy elements. In this paper, a new process was studied to improve mechanical properties of the surface layer of mechanical parts by modifying microstructure by combination of burnishing and annealing. Burnishing is usually used for surface finishing of machined surfaces of mechanical parts. At the same time, burnishing is effective to store the strain energy in the material, which induces static recrystallization occurs when it is adopted to annealing. Experiments were conducted to study effects of burnishing condtions and annealing condtions on the change of microstructure and hardness by recrystallization. Results showed possibility of arbitral control of the properties of surface of iron mechanical parts.

***Keywords*:** mechanical property, recrystallization, burnishing, annealing, iron.

INTRODUCTION

Mechanical parts are required to have various mechanical properties based on function of a machine, they are designed with a material having sufficient strength, toughness, hardness etc. so that it can satisfy the requirements. However, these mechanical parts are designed with margin in size in order to satisfy all the requirements, but it is not preferable for weight saving, miniaturization and resource saving. If mechanical properties of a mechanical part can be arbitrary modified in the manufacturing process, optimum design of mechanical parts that waste of resources are minimized can be realized. It is known that mechanical mechanical properties of steel products can be controlled by the TMCP (Thermo-Mechanical Control Process). This is based on the phenomenon that morphology of the crystal structure is changed by influence of the strain energy accumulated in the material and the heat treatment, whereby the material properties change. TMCP is applied to the production of high quality materials such as high strength steels and magnetic steel sheets. TMCP is able to control material properties without additional elements for alloying, and to produce various properties from the same material. Although, the TMCP have been developed for the production of primary materials such as steel sheets, the authors are studying a new TMCP for surface finishing of mechanical parts by combination of burnishing and annealing [1]. This paper reports effects of burnishing/annealing conditions on microstructure change and improvement of material properties of the surface of a mechanical part.

RESULTS AND CONCLUSIONS

A pure iron plate was used as the material. Since phase transformation does not occur up to 900 °C in pure iron, it is suitable as a model material to study microstructure change due to recrystallization. Burnishing test was conducted on the surface of the pure iron plate using the roller burnishing tool shown in figure 1, and thereafter heat treatment was applied to specimens cut out from the iron plate. The cross section of the specimen before and after the heat treatment was analyzed with an EBSD. In addition, the hardness was also measured, and change of mechanical properties were evaluated. Figure 2 shows the IPF maps of cross section of specimens annealed at 500 °C for 30 minutes after burnishing under various load. It is found from the figure that crystal grains under the burnished surface was refined by recrystallization. The depth of the affected layer increases with increase of the burnishing load. Figure 3 shows the influence of burnishing load on the average grain size of recrystallized grains generated by annealing. The average size of recrystallized grains decrease with increase of the burnishing load and burnishing time. These phenomena can be explained by the nucleation and grain growth mechanism that depends on the strain energy applied to the specimen by the burnishing process. Figure 4 shows the relationship between the reciprocal of the average recrystallized grain size and the hardness in each stage of the process. It is found that the specimen was hardened by burnishing and softened by heat treatment, and change of hardness can be explained by the Hall-Petch low. From these experimental results, it was shown that microstructure and mechanical properties of the pure iron product can be controlled by the burnishing and annealing conditions.

Figure 1 Roller burnishing tool

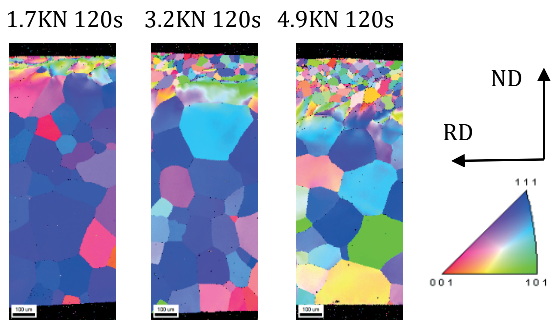

Figure 2 IPF [100] map of burnished specimen

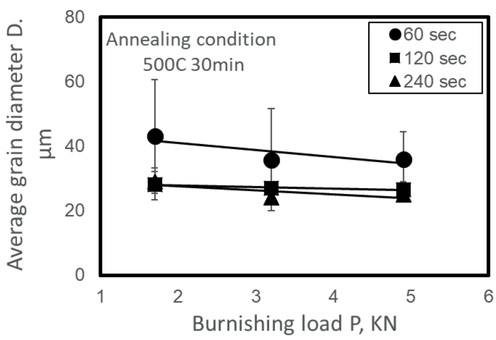

Figure 3 Effect of burnishing load on the average grain diameter

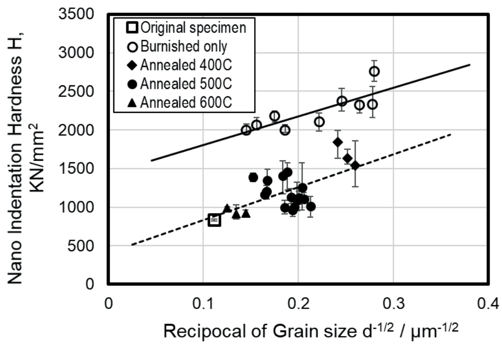

Figure 4 relationship between the reciprocal of the average recrystallized grain size and the hardness

ACKNOWLEDGMENTS

The authors gratefully acknowledge to research grant of AMADA foundation (AF-2016035).

REFERENCE

[1] Motoki Terano, Fan Zhang, Masahiko Yoshino: Influence of burnishing condition on static recrystallization of an iron sheet, Procedia Engineering, Volume 207,(2017), Pages 1850–1855

PAPER REF: 112

APPLICATION OF MASTER FLOW CURVES IN MODELLING POWDER INJECTION MOULDING

Petr Filip[1(*)], Berenika Hausnerova[2,3], Chiara Barretta[4]

[1]Institute of Hydrodynamics, Czech Academy of Sciences, Prague, Czech Republic
[2]Centre of Polymer Systems, University Institute, Tomas Bata University in Zlin, Zlin, Czech Republic
[3]Dept. of Production Engineering, Faculty of Technology, Tomas Bata University in Zlin, Zlin, Czech Republic
[4]Department of Chemical and Food Engineering, University of Salerno, Fisciano, Italy
[(*)]*Email:* filip@ih.cas.cz

ABSTRACT

Rheological modelling of compounds used in Powder Injection Moulding is complicated due to complexity of the primary materials (so called feedstocks). Even for a description of shear viscosity a number of adequate models are rather low due to high concentration of nano- or micro-particles in feedstocks. The problem gets more complicated as presence of surfactant is required for better packaging of powder particles. Hence, shear viscosity does not depend solely on powder content but subjects to surfactant participation as well. In the present contribution a master curve is proposed for a description of shear viscosity of a feedstock (no parameters are required to be determined) over sufficiently broad regions of both aluminium powder and stearic acid as a surfactant. The deviation from the measured values does not exceed an experimental error.

Keywords: Powder Injection Moulding, feedstock composition, viscosity, master curve.

INTRODUCTION

Powder Injection Moulding (PIM) is a very efficient method how to produce tiny items of very complex shapes with precision comparable with machining. PIM process consecutively passes through 4 basic steps starting with a preparation of evenly distributed feedstock (nano- or micro-particles, binder of organic substance with low melting point, additives (e.g. surfactant for better packaging -usually 50-55 %- of particles). Injection moulding represents the second step when the feedstocks are injected through microchannels to a complex shaped mould. Any defect initiated in this step cannot be corrected in the final steps (debinding and sintering). This emphasizes a necessity of a proper determination of shear viscosity of feedstocks as this quantity plays a crucial role in simulation of the whole PIM process.

For moderate or medium content of particles there has been proposed a series of empirical or phenomenological models (Kate, 2014). However, a situation gets much more complicated with an increasing concentration of solid particles in suspensions - the case corresponding to PIM technique. For higher packaging of particles a possibility to apply a responsible model is very limited. Moreover, with any change of powder or surfactant concentration there is a necessity to carry out new experiments and to optimize new values for the adjustable parameters appearing in the models. This rather awkward approach for viscosity prediction is possible to overcome by introducing the so called ‘master curve’ free of any adjustable parameters and continuously covering sufficient ranges of powder and surfactant concentrations.

RESULTS AND CONCLUSIONS

The used feedstocks are composed of two basic components:

- powder (MARTOXID® MR 70 produced by Martinswerk), dominant content of aluminium oxide (99.8 %), density attains 4.05 g/cm^3, particles diameter 0.1 to 3 μm;
- binder (3 components: low density poly(ethylene) Total LDPE 1200 MN 18 C (changing from 48 to 53 %), poly(ethylene) Escorene TM Ultra UL 40028CC (26 %), a paraffin wax produced by Dr. Kulich Pharma (21 %).

In addition, a plasticizer stearic acid Sigma-Aldrich contributing to better fluidity of the feedstocks, homogeneous distribution of aluminium microparticles in the binder and lower abrasion in the wall vicinity completed a feedstock up to 100 % (6 values 0 %, 1 %, ..., 5 % in such a way that the total with LDPE reaches 53 %). Summarizing, 36 combinations (volume fractions) of feedstocks were prepared differing in microparticle powder content (0, 10, 20, 30, 40, and 50 %) and content of stearic acid (0, 1, ..., 5 %).

Analysing the obtained experimental data it is possible to propose the following relation for approximation of expected values of shear viscosity

$$\log(\eta) = B1(SA\%, filling\%) + [B2(filling\%)] * [3 - \log(\dot{\gamma})],$$

where the additive member $B1$ depends only on the contents of stearic acid (SA%) and powder filling (filling%) (both in percentage) and the multiplicative member $B2$ is dependent only on powder filling (filling%). No parameters appear in $B1$ and $B2$:

$B1$ = log[(-0.7-1.61*exp(0.067*filling%))*(SA%)+30+12.5*exp(0.072*filling%)] ,

$B2$ = (log(1.11+0.002*filling%))/0.16.

These relations cover the entire range of powder filling (0 – 50) %, stearic acid content (0 – 5) %, and a range of the rate of shear deformation (100 – 1000 s^{-1}) with a mean deviation in 252 (6x6x7) measured points attaining 5.9 %, which does not exceed the maximum experimental error for shear measurements.

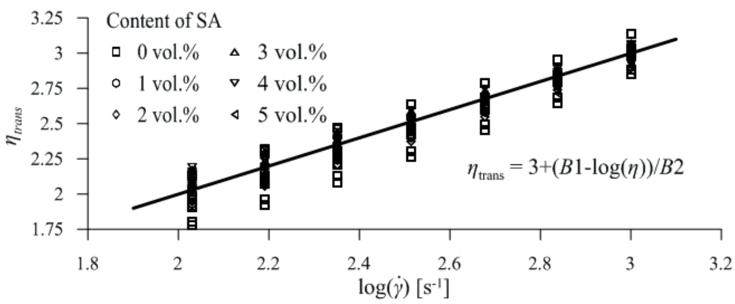

A course of the master curve including its comparison with the measured data is presented in Figure with transformed shear viscosity.

ACKNOWLEDGMENTS

The author (P. F.) wishes to acknowledge the Grant Agency CR for the financial support of Grant Project No. 17–26808S. The author (B.H.) appreciates the support by the Ministry of Education, Youth, and Sports of the Czech Republic - Program NPU I (LO1504).

REFERENCE

Kate KH, Enneti RK, Park SJ, German RM, Atre SV. Predicting powder-polymer mixture properties for PIM design. Crit. Rev. Solid State, 2014, 39, pp. 197–214.

PAPER REF: 113

INVESTIGATION OF THE STRAIN RATE HARDENING BEHAVIOUR OF GLASS FIBRE REINFORCED EPOXY UNDER BLAST LOADING

M.A. Louar[1(*)], B. Belkacem[2], H. Ousji[2,3], L. Pyl[3], J. Vantomme[2]

[1]Laboratoire de Dynamique des Systèmes Mécaniques, Ecole Militaire Polytechnique, Algiers, Algeria
[2]Department of civil and Material Engineering (COBO), Royal Military Academy, Brussels, Belgium
[3]Department of Mechanical Engineering and Materials (MEMC), Vrije Universitait Brussel, Brussels, Belgium
[(*)]*Email:* mohamedabderaouf.louar@emp.mdn.dz

ABSTRACT

This work investigates the use of blast loadings and inverse modelling for the identification of the strain rate hardening model parameters of fibre reinforced polymers. An experimental setup allowing the generation of known and predictable blast waves, leading to repeatable dynamic response in composite plates and the measurement of the displacement and strain fields, is developed. The dynamic response of the plates is measured by means of high-speed cameras and a 3D digital image correlation technique. A suitable numerical model that is able to reproduce the experimental conditions and predict the blast response of the plates is developed. Finally, the experimental measurements and the numerical calculation are combined through an inverse method in order to identify the strain rate hardening model parameters of the tensile and shear strengths of glass fibre reinforced epoxy.

Keywords: composite materials, inverse modeling, blast, high strain rate.

INTRODUCTION

The assessment of the dynamic response resulting from a blast wave impacting a structure is a complex task due to the intensity of the loading its transient nature, the high deformation rate and the intricate structure / blast wave interactions. Adequate material models and parameters are essential to a good prediction of the response of structures to dynamic loadings. Due to the limitations of the conventional experimental methods, obtaining high strain rate material parameters is arduous especially in the case of composite materials [1].

In this paper, an original method to estimate the strain rate hardening model parameters for in-plane tensile and shear strengths of laminated composites is developed. This method combines strain field measurements from 3D-DIC, FE calculations with the explicit solver of LS-DYNA and inverse modeling [2] to obtain these parameters. In order to reach high-strain rates, blast waves from an Explosive Driven Shock Tube are used to load glass fibre reinforced epoxy plates. The developed inverse method aims to minimize the difference between measured experimental data and calculated data by updating the strain rate hardening material model parameters using a Levenberg-Marquardt optimization algorithm. The obtained results are compared with data from literature and the agreement between them is encouraging.

RESULTS AND CONCLUSIONS

The strain rate is considered to have a scaling effect on the in-plane tensile and shear strengths of the laminated composite material (Equation 1). The optimisation aims to identify the two parameters C_t and C_s for the tensile and shear strengths respectively. The material used in the tests presented in this paper is glass fibre reinforced epoxy (GFRE). They are made of the glass-epoxy twill weave prepreg-HexPly® M10r with a fibre volume fraction of $v_f = 36{:}5\%$. They are produced using out-of-autoclave processing. The obtained results for the configurations listed in Table 1 are presented on Figure 1.

$$X_d = X_0\left(1 + C_x \log \frac{\dot{\varepsilon}}{\dot{\varepsilon}_0}\right) \quad (1)$$

where X_d is the dynamic material property at the strain rate $\dot{\varepsilon}$, X_0 is the quasi-static value of the material property obtained at a strain rate $\dot{\varepsilon}_0$ and C_x is the strain rate hardening model parameter to be identified.

Table 1- The experimental conditions for the GFRE blast tests

Set	Lay up	Dimensions [mm3]
1	$[0°]_2$	300x300x0.41
2	$[0°]_4$	300x300x0.82
3	$[0°,45°]_s$	300x300x0.82

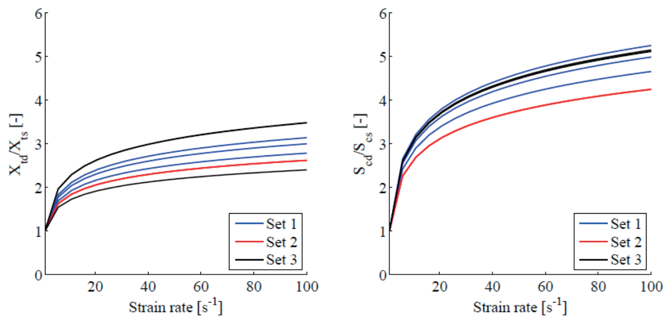

Fig. 1 - Tensile (left) and shear (right) strengths strain rate hardening curves for the three test series

As expected, the strain rate sensitivity of the shear strength is higher than the strain rate sensitivity of the tensile strength. However, even though the identified values are in the same order of magnitude than the values available in literature, the increase in the tensile and shear strengths seems exaggerated. In [3], the strain rate sensitivity of UD GFRE is discussed and the given values of the strain rate hardening model parameter for the longitudinal and the transverse tensile strength are 1.77 and 0.2 respectively. It has to be noted that these values are obtained for UD GFRE and it is known that woven fabrics have a higher strain rate sensitivity than UDs. Further investigation could improve the identification results.

REFERENCES

[1] B.C. Ray, D. Rathore, 2015, A Review on Mechanical Behavior of FRP Composites at Different Loading Speeds, Critical Reviews in Solid State and Materials Sciences 40:119-135.

[2] Spranghers, K., Vasilakos, I., Lecompte, D., Sol, H. and Vantomme, J., 2014, Identification of the plastic behaviour of aluminium plates under free air explosions using inverse methods and full- eld measurements, International Journal of Solid and Structures 51, 210-226.

[3] X. Wei, A. de Vaucorbeil, P. Tran, H.D. Espinosa, 2013, A new rate-dependent unidirectional composite model – Application to panels subjected to underwater blast, Journal of the Mechanics and Physics of Solids 61: 1305-1318.

PAPER REF: 114

INTEGRATION OF FAILURE CRITERIA FOR ANISOTROPIC MATERIALS INTO A NURBS-BASED-SIMP TOPOLOGY OPTIMIZATION ALGORITHM

Thibaut Roiné (*), Marco Montemurro(*), Giulio Costa, Jérôme Pailhès

Arts et Métiers ParisTech, I2M CNRS UMR 5295, F-33400, Talence, France

(*)*Email:* Thibaut.roine@ensam.eu, marco.montemurro@ensam.eu

ABSTRACT

The formulation of failure criteria in the framework of a particular SIMP topology optimization (TO) algorithm exploiting the features of Non-Uniform Rational B-Splines (NURBS) hypersurfaces is proposed in this work. Tsai-Wu (TW), Tsai-Hill (TH) and Hoffman (Ho) phenomenological criteria that allow identifying the failure for anisotropic materials as well as the well-known Huber-Henky-Von Mises (HHVM) for isotropic media are reformulated in the NURBS hypersurfaces framework and implemented into the problem formulation. The local behavior and the singularity of stresses can be easily handled thanks to the NURBS-based-SIMP method properties and a p-norm aggregation function. The effectiveness of the approach is proven on meaningful 2D and 3D benchmarks taken from the literature.

Keywords: NURBS hypersurfaces, Topology Optimization, Anisotropy, Failure criteria.

INTRODUCTION

With the recent development of additive layer manufacturing (ALM) techninology, 3D printing of composite materials becomes feasible. This implies the necessity of developing dedicated numerical tools and methodologies to design complex-geometry parts obtained through ALM process. During the last twenty years, several TO methods have been developed: along them the most used algorithm is the well-known Solid Isotropic Material with Penalization (SIMP) algorithm (Bendsoe and Sigmund, 2003). The main issue when dealing with the integration of failure criteria for anisotropic materials into the TO problem is the proper handling of the local information related to the stress field of each element. In particular two points must be faced: (a) what kind of penalization scheme should be considered for general anisotropic materials? (b) how should the failure criterion be integrated into the problem formulation? Although stress-based TO is a well-known problem, significant amount of studies (Bendsoe and Sigmund, 2003) focuses only on the HHVM criterion. However, the HHVM criterion is limited to isotropic materials and cannot be used for anisotropic ones. Indeed, to the best of the author's knowledge, only few works dealing with the integration of failure criteria for anisotropic materials into the TO problem can be found in literature (Mirzendehdel, 2018). Nevertheless, even when such a criteria are integrated into the SIMP method, the main issue is the significant discrepancy between the optimized results provided by the classical SIMP algorithm and the actual stress field evaluated on the reassembled geometry. This work takes advantages of the peculiar features of the NURBS-based-SIMP method developed at the I2M laboratory (Costa, 2018; Costa,2019) to formalise and integrate into the optimization process pertinent failure criteria for anisotropic media. Each criterion is reformulated in the context of NURBS hypersurfaces formalism and integrated as a constraint function into the problem formulation. The proposed approach fully exploits the advantages of the NURBS-based-SIMP approach: (i) the topology description relies on a purely geometric entity and it is unrelated to the mesh of the finite element model; (ii) the NURBS hypersurface local support acts as an implicitly defined filter zone; (iii) CAD-compatible solutions can be retrieved at the end of optimization process.

RESULTS AND CONCLUSIONS

The L-bracket benchmark is described in Fig. 1-(a) for a compliance minimization problem where the final volume must be lower or equal to a given fraction of the reference one and the function that denotes the generic failure criterion must be lower than 1.

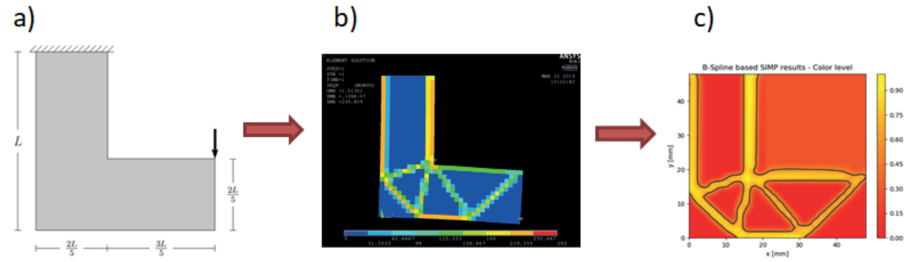

Material: Carbon/Epoxy Load: 450N Mesh: 48x48	Control Points: 27x27 NURBS Degrees: 2 Maximum stress: 240MPa

Fig. 1 – (a) The proposed benchmark: a L-bracket beam with a load distributed on 3 nodes. (b) Von Mises stress repartition. (c) The optimized cantilever beam topology and shape.

This study aims to integrate the failure criterion constraint into NURBS-based-SIMP topology optimization method. An example of optimised topology is given in Fig. 1. Further benchmarks and details of the method will be presented during the speech

ACKNOWLEDGMENTS

Thibaut Roiné is grateful to the region Nouvelle Aquitaine for supporting this research through the OCEAN-ALM project. Giulio COSTA is grateful to the support of the project COFFA ANR-17-CE10-0008 from the French National Research Agency (ANR).

REFERENCES

M. Bendsoe, O. Sigmund, J. Pailhes, Topology Optimization – Theory, Methods and applications. Springer, 2003.

G. Costa, M. Montemurro, J. Pailhes, A 2D topology optimization algorithm in nurbs framework with geometric constraints, *International Journal of Mechanics and Materials in Design,* 2018.

G. Costa, M. Montemurro, J. Pailhès. NURBS Hypersurfaces for 3D Topology Optimisation Problems. Mechanics of Advanced Materials and Structures, URL : https://doi.org/10.1080/15376494.2019.1582826, 2019 (in press).

A.M. Mirzendehdel, B. Rankouhi, K. Suresh, Strength-based topology optimization for anisotropic parts, Additive *Manufacturing,* 2018.

PAPER REF: 115

INTEGRATION OF STRUCTURAL DISPLACEMENT IN A NURBS-BASED SIMP TOPOLOGY OPTIMIZATION METHOD

Thibaut Rodriguez[12(*)], **Marco Montemurro**[1(*)], **Paul Le Texier**[2], **Jérôme Pailhès**[1]

[1] Arts et Métiers ParisTech, I2M CNRS UMR 5295, F-33400, Talence, France.

[2] CEA/CESTA (French Atomic Energy Commission), Route des Gargails, 33114 Le Barp, France.

[(*)] *Email:* thibaut.rodriguez@ensam.eu, marco.montemurro@ensam.eu

ABSTRACT

This work focuses on the formalisation of a general displacement function in the framework of a special topology optimisation (TO) algorithm. The formalism makes use of a Non-Uniform Rational Basis Splines (NURBS) hyper-surface to represent the pseudo-density field describing the part topology in the framework of the well-known Solid Isotropic Material with Penalisation (SIMP) approach. A general formulation of the structural displacement function (at any point of the structure) exploiting the advantages of NURBS hypersurfaces is proposed and its effectiveness is proven through 2D and 3D benchmarks.

Keywords: NURBS hyper-surface, SIMP, Topology Optimization, Structural displacement.

INTRODUCTION

As an emergent design method, TO presents multiple declinations. Among them, one of the most common TO approaches is the SIMP method which has been widely studied and used in the last three decades (Bendsoe and Sigmund, 2003). Several research works make use of the SIMP method to deal with various optimisation problems: compliance minimisation, mass minimisation, requirements on buckling loads and natural frequencies, etc… The SIMP method aims at computing a fictitious density for each element of a predefined mesh of the domain. Regardless of the problem nature, one of the main limitations of the classical SIMP approach is that the optimised topology is strongly mesh-dependent. Moreover, when the problem formulation includes several design requirements (especially those involving local responses like failure criteria, local displacement, damage phenomena, etc…) the optimisation constraints on the reassembled geometry (i.e. that obtained after a threshold operation on the pseudo-density field) are not met. Unlike the classical SIMP formulation, the NURBS-based SIMP method developed at the I2M laboratory (Costa et al. 2018, Costa et al. 2019) separates the pseudo-density field from the FE model mesh. More precisely for general 3D TO problems, a 4D NURBS hyper-surface is used to represent the pseudo-density field. In this way, the topology descriptor relies on a purely geometric entity which is fully CAD-compatible. In this background, the optimisation variables are the density at the control points and the associated weights, more details could be found in (Costa et al. 2019). In this study, the structural displacement requirement has been formulated in the framework of the NURBS-based SIMP approach. In particular, this requirement is often integrated into the problem formulation as an optimisation constraint and can be smartly exploited to study compliant mechanisms (Bendsoe and Sigmund, 2003). In the NURBS-based SIMP approach, the structural displacement function can be set as an objective or as a constraint function thanks to a flexible implementation. The formulation of such a requirement in the framework of NURBS based SIMP method takes full advantages of the properties of such geometric entities (in particular of the *local support property* of the NURBS blending functions).

RESULTS AND CONCLUSIONS

The effectiveness of the proposed method is proven on both 2D and 3D benchmarks. For the sake of brevity, only a 2D benchmark is illustrated in Fig. 1-(a). Fig. 1-(c) gives an example of optimised topology which is the solution of the following problem:

$$\min_{x} c(\mathbf{x})$$

$$\text{Subject to:}$$

$$\begin{cases} \dfrac{V(\mathbf{x})}{V_{ref}} = \Delta_V, \\ \dfrac{d_{A_y}^{\text{ref}} - d_{A_y}(\mathbf{x})}{d_{A_y}^{\text{ref}}} \geq 0 \end{cases} \tag{1}$$

where is the vector of design variables, is the compliance of the structure, is the volume, and the structural displacement of the point A along the *y*-axis. and are the reference values for the volume and the displacement, respectively.

(a)

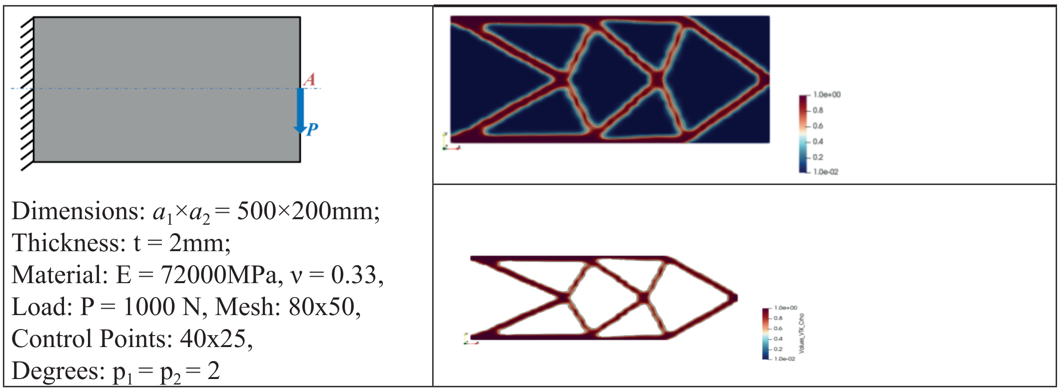

(b)

(c)

Fig. 1 – (a) 2D benchmark: a cantilever beam with a concentrated load. (b) The resulting NURBS surface representing the pseudo-density field. (c) The optimized reassembled geometry.

This study aims at showing the versatility and the true potential behind the NURBS-based SIMP method. Further benchmarks and details of the NURBS-based SIMP method will be presented during the speech to prove its effectiveness as well as the benefits of using a CAD-compatible geometric entity as a descriptor of the topology.

ACKNOWLEDGMENTS

The first author is grateful to region Nouvelle Aquitaine for supporting this research work through the OCEAN-ALM project.

REFERENCES

Bendsoe MP, Sigmund O, Topology optimization, theory, methods and applications, Springer Verlag Berlin Heidelberg, 2003.

Piegl L, Tiller W, The NURBS Book, Springer-Verlag, New York, 1997.

G. Costa, M. Montemurro, J. Pailhès. A 2D topology optimisation algorithm in NURBS framework with geometric constraints. *International Journal of Mechanics and Materials in Design*, v. 14 (4), pp. 669-696, 2018.

G. Costa, M. Montemurro, J. Pailhès. NURBS Hypersurfaces for 3D Topology Optimisation Problems. *Mechanics of Advanced Materials and Structures*, URL : https://doi.org/10.1080/15376494.2019.1582826, 2019 (in press).

PAPER REF: 116

METHODOLOGICAL APPROACH OF MAINTENANCE MANAGEMENT APPLIED TO A RESEARCH LABORATORY

Teresa Morgado[1,2,3,4(*)], Gilberto Santos[2]

[1]IPT – Polytechnic Institute of Tomar, Tomar, Portugal
[2]UNIDEMI - Research and Development Unit for Mechanical and Industrial Engineering, FCT NOVA - Faculty of Science and Technology, Universidade Nova de Lisboa, Lisboa, Portugal
[4]LNEC – Laboratório Nacional de Engenharia Civil, Lisboa, Portugal
[3]IPAC – Polytechnic Institute of Cávado e Ave, Braga, Portugal
[(*)]*Email:* tmorgado@ipt.pt

ABSTRACT

A research laboratory is a place of expensive calibrated equipment, standard operating procedures, hazard analysis, and quality management. Other than personnel-related costs, maintenance is generally the most expensive item in the laboratory operation budget. The pressures in the scientific communities will continue to motive research organizations to pursue research in the most efficient and cost effective manner possible. This work presents a methodological approach of maintenance management to apply to research laboratories. With this approach full service technics with core competencies in asset management, managed maintenance, validation and compliance services and disposition services are able to bundle service options to deliver higher quality at guaranteed lower costs while allowing the laboratory manager to focus on laboratory operations and business issues.

Keywords: maintenance management, research laboratories, quality, maintenance costs.

INTRODUCTION

A research laboratory is a place of expensive calibrated equipment, standard operating procedures, hazard analysis, and quality management (Kelly, 2006). Other than personnel-related costs, maintenance is generally the most expensive item in the laboratory operation budget. While the size of this of this expenditure makes it an attractive target for reduction, all laboratory managers recognize the limitations they face in achieving any real savings. Foregoing maintenance and repairs is usually not an option, they are a necessary cost of continued operation. Thus, cost reduction initiatives must extract operational and management efficiencies from the maintenance system without directly impact instrument reliability. Given the progress that has been made in controlling the cost of laboratory expendables and the effectiveness of the budget constraints in limiting discretionary expenditures improvements in maintenance management remain one of the few fertile areas to realize additional cost reductions through operational efficiencies.

There are three classic equipment management approaches (Oakland, 2014) that can be followed: Run-to-Fail (RTF), Preventive Maintenance Only (PM Only) and Full-Service Contract (FSC). All are valid, but it can achieve significant cost savings when it look at whether a given piece of equipment has been assigned the contract appropriate for its cost, criticality to the research at hand, age and nature of use.

Run-to-Fail is generally the most efficient approach for equipment and instruments for which replacement may be more cost-efficient than repair. Technically this approach does not require any maintenance contract at all, but it should be a conscious and structured choice nonetheless. To determine which pieces fall in this category, must be setting a replacement cost ceiling. If the replacement cost for a particular piece of equipment is below the ceiling cost, the RTF approach must be use because it will be more cost efficient to replace the item than to repair it. Other equipment that may be a good fit for RTF include those items that are well past their full depreciation point (age), frequently break down, or are infrequently use, unless they serve a critical function when needed.

Preventive maintenance on an item is almost always recommended by the original equipment manufacturer. This type of contract cover preventive maintenance does not cover labor or repairs when the equipment fails. PM only is generally well-suited for items with moving parts, liquid or gas flow, filters, or optical systems, yet not critical to day-today operations. Since researchers will invariably define everything as critical, the maintenance management must determine whether a piece of equipment is truly critical by looking at availability of an alternate piece of equipment, ability to generate data in another way, utilization and the cost of parts.

A Full-Service Contract typically covers preventive maintenance as well as all demand repairs, including parts and labor. Sometimes chosen as an “insurance policy” it can be a viable option both for high critical equipment and for less critical equipment that has one or two very expensive parts that, if they fails, would be burdensome to replace.

The pressures in the scientific communities will continue to motive research organizations to pursue research in the most efficient and cost effective manner possible. One way that this can be accomplished is to decrease the cost of R&D operations, including the maintenance of laboratory equipment and instruments. Properly categorizing the laboratory equipment support category as RTF, PM Only or Full Service can greatly reduce an organization’s operating costs.

CONCLUSIONS

Maintenance, a fundamental element of laboratory operation, is expensive and requires tedious administration to function effectively. This make it a prime candidate for outsourcing to one of the maintenance technical services. With the correct methodology applied to each laboratory, full service technics with core competencies in asset management, managed maintenance, validation and compliance services and disposition services are able to bundle service options to deliver higher quality at guaranteed lower costs while allowing the laboratory manager to focus on laboratory operations and business issues. In addition, a complete suite of metrics and reports provide feedback and assurance that the system is functioning properly.

REFERENCES

Oakland, J.. Total Quality Management and Operational Excellence: Text with Cases. United Kingdom, 2014.

Kelly A. Maintenance Management Auditing: In Search of Maintenance Management Excellence, Industrial Press Inc., 2006.

PAPER REF: 117

FREE VIBRATION ANALYSIS OF A RANDOM ORIENTED POROUS ALUMINUM BEAM

Oguz Kocar[1,2], H. Alper Ozyigit[1,2], Mehmet Yetmez[2(*)], Abdurrahim Temiz[3], Osman Ozdamar[4]

[1]Department of Mechatronics Engineering, Bulent Ecevit University, 67100 Zonguldak, Turkey
[2]Department of Mechanical Engineering, Bulent Ecevit University, 67100 Zonguldak, Turkey
[3]Department of Industrial Design Engineering, Karabuk University, 78050 Karabuk, Turkey
[4]Osmaneli Vocational School, Bilecik Seyh Edebali University, 11230 Bilecik, Turkey
[(*)]*Email:* yetmez@beun.edu.tr

ABSTRACT

In this study, Al 7075 alloy is considered to obtain (i) nonporous beam, (ii) uniformly oriented beam and (iii) random oriented beam. Dynamic characteristics of the three material models are obtained experimentally. Results show that differences of fundamental natural frequency and damping ratio among them are significant.

Keywords: porous metal, random orientation, free vibration, energy absorption, damping ratio.

INTRODUCTION

Due to its high strength, high natural frequency and high damping coefficient, porous metal materials are preferred for core layer of composites. Recently, pore orientation has been becoming a main role to improve mechanical properties of the porous metal materials, especially aluminum materials (Sritawat, 2017). Many procedures are used to analysis of such structures with respect to design procedures (Tang, 2018). It is clearly seen that because of the orientation effect, vibration characteristics are of great importance to determine design parameters easily. Displacement response function and damping ratio are actually two main important parameters of the porous metal beam to understand characteristic displacement field in frequency domain.

In this study, Al 7075 alloy is considered to obtain (i) nonporous beam, (ii) uniformly oriented bean and (iii) random oriented beam (see Figure 1). Then, dynamic characteristics of the three material models are obtained experimentally. Vibration measurements are conducted such a way that an impulse hammer with a force transducer (Model No: 5800B2, Dytran Instruments, Inc., USA) is used to excite each of the composite beams through the selected point. Then, the responses are obtained by an accelerometer (Model No: 3093B, Dytran Instruments, Inc., USA). The vibration measurements are completed using a microprocessor-based data acquisition system, namely SoMat™ eDAQ-lite and nCode GlyphWorks software (HBM, Inc., USA).

RESULTS AND CONCLUSIONS

The results from the modal testing are shown in Table 1. Differences of fundamental natural frequency and damping ratio among them are significant.

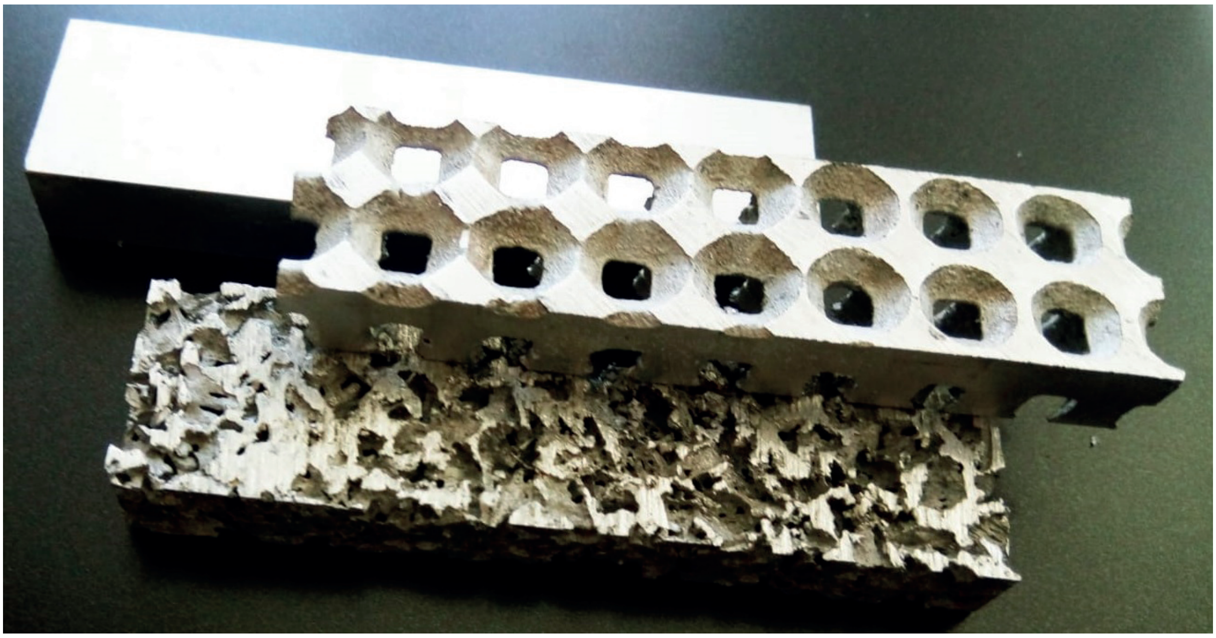

Figure 1 – Representation of 7075 aluminum beams with nonporous (lower top side), random oriented porous (lower bottom side) and uniformly oriented porous respectively

Table 1 – Modal testing analysis results of 7075 aluminum beams

Group	Fundamental frequency (Hz)	Damping ratio (Hz/Hz)
Nonporous	37.2	0.37
Uniformly oriented	17.1	0.56
Random oriented	29.4	0.41

REFERENCES

Sritawat K, Da C, Jie Y. Free vibration and elastic buckling of functionally graded porous beams reinforced by graphene platelets. Materials and Design, 2017, 116, p.656-665.

Tang H, Yang DH, Wang L, Liu Y, Wang J, Chen J. The ordered porous aluminium: modelling, preparation and properties with designed structures. Materials Science Forum, 2018, 933, p.148-155.

PAPER REF: 118

IMPROVEMENT OF MECHANICAL PROPERTIES OF TITANIUM ALLOY BY HIGH-DENSITY PULSED ELECTRIC CURRENT

Rui Iwase[1], Yuhki Toku[2], Yang Ju[2(*)]

[1]Graduate School of Engineering, Nagoya University, Nagoya, Japan
[2]Faculty of Engineering, Nagoya University, Nagoya, Japan
[(*)]*Corresponding email:* ju@mech.nagoya-u.ac.jp

ABSTRACT

This study focuses on the mechanical properties affected by applying high-density pulsed electric current (HPEC) in titanium alloy Ti-6Al-4V. It was confirmed that the hardness was decreased when we applied HPEC. Moreover in order to evaluate the effect of electrical stimulation. XRD analysis was employed to interpret the microstructure of the material with and without the application of HPEC. The rate of β phase in the material was increased by applying HPEC. As a result, we confirmed that the mechanical properties of titanium alloy were improved by applying HPEC due to the occurrence of phase transformation.

Keywords: Ti-6Al-4V, pulsed electric current, mechanical properties, elongation.

INTRODUCTION

As versatile material, titanium alloy has been used in many places such as aircraft parts, rocket parts and implants, etc. Currently, manufacturing such as hot working and heat treatment have been carried out in order to improve processibility of titanium alloy because cold working is difficult. However, those processes require high temperature and longtime steps, resulting in an increase in manufacture cost, which is an obstacle to use practically titanium alloy. In recent years, HPEC has been studied as a state of art method to repair defects of metallic materials, and to enhance the processibility (Hosoi, 2013, Conrad, 2000). This method has the merits that the processing steps are simpler and process time is shorter than the conventional method. It has been reported that this technique can improve the fatigue life of metal materials and repair fatigue cracks (Lin, 2008). In this work, the effect of HPEC on the mechanical properties of titanium alloy Ti-6Al-4V was investigated.

RESULTS AND CONCLUSIONS

As shown in Fig. 1, the average of hardness was decreased approximately 10.1% by applying HPEC with current density of 540A/mm^2. Fig. 2 shows the results of XRD analysis of the samples with and without applying HPEC. According to the analysis, the rate of α phase was decreased, by contrast, that of β phase was increased.

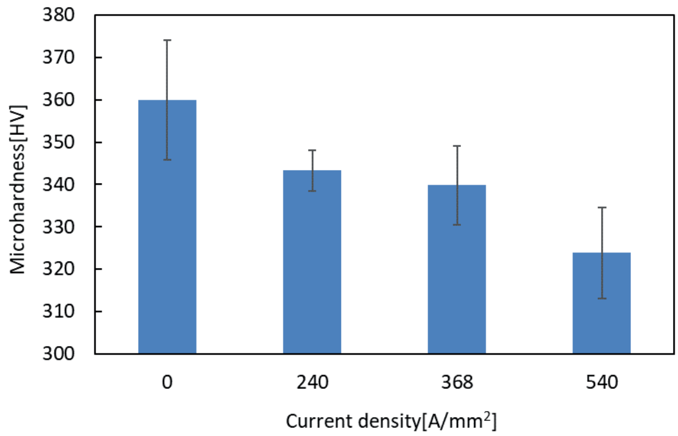

Fig. 1 The results of hardness test with and without applying HPEC.

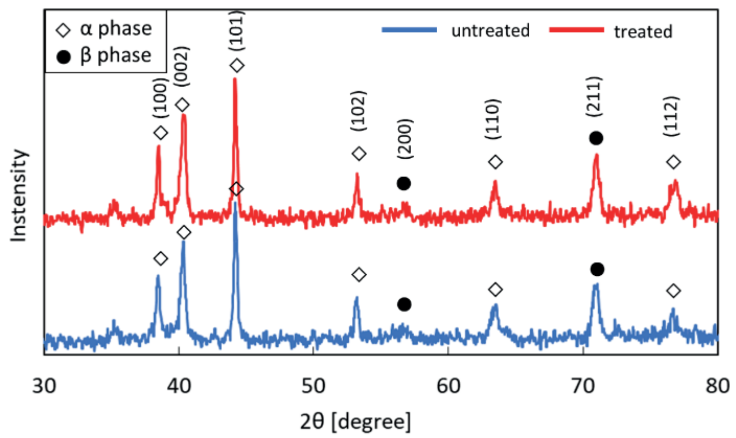

Fig. 2 The results of XRD analysis with and without applying HPEC.

Based on the above results, we confirmed that the mechanical properties were improved due to the occurrence of phase transformation by HPEC.

ACKNOWLEDGMENTS

This work was supported by the Japan Society for the Promotion of Science with Grants-in-Aid for Scientific Research (S) 17H06146.

REFERENCES

Hosoi A, Kishi T, Ju Y. Healing of fatigue crack by high-density electropulsing in austenitic titanium alloy treated with the surface-activated pre-coating. Materials, 2013, 6, p. 4213-4225.

Conrad H. Electroplasticity in metal and ceramics. Materials Science and Engineering A, 2000, 287, p. 276-287.

Lin H Q, Zhao Y G, Gao Z M, Han L G. Effects of pulse current stimulation on the thermal fatigue crack propagation behavior of CHWD steel. Material Science and Engineering A, 2008, 478, p. 93-100.

PAPER REF: 119

QCW LASER WELDING OF THIN ALUMINIUM AND COPPER SHEETS

Alessandro Fortunato[1*], Vincenzo Dimatteo[1], Flavia Lerra[1], Alessandro Ascari[1]

[1]Department of Industrial Engineering, University of Bologna, Italy

[(*)]*Email:* alessandro.fortunato@unibo.it

ABSTRACT

Laser welding of aluminium and copper thin sheets in lap-joint configuration by using a pulsed QCW Yb:Fiber laser was reported. The aim of this work is to understand how the laser parameters, such as peak power, pulse energy, pulse duration and feed rate affect the weld seam in order to identify a feasibility window. After a first microscope observation, different welding conditions were obtained: no-welding, partial penetration and full penetration. Parameters that allowed obtaining partial penetration were chosen to produce samples that have been mechanically characterized by micro hardness and tensile tests.

Keywords: Pulsed laser welding, aluminium, copper.

INTRODUCTION

In recent years, due to the limits on CO_2 emissions, the demand of electric vehicles (EVs) and hybrid-electric vehicles (HEVs) has increased. A battery pack for electric cars consists of hundreds of cells (Lithium-Ion cells), whose electrodes are made of aluminium (cathode) and copper (anode), connected together in series or in parallel. Therefore, a good weld bead is mandatory to achieve good performances. Fusion welding of aluminium and copper is difficult to obtain due to the significant differences in the chemical composition and physical properties of the base materials [1]. The goal is to have a reduced production time and high energy density focused in a small area as well as to have temperature gradients far away from the equilibrium and so to avoid intermetallic compounds formation. Many scientific studies focus on the use of laser sources in CW-mode, with spatial beam oscillation [2-3]; accordingly, no studies were found concerning the use of pulsed QCW sources in the welding of dissimilar thin sheet metals.

Samples were produced by using an IPG YLR-300-3000 QCW fiber laser with a near-infrared wavelength of 1070 nm in combinations with focusing lens placed at a focal distance of 90 mm with a spot diameter of 75 µm. The investigated materials are aluminium alloy EN-AW 1050 (99.5 %) in form of 0.45 mm thick sheet and pure copper C1020-HO (99.9% Cu) in form of 0.3 mm thick sheet with a thin layer of nickel (2.5 µm) electroplated. The sizes of the samples are 45 mm wide and 70 mm long, welded in overlap configuration with an overlap of 10 mm. A clamping system was designed in order to guarantee a correct adhesion at the interfaced between the sheets. No shielding gas was used. The parameters used are: pulse distance (0.1 mm), pulse energy (0.27÷0.7 J), peak power (550÷1800 W) and feed rate (40÷100 mm/s). After welding, the cross sections were prepared by hot resin mounting of the samples, grinded by sandpapers (different grits), polished with 1 and 0.5 µm alumina suspension and, finally, analyzed by optical microscope. The tensile strength tests of the welds were performed at room temperature in the testing machine INSTRON model 8033 at a crosshead speed of 0.025 mm/s. Vickers micro-hardness tests have been carried out with load time 20 s and the load of 100g, on the cross section in the longitudinal direction.

RESULTS AND CONCLUSIONS

Microscopic observation allowed identifying a process window reported in figure 1. No-welding condition was obtained with the highest feed rate and lowest pulse energy; increasing the pulse energy and reducing feed rate full penetration occurred. It is important to note how the parameters taken into account are closely related each other; during the trials, the average power of the source, in this case 300 W, has always been saturated.

Within the area where partial penetration was recorded, samples were chosen for mechanical characterization. When partial penetration occurred, mixing and presence of defects were reduced.

The maximum recorded tensile loads exceeded 100 kgf, with an interface width of 0.200 mm. Micro hardness tests showed an increase in hardness near the fused zone, reached values of 300÷400 HV.

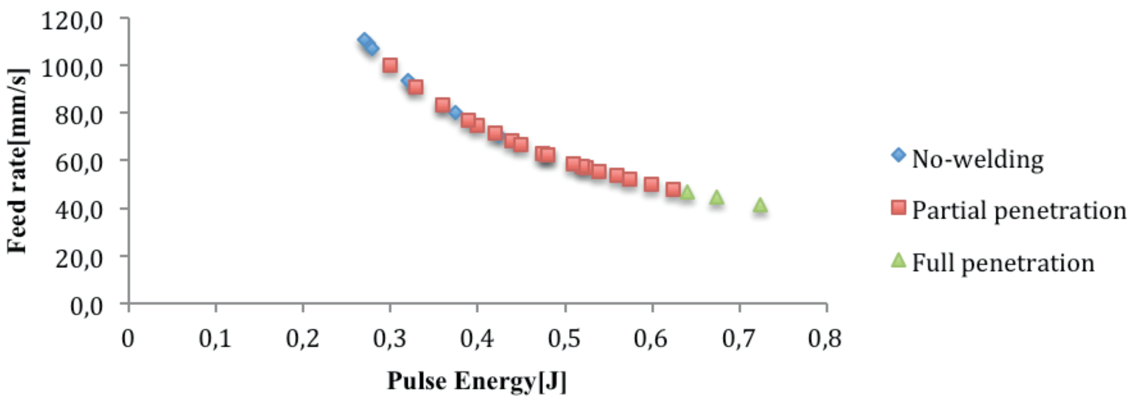

Fig. 1 – Process window

This study showed that a good weld seam can be obtained using pulse energy of 0.4÷0.7J, feed rate of 50÷75 mm/s and peak power of 1200÷1700 W. Further SEM analysis should be performed in order to characterize the intermetallic compounds formed as a result of the process.

REFERENCES

[1] Kah, Paul & Vimalraj, Cyril & Martikainen, Jukka & Suoranta, Raimo. (2015). Factors Influencing Al-Cu Weld Properties by Intermetallic Compound Formation. International Journal of Mechanical and Materials Engineering. 10. 10.1186/s40712-015-0037-8.

[2] Smith, S.; Blackburn, J; Gittos, M.; Bono, P.D.; Hilton, P. Welding of dissimilar metallic materials using a scanned laser beam. In proceedings of the 32nd International Congress on Applications of Lasers & Electro-Optics (ICALEO), Miami, FL, USA, 6-10 October 2013; pp. 6-10.

[3] Kraetzch, M; Standfuss, J.; Klotzbach, A.; Kaspar, J.; Brenner, B.; Beyer, E. Laser beam welding with high-frequency beam oscillation. Welding of dissimilar materials with brilliant fiber lasers. *Phys. Procedia* 2011**,***12, 142-149.*

PAPER REF: 120

VIBRATION ANALYSIS OF POROUS BIMORPH DOUBLY CURVED SHELLS FOR ENERGY HARVESTING APPLICATIONS

Mahmoud Askari[1(*)], Eugenio Brusa[1], Cristiana Delprete[1]

[1]Department of Mechanical and Aerospace Engineering (DIMEAS), Politecnico di Torino, Italy
[(*)]*Email:* mahmoud.askari@polito.it

ABSTRACT

The aim of this study is to develop an analytical solution to calculate the natural frequencies of a porous smart doubly curved shell considered for piezoelectric energy harvesting. The governing partial differential equations of motion are derived using Hamilton's principle and the Maxwell equation for both short- and open-circuit electrical conditions. Applying the Navier's solution results in an eigenvalue problem which permits to obtain the natural frequencies of the system. Finally, the effects of porosity and geometric parameters on the natural frequencies of the system are studied. The functionality of utilizing porous materials in energy harvesting applications is demonstrated by the relation between the obtained natural frequencies and porosity coefficient.

Keywords: piezoelectric energy harvesting, natural frequency, porous media, bimorph shell.

INTRODUCTION

Vibration-based piezoelectric energy harvesters can produce peak power when their resonance frequency matches the frequency of the input ambient vibration. Any difference between these two frequencies can lead to a significant decrease in produced power. Nevertheless, most of the existing energy harvesting configurations have a high resonance frequency compared to the frequencies of the typical ambient vibrations (Wei, 2017 and Yang, 2018). To overcome this drawback, porous materials could be useful in designing structures with lower resonant frequency specifically for harvesting applications where the weight of the structure is of concern.

The considered configuration is a porous bimorph shell as shown in Fig. 1. It is assumed that the porosity is asymmetrically distributed through the thickness of the core layer as presented by (Magnucka-Blandzi, 2008) and the outer layers are made of PZT-5H. First order shear deformation theory is used to obtain the governing equations of motion, and consequently the natural frequencies of the system are calculated analytically for a simply supported bimorph shell harvester.

RESULTS AND CONCLUSIONS

The effect of porosity on the short- and open-circuit resonance frequencies of the piezoelectric harvester is shown in Fig. 2(a). This figure simply demonstrates that the resonance frequency decreases as the porosity parameter increases and this behaviour is due to the induced reduction in the effective stiffness of the harvesting structure. In Fig. 2(b), the variation of the natural frequency with respect to the shell curvature is plotted for different values of the porosity parameter. The results which are related to a bimorph shell harvester in short-circuit electrical condition demonstrate that increasing the shell curvature causes a significant decrease in the value of resonance frequency for all considered porosity parameters.

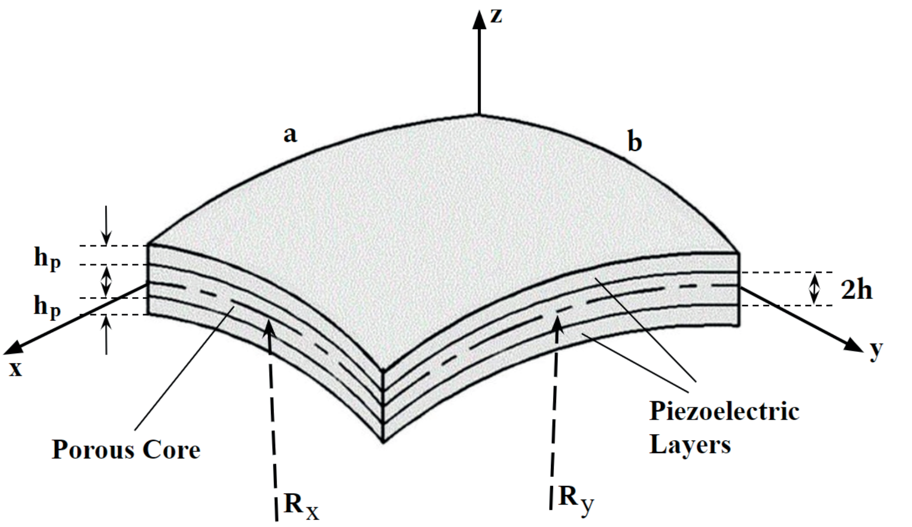

Fig 1. Schematic diagram of porous bimorph shell harvester

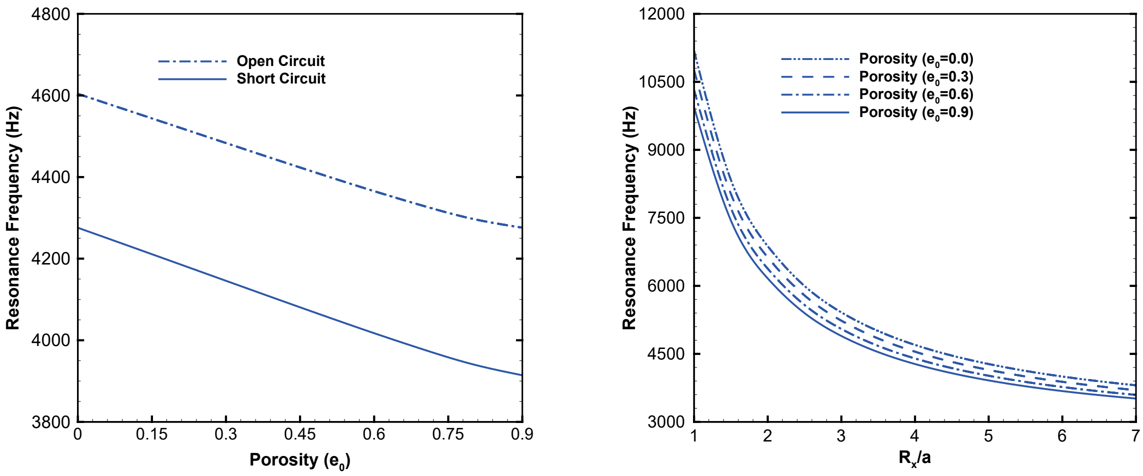

(a) (b)

Fig 2. Variation of the fundamental resonance frequency of the spherical harvester with respect to (a) porosity and (b) shell curvature (a=b=30 mm, $2h=h_p=0.135$ mm, $R_y/a=5$)

REFERENCES

Magnucka-Blandzi E. Axi-symmetrical deflection and buckling of circular porous-cellular plate. Thin Walled Structure, 2008, 46, p. 333-37.

Wei C, Jing X. A comprehensive review on vibration energy harvesting: Modelling and realization. Renewable and Sustainable Energy Reviews, 2017, 74, p. 1-18.

Yang Z, Zhou S, Zu J, Inman D. High-performance piezoelectric energy harvesters and their applications. Joule, 2018, 2, p. 642-697.

PAPER REF: 121

A MODEL FOR ENGINEERING DESIGN EDUCATION AND A CONTINUAL COURSE IMPROVEMENT METHOD

Marnie V. Jamieson[1(*)] **and John M. Shaw**[1]

[1]Department of Chemical and Materials Engineering (CME), University of Alberta, Edmonton, Canada
[(*)]*Email:* mvjamies@ualberta.ca and jmshaw@ualberta.ca

ABSTRACT

Teaching innovation, teamwork, leadership, and sustainable design are key deliverables for engineering programs and capstone design courses. Teaching engineering design requires instructors and students to work with ***complex*** problems. Engineering Accreditation Boards associated with the Washington Accord have been embracing performance-based outcomes known as graduate attributes and continual improvement processes. A learning culture supporting graduate attribute development and continual improvement can be cultivated to prepare engineering graduates for working in a world with complex problems. In this contribution we report on a model for engineering design education and a continual course improvement method.

Keywords: learning culture, innovation, teamwork, leadership, sustainable design, capstone design courses, graduate attributes, continual course improvement, metacognitive skill.

INTRODUCTION

Analysis of graduate attribute outcomes for an engineering course within an engineering program requires the examination of a complex system.[1] Complex systems may have a range of short term and long-term outcomes. They are characterized by multiple interacting factors where generalized formulas have limited applicability and where repeating an action or intervention might not produce the same outcome. The absolute and relative achievement of graduate attributes depends on multiple factors including prior student experiences, their metacognitive and professional skills, the learning effort they expend, the quality and quantity of their fundamental and socio-contextual knowledge bases. Students in a program may all graduate but it is unlikely they will attain the same level of graduate attribute achievement. The proposed engineering education and practice model (Figures 1 and 2) used with the continual course improvement method advocated in this work can help develop and improve engineering design course content and supports learning.

A case based integrated mixed methods design is used in this work to examine course and student outcomes, to identify *improvement actions* for subsequent iterations, and demonstrate student graduate attribute achievement. The work is briefly presented here. A more detailed elaboration is provided elsewhere (Jamieson, 2019). The engineering education and practice model was developed using qualitative analyses of interdisciplinary literature (Jamieson, 2019) and a continual improvement process (Jamieson 2016-2018). The application of the model provided guidance on the types of learning experiences required for individual students to excel and the process was instrumental in targeting course improvement areas.

[1] Complex system behaviour is distinguished from complicated system behaviour where outcomes can be reliably predicted from past behaviour with mathematical analysis (Clark, 2012).

DISCUSSION AND CONCLUSIONS

An engineering program of study is a complex system. Instructors *and* students change from iteration to iteration as they learn and reflect. Students and student cohorts can be influenced by previous work experience, class size, design teammates, course sequencing, extra curricular activities, life experience, performance in prior related courses, different instructors teaching prerequisite courses, economic factors, perceived career opportunities, and societal changes. The list of possible confounding factors is long. This observation lends support to the idea that students experience design courses uniquely even though there is a common course "reality" for all. Instructors are also subject to their own learning and changes as continual improvement processes are applied to multiple courses within a program. Learning activities and *tools for learning* change within the frameworks (illustrated in Figures 1 and 2) as students iterate through an open-ended complex design process in a community of practice.

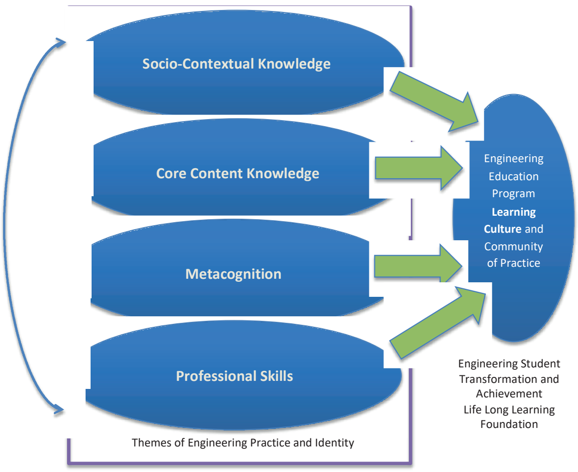

Figure 1. Proposed Engineering Education and Practice Theoretical Framework

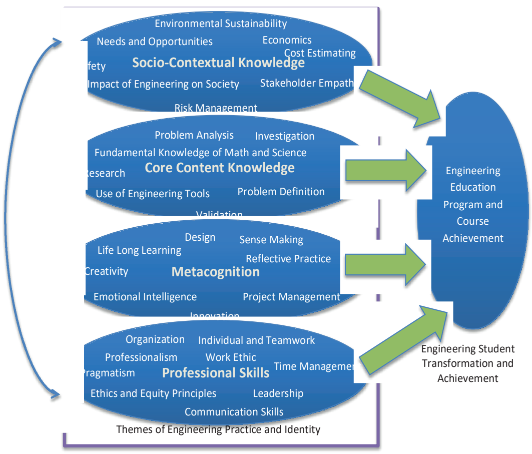

Figure 2. Proposed Engineering Education and Practice Conceptual Framework

Fig. 1 and 2 – Proposed Engineering Education and Practice Frameworks

The overall objective of the continual improvement process, outlined in Figure 3, is effective improvement action identification or status quo acceptability demonstration *over time*. Improvement actions are targeted to improve graduate attribute development during and at the end of an engineering program of study. The key criteria underlying assessment are listed in Table 1. Evidence based improvement actions can target course or program level improvements and should be supported by an analysis of outcomes at the course level. The method used to identify improvement actions should include multiple perspectives and should engage stakeholders. If no improvement actions are identified, the status quo can be justified - based on an outcome-based evidence assessment (CEAB, 2018).

We use a successive mixed method case study format to answer the continual improvement question "*What needs to be improved (if anything) and what are the improvement actions?*" after each iteration of the introductory and capstone Chemical Engineering process design courses. Implicit and explicit CEAB graduate attributes are inherently challenging to measure, because the attributes themselves are complex (Jamieson, 2019). A continual improvement process is an effective driver for identifying evidence-based learning activity changes and justifying maintaining the status quo in areas where no improvement actions are needed.

The proposed engineering education and practice frameworks generalize the themes of engineering education in order to guide successful program and design course curriculum development that supports lifelong learning and professional practice roles for engineering students as their careers develop. Frameworks also guide students to develop contextual and practice skills across the graduate attributes enabling more advanced graduate attribute achievement on completion of their engineering program.

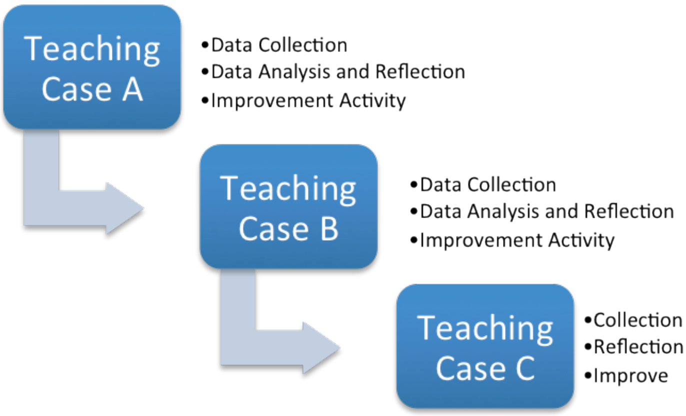

Fig. 3 – Sequential Case Study Mixed Method Continual Improvement Design
© ASEE 2019 M.V. Jamieson, J.M. Shaw, "A Continual Improvement Process for Teaching Leadership and Innovation within a Community of Practice," ASEE Annual Conference Proceedings, American Society for Engineering Education, Tampa, 16-19 June 2019.

Table 1 - Key evaluation criteria for a continual improvement process. © ASEE 2019 as above.

Criteria	**Process properties**
Identify improvement actions – evidence based – improvements must be informed by graduate attribute outcome assessment	Must be able to identify outcomes that need improvement. Assessment of learning activity efficacy: students & instructors. Requires mapping of graduate attributes to course learning outcomes
Used over time	Data collected, analysed and used to identify actions on a regular basis
Identify areas for improvement – learning activity and graduate attribute matching – is the assessment valid? Does it capture the attribute?	Stakeholder assessments – Community of practice: Student self-assessment (pre-post course); Input from industry advisors; input from instructors.
Measure the scope of the graduate attribute while minimizing measurement points	Assess each graduate attribute for scope – set a limit on redundancy – specific assessment points that span the attribute breadth
Justify keeping the status quo	Analyze data and compare from year to year and to a target value.
Stakeholder "buy in" - process becomes part of the *learning* culture of the institution	Process must be used to be valid. Flexible and adaptable to individual course needs
Consistency	An evidence driven course based process is an input to a consistent course reflection and program feedback process

ACKNOWLEDGMENTS

The authors gratefully acknowledge funding from The University of Alberta Provosts Digital Learning Committee as part of a Centre for Teaching and Learning led blended learning research project, and from the sponsors of the Natural Sciences and Engineering Research Council Industrial Research Chair in Petroleum Thermodynamics (Alberta Innovates - Energy and Environment Solutions, BP Canada Energy Corporation, ConocoPhillips Canada Resource

Corporation, Natural Sciences and Engineering Research Council of Canada (NSERC), Nexen Energy ULC, Shell Canada, Total E & P Canada, Virtual Materials Group Incorporated). This project received research ethics approval from the University of Alberta Research Ethics Board, No. *Pro00048272*. The authors also acknowledge with thanks the support of our community of practice – our students, our teaching team, our research community, and our industry participants. A special thank you to Michel Perrier, Sylvie Doré, Norma Nocente, and John Nychka for their (ongoing) helpful comments.

REFERENCES

Canadian Engineering Accreditation Board, "Canadian Engineering Accreditation Board: Accreditation Criteria and Procedures", Ottawa: Canadian Council of Professional Engineers, 2014 and Continual Improvement Rubric v3.2, 2018.

Clark, A.M., Briffa, T.G., Thirsk, L., Neubeck, L., Redfern, J., What football teaches us about complex health interventions *BMJ:* 2012, 345 (7888), pp. 25-27

Creswell, J. W., Educational research: Planning, conducting, and evaluating quantitative and qualitative research (2nd ed.). Upper Saddle River, NJ: Pearson, 2005.

Creswell, J. W., Poth, C.N., Qualitative Inquiry and Research Design: Choosing among five approaches. (4th ed.) Thousands Oaks: Sage Publications, 2018.

Jamieson, M.V., Shaw, J.M., A continual improvement process for teaching leadership and innovation within a community of practice. *Proceedings of The American Society for Engineering Education Annual Conference & Exposition*, Tampa Bay, Florida, 15-19 June 2019.

Jamieson, M.V., "Application of Blended and Active Learning to Chemical Engineering Design Instruction", 2016, University of Alberta

Jamieson, M.V., Shaw, J.M., Applications of peer teaching and deep learning in engineering education course design. *Proceedings of the 7th International Conference on Mechanics and Materials in Design* Albufeira, Portugal 11-15 June 2017.

Jamieson, M.V., Shaw, J.M., Applying metacognitive strategies to teaching engineering innovation, design, and leadership. *Proc. 2017 Canadian Engineering Education Conference (CEEA17)*, G. Evans (ed) (Toronto, Canada; 2017), 4-7 June 2017, Paper 045.

Jamieson, M.V., Shaw, J.M., Graduate attribute based continuous improvement in a blended learning engineering design course – a writing seminar case study. *Proc. 2018 Canadian Engineering Education Conference (CEEA18)*, P. Ostafichuk (ed) Vancouver, Canada; 3-6 June 2018, Paper 77.

Jamieson, M.V., Shaw, J.M., Learning to learn: Defining an engineering learning culture. *Proc. 2019 Canadian Engineering Education Conf. (CEEA19),* Ottawa, Canada, 9-12 June 2019, Paper 18.

Jamieson, M.V., Shaw, J.M., Pre and post course student self assessment of CEAB graduate attributes - A tool for outcomes assessment, student skill and course improvement. *Proc. 2016 Canadian Engineering Education Conf. (CEEA16)*, Halifax, Canada, 19-22 June 2016, Paper 037.

Jamieson, M.V., Shaw, J.M., Student and instructor satisfaction and engagement with blended learning in chemical engineering design. *Proc. 2017 CEEA Conf.,* Toronto, Canada, 2017, Paper 036.

Jamieson, M.V., Shaw, J.M., Teaching engineering innovation, design, and leadership within a community of practice. *Proc. 2018 Canadian Engineering Education Conf.,* June 2018, Paper 113.

PAPER REF: 122

NUMERICAL-EXPERIMENTAL CORRELATION OF DYNAMIC TEST OF A HONEYCOMB IMPACT ATTENUATOR FOR A FORMULA SAE VEHICLE

Andrea Vettorello(*) [1], Giuseppe Alessio Campo[1], Sergio Fanelli[1]

[1]Engineering Department "Enzo Ferrari" (DIEF), University of Modena and Reggio Emilia, Italy

(*) *E-mail:* andrea.vettorello@unimore.it

ABSTRACT

This work is focused on the investigation, the development, and the numerical-experimental correlations of a honeycomb Impact Attenuator (IA) for a Formula SAE (FSAE) prototype. Three different IA are studied and compared in order to obtain the optimal configuration, in accordance with the championship rules and the design constraints. The second part of the work concern the numerical-experimental correlation of the IA material, in particular the aluminum honeycomb. Finally, the development of the dynamic Finite Element model and the validation through the experimental crash test are presented.

Keywords: Impact Attenuator, Honeycomb, Crash Test, Finite Element modelling, FSAE.

INTRODUCTION

The design of efficient safety components in a FSAE racecar is one of the main challenges for the student team. This work is focused on the design of the IA and the Anti Intrusion Plate (AIP). The former absorbs the major part of kinetic energy in a frontal crash event and the latter protects the driver legs from any intrusion in the cockpit zone. The predictively of FE models of structural component is crucial in the automotive design (Lo Presti 2017- Mantovani 2017) even in FSAE.

The first design step of this work is the definition of the constraints, necessary to obtain a feasible solution. In case of a frontal impact event, the FSAE rules define the physical parameters necessary to achieve the approval of the IA system. Other constraints derive from the geometrical dimension of the design space. These constraints depend on the frontal section of the bulkhead and the free internal volume of the anterior bodywork. In the concept design phase, three different solutions are investigated and implemented: (*i)* stiff CFRP AIP and aluminum honeycomb crash-box, *(ii)* hollow cut pyramid welded on an aluminum plate, *(iii)* IA made up by four layers of honeycomb, linked together between thin CFRP plates.

The embodiment design phase starts from the numerical-experimental correlation of the materials employed. In particular, the aluminum honeycomb was modelled with homogenization technique as solid orthotropic material with equivalent mechanical properties (Gibson, 1997). The solution *(i)* is characterized by a light IA thanks to the huge specific energy absorption of aluminum honeycomb. On the other hand, *(ii)* presents a very light AIP, achieved orienting the load paths to the external edges of the bulkhead. The third configuration *(iii)* is a compromise between the previous solutions in terms of overall weight. Thus, the numerical dynamic crash test model and the experimental validation are performed. Finally, the results of solution *(iii)* are presented.

RESULTS AND CONCLUSIONS

Fig.1 presents the IA after the experimental test. As expected, the IA system passed the type approval for the competition. Fig.2 shows the validation of the dynamic model implemented. The parameters monitored and simulated are close to the real case.

Table 1 – Result comparison

Parameters	Simulated	Experimental	Error [%]
Average deceleration [g]	19.18	19.10	0.42
Max displacement [mm]	139.3	145.5	4.26
Time of impact event [ms]	37.3	37.8	1.32

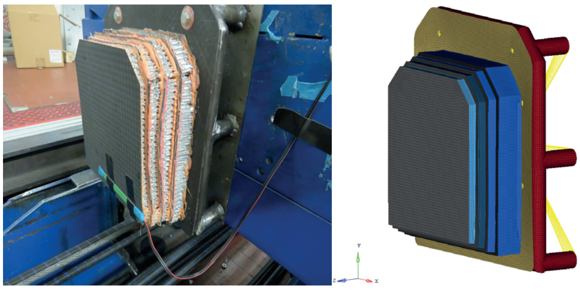

(a) (b)

Fig. 1 – Comparison after the crash test, experimental (a) and simulated (b)

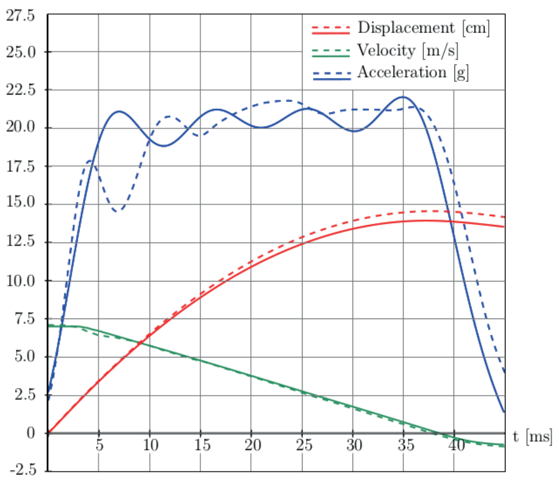

Fig. 2 – Validation of the dynamic model in terms of displacement, velocity and acceleration for experimental test (dashed curves) and Finite Element models (solid curves).

REFERENCES

Lo Presti, I., *et al.* (2017). Optimization Methodology for an Automotive Cross-Member in Composite Material. In *Key Eng Mater* (Vol. 754, pp. 291-294). Trans Tech Publications.

Mantovani, S., *et al.* (2017). Influence of manufacturing constraints on the topology optimization of an automotive dashboard. *Procedia Manufacturing*, *11*, 1700-1708.

Gibson, L. J.Ashby, M. F. (1997) 'Cellular solids', *Cambridge Solid State Science Series*, pp. 93-173.

PAPER REF: 123

EVALUATION OF THE CONTAMINATION OF VEGETABLES BOUGHT FROM DIFFERENT ALGERIAN MARKETS BY HEAVY METALS

Djeziri Mourad[1,2(*)], Didouche Yasmina-Fadhéla[3]

[1] Research Laboratory in Food Technology, Faculty of Engineering Sciences, University M'hamed Bougara of Boumerdes 35000, Algeria.
[2] Center for scientific and technical research in Physico-chemical analysis (CRAPC) Bou Ismail, Tipaza.
[3] Research Unit: Materials, Processes and Environment (UR / MPE), University of Boumerdes, 35000 Algeria.
[(*)] *Email:* mourad_djeziri@yahoo.fr

ABSTRACT

The contamination of vegetables by pollutants, especially heavy metals, is a major societal concern. Indeed, more and more crops are being planted in peri-urban areas sold in markets, and as a result can be impacted by past polluting industries or still in operation. This problem is global, and very few countries are spared. These contaminations may be related to soil pollution, or water used for irrigation. For lack of knowledge, many populations practice cultivation in territories with extremely high levels of pollution. The question of the transfer of these contaminants from the soil to the plants then appears paramount.

Key words: Vegetables, Heavy metals, Risk assessment, Atomic absorption spectrophotometry.

INTRODUCTION

Vegetables are a very important part of human nutrition. In addition to a potential source of important nutrients, they provide proteins, vitamins, iron and calcium that affect health (Arai, 2002). Leafy vegetables such as chards and lettuce growing on soils contaminated with heavy metals tend to accumulate large quantities of heavy metals, compared to those growing on non-contaminated soils because of they absorb these metals through their leaves (Al Jassir et al., 2005). The present study was carried out on vegetables of wide consumption in Algeria, bought from different markets. Knowledge about contamination of vegetables with heavy metals in these markets is not yet established.

RESULTS AND CONCLUSIONS

At the first glance we note a maximum value of iron Fe, which is of the order of 11.69 mg / Kg presented in the chard sold in the khemis el khechna market of boumerdes for the companion of 2016 and a minimum value of the order of 0.005 mg / Kg presented in the potato sold in the same market for the companion of 2017, which is logical hence the wealth of iron chard (stores iron) and the deficiency of the potato of the latter, something that is justified by works like (Naorem et al 2014), which found a value of 970.93 mg / kg in Swiss beech exceeding the permissible limits WHO / ML (mg / Kg) 425.00 mg / Kg, The consumption of these vegetables will give rise to health problems such as: the training of bone fractures, diarrhea, stomach pains, severe vomiting, reproductive failure, central nervous system damage and DNA, in addition to developments of cancers.

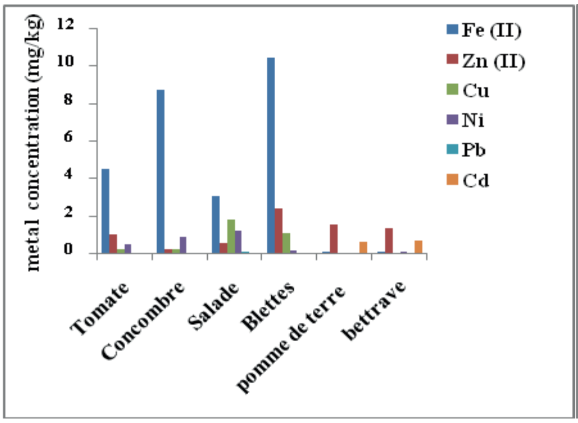

Fig 1- Concentrations of metals in market vegetables Khémis el khechna, Boumerdes Algeria (2015 sampling)

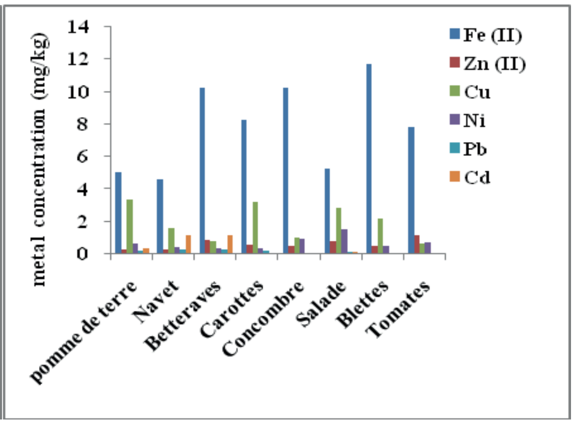

Fig 2- Concentrations of metals in market vegetables Khémis el khechna, Boumerdes Algeria (2016 sampling)

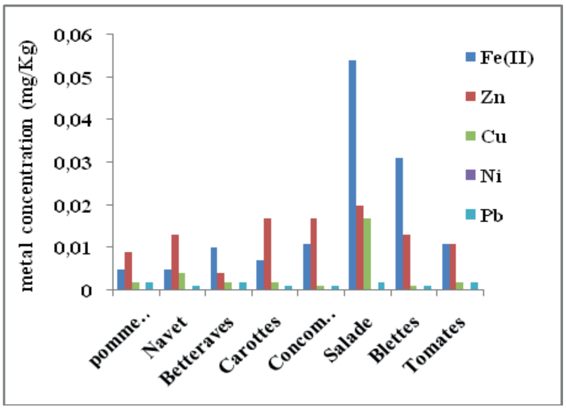

Fig 3- Concentrations of metals in market vegetables Khémis el khechna, Boumerdes Algeria (2017 sampling).

Table 1-Permissible limits of heavy metals in plants.

Permissible Limites	Cu	Pb	Zn	Cd	Fe	Ni
FAO/WHO (mg/Kg) Codex Alimentarius Commission (1984)	40.00	5.00	0.60	0.30	-	-
FAO (mg/l) recommended max. conc. Of trace elements for crop production (1985)	0.20	5.00	2.00	0.01	5.00	0.20
WHO/ML (mg/Kg) Under waste water irrigation	73.00	0.30	100	0.10	425.00	67.00
Mean heavy metal content (mg/Kg) of waste water samples taken from affect area	58.45	21.71	125.1	34.68	1873.6	63.94

CONCLUSION

The results presented here seem to show that vegetables with high foliage are much more impacted than root crops, as much of the contamination is done through irrigation water. In addition, when the mobility of metals with depth is low, the first centimeters of soil are enriched in metals and one can find the most important metal concentrations available. In addition, the consumption of some crops appears to pose an increased risk.

ACKNOWLEDGMENTS

My tanks go to these who helped this study.

REFERENCE

Al Jassir, M.S., A. Shaker and M.A. Khaliq. (2005). Deposition of heavy metals on green leafy vegetables sold on roadsides of Riyadh City, Saudi Arabea. B. Environ. Contam. Tox, 75: 1020-1027.

Arai, S. (2002). Global view on functional foods: Asian perspectives. Brit. J. Nutr., 88: S139 S143.

Naorem Mohendro Singh, Nongmaithem Rajen SinghA (2014). Quantitative Analysis of Heavy Metals in Vegetables Grown At Kakching-Wabagai Area, Thoubal District Manipur. PARIPEX - INDIAN JOURNAL OF RESEARCH. Volume : 3 Issue : 6.

PAPER REF: 124

EVALUATION OF FRACTURE TOUGHNESS OF ZIRCONIA OXIDE CERAMICS SUBJECTED TO WEDGE SPLITTING LOADING

Eremin Mikhail[1(*)], Evgenii Deryugin[1]

[1] Institute of Strength Physics and Materials Science SB RAS, Tomsk, Russia
[(*)] *Email:* eremin@ispms.tsc.ru

ABSTRACT

Evaluation of fracture toughness is one of the key problems related to understanding of crack resistance behavior of materials. In this work we investigate both experimentally and numerically the features of evolution stress and strain state of double cantilever specimen subjected to wedge splitting. The material under consideration is 3YSZ. The specimen has a chevron notch between cantilevers which maintains the stable manner of crack propagation. Experiments show that deviation from elastic behavior occurs during loading. The main hypothesis is that nonlinearity is due to martensitic phase transformation and propagation of crack. We build a mathematical model to describe these processes. The results of numerical simulation are in satisfactory agreement with experimental data.

Keywords: mode I fracture, fracture toughness, zirconia ceramics, martensitic transformation, numerical simulation, wedge splitting, double-cantilever specimen.

INTRODUCTION

Zirconia based ceramics have drawn much attention recently. Many articles are devoted to investigation of propagation of a single crack in infinite or finite region, examining wide range of parameters, e.g. notch radius [Gomes et al., 2006], material grading [Hbaieb et al., 2007], crack tip blunting caused by martensite transformation toughening [Kelly and Rose, 2002], phase field models are implemented to investigate a crack propagation [Kuhn and Muller, 2010]. One of the main tasks of mechanics and materials science is improvement of physical-mechanical properties of materials. It is necessary for certain range of practical applications. It is well known, that zirconia based ceramics are brittle and experience stress induced phase transformations. Numerous hardening techniques are applied to increase a fracture toughness of this material. One of such techniques is a stabilization of tetragonal phase at room temperature by adding of 3 mol. % of Y_2O_3. It is known that a stress induced martensitic transformation occurs in the apex of growing crack. In most of the cases, the crack growing is unstable. That is why we need to manufacture the specimens with special geometry to study the effect of hardening techniques on crack resistance of material. It gives an opportunity to study the hardening effect at stable manner of crack propagation. Related to that problem, specimens with chevron notch appeared to be an effective solution. When crack propagates along the chevron notch, the crack front width constantly increases which leads to the stable manner of crack propagation.

We investigated both experimentally and numerically the features of evolution of stress and strain state of double cantilever specimen subjected to wedge loading. Following section provides short summary of the results.

RESULTS AND CONCLUSIONS

Macroscopic loading diagram showed that there is a deflection from linear behaviour due to phase transformations and propagation of crack. Numerical simulation was carried out without explicit account for martensitic transformation, i.e. special equations for transformation of material in the apex of growing crack were not included in the model. However, before the local failure criterion is met, a small amount of inelastic strain is accumulated, which causes a relaxation of stresses. Comparison of experimental and numerical diagrams (Fig. 1a) show that blunting of crack due to accumulation of inelastic strain did not perform a necessary toughening of material and fracture toughness appeared to be underestimated for about 10%. However, crack path patterns in experiments and simulation are in good agreement (Fig. 1b, c).

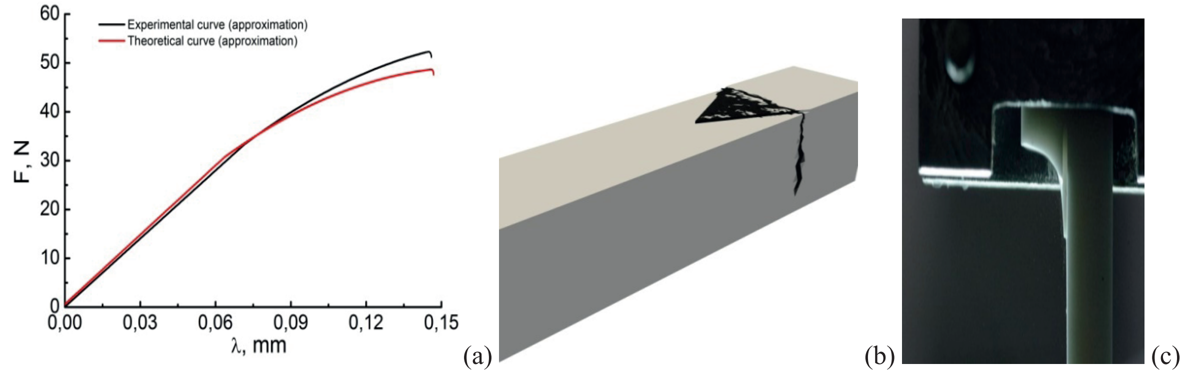

Fig. 1 - Comparison of loading diagrams Force – deflection (black – experiment, red - simulation),

Further study needs to account explicitly for martensitic transformation, which cause a volume jump of about 4% and consequent jump of compressive stresses which blunts the crack tip and leads to material toughening.

ACKNOWLEDGMENTS

The authors gratefully acknowledge the funding by Fundamental Research Program of the State Academies of Sciences for 2017-2020, line of research III.23 (mathematical formulation of the problem) and grant No. 17-08-00377 of Russian foundation for basic research.

REFERENCES

Gomes F., Guinea G., Elices M. Failure criteria for linear elastic materials with u-notches. International Journal of Fracture, 2006, 141 (1), pp. 99-113. doi:10.1007/ s10704-006-0066-7.

Hbaieb K., McMeeking R., Lange F. Crack bifurcation in laminar ceramics having large compressive stress. International Journal of Solids and Structures, 2007, 44 (10), pp. 3328-3343. doi:10.1016/j.ijsolstr.2006.09.023.

Kelly P., Rose L.F., The martensitic transformation in ceramics- its role in transformation toughening. Progress in Materials Science, 2002, 47 (5), pp. 463-557. doi: 10.1016/S0079-6425(00)00005-0.

Kuhn C., Muller R. A continuum phase field model for fracture. Engineering Fracture Mechanics, 2010, 77 (18), pp. 3625-3634. doi:10.1016/j.engfracmech.2010.08. 009.

PAPER REF: 125

PROPOSAL OF A NON-HERTZIAN MODEL FOR STUDYING CONTACT BETWEEN MOVING BODIES

Fabio Bruzzone, Tommaso Maggi, Claudio Marcellini, Carlo Rosso and Cristiana Delprete
Politecnico di Torino
Corso Duca degli Abruzzi, 10123 Torino (Italy)

ABSTRACT

In this paper a non-Hertzian model for studying behaviour of moving bodies in contact is presented. An already developed two-dimensional algorithm [*Rosso, 2019*] has been extended to the case of three-dimensional smooth contact phenomena. In this paper the friction contribution is neglected. Using an iterative cycle, the non-Hertzian contact algorithm calculates the pressure distribution and its maximum value in the local contact area between two generic bodies (any shape) in contact. It can analyse simultaneous contact areas in different parts of the same component, a fundamental aspect in case of meshing gears or bearings. The target of this study is to highlight the influence of micro-geometrical profile modifications on the contact stress and pressure. An explanation of the algorithm is shown in figure 1. To validate the model the results of pressure distribution of three different pair of gears are shown.

Keywords: gear contact, Hertzian model, contact pressure, contact deformation.

INTRODUCTION

The model requires three main inputs: the torque transmitted by the pinion; the material parameters, such as Young's modulus E and Poisson ratio v; the reciprocal positions of the two bodies in the initial rigid contact condition. This latter input is expressed by the Cartesian coordinates of the cloud points that describe the geometric shape of the surfaces in contact. When the rigid position of the two bodies is well defined, the algorithm starts to compute the pressure distribution imposing a first attempt indentation, in the form of a rigid displacement $d\theta$.

As bodies are getting in contact, the algorithm recognizes the simultaneous contact areas and the involved nodes; afterwards it calculates the pressure distributions according to the models of literature [Boedo, 2013 – Marmo, 2017].

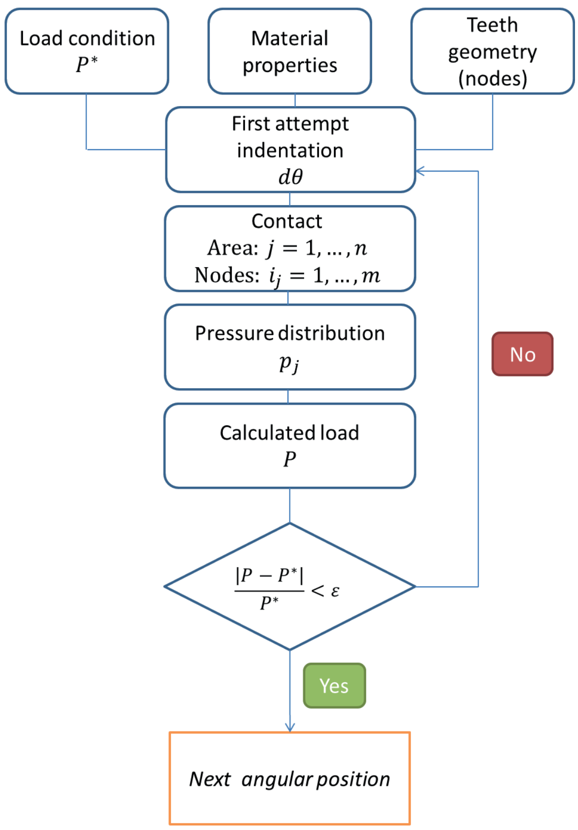

RESULTS AND CONCLUSIONS

To validate the model, three cases with different pairs of gears are presented: a pair of standard spur gears, a pair of crowned spur gears and a pair of helical gears.

Figures 2 and 3 show, for example, the pressure distributions exchanged by the teeth coupling, main result of the algorithm. The abscissa represents the direction along the face width of the tooth, while the vertical axis represents the tooth height.

For the first case, it noticeable that the contact covers all the face width from -10 mm to 10 mm of the two spur gears. Whereas in the second case the contact area is tighter along the face width but wider along the vertical axis.

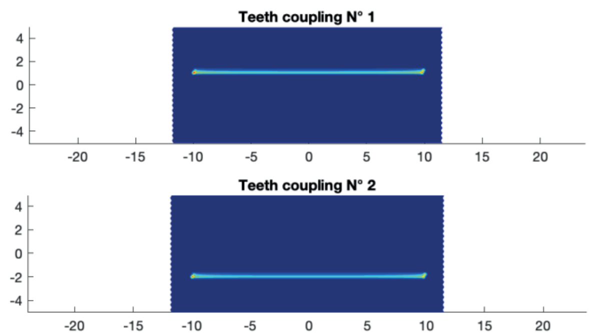

Figure 2: Double contact position in spur gears.

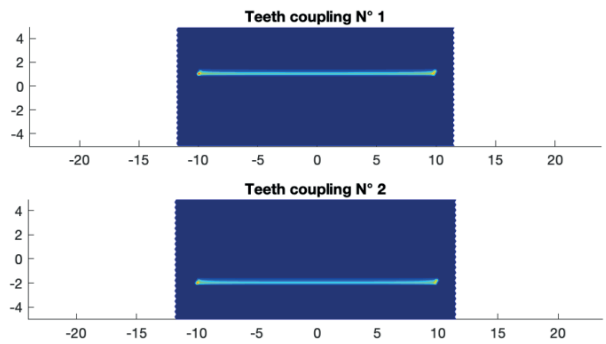

Figure 3: Double contact position in crowned gears.

In figure 4 three simultaneous teeth couplings are represented for the case of two helical gears. It is noticeable that the contact area is tilted with respect to the abscissa.

The algorithm can detect the pressure distributions along the tooth flank that decrease abruptly to zero at the tooth tip edge, where the flank ends.

Big advantage of such methodology is the possibility to have a precision of stress distribution like FEM analysis, but maintaining a very quick solution time and low computational effort.

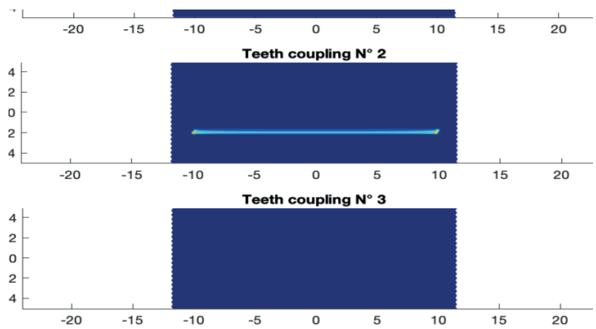

Figure 4: Triple contact position in helical gears.

REFERENCES

Rosso C., Bruzzone F., Maggi T., Marcellini C. “A proposal for semi-analytical model of teeth contact with application to gear dynamics”, *JSAE*, 2019

Marmo F., Toraldo F., Rosati A. “Numerical solution of smooth and rough contact problems”. *Meccanica*, 2017

Boedo S. “A corrected displacement solution to linearly varying surface pressure over a triangular region on the elastic half-space”, *Tribology International 60*, 2013.

PAPER REF: 126

BIOMIMETIC APPROACH, GENERATIVE DESIGN AND IRON-DOPED MATERIALS TO DEVELOP ADVANCED DEVICES FOR BIOMEDICAL APPLICATIONS

Antonio Gloria[1 (*)], Roberto De Santis[1], Teresa Russo[1], Saverio Maietta[2], Maria Richetta[3], Massimo Martorelli[2]

[1]Institute of Polymers, Composites and Biomaterials, National Research Council of Italy, Naples, Italy
[2]Department of Industrial Engineering, Fraunhofer JL IDEAS, University of Naples Federico II, Naples, Italy
[3]Department of Industrial Engineering, University of Rome Tor Vergata, Rome, Italy
[(*)]*Email*: angloria@unina.it

ABSTRACT

As reported in the literature, great efforts have been made in the development of prostheses and three-dimensional (3D) scaffolds for tissue regeneration, benefiting from progresses in the field of design, technologies and materials. Many devices have been designed and manufactured through conventional and advanced techniques. The aim of the current research was to report an approach in the design of multifunctional and smart devices, spanning from advanced prostheses to 3D hierarchical scaffolds for tissue regeneration.

Keywords: biomimetic design, generative design, additive manufacturing, iron-doped materials, biomedical applications.

INTRODUCTION

In the case of a degenerated tissue, medical practice generally involves several man-made devices to restore its function.

Over the past years, a great attention has been focused on the use of prostheses characterized by standard sizes.

Even though metals, ceramics and polymers have been widely employed to develop different kinds of prostheses, polymer-based composites have also been considered to overcome some drawbacks related to the use of conventional materials (Gloria et al., 2011; Martorelli et al., 2016). Combinations of metallic and non-metallic materials have also been considered.

However, the control of the process–structure–property relationship for the material plays an important role in the fabrication of biomedical devices featuring desired properties (Gloria et al., 2019).

In this context, the biomimetic approach has allowed to fabricate devices which are able to mimic the structure of the natural tissues, also reproducing the complex mechanical and functional behavior (Gloria et al., 2011).

Furthermore, the use of generative design and additive manufacturing has been explored to develop customized devices with tailored and improved properties for different applications (Lanzotti et al., 2015; De Santis et al., 2015; Martorelli et al., 2016).

RESULTS AND CONCLUSIONS

A pilot-scale production of biomimetic and customized prostheses was proposed by integrating different methodologies and technologies, such as computer tomography, filament winding, moulding and advanced fabrication methods (i.e., additive manufacturing).

A methodology for producing patient-specific prostheses and scaffolds for tissue engineering was also reported considering the combination of the reverse engineering approach (image capture and analysis techniques) with additive manufacturing technologies.

With regard to tissue engineering, 3D polymer-based scaffolds with different lay-down patterns were manufactured by FDM (Fused Deposition Modeling/3D fiber deposition technique).

Briefly, polymeric and nanocomposite pellets were heated using the cartridge unit on the mobile arm of a 3D plotter.

Specifically, polycaprolactone loaded with inorganic nanoparticles and iron-doped materials was also used to fabricate additively manufactured scaffolds by injecting/extruding the material through a needle.

3D morphologically controlled structures were optimized in terms of biological, mechanical and magnetic properties.

The effects of inorganic nanoparticles and iron-doped materials, as well as of the structural features, were properly studied.

REFERENCES

De Santis R, Russo A, Gloria A, D'Amora U, Russo T, et al. Towards the Design of 3D Fiber-Deposited Poly(ε-caprolactone)/Iron-Doped Hydroxyapatite Nanocomposite Magnetic Scaffolds for Bone Regeneration. J Biomed Nanotechnol, 2015, 11, p. 1236–1246.

Gloria A, Causa F, De Santis R, Tanner KE, Ambrosio L. A Multi-component Fiber-reinforced PHEMA-based Hydrogel/HAPEX™ Device for Customized Intervertebral Disc Prosthesis. J

Biomater Appl, 2011, 25, p. 795-810.

Gloria A, Maietta S, Richetta M, Ausiello P, Martorelli M. Metal Posts and the Effect of Material–Shape Combination on the Mechanical Behavior of Endodontically Treated Anterior Teeth. Metals, 2019, 9(2), 125. https://doi.org/10.3390/met9020125.

Lanzotti A, Del Giudice DM, Lepore A, Staiano G, Martorelli M. On the geometric accuracy of RepRap open-source three-dimensional printer. J Mech Des, 2015, 137, p. 101703-1 -101703-8.

Martorelli M, Maietta S, Gloria A, De Santis R, Pei E, Lanzotti A. Design and Analysis of 3D Customized Models of a Human Mandible. Procedia CIRP, 2016, 49, p.199–20.

PAPER REF: 128

ACTIVATION OF ALUMINUM DROSS USING A LIQUID GALLIUM-INDIUM EUTECTIC TREATMENT PROCESS

Jonathan Slocum[1(*)], Douglas Hart[1]

[1]Department of Mechanical Engineering, Massachusetts Institute of Technology (MIT), Cambridge, MA USA

ABSTRACT

Aluminum dross is a by-product of both primary and secondary aluminum production. Processing aluminum dross to extract entrapped aluminum is difficult and produces a harmful by-product known as salt cake, which is environmentally harmful, dangerous to handle, and often land-filled. In this paper aluminum dross is cold-worked and then treated with a heated gallium-indium eutectic, which activates the entrapped aluminum in the dross. The treated dross is then reacted in water to produce heat, hydrogen gas, and aluminum hydroxide. The heat and hydrogen can be used for industrial process or to generate electricity while the aluminum hydroxide can be processed back into aluminum. Thus this process could potentially replace current environmentally-harmful dross processing methods.

Keywords: Aluminum dross, gallium-indium eutectic, hydrogen generation, grain boundaries.

INTRODUCTION

Every year the world produces over 60 million tons of aluminum and demand is increasing [1]. From the aluminum production process comes an aluminum waste known as aluminum dross. Aluminum dross is produced by skimming the oxidized surface of molten aluminum in casting mills. Dross forms when molten aluminum wets and sticks to the aluminum oxide and salts in the furnace. When cooled, dross is a porous and sometimes malleable structure that is difficult to separate and process.

Currently, the world produces approximately 5 million tons of dross every year of which 80 percent is white dross, which contains approximately 15-70 wt.% Al [2][3]. Dross is processed in order to recover as much entrapped aluminum as possible. The leftover processing byproduct, known as salt cake, is difficult to dispose of in landfills as it is often flammable and can be dangerous to handle [4]. Disposing of salt cake in landfills in Europe is now banned, and in the United States disposes of nearly 1 million tons of salt cake which is landfilled every year [5]. Thus a more environmentally-friendly means of processing dross is needed.

In this study, tumbler dross[1] of unknown alloy content and 6061 alloy white dross were treated with a heated gallium-indium eutectic in order to activate any entrapped aluminum. This treatment process has already been shown to activate large pieces of pure aluminum that has been heavily cold worked [6]. The aluminum-gallium eutectic activates the entrapped aluminum by penetrating the grain boundaries and displacing oxide on the surface. Water is used to react with the aluminum in the treated dross to generate heat and hydrogen gas. The heat can be used for industrial processes and the hydrogen gas can be used for generating electricity. The remaining gallium-indium eutectic are byproducts of aluminum smelting and can be separated from the dross after it is reacted either by chemical or physical means such as centrifuging.

[1] Tumbler dross is an industry term for white dross which has been mechanically processed already to extract some raw aluminum

RESULTS AND CONCLUSIONS

Treated dross samples were reacted in an excess of water heated to approximately 80°C and the hydrogen was collected in an inverted column of water. Tumbler dross produced 14.63% ± 6.31% of the expected hydrogen yield while 6061 white dross produced 23.05% ± 4.68% of the expected hydrogen yield. Theoretical hydrogen yield was calculated assuming the entire mass of the dross piece was pure aluminum and did not account for the content of the dross that is non-reactive oxide and salt. This is because aluminum content varies greatly between each piece of dross, thus the calculated yields are relatively low compared to actual yield.

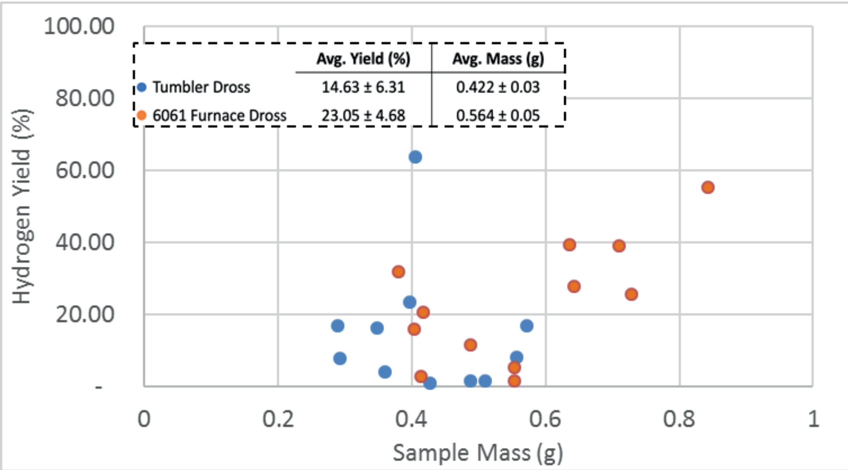

Figure 3 - *Hydrogen yields reacted samples of treated aluminum dross. Samples were reacted in an excess of water heated to 70°C until no further significant*

This study shows that aluminum dross activated with a gallium indium eutectic yielding promising amounts of hydrogen. When reacted in water, the treated dross disintrigates into a fine grain, making it easier to separate while also producing useable heat and hydrogen gas. Thus it is a potentially viable alternative to current environmentally-harmful processing methods.

ACKNOWLEDGMENTS

The authors would like to thank Bob Wagstaff for helping supply dross for this research.

REFERENCES

[1] 2020, A., 2018, "DEMAND FOR ALUMINUM IS GROWING WORLDWIDE" [Online]. Available: https://www.aluminium-messe.com/en/ALUMINIUM-2018/Demand-for-aluminium-is-growing-worldwide/758/.

[2] Adeosun, S. O., 2014, "Physical and Mechanical Properties of Aluminum Dross," Adv. Mater., **3**(2), p. 6.

[3] Shinzato, M. C., and Hypolito, R., 2005, "Solid Waste from Aluminum Recycling Process: Characterization and Reuse of Its Economically Valuable Constituents," Waste Manag., **25**(1), pp. 37–46.

[4] Majidi, O., Shabestari, S. G., and Aboutalebi, M. R., 2007, "Study of Fluxing Temperature in Molten Aluminum Refining Process," J. Mater. Process. Technol., **182**(1–3), pp. 450–455.

[5] Huang, X. L., Badawy, A. El, Arambewela, M., Ford, R., Barlaz, M., and Tolaymat, T., 2014, "Characterization of Salt Cake from Secondary Aluminum Production," J. Hazard. Mater., **273**, pp. 192–199.

[6] Slocum, J. T., and Hart, D. P., 2017, "Effects of Cold-Working Aluminum Prior to Activation via a Ga-In Eutectic.," *Proceedings of the 7th International Conference on Mechanics and Materials in Design*.

PAPER REF: 129

ADAPTATION OF THE ENGINEERING DESIGN PROCESS TO MEDICAL IMPLANTS

Rosaire Mongrain

[1]Department of Mechanical Engineering, McGill University, Montreal, Canada

[(*)]*Email:* rosaire.mongrain@mcgill.ca

ABSTRACT

In this work, we present the adaptation of the conventional design process applied to medical implants. The process needs to be expanded to include specific criteria related to the bio-integration (interaction of the implant with the surrounding biological tissue). Some of these design criteria constitute paradigm shifts which needs to be addressed. In particular, we put forward the failure modes that need to be shifted to the impact of the implant on the biological tissue.

Keywords: Design process, medical implant, failure modes, paradigm shift.

INTRODUCTION

Because our population is aging, there is an increasing need for artificial soft organs and tissue (e.g. cardiac tissue, joint replacement, skin, intervertebral disc, tendons, pelvic floor support) [1]. In fact, recent studies show that 15 million people in the United States carry medical implants. From a bio-engineering perspective, there are important geometrical and mechanical constraints that the synthetic replacements need to mimic to properly replace and integrate with the soft organs. Such technologies have to conform to highly complex anatomical shapes with curved surfaces [1] and three-dimensional features. The implants need to be compliant to function in conjunction with the soft tissue and avoid causing damaging local stresses (pressure, friction). The biomaterials used in these implants are directly interfacing with the surrounding soft tissues and organs [2] and bring specific problems linked with bio-compatibility. In particular, one important failure modes on the implant is foreign body reaction [3]. In addition, soft tissues exhibit mechanical characteristics that are more complex than most conventional engineering materials [4]. The large deformations of soft tissue subject the implant to important fatigue and failure complications.

RESULTS AND CONCLUSIONS

The design process for medical implants required to expand the conventional process with specific additional aspects [7]. In brief, 1) the Problem statement, needs the involvement of everyone that has a stake including medical doctors, biologists and nurses, 2) the Design specifications, needs the incorporation of the anatomical dimensions and physiological parameters, 3) the Concept design, requires to take into account large deformation and a changing environment (remodeling), 4) the Detail design, demands to address the biocompatibility and sterilization of the materials but more importantly, the paramount new failure mode is to preserve biological tissues and organs before the implant itself and 5) the Prototyping and testing require anatomically and physiologically correct reproducible conditions. In fact, mechanical properties have proven as important as biocompatibility properties and the expression “Mechanical Biocompatibility” has been coined [5]. Actually, deformation capability is considered even a more important criterion for highly deformable implants.

The introduction of these concepts at the undergraduate level will be illustrated with some examples.

ACKNOWLEDGMENTS

The authors gratefully acknowledge the funding by NSERC National Science and Engineering Council of Canada CDE 523735-18.

REFERENCES

1. Ghaffari R et al., Reinventing biointegrated devices, Materials Today 16(5): 156-157, 2013

2. Pillai CKS, Sharma CP, CRC Press, Woodhead, ed Sharma C, Absorbable Polymeric Surgical Sutures: Chemistry, Production, Properties, Biodegradability, and Performance ISBN 978-1-84569-509-5, 1-12, 2010

3. Bryers JD, Giachelli CM, Ratner BD, Engineering biomaterials to integrate and heal: The biocompatibility paradigm shifts, Biotechnol Bioeng. 109(8):1898-911, 2012

4. Freutel M et al., Finite element modeling of soft tissues: material models, tissue interaction and challenges.Clin Biomech (Bristol, Avon) 29(4):363-72, 2014

6. Mazza E, Ehret AE. Mechanical biocompatibility of highly deformable biomedical materials.J Mech Behav Biomed Mater, 48:100-12, 2015

7. Aitchison GA, Hukins DWL, Parry JJ, Shepherd DET, Trotman SG, A review of the design process for implantable orthopedic medical devices

PAPER REF: 130

THE MEANING AND THE VALUE AS TRIGGERS FOR DESIGNING SIGNIFICANT PRODUCT EXPERIENCES

Suzana Dias[1]; Ana Baptista[2]

[1] (IPCA) Polytechnic Institute of Cávado e Ave, ID+ Instituto de Investigação em Design, Media e Cultura / Polo IPCA, Portugal. Email: cdias@ipca.pt

[2] Queen Mary University of London, UK. Email: a.baptista@qmul.ac.uk

ABSTRACT

In this article we discuss the *value* and the *meaning* as a set of qualities that must complement functionality and external aspect of the objects as well as a tool for designers to access the very core of the otherness experience. In this reflection, we approach perspectives put forward by Donald Norman and Csikszentmihalyi. Within this symposium, we aim at contributing to exchange ideas into Design understood as an expanded field.

Keywords: Design, significant experience, value, meaning.

INTRODUCTION

Nowadays we live in a world where products, commodities and services have achieved high levels of satisfactory performance and results. In order to draw attention and to promote distinction between them, the challenge of design must focus not just in aesthetics and utilitarian aspects, because "today we want products that appeal to both cognition and emotion" as Donald Norman said. In fact today's expectation demands a new set of qualities as 'value' and 'meaning'.

If we want to achieve the integration of the products in people's real lives, we have to project material or immaterial results that effectively support people in their daily activities. So design solutions must trigger not only the *value* but also the *meaning* by the activation of both human dimensions: cognitive and senses. But, what do '*meaning*' and 'value' actually mean?

MEANING, PLESURE AND ENGAGEMENT

Remembering Csikszentmihalyi's long surveys on human behaviour, *meaning* is one of the three elements that can justify the sensation of a well-lived life – the life that goes beyond the 'normal' state of living. The other two are *pleasure* and *engagement*. The author understands *meaning* as a sensation "of being part of something" or as a "feeling of being linked to something bigger than ourselves" (Csikszentmihalyi, 2011). Carrying this perspective to the field of design, Donald Norman sets up the difference between *meaning* and *value:* if we activate the cognitive level – such as thought and memory – we are assigning meaning; if we activate the perceptive level – which means the senses – we are assigning value (Norman, 2004, p. 25).

However, to activate a feeling of well-being or a symbolic order, the cooperation and engagement of the other (the user) as the centre of the whole process is required as regarded by Csikszentmihalyi: "to be effective in conveying meaning, the owner has to be personally involved with the artefact. It was not enough that the object had been created by someone else; to be significant, the owner had to enter into an active symbolic relationship with it". He also concludes that the functionality and external aspect of the objects are relatively marginal to their meaning: "again, it was not the design quality of the piece that made it special, but what the person did with it, and what the interaction meant to the person" (Csikszentmihalyi, 1991, pp. 27-28). As he could ascertain through hundreds of interviews, the isolated qualities of the artefacts, such as aesthetical, formal or syntactical, were rarely mentioned as important factors of affective relation by the surveyed. Donald Norman seems to reinforce that perspective underlining that "what matters is the history of the interaction, the associations that people have with the objects, and the memories they evoke" (Norman, 2004, p. 46).

ENGAGEMENT AND INTERACTION

How can the *meaning* and the *value qualities* endorse a significant experience by design? The meaning comes from the engagement level between human-human or human-object during an interactive communication process. The concept of interaction design is not restricted to technological context. It is a broad term and it could be applied to two models: between artefact/object (as man-machine interaction), and between person/human, "on how human beings relate to other human beings through the mediating influence of products" (Buchanan, 2001). As Diltey explains, this interactive process is the very essence of the experience: "interaction is what makes the very nature of experience" (Dilthey, cit. by Cruz, 2009). In order to access the content of the user experience, that is a subjective and immaterial phenomenon, researchers such as Paul Bate and Glenn Robert consider *storytelling* a fundamental methodology. As posted by these authors, the information that one experience can't be accessed and perceived in 'real time'. It is only when it is turned into the conscience, that is, when it is digested and translated through language by the person that lived that experience that "words put meaning on that experience reflectively and retrospectively, and represent 'what I make of what I have lived through'" (Bate & Robert, 2006, p. 308). Only through this awareness of the experience, in a flux of collaboration with the user, the designers can integrate crucial components into the project creation.

For instance, two projects resulted from the attention given to the moment when the experience occurs: (i) *Social cups*, by Kristina Niedderer in 1999; and (ii) *Come a little closer,* by Nina Farkache (Droog Design) in 2001. Both examples promote a conscientious disruption by drawing attention to social behaviours, particularly uncomfortable social experiences, which are questioned. Both projects base their 'meaning' and 'value' by challenging the user to reflect about their emotions. More than a physical object, within these approaches the result creates an opportunity to create critical awareness. The user voluntarily accepts to be part of the 'game'.

It is also important to examine what Donald Norman sees as requirements to achieve a *significant experience*. The author observes that in order to design a well-succeeded solution, it is fundamental to recognise two important components: the skill of the designer, and the skill of the perceiver (Norman, 2004). The skill of the designer is required to project something in a complex and rich structure – something that can provide a variety of levels of interpretation in a dynamic experience without causing boredom, being too easy and expected, nor frustration, being too difficult and hermetic. On the other hand, it is required the skill of the perceiver, who ought to dedicate time and availability to the observation and thought (reflexive level) about the lived experience. It is in this second argument that the author draws attention to the importance of the motivation and necessary commitment of the other to allow a process with meaning and true participation.

CONCLUSION

With this set of ideas in mind, we defend that contemporary design must be understood as a process and not an end in itself. Design turned into a medium that provides a certain context where people can *play* the game. Today's designers must develop not only skills in the relational communication process but also experience design methodologies, that allow them a careful interpretation of the user *meanings* and *values*, in order to engage people into an active symbolic relationship with the 'game'. It is relevant to reinforce that to be effective in conveying valuable meaning, it is not enough that people create things by themselves nor it is required that designers master isolated aspects. What is quite important is the "history of the interaction" (Norman, 2004) what actually happens to people in terms of perception and memory during the communicative moment. Understanding that the designer needs to recognise the experience as an activity to collaborate with the user, the designer will integrate important components in the project throughout the process of creating a product.

REFERENCES

Bate, P., & Robert, G. (2006). *Experience-based design: From redesigned the system around the patient to co-designing services with the patient*. (pp. 307-310). Consult. nov. 2008. Retrieved from http://qualitysafety.bmj.com/content/15/5/307.full

Buchanan, R. (2001). Design research and the new learning. In *Design Issues*. Cambridge: MIT Press, *17*(4), pp.3-23.

Cruz, M. T. (2009). From participatory art forms to interactive culture: Towards a critique of the aesthetic economy. *The International Journal of Arts in Society, 4*. Retrieved from http://www.cecl.com.pt/workingpapers/files/ed16_interactive_culture.pdf

Csikszentmihalyi, M. (2011). *TEDxUChicago 2011 - Mihaly Csikszentmihalyi - Rules of engagement.* Consult. 18 jun. 2014. Retrieved from https://www.youtube.com/watch?v=7e1xU0-h9Y8

Csikszentmihalyi, M. (2004). *Flow, the secret to happiness*. Consult. 13 ago. 2013. Retrieved from http://www.ted.com/talks/mihaly_csikszentmihalyi_on_flow

Csikszentmihalyi, M. (1991). Design and order in everyday life. *Design issues, 8*(1), pp.26-34. Consult. 29 out. 2009. Retrieved from http://www.jstor.org/stable/1511451

Csikszentmihalyi, M., & Halton, E. (1981). *The meaning of things : Domestic symbols and the self*. Cambridge: Cambridge University Press.

Niedderer, K. (2007). Designing mindful interaction: The Category of the performative object. *Design Issues*, *23*(1), pp. 3-17. Retrieved from http://www.mitpressjournals.org/doi/pdf/10.1162/desi.2007.23.1.3

Niedderer, K. (2004). *Designing the performative object: A Study in designing mindful interaction through artefacts*. (Doctoral disseration). University of Plymouth.

Norman, D. (2009, outubro 2). The Transmedia design challenge: Co-creation. *Don Norman: Design for people.* Retrieved from http://www.jnd.org/dn.mss/the_transmedia_design_challenge_co-creation.html

Norman, D. (2004). *Emotional design: Why we love (or hate) every day things*. New York: Basic Books.

PAPER REF: 131

VIRTUAL DESIGN FOR ASSEMBLY

Davide Seminerio[1], Gianni Caligiana[1], Giampiero Donnici[1], Daniela Francia[1 (*)], Leonardo Frizziero[1], Alfredo Liverani[1]

[1]Department of Industrial Engineering (DIN), University of Bologna, Bologna, Italy

[(*)]*Email:* d.francia@unibo.it

ABSTRACT

Since 1980, analysis techniques have been implemented with the aim to guide designers towards the creation of products, which are easy to produce and assemble. This led to a revolution in the manufacturing industry, resulting in reduced product costs, improved quality, shorter time to market, lower inventory, fewer suppliers and many other improvements. This is to emphasize, first of all, the importance of paying attention to manufacturing and assembly problems, already in the initial stages of product design.

For the assembly to be done as effectively as possible, Design for Assembly (DFA) gives guidelines to direct the designer and evaluation methods that estimate the effectiveness of a product in its assembly. This paper has the purpose of identifying the optimal assembly sequence of a pressure reducing valve, studying its assembly effectiveness starting from its virtual modelling by CAD.

Keywords: Design for Assembly, Virtual Modelling, Assembly Sequence, CAD.

INTRODUCTION

The traditional design approach that paid attention to the design and manufacturing of the single pieces and not to the assembly process has to be overcome in order to design optimization. The design optimization method applied in this paper aimed at evaluating the effectiveness of the assembly of a two ways pressure regulation valve. A virtual model of the valve has been designed that reproduced the real valve with appraised and tested structural properties (Caligiana, 2017). Virtual modelling is useful to develop a functional and reliable ergonomics, without having to build a model in real scale, to design products in agreement with the customer's preference, with the possibility of previewing testing, to facilitate remote operations and control of equipment (Rosario, 1989, De Amicis, 2018).

The design for assembly (DFA) application on the valve is possible only by giving DFA tools to the designer teams to effectively analyse the ease of assembly of the products or sub-assemblies that are being modelled. Of all the quantitative assessment techniques, the best known are those of Hitachi, Boothroyd-Dewhurst and Lucas (Boothroyd, 1980, Miyakawa, 1990, Kroll, 1988). All three have been tested in the industrial world. These techniques are evaluative methods that analyse the assembly of the products, at an early stage of the design process; although they use the same philosophy, they differ in the way they quantitatively evaluate the project.

At first, the evaluation of the three methods applied to the pressure reducing valve compared some parameters that described the assembly efficiency to the piece as it is actually on the market. Once this is done, an alternative model of the valve has been proposed, following the guidelines to improve the design for better assembly, subsequently checking whether or not there will be an improvement in the assembly indicators.

RESULTS AND CONCLUSIONS

The studies carried out on the assembly of the valve according to the three methods have led, in any case, to an estimate of the very good assembly efficiency; for this reason, the piece resulted difficult to improve from a purely assembly point of view.

However, from the application of the theories of Boothroyd-Dewhurst and Lucas it can be noted that the valve can be optimized, reducing the parts that are not indispensable to the function of the valve itself, which are those components that concern the regulation system.

The model tested provides for an overall reduction of the pieces, passing from eleven to eight components: the changes were made to the register screw; in addition, the M8 nut, the rosettes and the upper nut have been eliminated, giving way to a single M8 nut with a built-in washer.

All the three DFA's methods have been applied to the new simplified model and the best result has been evidenced by the Lucas' method's application, that evidenced a great improvement in design efficiency; this implicated the improvement of the remaining indexes, both in the feed ratio and in the insertion ratio, as shown in Table 1.

Table 1 –Comparison between the two valve's models by LUCAS method's application

Model	Design Efficiency	Feeding Handling Ratio	Fitting ratio
Original valve	58%	1.57	4.07
Optimised valve	87%	1.27	3.16

CAD reproduction of the two-way relief valve allowed to appreciate the enormous potential of 3D virtual modeling, that enables products to be checked and tested without having to resort to their immediate prototyping: this aspect is decisive in the Design for Assembly because it facilitates the study in the early stage of design, with savings on costs and time.

REFERENCES

Caligiana G, Liverani A, Francia D, Frizziero L. Mechanical device with five-arms tested on service. Far East Journal of Electronics and Communications. 2017, 17(2), p. 327-349.

Rosario L.M. and Knight W.A. Design for Assembly Analysis: Extraction of Features from a CAD System Database. Annals of CIRP, 1989, 38(1), p. 13.

De Amicis R, Ceruti A, Francia D, Frizziero L, Simões B. Augmented Reality for virtual user manual. Int. Journal on Interactive Design and Manufacturing. 2018, 12(2), p. 689-697.

Boothroyd G. Product Design for Assembly. Department of Mechanical Engineering. University of Massachusetts, Amherst, 1980.

Miyakawa S, Ohashi T and Iwata M. The Hitachi New Assemblability Evaluation Method (AEM). Trans. of the North American Manufacturing Research Institution of SME, May 23-25, 1990.

Kroll E, LenZ E and Wolberg J. R. A Knowledge-based Solution to the Design for Assembly Problem. I Manufacturing Review, 1988, 1 (2).

PAPER REF: 132

VIRTUAL DISASSEMBLY EFFICIENCY'S EVALUATION

Simone Ponti[1], Gianni Caligiana[1], Giampiero Donnici[1], Daniela Francia[1 (*)], Leonardo Frizziero[1], Alfredo Liverani[1]

[1]Department of Industrial Engineering (DIN), University of Bologna, Bologna, Italy

[(*)]*Email:* d.francia@unibo.it

ABSTRACT

The technological progress in the last years caused an exponential increasing of goods produced and consequently a reduction in the useful life due to the obsolescence of the systems; this led to the increase of old waste and machinery that can become a potential risk for the environment. As a result, policies have been implemented for the proper disposal of wastes through the dismantling of various disused devices; this requires a peculiar attention to manage materials and to design choices totally aimed at optimizing production. In this context, the design for disassembly (DfD) aims at dealing with the dismantling and minimization of the wastes already during the design phase in the EOL cycle of a product. The activity described in this paper aims at optimising the disassembly of a virtual gearbox, starting from its CAD model. Some methods proposed by literature have been applied and combined in order to define three comparable parameters that can give a quantification to the disassembly efficacy. These are the disassembly sequence, the time taken to disassemble the product and the number of tool changes necessary to complete the sequence.

Keywords: Design for Disassembly, Virtual Modelling, Disassembly Sequence, CAD.

INTRODUCTION

DfD considers the future need to disassemble a product for repair, refurbish or recycle. Optimizing the disassembly sequence of mechanical systems is very useful in order to improve maintenance and recycling activities and to reduce costs, times and number of operations. In this work a virtual model of a typical mechanical system has been designed in order to evaluate the optimal disassembly sequence, by the application of three different methods validated in literature. The virtual model of a gearbox reproduced the real tested structural properties of the product. (De Amicis, 2018, Caligiana, 2017). The optimal disassembly sequence has been discussed by seeking the best compromise between the time taken for disassembly and the operations performed. Three different paths have been compared in order to grasp the differences in their modus operandi and to evaluate their interaction with the work environment and with the geometry of the component. The starting sequence is mainly based on the experience of the designer. The generation of the other sequences is based on (Mitrouchev, 2015, and Jianjun, 2008). The calculation of the disassembly time follows the method suggested by (Desai, 2003) that estimates the disassembly time through assigning some points which will then be converted into seconds. Three sequences have been compared in terms of time consumed and of tools changes required.

RESULTS AND CONCLUSIONS

Four subgroups of the gearbox have been defined and a starting disassembly sequence has been calculated based on the experience of the designer; two further sequences follows the

Mitrouchev's and Jianjun's methods. The four subgroups shown in Fig.1 are: A (3-2-28-29-27-2-4), B (23-8-9-7-26-23-24), C (21-13-19-11-12-21-10) and D (33-32-16-15-17-18-14-13-31).

Fig. 1 – The subgroups of parts of the total gearbox

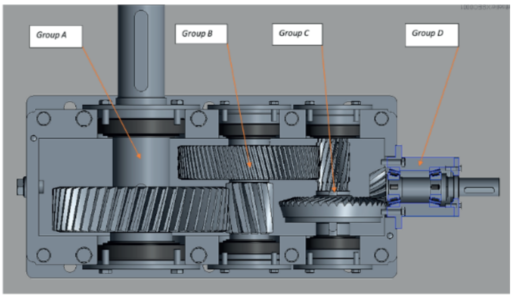

The disassembly sequences are collected in Table 1, as results about the time necessary to disassemble the gearbox and the number of tools' changes in the disassembly operations. The time taken to complete the disassembly have been calculated for each sequence. Also the tools changes required for each sequence has been calculated, because it influences the disassembly time as well.

Table 1 –The three methods' comparison for the optimal disassembly sequence

Method	Sequence	Time (min)	Tools changes
Designer	3-33-30-37-36-cop.A-5-42-6-25-34-39-35-38-39-40-45-20-22-gr.C-21-distB-19-11-12-21-10-gr.B-23-8-9-7-26-23-24-gr.A-2-28-29-27-2-4-16-32-15-17-18-14-13-14-31-41-43-44.	7.79	33
Mitrouchev	3-41-43-44-34-39-30-37-42-5-6-25-cop.A-36-gr.D-35-38-40-45-20-22-gr.A-gr.B-gr.C-1-2-28-29-27-4-23-8-9-7-26-23-24-21-dis.B-19-11-12-21-10-33-16-32-15-17-18-14-13-14-31	7.73	27
Jianjun	3-34-39-5-37-30-42-35-38-6-25-36-copA-gr.D-41-40-45-43-44-20-22grc-21-distB-19-11-12-21-10-grB-23-8-9-7-26-23-24-gr.A-2-28-29-27-2-4-33-16-32-15-17-18-14-13-14-31	7.78	32

As conclusion, the methodology described allowed to identify the best disassembly sequence, obtained through the Mitrouchev's method, as in terms of disassembly time as in terms of tools changes made. Such information can be strategic in the first stages of product development.

REFERENCES

De Amicis R, Ceruti A, Francia D, Frizziero L, Simões B. Augmented Reality for virtual user manual. Int. Journal on Interactive Design and Manufacturing. 2018, 12(2), p. 689-697.

Caligiana G, Liverani A, Francia D, Frizziero L. Mechanical device with five-arms tested on service. Far East Journal of Electronics and Communications. 2017, 17(2), p. 327-349.

Mitrouchev P, Wang C. G,.Lu L. X and Li G. Q. Selective disassembly sequence generation based on lowest level disassembly graph method. The International Journal of Advanced Manufacturing Technology, 2015, 80(1–4), p. 141–159.

Jianjun Y, Bin Y, Lei D, Chenggang L and Diqing H. International Journal of Advanced Manufacturing Technology 2008, 37(5), p. 599-604.

Desai A and Mital A. Evaluation of disassemblability to enable design for disassembly in mass production. International Journal of Industrial Ergonomics, 2003, 32(4), p.265-281.

PAPER REF: 133

THE COMPOSITE MATERIAL PROPERIES IN TECHNOLOGICAL SYSTEM MACHINE TOOL-CUTTING TOOL-WORKPIECE AND ENERGY EFFICIENCY

Zuzana Murčinková[1(*)], Jaromír Murčinko[2], Karol Vasilko[1]

[1]Faculty of Manufacturing Technologies with seat in Prešov, Technical University of Košice, Slovakia
[2]New Port Group, Lazaretská 23, 811 09 Bratislava
[(*)]*Email:* zuzana.murcinkova@tuke.sk

ABSTRACT

The paper presents the composites as a source of the energy efficiency improvement in the technological system machine tool-cutting tool-workpiece due to the fact that the cutting process is an energy-intensive process. Paper provides the experimental results of the damping properties measurement of composites and the analysis of energy consumption in terms of cutting conditions.

Keywords: lightweight factor, damping, friction coefficient, cutting process.

INTRODUCTION

The paper presents an idea of increasing the energy efficiency of a machine tool by means of decreasing the energetic losses by "inefficient" components and interfaces characterized by damping and friction as natural effects that can be minimized by use of composites and thin films. The main source of damping are the non-moving parts of machine tools (frames). Moreover, the weight of moving parts of machine tools is a main characteristic for energy saving. Furthermore, the low friction moving components interfaces minimizes the energy losses. The modern approaches for machine tool components designing are defined by use of composite material properties characterized by high damping and high natural frequency; large lightweight factor E/ρ (E is Young's modulus of elasticity, ρ density) typical properties of composites.

RESULTS AND CONCLUSIONS

The energy efficient components characterized by:

The large lightweight factor E/ρ of the moving parts. Our measurement showed that the energy efficient components are made of the composites such as the short carbon fiber ceramic composite C/SiC (Fig. 1, left) that is of the largest lightweight factor E/ρ and the shortest damping time comparing to standard materials (steel and aluminum alloy) and oxide ceramic Al_2O_3 (Murčinková Z., 2017). Moreover, the character of Fast Fourier Transformation spectrum without the sharp peaks predetermines, mainly short fiber composites, for dynamically loaded machine tool components (Murčinková Z., 2019).

High frequency and damped non-moving parts. As the factor E/ρ is large the natural frequency and damping properties are high. High frequency and damping (structural, material) of non-moving machine tool parts contribute to reduction of vibrations and stability of cutting process, Fig. 1, left. The vibrations as natural result of dynamic interaction between workpiece and machine tool are absorbed by machine frame or by energy absorbers to avoid the chatter.

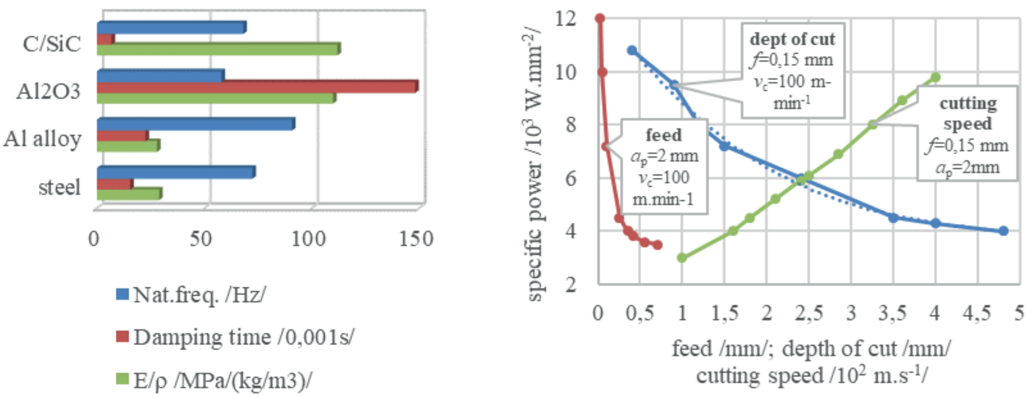

Fig. 1 – Some properties of materials (left) and specific power for turning (workpiece: steel C45; cutting tool sintered carbide P20 and coating TiC)

The low friction in interface interaction of individual components and sub-assemblies. A significant portion of the mechanical energy supplied to the cutting operation is consumed by frictional losses in range from 25-35% in the cutting zone (Vasilko, K., 2009). The coatings reduce cutting forces and provide longer tool life resulting in larger productivity and energy efficiency. The low friction coefficient (*f*) coatings (e.g. the diamond-like carbon (DLC) coatings: $f < 0{,}1$) improve the interface tribological conditions and decrease the amount of the generated heat. The application of nanocomposite coating with appropriate pre and post cutting edge preparation provides the energy saving up to 100% (Murčinková, Z. et al, 2017). The behavior on interface among individual coating layers and substrate is similar to behavior principles of fiber-matrix in composite.

The cutting process. It is an energy intensive process. The cutting process itself as direct interaction of cutting tool (its geometry and material) and material of workpiece can be source of energy reduction. There is even the independent from mechanical properties of machined material “force-free” cutting methods that are so called the “no-cutting tool” methods (laser, water jet, plasma etc.), however of very high energy consumption.

Fig. 1, right, shows a decrease in the consumed specific energy with an increase in both the depth of cut and the feed. This leads to a tendency to increase these parameters. However, there are the additional characteristics, such as machining accuracy, final surface quality and machining time.

ACKNOWLEDGMENTS

The authors would like to thank the Agency of Ministry of Education, Science, Research and Sport of the Slovak Republic for supporting this research (grant VEGA 1/0910/17).

REFERENCES

Murčinková Z, Kompiš V, Adamčík P, Dobrovič S, Murčinko J. Design of Fibrous Composite Materials for Saving Energy. In: Handbook of Composites from Renewable Materials: Volume 2: Design and Manufacturing. Beverly: Scrivener Publishing, 2017 P. 49-92.

Murčinková Z.Composite materials Micro and Macro Behaviour, Numerical Simulation and Experiment, Applications in Mechanical Engineering. Lüdenscheid: RAM-Verlag, 2018. p. 75.

Vasilko K. Teória a prax trieskového obrábania. COFIN, Prešov, 2009.

Murčinková Z, Vojtko I, Halapi M, Šebestová M. Damping properties of fibre composite and conventional materials measured by free damped vibration response. Advances in Mechanical Engineering, to be published.

PAPER REF: 134

CARBON-FIBRE/TITANIUM-MATRIX COMPOSITES: MICROSTRUCTURE AND MECHANICAL PROPERTIES

Sergei Mileiko*, Andrew Kolchin, Sergei Galyshev, Maxim Nikonovich, Viktor Kedrov
Institute of Solid State Physics of Russian Academy of Sciences, Chernogolovka, Russia
(*)*Email:* mileiko@issp.ac.ru

ABSTRACT

The paper describes the microstructure and mechanical properties of composites of the hierarchical microstructure *carbon fiber – titanium carbide layer – titanium containing eutectic - titanium*. Specific strength and Young's modulus values of such composites are much higher than those characteristics for metal alloys.

Keywords: fibrous composites, carbon fibre, titanium matrix, strength, Young's modulus.

INTRODUCTION

An effective reinforcing of a metal matrix with carbon fibres needs to use liquid metal fabrication route. Titanium alloys are most wanted matrix materials. However, direct contacting carbon fibre with molten titanium will lead to replacing carbon with titanium carbide and disappearing the strong reinforcement. An attempt to use an intermediate matrix, which has been Ti-Ti_5Si_3 eutectic, is known (Mileiko, 1995).

The Young's modulus of the composites obtained reached values 210 GPa, which was compatible with this characteristic of uni-direction GFRP containing high modules fibres (Mills, 1995). The composite density was just ~3.3 g/cm^3, and anisotropy of mechanical characteristic of all MMCs is much less than that of any FRP.

But the fabrication route developed that time did not allow controlling technological parameters sufficiently precisely. Hence, by now, the former fabrication technology has been modified to control the microstructure of the composites much more precisely. Here the microstructure, strength and fracture toughness of the composites are presented.

RESULTS AND CONCLUSIONS

The intermediate matrix in the present experiments was Ti-T_2Ni eutectic, the main matrix was titanium alloy VT1-0 (corresponds to ASTM Grade 2) with ultimate tensile strength between 350 and 500 MPa, the fibres of medium strength were produced by UMATEX.

The microstructure of the composites is presented in Fig.1, the non-brittle behavior of the composites is illustrated by load/displacement curve obtained in 3-point bending of a specimen. The critical stress intensity factor can be larger than 30 MPa·m$^{1/2}$.

The eutectic temperature in the Ti-T_2Ni system is about 950^{o}C, that allows to control temperature-time fabrication regimes to produce composites with a necessary thickness of the titanium carbide layer to affect the strength and elastic modulus values of the composites.

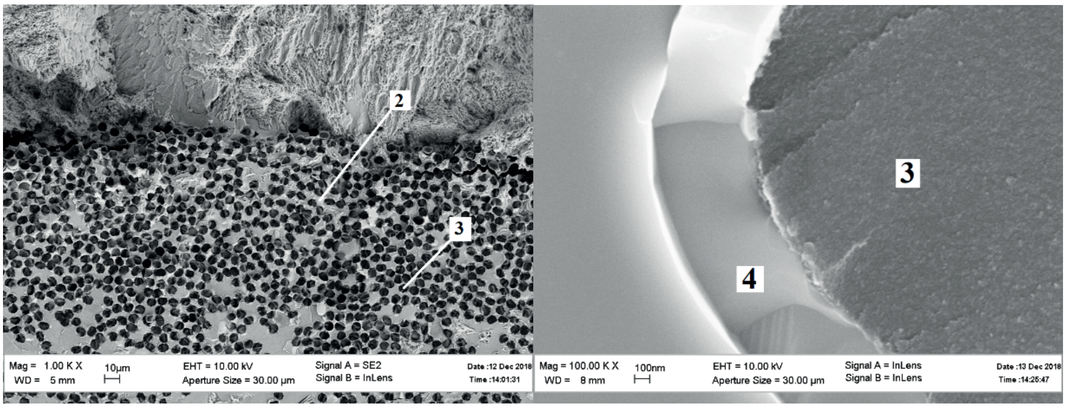

Fig. 1 – SEM micrographs of cross-sections of a composite specimen. 2: the intermediate matrix; 3: carbon fiber; 4: a layer of titanium carbide.

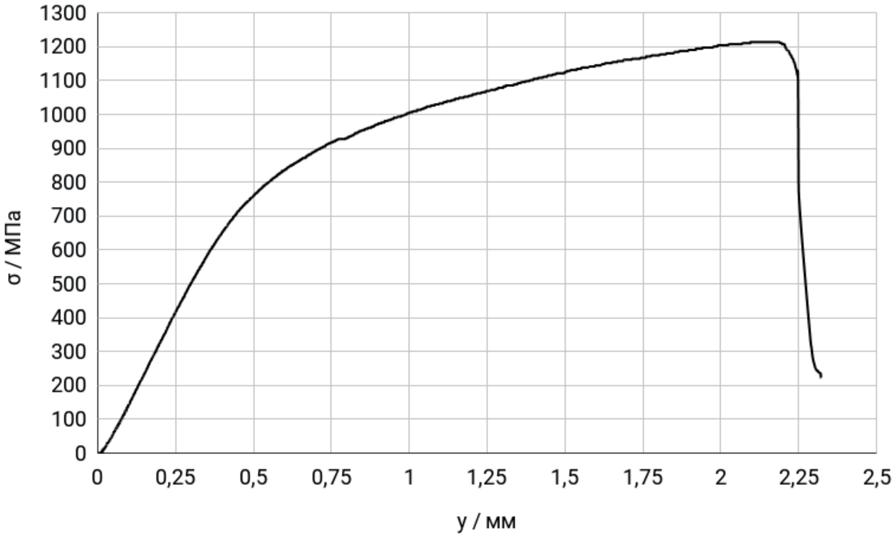

Fig. 2 – Stress/displacement curve of composite specimen tested in 3-point bending.

ACKNOWLEDGMENTS

The authors gratefully acknowledge the funding by Russian Foundation of Basic Research under grant 19-08-00804. A contribution to this work done by their colleagues Dr. AM Rudnev, Dr. NA Prokopenko, Mr VA Chmichev and Mr SA Abashkin is also acknowledged.

REFERENCES

Mileiko ST, Rudnev AM, Gelachov MV. Carbon-fibre/titanium-silicide-interphase/titanium-matrix composites - fabrication, structure and mechanical properties. Comp. Sci. and Technol, 1995, 55, p. 255-260.

Mills PJ, Smith PA. Carbon-fiber-reinforced plastics. In: Kelly A (ed) Concise Encyclopedia of Composite Materials. Elsevier, 1995, p. 43.

PAPER REF: 135

A NOVEL MICROSTRUCTURE OF OXIDE-FIBRE/MOLYBDENUM-MATRIX COMPOSITES

Andrew Kolchin, Nelly Prokopenko*, Olga Shakhlevich, Vyacheslav Prokopenko, Sergei Galyshev, Maxim Nikonovich, Sergei Mileiko

Institute of Solid State Physics of Russian Academy of Sciences, Chernogolovka, Russia

(*)*Email:* nelly@issp.ac.ru

ABSTRACT

The present mainstream in looking for metal-based heat resistant materials beyond nickel super-alloys is the developing of molybdenum alloys. The work, the results of which are to be presented at the conference, describes composites with oxide fibres and molybdenum alloy matrix similar to that under developing.

Keywords: composites, oxide fibre, molybdenum alloy matrix, high temperature strength, fracture toughness.

INTRODUCTION

Molybdenum alloys, which are now under developing, are strong and creep resistant. However, they are not sufficiently tough (Krueger, 2014; Moriyame, 2017). Oxide-fibre/molybdenum-matrix composites produced by the internal crystallization method (ICM) are characterized by high fracture toughness, but they are not sufficiently strong at temperatures above 1300^{o}C as a result of the usage of technically pure molybdenum that recrystallizes and lost its strength being heated up to a temperature of about 2000oC in the composite fabrication process (Mileiko, 2018). Hence, a method to introduce necessary phases into molybdenum matrix to be used in the ICM has been now developed and is to be described in the present paper.

RESULTS AND CONCLUSIONS

The ICM includes a stage of preparing the molybdenum matrix by diffusion bonding a set of molybdenum foil and wire to form continuous channels in the future matrix to be filled by oxides at the next stage of the fabrication process.

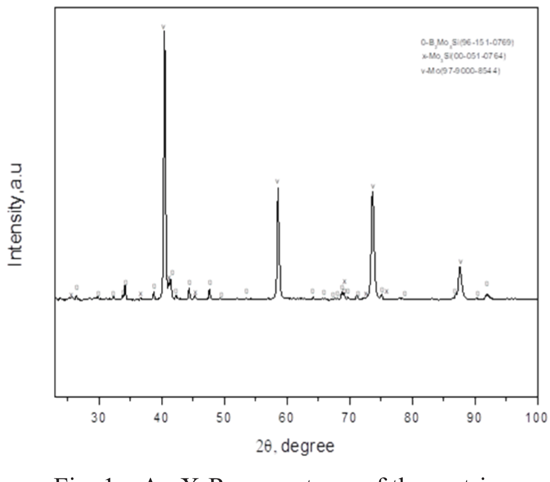

Fig. 1 – An X-Ray spectrum of the matrix.

At the present time, the ICM has been modified by introducing silicon and boron via a slurry containing those elements at the stage of preparing an assemblage of foil and wire. A heat treatment of the assemblage after diffusion bonding yields the molybdenum containing silicides and Mo_5SiB_2 phase, see Fig. 1.

Hardening molybdenum matrix in such a way leads to the oxide/molybdenum composites that have high temperature strength higher than those with pure molybdenum matrix (Fig. 2). The critical stress intensity factor for the composite specimens (Fig. 3) reaches values 15-17 MPa·m$^{1/2}$.

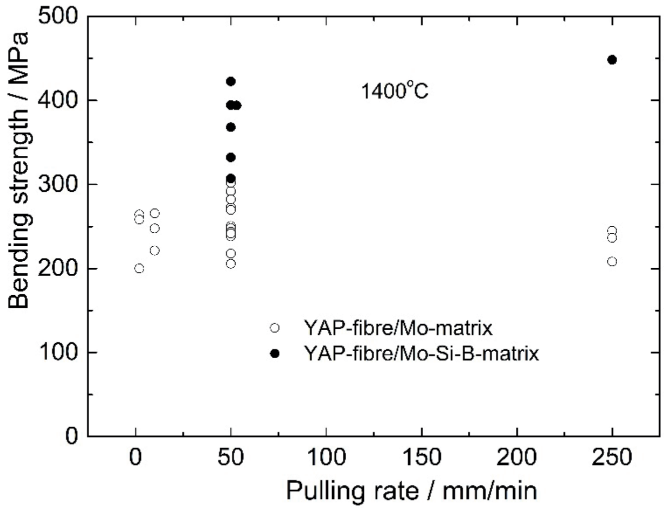

Fig. 2 – Strength at 1400°C of the composites with $YAlO_3$-based fibre and two types of the matrix versus crystallization rate of the fibre.

Fig. 3 – A composite specimen under testing to measure critical stress intensity factor.

ACKNOWLEDGMENTS

The authors gratefully acknowledge the funding by Russian Science Foundation, Project 16-19-10624. Also, they are thankful to Mr. S.A. Abashkin, Mr. V.A. Chumichev and Mrs. S.I. Kachurina for their help in the experiments.

REFERENCES

Krüger M, Jain P, Kumar KS, Heilmaier M. Correlation between microstructure and properties of fine grained Mo-Mo_3Si-Mo_5SiB_2 alloys. Intermetallics, 2014, 48, p. 10-18.

Mileiko ST, Chumichev VA. Mullite-zirconia-fibre/molybdenum-matrix composites: Strength and damage tolerance. Composites Part A, 2018, 112, p. 365-370.

Moriyama T, Yoshimi K, Zhao M, Masnou T, Yokoyama T, Nakamura J, Katsui H, Goto T. Room-temperature fracture toughness of MoSiBTiC alloys. Intermetallics, 2017, 84, p. 92-102

PAPER REF: 136

DESIGN OF A ROBOTIC TORQUE HANDLE FOR ORTHOPEDIC HAPTIC SIMULATION

Trevor Cotter[1(*)], Michael Grizenko-Vida[1], Mark Driscoll, PhD[1]

[1]Department of Mechanical Engineering, McGill University, Montreal, Canada
[(*)]*Email:* trevor.cotter@mail.mcgill.ca

ABSTRACT

This work addresses the current lack of robotic haptic torque devices in virtual reality and augmented reality (VR/AR) surgical training platforms. A torque handle that can augment existing haptic force devices has been designed to produce up to 3N-m of continuous torque at 38rpm. This device will be used to expand the scope and perceived realism of haptic simulation for orthopedic surgery.

Keywords: haptics, robotics, surgery, orthopedics, simulation

INTRODUCTION

To combat complications in medical procedures, simulators have been designed to train medical professionals. This technology incorporates haptic, or touch, feedback so that a virtual patient feels the same as an actual subject. This has been studied extensively in neurosurgery with haptic forces, but not with haptic torque feedback (Alotaibi, 2015; Holloway, 2015; Sawaya, 2017). Work has been done to measure torque during surgery, but it has not yet been adapted for haptic training platforms (Georgilas, 2018).

A target torque of 3N-m was established to mimic common orthopaedic load profiles. Tools used in orthopaedic torqueing applications with a minimum handle diameter of 28mm were identified. An Entact Robotics (Toronto, Canada) W3D device was chosen, which has existing hardware capacity to power a motor with 3A of continuous (6A peak) current. A Maxon (Sachseln, Switzerland) motor and gearbox was used to generate torque.

RESULTS AND CONCLUSIONS

The layout of the final torque handle design is shown in Figure 1. It consists of a motor (Maxon DCX Series 22W, 24V, 26mm OD), 3-stage planetary gearbox (Maxon 62:1 reduction), and 12 wire MOFLON slipring (Shenzhen, China) to accommodate the power and load-side encoders. The handle, which matches an existing orthopedic device, is bolted over the motor to secure and cover it. A sleeve (not shown in Figure 1) conceals the extending components for aesthetic purposes.

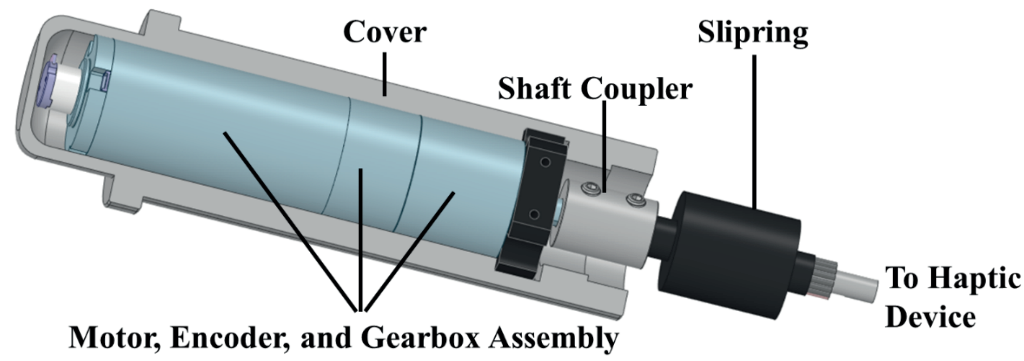

Figure 1 Diagram showing the hardware components of the haptic torque handle

This project shows robotic torque devices for haptic simulation can be designed for use with an existing haptic device to generate torques found in many orthopedic procedures. This technology can be adapted and modified for future application within orthopedic simulation and beyond.

ACKNOWLEDGMENTS

The authors thank the Natural Sciences and Engineering Research Council of Canada (NSERC) and Quebec Consortium for Industrial Research and Innovation in Medical Technology (MEDTEQ) as well as CAE Healthcare (Montreal, Canada) and DePuy Synthes Companies (Raynham, USA) for their research grant support. Entact Robotics is also acknowledged for their technical support.

REFERENCES

Alotaibi FE, AlZhrani GA, Sabbagh AJ, Azarnoush H, Winkler-Schwartz A, Del Maestro RF. Neurosurgical Assessment of Metrics Including Judgment and Dexterity Using the Virtual Reality Simulator NeuroTouch (NAJD Metrics). Surg Innov. 2015;22(6):636-642. doi:10.1177/1553350615579729

Georgilas I, Dagnino G, Tarassoli P, Atkins R, Dogramadzi S. Robot-Assisted Fracture Surgery: Surgical Requirements and System Design. In: Conference: 15th Annual Meeting Of The International Society For Computer Assisted Orthopaedic Surgery, CAOS 2015, At Vancouver, CA. Vol 46. Vancouver; 2018:1637-1649. doi:10.1007/s10439-018-2005-y

Holloway T, Lorsch ZS, Chary MA, et al. Operator experience determines performance in a simulated computer-based brain tumor resection task. Int J Comput Assist Radiol Surg. 2015;10(11):1853-1862. doi:10.1007/s11548-015-1160-y

Sawaya R, Bugdadi A, Azarnoush H, et al. Virtual Reality Tumor Resection: The Force Pyramid Approach. Oper Neurosurg. 2017. doi:10.1093/ons/opx189

PAPER REF: 137

IMPLEMENTING "QUICK-WINS" IN LEAN MANAGEMENT A CASE STUDY

Jorge Rodrigues[1], Jose Carlos Sá[1,2(*)], Francisco J. G. Silva[1], Luís Pinto Ferreira[1], Teresa Pereira[1],

[1]Department of Mechanical Engineering, School of Engineering, Polytechnic of Porto, Porto, Portugal
[2]School of Business Sciences, Polytechnic Institute of Viana do Castelo, Valença, Portugal
(*)*Email:* cvs@isep.ipp.pt

ABSTRACT

This study was undertaken at a Small and Medium-sized Enterprise (SME) in the metalworking sector, where Lean Management has been implemented through several Lean Tools (LT) and their variations. This study comprised two main goals. The first involved demonstrating which LT allow the highest impact during the implementation phase, thus producing great influence both in terms of organization and operational results, as well as in the context of employees' motivation. The second goal consisted of introducing procedure changes based on the Management of Human Resources through Lean Leadership tools.

By implementing these two objectives, one was able to achieve an increase of 8,5% in machine occupancy rate, and a reduction of 27,9% regarding the costs of defective products per hour.

***Keywords*:** Management by Objectives; KPI; Daily Kaizen; Visual Management; PDCA; 5S; 5 Whys; Yokoten; Brainstorming.

INTRODUCTION

During the months of November and December 2018, all the relevant existing data pertaining to the machining area of metalworking industry was compiled and analyzed. It was then divided into three categories: a) Adjustment to the area of manufacture/equipment; b) Management records and data; c) Lean Leadership.

By considering the tangible validation-worthy KPI, the project was set on two pillars: 1) the Production Rate; and 2) the Relation between Non-Quality/Production Hours. One then selected ten tools (Lean and Quality), the results of which would generate great impact within a 3-month period and in association with employees. The chosen tools allowed for changes in processes, manufacturing methods and cooperative management. After analyzing scientific articles and determining the company's stage of maturity, the following tools were selected for implementation: (1) Management by Objectives/SMART Objectives – Each worker's objectives were controlled weekly (2) KPI – A more generalized concept was transmitted to the entire company and its staff; (3) Daily Kaizen – besides being implemented in the production areas, it was also applied to cells; (4) Visual Management – reformulated to include cells; (5) PDCA – tool used in daily Kaizen to progress in problem solving; (6) Gemba Walk – the process was made to include the entire hierarchy, including the CEO; (7) 5S – introduction of the first 3 S to enable organizing spaces; (8) The "5 Whys"- to address the production of NCs (Non-Conformities) which require more complex solutions; (9) Yokoten: used to disseminate actions taken in the "5 Whys" throughout the area of manufacture; (10) Brainstorming – working with cell operators to find proposals for continuous improvement.

RESULTS AND CONCLUSIONS

After the implementation of the ten tools, the measurement of results have proven that some of the tools can be implemented effortlessly and rapidly. Since they are easily understood by workers and are managed by lean leadership tools, the operational results were highly positive, both in the occupancy rate of 8.5% (see Table 1) of machines, which was achieved in 3 months, as well as in the considerable increase of worked hours. Consequently, the relation of costs associated to non-quality per hours decreased significantly by 27.9% (see Table 2).

Table 1 –Productivity Rate

Productivity Rate	Average 2018	Goal for 1st Trimester 2019 (+5%)	Goal of 1st trimester 2019
Cell 1	56.5%	61.5%	64.2% **(+7.7%)**
Cell 2	56.1%	61.1%	66.3% **(+10.2%)**
Cell 3	54.6%	59.6%	64.8% **(+10.2%)**
Cell 4	43.5%	48.5%	49.5% **(+6.0%)**
Factory Average	52.7%	57.7%	61.2% **(+8.5%)**

Table 2 – Costs of Non Quality (NQ)/Production Hours

Costs of NQ / Production Hours	Average 2018	Goal for 1st Trimester 2019 (-10%)	Result of the 1st Trimester 2019
Manufacturing Area	0.61	0.55	0.44 **(-27,9%)**

REFERENCES

Alkhoraif, Abdullah; Rashid, Hamad; McLaughlin, Patrick. Implementing lean manufacturing principle in an automobile valve manufacturing industry with simulation analysis – a case study. DLSU Business & Economics Review. Jul2018, Vol. 28 Issue 1, p176-188. 13p.

J. C. Sá and J. Oliveira, "Generating Value With TQM and Six Sigma" in IRF2013 – 4th International Conference on Integrity, Reliability and Failure, Portugal, Madeira, (2013) 59-760.

J. Oliveira, J. C. Sá, A. Fernandes, "Continuous improvement through "Lean Tools" – An application in a mechanical company", Procedia Manufacturing 13 (2017) 1082-1089.

Li Zhu; Charlotta Johnsson; Martina Varisco; Massimiliano M.Schiraldi. Key performance indicators for manufacturing operations management – gap analysis between process industrial needs and ISO 22400 standard. Procedia Manufacturing Volume 25, 2018, Pages 82-88

Mudhafar Alefari; Konstantinos Salonitis; Yuchun Xu. The Role of Leadership in Implementing Lean Manufacturing. Elsevier B.V. Procedia CIRP, Volume 63, 2017, Pages 756-761

PAPER REF: 138

MATHEMATICAL MODELLING OF BLOOD FLOW WITH MAGNETIC NANOPARTICLES AS CARRIER FOR TARGETED DRUG DELIVERY IN A STENOSED ARTERY

Sreeparna Majee[1(*)], **G.C. Shit**[1]

[1]Department of Mathematics, Jadavpur University, Kolkata, India
[(*)]*Email:* sreeparnamajee@gmail.com

ABSTRACT

A systematic study on targeted drug delivery is carried out in an unsteady flow of blood infused with magnetic nanoparticles with an aim to understand the flow pattern and nanoparticle aggregation in a diseased arterial segment having stenosis. The magnetic NPs are supervised by magnetic field which is significant for therapeutic treatment of arterial diseases, tumor and cancer cells, and removing blood clots. Coupled thermal energy have also been analyzed by considering dissipation of energy because of the application of magnetic field and the viscosity of blood. Simulation technique used to solve the mathematical model is vorticity-streamfunction formulations in the diseased artery. An elevation in SLP (Specific loss power) is noted in the aortic blood stream when the agglomeration of nanoparticles is higher. This phenomenon has potential application in the treatment of hyperthermia. The study focuses on the lowering of WSS with increasing particle concentration at the downstream of the stenosis which depicts the vigorous flow circulation zone. This low shear stress regions prolong the residing time of the nanoparticles carrying drugs which soaks up the LDL deposition.

Keywords: Magnetic nanoparticles, Blood flow, Atherosclerosis, Hyperthermia

INTRODUCTION

Targeted drug delivery is a mechanism of delivering medication to an affected organism in a pattern that enhances the aggregation of the medication in the targeted tissue in cellular or subcellular level. The medium of delivery of drugs is largely dependent on nanomedicine, which employs nanoparticles, loaded with drugs and targeted to specific parts of the body where the disease persists, thereby avoiding interaction with healthy tissue. The significance of the targeted drug delivery system has an aim to confine, protract and a protected drug interaction with the diseased tissue. The targeted release system is primarily effective for minimizing the frequency of the drug dosages taken by the patient and its fluctuation in drug level. This method acts as a therapeutic agent for a prolonged period of time to a targeted diseased area within the body and prevents damage to the healthy tissue due to the drug inclusion. Several scientists are currently interested in the targeted drug delivery system due to its benefits towards capturing efficiency in the target area. Magnetically controlled drug targeting is the most widely used in drug delivery system, which combines drugs and ferromagnetic liquids to affect the target area.

RESULTS AND CONCLUSIONS

The results from Fig. 13 show the variation of dimensionless wall shear stress (skin-friction) along the length of the arterial segment with varying concentration of nanoparticles in the blood stream. It is observed that at the throat, wall shear stress increases and grows to a peak and falls sharply at the downstream of the stenosis. At the throat of the stenosis, wall shear stress increases with increasing concentration but the opposite trend is followed from the immediate downstream of the stenosis. In this figure, we have compared the shear stress with infused magnetic nanoparticles and no nanoparticles in the blood stream. The shear stresses in both cases have similar profile which shows that infusion of magnetic nanoparticles in the arteries does not cause any abnormalities in the flow behaviour. Moreover, the region of negative shear stress shows the radius of flow circulation eddies. This low shear stress regions have pathological significance and increasing concentration prolong the residing time of blood constituents that eventually flows into the arterial wall, which may cure the arterial disease.

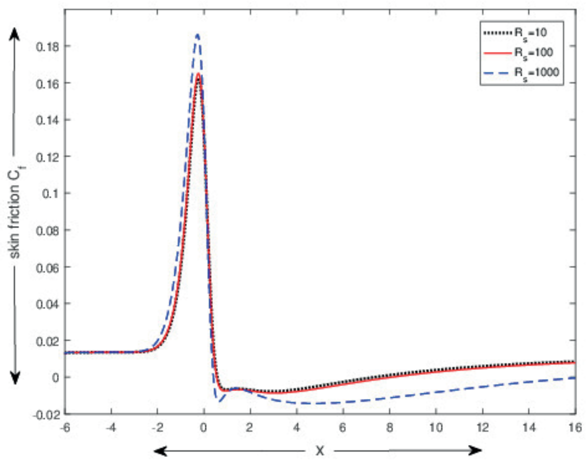

Fig. 1 - Result

ACKNOWLEDGMENTS

The authors gratefully acknowledge the funding by INSPIRE, Department of Science and Technology, India.

REFERENCES

E.P. Furlani, Magnetic Biotransport: Analysis and Applications, Materials 3 (2010) 2412-2446.

Q. Cao, X. Han, L. Li, Enhancement of the efficiency of magnetic targeting for drug delivery: development and evaluation of magnet system, J. Magn. Magn. Mater, 323 (2011) 1919-1924.

C. Kumar, F. Mohammad, Magnetic nanoparticles for Hyperthermia- Based therapy and controlled drug delivery, Adv. Drug Delivery Rev. 63 (2011) 789-808.

PAPER REF: 139

NUMERICAL ANALYSIS OF THE INFLUENCE OF REINFORCEMENT STRUCTURE ON THE DYNAMIC STRENGTH OF COMPOSITE CYLINDRICAL SHELLS

Nikolay Abrosimov[1], Nadezhda Novoseltseva[1], Francesco Dell'Isola[1(*)], Leonid Igumnov[1]

[1]Research Institute for Mechanics, National Research Lobachevsky State University of Nizhny Novgorod, Nizhny Novgorod, Russian Federation

(*)Email: abrosimov@mech.unn.ru

ABSTRACT

A technique of numerical analysis of the influence of reinforcement structure on the nature of the dynamic response and the process of layer-by-layer destruction of fiberglass cylindrical shells under an axisymmetric pulse loading is elaborated.

Keywords: composite materials, cylindrical shells, strength, numerical methods, pulse loading.

INTRODUCTION

An ever-increasing application of composite materials in creating structures of modern engineering stipulates a considerable interest in the study of specific features of their dynamic behavior and strength. In particular, composite materials are rather promising for protective load-carrying shells of chemical and nuclear reactors, designed to preserve their serviceability both in nominal operating modes and in emergency situations, accompanied by a sharp increase in impacts on the load-bearing elements. The basic load-bearing elements of such protective structures are, as a rule, composite cylindrical shells. The necessity to retain the serviceability of such structures subjected to intense pulse loadings imposes more stringent requirements on the models and the methods used for determining their strength, so that the calculation models could describe the simulated real processes more completely and comprehensively. The above-mentioned factors make it possible to conclude that investigation into dynamic response and strength of the pulse-loaded layered composite cylindrical shells based on the models describing both longitudinal and transverse wave processes in the composite material with a required accuracy are very topical. The kinematic model of deformation of a layered package is based on the non-classical theory of shells. An energetically consistent resolving system of the equations of the dynamics of composite cylindrical shells is obtained by minimizing the functional of total energy of the shell as a three-dimensional body. The numerical method for solving the formulated initial boundary-value problem is based on an explicit variational-difference scheme [1].

RESULTS AND CONCLUSION

The reliability and accuracy of the method considered was verified by comparing numerical calculations with experimental data [2] for a single loading of a cylindrical shell with free ends from inside by a pressure pulse induced by the burst of an explosive charge in its geometric center. Specific features of destruction of the shells with various reinforcement structures can be traced by analyzing their deformed configurations just before their failure, which are presented in Figure 1.

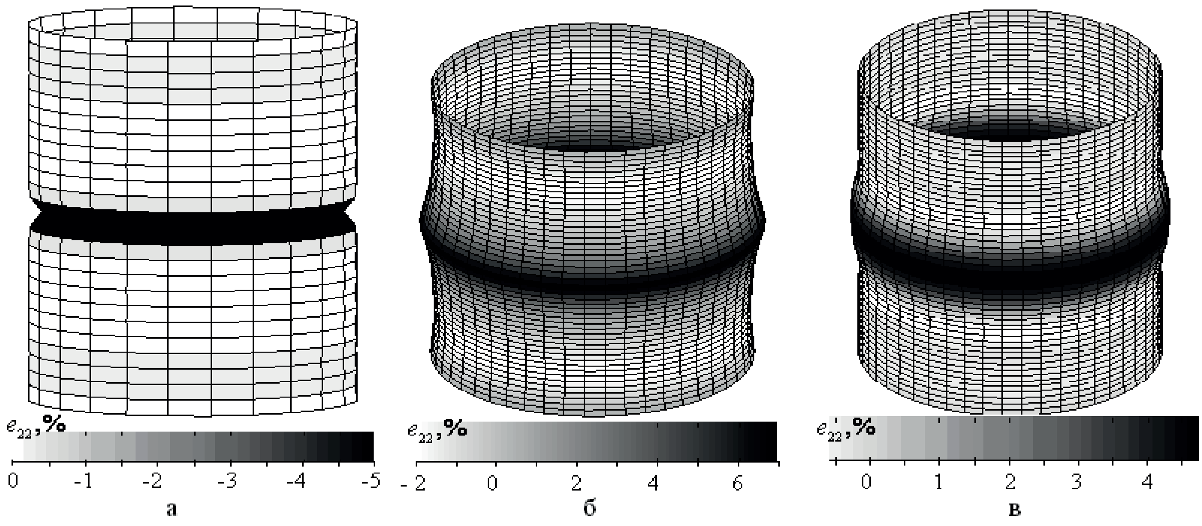

a) b) c)

Figure 1. Deformed configurations of shells with a circular (a), spiral (b), and combined reinforcement (c). The background here shows the intensity of circumferential strains.

In shells of the first type, their generatrix remained practically rectilinear, with a sharp crease in the central section. The shells of the second type are barrel-shaped, repeating the development along the generatrix of the pulse acting on the shell. The shells of the third type take a corrugated shape along the generatrix with a higher value of the corrugation in the central zone. It should be noted that the described scenario of numerical modeling of the process of layer-by-layer destruction of composite cylindrical shells with different reinforcement structures agrees well with experimental data [2].

ACKNOWLEDGMENTS

The development of the deformation model was financially supported by a grant from the Government of the Russian Federation (contract №14.Y26.31.0031), the development of failure model was financially supported by a grant of the Russian Science Foundation (16-19-10237-P).

REFERENCES

N.A. Abrosimov, V. G. Bazhenov, Nonlinear Problems of Dynamics of Composite Structures [in Russian], Izd. NNGU, N. Novgorod, 2002. p. 400.

A.G. Fedorenko, M.A. Syrunin, A.G. Ivanov Effect of the structure of reinforcement of oriented glass plastics on the strength of circular cylindrical shells in internal explosive loading // Mech. Comp. Mater. 1991. – № 4. p. 631-640.

PAPER REF: 140

NUMERICAL SIMULATION OF CRACK PROPAGATION IN A NOTCHED SPECIMEN UNDER CREEP CONDITIONS

Vasilii Gorokhov[1(*)], Sergey Kapustin[1], Yuriy Churilov[1], Svetlana Litvinchuk[1], Aleksandr Ipatov[1]

[1]Research Institute for Mechanics, National Research Lobachevsky State University of Nizhny Novgorod, Nizhny Novgorod, Russian Federation

[(*)]*Email:* vas-gor@rambler.ru

ABSTRACT

Numerical methods of research of processes of destruction of structures in the framework of the relations of mechanics of the damaged medium, enabling the analysis of behavior of structures, taking into account characteristics of processes of destruction, as at the initial generation stage and at the final stage of development of cracks. The results of the numerical study of the patterns of occurrence and development of cracks in a cylindrical sample with a concentrator at axial tension under high-temperature creep under the assumption of the viscous nature of the sample fracture are presented on the basis of the proposed technique.

Keywords: creep, mechanics of damaged medium, damage accumulation, fracture, stress concentrator, crack, finite element method.

INTRODUCTION

In the middle of the last century, the foundations of the approach of mechanics of the damaged medium to the description of creep and fracture processes were laid, in which a damage parameter was introduced, describing the state of the material from initially unbroken to completely destroyed (Rabotnov Yu. N., 1966; Kachanov L. M., 1974).

Modern approaches to solving structural strength problems are most widely used methods of linear and nonlinear fracture mechanics, engaged in the study of the final stage of destruction – the propagation of the main crack. Much less attention is paid to the study of the initial period of destruction associated with the accumulation of damage.

RESULTS AND CONCLUSIONS

In this paper, the study of the processes of elastic-viscoplastic deformation and destruction of structural materials is carried out on the basis of a composite hierarchical model of the damaged material in the framework of the relations of mechanics of the damaged medium (Kapustin S. A., 2015). To describe the processes of irreversible deformation of the material, a model of thermoplasticity with combined hardening and a flow-type thermal creep model based on the hypothesis of the existence of a creep surface and the gradient of the creep strain rate vector to it are used (Kapustin S. A., 2008). The process of origin and development of cracks in the structural element is modeled as follows. In the process of step-by-step solution of the problem in certain areas of the material structure can be born and develop damage zones, the intensity of which is characterized by a measure of damage ω. An increase in the measure in the physical node of the structure leads to a decrease in the elastic characteristics of the material and, thus, to a decrease in the resistance to deformation and redistribution of stresses in the volume of the material. By the time the limit value is reached in the node $\omega=\omega_f$, the material in the area of such a node ceases to resist further deformation, redistributing the previously perceived load on the nearest physical nodes. In the process of further development of damage destroyed are the following nodes. In this case, the interpolation of damage functions between adjacent destroyed nodes forms a line $\omega=\omega_f$, which corresponds to the trajectory of the fracture under study.

With the help of the developed methodological and software, a numerical study of the patterns of cracks in the sample with a concentrator under axial tension at a temperature of T=850ºC. In Fig.1 the dependences of the crack length *l* on the holding time *t* for different levels of tensile stresses are presented. In the figure, the number in the graph corresponds to the considered variant of the load level (in MPa).

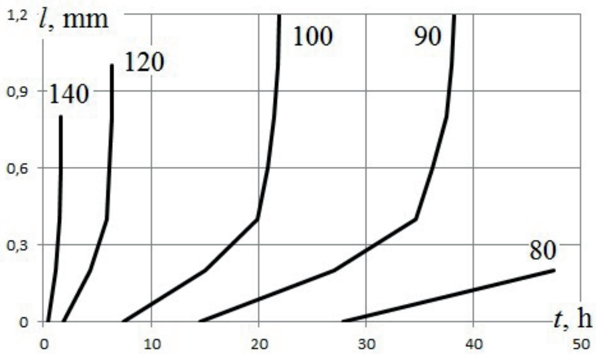

Fig. 1 - Crack length for different levels of tensile stresses

Also was obtained the dependence of the results of the calculations from the parameters of the FE-discretization of the sample in the center of the trajectory of the propagation of cracks.

ACKNOWLEDGMENTS

This work was supported by a grant from the Government of the Russian Federation (contract No. 14.Y26.31.0031)

REFERENCES

Kachanov L.M. Osnovy mekhaniki razrusheniya (in Rus.), Moscow, Nauka, 1974, 312 p.

Kapustin S.A., Kazakov D.A., Churilov Yu.A., Galushenko A.I., Vahterov A.M.. Eksperimentalno-teoreticheskoe izucheniye povedeniya izdeliy iz zharoprochnogo splava v usloviyah vysokotemperaturnoy polzuchesti (in Rus.), Problemy prochnosti i plastichnosti, 2008, 70, p. 98-108.

Kapustin S.A., Churilov Yu.A., Gorohov V.A. Modelirovanie nelineynogo deformirovaniya i razrusheniya konstrukciy v usloviyah mnogofaktornyh vozdeystviy na osnove MKE (in Rus.),Nizhniy Novgorod: Izd-vo Nizhegorodskogo gosuniversiteta im. N.I. Lobachevskogo, 2015, 347 p.

Rabotnov Yu.N. Polzuchest ehlementov konstrukciy (in Rus.), Moscow, Nauka, 1966, 752 p.

PAPER REF: 141

EXPERIMENTAL AND THEORETICAL STUDY OF THE DEFORMATION OF STAINLESS STEEL UNDER SOFT CYCLIC LOADING

Vasilii Gorokhov[1(*)], Sergey Kapustin[1], Yuriy Churilov[1], Dmitry Kazakov[1], Dmitry Zhegalov[1], Igor Vorobtsov[1]

[1]Research Institute for Mechanics, National Research Lobachevsky State University of Nizhny Novgorod, Nizhny Novgorod, Russian Federation
[(*)]*Email:* vas-gor@rambler.ru

ABSTRACT

A variant of the plasticity model is proposed, which allows describing the kinetics of plastic deformation of materials under different modes of low-cycle loading. In the model, the yield surface radius is represented as a function of temperature-dependent and accumulated plastic deformation, and the center coordinates are described by two evolutionary Armstrong-Frederick-Kadashevich Equations (Amstrong P. J., Frederick C. O., 1966; Kadashevich Yu.I., 1967), the first of which additionally introduced corrective material functions. Obtaining material functions of the model and checking its performance were carried out on the basis of the results of experimental study of the deformation process of a cylindrical sample under mild cyclic loading with control of the maximum and minimum values of forces in the cycle.

Keywords: Plasticity, soft loading, low-cycle deformation, yield surface, back stresses, numerical simulation, experiment.

INTRODUCTION

It was previously established (Bondar V. S., 2017) that the variants of plasticity models proposed in (Kapustin S. A., 2015) do not allow to correctly describe the quantitative dependence of the displacement and the change in the width of the plastic deformation loop on the number of cycles under soft cyclic loading. Other plasticity models (Chaboche J.-L., 2008; Bondar V. S., 2017) satisfactorily describe the displacement patterns of the plastic deformation loop. However, information on the possibility of describing the width of the plastic hysteresis loop kinetics within these models, which actually determine the cyclic component of the fracture energy, is practically absent.

RESULTS AND CONCLUSIONS

In the proposed version of the model, the radius of the flow surface C_p is represented as a function depending on the temperature T and the accumulated plastic deformation k_p. Back stresses are the sum of two types of back stresses, described by Armstrong-Frederick-Kadashevich-type evolutionary equations with additionally introduced corrective material functions. For certain values of the correction functions from the relations of the proposed model, it is possible to obtain a variant of the Bondar model relations without taking into account the back stresses of the third type and a variant of the Chaboche model with two Armstrong-Frederick-Kadashevich equations. The experiments were carried out on the Amsler HA 100 servo-hydraulic fatigue strength testing unit.

Obtaining the material parameters of the model and testing its performance were carried out on the basis of the results of an experimental study of the sample deformation process, made of 12X18H10T type material, with a cylindrical working part, under conditions of soft cyclic loading with control of the maximum and minimum forces in the cycle. In Fig. 1 shows a graph of the magnitude of the total deformations in the cycle $h(n)$ versus the number of cycles n. The results of numerical simulation are indicated in the figure by solid lines, the experimental results are shown by dots.

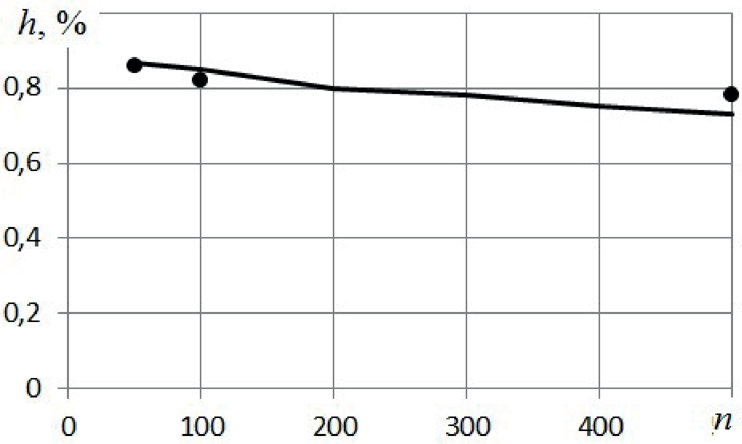

Fig. 1 - Magnitude of the total deformations in the cycle

The results show that the proposed model allows to describe well enough the main effects of plastic deformation of the material under soft asymmetric loading at n<500 cycles.

ACKNOWLEDGMENTS

This work was supported by a grant of the Russian Science Foundation (16-19-10237-P).

REFERENCES

Armstrong P.J., Frederick C.O. A mathematical represention of the multiaxial bauscinger effect. CEGB Report No. RD/B/N/ 731. 1966.

Bondar V.S., Abashev D.R., Petrov V.K. Comparative analysis of variants of plasticity theories under cyclic loading. PNRPU Mechanics Bulletin, 2017, no. 2, p. 23–44.

Chaboche J.-L. A review of some plasticity and viscoplasticity constitutive theories. Int. J. of Plasticity, 2008, 24. p. 1642–1692.

Kadashevich Yu.I. O razlichnykh tenzorno-lineynykh sootnosheniyakh v teorii plastichnosti (in Rus.), Issledovaniya po uprugosti i plastichnosti, Leningrad, Izd-vo LGU, 1967, 6, p. 3–-45.

Kapustin S.A., Churilov Yu.A., Gorohov V.A. Modelirovanie nelineynogo deformirovaniya i razrusheniya konstrukciy v usloviyah mnogofaktornyh vozdeystviy na osnove MKE (in Rus.),Nizhniy Novgorod: Izd-vo Nizhegorodskogo gosuniversiteta im. N.I. Lobachevskogo, 2015, 347 p.

PAPER REF: 142

METHODOLOGICAL APPROACH OF MAINTENANCE MANAGEMENT APPLIED TO A RESEARCH LABORATORY FOR COST REDUCTION

Teresa Morgado[1,2,3(*)], **Gilberto Santos**[4]

[1] UNIDEMI - Research and Development Unit for Mechanical and Industrial Engineering, FCT NOVA - Faculty of Science and Technology, Universidade Nova de Lisboa, Lisboa, Portugal

[2] LNEC – Laboratório Nacional de Engenharia Civil, Lisboa, Portugal

[3] IPT – Polytechnic Institute of Tomar, Tomar, Portugal

[4] Polytechnic Institute of Cávado e Ave, Barcelos, Portugal

[(*)] *Email:* t.morgado@fct.unl.pt; tmorgado@lnec.pt; tmorgado@ipt.pt

ABSTRACT

The pressures in the scientific communities will continue to motive research organizations to pursue research in the most efficient and cost effective manner possible. This work presents a methodological approach of maintenance management to apply to research laboratories. With this approach full service technics with core competencies in asset management, managed maintenance, validation and compliance services and disposition services are able to bundle service options to deliver higher quality at guaranteed lower costs while allowing the laboratory manager to focus on laboratory operations and business issues.

Keywords: maintenance management, research laboratories, quality, maintenance costs.

INTRODUCTION

A research laboratory is a place of expensive calibrated equipment, standard operating procedures, hazard analysis, and quality management (Kelly, 2006). Other than personnel-related costs, maintenance is generally the most expensive item in the laboratory operation budget. While the size of this of this expenditure makes it an attractive target for reduction, all laboratory managers recognize the limitations they face in achieving any real savings. Foregoing maintenance and repairs is usually not an option, they are a necessary cost of continued operation. Thus, cost reduction initiatives must extract operational and management efficiencies from the maintenance system without directly impact instrument reliability. Given the progress that has been made in controlling the cost of laboratory expendables and the effectiveness of the budget constraints in limiting discretionary expenditures improvements in maintenance management remain one of the few fertile areas to realize additional cost reductions through operational efficiencies.

There are three classic equipment management approaches (Oakland, 2014) that can be followed: Run-to-Fail (RTF), Preventive Maintenance Only (PM Only) and Full-Service Contract (FSC). All are valid, but it can achieve significant cost savings when it look at whether a given piece of equipment has been assigned the contract appropriate for its cost, criticality to the research at hand, age and nature of use.

Run-to-Fail is generally the most efficient approach for equipment and instruments for which replacement may be more cost-efficient than repair. Technically this approach does not require any maintenance contract at all, but it should be a conscious and structured choice nonetheless.

To determine which pieces fall in this category, must be setting a replacement cost ceiling. If the replacement cost for a particular piece of equipment is below the ceiling cost, the RTF approach must be use because it will be more cost efficient to replace the item than to repair it. Other equipment that may be a good fit for RTF include those items that are well past their full depreciation point (age), frequently break down, or are infrequently use, unless they serve a critical function when needed.

RESULTS AND CONCLUSIONS

Preventive maintenance on an item is almost always recommended by the original equipment manufacturer. This type of contract cover preventive maintenance does not cover labor or repairs when the equipment fails. PM only is generally well-suited for items with moving parts, liquid or gas flow, filters, or optical systems, yet not critical to day-today operations. Since researchers will invariably define everything as critical, the maintenance management must determine whether a piece of equipment is truly critical by looking at availability of an alternate piece of equipment, ability to generate data in another way, utilization and the cost of parts.

A Full-Service Contract typically covers preventive maintenance as well as all demand repairs, including parts and labor. Sometimes chosen as an “insurance policy” it can be a viable option both for high critical equipment and for less critical equipment that has one or two very expensive parts that, if they fails, would be burdensome to replace.

The pressures in the scientific communities will continue to motive research organizations to pursue research in the most efficient and cost effective manner possible. One way that this can be accomplished is to decrease the cost of R&D operations, including the maintenance of laboratory equipment and instruments. Properly categorizing the laboratory equipment support category as RTF, PM Only or Full Service can greatly reduce an organization’s operating costs. Maintenance, a fundamental element of laboratory operation, is expensive and requires tedious administration to function effectively. This make it a prime candidate for outsourcing to one of the maintenance technical services. With the correct methodology applied to each laboratory, full service technics with core competencies in asset management, managed maintenance, validation and compliance services and disposition services are able to bundle service options to deliver higher quality at guaranteed lower costs while allowing the laboratory manager to focus on laboratory operations and business issues. In addition, a complete suite of metrics and reports provide feedback and assurance that the system is functioning properly.

REFERENCES

Oakland, J.. Total Quality Management and Operational Excellence: Text with Cases. United Kingdom, 2014.

Kelly A. Maintenance Management Auditing: In Search of Maintenance Management Excellence, Industrial Press Inc., 2006.

PAPER REF: 143

CONTRIBUTIONS TO DISPLACEMENT AND RESISTANCE OF THE COMPONENTS OF THE MENISCUS-SUTURE COMPLEX IN TRANSTIBIAL MENISCAL ROOT REPAIR

Ana Pérez-Blanca[1(*)], María Prado Nóvoa[1], Belén Estebanez[1], Fernando Nadal[1], Alejandro Espejo-Reina[2], Marco Ceccarelli[3]

[1]Laboratory of Biomechanics, University of Malaga, Malaga, Spain
[2]Hospital Vithas Parque San Antonio, Malaga, Spain
[3]Department of Mechanical Engineering, University of Rome Tor Vergata, Italy
[(*)]*Email:* anaperez@uma.es

ABSTRACT

This work analyses in a porcine model the contributions of meniscal tissue, suture thread and meniscus-suture interaction to the permanent displacements generated at the repaired root after surgery to re-insert the posterior meniscal root using a transtibial pullout technique. Medial porcine menisci with a single suture applied at the posterior horn were subjected to cyclic and load-to-failure tests. Elongations of the different components of the meniscus-suture complex were determined applying photogrammetry. Results showed that after low intensity cyclic loading, the main contribution to permanent root displacements was due to the thread (51.2%), while no cutting of the suture through tissue occur at the interface. Under load-to-failure conditions, suture cutting started at a significantly higher load level (Suture Retention Strength, SRS), always before and close to the first local maximum of the load-elongation curve, and progressed rapidly afterwards causing the final failure of all specimens.

Keywords: biomechanical properties, posterior meniscal root, Transtibial pull-out repair, permanent displacements, Suture Retention Strength.

INTRODUCTION

Transtibial root repairs are frequent as meniscal root tears become increasingly recognized. Development of permanent root displacements in the early post-operative period should be minimized (Cerminara, 2014), to re-establish proper meniscal function (Stärke, 2010). To improve the surgical technique, a better knowledge of the contributions to displacement of the different components involved in the repair is necessary. This study focus in the mechanical behavior of the isolated meniscus-suture complex, including the characterization of SRS at the posterior meniscal horn, a fundamental tissue property for surgical repair success.

Nine isolated medial porcine meniscus-suture specimens were included. Posterior horns were sutured with a simple stitch of ultra-resistant N.2 thread at 5mm of the inner edge. Ink marks located at each component identified suture thread, insertion hole and surrounding tissue (Fig. 1(a)). Specimens were subjected to cyclic loading (1000 cycles of [10,30]N (Stärke, 2013) load at 0.5Hz) followed by load-to-failure test, while video-monitored with a digital camera (Stingray F-504B®, Allied Vision Technologies, Germany) synchronized with the testing machine. Photogrammetry based on a SIFT algorithm, was applied to extract normalized elongations of the different components from recorded images and to relate these elongations to force measured during the test (Fig. 1(b)). Residual displacements were computed as the difference in elongations at 10N, before the first cycle and after 1000 cycles.

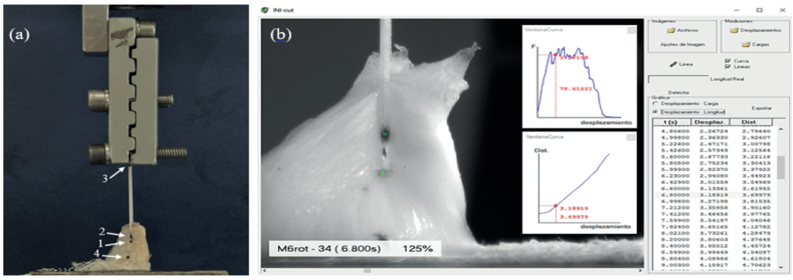

Fig. 1 - (a) Experimental setup. White arrows point out the ink marks on the different components. (b) Interface of the software Ini-cut, specifically develop to extract progression of elongations with loading from ink marks

RESULTS AND CONCLUSIONS

From cyclic test, the component that contributed the most to residual displacement was the thread with up to 51.20% of total residual displacement (Table 1). Tissue compaction at the interface contributed a 21.19%, but the suture did not cut through the tissue.

Table 1 – Initial length $\left(\mathbf{L}_{\mathbf{c}}^{0}\right)$ and residual displacement $\left(\Delta_{\mathbf{res,c}}\right)$ from cyclic tests

	Insertion hole		Suture thread		Meniscal tissue		TOTAL	
	Mean	(SD)	Mean	(SD)	Mean	(SD)	Mean	(SD)
L_c^0 **(mm)**	1.67	(0.51)	40.64	(5.63)	6.63	(1.45)	48.93	(5.31)
$\Delta_{res,c}$ **(mm)**	0.37	(0.25)	1.14	(0.70)	0.50	(0.35)	2.01	(0.90)
$\%\Delta_{res,c}$	21.19	(12.48)	51.20	(18.90)	27.61	(15.74)		

In load-to-failure, evolution of elongations showed a slope change at the same instant for all components (Fig. 2), coincident with the initiation of suture cutting through tissue in the images which occurred always close but before the first local maximum of the load-elongation curve (Fig. 2), at mean displacement of 3.2 mm and a mean load (SRS) of 97.5 N, a 10.2% lower than ultimate failure load (UFL). Once cut initiated, unpredictable permanent displacements generated, reaching a mean value of 6.9 mm at a UFL of 109.2N

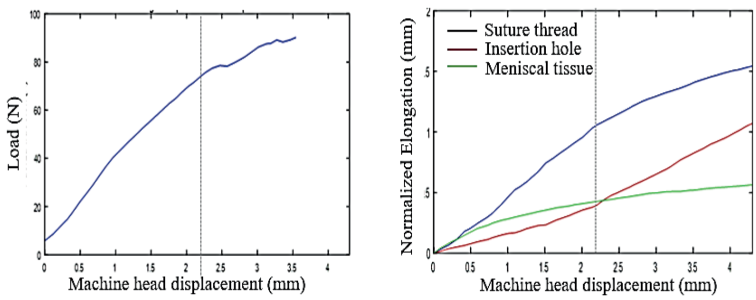

Fig. 1 – Mean curves from load-to-failure tests. Vertical lines mark tissue cut initiation.

In conclusion, suture thread contributes the most to permanent root displacements of the meniscus-suture complex in a porcine model under low intensity cyclic loading, and no cutting of the tissue occurs until SRS values of much higher intensity, after which cut progress rapidly.

REFERENCES

Cerminara AJ, LaPrade CM et al. Biomechanical evaluation of a transtibial pull-out meniscal root repair: challenging the bungee effect. Am J Sports Med, 2014, 42, p. 2988-2995

Stärke C, Kopf S, Grobel K, Becker R.The effect of a non-anatomical repair of the meniscal horn attachment on meniscal tension: a biomechanical study. Arthroscopy, 2010, 26, p. 358-365

Stärke C, Kopf S, Lippisch R, Lohman CH, Becker R. Tensile forces on repaired medial meniscal root tears. Arthroscopy, 2013, 29, p. 205-212

PAPER REF: 144

LASER CLADDING AS AN ADDITIVE MANUFATURING PROCESS AND DEVELOP OF THE NEW METALLIC ALLOYS

Teresa Morgado[1,2,3(*)]

[1] UNIDEMI - Research and Development Unit for Mechanical and Industrial Engineering, FCT NOVA - Faculty of Science and Technology, Universidade Nova de Lisboa, Lisboa, Portugal

[2] LNEC – Laboratório Nacional de Engenharia Civil, Lisboa, Portugal

[3] IPT – Polytechnic Institute of Tomar, Tomar, Portugal

[(*)]*Email:* t.morgado@fct.unl.pt; tmorgado@lnec.pt; tmorgado@ipt.pt

ABSTRACT

In XX century, in USA, LASER cladding process emerged with the purpose of improving the characteristics of metallic components' surfaces, mainly regarding the corrosion and wear resistance.

LASER cladding as an additive manufacturing process was developed, at the end of XX century, and allowed the manufacturing of complex components and tools in a short time. So, nowadays, LASER cladding technology includes various technological areas, namely the LASER technology, computer assisted production, robotic, automation, powder metallurgy, etc. Most of the scientific publications about LASER cladding applications refer mainly its use in materials from aerospace, medical and automotive industries.

In this work, an historical approach of LASER Cladding as additive manufacturing technique is presented, followed by a description of the principles of the LASER cladding and will end with a state of the art about the develop of new metallic alloys, in last years.

Keywords: LASER Cladding, Additive Manufacturing, Metallic alloys, innovation.

INTRODUCTION

LASER cladding technology was patented by Daniel S. Gnanamuthu in 4th of December of 1976, in the USA.

In the 1980s, LASER cladding has started to arouse industry's attention, having been identified as a process that presents great advantages in improving the corrosion and wear resistance of coatings over the conventional processes. The first report of its use in industry occurred in 1981, at Rolls Royce, in the coating of turbine blades components made by Nimonic that would be used in RB-211 jet engine, having its utilization extended to the leading companies in the engine production sector at that time. In the automotive industry, LASER cladding has also started to be applied in the engine valve coating as in the case of Fiat, Toyota and Mercedes-Benz (Gäbler, 2016).

In the last decade of the XX century, a large number of rapid prototyping and layered manufacturing methods of three-dimensional structures, that already used the principles of the cladding process, were introduced and patented, doing now part of the commercial available solutions (Toyerkani, 2005), (Sarin, 2014).

RESULTS AND CONCLUSIONS

According to Birger et al. (Birger, 2011), in LASER cladding area a large number of studies have been published related with the investigation of the application of different cladding mixtures in relation to the base materials on which they are applied, being one of the studied mixtures the nickel-base mixtures applied as powder mixtures for coating by LASER cladding. LASER cladding of magnesium alloys become a new area of interest in terms of research and, in the review article elaborated by Liu et al. (Liu, 2017), various studies are mentioned about the LASER cladding on magnesium alloys (working as substrate), as the case of studies that approach the optimization of the process parameters to this kind of alloys (LASER power, scanning velocity, beam focal position, feeding method, etc.) and the selection of the cladding materials that are going to be deposited on the substrate of magnesium alloys. These alloys are presented as one of the most promising lightweight structural materials and hence the interest in their improvement for other applications beyond those already recognized. As examples of some promising alloys that are also being studied, with published documentation, by Additive Manufacturing LASER cladding technique, are titanium alloys, more specifically the Ti-Ta, alloys (Morgado, 2015), (Valente, 2017), (Valente, 2019).

It is concluded that the Additive Manufacturing LASER cladding is a technology with great potentiality, in the development of new alloys and in the improvement of well-known alloys and, as well as, manufacturing process. It is a quick and precise process, whose operational parameters include the LASER power, scanning velocity, beam focal position, feeding method, just to name some. This is, the LASER cladding depends on the material (substrate and cladding material) and on the LASER cladding equipment characteristics (LASER, 2/3 axis table, powder feeder, nozzle, etc.) and consequently on the control of its operational parameters.

REFERENCES

F. Gäbler, «Cladding rises to the top Diode LASER cutting», Industrial LASER Solutions for Manufacturing, vol. 31, n. 2, pp. 16–18, Mar/Abr 2016.

E. Toyserkani, A. Khajepour, and S. F. Corbin, LASER Cladding. USA: CRC Press, 2005.

V. K. Sarin, D. Mari, L. Lianes, e C. E. Nebel, Eds., Comprehensive Hard Materials - Volume 1 Hardmetals. UK: Elsevier, 2014.

E. M. Birger, G. V. Moskvitin, A. N. Polyakov, and V. E. Arkhipov, «Industrial LASER cladding: current state and future», *Weld. Int.*, vol. 25, n. 3, pp. 234–243, 2011.

T. L. M. Morgado, H. Navas, and R. Brites, «Wear study of Innovative Ti-Ta alloys», *Procedia Struct. Integr.*, vol. 2, pp. 1266–1276, 2016.

C. Valente, «Study of the Mechanical Behaviour of a Titanium-Tantalum alloy, Ti10Ta, produced by LASER cladding» in Portuguese, Master Thesis, FCT, NOVA - Universidade Nova de Lisboa, Portugal, 2017.

C. Valente, J. Leunda, T. Morgado, A. Velhinho; «Mechanical Proprieties and fatigue behaviour of the Ti10Ta alloy»; Materiais 2019 - XIX Congresso da Sociedade Portuguesa de Materiais and X International Symposium on Materials, 14-17 April, 2019.

J. Liu, H. Yu, C. Chen, F. Weng, and J. Dai, «Research and development status of LASER cladding on magnesium alloys: A review», *Opt. LASERS Eng.*, vol. 93, pp. 195–210, 2017.

PAPER REF: 145
Topic: C – Fatigue and Fracture Mechanics
Sub-Topic: Damage Mechanics and Assessment

HYPOTHESIS FOR FAULT DYNAMIC MONITORING EVOLUTION IN RAILWAY SYSTEMS

Massimiliano Bruner[1], Fabio Croccolo[2(*)]

[1] Consultant Investigator for Italian Infrastructures and Transportation Ministry, Directorate General for railway and maritime investigations, Rome, Italy, massimiliano.bruner@outlook.it

[2(*)] General Director, Italian Infrastructures and Transportation Ministry, Directorate General for railway and maritime investigations, Rome, Italy, fabio.croccolo@mit.gov.it

ABSTRACT

The report presents the technical results of a survey carried out by the Directorate General for Railway and Maritime Investigations (DiGIFeMa). An investigation report was drafted in compliance with Legislative Decree n. 162/2007, identifying the technical causes, which have generated railway accidents and incidents and formulating specific recommendations, aimed at the continuous improvement of safety in rail transport. An extract from the official document published by the Ministry of Infrastructure and Transport is presented. The survey highlighted the importance of thermo-mechanical control procedures, interested in mechanical rotational devices (axles bushings) of railway vehicles. The results of the investigation proposed a monitoring procedure to be able to fallow the evolution speed of a mechanical fault, in addition to the usually comparison methodologies based on exceeding critical values.

Keywords: railway, vehicle, safety, monitoring.

INTRODUCTION

DiGIFeMa, the Investigative Body of the Ministry of Infrastructure and Transport, carries out technical-regulatory analysis on railway and maritime accidents, acting on the basis of Legislative Decree 10 August 2007, n. 162 [1] and of Legislative Decree 6 September 2011, n. 165. The first document implemented Directive 2004/49/EC on the safety of the Community Railways [2] and the second transposed Directive 2009/18/EC on the safety of maritime transport. In this context, DiGIFeMa has analysed and published in an Investigation Report [3] the studies related to a railway derailment that occurred in 2017, which involved an HS train (Fig. 1) used to transport passengers on a High-Speed line belonging to the National Railway Network.

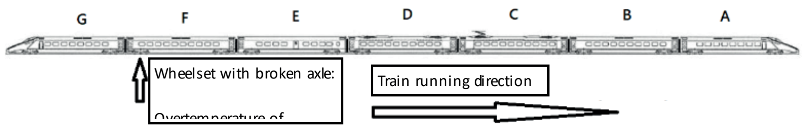

Fig. 1 – Side view of the rolling stock used for High-Speed passenger transport Italian National Railway Network: A, G: motorized driving cab; B, F: motorized passengers' car; C: trailing restaurant car; D, E: trailing passengers' cars (Source: [3])

The survey allowed to define all various stages of development of the event and to hypothesize technical problems. In particularly data analysis has highlighted that some faults in rotational devices (i.e.: wheelset bushings) of railway vehicles can assume different meaning if analysed from an evolution velocity point of view. This way to manage safety in railway operations could be connected to the monitoring methodology that Infrastructure Managers and Railway Undertaking usually follow: comparing actual single values with critical limits, both measured by wayside devices (RTB, Figgs. 2 and 3) and by on onboard devices.

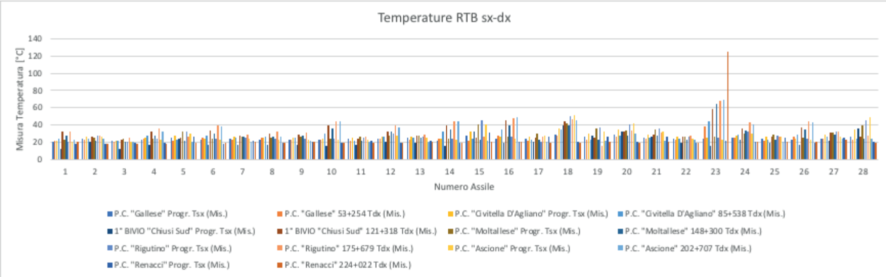

Fig. 2 – Train wheelsets left and right bushing temperature measured by wayside devices fixed along the railway HS line (Source: [3])

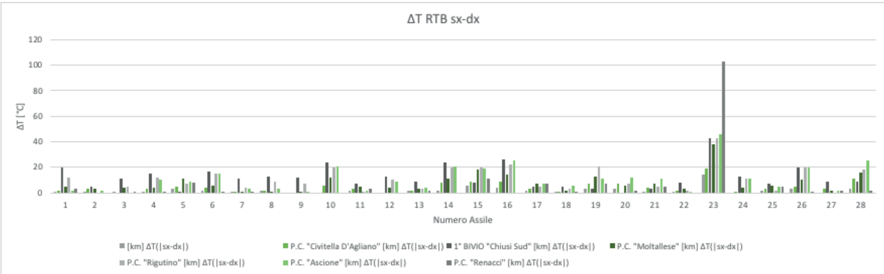

Fig. 3 – Train wheelsets left-right bushings difference temperature measured by wayside devices fixed along the railway HS line (Source: [3])

RESULTS AND CONCLUSIONS

The analysis of the survey evidences has identified the breaking of the wheelset axle as a direct cause of train derailment. During the journey on HS line, rolling of wheelset has become kinematically non-compliant due to the overtemperature of wheelset bushing bearings, as shown by the continuous rise in temperature, detected by the measurements of the wayside thermal monitoring devices. The DiGIFeMa Investigation Report proposed an interesting way to increase the railway running safety, based on a monitoring of the evolution rate (temporal thermal gradient) of the overheating phenomenon. This method could be combined with the existent ones applied on trains and on wayside, suggesting a "predictive" type of safety-related monitoring process.

REFERENCES

[1] Italian Legislative Decree August 10th 2007, n. 162, "Implementation of the directives 2004/49/CE and 2004/51/CE relating to the safety and development of the Community railways", Official Journal n. 234 of October 8th 2007 - Ordinary Supplement No. 199/L

[2] Directive n. 2004/49/EC of the European Parliament on the safety of the Community railways concerning the allocation of railway infrastructure capacity, to imposition of rights for the use of railway infrastructure and safety certification (Railway Safety Directive), G.U. April 30th, 2004, No. L 164.

[3] Ministry of Infrastructure and Transport, Directorate General for Railway and Maritime Investigations, Investigation Report, Accident: Train Es8510 Rolling Stock Etr600.004 Line: DD HS Roma-Firenze Occurred On 09.11.2017, published on 20th December 2018

PAPER REF: 146

AN ACOUSTIC RESONAT THERMOMETRY FOR MONITORING THE WATER TEMPERATURE

Hironori Tohmyoh[(*)], Shu Terashima, Masato Ito

Department of Finemechanics, Graduate School of Engineering, Tohoku University, Sendai, Japan
[(*)]*Email:* tohmyoh@ism.mech.tohoku.ac.jp

ABSTRACT

This work presents a new idea to measure the water temperature by ultrasound, where the acoustic resonance among the reflection plate, thin film and the water is utilized. The acoustic impedance of the water is temperature dependant, and related with this, the reflection coefficient at the plate/film/water interface shows the temperature dependency. The change in the reflection coefficient against the water temperature was examined, and the results are reported.

Keywords: ultrasound, acoustic resonance, reflection coefficient, water temperature.

INTRODUCTION

Measuring the temperature of liquid or gas contained in the pipe and vessel is required in many cases of application. Generally, the temperature of the object is measured by the thermocouple, and it requires the direct contact to the object. Therefore, the thermocouple should be placed inside the pipe and vessel for the above-mentioned purpose. On the other hand, infrared thermography can measure the temperature of the object in non-contact manner, but it is hardly to measure the temperature at the hidden location. So far, the acoustic resonance (Brekhovskikh, 1960), which occurs when sound passes through thin layer, is widely used to characterize the layered media. In our previous study, the acoustic properties of a polymer film were accurately measured by observing the acoustic resonance, which occurs at the reflection plate/film/outer environment interface (Tohmyoh, 2015). Though this study, we noticed that the reflection coefficient at the interface sensitively changes depending on the acoustic impedance of the outer environment.

Based on our findings, this presentation aimed to verify the possibility to measure the water temperature utilizing the acoustic resonance (Tohmyoh, 2019). The sound velocity and density of liquid and gas change against the temperature, and therefore, the acoustic impedance of them, which is given by the product of the sound velocity by the density, shows the temperature dependency (Del Grosso, 1972). When the acoustic impedance of water changes, the reflection coefficient at the reflection plate/film/water interface changes. With use of this, this presentation tried to monitor the change in the water temperature.

RESULTS AND CONCLUSIONS

Schematic of the experimental setup is shown in Figs. 1(a) and (b). Ultrasound emitted by an ultrasonic transducer was reflected at the back of the reflection plate, and received by the same transducer [Fig. 1(a)]. The amplitude spectrum, which was obtained by the frequency analysis of the received signal, is denoted as φ_0. Similarly, the amplitude spectrum of the echo reflected at the plate/film/water interface [Fig. 1(b)], is denoted as φ_1. The reflection plate was 0.3 mm thick Si plate, and a photoresist was used as thin film. In this study, φ_0 was obtained at the water temperature T = 25.7°C. Behaviors of φ_1 for various values of T were recorded, and the ratio γ (= φ_1 / φ_0) were determined.

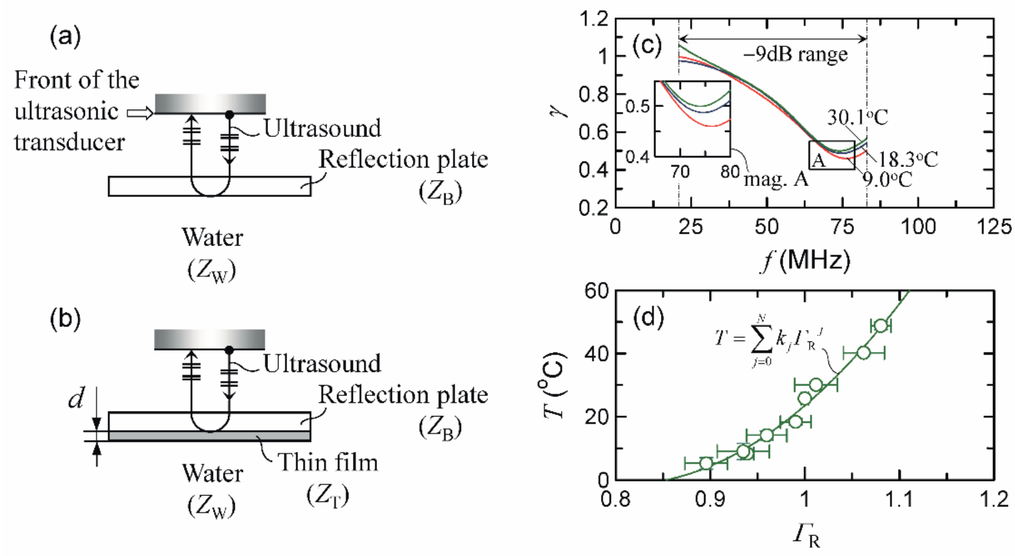

Fig. 1 - Two models for ultrasonic transmission in case of (a) without and (b) with thin film at the back of the reflection plate. (c) Examples of the amplitude ratio. (d) T vs. Γ_R. Reprinted with permission from Tohmyoh and Terashima. Copyright 2019 ASME.

Examples of γ for T = 9.0, 18.3 and 30.1°C are shown in Fig. 1(c) against the frequency f. Cleary, the values of γ take their minimum values, γ_R, at around 75 MHz. Form the magnified view around 75 MHz, γ_R is found to decrease with decrease in T. Relationship between T and the normalized value Γ_R, (= γ_R / γ_R^0) is shown in Fig. 1(d), where γ_R^0 is γ_R at T = 25.7°C, and good correlation between them can be seen. With use of this relationship, we monitor the change in the water temperature, and the results will be discussed in the presentation.

ACKNOWLEDGMENTS

This work was supported by JSPS KAKENHI Grant No. 18H01331.

REFERENCES

Brekhovskikh LM. Waves in Layered Media, Academic Press, New York, 1960.

Tohmyoh H, Sakamoto Y. Determination of acoustic properties of thin polymer films utilizing the frequency dependence of the reflection coefficient of ultrasound. Review of Scientific Instruments, 2015, 86, 114901.

Tohmyoh H, Terashima S. Trial for monitoring the water temperature utilizing the frequency dependence of reflection coefficient of ultrasound passing through thin layer. Transactions of the ASME, Journal of Nondestructive Evaluation, Diagnostics and Prognostics of Engineering Systems, 2019, 2, 021001, 6 pages.

Del Grosso VA, Mader CW. Speed of sound in pure water. The Journal of the Acoustical Society of America, 1972, 52, p. 1442-1446.

PAPER REF: 147

CLATTERING OF A FLEXIBLE BEAM FALLING ON A RIGID SURFACE

Sergey Shubin[1(*)], **Petr Gorelchenko**[2]
[1]Corning Scientific Centre, St. Petersburg, Russia
[2]Corning Research & Development Corporation, Corning, NY, USA
[(*)]*Email:* shubinsn@gmail.com

ABSTRACT

An analytical analysis is presented for a dynamic behavior of a flexible beam falling on a rigid surface. The analysis aims to describe multiple collisions of the beam with the surface (multiple contacts during event which the eyes observed like one impact) and clattering (subsequent impacts of opposite ends of the beam). Bernoulli-Euler theory is applied to describe a motion of the beam. It is assumed that a contact of the beam with the surface is carried through end points of the beam. The contact is simulated by linear springs. The whole process of the beam falling is divided into simple regimes: no contact with the surface; one contact point; two contact points. For each regime the solution is represented by a sum of eigenmodes. The complete solution has the form of sequence of the regimes. The developed approach allows us to evaluate trajectory and process time, bending modes, relative stresses and contact force from the beam-surface contact. The modeling could be performed for arbitrary orientation and initial velocities (both translational and rotational) of the beam.

Keywords: clattering, multiple collisions, impact, flexible beam.

INTRODUCTION

The problem of an impact between a rigid beam and a rigid surface has been subject to a great deal of research starting in 1895 by Painleve (Painleve, 1895) (see the review paper (Stewart, 2000) regarding this problem with a list of references therein), but clattering of the rigid beam which contacts the rigid surface were analyzed for a first time by Goyal et al. in 1998 (Goyal, 1998). This research allowed to find that when rigid beam is dropped onto the ground at a small angle, a velocity increase during the second impact might be two times of the first impact. It means that the second impact might be more dangerous than the first one, as an associated contact force might be greater. Later this model was modified in several ways to describe various effects. In work (Quercetti, 2002) analytical analysis of rigid beam clattering is performed for large impact angles. Comparison of analytical solution (discrete contact impact) with numerical (continuous contact impact) for falling rigid beam given in work (Shana, 2006). Numerical analysis of falling rigid beam with transversely attached harmonic oscillator is performed in (Baranyai, 2018).

In the current work we abandon an assumption of an absolutely rigid beam and consider clattering of a flexible beam. We estimated effects of a bending stiffness, mass, internal damping, contact stiffness and initial conditions to the dynamic response of the beam. Possible application of the model includes but not limited to a free fall event of a flexible object or a system or a device. The approach can also be used to design and evaluate for a shock absorbing system.

RESULTS AND CONCLUSIONS

The developed approach in an extreme case (assuming beam stiffness close to an infinitely rigid beam) agrees with the precursor model of a rigid rod (by Goyal et al.). In addition to that by considering a flexibility of the beam we were able to reveal and describe the following features of a drop event:

1. Bending deformation during clattering process. Which might be important for many applications such as reliability analysis, as large deformation may lead to damage.
2. It is shown that motion of the beam as rigid body co-aligned directionally with a flexural vibration may increase contact force. Opposite direction of the rigid motion and the flexural vibration instead lead to a decrease in the contact force. Thus, contact force associated with a second impact could be more than two times higher than the one for a first contact (as it is predicted by a rigid beam model).
3. The approach allowed us to evaluate duration of the contact during the beam clattering. The contact time is equally important parameter for the applications (for instance for reliability assessment) as the magnitude of the force.
4. Mason et al. in paper (Mason, 1935) showed that the impact that appear to be single to the naked eye may consists in reality of several collisions in rapid sequence. The number of multiple collisions depends on flexural rigidity and contact stiffness. The developed flexible beam model allowed us to explore this phenomenon as well.

The developed approach can be used as a general guideline in optimization process of products and equipment: the model allows to estimate flexural rigidity and contact stiffness to fulfill reliability requirements for the shock protection during drop.

REFERENCES

Baranyai T, Varkonyi L. Optimal mechanical design of electronic devices for shock protection. Transactions on Components, Packaging and Manufacturing Technology, 2018, 8, 9, p. 1533-1543.

Goyal S, Papadopoulos JM, Sullivan PA. The Dynamics of Clattering I: Equation of Motion and Examples. Journal of Dynamic Systems, Measurement, and Control, 1998, 120, p. 83-93.

Goyal S, Papadopoulos JM, Sullivan PA. The Dynamics of Clattering II: Global Results and Shock Protection. Journal of Dynamic Systems, Measurement, and Control, 1998, 120, p. 94-102.

Mason HL. Impact on Beams. ASME, 1935, 58, p. A55-A61.

Painleve P. Sur le lois du frottement de glissemment. C. R. Acad. Sci. Paris, 1895, 120, p. 83-93.

Quercetti T, Ballheimer V, Wieser G. Analytical, numerical, and experimental investigations on the impact behaviour of packagings for the transport of radioactive material under slap down conditions. J. Nucl. Mater., 2002, 3, p. 18-25.

Shana H, Sua J, Badiua F, Zhub J, Xub L. Modeling and simulation of multiple impacts of falling rigid bodies. Mathematical and Computer Modelling, 2006, 43, p. 592-611.

Stewart DE. Rigid-body dynamics with friction and impact. SIAM Rev., 2000, 42, 1, p. 3-39.

PAPER REF: 148

EFFECT OF HOT AND COLD START OF THE DIESEL ENGINE ON EMISSIONS

Aleš Dittrich[1(*)], Pavel Brabec[1], Josef Popelka[1], Celestýn Scholz[1]

[1]Technical University of Liberec, Liberec, Czech Republic

[(*)]*Email:* ales.dittrich@tul.cz

ABSTRACT

The paper deals with the influence of engine temperature and its operating fluids on the production of individual components of exhaust emissions. The experiments were performed for non-stationary modes according to EHK96 regulation - the so-called NRTC test. The concentrations of measured concentrations in the form of cumulative error are compared in the text.

Keywords: exhaust gas, nonstationary test, diesel engine, NRTC.

INTRODUCTION

The exhaust emission approval process of any vehicle or machine consists of a series of tests defined by legislation. Passenger and light commercial vehicles or motorcycles are tested as a whole. This is based on methodology and methods of testing. The situation is different for heavy-duty vehicles and non-road machines. [1] Individual components or internal combustion engines are tested as a single unit, so that other test procedures apply. In the second step, only the correct installation in the vehicle or machine is verified.

In the first step, it is therefore necessary to focus only on the internal combustion engine and several types of tests are required for its approval. The engine shall be tested separately, connected to a dynamometer test equipment capable of simulating the load. [2] The test cycle is dependent on the category and the determination of the engine. It is either a stationary NRSC test or a transient NRTC. [3]

The NRTC test (shown in Figure 1) is a 1238 seconds long transient driving cycle for mobile nonroad diesel engines developed by the US EPA in cooperation with the authorities in the European Union (EU). The test is used internationally for emission certification/type approval of nonroad engines. NRTC testing is required by a number of emission standards for nonroad engines, including the EU Stage III/IV regulation, the US EPA Tier 4 rule and Japanese 2011/13 regulations.

The NRTC is run twice, with a cold and a hot start, with a 20-minute soak period between the tests. The cold start weighting factors are 10% in the EU and 5% in the United States for the calculation of specific gaseous and particulate pollutants (expressed in g/kWh).

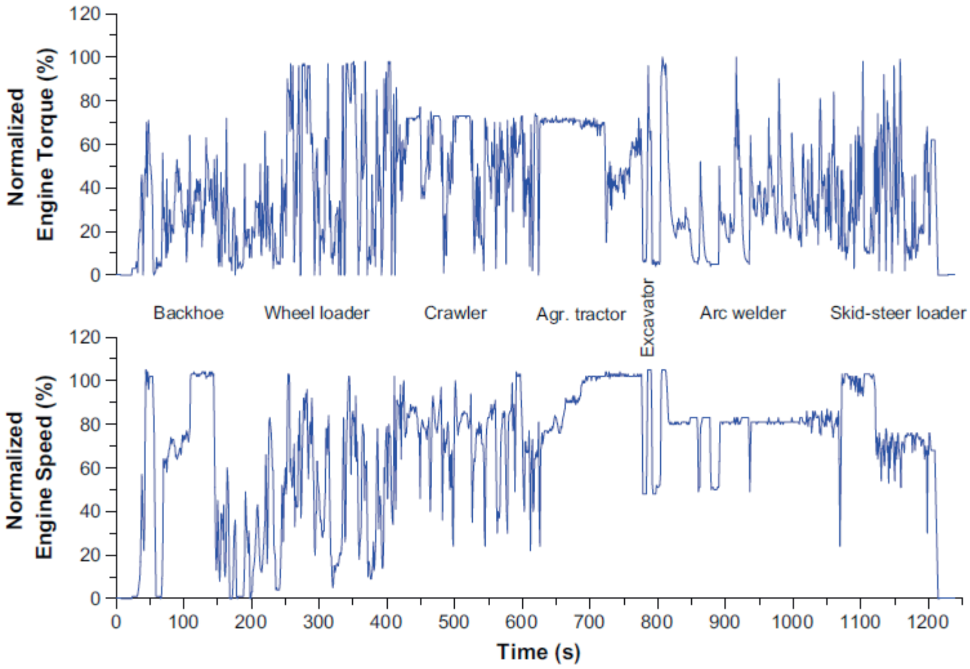

Fig. 1 - Engine speed and torque profile of the non-road NRTC composite transient cycle [3]

RESULTS AND CONCLUSIONS

Tested engine was installed at a test facility at the Department of Vehicles and Engines at Technical University of Liberec. The test station is equipped with a AC dynamometer ASD 235 M250. The dynamometer is controlled by the CMS control system under the Windows operating system, which allows the engine to operate according to a programmed test mode with electronic data collection of all standard engine operating variables. Special measuring equipment - Horiba Mexa-One (for gaseous exhaust emissions) was used for measurement.

ACKNOWLEDGMENTS

This publication was written at the Technical University of Liberec, Faculty of Mechanical Engineering with the support of the Institutional Endowment for the Long Term Conceptual Development of Research Institutes, as provided by the Ministry of Education, Youth and Sports of the Czech Republic in the year 2019.

REFERENCES

[1] Agreement: Concerning the Adoption of Uniform Technical Prescriptions for Wheeled Vehicles, Equipment and Parts which can be Fitted and/or be Used on Wheeled Vehicles and the Conditions for Reciprocal Recognition of Approvals Granted on the Basis of these Prescriptions; Addendum 95: Regulation No. 96

[2] Martyr A. J., Plint M. A. Engine testing - Theory and Practice. Third edition. Burlington, MA 01803, 2007. 242 p.

[3] Giakoumis E. G. Driving and Engine Cycles. Springer International Publishing, 2017. 193, 285 p.

PAPER REF: 149

NUMERICAL INVESTIGATION OF WEAR AND CAVITATION DAMAGE IN A HIGH PERFORMANCE ENGINE CONROD SMALL-END BEARING VIA ELASTOHYDRODYNAMIC ANALYSIS

Matteo Giacopini[1(*)], Andrea Ferretti[1], Daniele Dini[2], Luca Nicolò Mastrandrea[3]

[1]Engineering Department Enzo Ferrari (DIEF), University of Modena and Reggio Emilia, Modena, Italy

[2]Faculty of Engineering, Department of Mechanical Engineering, Imperial College London, London, United Kingdom

[3]Ferrari spa, Engine Simulation Department, Maranello, Italy

[(*)]*Email:* matteo.giacopini@unimore.it

ABSTRACT

This contribution presents the results of different elastohydrodynamic numerical simulations performed for the tribological analysis of the conrod small-end/piston pin coupling of a high performance internal combustion engine. In particular, both cavitation phenomenon and direct asperity contact occurrence are taken into consideration. Suitable damage indexes are proposed and employed to quantify the risk of cavitation damage and wear damage of the contacting surfaces. Comparisons versus experimental evidences registered during severe bench tests performed at an early stage of the design process of the engine are presented.

Keywords: conrod small-end, piston pin, lubrication, cavitation, asperity contact, wear, elastohydrodynamics.

INTRODUCTION

Lubricated contacts represent one of the main responsible of friction losses in internal combustion engines and they directly contribute to the definition of the engine efficiency. As a consequence, the development and the adoption of numerical methodologies for the analysis of lubricated couplings represents a pivotal aspect engine designers have to deal with.

In particular, the conrod small-end bearing is one of the most critical engine parts from a tribological point of view. The dominant effect for the lubrication of the conrod small-end is the film squeeze caused by the alternating combustion/inertial loads, while sliding hydrodynamic effects are usually negligible.

In high loaded applications, severe wear of the conrod small-end due direct asperity contact is usually present and it can affect the component reliability. A suitable *Direct Contact Damage Index* (*DCDI*), based on the maximum direct asperity contact pressure value is proposed and compared with experimental damage evidences:

$$DCDI = \max(p_a[j]) \; DCDI = \max(p_a[j]) \tag{1}$$

where p_a is the asperity contact pressure and j is the node index.

At the same time, the phenomenon of the damage caused by the onset and subsequent collapse of cavitation bubbles within the lubricant fluid film is analysed in detail. Despite the fact that a universally accepted theory does not exist, it is widely accepted that the cavitation damage occurs due to the rapid and violent collapse of the vapour bubbles in proximity of a solid boundary. In this contribution, a *Cavitation Damage Index* (*CDI*) is proposed, based on the bubble dimension evaluated just before the film reformation. In particular, considering that the bubble dimension is proportional to the void fraction and to the oil film height, the *CDI* can be defined as:

$$CDI = \frac{r[i-1,j]h[i-1,j]}{\Delta t} \quad if\ r[i,j] = 0\ and\ r[i-1,j] \neq 0$$
$$CDI = \frac{r[i-1,j]h[i-1,j]}{\Delta t} \quad if\ r[i,j] = 0\ and\ r[i-1,j] \neq 0 \qquad (2)$$

where r is the void fraction, h is the film thickness, Δt is the simulation time step, i is the time index and j is the node index.

RESULTS AND CONCLUSIONS

Figure 1 compares numerical results obtained in terms of *DCDI* with wear damage experimental evidences registered during severe bench tests of the engine. A perfect match is detected between numerical and experimental results.

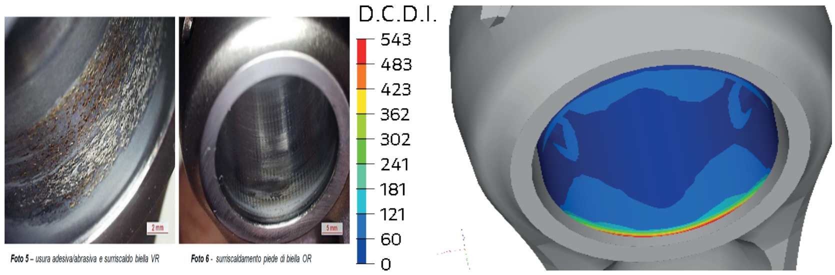

Fig. 1 – Direct Contact Damage Index (*DCDI*): comparison versus experimental evidences.

Figure 2 compares numerical results obtained in terms of *CDI* with cavitation damage experimental evidences registered during severe bench tests of the engine. Again, a good match is detected between numerical and experimental results.

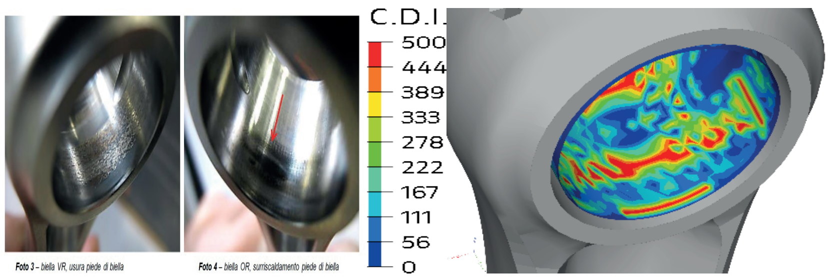

Fig. 2 – Cavitation Damage Index (*CDI*): comparison versus experimental evidences.

REFERENCES

Giacopini M., Fowell M.T., Dini D., Strozzi A. A mass-conserving complementarity formulation to study lubricant films in the presence of cavitation. Journal of Tribology, 2010, 132(4), 041702.

Bertocchi L., Giacopini M., Dini D. Analysis of the lubrication regimes at the small end and big end of a connecting rod of a high performance motorbike engine. In: American Society of Mechanical Engineers, Tribology Division, TRIB, 2012, p. 229-231.

Dini D., Mastrandrea L.N., Giacopini M., Bertocchi E. Numerical investigation of the cavitation damage in a high performance engine conrod big end bearing via a mass-conserving complementarity algorithm. In: Society of Tribologists and Lubrication Engineers Annual Meeting and Exhibition, 2014, 2, pp. 586-589.

PAPER REF: 150

DESIGN AND TESTS OF A Mg-BASED BIODEGRADABLE RIB-FIXATOR PROSTHESIS

Maria Richetta[1(*)], Alessandra Varone[1], Roberto Montanari[1], Marco Ceccarelli[1], Vincenzo Ambrogi[2]

[1] Department of Industrial Engineering, University of Rome "Tor Vergata", Rome, Italy
[2] Department of Surgical Sciences, University of Rome "Tor Vergata", Rome, Italy
[(*)]*Email:* richetta@uniroma2.it

ABSTRACT

The need to have biocompatible, biodegradable and osteoconductive implants for bone tissue applications has long emerged. Magnesium-based implants would seem to be able to meet these needs. Furthermore, they would only be temporarily necessary to guarantee mechanical support during tissue healing. The metal implants, currently in use, also have the major drawback of having to be removed by a second intervention. Repetition of the operation increases morbility and health costs, therefore the use of biodegradable metal implants, with good biocompatibility and adequate degradation rate, would make it possible to overcome the limits of conventional metal biomaterials and remove the second surgical intervention.

Keywords: Mg-based implants, Rib-fixator prosthesis, Corrosion rate, Strength, Load bearing, Tissue regeneration.

INTRODUCTION

Ribcage works as a perfect system conjugating resistance and flexibility. In the case of violent trauma involving more than one rib the ribcage can lose its integrity and this event can cause paradox movements during ventilation originating a serious problem physiologic called "flail chest". Ribs take at least 20 days for fracture repair and a system of fixation would be desirable during this period.

This is normally what can be done in all bone fracture but ribcage should be kept always mobile in order to allow breathing movements and cough, which are both vital functions [1]. Therefore a classic fixation system like plaster or external tutors cannot be feasible.

The problem is to find a system of fixation easy, flexible, atraumatic (thus respective of the intercostal nerve and intercostal artery, which flow underneath the inferior edge of the rib) and hopefully resorbable within a one-two months time [2]. This has represented a real challenge throughout the history of the traumatology and effective solutions have not yet been found.

In order to guarantee their healing, the broken bones must be firmly stabilized to avoid any slightest movement; furthermore any type of implant must be highly biocompatible to avoid inflammatory processes that hinder bone reconstruction. These requests are satisfied by prostheses made of stainless steel or titanium, however, in most cases, those implants are removed after a certain time to avoid bone degradation [3]. To reduce side effects it would be essential to have implants with mechanical bone-like characteristics, self-degradation and good adhesion to the bone tissue itself. In Table 1 the properties of the most studied materials for biodegradable plants are reported.

Table 1. Degradable Implants Materials. Basic Properties

Implant Materials	Degradation Speed	Physical and Corrosion Characteristics	Biological Effects	Ref.
Organic Polymers	Adjustable	Flexible Weak for load-bearing Implant swelling X-rays transparent	Inflammatory acidic hydrolysis products	(4)
Steel	Inert	Strong Suitable for load-bearing	Non-inflammatory	(5)
Titanium	Inert	Strong Suitable for load-bearing	Non-inflammatory	(5)
Iron - based	Very slow	Strong but irregular corrosion characteristics	Inflammatory iron hydroxide particles	(6)
Zinc-based	Slow	Suboptimal strength	Non-inflammatory	(7)
Magnesium-based	Rapid	Sufficient strength alloys Irregular pitting corrosion Corrosion coat formation	Non-inflammatory Bone friendly surface oxide layer	(8)

EXPERIMENTAL ANALYSIS

As emerges from the previous discussion, metallic alloys are extensively studied, in particular for orthopaedic applications. Among biodegradable metals, used in temporary implants for supporting tissue regeneration and healing, Fe, Mg and Zn alloys exhibit the best biocompatibility characteristics. However, some problems arise in vivo applications.

Corrosion products of Fe alloys accumulates and are not either metabolized or excreted at an appreciable rate, Zn alloys have relatively low mechanical properties while Mg alloys exhibit accelerate corrosion rate with hydrogen release leading to premature loss of mechanical prosthesis integrity and, in extreme conditions, gas embolism. On the other hand excessive magnesium corrosion may lead to a build-up of pressure in bone-enclosed cavities and may, therefore, stimulate bone growth in appropriate setups [9].

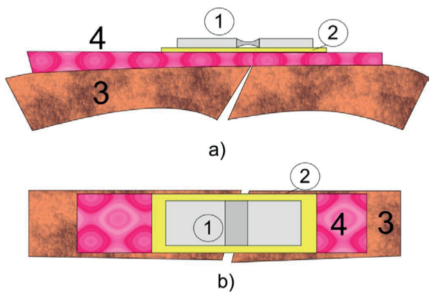

Fig. 1 - Design of the rib implant: a) side view; b) top view. (1 – implant plate, 2 – bio-adhesive glue, 3 – organic tissues, 4 – rib bone)

The promising results obtained so far suggest a bright future for biodegradable Mg-based orthopaedic implants. Given the increasing interest on this emerging biomaterials and intense effort to improve its properties for various clinical applications, in this work we will present our studies relative to new rib-fixator prosthesis.

Some Mg-based preliminary prostheses were realized and characterized in terms of: i) structure; ii) mechanical properties; iii) cohesion between the bio-adhesive, which connects the organic tissue underlying the prosthesis. In Fig. 1 a schematic view of the rib implant is reported. A rectangular plate of small thickness characterizes the rib implant in Fig. 1, with a flexural joint in the middle that will permit the plate inflection, following the rib movement during the breathing of a patient.

The rectangular plate is designed with proper size as for connecting the segment of a broken rib and facilitating the installation with a bio-glue through a minimal invasive surgery. In addition, its geometry is useful for a fair manufacturing using magnesium alloy. The problem of rib implants is studied for design purposes also by using experimental investigations like in [10,11] to search for new solutions that better fit with the biomechanics of the ribcage.

REFERENCES

Mineo T.C., Ambrogi V., Cristino B., Pompeo E., Pistolese C., Changing indications for thoracotomy in blunt chest trauma after the advent of videothoracoscopy, *J Trauma*. **1999**, *47*(6), 1088-1091.

Vu K.C., Skourtis M.E., Gong X., Zhou M., Ozaki W., Winn S.R., Reduction of rib fractures with a bioresorbable plating system: preliminary observations, *J Trauma*. **2008**, *64*(5), 1264-1269. doi: 10.1097/TA.0b013e3180340e31.

Sumner, D.R. Long-term implant fixation and stress-shielding in total hip replacement. *J. Biomech.* **2015**, *48*, 797–800.

Ceonzo K., Gaynor A., Shaffer L., Kojima K., Vacanti C.A., Stahl G.L. Polyglycolic acid-induced inflammation: Role of hydrolysis and resulting complement activation. *Tissue Eng.* **2006**, *12*, 301–308.

Perren S.M., Regazzoni P., Fernandez A.A. How to choose between the implant iaterials steel and titanium in orthopedic trauma surgery: Part 2—Biological aspects. *Acta Chir. Orthop. Traumatol. Cech.* **2017.**

Pierson D., Edick J., Tauscher A., Pokorney E., Bowen P., Gelbaugh J., Stinson J., Getty H., Lee C.H., Drelich J., et al. A simplified in vivo approach for evaluating the bioabsorbable behavior of candidate stent materials. *J. Biomed. Mater. Res. B Appl. Biomater.* **2012**, *100*, 58–67.

Yang H., Wang C., Liu C., Chen H., Wu Y., Han J., Jia Z., Lin W., Zhang D., Li W., et al. Evolution of the degradation mechanism of pure zinc stent in the one-year study of rabbit abdominal aorta model. *Biomaterials* **2017**, *145*, 92–105.

Zhao D., Witte F., Lu F., Wang J., Li J., Qin L. Current status on clinical applications of magnesium-based orthopaedic implants: A review from clinical translational perspective. *Biomaterials* **2017**, *112*, 287–302.

Noviana, D., Paramitha, D., Ulum, M.F., Hermawan, H. The effect of hydrogen gas evolution of magnesium implant on the postimplantation mortality of rats. *J. Orthop. Transl.* **2016**, *5*, 9–15.

Ramirez O., Ceccarelli M., Russo M., Torres-San-Miguel C.R., and Urriolagoitia-Calderon G., Experimental Dynamic Tests of Rib Implants, G. Carbone and A. Gasparetto (Eds.): Advances in Italian Mechanism Science- Proceedings of the Second International Conference of IFToMM Italy, MMS, Springer Nature Switzerland AG 2019, **2019**, *68*, 353–361. https://doi.org/10.1007/978-3-030-03320-0_38.

Aguilar L.A., Ceccarelli M., Torres-San-Miguel Ch. R., Urriolagoitia-Sosa G., and Urriolagoitia-Calderón G., Experimental Evaluation of Artificial Human Ribs, In: J.C.M. Carvalho et al. (eds.), Multibody Mechatronic Systems, Springer International Publishing AG **2018**, 434 – 433. DOI 10.1007/978-3-319-67567-1_41.

PAPER REF: 151

ENGINEERING OF BIOMEDICAL DEVICES WITH TAILORED FUNCTIONAL PROPERTIES

Chiara de Crescenzo[1 (*)], Saverio Maietta[2], Maria Richetta[1], Massimo Martorelli[2], Antonio Gloria[3]

[1]Department of Industrial Engineering, University of Rome "Tor Vergata", Rome, 00133, Italy
[2]Department of Industrial Engineering, Fraunhofer JL IDEAS - University of Naples Federico II, P.le Tecchio 80, 80125 Naples, Italy
[3]Institute of Polymers, Composites and Biomaterials - National Research Council of Italy, V.le J.F. Kennedy 54 - Mostra d'Oltremare Pad. 20, 80125 Naples, Italy
[(*)]*Email:* ch.decrescenzo@gmail.com

ABSTRACT

Over the past years, a great amount of research has been focused on the development of biomedical devices, benefiting from the advances in technologies (i.e., additive manufacturing) and design methods. The aim of the current research was to provide a further insight into the development of biomedical devices with tailored functional properties.

Keywords: generative design, design for additive manufacturing, metal devices, biomedical applications.

INTRODUCTION

Over the past years, great efforts have been made to design advanced systems as well as to develop surface modification strategies, thus enhancing the interaction between the devices and the surrounding tissues.

With regard to metal manufacturing, the relationship among microstructure, process parameters and mechanical properties is crucial in different areas (i.e., casting, sintering, welding, plastic forming) and usually involves traditional and advanced fabrication methods (Zhu et al., 2018; Fiorese et al., 2018; Geon et al., 2018).

Biomedical devices must possess mechanical and functional properties to satisfy specific requirements.

Metals like titanium and its alloys have been widely studied for biomedical applications. Specifically, titanium alloys are usually considered to fabricate dental and orthopedic devices, taking into account their excellent biocompatibility, high strength and good corrosion resistance. Interbody fusion devices for spinal applications, total hip replacements, bone screws and nails, parts of artificial heart valves have been developed using titanium alloys (Zhu et al., 2018; Fiorese et al., 2018; Geon et al., 2018; Deing et al., 2014).

The design of biomedical metal devices with desired properties clearly requires the control of the process–structure–property relationship for a material.

Conceptual designs and theoretical/experimental analyses have been used to assess the influence of geometry and material properties.

In this context, the possibility to design implants and scaffolds for tissue regeneration in the form of porous structures and lattices has been widely investigated. In brief, with regard to the design of 3D lattice structures, a “unit cell” may be adopted and a volume based on it may be built up. However, many methods are employed to develop 3D periodic structures, involving topology optimization and issues related to the implementation of different theories (i.e., homogenization).

Stress shielding effects, which are related to great mismatch between the elastic modulus of the implants and surrounding structures, generally cause bone atrophy and implant loosening.

Anyway, it is also well known that stress distributions are related to stiffness, which depends on shape and size as well as on an intrinsic mechanical property of the material (i.e., the Young’s modulus).

The aim of the current research was to provide a further approach in the development of engineered devices with tailored functional properties for biomedical applications, benefiting from the advances in technologies (i.e., additive manufacturing) and design methods.

RESULTS AND CONCLUSIONS

3D additively manufactured lattice structures were fabricated, starting from conceptual designs of porous devices with specific shapes and consisting of materials (i.e., cobalt-chromium, titanium and its alloys) with different Young’s modulus.

A computer-aided design (CAD) based approach was used to develop many kinds of structures with controlled morphology. Different cell units were designed varying pore size and strut diameter. SolidWorks® 2017 (Dassault Systemes, Paris, France) CAD system was used to perform the operations.

The design of porous devices was performed for the reduction of the implant stiffness in order to overcome the drawbacks (i.e., stress shielding effects, bone atrophy, implant loosening) related to the use of materials with Young’s moduli which are higher than those of natural tissues.

Topology optimization was also considered to define the optimal distribution of the material within the design domain, however satisfying the design constraints.

Results from theoretical/experimental analyses suggested that it is always possible to tailor the mechanical performance of porous devices, by properly varying the architectural features as well as the material–shape combination.

REFERENCES

Zhu M, Xu G, Zhou M, Yuan Q, Tian J, Hu H. Effects of Tempering on the Microstructure and Properties of a High-Strength Bainite Rail Steel with Good Toughness. Metals, 2018, 8, p. 484.

Fiorese E, Bonollo F, Battaglia E. A Tool for Predicting the Effect of the Plunger Motion Profile on the Static Properties of Aluminium High Pressure Die Cast Components. Metals, 2018, 8, p. 798.

Jeon G T, Kim KY, Moon J-H, Lee C, Kim W-J, Kim SJ. Effect of Al 6061 Alloy Compositions on Mechanical Properties of the Automotive Steering Knuckle Made by Novel Casting Process. Metals, 2018, 8, p. 857.

Deing A, Luthringer B, Laipple D, Ebel T, Willumeit R. A porous TiAl6V4 implant material for medical application. International journal of biomaterials, 2014.

PAPER REF: 152

MODELING FOR A MEDIAN CRACK IN BRITTLE PLATE WITH V-SHAPED NOTCH

Nikolai Antipin[1(*)], Alexander Freidin[1], Sergey Shubin[1], Petr Gorelchenko[2] and Daniil Belodubrovskii[1]
[1]Corning SNG, St.-Petersburg, Russia
[2]Corning Research & Development Corp., Corning, NY, USA
[(*)]*Email:* antipinkolya@yandex.ru

ABSTRACT

Fracture of a v-notched brittle plate with a median crack is studied. The notch is statically loaded by pressure that simulates contact pressure, or by displacement of the notch sides that simulates loading by a rigid wedge. Non-monotonous dependence of stress intensity factor (SIF) on the crack length and monotonous decrease are demonstrated in dependence on the loading type. The consequences of such behaviours are discussed and the influence of the plate thickness are examined.

Keywords: fracture mechanics, finite element analysis, v-notch, stress intensity factor, median crack, thin plate, brittle failure

INTRODUCTION

We study brittle fracture of a plate with a v-shaped notch with a crack at its vertex. At present, the methods used for the solution of the problems of fracture mechanics for cracked bodies are well developed. There are analytical solutions available for various brittle structures with different crack and loading scenarios. For example, a handbook for stress analysis of cracks (Hiroshi Tada, 2000) offers solutions for more than 200 fracture problems. The fracture problem of solids with a crack emanating from a vertex of a v-notch was studied in more details in number of works (e.g. Kazberuk, 2009; Savruk, 2010). The distinctive feature of those works is that the applied load is a tensile stress applied to the entire structure or point force applied to crack face.

In our work we focus on a pressure loading which is distributed over the notch surfaces and a prescribed displacement of the notch sides. Such loading scheme represents various types of contact loading of a v-notch. With the use of finite element numerical calculations, we examine how the plate thickness and loading type affect the dependence of the stress intensity factor (SIF) on the crack length. We demonstrate non-monotony dependence of SIF in the case of loading by pressure related with interconnection between the crack and rear surface. In the case of fixed displacement of the notch sides monotonous decrease of SIF is observed. We discuss the sources and consequences of such behaviors.

RESULTS AND CONCLUSIONS

The results of numerical simulations of the system of a v-notch and an associated underlying crack for the case of notch loading by pressure are shown in Fig. 1. The dependencies of SIF (y-axis) on the crack length (x-axis) are shown at various thicknesses of the plate. Three regimes are observed in this case. SIF decreases if the crack length increases at relatively small crack lengths. Then, after passing through the minimum which corresponds to the transient mode, SIF increases as the crack tip approaches to the rear surface of the plate. Crack length at which the dependence mode changes depend on the plate thickness. Such a behaviour may be explained by changing the crack loading: initially at small lengths we have a crack loaded by the forces induced by pressure at the notch sides. If the length increases, a couple produced by these forces begin to prevail. Such a behaviour is consistent with corresponding analytical formulas for loading by forces or the couple (Hiroshi Tada, 2000). If displacement of the notch sides is given then SIF decreases if the crack length increases.

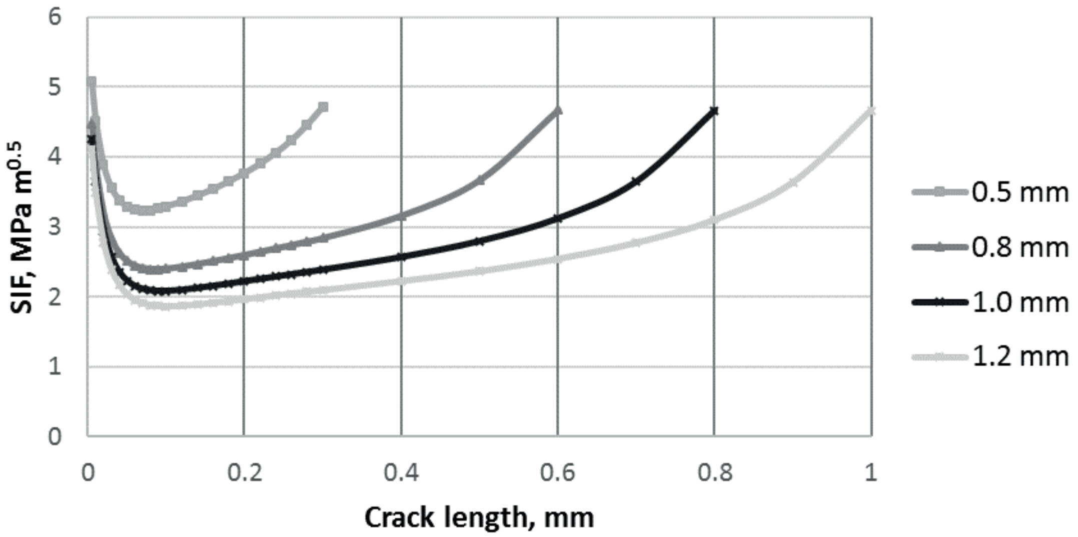

Fig. 1 – Stress intensity factor as a function of crack length for a number of plate thicknesses

A crack is stable if its length corresponds to the falling branch of the SIF dependence, even the crack is critical i.e. Irvin's or Griffith's criteria is satisfied. On the other hand the instability followed by fracture will take place if the crack is made somehow of the length which corresponds to the increasing branch for given notch, pressure and plate thickness.

The developed approach demonstrates the role of the plate thickness in fracture. It may allow us to explore various crack growth scenarios at various notches, loadings, including internal stresses, and material properties.

ACKNOWLEDGMENTS

The authors gratefully acknowledge Jason Harris, Kostja Koreshkov, Doris Lin and Josh Jacobs for the valuable discussions and provided experimental data.

REFERENCES

Hiroshi Tada; P. C. Paris; George Rankine Irwin. The Stress Analysis of Cracks Handbook (3rd ed.). American Society of Mechanical Engineers. February 2000.

Kazberuk A. Stress intensity factors for cracks at the vertex of a rounded v-notch, Material Science, Vol. 45, No. 5, 2009

Savruk M.P., Kazberuk A. Two-dimensional fracture mechanics problems for solids with sharp and rounded v-notches, International Journal of Fracture, 2010, p. 79-95

PAPER REF: 153

PROCESS OPTIMIZATION FOR THE AlSi7Mg0.6 ALLOY PRODUCED BY LASER-BASED POWDER BED FUSION

Lavinia Tonelli[1(*)], Erica Liverani[1], Giuseppe Valli[1], Alessandro Fortunato[1], Iuri Boromei[1], Lorella Ceschini[2]

[1] Department of Industrial Engineering (DIN), Alma Mater Studiorum - University of Bologna, Bologna (Italy)
[2] Department of Civil, Chemical, Environmental and Materials Engineering (DICAM), Alma Mater Studiorum - University of Bologna, Bologna (Italy)
[(*)]*Email:* lavinia.tonelli2@unibo.it

ABSTRACT

Additive Manufacturing (AM) technologies, such as Laser-based Powder Bed Fusion (LPBF), are one of the most promising processing routes, allowing the production of very complex shaped components. In case of aluminium components produced by LPBF a consistent weight reduction can be achieved fulfilling the needs of the automotive industry for fuel efficiency and emission reduction. However, in order to obtain high quality components, process and heat treatment conditions need a proper optimization, based on the peculiar microstructure resulting from LPBF. The aim of the present work is to identify the optimized process parameters for the production of AlSi7Mg0.6 alloy by LPBF.

Keywords: Additive Manufacturing, Laser Based Powder Bed Fusion, Aluminum alloy, AlSi7Mg

INTRODUCTION

Al-Si-Mg alloys are the most widely used casting alloys for the production of complex automotive components due to their high strength to weight ratio and excellent castability. Their mechanical properties directly depend on the microstructural features and solidification defects typical of the casting process (i.e. gas porosities, shrinkage cavities, oxide films, coarse SDAS) [1]. Artificial aging treatment (T6 condition) is typically applied to improve their mechanical strength, by precipitation of fine intermetallic compounds. Recently, the promising and innovative Additive Manufacturing (AM) technologies have been also applied to aluminum alloys, allowing to overcome some of the limits of the conventional processing routes. Indeed, the component can be built in freeform and, by adopting a topology optimization, very complex and ingenious design can be developed, adding material only where needed thus bringing to a further increase of the stiffness and strength to weight ratio [2]. In this view, the most promising AM technology is the Laser-based Powder Bed Fusion (LPBF), in which fine metallic spherical particles are processed, layer by layer, and melted with the aid of a laser beam. LPBF is a complex technology and the process parameters need a careful optimization in order to obtain high-density parts with a defect-free microstructure.

In view of the above, the present work aimed at defining the best process parameters for the production of high-density samples made of AlSi7Mg0.6 alloy produced by LPBF. Assessment of the quality of the produced samples was preliminary fulfilled by density and hardness measurements, then microstructure control was carried out by metallographic analyses using optical, scanning electron microscopy and X-ray diffraction.

EXPERIMENTAL PROCEDURE AND RESULTS

Process optimization aims to obtain full-density and defect free components and, in this view, a wide range of energy density values, resulting from different process parameters, were considered. As shown in Figure 1, by increasing the energy density, the density of samples increases accordingly. At high energy density correspond high values of laser power and low scanning velocities.

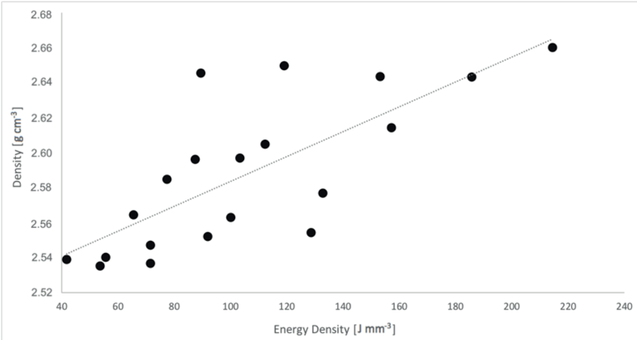

Figure 1: Density of LPBF samples as a function of applied energy density

The microstructure resulting from LPBF is very peculiar: due to the rapid solidification, a metastable microstructure with a sub-micron sized cellular grain is formed. An example of the microstructure, at low and high magnification, is given in Fig.2.

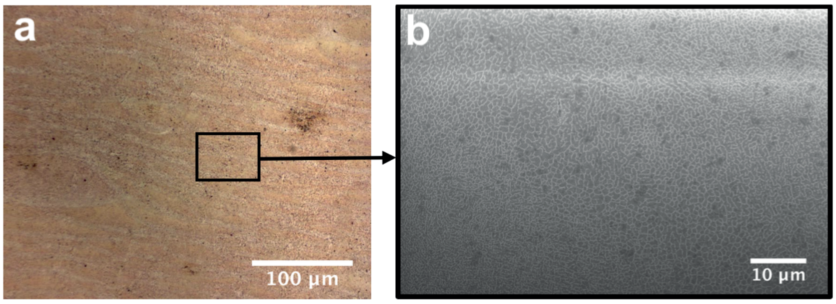

Figure 2: Representative microstructure of AlSi7Mg0.6 LPBF samples: a) optical micrograph at low magnification and b) scanning electron micrograph at high magnification

By reason of the peculiar microstructure, in the as-built condition near-full-density samples exhibit higher hardness than as-cast reference value and close to the heat-treated one, as shown in Table 1. After a period of about 1 month of natural aging, the hardness slightly increased.

Table 1: Hardness of LPBF A357 samples, compared to reference values for as-cast components

	A357 LPBF as-built	**A357 LPBF + natural aging**	**A357 as-cast**	**A357 cast + T6**
HB10	103.9 ± 1.95	105.3 ± 1.69	50-60	95-120

The study allowed to identify the best process conditions to use for the production of AlSi7Mg0.6 components by LPBF and an assessment of the heat treatment conditions was carried out.

REFERENCES

[1] L. Ceschini, Al. Morri, An. Morri, A. Gamberini, S. Messieri, Materials and Design 30 (2009), 4525-4531

[2] T. Debroy, H.L. Wei, J.S. Zuback, T. Mukherjee, J.W. Elmer, J.O. Milewski, A.M. Beese, A. Wilson-Heid, A. De, W. Zhang, Progress in Materials Science 92 (2018), 112-224

PAPER REF: 154

AUSTENITIC STAINLESS STEEL PLATES PRODUCED BY WIRE-AND-ARC ADDITIVE MANUFACTURING (WAAM): MICROSTRUCTURAL AND MECHANICAL CHARACTERIZATION

Lavinia Tonelli[1], Vittoria Laghi[2], Stefania Toschi[2], Alessandro Morri[1], Michele Palermo[2], Lorella Ceschini[2], Tomaso Trombetti[2]

[1] Department of Industrial Engineering (DIN), Alma Mater Studiorum - University of Bologna, Bologna (Italy)
[2] Department of Civil, Chemical, Environmental and Materials Engineering (DICAM), Alma Mater Studiorum - University of Bologna, Bologna (Italy)
(*)*Email:* lavinia.tonelli2@unibo.it

ABSTRACT

The present work provides a first overview of a wide experimental campaign recently carried out at the Topography and Structural Engineering Labs and at the Metallurgy Lab of the University of Bologna. The research aims at characterizing the microstructure and mechanical behaviour of 308LSi stainless steel plates produced by wire-and-arc additive manufacturing (WAAM) for structural engineering applications.

Keywords: Additive Manufacturing, Stainless Steel, Wire and Arc Additive Manufacturing, Microstructure, Mechanical behaviour.

INTRODUCTION

Additive Manufacturing (AM) technologies enable the fabrication of 3D complex parts by adding material, layer by layer, instead of subtracting it. Several AM processes can be used for a wide range of materials and for several applications. Among these, Wire Arc Additive Manufacturing (WAAM), allows the fabrication of metallic parts by melting a wire, with the aid of an electric arc, and depositing the melted material. Both the torch and the wire feedstock are computer-guided, so they can follow the designed path to build the component. Unlike other AM processes, WAAM does not require a closed chamber or a vacuum atmosphere to operate and it allows to work with high deposition rates (1-10 kg/hr) [1,2]. For these reasons, WAAM is a particularly appealing technology in the field of civil engineering for the fabrication of large structures [3]. Very recently, MX3D (NL) presented the first metal 3D-printed footbridge, to be mounted in Amsterdam city center by 2020, at the Dutch Design Week held in October 2018 in Eindhoven [4]. However, like all AM technologies, WAAM parts exhibit typical issues related to the process, such as residual stresses, distortions, poor surface quality, porosity, anisotropy. Therefore, in-depth microstructural and mechanical characterization has to be carried out, in order to highlight the actual potential of WAAM.

In the present work, 308LSi austenitic stainless steel plates produced by WAAM, with or without active cooling system, were characterized by tensile tests, microstructural and fractographic analyses, taking into account different samples orientations, longitudinal and transversal respect to the building direction.

RESULTS AND CONCLUSIONS

Representative images of the microstructure of WAAM plates, obtained by means of Optical (OM) and Scanning Electron Microscopes (SEM), are shown in Figure 1. At low magnification and in bright field (Figure 1a) the layered microstructure can be clearly recognized while, under polarized light (Figure 1b), the growing of columnar grains crossing-over layers, responsible for the anisotropy, is highlighted. SEM micrograph at higher magnification (Figure 1c) shows stringers of δ-ferrite in the austenitic matrix.

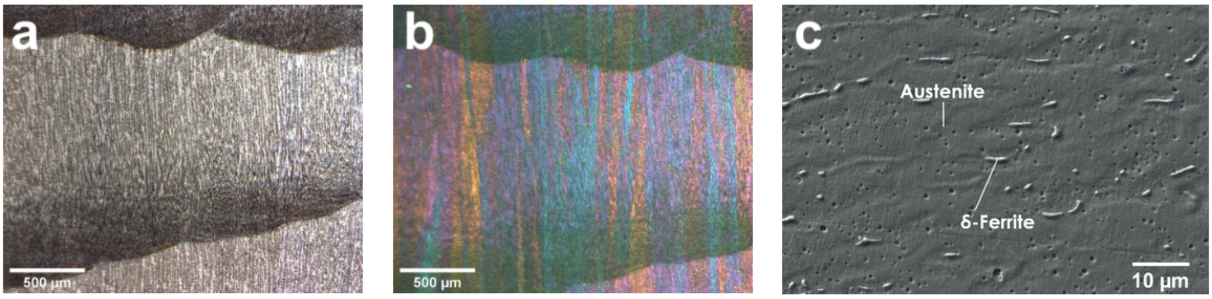

Figure 1: Microstructure of WAAM plates: a) OM bright field, b) OM under polarized light, c) SEM

The stress-strain curves [5], obtained by tensile tests carried out according to ISO EN 6892-1, show a considerable influence of the specimen orientation with respect to the printing deposition layer (i.e. longitudinal – *x*, along the printing layer and transversal – *y*, perpendicular to it).

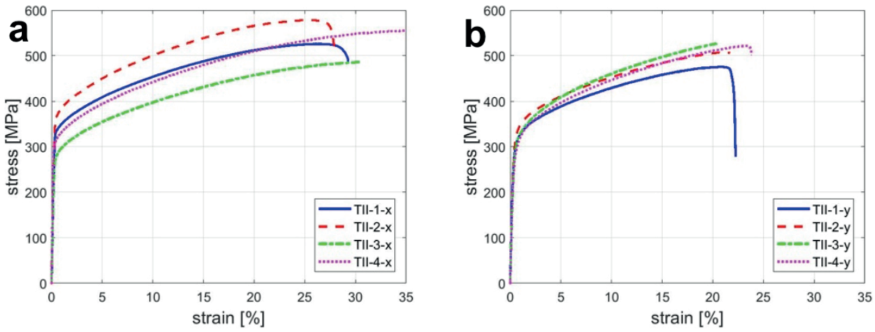

Figure 2: Tensile test results of WAAM plates: a) longitudinal (x direction), b) transversal (y direction)

ACKNOWLEDGMENTS

The support of Dutch company MX3D, which provided the tested materials, is gratefully acknowledged.

REFERENCES

[1] B. Wu, Z. Pan, D. Ding, D. Cuiuri, H. Li, J. Xu, J. Norrish, Journal of Manufacturing Processes, 35 (2018), 127-139

[2] C.R. Cunningham, J.M. Flynn, A. Shokrani, V. Dhokia, A.T. Newman, Additive Manufacturing 22 (2018), 672-686

[3] C. Buchanan, L. Gardner, Engineering Structures, 180 (2019):332-348.

[4] www.mx3d.com

[5] V. Laghi, M. Palermo, G. Gasparini, V.A. Girelli, T. Trombetti, Journal of Constructional Steel Research, (2018), under review.

PAPER REF: 155

RE-DIMENSIONING OF A WAREHOUSE LAYOUT A PRACTICAL CASE

Marlene Madureira(1), Jose Carlos Sá[1,2(*)], Manuel Pereira Lopes[1], Luís Pinto Ferreira[1], Teresa Pereira[3]

[1]Department of Mechanical Engineering, School of Engineering, Polytechnic of Porto, Porto, Portugal
[2]School of Business Sciences, Polytechnic Institute of Viana do Castelo, Valença, Portugal
[3]Design School, Polytechnique Institute Cavado Ave, Barcelos, Portugal
[(*)]*Email:* cvs@isep.ipp.pt

ABSTRACT

This study aims to design a new warehouse layout as a solution to the warehouse's main problem: lack of space to store all the materials in stock. Besides the existing warehouse building, which currently presents an unsuitable layout for the storage of large volumes, there is a second area right next to the first to increase the storage area. The two buildings were re-dimensioned to accommodate a great quantity of stock, enabling one to transform the warehouse building into an industrial warehouse with appropriate storage methods. The final layout increased the storage area by 64%, from a total of 1.471,41 m^2 to 2.414,22 m^2 overall.

Keywords: warehouse, layout, storage area.

INTRODUCTION

The warehouse focused upon in this paper supplies both the company's production lines as well as its clients. Nowadays, the space provided by the warehouse cannot accommodate the quantity of stock units which exist in the company. This has led to the occupation of secondary areas, which should not be congested. In addition to this situation, the materials handled by the warehouse are of different sizes and dimensions, a factor that makes space optimization even more difficult.

Since there was virtually no information pertaining to the storage of the materials in question, the study of materials was based on sampling through successive counts of the existent stock. This was only possible because production planning for the forthcoming years does not foresee a substantial increase in necessities. However, the company does have a short planning horizon as it depends on official tenders, which have rather limited timespans.

A new collection of data was carried out to register the current layout and the "AS IS" state, which resulted in a new warehouse map. A detailed study of project restraints was undertaken, thus supplying the primary information required to begin the layout design proposals. Six layout proposals were provided for each building.

RESULTS AND CONCLUSIONS

The selected layouts are shown in Fig. 1. One was able to increase the use of height space, which was one of the main issues in the current layout. Conventional racking and cantilever racking were also considered in warehouse A, while warehouse B (new building) is dedicated to the storage of picking material. Materials are thus segregated: small volumes are stored in warehouse B, and material of larger proportions and pallet sizes is stored in building A.

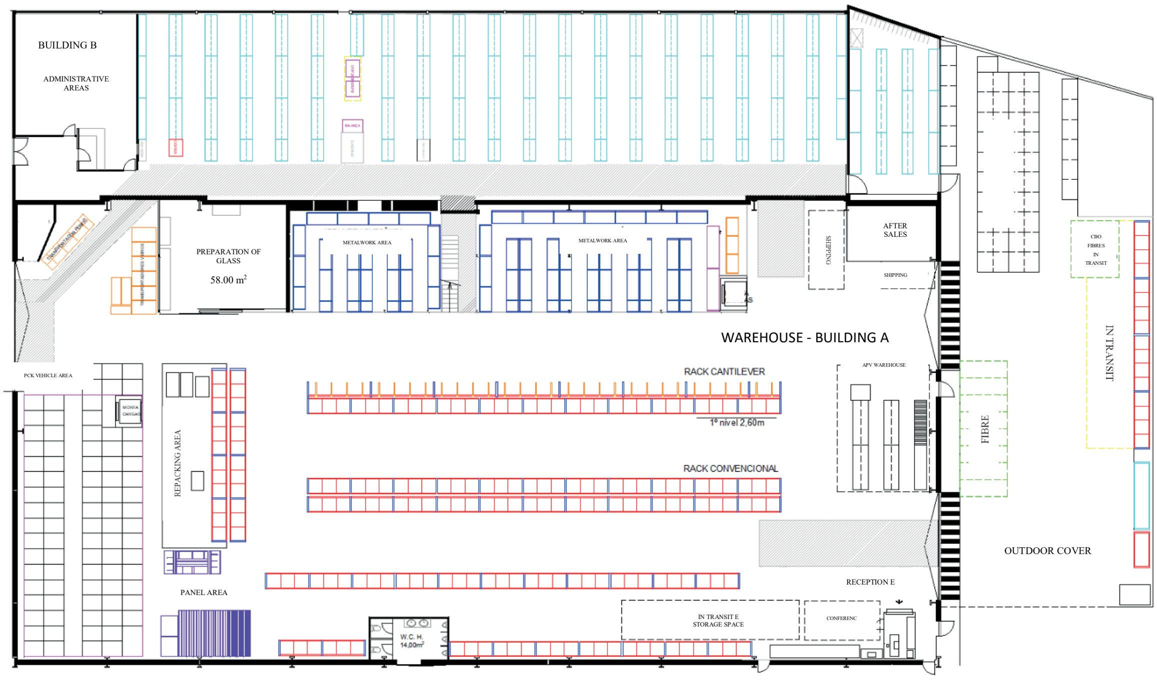

Fig. 1 Final layout

The new layout presents an increase of 218% in height storage, which was one of the main project goals. The proposal added 942,81 m² to the storage area, with an additional 64% in usable area, when compared to the present situation. However, some units had to be designated for storage in the covered zone at the entrance of the warehouse due to their excessive size. This would have limited the number of storage structures in the warehouse and restricted space units to other types of components.

Table 1 Comparison between the present layout and the new layout proposal

Comparison: Current state / New layout				
(m^2)	***Present layout***	***New layout***	***Difference***	***Earnings / Losses***
Storage area (floor)	928,26	685,97	-242,29	-26%
Occupied area (floor)	1323,66	1173,43	-150,23	-11%
Storage area (in height)	543,15	1728,25	1185,10	218%
Total storage area (floor + height)	1471,41	2414,22	942,81	64%
Circulation area	1457,74	1765,22	307,48	21%

ACKNOWLEDGMENTS

The author gratefully acknowledges the information provided by the company, which enabled the execution of this study.

REFERENCES

Karakis I., Tanyas M., Baskak M., 2018. “Hierarchical Warehouse Design Approach for Distribution Centres”. International Journal of Business and Management Invention.

Phumchusri N., Kitpipit P., 2017. “Warehouse Layout Design for an Automotive Raw Material Supplier”, Engineering Journal.

PAPER REF: 156

EXPERIMENTAL INVESTIGATION ON THE DAMPING PROPERTIES OF A POLYMER CONCRETE

Giulio Canella[1], Nicolò Vincenzi[2], Marco Troncossi[1,3(*)]

[1] CIRI-MAM – Interdepartmental Center for Industrial Research-Advanced Application in Mechanical Engineering and Materials Technology, University of Bologna, Viale del Risorgimento 2, 40136 Bologna, Italy

[2] GIULIANI – a Bucci Automations SpA Division, Via Granarolo 167, 48018 Faenza, Italy

[3] DIN – Dept. of Industrial Engineering, University of Bologna, Viale del Risorgimento 2, 40136 Bologna, Italy

[(*)]*Email:* marco.troncossi@unibo.it

ABSTRACT

The damping properties of a commercial polymer concrete are the subject of this study, which is aimed to investigate the material suitability as a filler of machine bed components to limit the vibration levels of machine tools and automatic machines working at high dynamics. Two main goals were targeted: (*i*) assessment of the elastodynamic effects due to the polymer concrete introduced into typical components of machine beds, in order to quickly evaluate its practical potential and (*ii*) determination of the damping parameter values to be set in numerical models which simulate the dynamic response of different design solutions of new machine architectures. The presentation will be focused on the methodological approach of the extensive experimental campaign that was carried out, also highlighting possible criticalities, and the main results achieved. The possible use of the polymer concrete as a viable solution to enhance the dynamic performance of the machines will be discussed.

Keywords: machine tool, vibration, damping, polymer concrete.

INTRODUCTION

The precision of automatic machines and machine tools is known to be highly hampered by an uncontrolled elastodynamic behavior of the machine components. With a particular focus on machine tools, vibrations and chatter can be triggered by several sources in a wide bandwidth (Altintas, 2012), e.g. by tool cutting forces and/or inertial loads associated with the rapid movements for spindle positioning, or even by external vibrations transmitted through the ground (Troncossi, 2009). If excessive, these vibrations can reduce the tool life, degrade the quality of the machined surfaces, and cause inacceptable tolerances of the final products. Limiting their effects is thus mandatory in high-performance machines (Munoa, 2016). One problem is that, just due to the variegated sources of vibrations, moving the system natural frequencies out of the excitation bandwidth could be difficult or even impossible. Hence, an effective way to improve the dynamic stability of the machine could be increasing its damping capability. Filling the structural components with proper materials (e.g. metal foam, polymer concrete) is a quite popular way to achieve the goal. In this context, an experimental investigation was performed to accurately characterize the damping properties of a commercial polymer concrete, targeted as a possible solution to be exploited in high-performance machine tools and automatic machines. The numerical data were required (*i*) to evaluate the actual effectiveness of the material and (*ii*) to obtain realistic values of the damping parameters involved in numerical models to properly predict the dynamic response of different design solutions of the machine architectures. To this aim, an extensive experimental campaign was performed on metal beams with hollow cross section filled with a damping core made of the polymer concrete EPUMENT 140/5. Natural frequencies and damping ratios (and static stiffness as well) were estimated and compared to the same properties of the corresponding hollow beams used as reference. For the sake of results robustness and reliability, many impact tests were performed on beams with diverse geometries and in different boundary conditions (free-free and one fixed support). The damping ratios (ζ) were calculated through both the "half-power bandwidth" and "logarithmic decrement" methods (Rao, 2004) after band-pass filtering the beam signal vibrations around the natural frequency of the first flexural mode (f_{n1}), which dominates the free response.

RESULTS AND CONCLUSIONS

The results of just one case are here reported, i.e. impact tests performed on a steel beam (section 100x50mm, length 750mm, thickness 5mm) excited in free-free condition. Five tests were performed for both the hollow and concrete-filled beams. Table 1 lists f_{n1} and ζ – estimated through the logarithmic decrement (δ) method – of the hollow and filled beams. Figure 1 shows the signals of the two beams free responses, filtered around f_{n1}. The dash lines spot the instants when the acceleration amplitudes drop to 5% of their maximum values. Just from the limited selection of the reported results, the suitability of the polymer concrete as a filler material of machine bed components to damp vibrations appears evident.

Table 1 – Modal parameters and logarithmic decrements of the two beams tested in free-free condition

Specimen	f_{n1} (Hz)	δ (-)	ζ (-)
Hollow beam	601	0.004	0.07%
Concrete-filled beam	501	0.020	0.33%

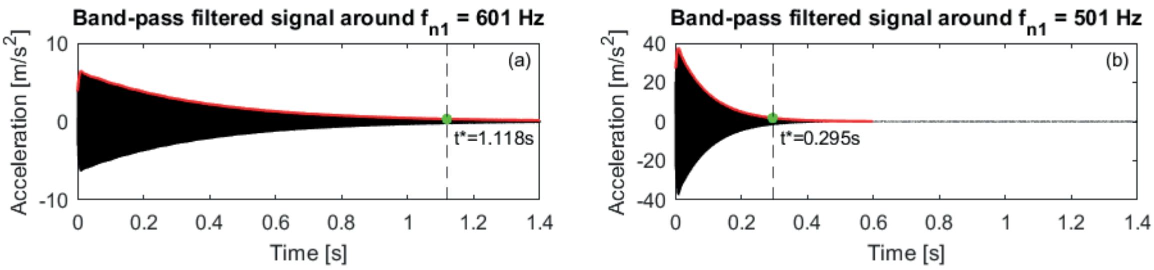

Fig. 1 – Filtered signals of the beam free responses: (a) hollow section ; (b) beam filled with polymer concrete

ACKNOWLEDGMENTS

The authors gratefully acknowledge the funding by the Operational Programme of the European Regional Development Fund of the Emilia-Romagna Region (ROP-ERDF 2014-2020, DGR 887/2018).

REFERENCES

Altintas Y. Manufacturing automation: metal cutting mechanics, machine tool vibrations, and CNC design. Cambridge University Press, Cambridge, 2012.

Troncossi M, Troiani E, Rivola A (2009). Design optimization of a laser cutting machine by elastodynamic modeling. Procs. of 9th ASME-ESDA, 7-9 July 2008, Haifa, Israel, p. 551-559.

Munoa J, Beudaert X, Dombovari Z, Altintas Y, Budak E, Brecher C, Stepan G. Chatter suppression techniques in metal cutting. CIRP Annals, 2016, 65(2), p. 785-808.

Rao SS. Mechanical Vibrations (5th Ed.). Prentice Hall, Upper Saddle River, 2004.

PAPER REF: 157

ENGINEERING DESIGN EDUCATION IN COMPUTATIONAL FLUID MECHANICS

S.I.S. Pinto[1,2(*)], **S.M. Zvacek**[3]

[1]Engineering Faculty, University of Porto, Porto, Portugal
[2]Institute of Science and Innovation in Mechanical and Industrial Engineering (LAETA-INEGI), Porto, Portugal
[3]Independent Consultant for Higher Education, SMZTeaching.com, Castle Rock, CO, United States
[(*)]*Email:* spinto@fe.up.pt

ABSTRACT

The goal of this work was to explore the possible effects of applying learning theories and the cognitive apprenticeship instructional model to a graduate engineering course. The professor learned about the cognitive apprenticeship model and associated learning theories while enrolled in a faculty development course, Engineering Education Theory and Practice. After a course revision using the cognitive apprenticeship model, the students reported excellent feedback relative to the teaching methods applied to the first module of the curricular unit Computational Fluid Mechanics of the Master Computational Mechanics at Engineering Faculty of University of Porto. This paper describes those results and the six teaching strategies incorporated in the revised module.

Keywords: engineering education, teaching methods, cognitive apprenticeship, computational fluid mechanics.

INTRODUCTION

The International Society for Engineering Education (IGIP) oversees a professional development curriculum designed to enhance the pedagogical skills of professors. The courses in this program encompass a wide array of topics within the teaching field at universities. One such course, Engineering Education Theory and Practice (EETP) was offered by the Faculty of Engineering of the University of Porto (FEUP) during the spring term of 2018. This work describes how one participant, a professor at FEUP, applied concepts from the course, specifically the cognitive apprenticeship instructional model (Collins et al., 1987), to the redesign of the first module of the Computational Fluid Mechanics (CFM) curricular unit of the Master of Computational Mechanics at FEUP.

The goal of a cognitive apprenticeship (CA) is to help students acquire and integrate cognitive and metacognitive strategies for using, managing, and discovering knowledge (Collins et al., 1987). The CA facilitates the growth and development of complex, expert-level problem-solving abilities. Students work with the assistance and guidance of those who are experienced in the subject, gradually taking on more difficult tasks as their need for support lessens (Dennen and Burner 2007). This instructional model is especially appropriate for graduate studies where learners are making the transition to careers in their chosen fields and faculty members can play a mentorship role in the process.

The CA model has been used to design a wide array of disciplines and in diverse learning environments. Some of the more recent examples of its use are in mathematical modelling (Wedelin and Adawi, 2015), software development (Christensen, 2016), and graduate-level statistics (Sadaati et al., 2015). Non-course-based applications of the CA are found in clinical practice for medical students (Stalmeijer et al., 2009), faculty development for online course design (Wiss et al., 2018), training for psychiatric rehabilitation providers (Bates et al. 2012), and mentoring doctoral research assistants (Maher et al., 2013), as just a few examples.

In 2018, one of the authors enrolled in the Engineering Education Theory and Practice (EETP) course, and began to associate theory with her teaching practice. She realized that the teaching methods of the CFM course unit could be improved by applying learning theories and procedures of validated instructional models for course design.

The first module of the course unit CFM was taught in 2017, before the EETP course was offered. With only her previous teaching experience (and good sense) as a guide and without the use of any formal pedagogic theory, the professor had applied a framework quite like the *cognitive apprenticeship* instructional model, based on *Collins et al.* (1987). The goal of this method is to help students acquire and integrate cognitive and metacognitive strategies for using, managing, and discovering knowledge (Collins et al.,1987).

While participating in the EETP course in 2018, this professor decided to align the activities of CFM with the cognitive apprenticeship approach in a more direct and purposeful manner. The revised first module of the course unit is built on the theoretical bases of behaviorism, cognitivism, and constructivism as the backbone of the instructional model. The relationships between the theories, the cognitive apprenticeship model, and the course components have guided the decisions of the professor to strengthen the course unit design.

RESULTS AND CONCLUSIONS

The CA instructional model of Collins et al. (1987) is divided into six teaching methods: *Modeling, Coaching, Scaffolding, Articulation, Reflection, and Exploration.* In the first, *Modeling*, the instructor demonstrates the tasks explicitly, so that students can later build a conceptual model of the process independently. In this curriculum unit of CFM, the professor showed the construction of the computational mesh, ran simulations, and analysed the desired results on the computer (displayed via projector), while students followed along on their computers. During *Coaching,* the professor gives feedback and hints to the students. For example, in the previous tutorial task, there was an ongoing discussion between the professor and students in which they could ask questions and get immediate guidance and feedback.

The teacher uses *Scaffolding* to support students with aspects of the tasks they cannot yet manage on their own. After the tutorial (with modelling and coaching) students were required to construct other computational meshes, other simulations, and other results on their own and the professor was available to assist only if necessary. The *Articulation* teaching method has the instructor question students to help them clarify their knowledge, reasoning or solving-processes in the domain. In the CFM unit, the professor asked students a series of questions related to the computational mesh reconstruction, such as, “Which is the accurate mesh? Tetrahedral? Hexahedral? Hybrid?” related to the simulation process, “Which the appropriate numerical method?” and related to the desired results “Which is the most important parameter that indicates atherosclerosis formation? TAWSS? OSI? RRT?” Students answer the questions to refine and restate their understanding and to form explicit conceptual models.

In *Reflection*, students consider their strengths and weaknesses, comparing their own problem-solving processes with those of an expert, of another student, and ultimately of an internal cognitive model of expertise. In an advanced phase of learning the CFM tasks, students look back and analyze their performance with a goal of moving toward the behavior of an expert, asking themselves questions such as, “Is RRT the hemodynamic parameter that most effectively shows the tendency to atherosclerosis appearance?”. Finally, during *Exploration*, students formulate and pursue personal learning goals and can frame interesting problems and take the initiative to solve them. In this final phase, students should be able to solve computational mechanics issues by themselves.

An anonymous survey about the six teaching methods of the CA was provided to the students who attended the CFM curricular unit in 2017 and in 2018. All of the student responded to the survey, and although these were very small groups (seven in 2017 and six in 2018) their answers revealed notably different points of view about the teaching methods used in each year.

Students were asked, for each of the six teaching methods, if the professor had included one or more of those strategies during the course and students answered on a scale of 1 “(No, not at all”) to five (“Yes, definitely”). Fig. 1 represents a summary of the answers of the students. The students from 2017 were less sure about the inclusion of the various instructional strategies, which is not surprising since the CA model was applied (unknowingly) in a somewhat sporadic manner.

Fig. 1 – Student responses to survey recognizing the use of the cognitive apprenticeship strategies.

Students were also asked to comment on the helpfulness of each method and to provide suggestions for improvement. In the *Modeling* step (Fig. 1a), two students of 2017 suggested that a more in-depth demonstration of the software should be emphasized, while all the students of 2018 totally agreed with the teaching step the way it was, focusing on “time-saving.” Students of 2017 and 2018 affirmed that Coaching was essential to clarify doubts while the professor explained the tasks. Students of 2018 were in agreement with this method, but fewer students of 2017 answered “Yes, definitely,” recognizing its use (Fig. 1b).

Students from 2017 and 2018 gave similar responses concerning the *Scaffolding* method (Fig. 1c). They remarked that this step was indispensable and agreed that students must perform examples of the tasks on their own with the support of the professor. A student from 2018, for example, commented that, “Working on your own lets you understand the deepness of what you have learnt in class, improving new skills and honing the ones you got from classes.” Two students from the 2017 group believed that the *Articulation* step (Fig. 1d) could be improved. One student remarked, “Allowing students to develop their own logic and being questioned more on why some decisions were made would absolutely be more beneficial.” In 2018, the professor asked a more diverse set of questions to help students clarify their thinking and all of the students were satisfied with this approach.

Three students of 2017 and one of 2018 felt that the *Reflection* step (Fig. 1e) should be improved, by providing more time to use the software so they could analyse their strengths and weaknesses.

The professor plans to improve this teaching method for the future, although the time allotted (two months, five hours per week) may limit how much this can be changed. When asked about the *Exploration* method (Fig. 1f), two students from the 2017 group focused on the problem of not being totally independent when using the software because of time limitations (again). An example comment was, “After the course, the student would have the basic knowledge about the software and the method. Not enough to solve real life problems.” Because of the time constraints already present, the professor chose to present more complex problems, thus giving the students more in-depth experience using the software. The feedback of students of 2018 was much more positive as a result.

In general, the students of 2018 had very good and positive opinions about the CA teaching method. These general results suggest that the EETP course, attended by the professor in 2018, led to more effective teaching methods. The professor became more aware of the relationship between the theoretical pedagogic methods and the practice. When teaching the course in 2018, the professor applied the cognitive apprenticeship model in a purposeful and intentional way and the answers of the student responses confirm its value.

ACKNOWLEDGMENTS

Authors gratefully acknowledge the Engineering Faculty of University of Porto, the students who attended the Computational Fluid Mechanics curricular unit of the Master in Computational Mechanics and answered the survey, and the Institute of Science and Innovation in Mechanical and Industrial Engineering.

REFERENCES

Bates FM, Dolce JN, Waynor WR. The cognitive apprenticeship model: Implications for its use in psychiatric rehabilitation provider training. Journal of Rehabilitation, 2012, 78, p. 5-10.

Collins A, Brown JS, Newman SE. Cognitive aprrenticeship : Teaching the craft of reading, writing and mathematics (Technical Report No. 403), 1987, Cambridge, MA : BBN Laboratories.

Christensen, H.B. Teaching devops and cloud computing using a cognitive apprenticeship and story-telling approach. Proceedings of the 2016 ACM Conference on Innovation and Technology in Computer Science Education, 2016, p. 174-179. New York: Association for Computing Machinery.

Dennen VP, Burner KJ. The cognitive apprenticeship model in educational practice. Handbook of Research on Educational Communications and Technology, 2007, p. 425-439.

Maher MA, Gilmore JA, Feldon DF, Davis TE. Cognitive apprenticeship and supervision of science and engineering research assistants. Journal of Research Practice, 2013, 9, p. 1-22.

Sadaati F, Tarmizi RA, Ayub AFM, Bakar KA. Effect of internet-based cognitive apprenticeship model (i-CAM) on statistics learning among postgraduate students. PLoS one, 2015, 10, p. 1-16.

Stalmeijer RE, Dolmans DH, Wolfhagen IH, Scherpbier AJ. Cognitive apprenticeship in clinical practice : Can it stimulate learning in the opinion of students ? Advances in Health Science Education, 2009, 14, p. 535-546.

Wedelin D, Adawi T. Teaching mathematical modelling and problem solving : A cognitive apprenticeship approach to mathematics and engineering education. International Journal of Engineering Pedagogy, 2014, 4, p. 49-55.

Wiss A, DeLoia J, Posey L, Waight N, Friedman L. Faculty development for online learning using a cognitive apprenticeship model. International Journal on Innovations in Online Education, 2018, 2.

PAPER REF: 158

DEEP ROLLING AND SHOT-PEENING TO IMPROVE THE TRIBOLOGICAL RESPONSE OF CONNECTING ROD SCREWS

D. Croccolo[1], M. De Agostinis[1], S. Fini[1], G. Olmi[1](*), L. Paiardini[1], F. Robusto[1]

[1]Department of Industrial Engineering (DIN), University of Bologna, Alma Mater Studiorum, Bologna, Italy
(*)*Email:* giorgio.olmi@unibo.it

ABSTRACT

This work deals with an experimental study on the frictional properties of connecting rod high strength screws. Considering that friction has a significant impact on the achievable preload for fixed and controlled tightening torque, the question of friction reduction was tackled by suitable surface treatments. Deep-rolling and shot-peening were involved in the campaign that proved the latter has a highly beneficial effect at reducing friction. Moreover, bearing friction coefficient is made barely steady versus repeated tightening in both lubricated and dry conditions.

Keywords: connecting rod, big hole bolts, tribology, shot-peening, deep-rolling.

INTRODUCTION

Connecting rod may be regarded as one of the most critical components in an engine. In fact, it transfers loads from the piston to the crankshaft and operates under high fatigue loads during service. Some previous studies have been focused on the failures of rods, which in turn caused engine catastrophic failures. The primary reasons for rod breakage were many times related to the fatigue cycling that triggered crack initiation in presence of high stress concentrations due to poor design (Witek, 2017). In some cases, failure occurrence could be related to rod big hole coupling by bolts, whose design or tightening may have triggered some issues. For instance, in (Witek, 2019), the authors pointed out that a too high tightening torque induced a too high preload. This caused, in turn, a high tensile stress concentration in the rod area close to the bolt hole, as well as a local bending effect, which led to the rod fatigue failure. In (Griza, 2009) it is highlighted it is usually desirable to tighten screws up to a remarkably high tightening torque, in order to achieve a sufficiently strong preload. In fact, the higher preload, the lower stress amplitude on the screw under the fatigue load in service condition. These two studies highlight that big hole bolt preload does have a significant impact on the screw behavior and on the rod response. On one hand, a too high preload may generate a too high load on the rod surface, thus weakening this component. On the other hand, a too low preload leads to an increment of the stress amplitude affecting the screw under fatigue, with consequent risk of bolt failure.

Previous studies from the same group (De Agostinis, 2016; Croccolo, 2017) have indicated that the bearing and the thread frictional coefficients have a strong impact on the achievable preload for a fixed tightening torque being controlled by a torque wrench upon fastening. In addition, specifically regarding connecting rod screws, it must be emphasized their fastening procedure requires a retightening, meaning that they are tightened, untightened and retightened again. Further retightening(s) may occur upon maintenance or refurbishment. Multiple tightening may also affect the tribological behavior, as the mating surfaces get gradually deteriorated with consequent wear that increases friction. Its underestimation or overestimation may lead for fixed applied torque to too low or too high preload. The subject of this research was the proper selection of suitable treatments having the capability of reducing friction and its variation with multiple tightening.

MATERIALS AND METHODS

This topic was tackled experimentally and the campaign involved MJ9 and MJ10 screws respectively made of 36 NiCrMo 16 and 42 CrMoV 5-7, in both lubricated and dry conditions, for a total amount of four experimental plans. Each of them investigated the impact on friction of three factors, i.e. deep rolling at the screw underhead fillet, shot-peening and multiple tightening. The first factor was regarded as on-off with deep rolling being performed before shot-peening. The latter was investigated over three levels: no peening, Z100 10-12 N and UFS70 10-12 N treatments. Finally, 1, 2 or 3 tightenings were considered, based on the most frequent number of tightenings in the screw life. The tests were conducted (with five replications) by a commercial test bench, in agreement with ISO 16047 (ISO 16047, 2005) for the determination of the total and of the bearing frictional coefficients (with reference to the treated zone). The results were then processed by the tools of three-factor ANOVA and F-test, to investigate the significance of the main effects and interactions.

RESULTS, DISCUSSION AND CONCLUSIONS

The outcomes indicate that shot-peening, as an effect of the generation of dimples and surface porosity with multiple contact points, is highly effective at lowering (up to 30%) the bearing frictional coefficient in both dry and lubricated conditions. In addition, shot-peening is able to make friction have a steady trend vs. repeated tightenings, when lubrication is applied (Fig. 1).

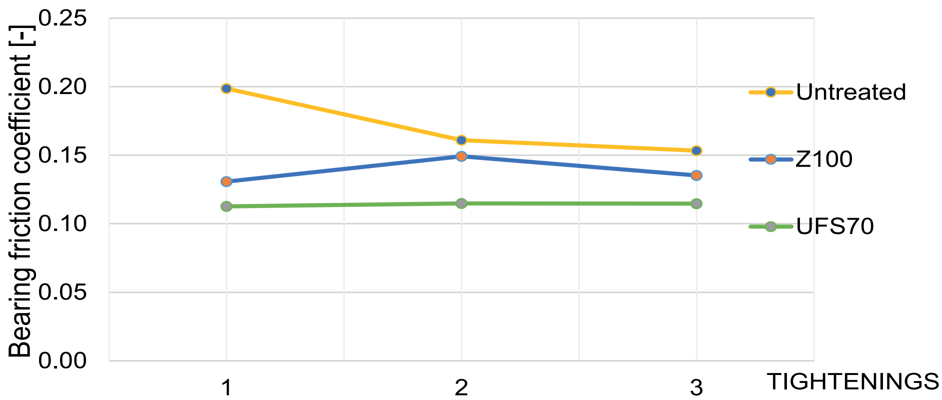

Fig. 1 – Bearing friction coefficients trends vs. repeated tightenings for unpeened and peened screws in lubricated conditions

In case of a dry surface (Fig. 2), the resulting trend is not flat, but the increase rate is reduced with respect to untreated screws. Deep rolling proved not to have effect on friction; however, it is also important, as it significantly affects the fatigue response, to be studied in a separate paper.

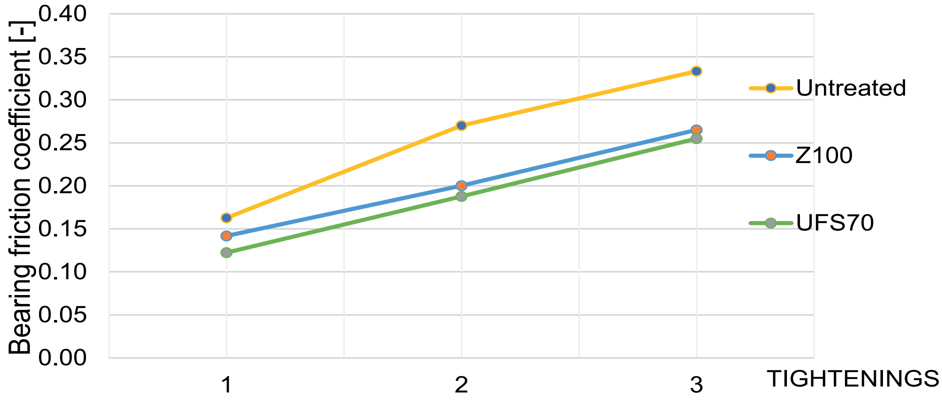

Fig. 2 - Bearing friction coefficient trends vs. repeated tightenings for unpeened and peened screws in dry conditions

REFERENCES

Witek L, Sikora M, Stachowicz F, Trzepiecinski T. Stress and failure analysis of the crankshaft of diesel engine. Engineering Failure Analysis, 2017, 82, p. 703-712.

Witek L, Zelek P. Stress and failure analysis of the connecting rod of diesel engine. Engineering Failure Analysis, 2019, 97, p. 374-382.

Griza S, Bertoni F, Zanon G, Reguly A, Strohaecker TR. Fatigue in engine connecting rod bolt due to forming laps. Engineering Failure Analysis, 2009, 16, p. 1542-1548.

De Agostinis M, Fini S, Olmi G. The influence of lubrication on the frictional characteristics of threaded joints for planetary gearboxes. Proceedings of the Institution of Mechanical Engineers, Part C: Journal of Mechanical Engineering Science, 2016, 230, p. 2553-2563.

Croccolo D, De Agostinis M, Fini S, Olmi G. Tribological properties of bolts depending on different screw coatings and lubrications: An experimental study. Tribology International, 2017, 107, p. 199-205.

International Organization for Standardization ISO 16047:2005(E). Fasteners - torque/clamp force testing. Geneva, Switzerland; 2005.

PAPER REF: 159

CONNECTING ROD SCREW TRIBOLOGICAL RESPONSE OPTIMIZED BY A PROPER CHOICE OF PEENING TREATMENT PARAMETERS

D. Croccolo[1], M. De Agostinis[1], S. Fini[1], G. Olmi[1](*), L. Paiardini[1], F. Robusto[1]

[1]Department of Industrial Engineering (DIN), University of Bologna, Alma Mater Studiorum, Bologna, Italy
(*)*Email:* giorgio.olmi@unibo.it

ABSTRACT

This work deals with an experimental study on the frictional properties of connecting rod high strength screws. It is a follow-up of a previous work: at the initial stage, a careful microscope analysis of the previously tested screws under tribological tests was carried out. These observations suggested that the peening treatment could be optimized by either increasing the shot size or decreasing the Almen intensity, thus achieving a better impact load distribution, as well as a surface roughness reduction. The results indicate that the modified peening parameters are able to lead to a significant drop of friction and to its steady trend versus repeated tightenings even in dry conditions.

Keywords: connecting rod, big hole bolts, tribology, shot-peening, repeated tightenings.

INTRODUCTION

The screws involved in the experimentation described in (Croccolo, 2019) underwent careful observations by stereoscopic microscope, as well as roughness measurements. In particular, the roughness measurements highlighted a quite high roughness, i.e. 1.5 and 2 μm for the two peening treatments (Z100 10-12 N and UFS70 10-12 N respectively), if compared to that of untreated screws (0.4mm). These results were obtained for both MJ9 and MJ10 threaded screws, regardless of their materials. This so high level of roughness was regarded as undesirable, as it was likely to have a detrimental effect on the fatigue response, considering also the high resistance class of the two screws (12.9), which could promote a high notch sensitivity. The microscope analyses (Fig. 1) were aimed at the estimation of the dimensions of dimples created by the shot impacts. These dimples were in the order of 85mm and 55mm for the Z100 and UFS70 treatments respectively. The morphology of the pitted surface and the retrieved dimensions indicated a remarkable amount of impacts with high impulsive load by a large quantity of very small sized shots that had significantly altered the surface. Therefore, as a follow-up of the previous research, further peening treatments were studied to achieve an acceptable value of roughness, not exceeding 1 mm. The expected results consisted in a further reduction of the bearing frictional coefficient both in dry ad in lubricated conditions, as well as a steady trend vs. repeated tightenings even without lubrication. Previous results from the literature (Witek, 2019; Griza, 2009) and by the same research group (De Agostinis, 2016; Croccolo, 2017) indicate that the tribological properties have a large effect on the achievable preload upon tightening under torque control. In addition, a not conformal (too low or too high) axial force may lead to bolt or rod failures.

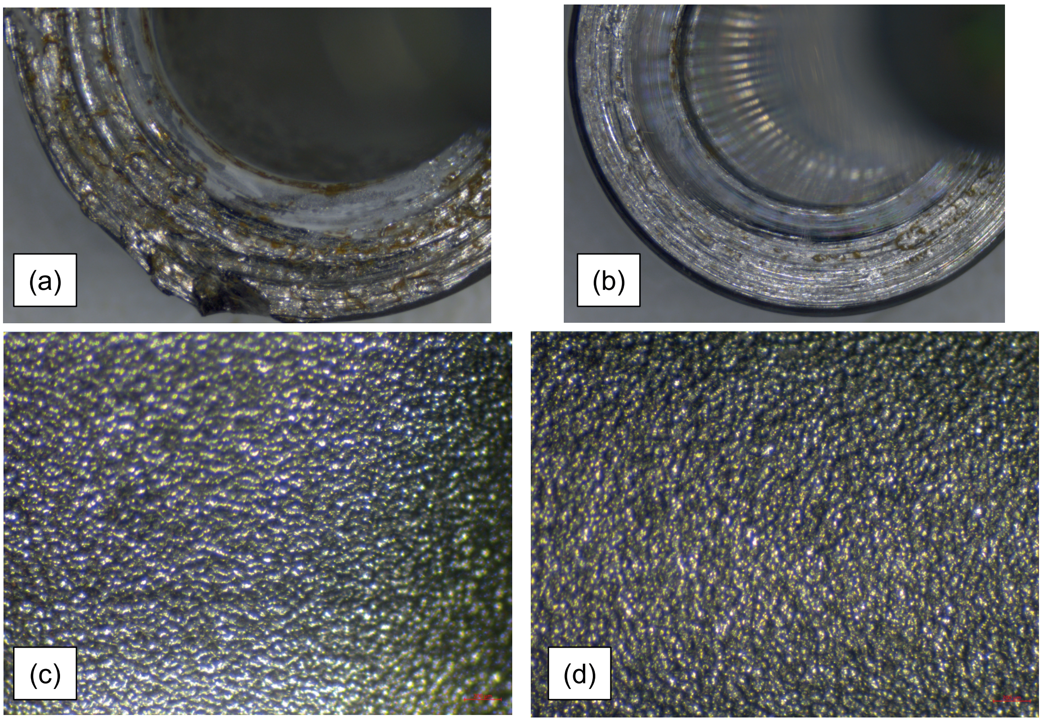

Fig. 1 – (a, b) Screw bearing after (respectively) tribological tests in dry and lubricated conditions; (c, d) surface morphology for (respectively) Z100 10-12N and UFS70 10-12N peening treatments

MATERIALS AND METHODS

The study was focused on 42 CrMoV 5-7 and involved MJ10 screws. The experimental, campaign was regarded as a two-factor design, accounting for the effects of shot-peening and or repeated tightening. Regarding the latter, 1, 2 or 3 repeated tightenings were considered. As for shot peening, the treatments Z100 4N and S110 8.8N were considered, as well as the reference (no treatment level). The aforementioned treatments had the rationale of increasing the shot size (thus achieving a better load distribution and reducing the impact concentrated load) and/or of reducing the Almen intensity. The effect of deep-rolling was not considered, as it previously proved not to affect friction (Croccolo, 2019). The tests were run (with five replications) in dry and lubricated conditions by the same test bench according to ISO 16047 (ISO 16047, 2005).

RESULTS, DISCUSSION AND CONCLUSIONS

The results indicate these shot-peening treatments are able to remarkably reduce friction at the bearing. In particular the outcomes, processed by the tools of two-factor ANOVA, indicate that shot-peening has a highly significant effect and that these two treatments are even better than the previous ones in (Croccolo, 2019) with friction decrease up to 50% with respect to untreated screws. Regarding the trend with respect to repeated tightenings, it is interesting to observe that, when the surfaces are lubricated, the bearing friction coefficient decreases as the number of tightenings increases. This outcome is presumably due to the effect of micro-dimples that retain wear debris and gradually released trapped lubricant. When the test is conducted in dry conditions (Fig. 2), the trend is flat, which indicates a stable tribological response: it means the same required preload can be accomplished only by controlling the tightening torque even after three tightenings. Therefore, these two treatments can be regarded as equivalent each other and among the best ones to provide an optimized tribological behavior to connecting rod screws.

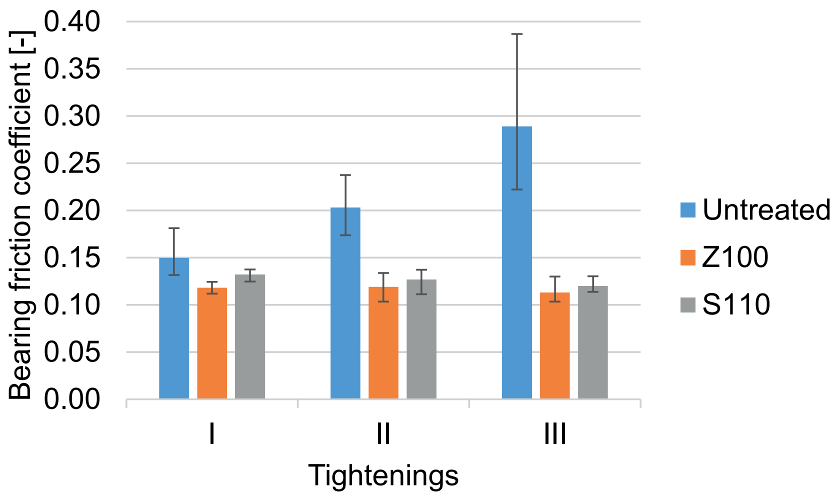

Fig. 2 – Bearing friction coefficient trends vs. repeated tightenings for unpeened and peened screws in dry conditions

REFERENCES

Croccolo D, De Agostinis M, Fini S, Olmi G, Robusto F. Deep rolling and shot-peening to improve the tribological response of connecting rod screws. Proceedings of M2D 2019, Bologna, Italy, 4th to 6th September 2019.

Witek L, Zelek P. Stress and failure analysis of the connecting rod of diesel engine. Engineering Failure Analysis, 2019, 97, p. 374-382.

Griza S, Bertoni F, Zanon G, Reguly A, Strohaecker TR. Fatigue in engine connecting rod bolt due to forming laps. Engineering Failure Analysis, 2009, 16, p. 1542-1548.

De Agostinis M, Fini S, Olmi G. The influence of lubrication on the frictional characteristics of threaded joints for planetary gearboxes. Proceedings of the Institution of Mechanical Engineers, Part C: Journal of Mechanical Engineering Science, 2016, 230, p. 2553-2563.

Croccolo D, De Agostinis M, Fini S, Olmi G. Tribological properties of bolts depending on different screw coatings and lubrications: An experimental study. Tribology International, 2017, 107, p. 199-205.

International Organization for Standardization ISO 16047:2005(E). Fasteners - torque/clamp force testing. Geneva, Switzerland; 2005.

PAPER REF: 160

WEAR BEHAVIOR OF AN ELECTRODEPOSITED NICKEL COATING ON A ZINC ALLOY

Dario Croccolo[1], Massimiliano De Agostinis[1], Stefano Fini[1], Giorgio Olmi[1], Francesco Robusto[1 (*)], Lavinia Tonelli[1]

[1]DIN, Department of Industrial Engineering, University of Bologna, Viale Risorgimento 2, Bologna, Italy
[(*)]*Email:* francesco.robusto@unibo.it

ABSTRACT

Nickel coating on zinc alloy is quite promising for the achievement of an additional wear improvement in corrosive environment. To investigate this point, block-on-ring tests were carried out. 5x5x20 mm^3 blocks were obtained from real locking components, made of ZP5 EN 12844 and coated by Zn/Cu1Ni5s ISO 1458. As counter material, an AISI 304 with a 40 mm diameter cylindrical geometry was used. Two load levels (5 and 15 N) and three coating thickness levels (low: 5 to 10 μm; medium: 10 to 15 μm; high: 15 to 20 μm) were considered. The sliding distance was set to 500 m and three replications per test condition were run as a total. The results, in terms of volume loss due to wear, were processed using the statistical tool of two-way ANOVA and Fisher-test. It was assessed that the wear rate is strongly affected by the applied load.

Keywords: Wear; nickel coating; sliding on cylinder test; two-way ANOVA.

INTRODUCTION

In the lock industries where the production batch is very high, in order to reduce the production costs, zinc alloys are frequently used. In particular die-casting components, made of low strength materials, are used. These components must sometimes withstand cyclic loads in corrosive environment. As explained in the European Standard 12209 [1], during the test of durability of the latch action, the lock must be mounted to a fixture, which is similar to a door. Afterwards, the door is opened by a force that is cyclically applied for several cycles. During this process, the components may experience a severe wear, due to the sliding between the components. Due to process cost, the most widespread procedure adopted to improve the wear resistance is to use electrodeposited nickel coatings on zinc alloys EN 12844 [2]. In fact, the combination of cheap materials as well of nickel coatings leads to cheaper products. The testing procedure according to the current standard is very expensive in terms of time and costs. In order to respond to this issue, Accelerated Life Tests can be a very promising alternative to more economically assess the reliability of the product. In order to accelerate the test, it is necessary to know the stress field in terms of von Mises stresses and contact pressures during the test. The main failure mechanisms involved during the tests are fatigue and wear. In fact, due to the wear of the latch the stresses in the other components increase, bringing to the failure of the mechanism. So, the wear behavior of electrodeposited nickel coating has been analyzed using a slider on cylinder wear test. Two different levels for the applied force were considered (5 N and 15 N) whereas 3 different levels for the coating thickness were considered (low: 5-10 mm, medium: 10-15 mm and high: 15-20 mm).

RESULTS AND CONCLUSIONS

During the tests, the applied force, the tangential force and the LVDT output signal were determined. It made it possible to investigate the evolution of the friction coefficient throughout a test. Typical trends of friction coefficient and of system wear versus distance are shown in Fig. 1. An abrupt transition, in terms of friction coefficient, was generally retrieved after 70-150 m. At the same distance, the system wear also significantly increases.

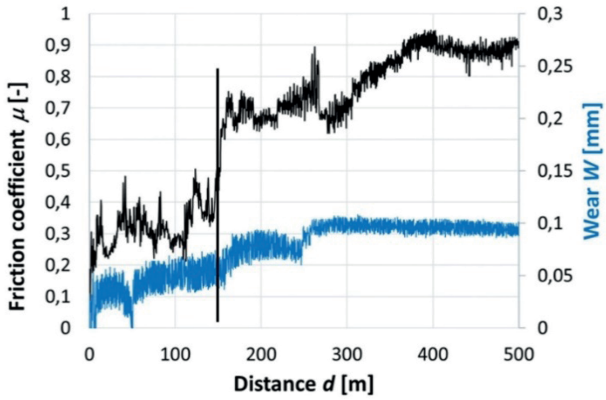

Fig. 1 – Wear test output

In order to detect the impact of each factor on the wear behavior of the studied coating, the results, in terms of wear volume lost (Fig. 2) during the test were treated by the statistical tools of two-way ANOVA and Fisher test. These tools make it possible to state if the factors involved in the experimental tests have a significant effect on the wear volume loss.

The outcome of the performed analysis indicate that the wear is strongly affected by the applied load (p-value=$2.4 \cdot 10^{-8}$). Furthermore, there is no significant effect of the coating thickness on the wear volume lost. This outcome, as mentioned before, suggests that the coating thickness is worn out completely during the first stages of the test. Finally, no significant interactions were found between applied load and coating thickness.

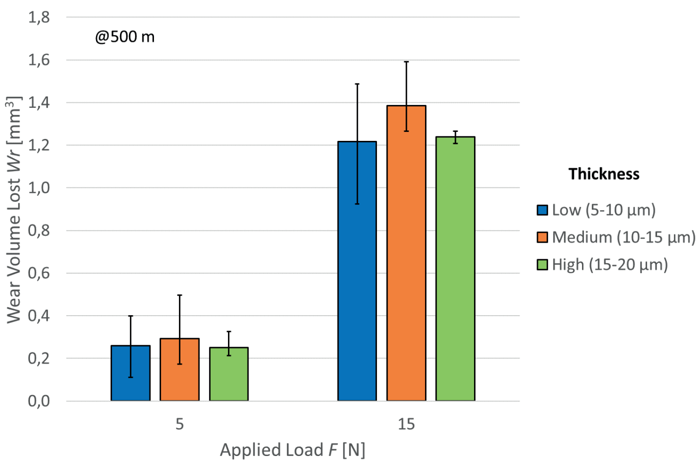

Fig. 2 – Wear volume lost at the end of the test

REFERENCES

[1] EN 12209 Building hardware – Mechanically operated locks and locking plates – Requirements and test methods; European Committee for Standardization: Brussels, 2016;

[2] EN 12844 Zinc and zinc alloys — Casting — Specification; European Committee for Standardization: Brussels, 1998;

PAPER REF: 161

DESIGN AND ANALYSIS OF ACTIVE SHOCK ABSORBER FOR CRASH ATTENUATION USING MAGNETO-RHEOLOGICAL FLUID

Alessandro Carrettin[1,2], Pieter Verberne[1], Shaker A. Meguid[1(*)], Dario Croccolo[2(**)]

[1]Mechanical and Aerospace Design Laboratory (MADL), University of Toronto, Toronto, Canada
[2]Dipartimento di Ingegneria Industriale, Università di Bologna, Bologna, Italy
[(*)]*Email:* meguid@mie.utoronto.ca
[(**)]*Email:* dario.croccolo@unibo.it

ABSTRACT

The focus of this study was to design a new magneto-rheological shock absorber (MRSA) that is capable of limiting the crippling impact force in car collisions. A number of possible conceptual designs were considered and a radial flow type MRSA was selected using a design matrix. Computer-aided FE simulations were conducted using ANSYS platform for the selected MRSA design to determine the magnetic circuit requirement. Crashworthiness analysis were also conducted, using LS-DYNA platform, to predict the energy absorption capabilities of the absorber. The results of our comprehensive design assessment reveal the feasibility of the MRSA and the validity of its use in crash boxes to reduce the severity of car collisions and the survivability of occupants.

Keywords: crashworthiness, magneto-rheological fluid, radial flow design.

INTRODUCTION

One of the most important safety features in a vehicle is an effective crash management system that is capable of absorbing the crash energy and reducing occupants' fatalities. These systems make use of effective crash boxes to absorb the crash energy. Key components in the crash box are the two collapsible thin walled tubes that absorb the majority of the impact energy. In order to optimize the crash response and energy absorption capabilities, different *active* shock reduction devices using magneto-rheological fluid have recently been proposed. In contrast to passive systems, the active MRSA will quickly determine the specific energy inputs and vary the stiffness of the crash box to mitigate the impact severity to the occupants during car collision. In this paper, we provide a number of conceptual designs and focus our attention on a selected design.

RESULTS AND CONCLUSIONS

The design specifications stipulated the following requirements. (a) Controllable active design of MRSA, (b) the crushing energy absorption should be controlled by adjusting the stiffness of the structure; (c) reduction of the collision kinetic energy, (d) MRSA should be responsive within 2-3 ms, (e) reliable and repeatable performance, (f) easy to manufacture and maintain and (g) cost effective.

Let us elaborate on items (c) and (d) above. From the legislative crash regulations of Europe and USA, the crash box has to be able to dissipate 100% of the kinetic energy during a frontal collision at 16 km/h. Since the average weight of a compact car is about 1350 kg, this means that 11.8 kJ has to be dissipated in the crash box. This means that during high speed impact

(48.3 km/h), neglecting the weight of the passengers, the crash box has to be able to dissipate 10% of the kinetic energy. Figure 1 shows an isometric view of the new radial flow MRSA. Details of all design concepts will be discussed during the presentation.

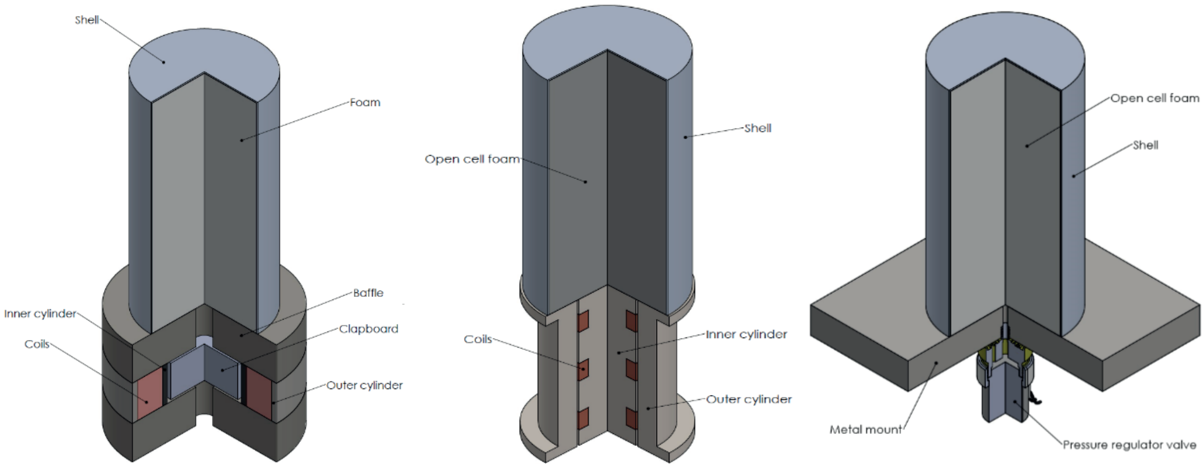

(a)Assembly of MRSA (b) Radial Flow Channels (c) Regulating Valve

Figure 1: Isometric views of the shock absorber with a pressure regulator valve

To design the magnetic circuit, the required number of coils and the amplitude of the current should be defined. To define these parameters, we ran a number of simulations considering: copper for coil materials and steel 1018 for the baffles, and the board. The outer cylinder was also made of steel 1018, to ensure high permeability and rapid demagnetization capabilities, while the inner cylinder is made of nonmagnetic 304 stainless steel. The variation of the controllable pressure drop due to the change of the magnetic field intensity is determined and analyzed. The required value of the magnetic field intensity is then identified using MATLAB. As expected, the pressure drop increases with the increase in the magnetic field intensity.

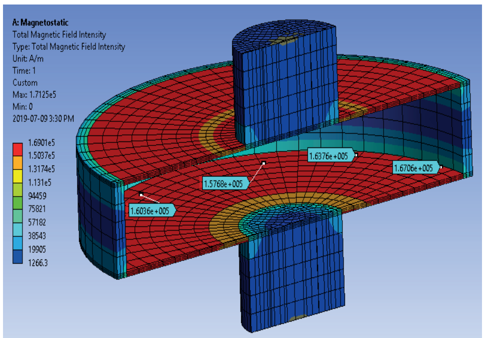

Figure 2: Response of magneto-rheological fluid to magnetic field intensity

CONCLUSIONS

We have conducted comprehensive design and analysis and devised a novel radial flow MRSA for crash attenuation. Our work reveals that the minimum value of the magnetic field needed to transmit 20 kN force to car chassis resulting from a crushing velocity of 4.17 m/s is 115 kA/m.

ACKNOWLEDGMENT

Alessandro Carrettin wishes to thank MADL of the University of Toronto for hosting him as "Visting Graduate Student" to conduct this research on MRSA for crash attenuation.

REFERENCES

David Woo et al, Frontal Crash Mitigation using MR Impact Damper for Controllable Bumper. Journal of Intelligent Material Systems and Structures, Vol. 18, 2007.
Choi, S.B., Han, Y.M, Magnetorheological Fluid Technology. Boca Raton: CRC Press, 2013.

PAPER REF: 162

THE COUPLED BEHAVIOUR OF PRECISION-GUIDED PROJECTILES SUBJECT TO PROPELLANT INDUCED SHOCK LOADS USING MULTIPHYSICS ANALYSIS

Pieter Verberne[1] and Shaker A. Meguid[1 (*)]

[1]Mechanical and Aerospace Design Laboratory (MADL), University of Toronto, Toronto, Canada
[(*)]*Email:* meguid@mie.utoronto.ca

ABSTRACT

Precision-guided projectiles (PGPs) are operated and guided by embedded electronic systems (EES). These PGPs are subjected to propellant induced shock loads often lead to the failure of the EES. In this study, we use multiphysics analysis of the launch process of PGPs accounting for propellant, PGP, confined volume and free space. In particular, we studied the entire launch process to observe local and global features of the setback, set forward pressure and acceleration histories using explicit axisymmetric Lagrangian-Eulerian finite element simulations. Furthermore, we examined the severity and frequency of the reflected waves as well as the springback of the PGPs resulting from these local oscillations as they exit the muzzle. Our results reveal the complex phenomena associated with the dynamic response of the PGPs and pressurization process resulting from the ignition of propellant during launch that are characterized by high oscillatory pressure profiles and projectile springback.

Keywords: Projectiles, Propellant, Shock, Multiphysics.

INTRODUCTION

Precision-guided projectiles (PGPs) are operated and guided by highly sophisticated embedded electronic systems (EES) that include onboard computers, GPS, micro-electro-mechanical systems and integrated circuitry. PGPs are subjected to severe shock loads resulting from the ignition of the propellant during their launch. Upon ignition, the combustion of the propellant produces high-pressure gases that lead to the acceleration of the projectile within the confined volume of the barrel. Such a launch process can be divided into two phases: the confined volume acceleration and free flight that are known as set back and set forward phases, respectively, with the transition between these two phases known as muzzle exit. During setback, the projectile is compressed due to the intense pressure loading from the combusted gases. However, at the muzzle exit, these gases are able to expand freely causing the base pressure and axial acceleration of the projectile to drop rapidly (Carlucci 2006).

This sudden decrease in loading causes the projectile to spring back inducing oscillation around its centre of gravity (Carlucci 2006). Since the barrel walls are no longer constraining the transverse movement of the projectile, the balloting accelerations in the set forward region increases to about the same intensity as the axial acceleration (Carlucci 2006). Consequently, these accelerations are transmitted to the EES, which causes great concern for the survivability of these components. It has been observed that the EES experience the greatest chance of failure at the muzzle exit and not at the maximum axial acceleration at setback (Carlucci 2006).There has been increased need to design PGPs to minimize failure of the EES. However, experimental testing is both expensive and time consuming with complex and at times unreliable highly specialized instrumentation leading to an interest in using numerical models (Chakka 2008). The numerical modelling has been split primarily two types of works, characterizing the propellant behaviour and the projectile response.

RESULTS AND CONCLUSIONS

Finite element, using Autodyn, was used to simulate the dynamics of the launch process. The system is composed of the propellant, the simplified PGP, the confined volume, and a free space extension (Fig. 1). The confined volume enables modelling of the flow and expansion of the gases during the acceleration of the projectile. The free space models the muzzle exit and the initial free flight of the projectile. More details specific to the individual components are discussed in the following subsections. Proper modelling of both the solid and fluid domains and the coupled interaction dictates the use of two different element types. Lagrangian-type solid elements were used for the modelling of the projectile. The fluid domain consisting of the propellant, confined volume, and free space were modelled using Eulerian-type elements. The discretised model showing these two element types is provided in Fig. 2.

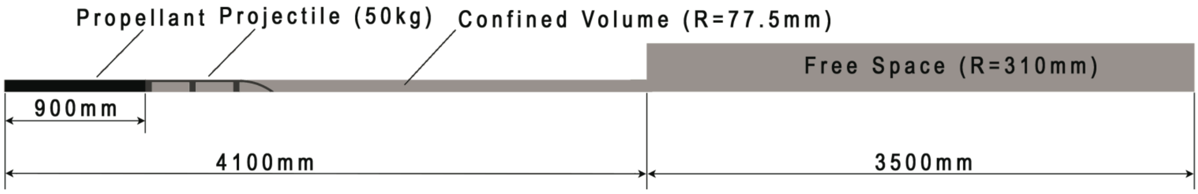

Fig. 1: Model description: geometry and materials

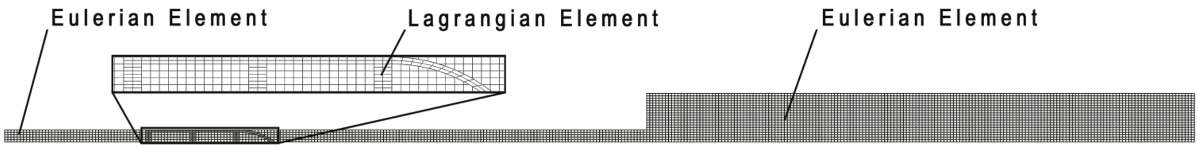

Fig. 2: Discretised mesh with Eulerian and Lagrangian domains

A comprehensive dynamic multiphysics axisymmetric Lagrangian-Eulerian finite element model is developed to study the launch process of PGPs. The model accounts for coupling and interactions effects between the different media. In addition, the flight state transition due to muzzle exit in terms of pressure and flow velocity is determined and discussed. Our results reveal the complex phenomena associated with the dynamic response of the PGPs and pressurization process resulting from the ignition of propellant during launch. It also gives an overall guidance as to the placement of the EES in PGPs.

ACKNOWLEDGMENTS

The authors gratefully acknowledge the funding by NSERC Grant # (RGPIN-2018-03804).

REFERENCES

Carlucci D, Cordes J, Hahn J, Frydman A. Electronics and the Gun Environment, Ferroelectrics, 2006a, 342, p. 193-204.

Chakka V, Tribia M, O'Toole B, Sridharala S, Ladkany S, Chowdhury M. Modeling and reduction of shocks on electronic components within a projectile, Int. J. of Impact Eng., 2008, 35, p. 1326-1338.

PAPER REF: 163

DYNAMIC RESPONSE OF BLADE SHEDDING UNDER PERIODIC IMPACT FORCE

Prayers A. Roy[1], **Shaker A. Meguid**[1(*)]

[1] Mechanics and Aerospace Design Laboratory, Department of Mechanical and Industrial Engineering, University of Toronto, Canada

(*)*Email:* meguid@mie.utoronto.ca

ABSTRACT

In this study, we examine the transient dynamic response of a rotating blade under periodic impact force at the tip of the blade due to unbalance created by blade shedding. The analytical formulation is derived assuming the blade to be non-uniform Timoshenko beam with nonlinear thickness variations. The deceleration of the rotor, because of blade shedding, is accounted for by subjecting the blade to a varying centrifugal force field. The transient analysis revealed significant effect of nonlinearity in the thickness and varying centrifugal force field on the dynamic response of the system.

Keywords: transient response, blade out, periodic impact force, non-uniform beam.

INTRODUCTION

Gas turbine engine manufacturers have always been concerned about the vulnerability of the engine to fully contain a failed blade within the engine casing and ensure the mechanical integrity requirements of the rotor. The problem is exacerbated by the pulsating contact between the blade and the casing as a result of the dynamic unbalance of the rotor (Haidari, 2008; Sinha, 2009). It is imperative that the dynamic stability of these blades are examined to ensure that no subsequent blade failures occur. In this study, the authors have presented an analytical formulation of the dynamic response of a blade based on Lagrangian mechanics taking into account nonlinearities associated with blade geometry, impact forces and centrifugal forces. The system envisaged is of a non-uniform rotating Timoshenko beam as a rotating blade under a periodic force at the tip as shown in Fig. 1. Coriolis coupling between axial and lateral displacements, rotary inertia and friction between the blade and the casing are also accounted for in the formulation.

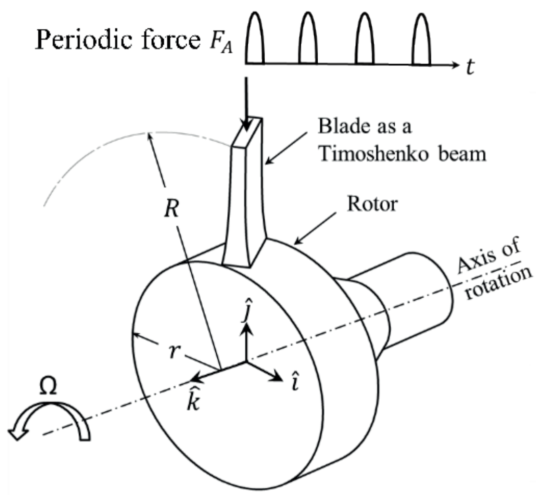

Fig. 1 – A schematic diagram of a rotating Timoshenko beam under periodic force at the tip

First, the parametric analysis of axial and lateral natural frequencies of the beam is performed to examine the effect of geometric nonlinearity and centrifugal force field on the dynamic characteristics of the beam. In the next step, the non-uniform beam is subjected to loading conditions as experienced in blade shedding for the evaluation of the transient response.

The tip of the beam is subjected to periodic sinusoidal pulses representative of the impact forces at the tip of the blade due to periodic contact with the casing. In addition, the effect of rotor deceleration is examined by subjecting the rotating blade to linear and nonlinear decaying centrifugal force field.

RESULTS AND CONCLUSIONS

The results of the selected case of an exponentially taper beam are presented here. Table 1 shows the variation of lateral natural frequencies of the beam in non-dimensional terms with the change in taper and rotational speed. The results show that the lateral natural frequencies decrease with the increase in the taper, except for the first lateral natural frequency which shows increasing trend with the increase in the taper. All later natural frequencies increase with the increase in the rotational speed.

Table 1 – Variation in lateral natural frequencies $\overline{\varpi}$ of a beam with taper ratio $\overline{h}$ and rotational speed $\overline{\Omega}$

	$\overline{\Omega}=5$					$\overline{\Omega}=10$				
$\overline{h}$	$\overline{\varpi}_1$	$\overline{\varpi}_2$	$\overline{\varpi}_3$	$\overline{\varpi}_4$	$\overline{\varpi}_5$	$\overline{\varpi}_1$	$\overline{\varpi}_2$	$\overline{\varpi}_3$	$\overline{\varpi}_4$	$\overline{\varpi}_5$
0	5.94	26.23	62.60	111.53	169.63	9.96	37.30	77.22	129.11	189.64
0.4	6.22	23.45	52.62	92.98	142.45	10.33	34.58	67.30	110.33	161.91
0.8	6.71	18.96	35.98	59.54	89.86	11.18	30.59	52.37	79.06	111.66

The effect of constant, linear and exponential decay of the centrifugal force field on the transient response of a beam under periodic pulsating force is shown in Fig. 2. The decaying centrifugal force field due to deceleration of the rotor increases the vibration by an order of magnitude and can severely affect the stability of the blade.

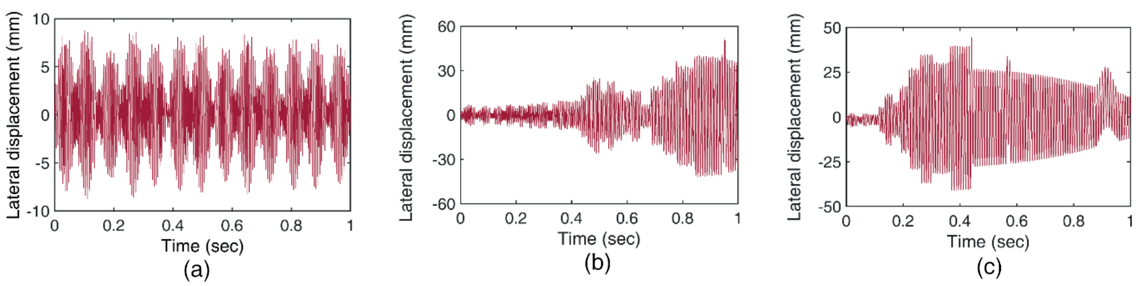

Fig. 2 – Effect of (a) constant, (b) linear, and (c) exponential decaying centrifugal force field on the transient response

ACKNOWLEDGMENTS

The authors gratefully acknowledge the funding by NSERC under grant number RGPIN-2018-03804.

REFERENCES

Heidari M, Carlson D, Sinha S, Sadeghi R, Heydari C, Bayoumi H, Son J. An efficient multi-disciplinary simulation of engine fan-blade out event using MD Nastran. 49th AIAA/ASME/ASCE/AHS/ASC Structures, Structural Dynamics, and Materials Conference, 2008, Schaumburg, IL, p. 2333.

Sinha, SK, Dorbala, S. Dynamic loads in the fan containment structure of a turbofan engine. Journal of Aerospace Engineering, 2009, 22(3), p. 260-269.

KEYWORD INDEX

Symbols

A

B

C

D

E

F

N

O

P

T

U

V

W

Y

Z